Advances in Polymer Science 271

Orlando J. Rojas *Editor*

Cellulose Chemistry and Properties: Fibers, Nanocelluloses and Advanced Materials

Springer

271
Advances in Polymer Science

Aims and Scope

The series Advances in Polymer Science presents critical reviews of the present and future trends in polymer and biopolymer science. It covers all areas of research in polymer and biopolymer science including chemistry, physical chemistry, physics, material science.

The thematic volumes are addressed to scientists, whether at universities or in industry, who wish to keep abreast of the important advances in the covered topics.

Advances in Polymer Science enjoys a longstanding tradition and good reputation in its community. Each volume is dedicated to a current topic, and each review critically surveys one aspect of that topic, to place it within the context of the volume. The volumes typically summarize the significant developments of the last 5 to 10 years and discuss them critically, presenting selected examples, explaining and illustrating the important principles, and bringing together many important references of primary literature. On that basis, future research directions in the area can be discussed. Advances in Polymer Science volumes thus are important references for every polymer scientist, as well as for other scientists interested in polymer science - as an introduction to a neighboring field, or as a compilation of detailed information for the specialist.

Review articles for the individual volumes are invited by the volume editors. Single contributions can be specially commissioned.

Readership: Polymer scientists, or scientists in related fields interested in polymer and biopolymer science, at universities or in industry, graduate students.

Special offer:
For all clients with a standing order we offer the electronic form of Advances in Polymer Science free of charge.

More information about this series at http://www.springer.com/series/12

Orlando J. Rojas
Editor

Cellulose Chemistry and Properties: Fibers, Nanocelluloses and Advanced Materials

With contributions by

S. Asaadi · M.N. Belgacem · K. Dazen · C. Fritz · A. Gandini · A.P. Gomes · R. Gonzalez · I.C. Gouveia · W.Y. Hamad · L.K.J. Hauru · T. Heinze · M. Hummel · H. Jameel · B. Jeuck · D.K. Johnson · K. Kafle · S.H. Kim · A.W.T. King · I. Kilpeläinen · C. Lee · Y. Ma · J.F. Mano · A. Michud · A. Moore · Y. Nishio · J. Oberlerchner · S. Park · A. Parviainen · A. Potthast · J.A. Queiroz · D. Reishofer · O.J. Rojas · T. Rosenau · C. Salas · J. Sato · H. Sixta · S. Spirk · K. Sugimura · M. Tanttu · P. Vejdovszky · T. Zweckmair

Springer

Editor
Orlando J. Rojas
Departments of Forest Biomaterials and
Chemical and Biomolecular Engineering
North Carolina State University
Raleigh, North Carolina
USA

Bio-based Colloids and Materials (BiCMat)
Department of Forest Products Technology
School of Chemical Technology
Aalto University, Espoo
Finland

ISSN 0065-3195 ISSN 1436-5030 (electronic)
Advances in Polymer Science
ISBN 978-3-319-26013-6 ISBN 978-3-319-26015-0 (eBook)
DOI 10.1007/978-3-319-26015-0

Library of Congress Control Number: 2016932497

Springer Cham Heidelberg New York Dordrecht London

Printed on acid-free paper

Springer International Publishing AG Switzerland is part of Springer Science+Business Media (www.springer.com)

Preface

This volume of *Advances in Polymer Science* is centered on the very timely topic of cellulose chemistry and properties and makes special emphasis on fibers, nanocelluloses and the development of advanced materials from such sources. The subject is important as polymer science and associated fields gravitate towards bio-based materials and products in developments current to the "bioeconomy". As such, ten expert groups were invited to provide their input in complementary areas and to draft a cohesive text that is now brought to fruitful completion and that I hope you find of interest and use.

The opening is by Thomas Heinze, from Friedrich Schiller University of Jena, who discusses the structure and properties of cellulose. It soon becomes obvious to the reader that cellulose is a fascinating polymer, making part of fibers and other structures that are ubiquitous in a variety of products and processes. Besides addressing the issue of solubility and chemical reactivity, bottom-up approaches to nanostructures of cellulose and the use of ionic liquids are presented. Both subjects are expanded in other chapters within this volume. It strikes the fact that while "cellulose" has been a topical subject, still there is a major need for better understanding of associated interactions and interfacial properties.

Antje Potthast and co-workers from the University of Natural Resources and Life Sciences in Vienna enlighten the volume with their discussion on the preparation and analysis of cello- and xylooligosaccharides. They provide a comprehensive and up-to-date overview about related preparation, separation, and analytical methods. This is extremely relevant to the sugar platform in biorefinery processes. On a higher structural scale, colleagues, also in Austria, David Reishofer and Stefan Spirk (Graz University of Technology), provide a comprehensive review towards understanding of cellulose accessibility, structure and function, with a particular focus on deuteration and allied methods, including small angle neutron scattering and 2H-NMR spectroscopy. Further on characterization of cellulose and its structures, a team led by Seong Kim and Sunkyu Park, from Penn State University, North Carolina State University and the National Renewable Energy Laboratory

expand on cellulose crystallinity and its measurements and correlations as determined by XRD, NMR, IR, Raman, and SFG.

Returning to the topic of ionic liquids but now looking into their deployment, a group led by Herbert Sixta and Michael Hummel, from Aalto University in Finland, introduces the production of man-made cellulosic fibers. They give a comprehensive account of opportunities and challenges. The summary of the reports on the preparation of pure cellulosic and composite fibers is complemented with an overview of the rheological characteristics and thermal degradation of cellulose-ionic liquid solutions, in light of the production of textile yarns and their applications. Recognizing that physical and chemical features in cellulose can be exploited to adjust its use, Alessandro Gandini and Mohamed Naceur Belgacem, from the Print Media and Biomaterials (Pagora) in Grenoble, expand on the topic of surface and in-depth modification of cellulose fibers and compile the most relevant advances achieved in the field. Their report includes cellulose nanocrystals (CNC), cellulose nanofibrils (CNF), microfibrillated cellulose (MFC) and bacterial cellulose (BC), as well as conventional lignocellulosic fibers.

Further on nanocellulose, as introduced in the previous contribution, our team in North Carolina and Aalto University, adds with a discussion on the importance of nanocellulose-protein interactions, including immobilization and synthesis of biocompatible materials. The topic is supplemented with the work of Isabel Gouveia and coworkers from five different research centers in Portugal, who discuss the biofunctionalization of cellulosic fibers with emergent antimicrobial agents, mainly using the layer-by-layer assembly approach.

Yoshiyuki Nishio and coworkers in Kyoto University as well as Wadood Hamad, from FPInnovations and University of British Columbia, introduce the fascinating topic of cellulose liquid crystals. Striking ordered structures are described for the design of functional material systems, mainly from cellulose nanocrystals. Both fundamental and applied research covering chiral nematic order and the development of photonic and semiconductor materials based on cellulose are offered.

To end, I would like to personally express my appreciation for the time and energy devoted by all contributing authors in making this project a reality. I am also very thankful for their patience as we approached the conclusion of this volume that took more time than expected. Also very deserving are the reviewers for their excellent service and feedback as well as the editorial team of *Advances in Polymer Science*, who assisted all of us through the process of editing and processing the manuscripts. I am confident the readers of this volume appreciate cellulose prospects and its outlook for future explorations. I also hope that the chapters are found informative and beneficial to those entering the field as well as those from academia and industry who are already familiar with cellulose, a fascinating natural polymer.

Raleigh, USA
Espoo, Finland

Orland J. Rojas

Contents

Adv Polym Sci (2016) 271: 1–52
DOI: 10.1007/12_2015_319

Published online: 10 September 2015

Cellulose: Structure and Properties

Thomas Heinze

Abstract Cellulose, a fascinating biopolymer and the most common organic compound on earth, is comprehensively reviewed. Details of its crystalline phases are given, starting with a description of molecular and supramolecular structures, including the hydrogen bond systems. Sources of this ubiquitous biopolymer are mentioned, with attention to the special properties of bacterially synthesized nanofibrous cellulose. Nanostructures obtained by disintegration of cellulose fibers (top-down approach) yielding nano- or microfibrillated cellulose and cellulose whiskers are the basis for novel materials with extraordinary properties. Moreover, nanofibers and nanoparticles can be made by special techniques applying the bottom-up approach. Efficient systems to dissolve cellulose by destruction of the hydrogen bond systems using ionic liquids and systems based on polar aprotic solvent and salt are described. Novel cellulose derivatives are available by chemical modification under heterogeneous or homogeneous conditions, depending on the cellulose reactivity. In particular, unconventional nucleophilic displacement reactions yielding products for high-value applications are highlighted. Novel amino cellulose derivatives showing fully reversible aggregation behavior and nanostructure formation on various materials are the focus of interest. Finally, "click chemistry" for the synthesis of novel cellulose derivatives is discussed.

Keywords Amino cellulose · Cellulose · Nanostructuring · Reactivity · Solubility · Structure · Supramolecular architecture

T. Heinze (✉)
Centre of Excellence for Polysaccharide Research, Institute of Organic Chemistry and Macromolecular Chemistry, Friedrich Schiller University of Jena, Humboldtstrasse 10, 07743 Jena, Germany
e-mail: Thomas.heinze@uni-jena.de

Contents

1 Introduction

Cellulose is the most abundant natural polymer in the biosphere, with a global production (and decomposition) of ~1.5×10^{12} tons per year, comparable to the planetary reserves of the main fossil and mineral sources [1]. In addition to the long-standing scientific interest in cellulose, the use of cellulose as renewable and biodegradable raw material in various applications is a proposed solution to the recent industrial challenge to successfully meet environmental and recycling problems [2]. Versatile structuring of cellulose by various routes of modification, including both physical and chemical methods, has enabled its use in a variety of applications (e.g., fillers, building and coating materials, laminates, papers, textiles, optical films, sorption media, viscosity regulators, and even advanced functional materials) [3].

The earliest systematic efforts that lead to the discovery of cellulose began in 1837 with the work of the French chemist Anselme Payen, who showed that various plant materials yielded a fibrous substance after purification with acid-ammonia treatment and extraction with water, alcohol, and ether. The French Academy finally named the resulting carbohydrate “cellulose” [4]. Nowadays, there are various processes used to isolate cellulose, for example, the alkaline, bisulfite,

and sulfate (kraft-) processes, in combination with thermal and mechanical treatments. The different processes result in varying fiber strengths of the pulp [5, 6].

The aim of this review is to discuss the different structural levels of cellulose and to describe important properties that result from this unique structure. Moreover, advanced micro- and nanostructural materials based on cellulose obtained by physical and hydrolytic treatments (top-down approaches) as well as the bottom-up elaboration of nanostructures by electrospinning and nanoprecipitation are highlighted. Finally, one of the most important paths for the design of highly engineered products, namely chemical modification of cellulose (particularly under homogeneous reactions conditions), is summarized with consideration of our own research in the field of chemical modification of cellulose by advanced organic chemistry.

2 Sources of Cellulose

Cellulose is distributed throughout nature in plants, animals, algae, fungi, and minerals (Fig. 1). However, the major source of cellulose is plant fiber. Cellulose contributes approximately 40% to the carbon fraction in plants, serving as structuring element within the complex architecture of their cell walls. Cellulose can occur in pure form in plants but it is usually accompanied by hemicelluloses,

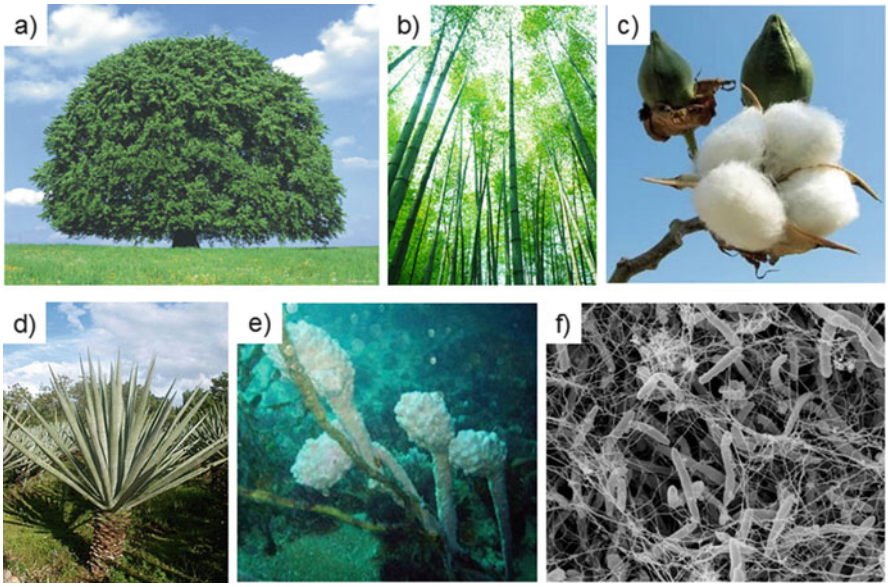

Fig. 1 Selection of important cellulose sources: (**a**) hard wood (beech tree), (**b**) bamboo, (**c**) cotton, (**d**) sisal, (**e**) tunicine, and (**f**) *Gluconacetobacter xylinum* (reproduced with permission from Schubert et al. [7])

lignins, and comparably small amounts of extractives. Wood contains about 40–50 wt% cellulose. Comparable amounts can be found in bagasse (35–45 wt%), bamboo (40–55 wt%), straw (40–50 wt%), and even higher in flax (70–80 wt%), hemp (75–80 wt%), jute (60–65 wt%), kapok (70–75 wt%), and ramie (70–75 wt %). Cotton is a fairly pure cellulose source, containing more than 90 wt% [8]. An impressive amount of cellulose is produced each year, not only in wood fiber from trees (ca. 1,750,000 kt world production) but also in annual plants such as bamboo (10,000 kt), cotton linters (18,450 kt), jute (2,300 kt), flax (830 kt), sisal (378 kt), hemp (214 kt), and ramie (100 kt) [9]. In addition, several fungi and green algae produce cellulose (e.g., *Valonia ventricosa*, *Chaetamorpha melagonicum*, *Glaucocystis*) and some (marine) animals such as ascidians contain cellulose in their outer membrane. Moreover, bacteria of the genera *Gluconacetobacter*, *Agrobacterium*, *Pseudomonas*, *Rhizobium*, and *Sarcina* can synthesize bacterial cellulose from glucose and various other carbon sources [10, 11]. Bacterial cellulose, which is produced directly as a fibrous network, contains no lignin, pectin, hemicelluloses, or other biogenic products; it is very highly crystalline and possesses a high degree of polymerization (DP).

3 Structure of Cellulose

3.1 Molecular Structure

Independent of the source, cellulose consists of D-glucopyranose ring units in the $^4C_1$-chair configuration, which exhibits the lowest energy conformation [12]. Such units are linked by β-1,4-glycosidic bonds that results in an alternate turning of the cellulose chain axis by 180°. Cellobiose with a length of 1.3 nm can be considered the repeating unit of cellulose [13]. Three reactive hydroxyl groups exist in each anhydroglucose unit (AGU) within the cellulose chain, a primary group at C6 and two secondary groups at C2 and C3 that are positioned in the plane of the ring (Fig. 2).

As is typical for a polymer formed by "polycondensation," the chain ends of the cellulose molecule are chemically different [14]. One end contains an anomeric C atom linked by the glycosidic bonds (nonreducing end) whereas the other end has a D-glucopyranose unit in equilibrium with the aldehyde function (reducing end group).

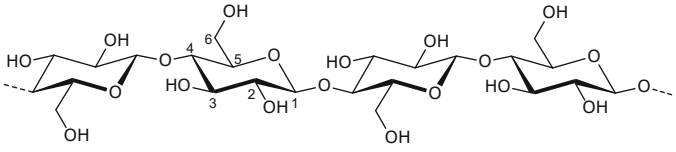

Fig. 2 Representation of a cellulose molecule

Changes in the molecular structure originate from reactions leading to hydrolysis or oxidation of the cellulose chain. Such reactions mainly occur on the surface of the fibrils or in amorphous regions.

The DP of native cellulose of various origins is in the range of 1,000–30,000, which corresponds to chain lengths of 500–15,000 nm. The cellulose samples that are obtained by isolation methods possess DP values ranging between 800 and 3,000 [13]. Cellulose samples are polydisperse, thus, the DP is an average value. There are several techniques that can give information about the molar masses and their distribution, including viscosity measurements, size-exclusion chromatography, and light scattering.

3.2 Hydrogen Bonding

Cellulose possesses various systems of hydrogen bonds, which have a significant influence on properties [15]. For instance, the limited solubility in most solvents, the reactivity of the hydroxyl groups, and the crystallinity of cellulose samples originate from strong hydrogen bonding systems. Cellulose also contains hydrophobic areas (around the C atoms) that have a certain influence on the overall properties, including solubility.

The three hydroxyl groups of the AGU, the oxygen atoms of the D-glucopyranose ring, and the glycosidic linkage interact with each other within the chain or with another cellulose chain by forming intramolecular and intermolecular hydrogen bonds. The hydrogen bonds give rise to various three-dimensional arrangements.

Infrared (IR) [16, 17] and solid state ^{13}C-NMR spectroscopy [18] revealed that the OH group at C3 and adjacent ether oxygen of the AGU units form intramolecular bonds together with those between the oxygen atoms in the hydroxyl group at C6 and neighboring hydroxyls linked to C2. Together with the β-glycosidic covalent linkage, the intramolecular hydrogen bonds are responsible for the rigidity or stiffness of the cellulose polymer [13]. As a result, highly viscous solutions are produced from cellulose relative to those obtained from equivalent polysaccharides bonded by α-glycosidic linkages. This also leads to a high tendency to crystallize or to form fibrillar structures.

Intermolecular hydrogen bonding is responsible for the strong interaction between cellulose chains. The bonds are produced between adjacent cellulose macromolecules located along the (002) plane in the crystal lattice of cellulose I (native cellulose), mainly between the oxygen atom in C3 and the OH at C6 (see Sect. 3.3) [19]. Together, the hydrogen bonding, weak C–H–O bonds, and hydrophobic interactions are responsible for the assembly of cellulose in layers, as elucidated by synchrotron X-ray and neutron diffraction experiments [20].

Cellulose II (see Sect. 3.3) shows a different hydrogen bonding system. Because of the existence of an intermolecular hydrogen bond between the OH groups of C6 and C2 of another chain, the intramolecular bonding of OH in C2 is avoided and an

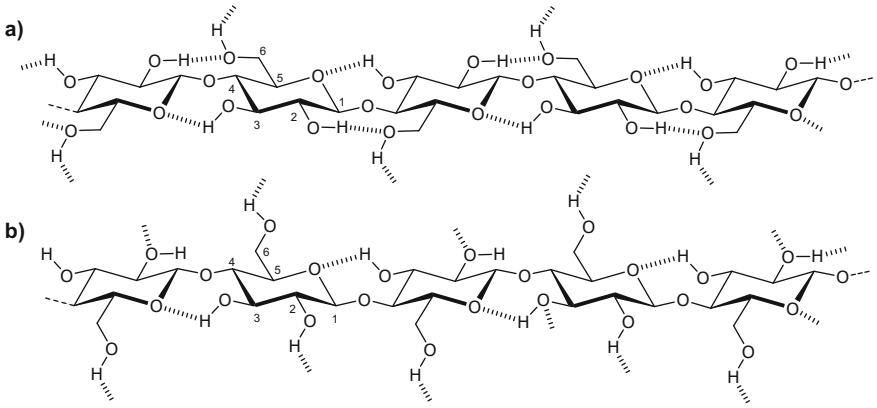

Fig. 3 Hydrogen bonding system of (**a**) cellulose I and (**b**) cellulose II (reproduced with permission from Tashiro and Kobayashi [22], copyright 1991, with permission from Elsevier)

intermolecular hydrogen bond of OH–C2 to OH–C2 of the next chain is formed [21]. In comparison to cellulose I, the cellulose II molecules are more densely packed and strongly interbonded and, therefore, cellulose II is less reactive, as commonly observed [13]. Figure 3 shows a scheme of the hydrogen bonding system in cellulose I and II.

3.3 Crystal Modifications

The regular structure of cellulose leads to X-ray diffraction patterns that reveal its degree of crystallinity. There were a number of inconsistencies in the crystalline structure described for different cellulose modifications after certain treatments [23]. X-ray and NMR experiments confirmed the dimorphism [24]. X-ray diffraction patterns and solid-state ^{13}C-NMR revealed cellulose conformations (Figs. 4 and 5) that were used to elucidate the detailed crystalline structure and the basis for transformation in the various allomorphs [25].

Celluloses from different sources possess comparable crystallinity (i.e., modifications of cellulose I). However, solid state ^{13}C-NMR studies revealed that cellulose can crystallize with varying proportions of two different phases, named cellulose I_α and I_β. Plant cellulose mainly consists of cellulose I_β, whereas cellulose produced by primitive organisms crystallizes in the I_α phase. The monoclinic unit cell of cellulose I_α with a space group $P2_1$ consists of two cellulose molecules, each containing a cellobiose unit in the 002 corner plane and 002 center plane in a parallel fashion [19]. Cellulose I_β corresponds to a triclinic symmetry with space group P_1 containing one chain in the unit cell, as schematically displayed in Fig. 6a.

Cellulose I can be transformed into the thermodynamically stable crystalline form of cellulose II by regeneration from the dissolved state or mercerization.

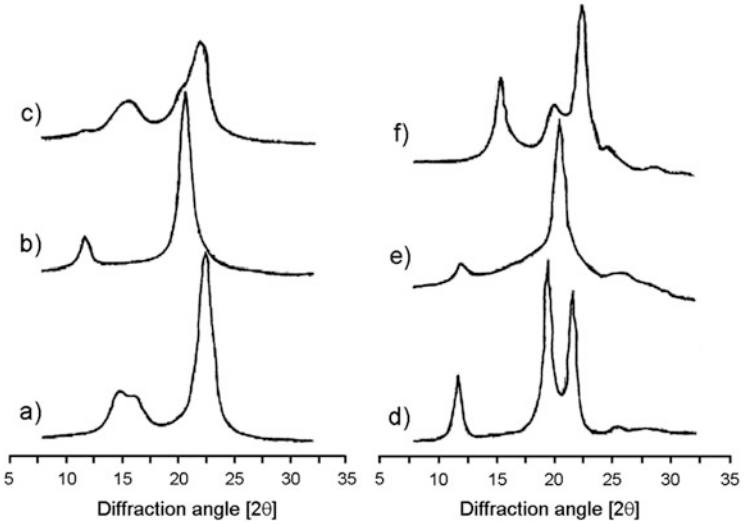

Fig. 4 X-ray diffraction patterns of (**a**) cellulose I_β, (**b**) cellulose III_I, (**c**) cellulose IV_I, (**d**) cellulose II, (**e**) cellulose III_{II}, and (**f**) cellulose IV_{II} (adapted from Isogai et al. [25], copyright 1989 with permission from American Chemical Society)

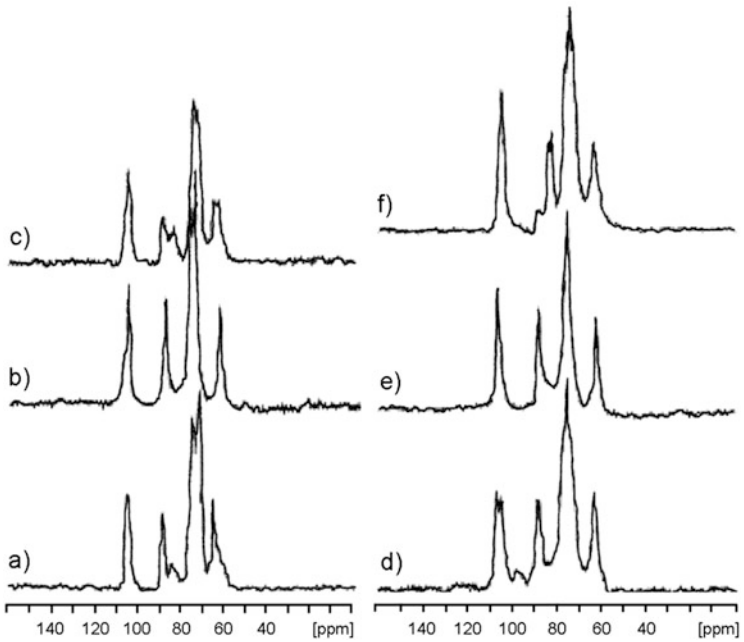

Fig. 5 Solid state ^{13}C-NMR spectra of (**a**) cellulose I_β, (**b**) cellulose III_I, (**c**) cellulose IV_I, (**d**) cellulose II, (**e**) cellulose III_{II}, and (**f**) cellulose IV_{II} (adapted from Isogai et al. [25], copyright 1989 with permission American Chemical Society)

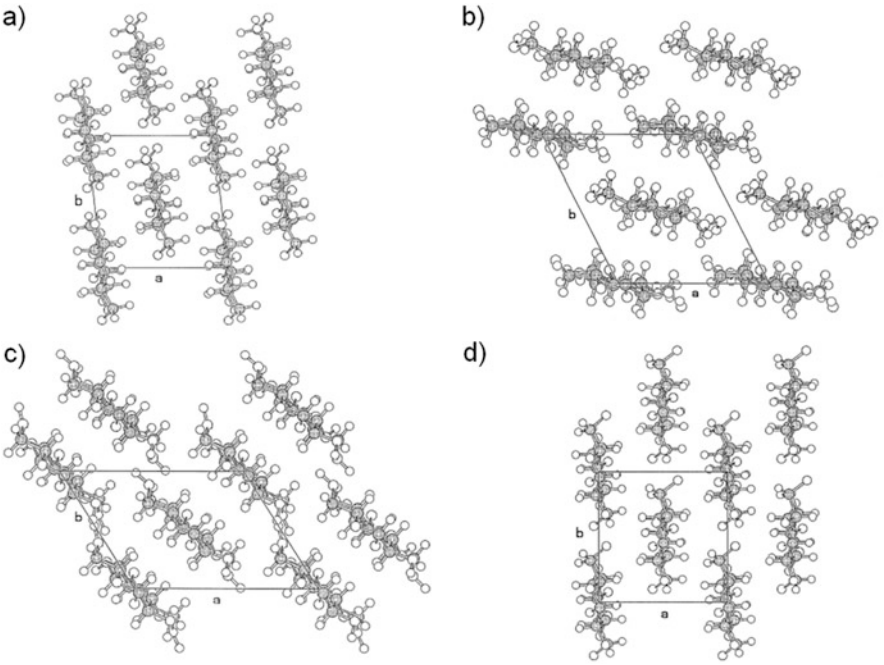

Fig. 6 Models of (**a**) cellulose I_β, (**b**) cellulose II, (**c**) cellulose III_I, and (**d**) cellulose IV_I (reproduced from Zugenmaier [26], copyright 2001, with permission from Elsevier)

Mercerized cellulose II can easily be achieved by treatment of cellulose with alkali at concentrations >18 wt% and subsequent thorough washing. The irreversible transition to cellulose II is used for improving the quality of natural fibers and yarns. Moreover, the treatment of cellulose with aqueous alkali (mainly aqueous sodium hydroxide) is the key step for activating the polymer prior to heterogeneous chemical modification, particularly for commercial etherification. The structure of cellulose II was revised by neutron fiber diffraction analysis [27]. Two chains of cellulose are located antiparallel on the 2_1 axis of the monoclinic cell (Fig. 6b), while the chains are displaced relative to each other by about one fourth of the AGU.

The treatment of cellulose I and II with liquid ammonia and certain amines results in the formation of cellulose III_I and III_{II}, respectively, possessing the same unit cell [26]. The structures can easily be reconverted into cellulose I or II by mild heating. The crystalline structure of cellulose III_I can be described as a one-chain unit cell and a $P2_1$ space group, with the cellulose chain axis on one of the 2_1 screw axes of the cells [28]. A single chain of cellulose III_I is similar to one of the two chains existing in a crystal of cellulose II.

Cellulose III can be transformed into cellulose IV_I or IV_{II} in glycerol at high temperatures, depending on the starting materials used. However, the conversion is

never quantitative, which complicates complete analysis of the crystallinity [29]. The space group P_1 is assumed for both structures.

In addition to the crystalline domains, there are also amorphous or noncrystalline regions in cellulose, which influence the physical and chemical properties of celluloses [30]. Interactions between solid cellulose and water, enzymes, and reactive or adsorptive substances occur first at the noncrystalline, amorphous domains or at the surface of cellulose crystals. Entire amorphous cellulose samples can be prepared by ball-milling of cellulose [31], deacetylation of cellulose acetate under nonaqueous alkaline conditions [32], or precipitation from nonaqueous cellulose solutions into nonaqueous media avoiding stress [33]. However, the amorphous structures are usually unstable in the presence of water and form partly crystalline cellulose II. Interestingly, it was found that Raman and solid state ^{13}C-NMR spectra of amorphous and highly crystalline cellulose IV_{II} are almost identical, which confirms the similarity of the secondary structures of the two cellulose types [34].

Regarding the use of cellulose and its chemical derivatization, the crystal structures of cellulose I and II are important. As far as this author knows, there are no established technical processes nor cellulose-based products using or possessing any other crystalline structures.

3.4 Morphology

3.4.1 Plant Cellulose

Cellulose is organized in parallel assemblies of elementary crystallites, which organize into fibers via hydrogen bonding [13]. Whereas areas of lower order or noncrystalline regions contain turns between neighboring chains, ordered crystallites pack cellulose chains folded in a longitudinal direction. The less ordered regions display a relatively lower density and more random orientation [35]. The cellulose chains arrange as a basic fibrillar unit, the so-called elementary fibrils, which have been reported to be 100 nm in length and have a characteristic lateral dimension of 1.5–3.5 nm [1]. Such elementary fibrils are further assembled as fibrillar bundles, called microfibrils, with widths in the range of 10–30 nm. Also, microfibrillar bands form, of the order of 100 nm in width and lengths of hundreds of nanometers or even a few microns (Fig. 7). Such fibrillar architectures are characteristic of both native and manmade fibers [13]. However, in plant cell walls, a sheath of amorphous cellulose, which is surrounded by hemicelluloses, further covers the microfibrils [9].

Fibers from different sources display different morphologies and dimensions. For example, cotton fibers are twisted (Fig. 8a) whereas those from spruce wood are generally untwisted (Fig. 8b). In contrast, fibers from bast plants are straight and round (Fig. 8c). Interestingly, they all share an internal structure made up of multiple cell wall layers. During the growth period, plant fibers develop a primary

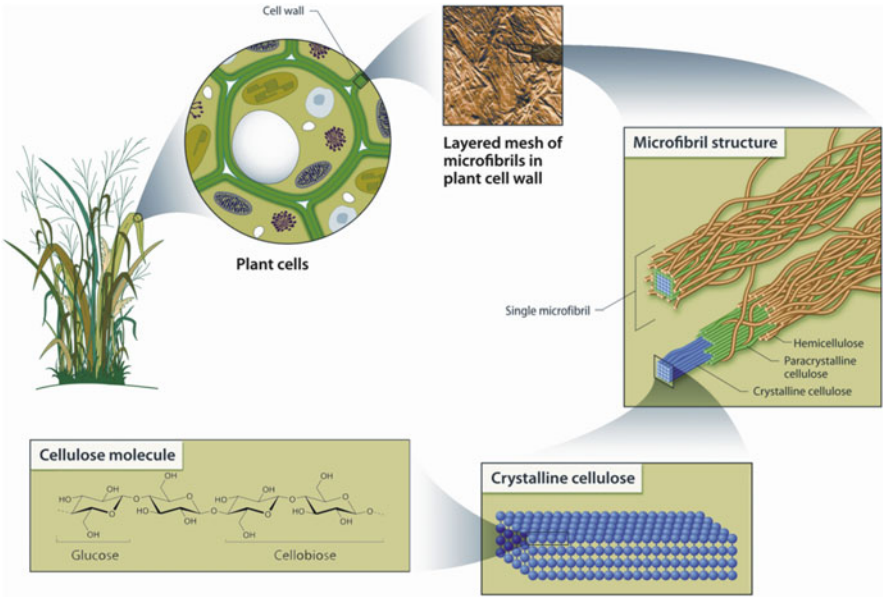

Fig. 7 Association of cellulose molecules in the plant cell wall (reproduced from https://public.ornl.gov/site/gallery/detail.cfm?id=181&topic=&citation=&general=Cellulose&restsection=all, U.S. Department of Energy Genomic Science program, http://genomicscience.energy.gov)

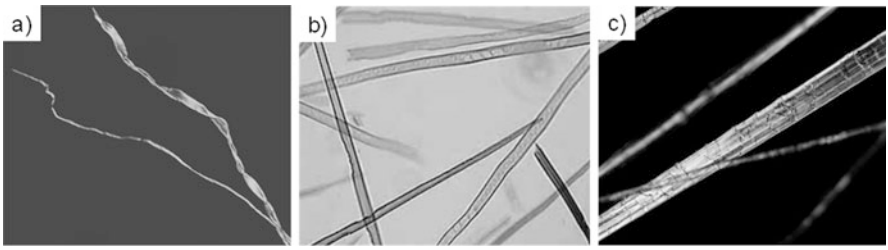

Fig. 8 Micrographs of (**a**) twisted cotton fibers, (**b**) tracheids of spruce wood, and (**c**) straight fibers of ramie (reproduced with permission from Ioelovich and Leykin [36])

cell wall layer (P) that is much thinner than the secondary wall (S), which is formed on its inner side. Further inside, the tertiary cell wall (T) is exposed to an open, hollow area or lumen resulting in typical hollow, cylinder-like plant cells. The cell wall thickness and length of plant fibers are about 4–6 30 μm and 15–30 μm, respectively. The P and T layers contain disordered cellulose nets with dimensions of ~100 nm. The swelling characteristics of fibers (as well as their physical and chemical properties) are influenced by the configuration, composition, and structure of the P layer, which contains microfibrils criss-crossed onto each other to make a network-like helical structure. The secondary layer (~3–5 μm thickness) comprises

three sublayers (S1, S2, and S3) of which S2 is the thickest (2–4 μm). The S2 layer contains microfibrils arranged parallel to each other and oriented at a given average helical angle with respect to the fiber axis, the so-called microfibril angle. It is noteworthy that the tensile strength of the fibers correlates inversely with the microfibril angle [36]. The fibers also display a variety of features and defects that facilitate chemical attack and mechanical failure, including pores or openings (pits), cracks, damage sites, compression failures, nodes, and thinning regions.

The fibrillar arrangement of regenerated cellulose is different; manmade fibers also consist of elementary fibrils but with a random location in the supramolecular structure [37]. Applying a precipitation process without shear forces, the crystallites are randomly distributed in a semi-amorphous matrix, whereas in a film-forming procedure the crystallites are positioned parallel to the film surface with an orientation in the direction of the draw [38]. The crystallites are aligned with the longitudinal axis in the direction of stretch in regenerated cellulose fibers, but with a certain transverse nonuniformity that depends on the spinning conditions applied.

3.4.2 Morphology of Bacterial Cellulose

Compared with plant cellulose, bacterial cellulose (BC) is very pure (contains no hemicelluloses and lignin) and only a very low amount of carbonyl and carboxyl moieties are present [7]. BC possesses high crystallinity (more than 80%), excellent water absorption capacity, and extraordinary mechanical strength, particularly in the wet state, resulting mainly from the presence of nanofibrils of BC rather than microfibers of plant cellulose (see Sect. 4). An important advantage of BC is its in situ moldability (i.e., shaping during biosynthesis) [39].

BC consists of a three-dimensional network of ultrafine cellulose fibrils with a diameter in the range of 80–150 nm and can contain up to 99% water in the initial never-dried state. In addition, the DP value of BC is high, with values of up to 10,000 [40].

Under static culture conditions, layers (sheets) of BC of up to several centimeters thickness are formed on the surface of the culture medium. It is important to control the pH because the accumulation of gluconic-, acetic-, or lactic acids in the culture broth decreases the pH far below the optimum for growth and cellulose production [41]. In the 1980s, Johnson & Johnson (New Brunswick, USA) started to commercialize sheets of BC on large scale for the treatment of different wounds [42, 43]. Independently, a Brazilian company, BioFill Produtos Biotecnologicos (Curitiba, PR Brazil), created a new wound healing system based on BC [1, 44, 45]. At present, commercial products such as Suprasorb X® are distributed by Lohmann & Rauscher (Neuwied, Germany).

In contrast to stationary culture conditions, various reactors (e.g., the rotating disk fermenter) were developed to produce BC under agitated culture conditions that prevent conversion of cellulose-producing strains into cellulose-negative mutants. Morphological differences between the cellulose produced by static and

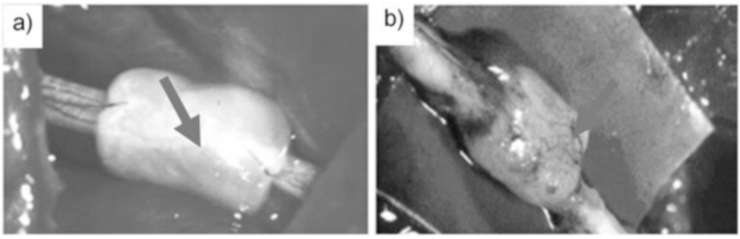

Fig. 9 Sciatic nerve of a rat with a BASYC® tube as protective cover (**a**) immediately and (**b**) 10 weeks after the operation (reproduced from Klemm et al. [47], copyright 2006 with permission from Springer)

agitated cultures contribute to varying degrees of crystallinity, crystalline sizes, and cellulose I_α content. The crystallinity index is closely related to the I_α content [46].

Shaping of BC in a static culture by applying a template matrix can yield different shapes, including tubes of different length, wall thickness, and inner diameter (e.g., BASYC® bacterial synthesized cellulose tubes). The roughness of the BASYC® tubes in the wet state resembles blood vessels and ranges between 7 and 14 nm. Their tremendous mechanical strength provides the stability necessary for microsurgical preparation and to withstand the blood pressure of the living body (Fig. 9) [1, 47].

4 Nanostructures of Cellulose and Their Properties

Natural cellulose can be transformed into micro- and nanoscale materials by applying specific top-down approaches, yielding defined products such as microcrystalline cellulose, microfibrillar cellulose, and whiskers (see Fig. 10) [48].

The micro- and nanoscale materials mainly differ in DP and crystallinity according to the disintegration technique used and, consequently, differ in shape. Figure 11 shows examples of micro- and nanoscaled cellulose samples in comparison with native bacterial cellulose.

4.1 Microcrystalline Cellulose

Microcrystalline cellulose (MC) is a fine, white, and odorless crystalline powder (commercial products include Avicel®, Heweten®, Microcel®, Nilyn®, and Novagel®) used in pharmaceutical (tablet binder), food (rheology control), and paper applications as well as in composite manufacturing [49]. MC is commercially produced by treatment of biomass with aqueous sodium hydroxide to remove other constituents [50], followed by acidic hydrolysis. During hydrolysis, the DP of cellulose decreases with hydrolysis time until reaching a plateau value called

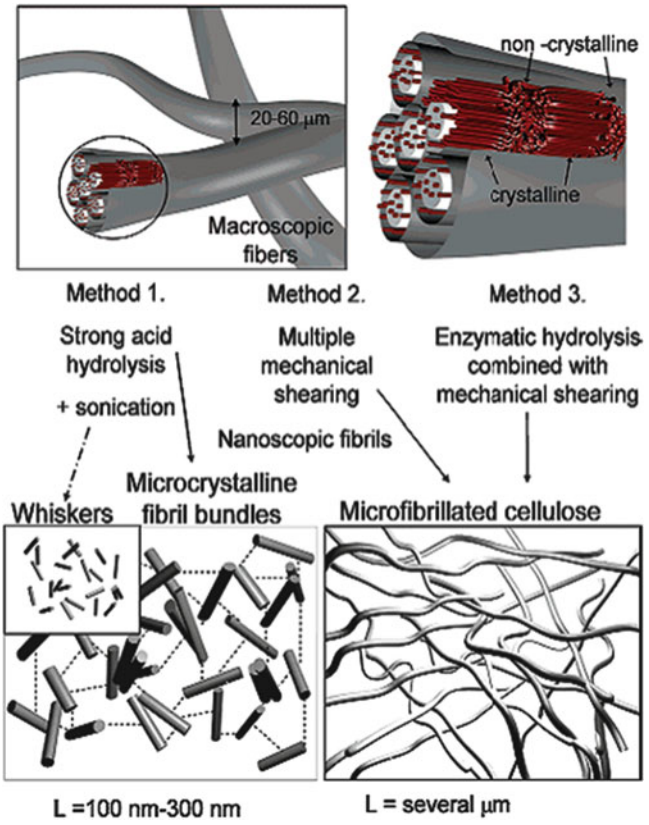

Fig. 10 Mechanical treatment and hydrolysis as top-down approaches for preparing nanoscale cellulosic materials (reprinted from Pääkköö et al. [48], copyright 2007 with permission from American Chemical Society)

"level off DP" (LODP), which ranges between 25 and 300 depending on the cellulose source [51]. The hydrolysis takes place in the less crystalline regions, leaving a solid residue that is water-insoluble and crystalline. As a result of the motion freedom of the hydrolyzed crystallites, structures are produced that have larger dimensions than the original microfibrils [35] forming a stable aqueous dispersion upon vigorous stirring. However, colloidal destabilization of the small crystalline domains can occur upon removal of acid by dialysis followed by spray-drying [52]. In such dry form, MC morphology varies from stubby to fibrillar. Importantly, sulfate half-ester moieties are introduced on the microcrystals (sulfur content 0.5–2%) when sulfuric acid is used for hydrolysis [53, 54]. The negative charge developed in aqueous media by these groups is the main contributor to colloidal stability of the dispersion, and its viscosity has been found to strongly depend on the charge density [55]. HCl is the hydrolytic medium of choice if MC is to be produced for applications that require the absence of electrostatic charges

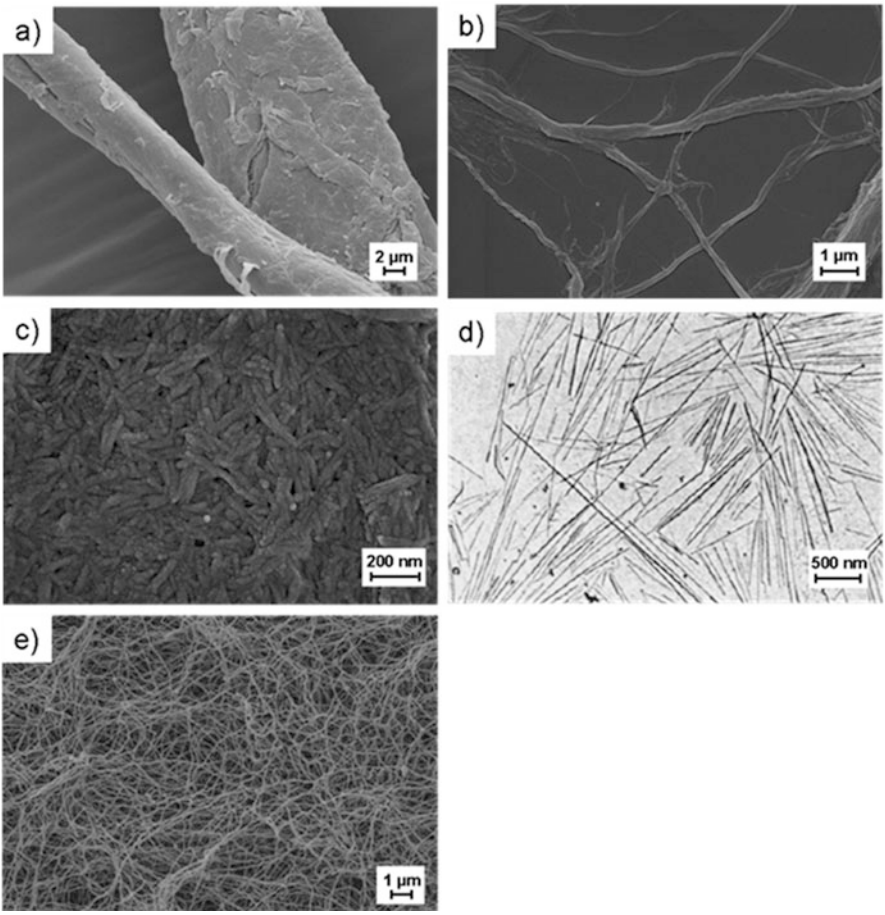

Fig. 11 Scanning electron micrographs of (**a**) fibers of cotton linters, (**b**) microfibrillar cellulose, (**c**) microcrystalline cellulose, (**d**) tunicate whiskers (reproduced from Eichhorn et al. [9], copyright 2001 with permission from Springer) and (**e**) bacterial cellulose

(e.g., in order to enhance enzyme interactions, binding, and attack). Such HCl-hydrolyzed MC is uncharged and can be of similar shape and size to that from sulfuric acid hydrolysis (Fig. 12). Concentrated dispersions of MC obtained with HCl show thixotropy (concentration >5%) whereas antithixotropic behavior is displayed at lower concentrations (<0.3%).

MC cellulose crystallites (and also cellulose nanocrystals or whiskers, see Sect. 4.2) self-assemble in water into chiral nematic phases of a given pitch, P, that reflect circularly polarized light of the same handedness. The value of P is in the order of the wavelength of visible light, giving rise to interesting interactions under illumination. Furthermore, above a critical concentration the cellulose crystallites evolve spontaneously into chiral nematic liquid crystals in water, which upon drying

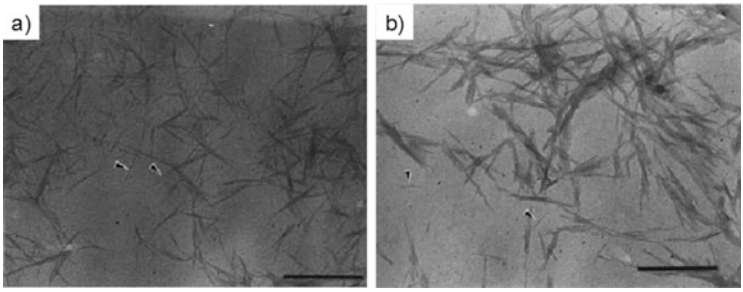

Fig. 12 Transmission electron micrograph of microcrystalline cellulose prepared by treatment with (**a**) H_2SO_4 and (**b**) HCl, with typical single microcrystals marked by *arrowheads*. *Scale bars* indicate 500 nm (reproduced from Araki et al. [53], copyright 1998 with permission from Elsevier)

form regularly twisted fibril layers that resemble the structural organization that evolves in nature [56, 57].

For the synthesis of new cellulose derivatives at the laboratory scale, MC is a convenient starting material of very high purity and sufficiently low viscosity, for example, to acquire well-resolved liquid state NMR spectra for structural analysis.

4.2 Cellulose Whiskers

Intense hydrolysis of cellulose results in crystallites that assemble into rigid rodlike cellulose particles, namely cellulose whiskers, after treatment with ultrasound [50]. Their preparation is also possible using high-energy mechanical treatments that cleave the amorphous parts by mechanical disintegration of a cellulose suspension. An enzymatically produced precursor yields whiskers in a more efficient two-step process [48]. Enzymatic hydrolysis is milder than the more aggressive acid hydrolysis and yields whiskers that are relatively longer and more entangled, resulting in a hydrogel network that possesses much greater strength. Cellulose nanocrystals take rodlike shapes with a typical width of a few nanometers and length of the order of hundreds of nanometers [50]. Such dimensions depend on the cellulose source and amorphous cellulose content, and are thus influenced by the conditions used during hydrolysis. Cellulose nanocrystals display a small number of defects and show no signs of chain folding. A large elastic modulus (~150 GPa) and strength (~7 GPa) have been typically calculated or determined for cellulose nanocrystals, which also possess a very low thermal expansion coefficient ($\sim 10^{-7}$ K^{-1}) [58, 59]. The small nanocrystals can form an isotropic dispersion, whereas larger particles separate into an anisotropic, bottom phase as the concentration increases [60]. Whiskers obtained from tunicate cellulose can be separated by ultracentrifugation using a saccharose gradient [61].

The stability of cellulose whiskers is strongly influenced by the size polydispersity, the dimensions of the particles, and their surface charge. Suspensions of

whiskers prepared with H_2SO_4 (negatively charged) are more stable as a result of electrostatic repulsion [62] than whiskers obtained by hydrolysis with HCl (neutral particles).

The rigid and rodlike nature of cellulose I nanocrystals leads to macroscopic birefringence under observation with crossed polarizers [63]. At low concentrations, cellulose nanocrystals are randomly oriented in water and appear as oval or spherical features [64]. As the concentration is increased, the nanocrystals self-assemble along a vector to yield a typical cholesteric liquid crystalline phase. The chiral nematic order can be retained upon removal of water and results in iridescent films, the color of which can be easily tuned by changing the salt concentration, pH, and temperature of the suspension [65]. At higher ionic strength (e.g., by addition of HCl, NaCl, or KCl), the electrical double-layer effect is screened out and the chiral interactions become stronger. The counter-ion also effects the interactions between particles. In the presence of protons, the cellulose suspensions form ordered phases at the lowest critical concentration. Application of a magnetic field during drying of cellulose films results in perfect orientation of the whiskers, leading to colored materials that can be used as security paper. The color change depends on the viewing angle, which is useful for production of optically variable coatings and inks. Figure 13 shows different domains of the cellulose nanocrystals, suggesting an ordered phase (Fig. 13a) and a well-defined cholesteric phase (Fig. 13b) [35]. Under an external magnetic field, small angle neutron scattering (SANS) experiments indicate that the cholesteric axis of the chiral nematic phase aligns with the magnetic field [66]. Along the cholesteric axis, the distance between the cellulose particles is shorter than perpendicular to it. This evidence suggests a helical twist of the cellulose whiskers.

In cellulose-based nanocomposites, whiskers give excellent properties because their regular and precise rigid-rod shape improves the mechanical characteristics of a variety of natural and synthetic materials. The nanocomposites show significantly enhanced mechanical properties as a result of formation of a rigid whiskers network, even when the whiskers content is only a few percent [67, 68].

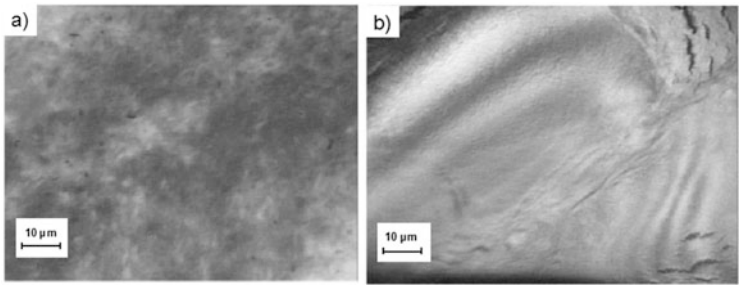

Fig. 13 Cross-polarized optical microscopy images of tunicate whiskers (**a**) at initial ordered phase and (**b**) at cholesteric phase (reproduced from de Souza Lima and Borsali [35], copyright 2004 with permission from John Wiley and Sons)

Cellulose nanocrystals can be dispersed in polar aprotic solvents such as dimethyl sulfoxide (DMSO) and *N*,*N*-dimethylformamide (DMF), for example, for the preparation of films displaying birefringence [69]. Dispersions in dichloromethane allow film-casting with poly(ε-caprolactone) leading to completely biobased composites that possess higher melting and crystallization temperatures, as well as higher glass transition temperatures compared with poly (ε-caprolactone). Poly(β-hydroxyalkanoate), cellulose acetate butyrate, starch, poly (vinyl chloride), polyamide 6, latex, poly(vinyl alcohol), and other synthetic and natural macromolecules have been blended with cellulose whiskers to reinforce the systems [35, 67, 68, 70–76].

Cellulose whiskers can increase the crystallinity of the matrix, with cellulose particles probably acting as a nucleating agent. The nucleating effect is mainly governed by the surface characteristics, whereas unmodified whiskers have the largest nucleation effect [77].

4.3 Microfibrillated Cellulose

Wood pulp is disintegrated by applying high shear force for the preparation of microfibrillated cellulose (MFC). The fibers are moderately degraded and opened into their substructural fibrils and microfibrils [78]. The fibrils and fibril aggregates are highly entangled, inherently connected, and form mechanically strong networks and gels. The inherent interactions result in much stronger gels than those formed only by weak hydrogen bonds between water and fibrils. Various pretreatments, such as mild carboxymethylation, enable MFC to be obtained by a less energy-consuming shearing [79]. Subsequent ultrasound results in smaller and charged MFC. The combination of mild enzymatic hydrolysis with high-pressure shear forces can be used as an additional method for the preparation of MFC with controlled diameter in the nanoscale range. Mercerization can also be an appropriate treatment [80].

MFC can be used to produce patterned surfaces using lithographic techniques [81]. In these cases, MFC improves homogeneity and stability, which is important in various applications. Microcontact printing of oppositely charged poly(ethylene imine) (PEI) on a surface of PEI/poly(styrene sulfonate) followed by MFC treatment (Fig. 14a), or on a PEI-coated poly(dimethyl siloxane) stamp, produces geometric patterns (Fig. 14b). Such surfaces can be used in the development of membranes and filters because the pore geometry and size can be controlled by selection of the appropriate microstamp pattern.

MFC can be chemically modified with different reagents, including *N*-octadecyl isocyanate and others that enable combination with synthetic polymers and produce precursor materials for film casting [82]. Charged groups, reactive vinyl moieties, and polymer chains can be installed on the surface of MFC via treatment with maleic anhydride, glycidyl methacrylate, and succinic anhydride [83]. Hydrophobization via acetylation, silanization, and carboxymethylation as well as corona or

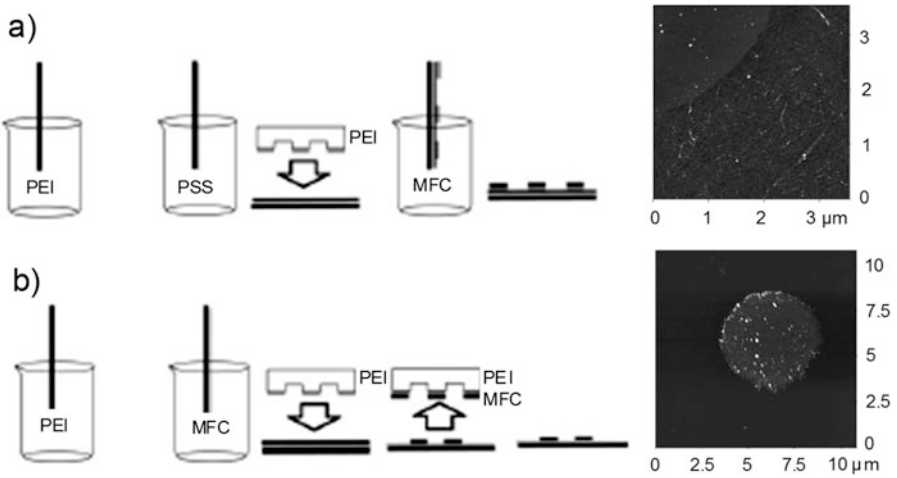

Fig. 14 (**a**) Selective adhesion technique using poly(ethylene imine) (*PEI*) and poly(styrene sulfonate) (*PSS*) to pattern microfibrillated cellulose (*MFC*). (**b**) Lift-off technique, where MFC is partially removed by a PEI-modified stamp. Representative atomic force micrographs are also included (reproduced from Werner et al. [81], copyright 2008 with permission from Royal Society of Chemistry)

plasma treatment can be used to adapt microfibrillated cellulose for given applications [84–88], including oil-in-water emulsions and others.

5 Bottom-up Approaches to Nanostructures of Cellulose

5.1 Electrospinning of Cellulose and Cellulose Derivatives

The electrospinning technique is widely used for the production of nanofibers, which opens a route for production of materials with high effective surface areas [89]. Nanofibers can be produced from different polymers and have applications in various fields, namely biomedicine, composites, filters, catalysts, and textiles [90–92]. Nanofibers regulate water vapor and wind permeability and can improve the thermal isolation of textiles. Moreover, they can possess special properties such as aerosol-filtration, binding of chemical and biological contaminants, or improved surfactant release [93]. Air cleaning of contaminated environments is a typical example of their application [94].

Cellulose dissolved in DMA/LiCl, *N*-methylmorpholine-*N*-oxide (NMMNO) [95], ionic liquids (e.g., BMIMCl) [96], or sodium hydroxide/water/urea [97] can be transferred to nanofibers of different morphology by electrospinning.

Although electrospinning of polyelectrolytes from aqueous solutions is not successful in the majority of cases, water-soluble and bioactive nanofibers of

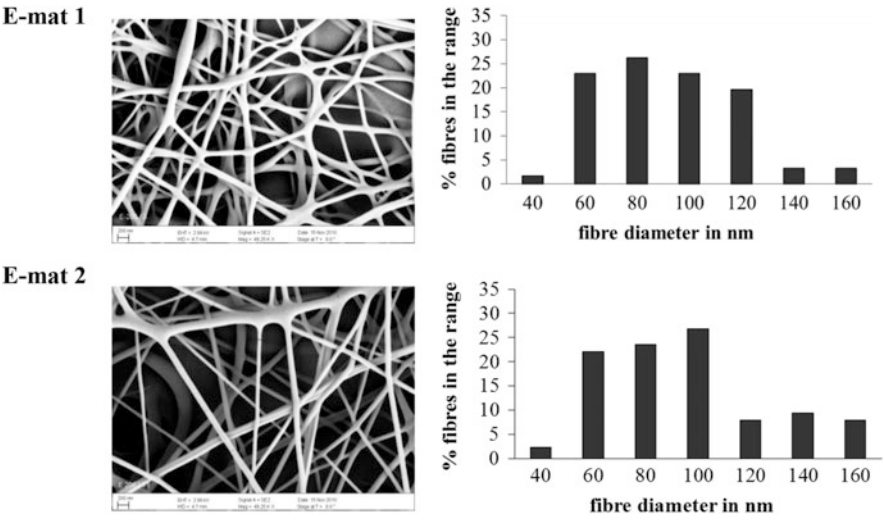

Fig. 15 Scanning electron micrographs of the nanofiber webs of 6-deoxy-6-trisaminoethylamino cellulose/polyvinyl alcohol in the ratio 1:15 (*E-mat 1*) and TEAE cellulose/PVA at 1:18 (*E-mat 2*)

amino cellulose can be prepared using blended solutions of a typical amino cellulose, 6-deoxy-6-trisaminoethyl-amino (TEAE) cellulose, and polyvinyl alcohol (PVA), as shown in Fig. 15. The nanofibers show high antimicrobial activity against *Staphylococcus aureus* and *Klebsiella pneumoniae* [98].

5.2 Nanospheres

Nanoscaled particles can be obtained from different cellulose esters, including commercially available cellulose acetates, cellulose acetate propionate, and cellulose acetate butyrate, and also from some organo-soluble cellulose ethers. Methods commonly used are emulsification solvent evaporation and the low-energy method of solvent displacement by dialysis, inducing nanoprecipitation [99]. Comparing the methods, a large amount of small and uniform nanoparticles can be obtained by the emulsification solvent evaporation procedure, whereas solvent displacement yields narrowly distributed particles. Typical particles obtained from cellulose acetate are shown in Fig. 16 [100]. Dialysis is easy to use and therefore appropriate for laboratory-scale studies. Moreover, very pure suspensions of the nanoparticles can be obtained.

It is important to point out that even spherical nanoparticles of polymers containing hydrophilic moieties such as 6-deoxy-6-(ω-aminoalkyl)aminocellulose-carbamates can be prepared. Such nanoparticles are of particular interest because they possess primary amino groups that can be more easily modified than OH moieties. Thus, labeling with rhodamine B isothiocyanate is simple and does not

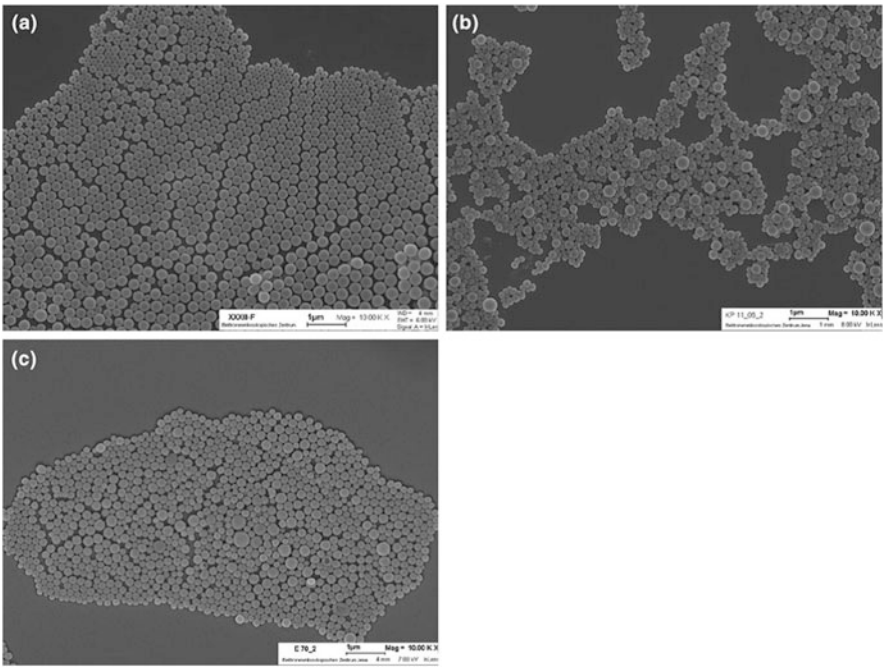

Fig. 16 Field-emission scanning electron micrographs of nanoparticles prepared by (**a**) emulsification–evaporation of cellulose triacetate (CTA) (150 W, 10 s, cW 25 mg/mL), (**b**) by dialysis of CTA (cW 4 mg/mL), and (**c**) by dropping water into a solution of CA, DS 2.45 (cW 6 mg/mL, V(H_2O) 70 mL, rate 10 mL/min)

change the size, stability, or shape of the nanoparticles. Incorporation of such nanoparticles into human foreskin fibroblasts BJ-1-htert and breast carcinoma MCF-7 cells could be successfully carried out without any transfection reagent [101].

Although an organo-soluble cellulose derivative must be used for the technique of nanoprecipitation, even pure cellulose nanoparticles can be prepared. Using trimethylsilyl cellulose (TMSC), the formation of nanoparticles by dialysis of the organic solvent against water is accompanied by complete removal of the TMS functions. Analysis of particle size distribution shows that cellulose particles with a size of 80–260 nm are accessible in this simple manner [102]. Aqueous suspensions of the pure, spherical cellulose nanoparticles are storable for several months without any demixing. Covalent labeling of the cellulose nanoparticles with FITC has no influence on particle size, shape, and stability. The particles can be sterilized and suspended in biological media without structural changes. As can be seen in Fig. 17, FITC-labeled cellulose nanoparticles can penetrate into living human fibroblasts by endocytosis without transfection reagents or attachment of a receptor molecule, as shown by means of confocal laser scanning microscopy [103].

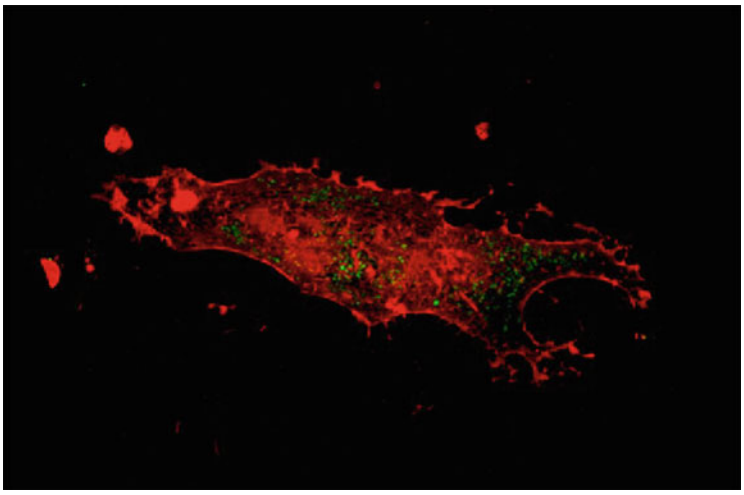

Fig. 17 Confocal micrograph overlay of 21 stacks of human fibroblasts (*red* cell membrane) incubated with FITC-labeled cellulose nanoparticles

6 Solubility of Cellulose

As a result of the extended hydrogen bonds between the cellulose chains, special media and procedures must be applied to dissolve cellulose. Today, solvents are divided into derivatizing solvents (forming covalent bonds of low stability with the polymer) and nonderivatizing solvents (interacting only physically with the polymer). At the industrial scale, cellulose nitrate as a soluble and, thus, formable cellulose derivative can be used. It should be pointed out that cellulose nitrate is a relatively stable cellulose derivative so introduction of ester moieties for "derivatizing dissolution" is somewhat questionable, although regeneration is easy to achieve. The invention of a mixture of copper(II) hydroxide and aqueous ammonia for dissolving cellulose, with subsequent precipitation in dilute sulfuric acid, was followed by probably the most important large-scale technical process in fiber production, the viscose process. Cellulose is transformed into cellulose xanthogenate, with subsequent spinning of the solution in aqueous sodium hydroxide. The Lyocell process is an environmentally friendly alternative to the viscose process, whereby cellulose is dissolved physically in *N*-methylmorpholine-*N*-oxide monohydrate and regenerated in water [104].

The majority of cellulose solvents known today are only applied at the laboratory scale although there are some semitechnical trials being carried out for fiber spinning using novel solvents such as ionic liquids (ILs). Until now there has been no homogeneous chemical modification carried out at technical scales.

6.1 Polar Aprotic Solvents in Combination with Electrolytes

Binary mixtures of organic liquids and inorganic or organic electrolytes are the most-used solvents for cellulose. Typical examples are *N*,*N*-dimethylacetamide (DMAc), *N*-methyl-2-pyrrolidinone, 1,3-dimethyl-2-imidazolidinone in combination with LiCl, and DMSO with tetra-*n*-butylammonium fluoride × $3H_2O$ [105].

In these solvents, there are ions that can efficiently interact with hydrogen bonds and liquids that can solvate polar polymers such as cellulose. The essential factors required for dissolution of cellulose include:

1. Solubility of a sufficient amount of electrolyte in the organic liquid
2. Adequate stability of the electrolyte/solvent complex
3. Cooperative action of the solvated ion-pair on cellulose hydrogen bonds
4. Sufficient basicity of the anion [106]

For example, to obtain a 3 wt% solution of cellulose in DMAc requires about 4 wt% LiCl, whereas 10 wt% LiCl is needed to dissolve it in DMF. This agrees with the fact that LiCl forms a stronger complex with the former solvent [107]. By contrast, NaCl is not appropriate because it is insoluble in DMAc and DMF. The strength of cation–solvent association of alkali metal chlorides in DMAc and DMF is in the order $Li^+ > Na^+ > K^+ > Cs^+$(as determined by electrospray ionization mass spectroscopy). For LiCl, the strength of cation–solvent association is in the order *N*,*N*-dimethylpropionamide > DMAc ≫ DMF. That is, the association increases as a function of increasing negative charge on the oxygen atom of the C=O group of the solvent [108, 109]. For DMAc, LiCl is more efficient than LiBr for dissolving cellulose, because the later halide ion is less basic than the former.

In general, to design new solvents of this type, the requirements mentioned must be fulfilled. Thus, it was found that quaternary tetraalkylammonium chlorides with one long alkyl chain dissolve in various organic solvents and constitute a new class of cellulose solvents. In contrast to the well-established solvent DMAc/LiCl, cellulose dissolves in DMA/quaternary ammonium chlorides without any pretreatment (Fig. 18). Consequently, use of the new solvent avoids some of the disadvantages of DMAc/LiCl [110].

Highly surprising is the finding that cellulose dissolves quickly even in a mixture of acetone/triethyloctylammonium chloride containing 9 parts of the salt and 20 parts of the organic liquid. No pretreatment or activation of the cellulose is necessary. This has not yet been reported for binary acetone/salt mixtures, including ILs, where acetone has been found to cause immediate cellulose precipitation [111]. Further increase in the amount of triethyloctylammonium chloride does not have an adverse effect on the solution. The ^{13}C-NMR spectrum measured for cellulose dissolved in acetone/triethyloctylammonium chloride verifies that the biopolymer is dissolved without being chemically modified (nonderivatizing solvent) as is the case for all solvents of this class (Fig. 19). Nevertheless, the solvent LiCl/DMAc is still the most extensively employed because it is capable of

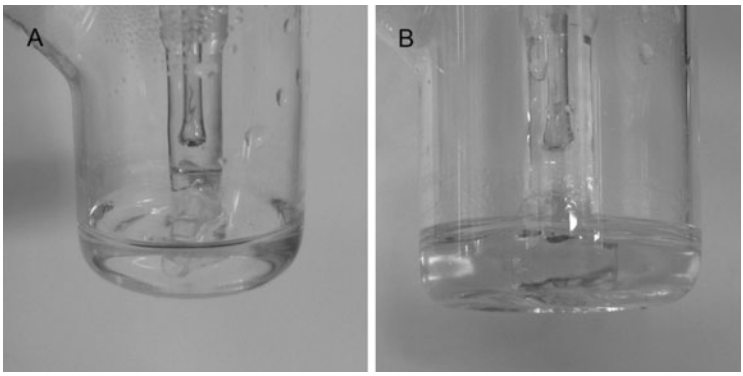

Fig. 18 Cellulose dissolved in *N,N*-dimethylacetamide/triethyloctylammonium chloride after dissolution (**a**) and after 24 h (**b**)

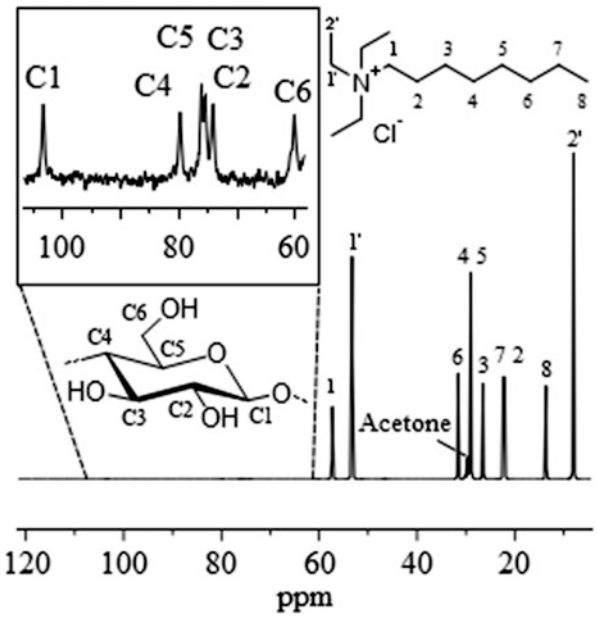

Fig. 19 ^{13}C-NMR spectrum (100 MHz, acetone-d_6) of cellulose in acetone-d_6/triethyloctylammonium chloride

dissolving different celluloses, including samples of high DP and index of crystallinity (e.g., cotton linters and even bacterial cellulose).

The combination of DMSO and tetra-*n*-butyl ammonium fluoride $\times$ $3H_2O$ (TBAF $\times$ $3H_2O$, premixed) dissolves cellulose very efficiently without any pretreatment as a result of the fact that the fluoride ion is a harder base than the chloride ion (LiCl/DMAc). Furthermore, the cation is voluminous and hence acts as

a "spacer," preventing re-attachment [105, 112]. For instance, clear solutions of microcrystalline cellulose were obtained in 15 min at room temperature, whereas fibrous sisal required 30 min at room temperature plus 60 min at 60°C [113].

The commercially available, stable TBAF contains 3 mole of water. The water may influence the chemical modification of dissolved cellulose because of hydrolysis of the reagent. However, the cellulose solution can be partially dehydrated by distilling off about 30% of the solvent before addition of the reagent (e.g., acetic anhydride). The esterification yields products of higher degree of substitution (DS) [113].

Complete dehydration of TBAF × $3H_2O$, resulting in the water-free salt, is impossible because anhydrous TBAF is unstable and undergoes rapid E2 elimination, resulting in the formation of hydrogen difluoride anions [114]. However, preparation of anhydrous TBAF in situ by reacting tetra-*n*-butylammonium cyanide with hexafluorobenzene in dry DMSO has been described [115]. Freshly prepared water-free DMSO/TBAF solution, even in the presence of the by-product hexacyanobenzene, dissolves cellulose very easily. In the water-free solvent, dissolution of bleached cotton fibers with very high DP of 3,743 occurs within a short time, as visualized by optical microscopy (Fig. 20, [116]).

Other ammonium salts have been studied as electrolytes in DMSO-based cellulose solvents, namely tetramethylammonium fluoride (TMAF) and benzyltrimethylammonium fluoride monohydrate (BTMAF × H_2O). At room temperature, 0.94 mol/L TBAF × $3H_2O$ could be dissolved in DMSO, but only 0.025 mol/L of

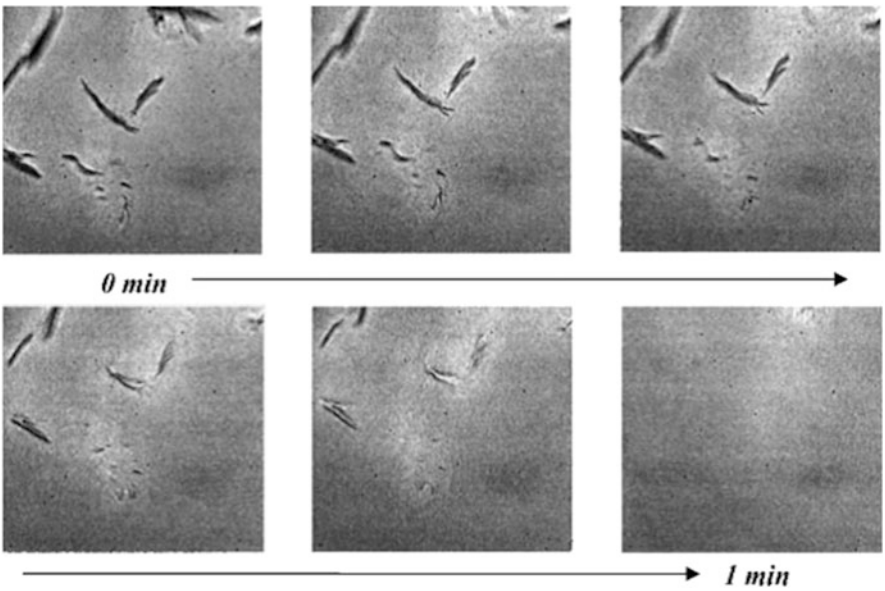

Fig. 20 Optical micrographs showing the dissolution of bleached cotton fibers in dimethyl sulfoxide/water-free tetrabutylammonium fluoride (10 wt%) at 35°C

BTMAF × H_2O dissolves at room temperature, and 0.142 mol/L at 90°C. TMAF is insoluble in DMSO.

Up to 1 wt% of cellulose is soluble in DMSO/BTMAF × H_2O by heating the system to 85°C to maintain an adequate fluoride ion concentration. A minimal amount of 2.2 fluoride ions per AGU is needed. In the case of TBAF × $3H_2O$, the relation between the fluoride ions and AGU depends on the DP of the cellulose (as also known for DMAc/LiCl). Thus, for microcrystalline cellulose (Avicel, DP 332) a ratio of 1:1 (salt/cellulose) is appropriate, whereas for spruce sulfite pulp (DP 600) and cotton linters (DP 1,198) a ratio of 3:1 is needed.

These results again substantiate the simple approach mentioned above for creation of new solvents for cellulose. Following such an approach, another solvent was found very recently; almost anhydrous dibenzyldimethylammonium (BMAF × $0.1H_2O$) in DMSO dissolves microcrystalline and fibrous celluloses [117].

It should be pointed out that clear cellulose solutions are not necessarily molecularly dispersed, but may contain aggregates of still-ordered cellulose molecules [118]. These aggregates were described as forming a "fringed" micellar structure (Fig. 21a) composed of laterally aligned chains, forming a rather compact and possibly geometrically anisotropic core that is immiscible in the solvent. The solvated amorphous cellulose chains form "coronas" at both ends of the particles [119]. The thickness of the coronas and the number of molecular chains forming the aggregate increase as a function of both cellulose concentration and the interfacial tension between the solvent and particle core [120]. Monodisperse solutions of cellulose molecules with small (Fig. 21b), and large (Fig. 21c) DP produced typical features. The length of the short cellulose chain is practically equal to its persistent length, (i.e., there is neither chain coiling nor interaction with other chains). The flexibility of the long chain polymer allows the formation of strong intramolecular hydrogen bonds, provided that the OH groups reside for some time within a "critical

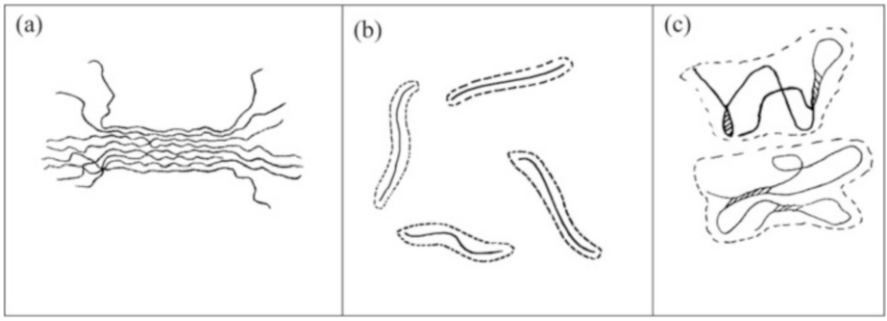

Fig. 21 Cellulose structures in solution: (**a**) "fringed" micellar structure, (**b**, **c**) possible chain conformations of celluloses of different DP. Intramolecular hydrogen bonding is possible for high molecular weight cellulose (**c**)

distance" of each other (ca. 0.3 nm), sufficient for van der Waals forces to operate (Fig. 21c) [121]. As a result, the properties of cellulose (DP, crystallinity, and concentration) affect its solution state and, hence, its derivatization. For the same cellulose, the accessibility of the OH groups increases with decreasing solution concentration. For different celluloses, at a given concentration, only the outer surface of the fringed micellar core is accessible and the area of this part decreases with DP and crystallinity.

Regarding chemical modification, molecularly dispersed solutions are not needed. Moreover, as a result of the change in structure of the cellulose derivative compared with the starting material, and considering the DS, the different structures formed during the course of reaction have different interactions with the solvent components. In some cases the reaction systems can become microheterogeneous, and possibly even complete gelation or precipitation can occur.

6.2 Ionic Liquids

The first ionic liquids (ILs) used for esterification of cellulose were *N*-alkylpyridinium halides, especially *N*-ethylpyridinium chloride (EPyCl) and *N*-benzylpyridinium chloride (BPyCl) [122]. Nevertheless, the most promising ILs for the modification of cellulose are the salts of 1-alkyl-3-methylimidazolium. In 2002, it was shown that such ILs could open new paths for the shaping of polysaccharides [123, 124]. Additionally, they could lead to commercially relevant routes toward homogeneous cellulose chemistry, which would significantly broaden the number of tailored cellulose derivatives. Meanwhile, a huge number of cellulose-dissolving ILs are now known and discussed in various recent reviews (e.g., [125] and references cited therein), and the number of reported low melting organic salts is growing rapidly (Fig. 22). Nevertheless, according to the literature [126, 127] and our own experience, cellulose can be dissolved in ILs with imidazolium, ammonium, and pyridinium. Only organic salts with asymmetric cations give melts that can interact with the backbone of cellulose. Neither sulfonium nor phosphonium salts have so far been able to dissolve cellulose. Dissolution of cellulose in pyridinium salts must be performed under protective gas otherwise degradation results [128]

1-Ethyl-3-methylimidazolium acetate (EMIMAc) ILs have the advantage of not having a reactive side group, such as the unsaturated function of the 1-allyl-3-methylimidazolium (AMIM) ion. Moreover, EMIMAc is considered to be nontoxic, noncorrosive, and even biodegradable. However, EMIMAc reacts with the reducing end groups of cellodextrins, according to the formula depicted in Fig. 23, giving a hemiacetal-type structure [129–131].

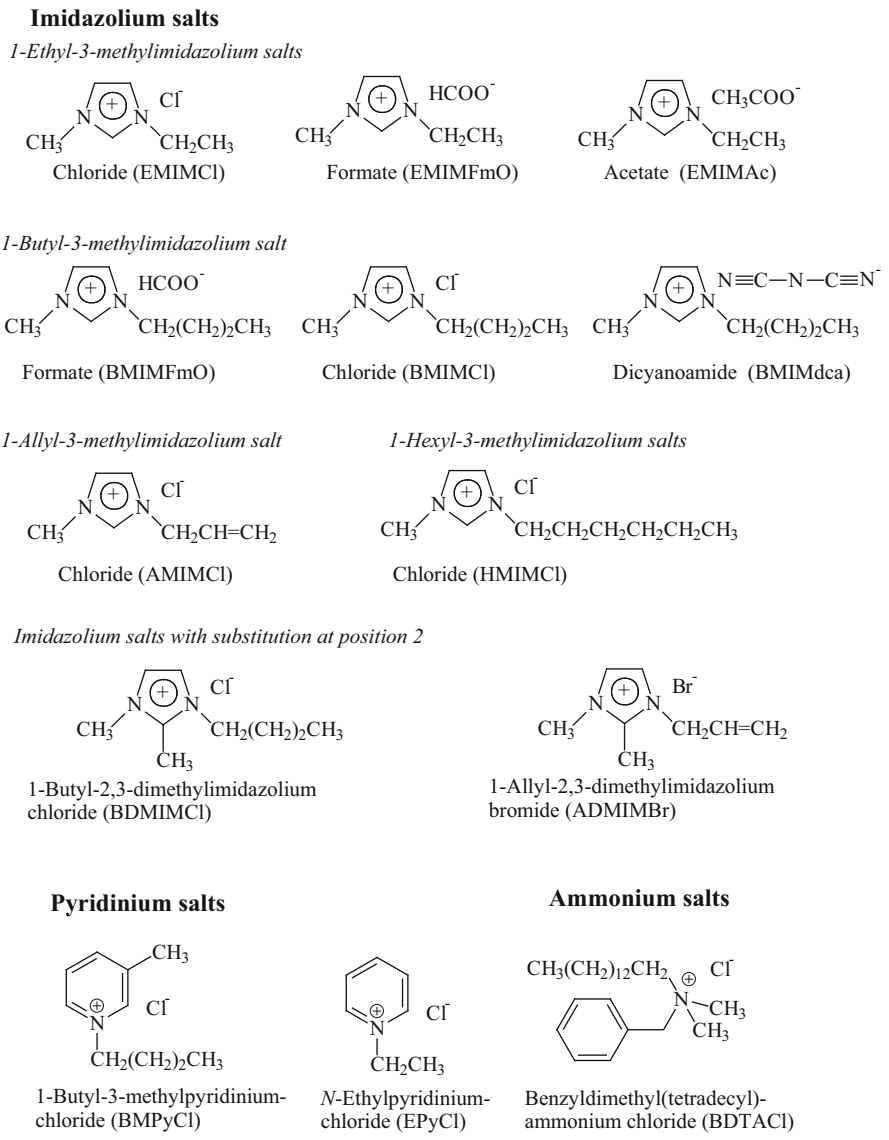

Fig. 22 Examples of ionic liquids suitable for dissolving cellulose

The dissolution mechanism is still the subject of ongoing research. 1-Alkyl-3-methylimidazolium-based ILs yield clear solutions after 15 min without activation of the cellulose. The solubility of cellulose in such ILs is directly related to the length of the alkyl chain. But, the solubility does not regularly decrease with increasing length of the alkyl chain. An odd–even effect was determined for short alkyl chains [132].

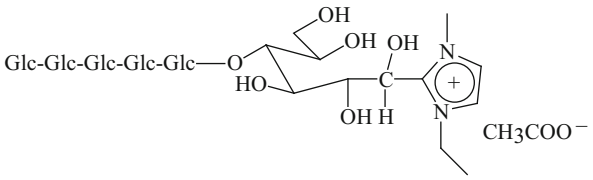

Fig. 23 Structure proposed for conversion of the reducing end group of cellodextrins with 1-ethyl-3-methylimidazolium acetate

Although there is a very high potential for a commercial application of ILs, it is clearly obvious that ILs also possess various disadvantages and further research and development is needed.

6.3 Aqueous Alkali (Base)-Containing Solvents

Mercerization, the treatment of cellulose with aqueous solution of bases such as NaOH, is one of the most important processes prior to cellulose etherification. The phase diagram established by Sobue et al. suggests that there is a dissolution zone of cellulose in aqueous NaOH at a concentration of 7–10% at temperatures below 268 K (Fig. 24, [133]).

Complete dissolution of microcrystalline cellulose in aqueous NaOH is possible [134]. However, linters cellulose had limited solubility (26–37%) applying the same procedure. Kamide and coworkers have applied steam explosion treatments in order to dissolve pulp directly in NaOH [135–139]. In technical papers, they claim that a solution of 5% of steam-exploded cellulose in 9.1% NaOH at 4°C, spun into 20% H_2SO_4 at 5°C, yielded fibers but of poor quality.

Recently, the dissolution and modification of cellulose in mixtures of an aqueous base with urea and thiourea has been the focus of interest [140–143]. Cellulose can be dissolved in an aqueous solution of NaOH (7 wt%)/urea (12 wt%). Starting from a precooled mixture at −12°C, cellulose dissolves within 2 min. The urea hydrates could possibly be self-assembled at the surface of the NaOH hydrogen-bonded cellulose [144]. The solutions are rather unstable and sensitive to temperature, polymer concentration, and storage time [145, 146]. Alternatives include LiOH/urea [147, 148] and NaOH/thiourea [149]. TEM images and wide-angle X-ray diffraction (WAXD) provide experimental evidence for the formation of a worm-like cellulose inclusion complex surrounded by urea (Fig. 25).

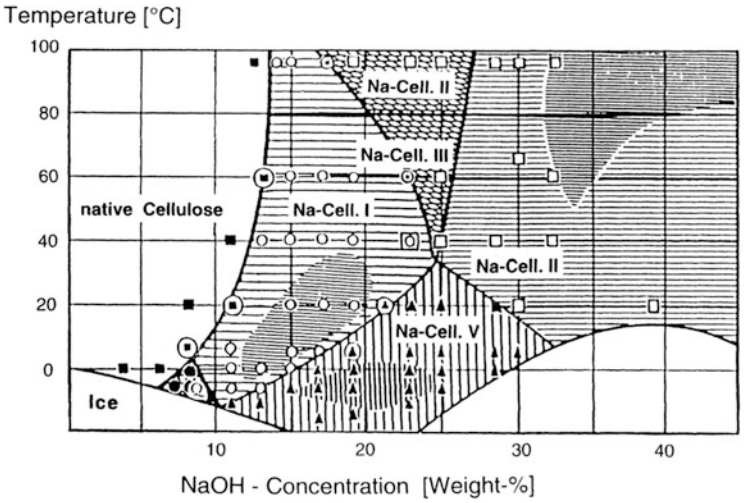

Fig. 24 Phase diagram of ternary cellulose/NaOH/water system

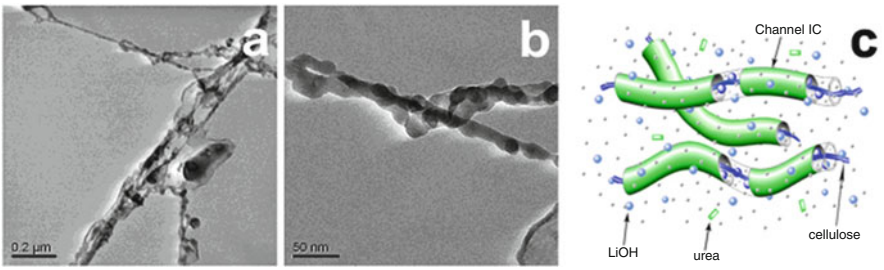

Fig. 25 (**a**, **b**) Transmission electron micrographs of cellulose at concentration of 4.0×10^{-4} g mL^{-1} in aqueous 4.6 wt% LiOH/15 wt% urea. (**c**) Model of inclusion complex

7 Chemical Reactivity

Glucan cellulose was used as a precursor for chemical modification even before its polymeric nature was accepted and well understood. The reactive groups are the hydroxyl moieties. Cellulose nitrate (misnomer, nitrocellulose) of high nitrogen content was an important explosive. Partially nitrated cellulose ester was used as a "plastic" (trade name Celluloid) and is still produced commercially [150]. Methyl-, ethyl-, and hydroxyalkyl ethers as well as cellulose acetate are cellulose products that remain important even decades after their discovery. The same applies to other cellulose products carrying a variety of functional groups, such as ethylhydroxyethyl and hydroxypropylmethyl cellulose, acetopropionates, acetobutyrates, and acetophthalates. Ionic cellulose ethers were introduced a long

time ago and commercial production of the most important ionic cellulose ether, carboxymethyl cellulose (CMC), began in the 1920s [151].

The preparation of commercial cellulose derivatives is exclusively carried out under heterogeneous reaction conditions. In the case of acetylation, the cellulose acetate formed may dissolve during the course of reaction, thus it is not considered a homogeneous reaction.

However, the dissolution of cellulose *prior* to chemical reaction offers a great opportunity for the design of novel and unconventional cellulose derivatives by homogeneous phase chemistry. For homogeneous phase chemistry, either nonderivatizing or derivatizing solvents can be used. In the case of derivatizing solvents, both conversion of the soluble intermediate formed during dissolution and modification of the isolated intermediate (which is re-dissolved in an organic solvent such as DMSO or DMF) are considered homogeneous reactions. By contrast, neither chemical modification of soluble but "stable" cellulose derivatives such as cellulose acetate in DMSO nor chemical modification of cellulose under dissolution of the cellulose derivative formed (as a result of the conversion) are included in the context of homogeneous phase chemistry. In the following section, the synthesis of some cellulose derivatives is discussed.

7.1 Homogeneous Modification of Cellulose

7.1.1 Acylation of Cellulose

Although a wide variety of solvents for cellulose have been developed and investigated in recent years, only a few have shown the potential for controlled and homogeneous functionalization of the polysaccharide (Table 1) [157]. Limitations to the application of solvents result from high toxicity, high reactivity of the solvents leading to undesired side reactions, and loss of solubility during reactions. The latter results in inhomogeneous mixtures through formation of gels and pastes,

Table 1 Solvents and reagents exploited for the homogeneous acetylation of cellulose

Solvent	Acetylating reagent	DS_{max}[a]	Reference
N-Ethylpyridinium chloride	Acetic anhydride	Up to 3	[122]
1-Allyl-3-methyl-imidazolium chloride	Acetic anhydride	2.7	[152]
N-Methylmorpholine-*N*-oxide	Vinyl acetate	0.3	[153]
DMAc/LiCl	Acetic anhydride	Up to 3	[154, 155]
	Acetyl chloride	Up to 3	
DMI/LiCl	Acetic anhydride	1.4	[156]
DMSO/TBAF	Vinyl acetate	2.7	[105, 113]
	Acetic anhydride	1.2	

DMAc *N*,*N*-Dimethylacetamide, *DMI* 1,3-dimethyl-2-imidazolidinone, *DMSO* dimethyl sulfoxide, *TBAF* tetra-*n*-butylammoniumfluoride trihydrate

[a]Maximum degree of substitution

which are difficult to mix, and even through formation of de-swollen particles of low reactivity, which settle out in the reaction medium.

Homogeneous reaction conditions give the opportunity for esterification with state of the art reagents, for example, after in situ activation of carboxylic acids, which is characterized by reacting the carboxylic acid with a reagent to form an intermediate, highly reactive carboxylic acid derivative. The carboxylic acid derivative can be formed prior to reaction with the polysaccharide or converted directly in a one-pot reaction. Modification of cellulose with carboxylic acids after in situ activation has made a broad variety of new esters accessible, because common reactive derivatives such as anhydrides or chlorides are not accessible for numerous acids (e.g., unsaturated or hydrolytically instable acids). The mild reaction conditions applied for in situ activation avoids side reactions such as pericyclic reactions, hydrolysis, and oxidation [158]. For example, a reaction with enormous potential for cellulose modification is the homogeneous one-pot reaction after in situ activation of carboxylic acids with *N*,*N*′-carbonyldiimidazole (CDI), which has been well known in bioorganic chemistry since 1962 [159]. The reactive imidazolide of the acid is generated, and the by-products CO_2 and imidazole are nontoxic (Fig. 26). The pH is almost constant during the conversion, resulting in negligible chain degradation. In comparison to dicyclohexylcarbodiimide (DCC), the application of CDI is much more efficient, avoids most of the side reactions, and allows the use of DMSO (a good solvent for most complex carboxylic acids).

7.1.2 Sulfation of Cellulose

Although studied for decades, sulfation of cellulose is still of interest because the products show pronounced bioactivity and can be used for self-assembly systems such as polyelectrolyte complexes. A very elegant method offers the sulfation of cellulose dissolved in ILs. Cellulose dissolved in BMIMCl/co-solvent mixtures can be easily converted into cellulose sulfate (CS) by using SO_3-Py, SO_3-DMF, or $ClSO_3H$ [160]. Highly substituted CS with DS values up to 3 has been reported for sulfation in BMIMCl at 30°C [161]; however, it should be noted that cellulose/IL solutions slowly turned solid upon cooling to room temperature, depending on the cellulose and moisture content. Synthesis of CS with an even distribution of sulfate groups along the polymer chains requires a dipolar aprotic co-solvent that drastically reduces the solution viscosity and does not significantly influence the reactivity of the sulfating agent [162]. At a 2:1 molar ratio of SO_3-DMF/AGU, the sulfation of microcrystalline cellulose in BMIMCl and BMIMCl/DMF mixtures leads to comparable DS values of about 0.86. Whereas CS synthesized without co-solvent is insoluble, the other readily dissolves in water.

Homogeneous sulfation of cellulose in IL allows tuning of CS properties simply by adjusting the amount of sulfating agent and choosing different types of cellulose. If conducted at room temperature, the reaction leads only to minor polymer degradation. This makes the procedure valuable for the preparation of water-soluble CS over a wide DS range. In particular, capsules of CS with low DS can

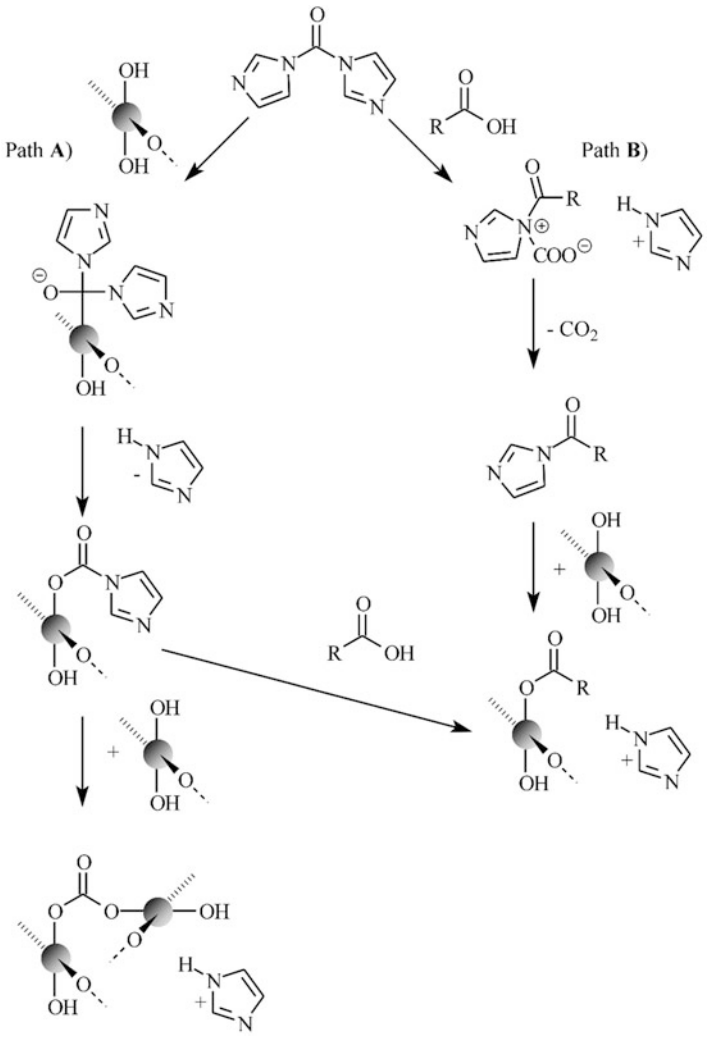

Fig. 26 Mechanism of activation of carboxylic acids with *N*,*N*′-carbonyldiimidazole

be prepared efficiently in IL/co-solvent mixtures and are of interest for bioencapsulation applications [162].

7.1.3 Structural Design of Cellulose by Nucleophilic Displacement Reactions

In addition to typical modification of the hydroxyl groups of cellulose, chemical modification can be carried out by reaction at the C atoms of the AGU. Nucleophilic displacement (S_N) reactions with cellulose are based on the transformation of

Table 2 Typical products of nucleophilic displacement reactions of cellulose tosylate

Reagent	Product	Reference
$Na_2S_2O_3$	6-Deoxy-6-*S*-thiosulfato cellulose	[165]
$NaSCH_3$,	6-Deoxy-6-thiomethyl-2,3-di-carboxymethyl cellulose	[166]
$NaSO_3$	Sodium deoxysulfate-*co*-tosylate cellulose	[167, 168]
NaN_3	6-Deoxy-6-azido cellulose	[169]
Iminodiacetic acid	6-Deoxy-6-iminodiacetic acid cellulose sodium salt	[170]
Triethylamine	6-Deoxy-6-triethylammonium cellulose	[171]
N,*N*-Dimethyl-1,3-diaminopropane	6-Deoxy-6-(*N*,*N*-dimethyl-3-aminopropyl)ammonium cellulose	[171]
2,4,6-Tris(*N*,*N*-dimethylaminomethyl)phenol	6-Deoxy-6-(2,6-di(*N*,*N*-dimethylaminomethyl)phenol)-4-methyl-*N*,*N*-dimethylamino cellulose	[171]
R(+)-, *S*(−)-, and racemic 1-phenylethylamine	6-Deoxy-6-(1-phenylethyl)amino cellulose	[172]
Aminomethane	6-Deoxy-6-methylamino cellulose	[173]

hydroxyl groups of the biopolymer to a good leaving group, mainly by tosylation [163, 164]. A broad variety of cellulose derivatives are accessible, as summarized in Table 2. The S_N reaction occurs almost exclusively at the primary position of the repeating unit, most probably for steric reasons. The S_N of a tosylate moiety occurs via a S_N2 mechanism (i.e., a transition state appears containing five atoms that is hardly formed at the secondary positions of the modified AGU).

7.2 Amino Cellulose

Conversion of cellulose tosylate with diamines or oligoamines yields polymers of the type P-CH_2-NH-(X)-NH_2 (P = cellulose; X = alkylene, aryl, aralkylene, or oligoamine) at position 6 (Fig. 27). These cellulose derivatives can form transparent films and can be used for the immobilization of enzymes such as glucose oxidase, peroxidase, and lactate oxidase. The products are useful as biosensors. Soluble and film-forming cellulose derivatives with redox–chromogenic and enzyme-immobilizing 1,4-phenylenediamine groups have been reported [174–178].

Thus, it is possible to design amino celluloses with properties that differ in, for example, the distance of the terminal NH_2 groups from the cellulose backbone (spacer effect), basicity, and reactivity. Moreover, di- and oligoamines provide different properties such as pH value and charge distribution, control of hydrophilic/lipophilic balance, and redox–chromogenic properties. Chromogenic properties (electron mediator) play an important role in the use of amino cellulose derivatives as transducers in the field of biosensors [179].

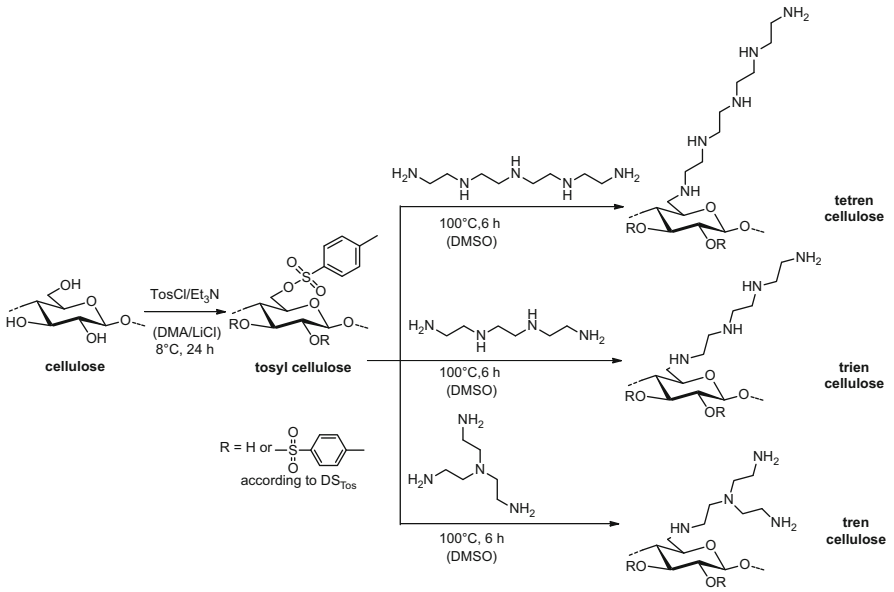

Fig. 27 Reaction path for the synthesis of 6-deoxy-6-amino cellulose ester derivatives by nucleophilic displacement of tosyl cellulose

Because of the multifunctionality of cellulose and the stability of tosylates, modification of the secondary OH groups prior to the S_N reaction can also be carried out to design the properties of the products. The OH groups at positions 2 and 3 are preferably esterified to adjust the properties, including the solubility of the polymer. Whereas amino celluloses possessing mainly OH groups at the secondary positions are water soluble, the additionally esterified polymer derivatives are soluble in organic solvents such as DMAc and can form nanoparticles (see Sect. 5.2).

6-Deoxy-6-amino cellulose forms multiple oligomeric species that were discovered using the hydrodynamic technique of analytical ultracentrifugation as a probe. For every amino cellulose studied, the sedimentation coefficient distributions indicate 4 or 5 discrete species, with a stepwise increase in sedimentation coefficient. This was found in every case across a range of six different solute loading concentrations (from 0.125 to 2.0 mg/mL). For example, the lowest sedimentation coefficient of 6-Deoxy-6-(2-(bis(2-aminoethyl)aminoethyl)amino) cellulose was 1.8 Svedberg (S). Additional species sedimenting at peak maxima of 2.8, 4.0, 5.1 and 6.5 S were also clearly found (Fig. 28).

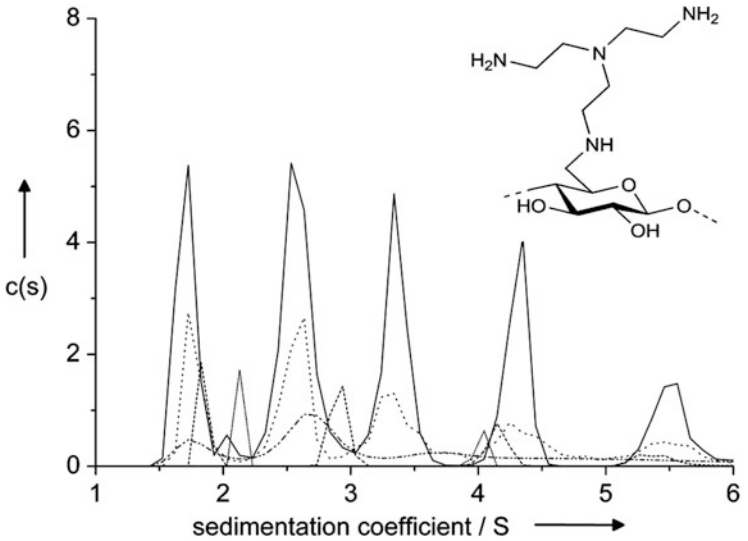

Fig. 28 Representative sedimentation coefficient distributions of 6-deoxy-6-(2-(bis(2-aminoethyl)aminoethyl)amino) cellulose $DS_{Amine} = 0.60$, at various concentrations: *solid* (——) 2.0 mg/mL; *dash* (– –) 1.0 mg/mL; *dot* (·····) 0.5 mg/mL; *dash dot* (– · – ·) 0.25 mg/mL; *short dot* (·····) 0.125 mg/mL. Sedimentation velocity patterns from the Rayleigh interference optical system of the Beckman XL-I ultracentrifuge were analyzed using the SEDFIT procedure of Schuck and Dam [180]. Sedimentation coefficients were extrapolated to zero concentration to correct for non-ideality effects [181]

It is obvious that even a fully reversible self-association (tetramerization) within this family of 6-deoxy-6-amino celluloses can occur (Fig. 29). Remarkably, these carbohydrate tetramers are then seen to associate further in a regular way into supramolecular complexes.

This behavior was found for the first time for carbohydrates, whereas it is well known for polypeptides and proteins such hemoglobin and its sickle cell mutation [182]. The large self-assembling cationic structures render them possible candidates for mimicking the properties of histones and using as condensing or packing agents in DNA-based therapies [183]. Most importantly, however, our traditional perceptions as to what is “protein-like” and what is “carbohydrate-like” behavior may need to be reconsidered [184].

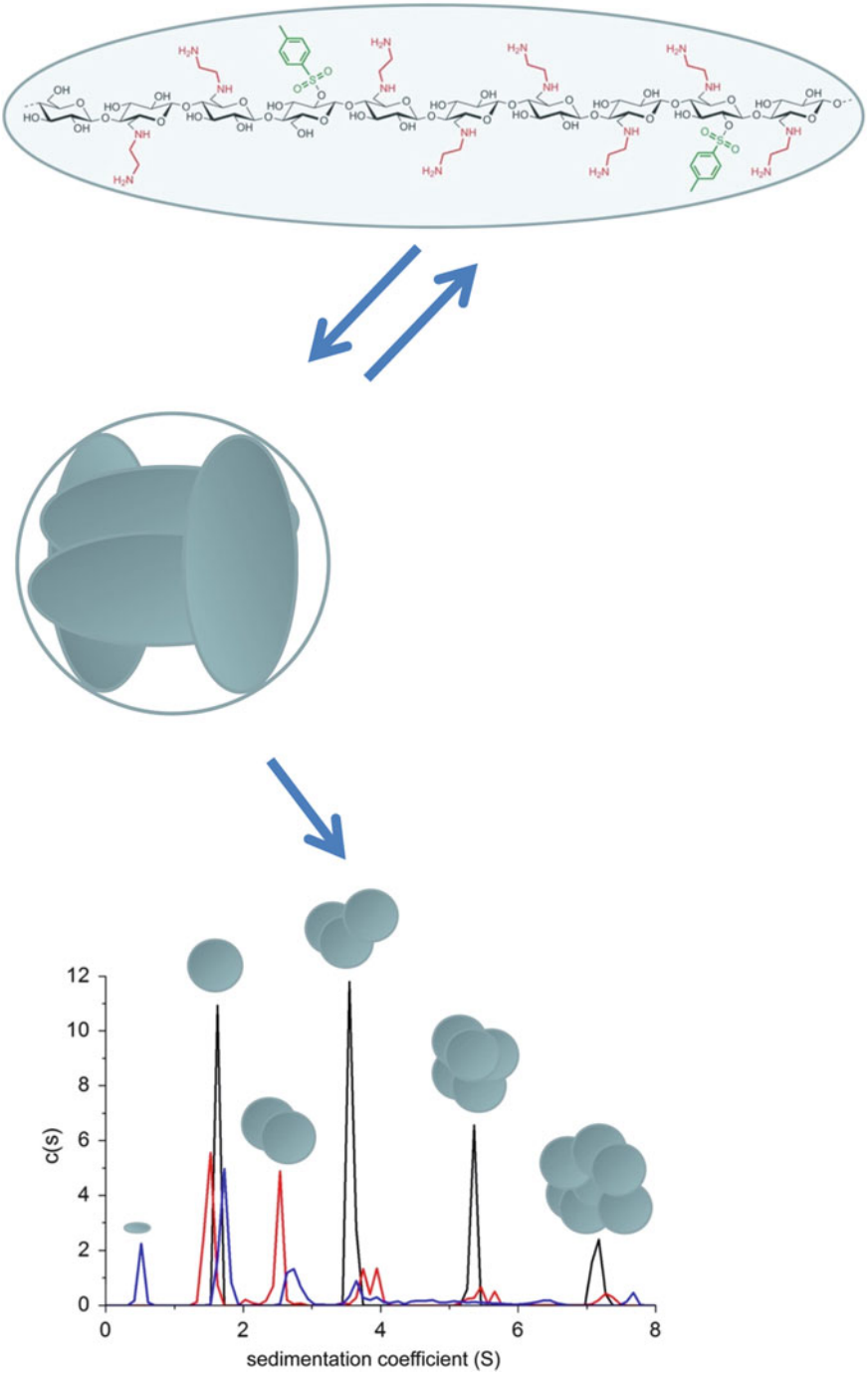

Fig. 29 Reversible tetramerization and further higher-order association of the polysaccharide 6-deoxy-6-(*ω*-aminoethyl)aminocellulose (AEA cellulose). *Top*: Monomer unit of DP ~10, degree

7.3 Reactions of 6-Deoxy-6-Azido Cellulose

S_N reaction of tosyl cellulose with sodium azide and subsequent copper-catalyzed Huisgen reaction (click chemistry) is another promising path to new cellulose derivatives not accessible by conventional etherification and esterification. Thus, 1,4-disubstituted 1,2,3-triazols formed as linker yield novel cellulose derivatives with methylcarboxylate, 2-aniline, 3-thiophene, and acetylenecarboxylic acid dimethyl ester moieties without any side reaction, with a conversion of up to 98% (Fig. 30) [185, 186].

The chemoselective introduction of dendrons into cellulose is achieved by homogeneous reaction of 6-deoxy-6-azido cellulose with propargyl-polyamidoamine (PAMAM) dendrons in DMSO and ILs or heterogeneously in methanol in the presence of $CuSO_4 \cdot 5H_2O$/sodium ascorbate (Fig. 31) [187–189].

The HSQC-DEPT NMR spectrum of second generation PAMAM-triazolo cellulose (DS 0.59) allows complete assignment of the signals of the protons of the substituent in ^{1}H-NMR spectra (Fig. 32).

In Fig. 33, a comparison of ^{13}C-NMR spectra of first, second, and third generation PAMAM-triazolo cellulose synthesized in EMImAc demonstrates the possibility to assign the signals of the dendrons and the AGU. However, the intensity of the peaks of the carbon atoms of the repeating unit decreases as a result of the large number of branches and corresponding carbon atoms.

Even water-soluble deoxy-azido cellulose derivatives are accessible by carboxymethylation, applying 2-propanol/aqueous NaOH as medium [190]. The carboxymethyl deoxy-azido cellulose provides a convenient starting material for the selective conversion by Huisgen reaction, yielding water-soluble carboxymethyl 6-deoxy-(1-*N*-(1,2,3-triazolo)-4-PAMAM) cellulose derivatives of first to third generation (Fig. 34).

Chemoselective synthesis of dendronized cellulose could be a path not only to regioselective functionalization of propargyl cellulose in position 6 [191] but also to functionalization at position 3 [192]. By nucleophilic displacement of 6-*O*-tosylcellulose (DS 0.58) with propargyl amine, 6-deoxy-6-aminopropargyl cellulose is formed and provides an excellent starting material for reaction, including dendronization of cellulose by the Huisgen reaction to yield 6-deoxy-6-amino-

Fig. 29 (continued) of substitution at C-6 $DS_{Amine} = 0.83$, and degree of substitution at C-2 of tosyl residues $DS_{Tosyl} = 0.2$, yielding molar mass $M \sim 3{,}250$ g/mol and sedimentation coefficient $s \sim 0.5$ S. *Middle*: Assembly into tetramers with $M \sim 13{,}000$ g/mol and $s \sim 1.7$ S. *Lower*: Sedimentation coefficient distribution for AEA cellulose at different concentrations: 2.0 (*black*), 1.0 (*red*), 0.75 (*blue*), 0.25 (*green*), and 0.125 mg/mL (*pink*). Based on the $s \sim M^{2/3}$ scaling relationship, the supermonomers associate into supertrimers, superhexamers, and super-9-mers. There is also evidence for some superdimers, although they were not evident at the highest loading concentration. The proportion of supermonomers drops relative to the higher-order species indicates partial reversibility, even with the higher-order association

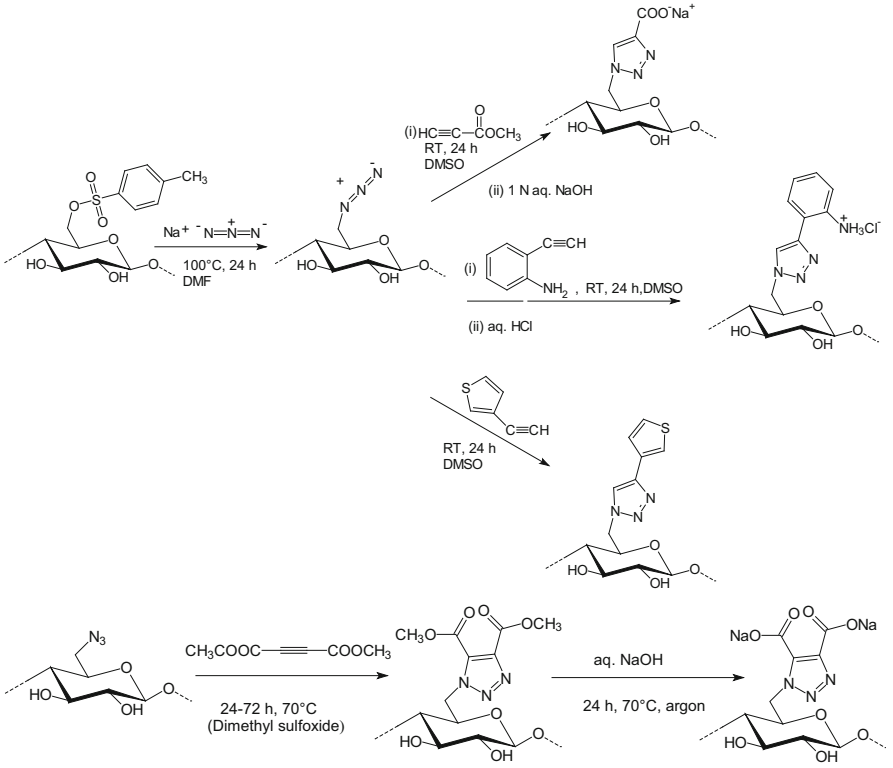

Fig. 30 Reaction path for synthesis of 6-deoxy-6-azido cellulose and subsequent copper-catalyzed Huisgen reaction of 1,4-disubstituted 1,2,3-triazols used as linker for the modification of cellulose with methylcarboxylate, 2-aniline, 3-thiophene moieties, and acetylenecarboxylic acid dimethyl ester

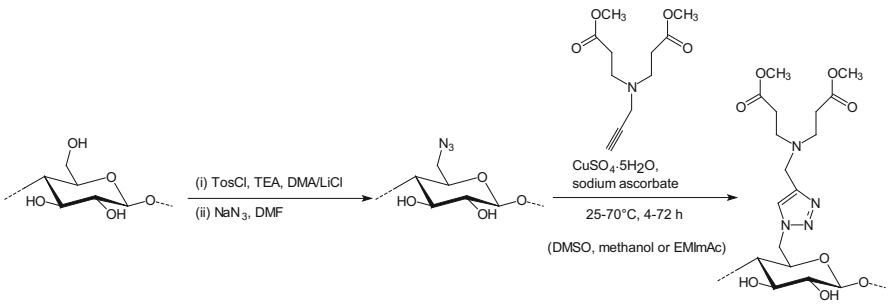

Fig. 31 Reaction path for conversion of cellulose with first generation propargyl-PAMAM dendron via tosylation, nucleophilic displacement by azide, and conversion with the dendron

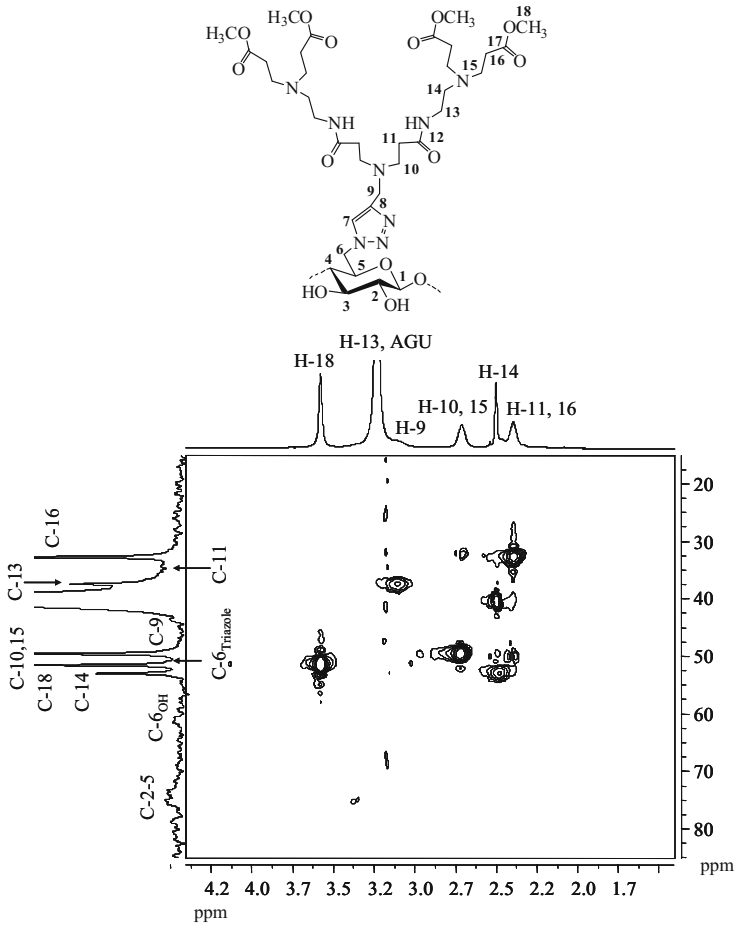

Fig. 32 HSQC-DEPT NMR spectrum of second generation PAMAM-triazolo cellulose (DS 0.59). *AGU* anhydroglucose unit. Adapted from [187]

(4-methyl-(1,2,3-triazolo)-1-propyl-polyamido amine) cellulose derivatives (Fig. 35).

3-Mono-*O*-propargyl cellulose can be produced by reaction of 2,6-di-*O*-thexyldimethylsilyl cellulose with propargyl bromide in the presence of sodium hydride, followed by subsequent treatment with tetrabutylammonium fluoride trihydrate for complete removal of the silicon-containing moieties of 3-mono-*O*-propargyl-2,6-di-*O*-thexyldimethylsilyl cellulose. Cu-catalyzed Huisgen reaction with azido-propyl-polyamidoamine of first and second generation dendrons leads to cellulose regioselectively functionalized with 3-*O*-(4-methyl-1-*N*-propyl-polyamidoamine-(1,2,3-triazole)) ([192], Fig. 36).

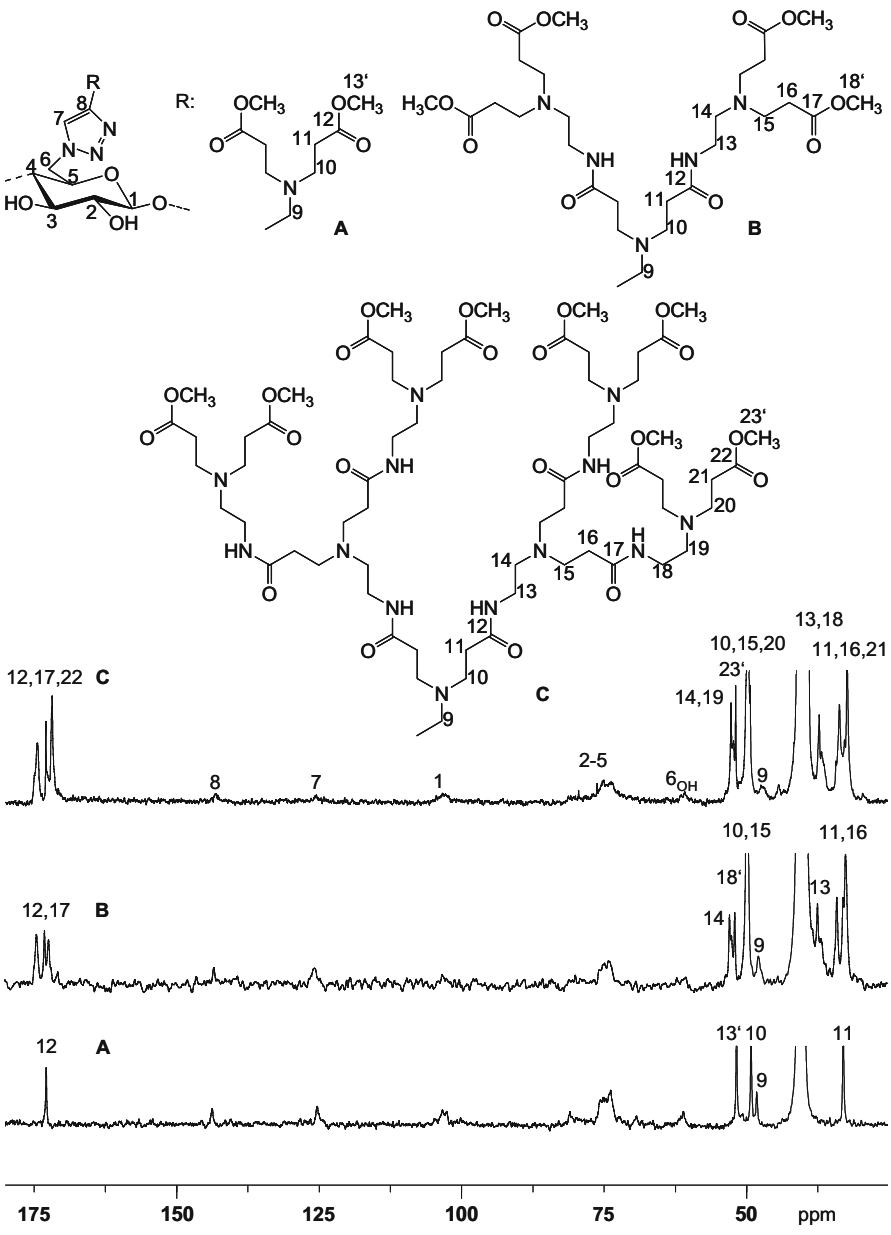

Fig. 33 ^{13}C-NMR spectra of first (DS 0.60, *A*), second (DS 0.48, *B*), and third (DS 0.28, *C*) generation PAMAM-triazolo cellulose in DMSO-d_6 at 60°C

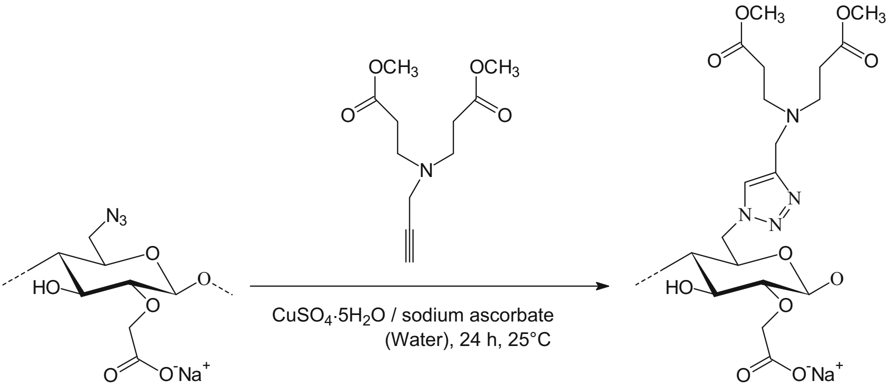

Fig. 34 Homogeneous conversion of carboxymethyl 6-deoxy-6-azidocellulose (DS_{Azide} 0.81, DS_{CM} 1.25) with first generation propargyl-polyamidoamine dendron via the copper-catalyzed Huisgen reaction

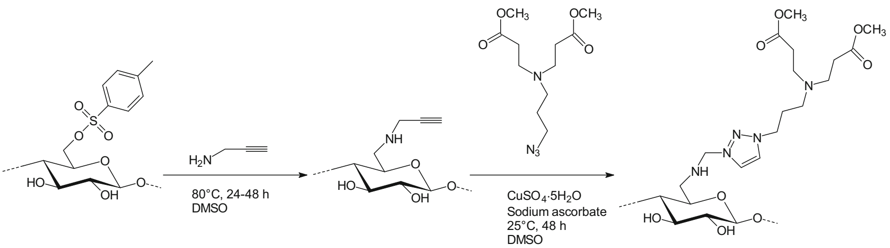

Fig. 35 Reaction path for the synthesis of 6-deoxy-6-amino-(4-methyl-(1,2,3-triazolo)-1-propyl-polyamido amine) cellulose derivatives of first generation (DS 0.33) via 6-deoxy-6-aminopropargyl cellulose

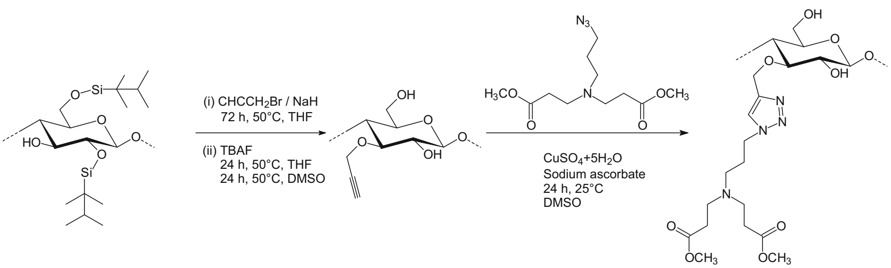

Fig. 36 Synthesis reaction of first generation 3-*O*-(4-methyl-1-*N*-propyl-polyamidoamine-(1,2,3-triazole)) cellulose via 3-*O*-propargyl cellulose

7.4 Cellulose Carbonate as Reactive Intermediate

Polysaccharide aryl carbonates are easily accessible reactive derivatives useful for a variety of reactions [193]. Easily soluble cellulose aryl carbonates can be synthesized by applying phenyl chloroformate, phenyl fluoroformate, and *p*-NO_2-phenyl chloroformate under homogeneous reaction conditions with DMAc/LiCl as reaction medium. Pyridine should be used instead of triethylamine to reduce the nucleophilicity of the hydroxyl groups of the polymer and to exclude formation of cyclic or intermolecular carbonates [194–196].

The synthesis of cellulose phenyl carbonates in the IL 1-butyl-3-methylimidazolium chloride/pyridine is even more efficient. The DS can be controlled, and completely functionalized products are available as a result of the less pronounced side reactions than with tertiary amide solvents [197].

A variety of novel cellulose derivatives are accessible based on cellulose phenyl carbonate. For instance, poly-zwitterions can be produced (Fig. 37). Cellulose phenyl carbonate can be allowed to react with equimolar amounts of β-alanine ethyl ester and *N-tert*-butoxycarbonyl-1,2-ethanediamine. The aminolysis produces (3-ethoxy-3-oxopropyl-*N*-Boc-2-aminoethyl) cellulose carbamate with a $DS_{alanineester}$ of 0.88 and a $DS_{Boc-EDA}$ of 0.95. Thus, there is indication of similar reactivity of the amines, together with a very high conversion (95% of the carbonate moieties into carbamate).

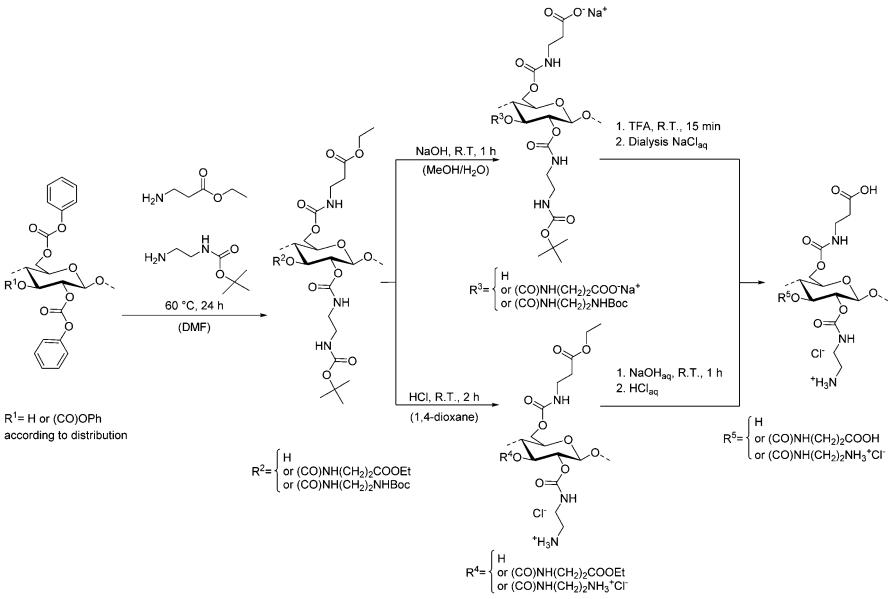

Fig. 37 Reaction scheme for the synthesis of anionic, cationic, and ampholytic cellulose carbamate

A polyanion, polycation, and poly-zwitterion can be obtained from cellulose carbamate because of the orthogonal protecting groups. Synthesis of (2-carboxyethyl-*N*-Boc-2-aminoethyl) cellulose carbamate by alkaline cleavage of the ethyl ester has been carried out homogeneously in methanolic/aqueous NaOH solution to mediate the solubility of educt and product. By applying gaseous hydrogen chloride, acidic cleavage of the Boc group leads to the polycation. Also, (2-carboxyethyl-2-aminoethyl) cellulose carbamate, a poly-zwitterion, can be produced by acidic treatment of the polyanion.

8 Conclusions

Cellulose is the most important renewable resource and a unique polymer in terms of its structure and properties. Because of its unique properties, cellulose can serve as starting material for various products and processes for a sustainable world and the development of a country's bioeconomy. Physical and chemical modification reactions yielding fibers, film, sponges, and cellulose ethers and esters are of high commercial importance today. However, research and development in the field of nanostructuring of cellulose and cellulose derivatives, homogeneous chemistry with cellulose applying various solvents (including molten salts, ionic liquids, and water-based systems) can open new avenues for product design with modern organic chemistry. It can be expected that homogeneous phase chemistry will enter the technical scale in the future. Not only chemical modification of the bulk, but also surface modification (i.e., products with low DS) can provide important novel materials. Last but not least, as discussed in this review paper, depending on its nano- and microstructured architectures, versatile characteristics of the biopolymer cellulose can be achieved and addressed to a specific function. Consequently, cellulose is a promising and broadly applicable material not only (as commonly known) in the paper and textile industries but also for medical and pharmaceutical devices, among others. The applications of nano- and microstructured cellulose can further be broadened by chemical and physical surface treatments.

However, there is still a need for research and development investment in science and engineering to produce advanced and cost-competitive cellulose nanoscale products. It is necessary to obtain a better understanding of the adhesion interactions beyond hydrogen bonding, including mechanical interlocking and interpenetrating networks, on a fundamental level to improve the interfacial properties of cellulose composite materials.

From the author's point of view, cellulose and other polysaccharides and their derivatives obtained by physical, biological, and chemical processes and combinations thereof have a bright future.

Acknowledgements Dr. Andreas Koschella is thankfully acknowledged for his efforts in preparing the manuscript.

References

1. Klemm D, Heublein B, Fink H-P et al (2005) Cellulose: fascinating biopolymer and sustainable raw material. Angew Chem Int Ed 44:3358–3393
2. Mohanty AK, Misra M, Hinrichsen G (2000) Biofibres, biodegradable polymers and biocomposites. An overview. Macromol Mater Eng 276(277):1–24
3. Heinze T, Liebert T (2012) Celluloses and polyoses/hemicelluloses. In: Matyjaszewski K, Möller M (eds) Polymer science: a comprehensive reference, vol 10. Elsevier, Amsterdam, pp 83–152
4. Payen A (1839) Composition de la matière ligneuse. Comptes Rendus 8:51–53
5. Young RA (1994) Comparison of the properties of chemical cellulose pulps. Cellulose 1:107–130
6. Sixta H (ed) (2006) Handbook of pulp. Wiley-VCH, Weinheim
7. Schubert S, Schlufter K, Heinze T (2011) Configurations, structures, and morphologies of cellulose. In: Popa V (ed) Polysaccharides in medicinal and pharmaceutical applications. iSmithers, Shrewsbury, pp 1–55
8. Hon DN-S (1996) Cellulose and its derivatives: structures, reactions, and medical uses. In: Dumitriu S (ed) Polysaccharides in medical applications. Marcel Dekker, New York, pp 87–105
9. Eichhorn SJ, Baillie CA, Zafeiropoulos N et al (2001) Current international research into cellulosic fibers and composites. J Mater Sci 36:2107–2131
10. Vandamme EJ, De Baets S, Vanbaelen A et al (1998) Improved production of bacterial cellulose and its application potential. Polym Degrad Stab 59:93–99
11. Jonas R, Farah LF (1998) Production and application of microbial cellulose. Polym Degrad Stab 59:101–106
12. Rao VSR, Sundararajan PR, Ramakrishnan C et al (1967) Conformational studies of amylose. In: Ramachandran GN (ed) Conformation of biopolymers, vol 2. Academic, London, pp 721–737
13. Krässig HA (1993) Cellulose: structure, accessibility and reactivity. Gordon and Breach Science, Yverdon
14. Perez S, Mazeau K (2005) Conformations, structures, and morphologies of celluloses. In: Dumitriu S (ed) Polysaccharides: structural diversity and functional versatility. Marcel Dekker, New York, pp 41–68
15. Kondo T (1997) The relationship between intramolecular hydrogen bonds and certain physical properties of regioselectively substituted cellulose derivatives. J Polym Sci A Polym Chem 35:717–723
16. Liang CY, Marchessault RH (1959) Infrared spectra of crystalline polysaccharides. I. Hydrogen bonds in native celluloses. J Polym Sci 37:385–395
17. Michell AJ (1988) Second derivative FTIR spectra of celluloses I and II and related mono- and oligosaccharides. Carbohydr Res 173:185–195
18. Kamide K, Okajima K, Kowsaka K et al (1985) CP/MASS (cross-polarization/magic angle sample spinning] carbon-13 NMR spectra of cellulose solids: an explanation by the intramolecular hydrogen bond concept. Polym J 17:701–706
19. Gardner KH, Blackwell J (1974) Structure of native cellulose. Biopolymers 13:1975–2001
20. Nishiyama Y, Langan P, Chanzy H (2002) Crystal structure and hydrogen-bonding system in cellulose Iβ from synchrotron x-ray and neutron fiber diffraction. J Am Chem Soc 124:9074–9082
21. Kondo T (2005) Hydrogen bonds in cellulose and cellulose derivatives. In: Dumitriu S (ed) Polysaccharides: structural diversity and functional versatility, 2nd edn. Marcel Dekker, New York, pp 69–98
22. Tashiro K, Kobayashi M (1991) Theoretical evaluation of three-dimensional elastic constants of native and regenerated celluloses: role of hydrogen bonds. Polymer 32:1516–1526

23. Sarko A, Muggli R (1947) Packing analysis of carbohydrates and polysaccharides. III. Valonia cellulose and cellulose II. Macromolecules 7:486–494
24. Atalla RH, VanderHart DL (1984) Native cellulose: a composite of two distinct crystalline forms. Science 223:283–285
25. Isogai A, Usuda M, Kato T et al (1989) Solid-state CP/MAS carbon-13 NMR study of cellulose polymorphs. Macromolecules 22:3168–3172
26. Zugenmaier P (2001) Conformation and packing of various crystalline cellulose fibers. Prog Polym Sci 26:1341–1417
27. Langan P, Nishiyama Y, Chanzy H (1999) A revised structure and hydrogen-bonding system in cellulose II from a neutron fiber diffraction analysis. J Am Chem Soc 121:9940–9946
28. Wada M, Heux L, Isogai A et al (2001) Improved structural data of cellulose IIII prepared in supercritical ammonia. Macromolecules 34:1237–1243
29. Gardiner ES, Sarko A (1985) Packing analysis of carbohydrates and polysaccharides. 16. The crystal structures of celluloses IV_I and IV_{II}. Can J Chem 63:173–180
30. Isogai A (1994) Allomorphs of cellulose and other polysaccharides. In: Gilbert RD (ed) Cellulosic polymers: blends and composites. Hanser, Munich, p 1
31. Hermans PH, Weidinger A (1946) Recrystallization of amorphous cellulose. J Am Chem Soc 68:1138
32. Wadehra IL, Manley RSJ (1965) Recrystallization of amorphous cellulose. J Appl Polym Sci 9:2627–2630
33. Schroeder LR, Gentile VM, Atalla RH (1986) Nondegradative preparation of amorphous cellulose. J Wood Chem Technol 6:1–14
34. Atalla RH, Ellis JD, Schroeder LR (1984) Some effects of elevated temperatures on the structure of cellulose and its transformation. J Wood Chem Technol 4:465–482
35. de Souza Lima MM, Borsali R (2004) Rodlike cellulose microcrystals: structure, properties, and applications. Macromol Rapid Commun 25:771–787
36. Ioelovich M, Leykin A (2008) Cellulose as a nanostructured polymer: a short review. Bioresources 3:1403–1418
37. Welch LM, Roseveare WE, Mark H (1946) Fibrillar structure of rayon fibers. Ind Eng Chem 38:580–582
38. Sisson WA (1940) X-ray studies of crystallite orientation in cellulose fibers. III. Fiber structures from coagulated cellulose. J Phys Chem 44:513–529
39. Klemm D, Schumann D, Udhardt U et al (2001) Bacterial synthesized cellulose – artificial blood vessels for microsurgery. Prog Polym Sci 26:1561–1603
40. Yoshinaga F, Tonouchi N, Watanabe K (1997) Research progress in the production of bacterial cellulose by aeration and agitation culture and its application as a new industrial material. Biosci Biotechnol Biochem 61:219–224
41. Kongruang S (2008) Bacterial cellulose production by Acetobacter xylinum strains from agricultural waste products. Appl Biochem Biotechnol 148:245–256
42. Ring DF, Nashed W, Dow T (1987) Microbial polysaccharide articles and methods of production. US Patent 4,655,758, 7 Apr 1987
43. Ring DF, Nashed W, Dow T (1986) Liquid loaded pad for medical applications. US Patent 4,588,400, 13 May 1986
44. Farah LF (1990) Process for the preparation of cellulose film, cellulose film produced thereby, artificial skin graft and its use. US Patent 4,912,049, 27 Mar 1990
45. Czaja W, Krystynowicz A, Bielecki S et al (2006) Microbial cellulose-the natural power to heal wounds. Biomaterials 27:145–151
46. Watanabe K, Tabuchi M, Morinaga Y et al (1998) Structural features and properties of bacterial cellulose produced in agitated-culture. Cellulose 5:187–200
47. Klemm D, Schumann D, Kramer F et al (2006) Nanocelluloses as innovative polymers in research and application. Adv Polym Sci 205:49–96

48. Pääkkö M, Ankerfors M, Kosonen H et al (2007) Enzymatic hydrolysis combined with mechanical shearing and high-pressure homogenization for nanoscale cellulose fibrils and strong gels. Biomacromolecules 8:1934–1941
49. Samir MASA, Alloin F, Dufresne A (2005) Review of recent research into cellulosic whiskers, their properties and their application in nanocomposite field. Biomacromolecules 6:612–626
50. Dufresne A (2008) Polysaccharide nano crystal reinforced nanocomposites. Can J Chem 86:484–494
51. Steege H-H, Philipp B (1974) Production, characterization, and use of microcrystalline cellulose. Zellst Pap 23:68–73
52. Bondeson D, Mathew A, Oksman K (2006) Optimization of the isolation of nanocrystals from microcrystalline cellulose by acid hydrolysis. Cellulose 13:171–180
53. Araki J, Wada M, Kuga S et al (1998) Flow properties of microcrystalline cellulose suspension prepared by acid treatment of native cellulose. Colloid Surf A Physicochem Eng Asp 142:75–82
54. Dong XM, Revol JF, Gray DG (1998) Effect of microcrystallite preparation conditions on the formation of colloid crystals of cellulose. Cellulose 5:19–32
55. Araki J, Wada M, Kuga S et al (1999) Influence of surface charge on viscosity behavior of cellulose microcrystal suspension. J Wood Sci 45:258–261
56. de Vries HI (1951) Rotatory power and other optical properties of certain liquid crystals. Acta Crystallogr 4:219–226
57. Revol J-F, Bradford H, Giasson J et al (1992) Helicoidal self-ordering of cellulose microfibrils in aqueous suspension. Int J Biol Macromol 14:170–172
58. Kroon-Batenburg LMJ, Kroon J, Northolt MG (1986) Chain modulus and intramolecular hydrogen bonding in native and regenerated cellulose fibers. Polym Commun 27:290–292
59. Nishino T, Matsuda I, Hirao K (2004) All-cellulose composite. Macromolecules 37:7683–7687
60. Odijk T, Lekkerkerker HNW (1985) Theory of the isotropic-liquid crystal phase separation for a solution of bidisperse rodlike macromolecules. J Phys Chem 89:2090–2096
61. de Souza Lima MM, Borsali R (2002) Static and dynamic light scattering from polyelectrolyte microcrystal cellulose. Langmuir 18:992–996
62. Angellier H, Putaux J-L, Molina-Boisseau S et al (2005) Starch nanocrystal fillers in an acrylic polymer matrix. Macromol Symp 221:95–104
63. Marchessault RH, Morehead FF, Walter NM (1959) Liquid crystal systems from fibrillar polysaccharides. Nature 184:632–633
64. Revol JF, Godbout L, Dong XM et al (1994) Chiral nematic suspensions of cellulose crystallites; phase separation and magnetic field orientation. Liq Cryst 16:127–134
65. Revol JF, Godbout L, Gray DG (1998) Solid self-assembled films of cellulose with chiral nematic order and optically variable properties. J Pulp Paper Sci 24:146–149
66. Orts WJ, Godbout L, Marchessault RH et al (1998) Enhanced ordering of liquid crystalline suspensions of cellulose microfibrils: a small-angle neutron scattering study. Macromolecules 31:5717–5725
67. Favier V, Canova GR, Cavaillé JY et al (1995) Nanocomposite materials from latex and cellulose whiskers. Polym Adv Technol 6:351–355
68. Favier V, Chanzy H, Cavaillé JY (1995) Polymer nanocomposites reinforced by cellulose whiskers. Macromolecules 28:6365–6367
69. Viet D, Beck-Candanedo S, Gray DG (2007) Dispersion of cellulose nanocrystals in polar organic solvents. Cellulose 14:109–113
70. Dubief D, Samain E, Dufresne A (1999) Polysaccharide microcrystals reinforced amorphous poly(β-hydroxyoctanoate) nanocomposite materials. Macromolecules 32:5765–5771
71. Dufresne A, Kellerhals MB, Witholt B (1999) Transcrystallization in Mcl-PHAs/cellulose whiskers composites. Macromolecules 32:7396–7401

72. Angles NM, Dufresne A (2000) Plasticized starch/tunicin whiskers nanocomposites. 1. Structural analyses. Macromolecules 33:8344–8353
73. Grunert M, Winter WT (2002) Nanocomposites of cellulose acetate butyrate reinforced with cellulose nanocrystals. J Polym Environ 10:27–30
74. Chazeau L, Cavaillé JY, Perez J (2000) Plasticized PVC reinforced with cellulose whiskers. II. Plastic behavior. J Polym Sci B Polym Phys 38:383–392
75. Revol JF (1982) On the cross-sectional shape of cellulose crystallites in Valonia ventricosa. Carbohydr Polym 2:123–134
76. Correa AC, Morais Teixeira E, Carmona VB et al (2014) Obtaining nanocomposites of polyamide 6 and cellulose whiskers via extrusion and injection molding. Cellulose 21:311–322
77. Mathew AP, Dufresne A (2002) Morphological investigation of nanocomposites from sorbitol plasticized starch and tunicin whiskers. Biomacromolecules 3:609–617
78. Turbak AF, Snyder FW, Sandberg KR (1982) Suspensions containing microfibrillated cellulose. EP 19810108847, 12 May 1982
79. Wagberg L, Decher G, Norgren M et al (2008) The build-up of polyelectrolyte multilayers of microfibrillated cellulose and cationic polyelectrolytes. Langmuir 24:784–795
80. Li Y, Li G, Zou Y et al (2014) Preparation and characterization of cellulose nanofibers from partly mercerized cotton by mixed acid hydrolysis. Cellulose 21:301–309
81. Werner O, Persson L, Nolte M et al (2008) Patterning of surfaces with nanosized cellulosic fibrils using microcontact printing and a lift-off technique. Soft Matter 4:1158–1160
82. Siqueira G, Bras J, Dufresne A (2009) Cellulose whiskers versus microfibrils: influence of the nature of the nanoparticle and its surface functionalization on the thermal and mechanical properties of nanocomposites. Biomacromolecules 10:425–432
83. Stenstad P, Andresen M, Tanem BS et al (2008) Chemical surface modifications of microfibrillated cellulose. Cellulose 15:35–45
84. Dong S, Sapieha S, Schreiber HP (1993) Mechanical properties of corona-modified cellulose/polyethylene composites. Polym Eng Sci 33:343–346
85. Cavaille JY, Chanzy H, Fleury E et al (1997) Surface-modified cellulose microfibrils, method for making the same, and use thereof as a filler in composite material. US Patent 6,117,545, 12 Sept 2000
86. Cash MJ, Chan AN, Conner HT et al (1999) Derivatized microfibrillar polysaccharide. US Patent 6,602,994, 5 Aug 2003
87. Gousse C, Chanzy H, Excoffier G et al (2002) Stable suspensions of partially silylated cellulose whiskers dispersed in organic solvents. Polymer 43:2645–2651
88. Agarwal M, Lvov Y, Varahramyan K (2006) Conductive wood microfibres for smart paper through layer-by-layer nanocoating. Nanotechnology 17:5319–5325
89. Greiner A, Wendorff JH (2007) Electrospinning: a fascinating method for the preparation of ultrathin fibers. Angew Chem Int Ed 46:5670
90. Reneker DH, Chun I (1996) Nanometer diameter fibers of polymer, produced by electrospinning. Nanotechnology 7:216–223
91. Frenot A, Chronakis IS (2003) Polymer nanofibers assembled by electrospinning. Curr Opin Colloid Interface Sci 8:64–75
92. Xie J, Li X, Xia Y (2008) Putting electrospun nanofibers to work for biomedical research. Macromol Rapid Commun 29:1775–1792
93. Li F, Zhao Y, Song Y (2010) Core-shell nanofibers: nano channel and capsule by coaxial electrospinning. In: Kumar A (ed) Nanofibers. InTech, Rijeka, pp 419–438
94. Scholten E, Bromberg L, Rutledge GC, Hatton TA (2011) Electrospun polyurethane fibers for absorption of volatile organic compounds from air. ACS Appl Mater Interfaces 10:3902–3909
95. Kim C-W, Kim D-S, Kang S-Y et al (2006) Structural studies of electrospun cellulose nanofibers. Polymer 47:5097–5107

96. Viswanathan G, Murugesan S, Pushparaj V et al (2006) Preparation of biopolymer fibers by electrospinning from room temperature ionic liquids. Biomacromolecules 7:415–418
97. Qi H, Sui X, Yuan J et al (2010) Electrospinning of cellulose-based fibers from NaOH/urea aqueous system. Macromol Mater Eng 295:695–700
98. Römhild K, Wiegand C, Hipler UC et al (2013) Novel bioactive amino-functionalized cellulose nanofibers. Macromol Rapid Commun 34:1767–1771
99. Hornig S, Heinze T (2008) Efficient approach to design stable water-dispersible nanoparticles of hydrophobic cellulose esters. Biomacromolecules 9:1487–1492
100. Wondraczek H, Petzold-Welcke K, Fardim P et al (2013) Nanoparticles from conventional cellulose esters: evaluation of preparation methods. Cellulose 20:751–760
101. Nikolajski M, Wotschadlo J, Clement JH et al (2012) Amino-functionalized cellulose nanoparticles: preparation, characterization, andinteractions with living cells. Macromol Biosci 12:920–925
102. Kostag M, Köhler S, Liebert T et al (2010) Pure cellulose nanoparticles from trimethylsilyl cellulose. Macromol Symp 294(2):96–106
103. Liebert T, Kostag M, Wotschadlo J et al (2011) Stable cellulose nanospheres for cellular uptake. Macromol Biosci 11:1387–1392
104. Heinze T, Liebert T (2001) Unconventional methods in cellulose functionalization. Prog Polym Sci 26:1689–1762
105. Heinze T, Dicke R, Koschella A et al (2000) Effective preparation of cellulose derivatives in a new simple cellulose solvent. Macromol Chem Phys 201:627–631
106. El Seoud OA, Heinze T (2005) Organic esters of cellulose: new perspectives for old polymers. In: Heinze T (ed) Polysaccharides I, structure, characterization and use, vol 186, Advances in polymer science. Springer, Berlin, pp 103–149
107. Morgenstern B, Berger W (1993) Investigations about dissolution of cellulose in the lithium chloride/N, N-dimethylformamide system. Acta Polym 44:100–102
108. Silva AA, Laver ML (1997) Molecular weight characterization of wood pulp cellulose: dissolution and size exclusion chromatographic analysis. Tappi J 80:173–180
109. Striegel A (1998) Theory and applications of DMAc/LiCl in the analysis of polysaccharides. Carbohydr Polym 34:267–274
110. Kostag M, Liebert T, El Seoud OA et al (2013) Efficient cellulose solvent: quaternary ammonium chlorides. Macromol Rapid Commun 34:1580–1584
111. Gericke M, Liebert T, El Seoud OA et al (2011) Tailored media for homogeneous cellulose chemistry: ionic liquid/co-solvent mixtures. Macromol Mater Eng 296:483–493
112. Berger W, Keck M, Philipp B (1988) On the mechanism of cellulose dissolution in nonaqueous solvents, especially in O-basic systems. Cellul Chem Technol 22:387–397
113. Ciacco GT, Liebert TF, Frollini E et al (2003) Application of the solvent dimethyl sulfoxide/tetrabutyl-ammonium fluoride trihydrate as reaction medium for the homogeneous acylation of Sisal cellulose. Cellulose 10:125–132
114. Sharma RK, Fry JL (1983) Instability of anhydrous tetra-n-alkylammonium fluorides. J Org Chem 48:2112–2114
115. Sun H, DiMagno SG (2005) Anhydrous tetrabutylammonium fluoride. J Am Chem Soc 127:2050–2051
116. Köhler S, Heinze T (2007) New solvents for cellulose: dimethyl sulfoxide/ammonium fluorides. Macromol Biosci 7:307–314
117. Casarano R, Pires PAR, El Seoud OA (2014) Acylation of cellulose in a novel solvent system: solution of dibenzyldimethylammonium fluoride in DMSO. Carbohydr Polym 101:444–450
118. Burchard W (1993) Macromolecular association phenomena. A neglected field of research? Trends Polym Sci 1:192–198
119. Schulz L, Burchard W, Dönges R (1998) Evidence of supramolecular structures of cellulose derivatives in solution. In: Heinze T, Glasser WG (eds) Cellulose derivatives: modification, characterization, and nanostructures, vol 688, ACS symposium series. American Chemical Society, Washington DC, pp 218–238

120. Morgenstern B, Kammer H-W (1999) On the particulate structure of cellulose solutions. Polymer 40:1299–1304
121. Menger FM (1993) Enzyme reactivity from an organic perspective. Acc Chem Res 26:206–212
122. Husemann E, Siefert E (1969) N-Ethylpyridinium chloride as solvent and reaction medium for cellulose. Makromol Chem 128:288–291
123. Swatloski RP, Spear SK, Holbrey JD et al (2002) Dissolution of cellulose with ionic liquids. J Am Chem Soc 24:4974–4975
124. Swatloski RP, Rogers RD, Holbrey JD (2003) Dissolution and processing of cellulose using ionic liquids, cellulose solution, and regenerating cellulose. World Patent 2003029329 A2, 10 April 2003
125. Gericke M, Fardim P, Heinze T (2012) Ionic liquids – promising but challenging solvents for homogeneous derivatization of cellulose. Molecules 17:7458–7502
126. El Seoud OA, Koschella A, Fidale LC et al (2007) Applications of ionic liquids in carbohydrate chemistry: a window of opportunities. Biomacromolecules 8:2629–2647
127. Zhu S, Wu Y, Chen Q et al (2006) Dissolution of cellulose with ionic liquids and its application: a mini-review. Green Chem 8:325–327
128. Barthel S, Heinze T (2006) Acylation and carbanilation of cellulose in ionic liquids. Green Chem 8:301–306
129. Liebert T (2008) Innovative concepts for the shaping and modification of cellulose. Macromol Symp 262:28–38
130. Ebner G, Schiehser S, Potthast A et al (2008) Side reaction of cellulose with common 1-alkyl-3-methylimidazolium-based ionic liquids. Tetrahedron Lett 49:7322–7324
131. Handy ST, Okello M (2005) The 2-position of imidazolium ionic liquids: substitution and exchange. J Org Chem 70:1915–1918
132. Erdmenger T, Haensch C, Hoogenboom R et al (2007) Homogeneous tritylation of cellulose in 1-butyl-3-methylimidazolium chloride. Macromol Biosci 7:440–445
133. Sobue H, Kiessig H, Hess K (1939) The system: cellulose-sodium hydroxide-water in relation to the temperature. Z Phys Chem B43:309–328
134. Isogai A, Atalla RH (1998) Dissolution of cellulose in aqueous NaOH solutions. Cellulose 5:309–319
135. Yamashiki T, Kamide K, Okajima K (1990) New cellulose fiber from aqueous alkali cellulose solution. In: Kennedy JF, Phillips GO, Williams PA (eds) Cellulose sources and exploitation. Ellis Horwood, London, pp 197–202
136. Yamashiki T, Matsui T, Saitoh M et al (1990) Characterization of cellulose treated by the steam explosion method. Part 1. Influence of cellulose resources on changes in morphology, degree of polymerization, solubility and solid structure. Br Polym J 22:73–83
137. Yamashiki T, Matsui T, Saitoh M et al (1990) Characterization of cellulose treated by the steam explosion method. Part 2: effect of treatment conditions on changes in morphology, degree of polymerization, solubility in aqueous sodium hydroxide, and supermolecular structure of soft wood pulp during steam explosion. Br Polym J 22:121–128
138. Yamashiki T, Matsui T, Saitoh M et al (1990) Characterization of cellulose treated by the steam explosion method. Part 3: effect of crystal forms (cellulose I, II and III) of original cellulose on changes in morphology, degree of polymerization, solubility and supermolecular structure by steam explosion. Br Polym J 22:201–212
139. Yamashiki T, Matsui T, Kowsaka K et al (1992) New class of cellulose fiber spun from the novel solution of cellulose by wet spinning method. J Appl Polym Sci 44:691–698
140. Zhou J, Zhang L (2000) Solubility of cellulose in sodium hydroxide/urea aqueous solution. Polym J 32:866–870
141. Cai J, Zhang L (2005) Rapid dissolution of cellulose in LiOH/urea and NaOH/urea aqueous solutions. Macromol Biosci 5:539–548
142. Cai J, Liu Y, Zhang L (2006) Dilute solution properties of cellulose in LiOH/urea aqueous system. J Polym Sci B Polym Phys 44:3093–3101

143. Egal M, Budtova T, Navard P (2008) The dissolution of microcrystalline cellulose in sodium hydroxide-urea aqueous solutions. Cellulose 15:361–370
144. Cai J, Zhang L, Liu S et al (2008) Dynamic self-assembly induced rapid dissolution of cellulose at low temperatures. Macromolecules 41:9345–9351
145. Cai J, Zhang L (2006) Unique gelation behavior of cellulose in NaOH/Urea aqueous solution. Biomacromolecules 7:183–189
146. Qi H, Chang CY, Zhang L (2008) Effects of temperature and molecular weight on dissolution of cellulose in NaOH/urea aqueous solution. Cellulose 15:779–787
147. Liu S, Zhang L (2009) Effects of polymer concentration and coagulation temperature on the properties of regenerated cellulose films prepared from LiOH/urea solution. Cellulose 16:189–198
148. Cai J, Zhang L, Chang C et al (2007) Hydrogen-bond-induced inclusion complex in aqueous cellulose/LiOH/urea solution at low temperature. ChemPhysChem 8:1572–1579
149. Ruan D, Lue A, Zhang L (2008) Gelation behaviors of cellulose solution dissolved in aqueous NaOH/thiourea at low temperature. Polymer 49:1027–1036
150. Balser K, Hoppe L, Eicher T et al (1986) Cellulose esters. In: Gerhartz W, Yamamoto YS, Campbell FT et al (eds) Ullmanns's encyclopedia of industrial chemistry, vol A5, 5th edn. Wiley-VCH, Weinheim, p 419
151. Brandt L (1986) Cellulose ethers. In: Gerhartz W, Yamamoto YS, Campbell FT et al (eds) Ullmann's encyclopedia of industrial chemistry, vol A5, 5th edn. Wiley-VCH, Weinheim, p 461
152. Wu J, Zhang J, Zhang H et al (2004) Homogeneous acetylation of cellulose in a new ionic liquid. Biomacromolecules 5:266–268
153. Klohr EA, Koch W, Klemm D et al (2000) Manufacture of regioselectively substituted esters of oligo- and polysaccharides. DE Patent 19951734, 07 Sept 2000
154. Ibrahim AA, Nada AMA, Hagemann U et al (1996) Preparation of dissolving pulp from sugarcane bagasse, and its acetylation under homogeneous solution condition. Holzforschung 50:221–225
155. Heinze T, Liebert TF, Pfeiffer KS et al (2003) Unconventional cellulose esters: synthesis, characterization, and structure property relations. Cellulose 10:283–296
156. Takaragi A, Minoda M, Miyamoto T et al (1999) Reaction characteristics of cellulose in the lithium chloride/1,3-dimethyl-2-imidazolidinone solvent system. Cellulose 6:93–102
157. Heinze T, Glasser WG (1998) The role of novel solvents and solution complexes for the preparation of highly engineered cellulose derivatives. ACS Symp Ser 688:2–18
158. Heinze T, Liebert T, Koschella A (2006) Esterification of polysaccharides. Springer, Berlin
159. Staab HA (1962) New methods of preparative organic chemistry IV. Syntheses using heterocyclic amides (azolides). Angew Chem Int Ed 1:351–367
160. Gericke M, Liebert T, Heinze T (2009) Interaction of ionic liquids with polysaccharides – 8. Synthesis of cellulose sulfates suitable for symplex formation. Macromol Biosci 9:343–353
161. Wang Z-M, Li L, Xiao K-J et al (2009) Homogeneous sulfation of bagasse cellulose in an ionic liquid and anticoagulation activity. Bioresour Technol 100:1687–1690
162. Gericke M, Liebert T, Heinze T (2009) Polyelectrolyte synthesis and in situ complex formation in ionic liquids. J Am Chem Soc 131:13220–13221
163. Petzold-Welcke K, Michaelis N, Heinze T (2009) Unconventional cellulose products through nucleophilic displacement reactions. Macromol Symp 280:72–85
164. Heinze T, Petzold-Welcke K (2012) Recent advances in cellulose chemistry. In: Habibi Y, Lucia LA (eds) Polysaccharide building blocks: a sustainable approach to the development of renewable biomaterials. Wiley, Hoboken, pp 1–50
165. Klemm D (1998) Regiocontrol in cellulose chemistry: principles and examples of etherification and esterification. In: Heinze TJ, Glasser EG (eds) Cellulose derivatives: modification, characterisation, and nanostructures, vol 688. American Chemical Society, Washington DC, pp 19–37

166. Wenz G, Liepold P, Bordeanu N (2005) Synthesis and SAM formation of water soluble functional carboxymethylcelluloses: thiosulfates and thioethers. Cellulose 12:85–96
167. Arai K, Aoki F (1994) Preparation and identification of sodium deoxycellulosesulfonate. Sen'i Gakkaishi 50:510–514
168. Arai K, Yoda N (1998) Preparation of water-soluble sodium deoxycellulose sulfonate from homogeneously prepared tosyl cellulose. Cellulose 5:51–58
169. Liu C, Baumann H (2002) Exclusive and complete introduction of amino groups and their N-sulfo and N-carboxymethyl groups into the 6-position of cellulose without the use of protecting groups. Carbohydr Res 337:1297–1307
170. Heinze T (1998) New ionic polymers by cellulose functionalization. Macromol Chem Phys 199:2341–2364
171. Koschella A, Heinze T (2001) Novel regioselectively 6-functionalized cationic cellulose polyelectrolytes prepared via cellulose sulfonates. Macromol Biosci 1:178–184
172. Heinze T, Koschella A, Magdaleno-Maiza L et al (2001) Nucleophilic displacement reactions on tosyl cellulose by chiral amines. Polym Bull 46:7–13
173. Knaus S, Mais U, Binder WH (2003) Synthesis, characterization and properties of methylaminocellulose. Cellulose 10:139–150
174. Tiller J, Berlin P, Klemm D (1999) Soluble and film-forming cellulose derivatives with redox-chromogenic and enzyme immobilizing 1,4-phenylenediamine groups. Macromol Chem Phys 200:1–9
175. Tiller J, Berlin P, Klemm D (2000) Novel matrices for biosensor application by structural design of redox-chromogenic aminocellulose esters. J Appl Polym Sci 75:904–915
176. Berlin P, Klemm D, Tiller J et al (2000) A novel soluble aminocellulose derivative type: its transparent film-forming properties and its efficient coupling with enzyme proteins for biosensors. Macromol Chem Phys 201:2070–2082
177. Berlin P, Klemm D, Jung A et al (2003) Film-forming aminocellulose derivatives as enzyme-compatible support matrices for biosensor developments. Cellulose 10:343–367
178. Becher J, Liebegott H, Berlin P et al (2004) Novel xylylene diaminocellulose derivatives for enzyme immobilization. Cellulose 11:119–126
179. Jung A, Berlin P (2005) New water-soluble and film-forming aminocellulose tosylates as enzyme support matrices with Cu^{2+}-chelating properties. Cellulose 12:67–84
180. Dam J, Schuck P (2005) Sedimentation velocity analysis of heterogeneous protein-protein interactions: sedimentation coefficient distributions c(s) and asymptotic boundary profiles from Gilbert-Jenkins theory. Biophys J 89:651–666
181. Heinze T, Nikolajski M, Daus S et al (2011) Protein-like oligomerisation of carbohydrates. Angew Chem Int Ed 50:8602–8604
182. Ferrone FA, Hofrichter J, Eaton WA (1985) Kinetics of sickle hemoglobin polymerization. II. A double nucleation mechanism. J Mol Biol 183:611–631
183. Teif VB, Bohinc K (2011) Condensed DNA: condensing the concepts. Prog Biophys Mol Biol 105:208–222
184. Nikolajski M, Heinze T, Adams GG et al (2014) Protein–like fully reversible tetramerisation and super-association of an aminocellulose. Sci Rep 4:3861
185. Liebert T, Hänsch C, Heinze T (2006) Click chemistry with polysaccharides. Macromol Rapid Commun 27:208–213
186. Koschella A, Richter M, Heinze T (2010) Novel cellulose-based polyelectrolytes synthesized via the click reaction. Carbohydr Res 345:1028–1033
187. Pohl M, Schaller J, Meister F et al (2008) Selectively dendronized cellulose: synthesis and characterization. Macromol Rapid Commun 29:142–148
188. Heinze T, Schöbitz M, Pohl M et al (2008) Interactions of ionic liquids with polysaccharides: IV. Dendronization of 6-azido-6-deoxy cellulose. J Polym Sci A Polym Chem 46:3853–3859
189. Schöbitz M, Meister F, Heinze T (2009) Unconventional reactivity of cellulose dissolved in ionic liquids. Macromol Symp 280:102–111

190. Pohl M, Morris GA, Harding SE et al (2009) Studies on the molecular flexibility of novel dendronized carboxymethyl cellulose derivatives. Eur Polym J 45:1098–1110
191. Pohl M, Heinze T (2008) Novel biopolymer structures synthesized by dendronization of 6-deoxy-6-aminopropargyl cellulose. Macromol Rapid Commun 29:1739–1745
192. Fenn D, Pohl M, Heinze T (2009) Novel 3-O-propargyl cellulose as a precursor for regioselective functionalization of cellulose. React Funct Polym 69:347–352
193. Elschner T, Ganske K, Heinze T (2013) Synthesis and aminolysis of polysaccharide carbonates. Cellulose 20:339–353
194. Pourjavadi A (2011) Synthesis of soluble N-functionalized polysaccharide derivatives using phenyl carbonate precursor and their application as catalysts (Erratum to document cited in CA156:339191]. Starch 63:820
195. Hayashi S (2002) Synthesis and properties of cellulose carbonate derivatives. Kobunshi Ronbunshu 59:1–7
196. Sanchez Chaves M, Arranz F (1985) Water-insoluble dextrans by grafting, 2. Reaction of dextrans with n-alkyl chloroformates. Chemical and enzymic hydrolysis. Makromol Chem 186:17–29
197. Elschner T, Kötteritzsch M, Heinze T (2014) Synthesis of cellulose tricarbonates in 1-butyl-3-methylimidazolium chloride/pyridine. Macromol Biosci 14:161–165

Adv Polym Sci (2016) 271: 53–92
DOI: 10.1007/12_2015_306

Published online: 20 May 2015

Preparation and Analysis of Cello- and Xylooligosaccharides

Philipp Vejdovszky, Josua Oberlerchner, Thomas Zweckmair, Thomas Rosenau, and Antje Potthast

Abstract This review provides a general overview of preparation, separation, and analytical methods for cello- and xylooligosaccharides. Arising as side-stream products of different biorefinery processes, these compounds have increasingly gained the interest of researchers and engineers in the last few decades. Beside their application as additives in the food, feed, and pharmaceutical industries, these oligomeric carbohydrates are of key importance as model compounds for studying the dependence of physicochemical properties on the degree of polymerization (DP). First, different preparation methods for mixtures of oligosaccharides with DPs between 1 and 30 are discussed. These methods include acetolysis, acid and enzymatic hydrolysis, and glycoside synthesis. Then, separation techniques, including size exclusion chromatography, normal phase and hydrophilic interaction chromatography, and chromatography on cation exchange resins, are presented. Analysis of oligosaccharides by different techniques is described.

Keywords Cellooligosaccharides • Cellulose • Cellulose hydrolysis • Chromatography of cellooligosaccharides • Synthesis of cellooligosaccharides • Xylan • Xylan hydrolysis • Xylooligosaccharides

Contents

P. Vejdovszky, J. Oberlerchner, T. Zweckmair, T. Rosenau, and A. Potthast (✉)
Division of Chemistry of Renewable Resources, Department of Chemistry, University of Natural Resources and Life Sciences (BOKU) Vienna, Muthgasse 18, 1190 Vienna, Austria
e-mail: antje.potthast@boku.ac.at

1 Introduction

Celluloses and heteropolysaccharides (or hemicelluloses) are among the most abundant natural materials on earth. Together they form the polysaccharide fraction of the plant cell wall, where they provide structural integrity and act as a barrier between the inside and the outside of the cell. In addition, hemicelluloses can be used as a seed storage carbon source and as a mobile carbon source in the non-reproductive tissues of some plants [1]. The practically inexhaustible nature and unique properties of these polysaccharides from the perspective of a strongly increasing demand for sustainable, re-growing resources make them a raw material of great interest for researchers and engineers. The history of the industrial utilization of cellulose in particular is long and diverse, reaching from its application as a raw material in the pulp, paper, and fiber industry to a source of carbon and chemical energy in biotechnological processes, to its use in (anti-nutritional) food additives and in high-tech applications (e.g., as the stationary phase in column chromatography). Furthermore, the chemical replacement of hydroxyl groups of the polymer chain with different substituents provides the possibility to generate materials with new characteristics. In this context, cellulose ethers, esters, nitrates, and acetates are the most prominent types of derivatives that give the polymer different, interesting new features, such as film- and gel-forming properties [2, 3]. Hemicelluloses, although less known, are also of commercial significance because they can impart important properties to many food and feed products [4]. Figure 1 depicts the structures of cellulose and xylan, a certain type of hemicellulose.

"Biorefinery" is a general term for the conversion of natural (plant) feed stock materials to products of higher value. Many process strategies for the degradation and/or transformation of cellulose and hemicellulose to desired compounds have been developed and successfully applied [5]. In this regard, the hydrolysis of polysaccharides to their monomeric building units can be subjected to fermentation processes with a large variety of potential end products (e.g., bioethanol, biogas, propanol, acetic acid), or can be chemically treated to produce platform chemicals such as furfural and furan. However, the oligomeric degradation products, which can be seen as intermediates of a total hydrolysis of the polymers, are not given similar consideration, in spite of their potentially great importance in present and future technologies.

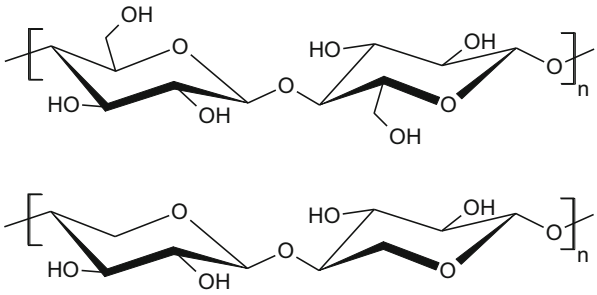

Fig. 1 Molecular structure of cellulose (*top*) and xylan (*bottom*)

With respect to the degree of polymerization (DP), oligosaccharides fall between the monosaccharides and the corresponding polysaccharides. There is no exact definition, that is, no DP limit above which they are referred to as a polymer and below which as oligomers. However, a very common distinctive feature is the solubility in water, which means that with reference to cellulose, the water-soluble saccharides ($DP \leq 8$) are referred to as cellooligosaccharides, and the insoluble saccharides having a higher DP are called polysaccharides. This strict demarcation, justified solely by the solubility in water, is very often not useful, because other DP-dependent physicochemical properties do not change as suddenly. In this review, the term "oligosaccharide" is regarded in a broader sense, meaning saccharides having DP values up to about 30–35. These higher oligosaccharides and short-chain celluloses are of central significance for the elucidation of physicochemical properties in relation to the DP [6, 7]. Studies of homologous series of cellooligosaccharides (also referred to as cellodextrins) that asymptotically approach a polymeric structure provide insight into the macromolecule character of celluloses with increasing chain length [6, 8]. Oligosaccharides with a defined DP can be used as a simple model for cellulose in structural investigations [8, 9]. In addition, cellodextrins are considered to be useful substrates for the study of cellulose hydrolysis and can also be used in the screening of cell cultures for specific cellulase activities and in induction studies of microbial cellulase expression [10]. Oligosaccharides originating from cellulose are used in the food industry as anti-nutritional additives and have potential application in the pharmaceutical industry as coating agents for the controlled release of active ingredients. There is also a broad area of application for xylooligosaccharides, reaching from the pharmaceutical to the food and feed industries [11].

Several methods for the generation of cellooligosaccharides have been developed during the past century, and can principally be divided into two basic strategies: (1) fragmentation of polymers to shorter chain lengths by partial hydrolysis, and (2) synthesis of oligomers by selective condensation of smaller saccharides. The latter procedures inherit difficulties with regard to the stereo- and regioselectivity of the reactions, because the synthesis of natural polymers such as polysaccharides necessitates a precise steric control of the polymerization [12]. Section 2 of this review is dedicated to the variety of preparation methods for cello- and xylooligosaccharides.

Unfortunately, the methods for analysis of these compounds are still not well developed. Although mono- and disaccharides as well as polysaccharides can be

analyzed by different means relatively easily (e.g., gas chromatography for the small sugars and gel permeation chromatography for the polymers) proper techniques for saccharides with a DP range between 10 and 50 do not exist. The separation of cellooligosaccharides according to their DP to obtain monodisperse fractions (or at least fractions with a very narrow molecular weight distribution) of oligosaccharide mixtures is currently still a subject of research. The reason for this is that the physicochemical properties of cellodextrins, including molecular dimensions, molecular weight, and melting points, alter very slowly with a change in chain length, leaving effective separation with respect to the DP as challenge for scientists. Therefore, Sect. 3 of this review is dedicated to the different chromatographic and other separation methods that have the potential to solve this problem and to other analytical procedures for the characterization of these compounds.

In order to overcome these difficulties, strategies have to be worked out for the preparation of cello- and xylooligosaccharides in the 10–50 DP range that are homogeneous with regard to molecular weight. These can then be used as standard

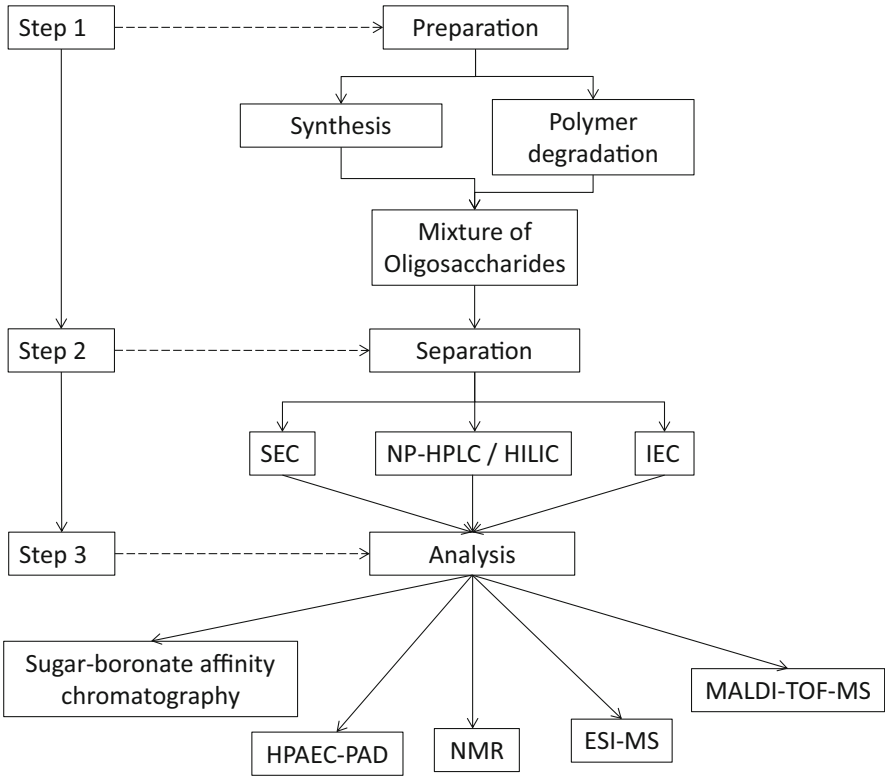

Fig. 2 Principal scheme for the generation of homogeneous oligosaccharides. *SEC* size-exclusion chromatography, *NP-HPLC* normal phase high-performance liquid chromatography, *HILIC* hydrophilic interaction chromatography, *IEC* ion exchange chromatography, *HPAEC-PAD* high-performance anion exchange chromatography coupled with pulsed amperometric detection, *NMR* nuclear magnetic resonance, *ESI-MS* electrospray ionization mass spectrometry, *MALDI-TOF-MS* matrix-assisted laser desorption/ionization time-of-flight mass spectrometry

compounds for the development of analytical methods. The principal scheme for such an effort essentially consists of three steps, as illustrated in Fig. 2. Step 1 is preparation of an oligosaccharide mixture, either by hydrolysis of the parent polymers or polymerization of the corresponding monomers. Step 2 is separation according to the DP. Step 3 is analysis of the separated fractions in terms of structure and purity. Although several publications, including some review papers, describe one of these three steps, to the best knowledge of the authors there is no general account fully covering this topic. The intention of this review is therefore to provide the reader with a broad comprehensive overview of the variety of techniques that exist for the production of cello- and xylooligosaccharides, particularly at a preparative scale; to provide a summary of the different methods for their separation according to molecular weight; and to survey the different possibilities for analysis.

2 Preparation of Oligosaccharides from Celluloses and Hemicelluloses

2.1 Synthesis of Oligosaccharides

One possibility for the generation of oligosaccharides from cellulose or hemicellulose is to synthesize them from their monomeric or, in the case of cellulose, dimeric building units. This requires the formation of a new glycosidic bond between a glycosyl donor and a glycosyl acceptor (i.e., the growing oligosaccharide). In order to synthesize a desired oligomer, it has to be ensured that the linkage is formed regio- and diastereoselectively. In this context, the high number of glycosidic links that can be possibly created is a major complexity of the problem. Because the electrophilic attack of the anomeric carbon of the donor molecule at a hydroxyl oxygen of the (non-protected) acceptor can principally take place at any of the free OH groups, the number of potential oligosaccharide products rises drastically with an increase in DP. In order to force the coupling reaction exclusively toward a specific glycosidic bond (e.g., in the case of cellooligomers, the reaction of the anomeric carbon of the donor with the terminal 4-OH of the acceptor) it was necessary to develop strategies to make the reaction regioselective (i.e., to avoid the formation of "wrong" bonds). In addition to this problem of regioselectivity, the stereochemistry of the hydroxyl group at C1 raises another difficulty. In solution, pyranoses display an equilibrium between their α- and β-configurations, which consequently leads to the formation of both the α- and β-forms of the glycosidic bond. Efforts to synthesize (pure) cellooligosaccharides, which require generation of the desired β-(1,4)-glycosidic linkage only, therefore have to include routes that help to make the reaction both regio- and stereoselective. In this regard, several strategies have been developed, with different degrees of success. They can be divided into two groups: those that use an enzyme as a catalyst, and those that

do not. Historically, the latter approach appeared earlier and is therefore discussed first.

2.1.1 Chemical Synthesis

The targeted chemical synthesis of cellooligosaccharides (or any except "non-random" oligosaccharides) necessitates the introduction of blocking groups that prevent the formation of undesired glycosidic bonds. This means that those OH groups that should not participate in the glycosidic linkage must be substituted in such a manner that electrophilic attack at the hydroxyl oxygen cannot take place. In addition to this, the anomeric C atom of the glycosyl donor must be activated in order to favor coupling reactions (see Fig. 3). The classical Koenigs–Knorr method, developed in 1901 [13] and continuously improved later, achieves this activation by the formation of glycosyl halides (mainly bromides and chlorides), and the reaction with the acceptor takes place in the presence of heavy-metal salts (preferably Ag salts). Pfaeffli et al. [14], for example, successfully synthesized the disaccharide isomaltose by coupling the glucose derivatives 2,3,4-tri-*O*-benzyl-1-thio-β-D-glucopyranoside as acceptors and 6-*O*-acetyl-2,3,4-tri-*O*-benzyl-α-D-glucopyranosyl chloride as donors, resulting in a disaccharide product containing 72% of the desired α-(1,6)-configuration, but also 28% of the β-anomeric gentiobioside. The halide at C1 of the donor works as an activator for the anomeric carbon and is the leaving group during formation of the glycosidic bond, whereas the benzyl groups and the acetyl group at C6 of the donor act as protecting groups for the positions that should not be involved in the linkage.

In 1973, Schuerch [15] reviewed approaches to the chemical synthesis of polysaccharides and divided the problem into two main areas. On the one hand was the stepwise synthesis of complex oligo- and polysaccharides by a consecutive series of reactions, forming one new regio- and stereoselectively correct bond at a time. On the other hand were the ring-opening propagation (see Fig. 4) and condensation reactions, which are more suitable for the generation of homooligosaccharides (e.g.,

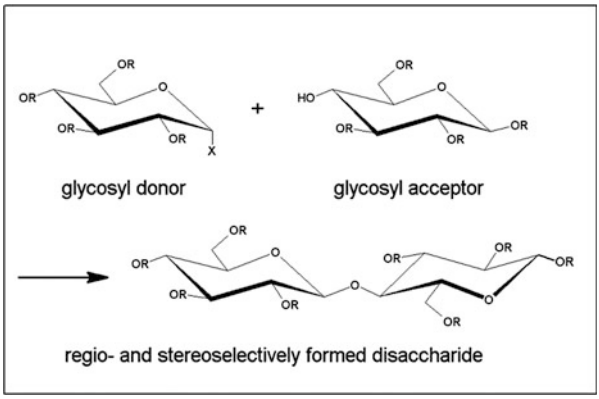

Fig. 3 Glycosidation is formation of a glycosidic bond between glycosyl donor and glycosyl acceptor with the aid of protecting groups (*R*) and an activating group (*X*)

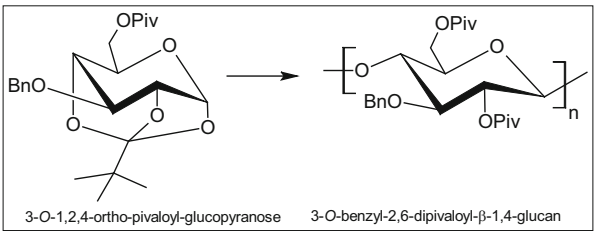

Fig. 4 Typical ring-opening polymerization starting from a glucose 1,2,4-orthopivalate as the precursor

cellooligosaccharides) and polymers of simple repeating sugar units (as well as polysaccharides with a random sequence of monomers). The latter type of approach is discussed in more detail next.

In the 1950s and 1960s some efforts were made to generate stereoregular oligosaccharides and polysaccharides through self-condensation of carbohydrate derivatives with ester functions as blocking agents. Haq et al. [16], for example, published in 1956 the first chemical synthesis of an α-(1,2)-linked glucoside out of 1,2-anhydro-3,4,6-tri-*O*-acetyl-α-D-glucopyranose. The reaction, however, displayed a lack of stereoselectivity, leading to a variety of di- and oligosaccharide side products. In the same year, the authors reported [17] the chemical synthesis of a homologous series of β-(1,6)-D-glucopyranans up to a DP of 9 using 2,3,4-tri-*O*-acetyl-α-D-glucopyranosyl bromide as the monomeric glycosyl donor and Ag_2O as the catalyst. However, isomer formation occurred and the yields were very low (<1%). More than a decade later, McGrath et al. [18] made similar attempts at regio- and stereoselective preparation of oligo- and polysaccharides, showing again that the drawbacks were poor stereoselectivity and a very low yield in general. Thus, there are obviously two main disadvantages [15] in attempts at polymerization via self-condensation using ester derivatives of the carbohydrates as building blocks: (1) The ester groups tend to migrate, which leads to formation of isomeric structures within the oligo- or polymer. (2) The achieved yields and degrees of polymerization are generally low as a result of side reactions, which cause chain termination. A more promising approach, especially for the generation of cellooligosaccharides, was shown by Husemann et al. [19] in 1966, using glucose 2,3,6-tri-carbanilate as the monomer with P_2O_5 as the catalyst. The study demonstrated the formation of unbranched polysaccharides with a DP of up to 60, displaying β-(1,4)-glycosidic linkages between the glucopyranosyl monomers only. However, the major drawback to this effort was the extremely long time (over 10 days) required for the preparation.

A different approach to stereo- and regioselective polymerization of carbohydrate derivatives to obtain desired oligo- and polysaccharides was introduced by Kochetko et al. [20, 21] using a different mechanism, ring-opening polymerization. The use of cyclic orthoester derivatives of different sugar monomers without free OH groups, in the presence of $HgBr_2$ as a catalyst and an alcohol initiator, led to the formation of polysaccharides of comparatively high DPs of between 23 and 60 at high yields of 20–50%. The achieved molecular weight was dependent on the ratio of monomer to initiator, and the reaction rate of polymerization was dependent on

the amount of catalyst used. However, these methods still showed weaknesses in terms of regioselectivity, resulting in the occurrence of some random links and branches in the final product mixture. In 1970, Masura et al. [22] investigated the propagation of a polysaccharide using the cellobiose derivative 1,6-anhydro-2,3-di-*O*-benzyl-4-*O*-(2,3,4,6-tetra-*O*-benzyl-β-D-glucopyranosyl)-β-D-glucopyranose as a dimeric building unit with the aid of a Lewis acid as the catalyst. The ring-opening polymerization of 1,6-anhydro-2,3,4-tri-*O*-benzyl derivatives of monomeric β-D-pyranosides had been studied in the same laboratory in earlier years [23–28], and investigators managed to stereoselectively synthesize oligo- and polysaccharides of relatively high DPs (150–350). In this context, the temperature at which polymerization took place as well as the choice of Lewis acid had a strong impact on the DP finally reached and the stereoselectivity of the prolongation reaction [24, 28]. With this experience, the authors managed to build derivatized product polymers out of the 1,6-anhydro-cellobiose benzyl ether derivative, with number average molecular weights of $6–7 \times 10^3$ g mol^{-1}. Again, the choice and concentration of Lewis base (PF_5 was the most suitable), as well as the temperature and the initial substrate concentration, had significant impact on the stereoselectivity and DP. A final debenzylation resulted in stereoisomerically pure 4-β-D-glucopyranosyl-(1, 6)-α-D-glucopyranan containing between 14 and 16 D-glucose units at yields of up to 70%.

In his review, Schmidt [12] offered an overview of different alternatives to the classical Koenigs–Knorr method that poses some major disadvantages [12], including harsh conditions during formation of the glycosyl halide, low thermal stability and tendency for hydrolysis of the glycosyl halides, and the potential hazard of heavy-metal salts. Two methods for monomer derivatization were presented as being most suitable for the stereo-controlled formation of glycosidic bonds: (1) direct 1-*O*-alkylation of sugars, which eases the generation of saccharides by using a comparatively simple method [29], and (2) the trichloroacetimidate method, resulting in stable *O*-glycosyl trichloroacetimidates with high glycosylation potential in a stereo-controlled manner.

As a consequence of the enormous number of possible ways that carbohydrates can be linked to one another by glycosidic bonds, every chemical oligosaccharide synthesis requires deep knowledge of reaction mechanisms and experimental methods. Different reactivities and stereoselectivities of glycosyl donors and acceptors, induced by altering the through-space steric interactions and amphiphilic properties of protecting groups and neighboring groups, render the development of generalized methods almost impossible [12]. Therefore, it is no wonder that it took until the early 1980s before reports of the first synthesis of pure β-(1,4)-linked cellooligosaccharides were published by Schmidt [30] and Takeo [31], although yields were not very high. In the first case, cellotetraose was synthesized using the α-trichloroacetimidate of 2,3,4,6-tetra-*O*-acetylglucopyranose as donor and 1,6-anhydro-β-D-glucopyranose carrying benzyl protecting groups at the 2-*O*- and 3-*O* positions as initial acceptor in a stepwise procedure. In the latter procedure, cellobiose, cellotriose, and cellotetraose were synthesized via the Koenigs–Knorr method using benzyl ethers as protecting groups and bromide as the activating

reagent. In their "Synthetic studies of cellulose" series of articles, Takano et al. systematically investigated the impact of substituting groups on the stereoselectivity of the glycosylation reaction [32–34] and evaluated different starting materials for the convergent synthesis of cellooligosaccharides [35, 36]. The authors primarily focused on the use of α-imidates as donors, testing different substitution patterns (acetyl or benzyl groups) on both the donor and the acceptor, and were finally able to establish some general principles for the effect of substituents on linkage formation: (1) The substituent at position 3-*O* is crucial, which was in agreement with an earlier publication by Sina [37]. A benzyl group there leads to β-glycosylation in an extremely high yield, whereas an acetyl function at this position results in the predominant formation of the α-glycoside in significantly lower yields. (2) The character of the protective group at 4-*O* of the α-imidate (donor) also has a significant impact on bond formation. Electron-withdrawing functions (e.g., acyl groups) there lead to an increase in the stability of the donor, but on the other hand to a lower β-glycoside yield. In contrast, electron-donating ether groups (in particular benzyl and *p*-methoxybenzyl) result in a high yield of the β-glycoside. In conclusion, 2,6-di-*O*-acetyl-3-*O*-benzyl-4-*O*-*p*-methoxybenzyl-α-D-glucopyranoside was named as the most suitable α-imidate glycosyl donor for the stereoselective formation of β-(1,4)-glycosidic linkages between glucose derivatives [34].

In an effort to gain information about the impact of the type of derivatization on the yield of cellooligosaccharides, Nishimura et al. [38] compared different glycosyl donors for the synthesis of cellotetraose. The highest yield of more than 70% was found when working with the 4-*O*-acetyl trichloroacetimidate form as the glycosyl donor. The authors found that the reactivity of donor and acceptor decreases with an increase in chain length [38]. When trying to overcome this problem with a higher amount of catalyst (BF_3 etherate) or higher reaction temperatures, side reactions such as glycosyl fluoride formation and cleavage of the *p*-methoxy-benzyl groups (temporary *O*-4′ protective group on the donor) occurred. The use of acetyl groups instead of *p*-methoxy-benzyl groups significantly enhanced the outcome, so that the aforementioned high yields could be reached [38]. In a subsequent publication, Nishimura [7] and his team presented a high-yield β-glycosylation using a convergent synthetic method between a cellotetraosyl donor and acceptor, resulting in the formation of a cellooctaose derivative. The one-step anhydrous glycosylation was performed under high vacuum to minimize imidate side reactions (e.g., hydrolysis, glycosyl fluoride formation), using pivaloyl, allyl, and benzyl functions as protecting groups. After the reaction, these groups were replaced by acetyl groups, which were removed in a last step to give pure cellooctaose with a yield of 87%. In 1996 Nakatsubo et al. [39] succeeded in performing the first cellooligosaccharide synthesis via cationic ring-opening polymerization. The reaction, performed with 3,6-di-*O*-benzyl-α-D-glucose 1,2,4-orthopivalate and the aid of a triphenylcarbenium tetrafluoroborate initiator, was shown to be highly stereoselective. The number-average molecular weight of the product was 8.3×10^3 g mol^{-1}, which corresponds to a DP of approximately 20. Complete removal of the protective group via temporary

acetylation resulted in the underivatized cellooligosaccharide product. Later, it was again Nishimura who presented the first stepwise synthesis of a homologous series of cellulose analogs [8, 40]. The authors conducted sugar chain prolongation via stepwise additions of cellotetraosyl units, thus investigating the same pattern of protective and activating groups as in their previous work [7]. In this way, a DP of up to 20 for the acetylated end product was reached, with an overall yield of 37%.

In 2009, Adelwöhrer et al. [41] reported the successful synthesis of ^{13}C-perlabeled cellulose through an approach involving cationic ring-opening polymerization. As precursor, the authors used 3-*O*-benzyl-$^{13}C_6$-glucopyranose 1,2,4-orthopivalate and obtained fully labeled ^{13}C-cellulose as the cellulose II allomorph, with a DP of 40 and an overall yield of 28%. In conclusion, despite great advances in chemosynthetic methods during recent decades, the strategies of conventional chemical synthesis of cellooligosaccharides have not yet produced fully satisfying results in terms of either time and work intensity or the regio- and stereospecificity of the products. In order to find ways to produce these compounds by polymerization of smaller saccharides in useful amounts within reasonable preparation times, different approaches applying enzymatic catalysis in combination with conventional chemical approaches may be the answer.

2.1.2 Chemo-Enzymatic Synthesis

Another way to produce cellooligo- and cellopolysaccharides is to synthesize them with the aid of an enzyme that can catalyze formation of the glycosidic bond. The main advantage of these procedures is that enzymes in general work in an extremely specific manner, which means that, for the generation of polysaccharides, the glycosides are produced with high regio- and stereoselectivities. This major characteristic of enzymes is of great advantage in oligo- and polysaccharide synthesis, making chemo-enzymatic approaches superior to conventional chemical approaches for three main reasons: (1) The laborious introduction of protective groups and subsequent deprotection after the product is formed becomes obsolete because of the high regioselectivity of the biocatalyst, so that an underivatized polymer can be created directly [42–44]. (2) The reactions can be performed under mild conditions of temperature, pH, and salt concentration and the conversion rates are comparatively fast [43, 44]. (3) The use of potentially harmful catalysts (e.g., heavy metals) can be avoided, and undesired side reactions generally do not occur [43, 44]. Since the early 1990s, the application of enzymes in polysaccharide synthesis has undergone a massive upsurge [45]. Many of these efforts have in common that the design of an activated donor molecule is required. According to Pauling [46], enzymatic reactions can happen under very mild conditions because of the formation of an intermediate enzyme–substrate complex, which is energetically favored over the free substrate. This so-called stabilization of the transition state allows an increase in reaction rate of several orders of magnitude by decreasing the activation energy of the reaction. Another convenient characteristic of enzymes is that they are able to catalyze their reaction not only on the natural

substrate, but also on artificial substrates that closely resemble their natural relative. In this context, Kobayashi et al. [44, 47–49] suggested that, for an effective polymerization to polysaccharides, it is possible to design such an altered substrate, a so-called transition-state analog substrate (TSAS), that is readily incorporated into the active site of the enzyme and, later, rapidly attached to the growing polymer chain. The enzymes involved in these efforts can be divided into two main classes [43]: (1) glycoside hydrolases, which catalyze hydrolytic cleavage of the glycosidic bond and the back reaction (i.e., formation of such a linkage), and (2) transferases or, specifically, glycosyltransferases, which catalyze the transfer of a carbohydrate monomer moiety (glycoside donor) to a glycoside acceptor. In the following sections, these two types of enzymes are discussed in more detail with regard to their applicability in oligo- and polysaccharide synthesis.

Glycoside Hydrolases

Glycoside hydrolases (EC 3.2.1) are enzymes designed by nature for the catalytic degradation of oligo- and polysaccharides. However, as for any enzyme their reactions are principally reversible, so that, under appropriate conditions (especially regarding water activity), they can also catalyze the reverse reaction (i.e., the formation of a glycosidic bond between a glycosyl donor and an acceptor). As extracellular (secreted) enzymes, they display some major technical advantages, including good stability in aqueous solution, easy accessibility in terms of purification, and a relatively low price [44]. With regard to the substrate, these hydrolases can be categorized into two major groups: those that attack the polymer chain at the end, releasing one monomer at a time (referred to as "exo-types"), and those that cleave the chain at a random position somewhere in the middle, leading to fragments of the original polysaccharide chain (called "endo-types") [50]. The latter have proved to be far more suitable for enzymatic polymerization to polysaccharides [49], a result of the different topology of their catalytic domain, which is shaped like a cleft rather than a tunnel. Two common ways of activating the glycosyl donor have been described in the literature. They not only differ in the type of derivatization but also in the character of the polymerization reaction. The first method involves activation by a fluoride atom to give glycosyl fluorides, which lead to a polycondensation type of polymerization. The second method involves activation of C1 by introduction of an oxazoline group, resulting in a ring-opening polymerization [44]. Although both of these artificial substrates are readily recognized by the cellulase, the former displays some important advantages [42–44, 51]: (1) The size of the fluoride atom closely resembles the size of an OH group, minimizing interfering steric effects; (2) Glycosyl fluorides are the only glycosyl halides that are stable in an unprotected form, allowing the reaction to be performed in aqueous media. (3) Fluoride is a very good leaving group, widely used in chemical synthesis. Because glycosyl fluorides are the main substrate used for the generation of cello- and xylooligosaccharides, the focus of this review is on activation by fluoride, whereas the other type of activation is not discussed further.

Kobayashi et al. [52, 53] were the first to publish the successful synthesis of cellulose by polycondensation, using an endocellulase as catalyst and β-D-cellobiosyl fluoride as the activated donor molecule. The reason for the use of the disaccharide donor (rather than monomeric β-D-glucopyranoside) was that this substrate is more readily recognized by the enzyme, resulting in faster polymerization. A mixture of an organic solvent and an aqueous buffer was selected as reaction medium in order to avoid excessive water activity, which would favor hydrolytic cleavage of the glycosidic links. In this regard, a 5:1 mixture of acetonitrile and acetate buffer (pH 5) was found to result in the best polymer yields, up to 54% for water-insoluble fractions (i.e., DP > 8). The highest DP achieved during these efforts was 22. The suggested reaction mechanism for this polymerization is as follows [52]: In a first step, a cellobiosyl–enzyme intermediate or, alternatively, a glycosyloxocarbenium ion is formed under elimination of the fluoride anion at the active site of the enzyme. In a second step, this highly reactive intermediary compound is attacked by the terminal 4-OH oxygen of the growing polymer chain (carrying a fluoride group at its C1 end), which is located at a sub-site of the catalyst. The stereoselectivity of the reaction is achieved by a "double inversion" of the anomeric site of the donor, and thus a "net retention" of the β-conformation, leading to exclusively β-(1,4)-glycosidic linkages.

Another huge benefit of using these enzymes in polysaccharide synthesis is that it is also possible to produce functionalized polymers with exactly defined structures, not only in terms of stereo- and regioselectivity of the glycosidic bonds, but also regarding the regioselectivity and distribution of the substituents [43], which makes these methods superior to conventional chemical modification techniques. For example, a modified cellooligomer carrying methyl groups exclusively at C6 was synthesized by Okamoto et al. [54] using 6,6′-di-*O*-methyl-β-cellobiosyl fluoride derivatives as substrates for a cellulase from *Trichodermaviride*. The resulting cellulose derivate displayed a unique structure that is not achievable by the conventional chemical modification of cellulose polymers. Similarly, Izumi et al. [55] reported the successful synthesis of a 2-*O*-methylated derivative of a cellooligosaccharide. Furthermore, the application of hydrolases in polysaccharide synthesis is not restricted to the generation of homopolymers. Shoda et al. [56] used an endoglucanase for the enzymatic polymerization of α-(1,6)-xylopyranosyl-β-cellobiosyl fluoride as monomer to an artificial xyloglucan oligomer, with α-(1,6)-xylopyranosyl residues linked to the alternating glucose residues in the main chain. Fujita et al. [57] presented a xylanase-catalyzed polymerization of the unnatural monomer 4-*O*-β-D-xylopyranosyl-β-D-glucopyranosyl fluoride, resulting in a novel polysaccharide having a glucose–xylose repeating unit (i.e., a cellulose–xylan hybrid polymer), again demonstrating the great potential of these enzymes in polysaccharide synthesis.

At this point it should be mentioned that the use of glycoside hydrolases for these efforts has one major disadvantage: they are actually designed by nature to catalyze the opposite reaction (i.e., the hydrolytic cleavage of the glycosidic bond). To suppress this undesired reverse reaction, the water activity in the media has to be kept at a low value. Thus, the choice of solvent mixture is of crucial importance. As

demonstrated by Kobayashi et al. [52] and several publications thereafter, a combination of acetonitrile and aqueous buffer is the most suitable system in this regard. However, a more effective way of overcoming this problem can be found by means of genetic engineering, using mutant cellulases [58] that are less prone to cleave the glycosidic bonds. A common strategy in this regard is to produce a cellulase that is lacking the so-called cellulose binding domain, which is required to perform the hydrolysis reaction on a solid substrate [44]. However, these methods are not discussed in detail in this review. A very useful publication for starting a literature research on the topic of genetically engineered cellulases is chapter 4 of Kadokawa's review [43] on enzymatic polysaccharide synthesis.

A somewhat different approach to cellulose synthesis using a hydrolytic enzyme for the formation of the β-(1,4)-glycosidic bond was published recently by Egusa et al. [59, 60]. In contrast to the aforementioned efforts, a non-aqueous solvent was used as the reaction media, namely a solution of LiCl in *N*,*N*-dimethylacetamide (DMAc). This solvent system has been known for a long time and is commonly used for the dissolution of cellulose [61]. Most enzymes, including cellulases, are usually not stable and therefore not able to catalyze their reaction in this environment. In order to preserve catalytic activity, the enzyme was treated with a non-ionic surfactant (dioleyl-*N*-D-glucono-L-glutamate), which kept it stable in this aprotic medium. With the aid of this so-called surfactant-enveloped enzyme (SEE) and a protic acid co-catalyst, the investigators were able to generate artificial cellulose with chain lengths of up to 120 anhydroglucose monomers. A great virtue of this method is that the "reversed hydrolysis" works without any pre-activation of the glycoside donor (or acceptor), that is, natural, untreated cellobiose can be used directly for the polycondensation.

Glycosyltransferases

In nature, polysaccharides are synthesized via catalytic action of glycosyltransferases, which catalyze the formation of a glycosidic bond using an activated glycosyl donor in which the OH group at C1 is substituted by a phosphate function [62]. According to the nature of the substitution to be recognized by the enzyme, there are two main types of glycosyltransferases: (1) those that are dependent on sugar mono- or diphosphonucleotides as donor substrates, referred to as Leloir-glycosyltransferases or glycoside synthases; and (2) those that utilize sugar-1-phosphates, sugar-1-pyrophosphates, or sugars linked to a lipid via phosphoester or phosphodiester linkage, referred to as non-Leloir-glycosyltransferases or phosphorylases [63]. In both cases, the anomer configuration of the activated donor displays the α-isomeric form. In the following sections, the two types of enzymes are discussed in more detail and examples of their application in oligosaccharide synthesis are given.

Leloir-Glycosyltransferases

Leloir-glycosyltransferases (very often referred to as glycoside synthases) employ the high energy bond of the glycosyl nucleotide donors (usually UDP–monosaccharides) to provide the free energy needed for formation of the glycosidic bond [42, 63]. The highly negative ΔG of the substrate phosphorolysis renders the reaction practically irreversible in the synthesis direction. Plant cell wall cellulose is synthesized by the enzyme cellulose synthase situated in the cell membrane [64]. The catalytically active enzyme exists as a complex of six subunits of six single enzymes, together shaping a rosette-like structure [65]. Their location in the membrane highlights a major disadvantage of employing these enzymes for in vitro oligosaccharide synthesis. The location complicates purification of the active enzyme, making these biological catalysts quite expensive compared with, for example, hydrolases [44]. Another drawback, arising from their existence as *trans*-membrane proteins, is their decreased stability in solution [44, 66]. Additionally, nucleoside diphosphates act as inhibitors of these enzymes, which has to be overcome either by the exploitation of phosphatases to degrade the nucleotides [67] or, alternatively, by in situ regeneration of sugar nucleotides with the aid of pyrophosphorylases [68]. In spite of these hindrances, some successful applications of Leloir-glycosyltransferases have been reported. Rosette-like particles corresponding to the rosettes of the plasma membrane were isolated from mixtures of synthesizing complexes from mung beans by means of gel electrophoresis [64] and used for the synthesis of cellulose with UDP–glucose as a substrate [69]. Futaki and Mizumo [70] reported the preparation of high molecular weight complexes with β-(1,4)- and β-(1,3)-synthase activity from azuki bean epicotyls. A further purification by affinity chromatography with anti-tubuline as a ligand [71] resulted in the isolation of a pure β-(1,4)-glycan synthase (i.e., cellulose synthase), that could be used for in vitro synthesis experiments. A mechanism of the cellulose synthase reaction was suggested by Saxena et al. [72]: nucleophilic attack of the C4-OH group of the non-reducing chain end at the α-C1 position of the UDP–glucose substrate takes place via a single displacement mechanism with inversion of the anomer configuration, resulting in the formation of β-(1,4)-linkages. A consecutive polymerization is achieved by the so-called two-residue addition model, whereby simultaneous coupling of two monosaccharide monomers occurs successively during chain propagation.

Non-Leloir Glycosyltransferases (Phosphorylases)

In general, sugar-nucleotide-independent glycosyltransferases, often referred to as phosphorylases, catalyze the transfer of a monosaccharide moiety from a poly- or oligosaccharide, or from a nucleoside to an orthophosphate ion, in other words, phosphorolysis of the glycosidic bond. The bonding energy of the resulting sugar-1 phosphate is low enough to make the reaction practically reversible [63]. Consequently, in nature these enzymes are involved in both the degradation and synthesis

of polysaccharides. They all have in common that they catalyze an exo-wise phosphorolysis at the non-reducing end [42, 43, 63] and work in a very strict regiospecific manner, cleaving only "their" type of glycosidic bond [63]. They can be classified either according to the anomeric form of the glycosidic bond they cleave (the anomeric form of the glycosyl-1-phosphate product [63]) or by the reaction mechanism, that is, whether an anomeric retention or an inversion occurs during the catalysis [63]. Phosphorylases are usually named after the substrate to be degraded and, since the first was found almost 100 years ago [73], many phosphorylases have been discovered in a huge number of different organisms. In the field of cellooligomer synthesis, the so-called cellobiose-phosphorylase (EC 2.4.1.20) and, even more so, cellodextrin-phosphorylase (EC2.4.1.49) are of interest. The former catalyzes the reversible cleavage of cellobiose yielding α-glucose-1-phosphate (inversion mechanism) and glucose and can be found in bacteria capable of metabolizing cellulose [74]. The enzyme recognizes the β-anomeric OH group at the reducing end, but only of oligos with a maximum DP of 3 [63]. Thus, the enzyme is not suitable for the generation of higher cellooligosaccharides; nevertheless, it has been successfully used for the generation of trimers [63]. Cellodextrin-phosphorylases, on the other hand, are adequate for the synthesis of cellooligos larger than this, because of their ability to recognize longer chains. Similarly, they catalyze the cleavage of a monosaccharide moiety by an inversion mechanism, releasing α-glucose-1-phosphate and a cellodextrin chain shortened by one monomer [75]. They have only been found in *Clostridia*, which also express cellobiose-phosphorylase [76]. With regard to the back reaction (i.e., glycosidic bond synthesis), they cannot recognize glucose as a substrate, but different types of aryl-β-glucosides and β-glucosyl-disaccharides are properly transferred to the elongating oligosaccharide chain [75]. With their aid, different cellooligosaccharide analogs have been synthesized that can be used as artificial inhibitors for cellulases [77]. Samain et al. [66] reported the phosphorylase-mediated synthesis of crystalline non-substituted cellodextrins as well as cellodextrins substituted at their reducing end (depending on the primer used; see below). The enzyme employed has been isolated from *Clostridium thermocellum* grown on cellulose-based media, inducing the expression of cellobiose-phosphorylase as well as cellodextrin-phosphorylase. The authors exploited an interesting feature of cellodextrin-phosphorylases, namely their ability to synthesize cellooligomers when the enzymes are incubated with a primer ($Glc_{n\ (n\geq 2)}$; e.g., cellobiose) and glucose-1-phosphate to produce Glc_{n+1} and pyrophosphate [78]. In order to remove cellulase activity, the enzyme was purified from cell extracts by precipitation with protamine sulfate and subsequent fractionation with ammonium sulfate. The non-substituted crystalline cellodextrins produced with the aid of this isolate were shown to have an average DP of 8, with crystal structures closely resembling those of low molecular weight cellulose II. It was suggested that the chain elongation does not proceed beyond a DP value of 8 as a result of immediate dissociation of enzyme and oligosaccharide chain after every monomer addition. Therefore, the enzyme requires its substrate to be in aqueous solution [66], which is not possible for non-substituted cellooligomers above a chain length of eight. A similar observation was made earlier by Ziegast et al. [79]

for a potato amylose phosphorylase, additionally supporting this suggestion of an immediate dissociation.

2.2 *Generation of Oligosaccharides by Degradation of Polymers*

For the generation of cellooligosaccharides through degradation of cellulose, a variety of methods was developed during the last century [80, 81]. The breakdown of long polysaccharide chains into smaller fragments requires hydrolytic cleavage of the glycosidic bonds, which can be achieved using different chemical catalysts (usually acids) or specific hydrolytic enzymes (cellulases). The two most prominent methods in this regard are fragmentation of cellulose by acetolysis [82], applying a mixture of acetic acid, acetic anhydride, and concentrated sulfuric acid, and direct acid hydrolysis using hydrochloric acid [83]. The methods, especially those employing halogen acids, rely on the reduction of cellulose crystallinity to render it more amorphous and thus easier to hydrolyze at temperatures where sugar degradation plays a very minor role [84]. Furthermore, a number of direct hydrolysis techniques has been reported that exploit different acids (including sulfuric acid [10], mixtures of hydrochloric and sulfuric acid [85], and weak acids such as pivaloyl acid (pivaloylysis) [86]) and methods that apply water under supercritical conditions [87] without using any chemical catalyst. For many of these methods, a thorough control of process parameters, especially acid concentration, temperature, reaction time, and the nature of the acids and solvents is crucial in order to avoid the formation of unwanted side products [88]. These approaches are discussed in more detail in the following sections.

2.2.1 Acetolysis

The degradation of cellulose by applying a mixture of glacial acetic acid, acetic anhydride, and concentrated sulfuric acid was originally developed by Hess et al. [82] in 1935 and then further explored in several publications, for example by Miller et al. [83], Dickey and Wolfrom [89], Wolfrom and Dacons [90], and Wolfrom and Thompson [91]. The main product compounds of the hydrolysis are peracetylated cellooligosaccharides. In the original form, the hydrolysis mix consists of the three compounds in a ratio of 10:10:1 (acetic acid:acetic anhydride: sulfuric acid) containing about 10–12% (w/w) cellulose. Because contact of the acid with the cellulose substrate is strongly exothermic, the reaction mixture has to be kept below a temperature of 40°C by external cooling. The hydrolysis reaction is allowed to proceed for 60 h before it is quenched by transferring the now pale yellowish cellulose solution into ice-cold water, which precipitates the mixed acetylated oligosaccharides. The cellooligosaccharide acetates are then washed

with H_2O, the excess acid neutralized with $NaHCO_3$, the precipitate washed again with H_2O, dried, and then suspended in anhydrous methanol. The suspension is then filtered, the filtrate evaporated until dry, and the gummy white residue dissolved in a small amount of hot chloroform. In a final step, this solution is transferred into an excess of ice-cold hexane in order to re-precipitate the acetylated cellooligosaccharides, which are dried in a vacuum oven to obtain a solid, pure form. Using this method, the DP of the isolated oligomers ranged from 1 to 6 [80, 89]; a value of 7 has also been reported [90]. Oligomers of higher chain length are present in the product in very low amounts, if at all. The yield of acetylated oligosaccharides is around 32% (w/w), related to the amount of cellulose used [80].

In order to address the preparation of cellooligosaccharides with higher degrees of polymerization, Kaustinen et al. [92] presented a method for selective acetolysis of cellulose to DPs ranging from 18 to 100. The study was inspired by a method originally developed by Frith [93] in an effort to determine the kinetics of the acid-catalyzed acetylation of cellulose. The reaction mixture contains glacial acetic acid, acetic anhydride, and dichloromethane in a ratio of 1:4:6 and either sulfuric or perchloric acid as the catalyst. The amount of cellulose used should be around 3% (w/w). Through variation of the reaction parameters (i.e., type and concentration of catalyst, temperature, and time), different product compounds with regard to the average DP of the peracetylated polysaccharides can be achieved, ranging from DP 18, when hypochloric acid at the highest concentration is used, to DP 100, when sulfuric acid at the lowest concentration is used [92]. The products are isolated by increasing the pH with sodium acetate, which precipitates the oligosaccharides. The grainy, yellowish cellulose triacetate is subsequently washed first with water and then with methanol to remove smaller (water-soluble) saccharides and the yellow color. The yield with regard to the amount of cellulose powder employed was as high as 90% (w/w) [92].

2.2.2 Direct Acid Hydrolysis

Hydrochloric Acid

The preparation of cellooligosaccharides from cellulose by applying hydrochloric acid was first reported by Zechmeister et al. [94] in 1931, later explored by Jermyn [95], and published with modifications by Miller et al. [83, 96, 97], Hamacher et al. [88], and Huebner et al. [98]. The procedure starts with a pre-wetting of cellulose powder in saturated HCl (37% w/w) solution at room temperature, which favors homogeneity in the subsequent stages. The suspension is then treated with fuming HCl at 0°C, resulting in a homogeneous, viscous, yellowish solution containing about 10% cellulose. The HCl concentration needed for complete dissolution is about 40% (w/w) [81], which is achieved by bubbling HCl gas through the saturated solution. The hydrolysis reaction is usually performed for

1–3 h. Again, an efficient cooling system is required in order to avoid formation of unwanted side products. The reaction parameters (time, temperature, and HCl concentration) have a strong impact on the relative yield for different (with regard to their chain length) oligomers [81]. However, rigorous control of those parameters is difficult because of the strong exothermic character of the acid–cellulose contact and the use of an oversaturated HCl solution. In 1960, Miller [83] had already shown that the rate of hydrolysis is linear and that the yield of cellodextrins attains a maximum after 2 h of reaction time. The optimal time and temperature for the preparation of cellodextrins has been determined empirically by several authors, and mathematical models for the degradation kinetics of acid-catalyzed hydrolysis have been proposed [99]. However, the reproducibility of these is rather limited as a result of the above-mentioned complexity of parameter control. After the degradation, the solution has to be neutralized, which is required for subsequent separation procedures and also increases the stability of the cellodextrins [81].

The most common method for increasing the pH is direct neutralization with $NaHCO_3$ [83, 96, 97], which has the disadvantage of producing huge amounts of NaCl. Two alternatives have therefore been developed: (1) preliminary HCl removal by vacuum suction before the neutralizing agent is added [98], necessitating trapping of the evaporated hydrochloric acid gas, and (2) a rather laborious but effective washing procedure with 1-propanol and ethanol [88], which allows the simultaneous removal of excess acid and the main hydrolysis products, glucose and cellobiose. Another possibility would be the application of an anion exchange resin [80], which has the drawback of temperature gradients in the resin bed as a result of the high acid concentration employed. The DP of the isolated cellooligosaccharides does not exceed a value of 7; saccharides of a higher chain length are only present, if at all, in insignificant amounts. The relative yields of the different cellooligosaccharide species are about 13–23% (w/w) [80] with respect to the cellulose amount employed and are also dependent on the method of neutralization after hydrolysis.

With the above-described methods of direct acid hydrolysis using highly concentrated HCl, it is not possible to prepare cellooligosaccharides with a DP above 8 in reasonable amounts, because these fractions are usually removed together with the larger fractions during the procedures. According to Isogai et al. [100], higher cellooligomers can be isolated from cellulosic starting materials by performing the hydrolysis reaction in a heterogeneous state, exploiting the fact that when celluloses are hydrolyzed in dilute acids at high temperatures they display a rapid and drastic decrease in chain length until they reach a constant value, referred to as the level-off degree of polymerization (LODP) [101]. This LODP behavior is thought to be related to the size of the crystalline zones along the cellulose fiber and is therefore dependent on the species and tissue from which the cellulose originates [102]. When alkali-treated native and regenerated celluloses were subject to hydrolysis with 1 M HCl solutions at 105°C for 3 h, the degraded samples (regardless of their origin) showed bimodal size exclusion chromatography

(SEC) elution patterns, indicating the presence of a predominant high molecular mass fraction and a minor low molecular mass fraction [100]. The DP values of the former ranged from 35 to about 100; those of the minor fraction from 18 to 24.

Sulfuric Acid

The fact that cellodextrins are formed as intermediates by the action of concentrated sulfuric acid has been known for a long time [10, 103], but it took until 1984 that Voloch et al. [10] presented a method for the production of cellooligosaccharides by direct acid hydrolysis employing concentrated sulfuric acid. An 80% (w/w) H_2SO_4 solution is added to crystalline cellulose to a comparatively high final concentration of 2 g cellulose per milliliter of hydrolysis solution. Again, because of the exothermic contact of the acid and the polysaccharide, both have to be pre-cooled, and this is performed in an ice-water bath. After stirring for a few minutes, the acid is diluted with water to a H_2SO_4 concentration of 33% (w/w) and the reaction mixture is transferred to a water bath at 70°C where the hydrolysis reaction is allowed to proceed for 14 min. The reaction is quenched by the addition of pre-cooled absolute ethanol and the hydrolyzate, having a dark brown color and containing some unreacted solids, is transferred to an ice-water bath. The color can be removed by adsorption on activated charcoal (pre-wetted with ethanol) and subsequent filtration, resulting in a clear, yellowish solution. The ethanol concentration is then increased to 93–95%, which results in precipitation of the cellodextrins. Excess acid is removed by washing the white precipitate with ethanol. The solids are then dried. The merit of the precipitation with ethanol lies in the fact that glucose and cellobiose, as the main degradation products, stay in solution to a predominant extent whereas oligosaccharides with a $DP \geq 3$ are precipitated. The DP range of the oligomers isolated in this way is from 3 to about 8, and the yield related to the amount of cellulose used around 1.5% (w/w), which is significantly below [10, 81] the value reached by the method employing fuming HCl.

As reported (amongst others) by Kim et al. [104], cellulosic starting materials can be degraded under so-called extremely low acid conditions at elevated temperatures above 200°C. The degradation reactions are performed in different types of reactors with sulfuric acid concentrations as low as 0.07%(w/w), resulting in glucose yields of up to 91% (w/w) with regard to the amount of cellulose used. However, the study focused on the maximization of fermentable monomer yield. A separate investigation focusing on the impact of reaction parameters (especially time and temperature) on the molar mass distribution of the product compound could provide valuable information for the development of new strategies for cellooligosaccharide preparation.

Mixed Acid Hydrolysis

The method of cellodextrin preparation employing a mixture of concentrated hydrochloric acid and concentrated sulfuric acid was first reported by Zhang et al. [85] in 2003. The method somewhat circumvents the disadvantages of the above-described methods, such as the application of fuming HCl in Miller's method [83], the rather time-consuming procedure when cellulose is degraded by acetolysis [82], and the comparatively low yields when concentrated H_2SO_4 is applied [10]. It was shown that the optimal ratio of HCl (37% w/w) to H_2SO_4 (98% w/w) for the production of cellodextrins is 4:1 [85]. Higher amounts of the latter lead to fast formation of by-products by oxidation, as indicated by the occurrence of a black color in the hydrolyzate. Lower amounts significantly increase the time needed to obtain a clear hydrolyzate, to over 12 h. The acids are added in a pre-cooled state, and the hydrolysis reaction is then performed at room temperature. The optimal reaction time was determined to be between 3 and 5.5 h, after which the amount of glucose formed is gradually increasing, while the already formed cellodextrins are successively degraded. The hydrolyzate develops a yellowish color during the reaction, which is stopped by transferring the solution into an excess amount of acetone at –20°C, resulting in abundant formation of a white precipitate consisting of water-soluble cellodextrins as well as cellodextrins with a higher DP. The smaller compounds are extracted by centrifuging, washing the pellet with water, and re-centrifuging, resulting in a clear supernatant containing components with a DP of 1–6 (only very low amounts of DP 7 and 8) and a pellet containing the larger fractions. Because the study focused on the preparation of water-soluble cellodextrins, the higher cellooligosaccharides were not discussed further. Analysis of the remaining pellet, especially with regard to the molar mass distribution, could provide useful information on the interdependency of reaction parameters (acid concentrations, time, and temperature) and the formation of cellooligosaccharides with a higher DP. However, the study revealed that, for the smaller fractions (DP 3–6), yields of about 23% related to the cellulose amount employed were reached after a reaction time of 5.5 h. The individual yields for certain species are strongly dependent on the reaction time, favoring lower DPs after longer reaction times. Table 1 summarizes and compares the different hydrolytic preparation methods discussed.

Other Acids

In addition to the above-described methods using the common strong acids HCl and H_2SO_4, which are the most frequently mentioned in the literature, some other strategies for the degradation of cellulose by acid hydrolysis have been developed. However, most of these comparatively recent investigations focus on the yield maximization of fermentable sugars, and consequently parameter optimization for

Table 1 Preparation of cellooligosaccharides by polymer degradation with the aid of acids

	Acetolysis	Selective acetolysis	Concentrated HCl	Diluted HCl	H_2SO_4	Mixed HCl/H_2SO_4
DP range	1–7	18–100	1–7	18–24/35–100[a]	3–8	1–6
Yield (%)[b]	~32	90	100	–	~1.5	23[c]
Reaction time (h)[d]	>60	1–11	1–3	3	<0.5	3–5.5
Comments	Peracetylated product	Peracetylated product	Difficult reaction control	Heterogeneous reaction	–	–
References	[81, 90, 91]	[92]	[84, 89, 95–99]	[101]	[10]	[85]

[a]Molecular weight distribution of the two fractions is dependent on the type of cellulose used
[b]Yields are given as the ratio of mass of the isolated oligomers over the mass of the employed cellulose/cellulose acetate
[c]Value for the fraction DP 3–6
[d]Net hydrolysis reaction time; subsequent precipitation, neutralization, or purification steps are not included

the preparation of cellooligosaccharides is not part of these publications. Nevertheless, as these methods could potentially be useful for the production of oligomers, for the sake of completeness the most important ones are included in this review. Harmer et al. [105], for example, reported a process giving monosaccharides in high yields from biomass that employed a combination of sulfuric and phosphoric acid at elevated temperatures of about 200°C. The two-step strategy is characterized by a preliminary decrystallization and subsequent hydrolysis of the biomass to glucose and xylose at a conversion ratio of about 90% (w/w). The application of formic acid for the hydrolysis of organosolv-derived pulp at temperatures of 180–220°C was published by Kupiainen et al. [106]. As expected, they found the glucose yields from fibrous cellulose (pulp) to be significantly higher than those obtained from microcrystalline cellulose, which is often used as a model compound for cellulose hydrolysis. A comparison of different dicarboxylic acids with regard to their ability to hydrolytically degrade cellulose was presented by Mosier et al. [107]. It was shown that maleic acid is an especially suitable catalyst for the rupture of the glycosidic bond, because the degradation of microcrystalline cellulose was as effective as with dilute sulfuric acid but only a very small amount of glucose degradation was seen. The lower pK_a value of dicarboxylic acids compared with their monocarboxylic relatives is thought to be the explanation for their better performance as catalysts in polysaccharide degradation [108].

The application of maleic acid and oxalic acid at high salt concentrations was tested by vom Stein et al. [108]. Introducing a high ionic strength by addition of 30% (w/w) NaCl to the catalyst solution allowed the hydrolysis reaction to be performed under comparatively mild conditions (100–125°C), which advantageously results in less thermal decomposition of the sugar. The action of the salt is presumably similar to the action of ionic liquids, helping to break the dense H-bond network of cellulose fibers and thus making the glycosidic bonds better accessible to the catalyst molecules. Production of soluble cellooligomers with yields of up to 5% (w/w) with respect to the amount of cellulose initially employed, at concentrations of 0.25 and 1 g L^{-1}, depending on the type of cellulose, temperature, reaction time, and type and amount of catalyst used, can be reached. Amarasekara et al. [109] presented a study comparing different alkyl/aryl sulfonic acids, especially with sulfuric acid of the same acid strength. They were able to reach yields of up to 30.3% of total reducing sugars (i.e., glucose + soluble oligosaccharides) using 4-biphenylsulfonic acid as a catalyst (160°C, reaction time of 3 h), which is significantly above the value of 21.7% when aqueous sulfuric acid is used. A somewhat radically different approach to the preparation of cellulosic oligosaccharides from cellulose was reported by Redlich et al. [86, 110]. The process, referred to as pivaloylysis, was developed with the aim of generating oligosaccharides under mild conditions with regard to temperature as well as type of catalyst in order to prevent the formation of undesired side products. The hydrolysis is conducted on fully acetylated cellulose with pivalic anhydride and boron trifluoride etherate in dichloromethane at 40°C. Variation of the reaction time allows the specific yield for certain oligomers to be controlled, favoring smaller DPs after longer times and vice versa. Yields for the total amount of acetylated

cellooligosaccharides with a DP range of 1–8 are typically very high (~0.83 g g^{-1} cellulose acetate). However, the method has some major disadvantages, first and foremost the fact that the reaction has to be conducted in the strict absence of water, severely complicating the experimental work, and with long reaction times of about 40–50 h.

2.2.3 Hydrothermal Treatment

As reported by several authors (see, for example, [87, 111–114]), it is possible to hydrolytically degrade cellulose in pure H_2O without using any catalytic agents such as acids or enzymes. Zhao et al. [87] reported a procedure for oligosaccharide generation by supercritical hydrolysis of cellulose and lignocellulose. The authors developed a combined supercritical/subcritical technology that they used as a method for pretreatment and hydrolysis of the starting material. The supercritical step yields mainly oligosaccharides (in addition to some monosaccharides and their degradation products), whereas in the second, subcritical step these oligomers are further hydrolyzed to glucose. That subcritical conditions are more effective than supercritical conditions with regard to glucose production concurs with a publication by Ehara et al. [115]. However, as reported by Jin et al. [116], the decomposition rate of glucose under subcritical conditions is significantly higher than the rate of cellulose hydrolysis, rendering the production of glucose under these conditions complicated. The combined method used by Zhao et al. circumvents these difficulties by "pre-degrading" the cellulose to oligomers under supercritical conditions.

With regard to the production of cellooligosaccharides, the best reaction conditions were found to be a temperature of 380°C and a reaction time of 16 s, with an initial concentration of microcrystalline cellulose of 2.4% (w/w) in deionized water. Using these conditions, 40% (w/w) of the employed cellulose can be converted to cellooligosaccharides with a DP range of 2–6; 24% (w/w) are converted to glucose. The residual amount consists to a large extent of glucose decomposition products. Whether these methods applying supercritical conditions for cellulose degradation can be adjusted for the production of cellooligosaccharides having higher DPs is highly questionable, because the hydrolysis in the supercritical environment is extremely fast [87] and thus thorough control seems almost impossible. Griebl et al. [117] presented a procedure for the formation of xylooligosaccharides through the hydrothermolysis of xylan derived from the steeping-lye of the viscose process. The hydrothermal treatment, conducted at varying temperatures between 120°C and 180°C, resulted in a soluble fraction containing mainly neutral and acidic xylooligosaccharides, and an insoluble fraction that was predominantly highly crystalline cellulose. The DP of the neutral xylooligosaccharides could be varied in a wide range from approximately 1 to 15 by altering the reaction conditions (time and temperature). The isolated acidic fraction displayed a DP range of 3–17.

2.2.4 Enzymatic Degradation

The application of enzymes that are designed by nature to rupture glycosidic bonds for the production of mono- and oligosaccharides from polysaccharides seems obvious at a first glance. However, their employment is not as simple as the use of chemical catalysts, because enzymes need to be purified from cell extracts in laborious procedures and are sensitive to environmental conditions (pH, temperature, and presence of inhibitors) that can alter their activity or even denature them. Moreover, in nature cellulose is not degraded by just one enzyme, but by a combination of three classes of enzymes working together in a synergistic manner [118] to produce sugars that can be metabolized by the corresponding microorganisms [65]. An effective process requires enzyme preparations with the highest possible activity and a cellulosic substrate with sufficiently high reactivity. The commercial availability of purified cellulases with reasonably high activity was practicably negligible before the 1980s and the crude products contained high amounts of impurities in the form of other proteins and had a high price [119]. Therefore, it is no wonder that methods exploiting these biocatalysts for the degradation of polysaccharides had been developed long after the conventional chemical procedures.

A pioneering work in the field of enzymatic hydrolysis of cellulose was published by Reese et al. [119, 120], who made the requirement of a complex of enzymes for the depolymerization of cellulose to glucose commonly accepted [121]. In 1963, the authors described a procedure for the production of cellobiose and cellotriose, employing a cellulolytic filtrate isolated from the supernatant of a *Trichoderma viride* culture grown on cellulosic media [119]. The advantage of the application of enzymes is that the hydrolysis reaction can be performed under very mild conditions with respect to temperature and pH, which avoids the formation of unwanted side products and leaves other components unaltered. Because the generation of sugar decomposition compounds (which often have an inhibiting effect on fermentation processes) is avoided, glucose solutions resulting from enzymatic digestions are very well applicable as substrates for biotechnological processes. For that reason, the vast majority of methods developed focused on the maximization of glucose formation, leaving the formation of oligomeric intermediates relatively untouched. Recent and by no means exhaustive examples of the rare exceptions in this regard are given in the following paragraph. For a deeper insight into the state-of-the-art production of cellulolytic enzymes and their potential in technical applications, the reader is referred to a review by Wang et al. [122] and, for a more biological viewpoint on the topic, to a review by Lynd et al. [65].

Andersen et al. [121] studied the synergy and the interactions of the three enzyme classes with respect to the impact of individual concentrations on the hydrolysis pattern of the product mixture (i.e., the relative amounts of glucose and oligosaccharides formed). The authors performed assays with binary and ternary enzyme cocktails on two different cellulosic substrates, a microcrystalline cellulose and a cellulose pretreated by swelling in phosphoric acid. As expected, the

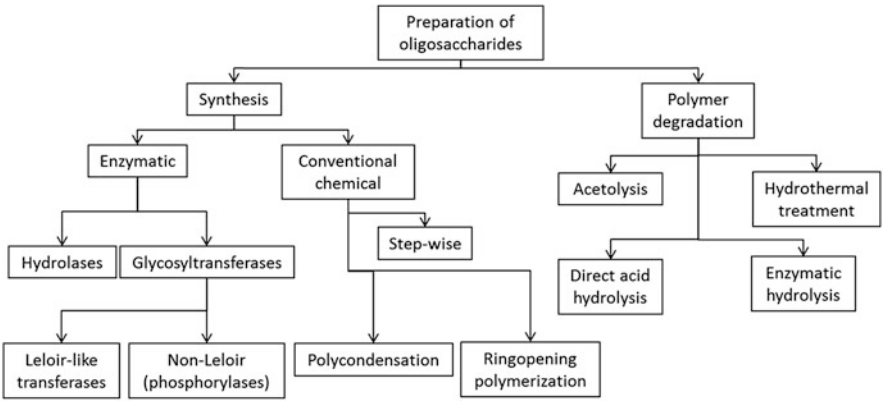

Fig. 5 Preparation of oligosaccharides from celluloses and hemicelluloses

highest yield of soluble oligosaccharides, with a DP range of 1–6, was achieved when working with a relatively low enzyme concentration of 0.1 μM. Interestingly, the relative amount of individual oligomers formed was dependent on the type of cellulose substrate used. A procedure for the coproduction of oligosaccharides and glucose from corncobs was published by Garrote et al. [11]. In a first step, the raw material containing mainly cellulose and hemicellulose (xylan) is subject to autohydrolysis at elevated temperatures of 202–216°C, during which most of the xylan is degraded to xylooligosaccharides. After this hydrothermal step, the reaction mixture consists of a liquid part (referred to as liquor) containing the soluble xylooligosaccharides as well as soluble compounds not originating from the hemicellulose fraction and side products, and a solid fraction consisting predominantly of cellulose. This insoluble part is then subject to enzymatic hydrolysis by cellulases in order to produce fermentable glucose. Under optimal conditions, a maximum xylooligosaccharide yield of 32.2% (w/w) of the dry substance of the raw material can be achieved, while the conversion of cellulose to glucose is almost quantitative, resulting in glucose solutions with concentrations of up to 97.2 g L^{-1}. Rydlund et al. [123] reported the preparation of neutral and acidic oligosaccharides derived from the hemicellulosic fraction of an unbleached birch Kraft pulp with the aid of an endoxylanase from *Trichoderma reesei*. They were able to show that the mixture of hydrolysis products after 24 h at 40°C consists of a neutral fraction (mainly xylose, xylobiose, and xylotriose) and an acidic fraction, bearing α-(1,2)-linked uronic acid groups attached to the xylose unit adjacent to the non-reducing chain end, with a DP of up to 5.

An overview of the different strategies for the preparation of cello- and xylooligosaccharides is given in Fig. 5, summarizing both the synthetic and the degradation approaches.

3 Separation and Analysis of Oligosaccharides

The separation of cello- and xylooligosaccharides according to their DP is a challenging task. Nevertheless, several methods exploiting different separation mechanisms have been developed during the last few decades. On a preparative scale, the most commonly used techniques, according to the literature, are: (1) SEC on particulate polyacrylamide or crosslinked dextran gels [80, 81, 85, 88, 124–129]; (2) partition/adsorption chromatography on charcoal, untreated charcoal–celite, or stearic-acid treated charcoal–celite columns [80, 83, 96] and on cellulose-based stationary phases [80, 130]; (3) hydrophilic interaction chromatography (HILIC) and normal phase high-performance liquid chromatography (NP-HPLC) on silica gels, amino-bonded silica columns, or matrices with copolymer-bonded cyclodextrins [80, 89, 131, 132]; and (4) ion exchange chromatography on cation exchange resins with sulfo-groups coupled with metal counter ions (e.g., Ca^{2+}, Li^{+}, Ag^{+}, Na^{+}, Pb^{2+}) or hydronium ions [10, 80, 98, 133]. For analytical purposes, especially for purity investigations on isolated fractions homogenous with respect to the DP, a variety of methods exist. In this regard, metal-loaded cation exchangers (e.g., sulfonated styrene-divinylbenzene copolymers with Ca^{2+}, Li^{+}, Ag^{+}, Na^{+}, or Pb^{2+}) are widely used stationary phases that can be used for the analysis of non-derivatized oligosaccharides in different operation modes, such as ion exchange, ion exclusion, and ligand exchange [134]. Furthermore, separation of saccharides as their borate complexes on anion exchange resins has been shown to be a powerful technique for the detection and quantification of impurities [81, 88, 124].

High-performance anion exchange chromatography coupled with pulsed amperometric detection (HPAEC-PAD), where the sugars are transformed into their oxyanionic forms at high pH, is another potent method for the analysis of closely related oligosaccharides, which was reviewed recently by Corradini et al. [134]. As reported by Weith et al. [135] and later by Liu et al. [136], sugar boronate affinity chromatography can also be applied as a useful separation method for carbohydrates, exploiting the formation of cyclic diesters between *cis*-diols (sugars) with borate bound to the stationary phase. In principle, oligosaccharides can also be separated by means of classical reversed phase chromatography employing alkylated silica gels [137–139]. However, the chromatograms are often difficult to interpret because anomers of each oligosaccharide are separated. Because these methods have not been much used for the separation of cello- or xylooligosaccharides, reversed phase HPLC techniques are not discussed further in this review.

Especially for analytical purposes, capillary zone electrophoresis (CZE) is another possibility for the study of oligosaccharides derived from xylan or cellulose, provided that they can be dissolved in the used background electrolyte. Rydlund et al. [140], for example, demonstrated the separation efficiency of CZE on xylooligosaccharides. The separation was performed in a concentrated alkaline borate buffer in a fused-silica capillary column at constant power supply (1,200 mW), with on-column UV-detection at 245 nm. A pre-column derivatization was carried out by reductive amination with 6-aminoquinoline (6-AQ) and the

saccharides were separated as their borate complexes. The method was found to have a relatively low minimum concentration limit in the micromolar range, which corresponds to the limit of detection in the femtomolar range. Xylooligomers up to the hexaose were separated with baseline resolution. Sartori et al. [141] applied CZE for the separation of xylo- and cellooligosaccharides derived from alkaline degradation of the parental polymers after pre-column derivatization with *p*-aminobenzonitrile (UV tag). Cellooligomers up to the heptaose were efficiently separated by this method. A high borate concentration was needed in both cases, because electrophoretic mobility is a function of the net negative charge and thus of the extent of borate complex formation. On the other hand, the mobility decreases with the size of the analyte molecules; thus smaller molecules elute first followed by the larger molecules. Furthermore, CZE was demonstrated to be a useful technique for the structural elucidation of wood-derived polysaccharides with respect to their degradation products after hydrolysis, especially when combined with mass spectrometry [123, 142].

Once fractions are obtained that are homogeneous with respect to the DP, or at least have a very narrow molecular weight distribution, they can be further analyzed with regard to structural homogeneity and the presence of impurities having the same molecular weight by means of mass spectrometry (see, for example, [6, 123, 128, 142]) and nuclear magnetic resonance (NMR) spectroscopy (see, for example, [6, 86, 123, 142–144]). For a detailed overview of the mass spectroscopic characterization of oligo- and polysaccharides and their derivatives, the reader is referred to the comprehensive review by Mischnick [145]. In the following sections, some of the above-mentioned separation methods are discussed in more detail, with a slight emphasis on those that can be applied in preparative efforts.

3.1 Size Exclusion Chromatography

Size exclusion chromatography (SEC), also referred to as gel permeation chromatography (GPC), is a technique that allows the separation of analytes according to their hydrodynamic volume. The method is widely used in polymer analysis for the determination of molar mass distributions, in biochemical laboratories for protein or nucleic acid purification, and it is also applied for the investigation of oligosaccharides. In contrast to other chromatographic methods, no enthalpic interaction between analytes and the column material should occur. The stationary phase usually consists of a porous particulate or continuous gel with clearly defined pore sizes. Depending on their hydrodynamic volume, which is an expression of their size in solution, the molecules to be analyzed have different abilities to enter these pores. Small molecules are able to penetrate the pores of the stationary phase, whereas larger molecules (with a higher hydrodynamic radius) leave the column without entering the pores. In other words, the extent to which a molecule can freely diffuse into the pore volume determines its duration in the column. Molecules that are too large to enter the pores elute when the void volume of the column is reached.

Those that are small enough to diffuse in a completely free manner elute with the total elution volume of the column. According to Churms [126], the optimal column length is between 50 and 100 cm (4–8 mm internal diameter), which can be achieved by connecting two or more shorter columns in series. The method has been applied to the separation of cellooligosaccharides in several studies [126].

Polyacrylamide (PAA) gels are the most frequently used stationary phases in these efforts, because they are advantageous in terms of selectivity, resolution, low band broadening, and linearity between the logarithm of the distribution coefficients and the DP [81, 126]. The main drawback of using PAA gels (e.g., BioGel P-2, P-4, or P-6; Bio-Rad, Richmond, CA, USA) lies in the lack of resistance to high pressures, resulting in long separation times of 24 h and more [81, 126]. To overcome this problem, gels have been developed that are capable of withstanding higher pressures, including Trisacryl GF05 (LKB, Bromma, Sweden), which is a crosslinked polymer of *N*-acryloyl-2-amino-2-hydroxymethyl-1,3-propanediol [146], and Toyopearl HW-40S (Toyo Soda, Tokyo, Japan), a hydroxylated-methacrylic polymer [147]. Furthermore, the successful application of diol-modified silica for the separation of oligogalacturonic acids with a DP range of 2–19 was reported by Naohara et al. [148]. However, these high-performance techniques are inferior to conventional SEC with regard to resolution, as reviewed by Churms [149].

Hamacher et al. [88] reported the separation of cellooligosaccharides (DP 1–8), obtained by hydrochloric acid hydrolysis and acetolysis, at a preparative scale using PAA (BioGel P-4; Bio-Rad, Richmond, CA, USA) columns with a total length of 210 cm (5 cm internal diameter) and double-distilled water at 65°C as the eluent. The dry gel had to be especially wind-sieved in advance to give the desired narrow range of particle sizes. Detection was performed with a differential refractive index (RI) detector. Additionally, the system was calibrated with D-glucose eluting at the inner volume of the column and dextran 70 (molecular weight $\sim 7 \times 10^4$ g mol^{-1}) eluting at the void volume. With this set-up, separation up to the cellooctaose was possible with a good resolution, and re-chromatography of the fractions indicated products of uniform molecular weight. However, the time needed for this procedure was more than 22 h. In addition, it was shown that the fractions, although apparently homogeneous according to SEC, contained some side products arising from the harsh conditions during cellulose degradation and possibly also during SEC [124], which was shown by sugar borate chromatography (see Sect. 3.3.2). Similar procedures have been reported by Schmid et al. [124, 125] and Pereira et al. [81]. The procedure can be somewhat advanced by the introduction of the "recycle-SEC" technique [124], which allows a separation of cellooligosaccharides up to a DP of 12. Zhang et al. [85] combined a PAA column (100×5 cm) with a cation exchange column (see Sect. 3.3.1) and efficiently separated water-soluble cellooligomers, obtained through mixed acid hydrolysis, up to a DP of 8 in gram quantities within less than 30 min, demonstrating the good performance of this method in terms of productivity on a preparative scale. In a comparative study, Akpinar et al. [80, 81] tested different chromatographic techniques for the separation of cellodextrins, including SEC on the polyacrylamide gel BioGel P-2. In this

case, SEC was shown to be inferior to other methods, especially adsorption chromatography on charcoal–celite. An effective separation was only possible up to the hexaose and the preparation times were longer than in the case of other methods. However, separation of cellooligosaccharides with a higher DP (10–50) was not addressed by the aforementioned efforts, which is a consequence of the preparation methods, during which these compounds are removed together with the polymer fraction.

Kaustinen et al. [92], who developed the method of selective acetolysis, allowing the preparation of cellooligosaccharides with a defined DP of 18–100 by altering the reaction conditions, used SEC on a silica-based material to determine the molecular weight of their product hydrolysates. Elution was performed with 1:1 (v/v) 1,4-dioxane and 1,2-dichloroethane. Fractions with a molecular weight ranging from 8,000 to 24,000 g mol^{-1} (peracetylated saccharides), corresponding to DP values of approximately 30–100, were isolated. However, as can be demonstrated, the separation performance decreases with a decline in DP, indicating the particular difficulty of analyzing cellooligosaccharides with a DP between 10 and 50. Isogai et al. [100] prepared cellooligomers by dilute HCl hydrolysis that had DPs of 18–24 and 35–100 (depending on the DP of the cellulose used). The authors also used SEC to characterize the hydrolyzates. The water-insoluble oligosaccharides were dissolved in 8% LiCl in *N*,*N*-dimethylacetamide (DMAc) and analyzed on a styrene-divinylbenzene copolymer gel (KD-803; Shodex, Japan) with 1% LiCl/DMAc as the mobile phase. Detection was performed with a combination of a differential refractive index detector and multi-angle laser light scattering (MALLS) to obtain the molecular weight distributions of the products. Fraction collection, which would allow obtaining solutions of cellooligosaccharides with a very narrow molecular weight distribution, however, was not performed.

The SEC analysis of xylan and xylooligosaccharides was reported by several authors, for example, Rasmussen et al. [150] and Deery et al. [128]. Rasmussen [150] used a polymer-based aqueous SEC column (300 × 8 mm, Shodex SB-806 HQ; Showa Denko K.K., Tokyo, Japan) for monitoring the enzyme-catalyzed hydrolysis of xylan substrates. Quantitative profiling of the reaction mixture was performed with 0.1 M sodium acetate as the eluent and an RI detector, using standard compounds (pullanans, xylohexaose, xylose, and dextrans) as molecular weight markers for column calibration. Deery [128] reported the combination of SEC and different mass spectrometry techniques for the characterization of arabinoxylan fragments derived by either acid or enzyme-catalyzed hydrolysis. The polymer-based aqueous SEC columns (PL Aquagel-OH 30 8 μm, 300 × 7.5 mm; Polymer Laboratories, Church Stretton, UK) were calibrated with dextran standards. The mass spectrometry detection methods applied were on-line electrospray ionization mass spectrometry (ESI-MS) and off-line matrix-assisted laser desorption/ionization time-of-flight mass spectrometry (MALDI-TOF MS).

3.2 Normal Phase HPLC and Hydrophilic Interaction Chromatography

Normal phase high-performance liquid chromatography (NP-HPLC) and hydrophilic interaction chromatography (HILIC) are operation modes in which a polar stationary phase is used in combination with a less polar mobile phase for the chromatography of apolar substances. As reviewed by Churms [149], the stationary phases predominantly used for the separation of carbohydrates by partition and/or adsorption in normal phase chromatography can be divided into three groups: (1) silica gels having their surface covered with hydrated hydroxyl groups, (2) matrices in which polar phases are covalently bound to silica gels, and (3) methods based on polymers with polar functional groups. The application of microparticulate silica gels with spherical particles of an average size of 3–5 μm in a packing of homogeneous beads results in good chromatographic efficiency. The material can be used in its unmodified form or with polar groups attached to the gel network. In this regard, aminopropyl silica packings were widely used [149] for the separation of carbohydrates, in spite of the major drawback that reducing sugars react with the amino groups, which leads to loss of analytes and deactivation of the column.

As alternative bonded-phase packings, bonded amide, cyano, diol, and polyol phases have to be mentioned. Furthermore, Alpert [151] suggested the application of a novel stationary phase, in which ethanolamine is incorporated into a coating of polysuccinimide covalently bound to silica. Unmodified silica gel was successfully used for the separation of acetylated cellooligosaccharides in the middle of the past century [89]. In their comparative study of different cellooligosaccharide preparation and separation methods, Akpinar et al. [80] also tested separation by normal phase chromatography on silica gel. Using a 1:1 (v/v) mixture of ethyl acetate and toluene as the eluent, they were able to effectively purify (on a preparative scale) peracetylated cellooligomers (obtained by acetolysis) up to hexaose, and also successfully applied the system for the separation of both acetylated and deacetylated cellooligomers on an analytical scale. Armstrong et al. [152] introduced silica packings bearing cyclodextrins for the analytical separation of carbohydrates, especially for the distinction of isomers. Simms et al. [132] applied β-cyclodextrin columns for the separation of neutral oligosaccharides derived from cellulose, xylan, and other polysaccharides. They used a Cyclobond I column (250×4.6 mm; Rainin Instrument, Woburn, MA, USA) with a matrix of β-cellodextrin molecules coupled to 5 μm spherical silica gel particles via a 10-atom spacer arm, acetonitrile–water mixtures as eluents, and a differential refractometer as detection system. The authors found a clear dependence of the retention behavior on the monosaccharide composition and the types of glycosidic linkages present in the saccharides. The cellodextrin separation material was shown to be similar in selectivity to aminoalkyl-bonded silica gels but superior in durability. Berthod et al. [131] investigated cyclodextrin columns with regard to the separation mechanism of oligosaccharides from different origins including cello-

and xylooligosaccharides. They used commercial cellooligomer standards up to a DP of 5 and xylooligomer standards up to a DP of 6. It was shown that partitioning between the mobile (different acetonitrile–water mixtures) and the stationary phase and hydrogen bonding are the two possible mechanisms responsible for carbohydrate retention in these columns. For detection, an RI detector as well as a UV detector operated at 190 nm were employed.

Because the solubility of silica in aqueous solutions increases rapidly above a pH of 8 and below a pH of 2 and is, moreover, dependent on the concentration of water and buffer [149], the application of the aforementioned materials is somewhat restricted. To overcome this problem, polymer-based sorbents that are stable in environments of very high or very low pH have been developed [149]. The materials must be able to withstand the high pressures and flow rates applied in HPLC methods without deformation, shrinking, or swelling with the solvent. Important examples of such macroporous polymers carrying polar functional groups used for HILIC of carbohydrates are highly crosslinked sulfonated polystyrene cation exchange resins and vinyl polymers. Mobile phases for partition chromatography on silica materials include different organic solvents (very often acetonitrile) mixed with water in different ratios for adsorption chromatography of carbohydrate derivatives on silica [149].

A widely used detection system for HILIC of sugars is the RI detector. However, although the detection limits have improved in recent years, RI detectors display a major drawback, namely their sensitivity to changes in solvent composition. Thus the elution of higher oligosaccharides, which usually requires a gradient elution mode, cannot be followed with this detection system. Evaporative light-scattering (ELS) detection, which is compatible with changing solvent compositions, has therefore emerged as a good alternative [153], extending the upper limit of the resolution of oligosaccharides to a higher DP. ELS detectors are able to detect sugars and alditols with much higher sensitivity than RI detectors. They have great baseline stability and are independent of changes in temperature [153]. The authors recently tested the application of an ELS detector for the detection of fully acetylated cellooligosaccharides with a higher DP obtained by acetolysis of

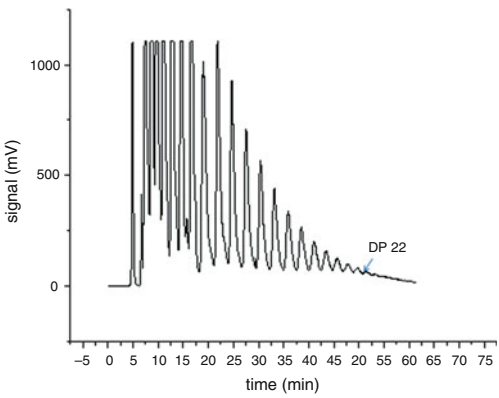

Fig. 6 Evaporative light-scattering detection of acetylated cellooligosaccharides after normal phase separation on a silica-based column

microcrystalline cellulose. Separation was realized with a normal phase silica column up to a DP of 22. Eluents were ethyl acetate and toluene. A linear gradient starting with 70% of the former to 100% within an hour was used. The results can be seen in Fig. 6.

It was demonstrated that detection of even very low amounts of cellooligomers is possible using an ELS detector, and that a good separation of compounds having a DP of up to 22 is easily feasible using NP-HPLC in gradient elution mode with common solvents.

Other possibilities for effective detection of the analytes after silica or silica-based chromatography is pre-column derivatization introducing chromophoric or fluorescent groups into the analytes, and post-column derivatization allowing fluorescence, UV, or electrochemical detection systems [149].

Adsorption chromatography on charcoal–celite columns is a widely used and effective technique for the preparative separation of cellooligosaccharides. The method, displaying the benefit of an inexpensive column material and easily available elution solvents, has been known for a long time and was used in early attempts of oligosaccharide separation by, for example, Miller et al. [83]. Separation of analyte molecules is achieved by adsorption on the charcoal surface, while the celite is used to improve the flow characteristics of the charcoal, which is necessary because of the granulation of the charcoal [80]. For a given series of homologous oligosaccharides, retention is a function of the molecular weight, because the extent of adsorption increases strongly and regularly with an increase in molecular weight. Once oligosaccharides are adsorbed in the stationary phase, they can be desorbed by using a water → ethanol gradient. In order to improve desorption and eliminate re-adsorption of oligomers with a higher DP, the charcoal is often treated with stearic acid [80]. It was demonstrated [80, 83] that, with this method, oligomers of DP 1–7 can be separated with good resolution. However, adsorption chromatography with charcoal–celite columns displays some major drawbacks. First of all, the time needed for a separation run is extremely long (several days), because the packing is not able to resist high pressures. Once used, the separation capability of the material is diminished, so that a new adsorbent material has to be prepared before each run [98].

A comparatively newly developed stationary phase for the fractionation of cellooligosaccharides was developed by Akpinar et al. [130] using a cellulose-based material for adsorption chromatography with water–ethanol mixtures as eluents. This method exploits the affinity of the oligomers to their parent polymers. The main advantage lies in the fact that cellulose is a relatively inexpensive material that is readily available at cellooligosaccharide processing facilities, and that these columns can easily be regenerated by purging with water. However, with regard to the separation performance, the cellulose-based columns are considerably inferior to other systems, allowing an effective fractionation only in terms of separating oligomers above DP 4 from smaller oligomers.

3.3 Ion Exchange Columns

3.3.1 Cation Exchange Resins

The use of cation exchange resins, such as sulfonated polystyrene-divinylbenzene copolymer matrixes, has been shown by several authors to be a powerful technique for oligosaccharide separation at both analytical and preparative scales [10, 80, 81, 124, 125, 133]. The mode of action of these columns combines a variety of separation mechanisms, including ion exclusion, ion exchange, ligand exchange, size exclusion, reversed phase, and normal phase partitioning, and is referred to as ion-moderated partitioning [154]. The application of such stationary phases for the HPLC of cellooligosaccharides was introduced by Ladisch et al. [155] using Ca^{2+} as a fixed counter ion, and later by Bonn et al. [156] employing Ag^{+} counter ions. Both methods were developed for analytical scale separation and were found to have a good scale-up potential for the production of cellooligosaccharides in larger amounts [157]. Since then, these materials have been widely used for the chromatographic separation of oligosaccharides. Ladisch et al. [133], for example, used a cation exchange resin in its Ca^{2+} form to separate cellodextrins from DP 1 to DP 7 effectively within 30 min using water as the eluent and a differential RI detection system. The same authors combined a strong cation exchange resin (Ca^{2+}) column with a SEC column for a one-step desalting and separation procedure for the preparation of pure component solutions of cellooligosaccharides of DP 2–7 [98]. Pereira et al. [158] employed a styrene-divinylbenzene cation exchange matrix with Ca^{2+} as counter ion and H_2SO_4 as the eluent for the separation of cellodextrins obtained according to Voloch method [10]. The analytical column combined with an RI detector was shown to be suitable for the analysis of submicrogram quantities of oligosaccharides. Zhang et al. [85] also combined a strong cation exchange column (29×5 cm internal diameter) in its Ca^{2+} form with a SEC column (100×5 cm internal diameter) and water as the mobile phase. Through their procedure, a separation of cellodextrins of DP 1–8 at a preparative scale was possible; however, a major drawback of the method was the long run time of about 24 h. In a comparative study by Akpinar et al. [80], cation exchange resins were also tested regarding their cellooligosaccharide separation capabilities. A polystyrene-divinylbenzene stationary phase in its Ag^{+} form was used with water as the eluent and was able to resolve cellooligosaccharides up to the hexaose in less than 1 h.

Table 2 gives an overview of the most important chromatography procedures used for the separation of cellooligosaccharides at a preparative scale.

3.3.2 Anion Exchange Chromatography

Anion exchange chromatography of sugar-borate complexes is one procedure used for analysis of oligosaccharides. For analytical purposes carbohydrates can be

Table 2 Preparative separation techniques for cellooligosaccharides

Chromatography mode	Stationary phase	Mobile phase	Separation range	Comments	References
SEC	Polyacrylamide	Water	1–8	Long run times	[88]
	Polyacrylamide	Water	1–12[a]	Long run times	[124]
	Polyacrylamide	Water	1–8	Connected in series with a CIEX column	[85]
	Silica-based	1:1 (v/v) *p*-diosane: 1,2-dichloroethane	30–100[b]	–	[92]
	Styrene-divinylbenzene copolymer gel	1% LiCl in DMAc	18–100	No fractionation performed	[100]
NP-HPLC/ HILIC	Silica based	1:1 (v/v) ethylacetate: toluene	1–6	–	[80]
		Acetonitrile–water mixtures	1–5	–	[131, 132]
Adsorption	Charcoal/celite-based	Water–ethanol gradient	1–7	Long run times, column material not reusable	[80, 83]
	Cellulose-based	Water–ethanol mixtures	≤4 from larger oligomers	–	[130]
Ion moderated	Styrene-divinylbenzene copolymer-based	Water	1–7	–	[133]
	Styrene-divinylbenzene copolymer- and Polyacrylamide-based	Water	1–8	Connected in series with a SEC-column	[85]

[a]Recycle-SEC mode (rechromatography of eluted solution)
[b]Fractions were not monodisperse but displayed a narrow molecular weight distribution

separated in anion exchange columns after transformation to their corresponding borate complexes. Oligosaccharides that have been purified by other methods can be further investigated as potential side components of the mixture by these means. Hamacher et al. [88] used an anion exchange resin for the detection of structural heterogeneities of cellooligomers that were homogeneous according to SEC. They used a strong-base anion exchange resin (DURRUM DA-X4-20) at 60°C with dimension of 0.6×30 cm and applied a two-step borate buffer elution followed by a regeneration and equilibration procedure to separate the borate complexes of the oligosaccharides. As a detection system, a post-column derivatization strategy with orcinol–sulfuric acid reagent was used, followed by measurement of the absorbance at 420 nm. The authors reported the presence of several other oligomers in the sample solutions. These secondary components were found to contain at least one monomeric unit that was structurally different from glucose. Similar results were published by several other authors, for example, Schmid et al. [124, 125] and Pereira [81].

HPAEC-PAD is another powerful method of sugar analysis and exploits the fact that carbohydrates are weak acids with pK_a values between 12 and 14 and can thus be transformed into their oxyanion form under strongly alkaline conditions and then readily separated in anion exchange columns. After passing through the column, the anions can be detected directly by pulsed amperometric detection, typically using platinum electrodes operated in a three-step potential wave form, which provides the ability for effective detection and simultaneous prevention of electrode fouling [159]. However, strongly alkaline solutions in combination with sugar analysis are often problematic because of possible degradation and β-fragmentation reactions, which can alter the product distribution of the sample considerably; this also applies to HPAEC, as discussed below. Corradini et al. [134] reviewed the application of HPAEC-PAD for the analysis of carbohydrates of interest in food science. The method, which is applied in a variety of routine monitoring and research applications, offers the possibility to separate all classes of alditols, aminosugars, mono-, oligo-, and polysaccharides according to structural features including size, composition, anomericity, and type of glycosidic bonds. A major requirement for the stationary phases is the ability to maintain stability at very high pH values, which is, for example, the case for quaternary ammonium-bonded pellicular anion exchange materials. The method inherits the advantage of good performance in terms of selectivity and efficiency. Furthermore, the method avoids common detection problems, such the sensitivity of RI detectors to the changing eluent composition and absorption of UV light by the solvent when using a UV detector. The main separation parameters with regard to the analyte molecules are DP and linkage position, which means that, for a series of homologous oligosaccharides, retention is directly proportional to the DP and indirectly proportional to the pK_a in a regular and predictable manner.

For the separation of oligosaccharides, CarboPac PA100 and PA200 (Dionex) are widely used columns, usually operated in a sodium acetate gradient elution mode. Griebl et al. [117], for example, used HPAEC-PAD as an analysis method for the characterization of the SEC fractions of the hydrolyzate obtained by

hydrothermolysis of xylan. The column was a DionexCarboPac PA100 with dimensions of 4×250 mm. The system was calibrated with xylooligosaccharide standards having DPs of up to 6 and fucose as internal standard. Higher xylooligosaccharides had to be quantified by extrapolation because of the non-availability of standards. Elution was performed in gradient mode starting with pure 0.15 M NaOH, to 0.15 M NaOH plus 0.5 M NaOAc.

3.4 Sugar Boronate Affinity Chromatography

Sugar boronate affinity chromatography was first introduced by Weith et al. [135] in 1970. The stationary phase usually consists of phenyl-boronate-agarose with immobilized boronate ligands, which display great specificity for a wide variety of compounds containing *cis*-diols (e.g., nucleosides, nucleotides, and carbohydrates). The separation principle of these columns is an esterification reaction between the boronate ligands and *cis*-diols [136]. Boronate, usually having a trigonal planar geometry, can be hydroxylated under alkaline conditions, resulting in a tetrahedral boronate anion that is able to react with the *cis*-diol analytes. The product diester can then be hydrolyzed by decreasing the pH, reversing the reaction. The method has been used in many publications for the separation of different mono- and oligosaccharides and for the analysis of purified cellodextrin fractions. Schmid et al. [124, 125], for example, used sugar boronate affinity chromatography for the purification of cellooligomers obtained by acetolysis or direct acid hydrolysis that were homogenous with regard to their DP according to SEC. The authors used preparative phenyl boronate-agarose columns (PBA 60; Amicon, Danvers, MA, USA) with dimensions of 100×0.9 cm internal diameter and 100 mM $(NH_4)_2CO_2$ buffer (pH 10.5) as the mobile phase. The method was shown to be very effective for detecting impurities and for preparative purification procedures. The impurities, often characterized by having at least one monomer different to glucose, could not be separated or even detected by other methods such as SEC or HPLC on cation exchange resins, demonstrating the unique power of sugar boronate affinity chromatography.

4 Summary and Outlook

Cello- and xylooligosaccharides with a DP between 2 and approximately 30 offer a wide field of potential applications. In addition to their use as anti-nutritional additives in the food industry and their employment as coating agents in the pharmaceutical industry, oligomeric compounds originating from cellulose in particular are of greatest interest for research on physicochemical properties as a function of DP, for structural and macromolecular investigations, as well as for studies of (enzymatic) cellulose hydrolysis. They are also gaining increasing

importance as intermediates in current biorefinery scenarios. In this regard, it is of central significance to have procedures available that allow the production of cello- and xylooligosaccharides with a defined DP that can be used as standard compounds in analytical efforts. Nevertheless, targeted techniques to generate these compounds at a preparative scale and, even more demanding, to separate them according to their DP and analyze the obtained fractions have not been fully developed. Principal strategies for the preparation of oligosaccharides are either enzymatic or conventional syntheses using the respective monomers as starting material or partial hydrolysis of the parent polymers, which can be achieved with the aid of different acids or enzymes. For the separation of the mixtures of oligomers obtained in this way, different chromatography modes have been evaluated; SEC and NP-HILIC have turned out to be the most promising techniques. Remarkably, most publications dealing with the degradation of cellulose and hemicellulose focus on the production of monomeric sugars or very short-chained oligosaccharides that can be subjected to fermentation processes. This is probably the reason why the preparation, separation, and analytical methods for oligomers having a DP between 8 and 30 are still in the early stage of development. Future studies should elucidate which methods are the most suitable for isolation of cello- and xylooligosaccharides and how they can be advanced.

References

1. Hoch G (2007) Funct Ecol 21:823
2. Klemm D (1998) Comprehensive cellulose chemistry, vol 2. Wiley-VCH, Weinheim
3. Klemm D, Heublein B, Fink HP, Bohn A (2005) Angew Chem Int Ed Engl 44:3358
4. Scheller HV, Ulvskov P (2010) Annu Rev Plant Biol 61:263
5. Ullmann's encyclopedia of industrial chemistry. 2011, Wiley-VCH, Weinheim
6. Buchanan CM, Hyatt JA, Kelley SS, Little JL (1990) Macromolecules 23:3747
7. Nishimura T, Nakatsubo F (1996) Carbohydr Res 294:53
8. Nishimura T, Nakatsubo F (1996) Tetrahedron Lett 37:9215
9. Raymond S, Heyraud A, Qui DT, Kvick A, Chanzy H (1995) Macromolecules 28:2096
10. Voloch M, Ladisch MR, Cantarella M, Tsao GT (1984) Biotechnol Bioeng 26:557
11. Garrote G, Yanez R, Alonso JL, Parajo JC (2008) Ind Eng Chem Res 47:1336
12. Schmidt RR (1986) Angew Chem Int Ed Engl 25:212
13. Koenigs W, Knorr E (1901) Ber Dtsch Chem Ges 34:957
14. Pfaffli PJ, Hixson SH, Anderson L (1972) Carbohydr Res 23:195
15. Schuerch C (1973) Acc Chem Res 6:184
16. Haq S, Whelan WJ (1956) Nature 178:1222
17. Haq S, Whelan WJ (1956) J Chem Soc 4543-4549
18. Mcgrath D, Lee EE, Ocolla PS (1969) Carbohydr Res 11:461
19. Husemann E, Muller GJM (1966) Makromol Chem 91:212
20. Kochetko NK, Kudryash LI, Chlenov MA, Chizhov OS (1968) Dokl Akad Nauk SSSR 179:1385
21. Kochetko NK, Bochkov AF, Yazlovet IG (1969) Carbohydr Res 9:49
22. Masura V, Schuerch C (1970) Carbohydr Res 15:65
23. Frechet J, Schuerch C (1969) J Am Chem Soc 91:1161
24. Ruckel ER, Schuerch C (1966) J Org Chem 31:2233

25. Ruckel ER, Schuerch C (1966) J Am Chem Soc 88:2605
26. Ruckel ER, Schuerch C (1967) Biopolymers 5:515
27. Uryu T, Libert H, Zachoval J, Schuerch C (1970) Macromolecules 3:345
28. Zachoval J, Schuerch C (1969) J Am Chem Soc 91:1165
29. Schmidt RR, Moering U, Reichrath M (1980) Tetrahedron Lett 21:3565
30. Schmidt RR, Michel J (1982) Angew Chem Int Ed Engl 21:72
31. Takeo K, Okushio K, Fukuyama K, Kuge T (1983) Carbohydr Res 121:163
32. Takano T, Nakatsubo F, Murakami K (1988) Cell Chem Technol 22:135
33. Takano T, Harada Y, Nakatsubo F, Murakami K (1990) Mokuzai Gakkaishi 36:212
34. Takano T, Harada Y, Nakatsubo F, Murakami K (1990) Cell Chem Technol 24:333
35. Nishimura T, Takano T, Nakatubo F, Murakami K (1993) Mokuzai Gakkaishi 39:40
36. Nakatsubo F, Takano T, Kawada T, Someya H, Harada T, Shiraki H, Murakami K (1985) Mem Coll Agric Kyoto Univ 127:37
37. Sinay P (1978) Pure Appl Chem 50:1437
38. Nishimura T, Nakatsubo F, Murakami K (1994) Mokuzai Gakkaishi 40:44
39. Nakatsubo F, Kamitakahara H, Hori M (1996) J Am Chem Soc 118:1677
40. Nishimura T, Nakatsubo F (1997) Cellulose 4:109
41. Adelwohrer C, Takano T, Nakatsubo F, Rosenau T (2009) Biomacromolecules 10:2817
42. Kobayashi S, Sakamoto J, Kimura S (2001) Prog Polym Sci 26:1525
43. Kadokawa J (2011) Chem Rev 111:4308
44. Kobayashi S (2007) Proc Jpn Acad Ser B 83:215
45. Kaplan DL, Dordick J, Gross RA, Swift G (1998) ACS Symp Ser 684:2
46. Pauling L (1946) Chem Eng News 24:1375
47. Kobayashi S, Kiyosada T, Shoda S (1996) J Am Chem Soc 118:13113
48. Kobayashi S (1999) J Polym Sci Polym Chem 37:3041
49. Kobayashi S, Makino A (2009) Chem Rev 109:5288
50. Crout DHG, Vic G (1998) Curr Opin Chem Biol 2:98
51. Williams SJ, Withers SG (2000) Carbohydr Res 327:27
52. Kobayashi S, Kashiwa K, Kawasaki T, Shoda S (1991) J Am Chem Soc 113:3079
53. Kobayashi S, Shoda S (1995) Int J Biol Macromol 17:373
54. Okamoto E, Kiyosada T, Shoda SI, Kobayashi S (1997) Cellulose 4:161
55. Kadokawa J-I (ed) (2009) Interfacial researches in fundamental and material sciences of oligo- and polysaccharides. Transworld Research Network, Kerala
56. Shoda S (1999) Glycoconj J 16:S3
57. Fujita M, Shoda S, Kobayashi S (1998) J Am Chem Soc 120:6411
58. Fort S, Boyer V, Greffe L, Davies G, Moroz O, Christiansen L, Schulein M, Cottaz S, Driguez H (2000) J Am Chem Soc 122:5429
59. Egusa S, Goto M, Kitaoka T (2012) Biomacromolecules 13:2716
60. Egusa S, Kitaoka T, Goto M, Wariishi H (2007) Angew Chem Int Ed Engl 46:2063
61. Burchard W, Habermann N, Klufers P, Seger B, Wilhelm U (1994) Angew Chem Int Ed Engl 33:884
62. Taniguchi N, Honke K, Fukuda M (eds) (2002) Handbook of glycosyltransferases and related genes. Springer, Tokyo
63. Kitaoka M, Hayashi K (2002) Trends Glycosci Glycotechnol 14:35
64. Kudlicka K, Brown RM (1997) Plant Physiol 115:643
65. Lynd LR, Weimer PJ, van Zyl WH, Pretorius IS (2002) Microbiol Mol Biol Rev 66:506
66. Samain E, Lancelonpin C, Ferigo F, Moreau V, Chanzy H, Heyraud A, Driguez H (1995) Carbohydr Res 271:217
67. Unverzagt C, Kunz H, Paulson JC (1990) J Am Chem Soc 112:9308
68. Wong CH, Halcomb RL, Ichikawa Y, Kajimoto T (1995) Angew Chem Int Ed Engl 34:412
69. Salmon S, Hudson SM (1997) J Macromol Sci R M C C37:199
70. Mizuno K, Kobayashi E, Tachibana M, Kawasaki T, Fujimura T, Funane K, Kobayashi M, Baba T (2001) Plant Cell Physiol 42:349

71. Mizuno K (1994) Plant Cell Physiol 35:1149
72. Saxena IM, Brown RM, Fevre M, Geremia RA, Henrissat B (1995) J Bacteriol 177:1419
73. Nelson DL, Cox MM (2008) Lehninger principles of biochemistry, 5th edn. W.H. Freeman, New York
74. Yernool DA, McCarthy JK, Eveleigh DE, Bok JD (2000) J Bacteriol 182:5172
75. Sheth K, Alexande JK (1969) J Biol Chem 244:457
76. Reichenbecher M, Lottspeich F, Bronnenmeier K (1997) Eur J Biochem 247:262
77. Kawaguchi T, Ikeuchi Y, Tsutsumi N, Kan A, Sumitani JI, Arai M (1998) J Ferment Bioeng 85:144
78. Alexander JK (1972) Vol. 28
79. Ziegast G, Pfannemuller B (1987) Carbohydr Res 160:185
80. Akpinar O, Penner MH (2008) J Food Agric Environ 6:55
81. Pereira AN, Mobedshahi M, Ladisch MR (1988) Methods Enzymol 160:26
82. Hess K, Dziengel K (1935) Ber Dtsch Chem Ges 68:1594
83. Miller GL, Dean J, Blum R (1960) Arch Biochem Biophys 91:21
84. Wright JD, Power A (1986) J Biotechnol Bioeng Symp 15:511
85. Zhang YHP, Lynd LR (2003) Anal Biochem 322:225
86. Arndt P, Gerdes R, Huschens S, Pyplo-Schnieders J, Redlich H (2005) Cellulose 12:317
87. Zhao Y, Lu WJ, Wang HT (2009) Chem Eng J 150:411
88. Hamacher K, Schmid G, Sahm H, Wandrey C (1985) J Chromatogr 319:311
89. Dickey EE, Wolfrom ML (1949) J Am Chem Soc 71:825
90. Wolfrom ML, Dacons JC (1952) J Am Chem Soc 74:5331
91. Wolfrom ML, Thompson A (1963) Methods Carbohydr Chem 3:143
92. Kaustinen HM, Kaustinen OA, Swenson HA (1969) Carbohydr Res 11:267
93. Frith WC (1963) Tappi 46:739
94. Zechmeister L, Toth G (1931) Ber Dtsch Chem Ges 64:854
95. Jermyn MA (1957) Aust J Chem 10:55
96. Miller GL (1960) Anal Biochem 1:133
97. Miller GL (1963) Methods Carbohydr Chem 3:134
98. Huebner A, Ladisch MR, Tsao GT (1978) Biotechnol Bioeng 20:1669
99. Moiseev YV, Khalturinskii NA, Zaikov GE (1976) Carbohydr Res 51:39
100. Isogai T, Yanagisawa M, Isogai A (2008) Cellulose 15:815
101. Hakansson H, Ahlgren P (2005) Cellulose 12:177
102. Klemm D, Philipp B, Heinze T, Heinze U, Wagenknecht W (1998) Comprehensive cellulose chemistry, vol 1, Fundamentals and analytical methods. Wiley-VCH, Weinheim
103. Saeman JF, Moore WE, Millett MA (1963) Methods Carbohydr Chem 3:54
104. Kim JS, Lee YY, Torget RW (2001) Appl Biochem Biotechnol 91–3:331
105. Harmer MA, Fan A, Liauw A, Kumar RK (2009) Chem Commun 2009(43):6610. doi: 10.1039/b916048e
106. Kupiainen L, Ahola J, Tanskanen J (2010) Ind Eng Chem Res 49:8444
107. Mosier NS, Sarikaya A, Ladisch CM, Ladisch MR (2001) Biotechnol Prog 17:474
108. Vom Stein T, Grande P, Sibilla F, Commandeur U, Fischer R, Leitner W, Dominguez DMP (2010) Green Chem 12:1844
109. Amarasekara AS, Wiredu B (2012) Appl Catal A Gen 417:259
110. Arndt P, Bockholt K, Gerdes R, Huschens S, Pyplo J, Redlich H, Samm K (2003) Cellulose 10:75
111. Saka S, Ueno T (1999) Cellulose 6:177
112. Ogihara Y, Smith RL, Inomata H, Arai K (2005) Cellulose 12:595
113. Sasaki M, Kabyemela B, Malaluan R, Hirose S, Takeda N, Adschiri T, Arai K (1998) J Supercrit Fluid 13:261
114. Sasaki M, Fang Z, Fukushima Y, Adschiri T, Arai K (2000) Ind Eng Chem Res 39:2883
115. Ehara K, Saka S (2002) Cellulose 9:301
116. Jin FM, Zhou ZY, Enomoto H, Moriya T, Higashijima H (2004) Chem Lett 33:126

117. Griebl A, Lange T, Weber H, Milacher W, Sixta H (2006) Macromol Symp 232:107
118. Zhang YHP, Lynd LR (2004) Biotechnol Bioeng 88:797
119. Reese ET, Mandels M (1963) Methods Carbohydr Chem 3:139
120. Reese ET (1976) Biotechnol Bioeng Symp 6:9
121. Andersen N, Johansen KS, Michelsen M, Stenby EH, Krogh KBRM, Olsson L (2008) Enzyme Microb Technol 42:362
122. Wang M, Li Z, Fang X, Wang L, Qu Y (2012) Adv Biochem Eng Biotechnol 128:1
123. Rydlund A, Dahlman O (1997) Carbohydr Res 300:95
124. Schmid G, Biselli M, Wandrey C (1988) Anal Biochem 175:573
125. Schmid G (1988) Methods Enzymol 160:38
126. Churms SC (1996) J Chromatogr A 720:151
127. John M, Trenel G, Dellweg H (1969) J Chromatogr 42:476
128. Deery MJ, Stimson E, Chappell CG (2001) Rapid Commun Mass Spectrom 15:2273
129. Sabbagh NK, Fagerson IS (1976) J Chromatogr 120:55
130. Akpinar O, McGorrin RJ, Penner MH (2004) J Agric Food Chem 52:4144
131. Berthod A, Chang SSC, Kullman JPS, Armstrong DW (1998) Talanta 47:1001
132. Simms PJ, Haines RM, Hicks KB (1993) J Chromatogr 648:131
133. Ladisch MR, Huebner AL, Tsao GT (1978) J Chromatogr 147:185
134. Corradini C, Cavazza A, Bignardi C (2012) Int J Carbohydr Chem 2012:487564. doi: 10.1155/2012/487564
135. Weith HL, Wiebers JL, Gilham PT (1970) Biochemistry 9:4396
136. Liu X-C, Scouten WH (2000) Methods Mol Biol 147:119
137. Verhaar LAT, Kuster BFM, Claessens HA (1984) J Chromatogr 284:1
138. Cheetham NWH, Sirimanne P, Day WR (1981) J Chromatogr 207:439
139. Brons C, Olieman C (1983) J Chromatogr 259:79
140. Rydlund A, Dahlman O (1996) J Chromatogr A 738:129
141. Sartori J, Potthast A, Ecker A, Sixta H, Rosenau T, Kosma P (2003) Carbohydr Res 338:1209
142. Hilz H, de Jong LE, Kabel MA, Schols HA, Voragen AGJ (2006) J Chromatogr A 1133:275
143. Sartori J, Potthast A, Rosenau T, Hofinger A, Sixta H, Kosma P (2004) Holzforschung 58:588
144. Flugge LA, Blank JT, Petillo PA (1999) J Am Chem Soc 121:7228
145. Mischnick P (2012) Adv Polym Sci 248:105
146. Hagel L, Janson JC (1992) J Chromatogr Libr 51A:A267
147. Goso Y, Hotta K (1990) Anal Biochem 188:181
148. Naohara J, Manabe M (1992) J Chromatogr 603:139
149. Churms SC (1996) J Chromatogr A 720:75
150. Rasmussen LE, Meyer AS (2010) J Agric Food Chem 58:762
151. Alpert AJ (1990) J Chromatogr 499:177
152. Armstrong DW, Jin HL (1989) J Chromatogr 462:219
153. Clement A, Yong D, Brechet C (1992) J Liq Chromatogr 15:805
154. Jupille T, Gray M, Black B, Gould M (1981) Am Lab 13:80
155. Ladisch MR, Tsao GT (1978) J Chromatogr 166:85
156. Bonn G, Pecina R, Burtscher E, Bobleter O (1984) J Chromatogr 287:215
157. Hicks KB, Hotchkiss AT, Sasaki K, Irwin PL, Doner LW, Nagahashi G, Haines RM (1994) Carbohydr Polym 25:305
158. Pereira AN, Kohlmann KL, Ladisch MR (1990) Biomass 23:307
159. Hughes S, Johnson DC (1981) Anal Chim Acta 132:11

Adv Polym Sci (2016) 271: 93–114
DOI: 10.1007/12_2015_321

Published online: 10 July 2015

Deuterium and Cellulose: A Comprehensive Review

David Reishofer and Stefan Spirk

Abstract This contribution summarizes achievements in the understanding of cellulose accessibility, structure, and function with a particular focus on its interactions with deuteration. This review is the first to explicitly devote a discussion to deuteration of cellulose and highlights remarkable new findings in cellulose research as a result of the development of new experimental approaches, from simple weighing of deuterated samples to sophisticated techniques such as small angle neutron scattering and ^{2}H-NMR spectroscopy.

Keywords Accessibility · Cellulose · Crystallinity · Deuteration · Infrared spectroscopy

Contents

D. Reishofer and S. Spirk (✉)
Institute for the Chemistry and Technology of Materials, Graz University of Technology, Graz, Austria
e-mail: stefan.spirk@tugraz.at

1 Initial Efforts in Cellulose Deuteration

The first report on deuteration experiments with cellulose dates back to the early 1930s when Bonhoeffer [1] investigated the reaction of heavy water and cellulose. More than a polymer scientist, Bonhoeffer can be considered an electrochemist who during his career studied processes occurring at electrode interfaces. It is not surprising that he was not very interested in the structural details and arrangements of cellulose but rather in the (electro)chemical behavior and reactivity of D_2O itself, particularly its interaction with platinum electrodes. His experiments did not address the understanding of the polymeric structure of cellulose, determined by Staudinger some years before in 1920 [2]. On the basis of viscosity measurements, Staudinger found the supramolecular structure of cellulose to be a linear arrangement of the polymeric molecule. Soon after Staudinger's discovery, the amorphous-crystalline nature of cellulose was investigated by means of electron diffraction and X-ray scattering experiments. These methods prompted discussions on the potential differences in reactivity of crystalline and amorphous domains and the methods to be used for such explorations. One of the first attempts to measure reactivity differences was made by Goldfinger et al. [3], who showed that there are two rate constants in the course of oxidation of various cellulose samples with periodate solutions. The rate constants differed significantly, and the faster of these has been determined to take place preferentially in the amorphous domains, whereas the second is related to the crystalline domains. In the second attempt to investigate reactivity differences, thallous ethylate was used to treat cellulose in a variety of solvents. As it turned out, only a fraction of the hydroxyl groups of cellulose were converted into the thallium salt while the others remained unchanged. Besides these two reactions, a third oxidative degradation method was employed to analyze the rate constant of CO_2 evolution; it was observed that rapid linear degradation was followed by a much slower reaction until stable equilibrium was reached. As we know today, the plateau value they observed is connected to the leveling-off degree of polymerization (LODP), which is a very important characteristic in the course of cellulose nanocrystal preparation.

However, all the methods employed thus far were laborious, the analyses were pretty complicated, and most importantly they were destructive. Champetier and Villard [4] were the first to recognize the potential importance of Bonhoeffer's observation and performed the first detailed studies on exchange reactions of cellulose. However, one of the problems in their experimental setup was the exposure of samples to ambient atmosphere during analyses, which affected interpretation of the obtained results because of rehydrogenation of the samples. Analyses of samples at that time were performed using gravimetry, taking advantage of the difference in density between D_2O and H_2O; the accuracy was in the range of 5%. It took another 10 years until Frillette et al. [5] revived the idea of employing D_2O for the characterization of cellulosic samples. They used a variety of different sources such as cotton, cotton linters, viscose rayon fibers, and wood fibers and studied the exchange reaction as a function of the pH value and, to some extent, the

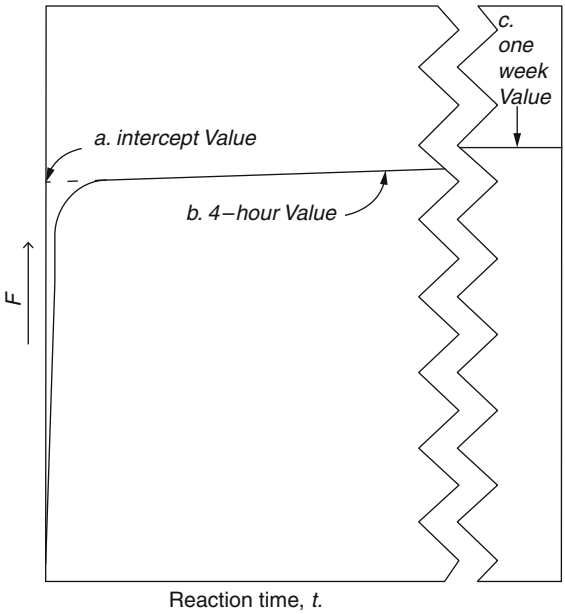

Fig. 1 Generalized reaction curve and characterization values in the deuteration of cellulose samples made by Mark and colleagues: *a* intercept of the horizontal portion of the curve extrapolated to zero time, *b* at 4 h, and *c* at 1 week [5]

temperature. In order to avoid ambiguous results, they took great care to prevent the samples from rehydrogenation by carrying out the experiments in a dry box. For all samples, very similar curves were obtained that featured a fast exchange at the beginning of the reaction (ca. 1 h), followed by a slow second phase that lasted several hours until a stable plateau was reached. Because the curves looked very similar in shape, the authors tried to extract information that could be potentially useful for further characterization of the cellulose samples, in particular the degree of crystallinity. This was done by extrapolating the plateau part of the curve to zero time, yielding the "*a*" value. Other values used were the "*b*" value (degree of exchange after 4 h) and the "*c*" value (exchange after 1 week) (Fig. 1).

The authors already had a good idea of the supramolecular structure of cellulose, even several years before the Fringe model was introduced. They proposed that the amorphous domains of cellulose were easily accessible to water whereas the crystalline domains were not. From their obtained data, they made a distinction between the two domains by considering the role of surface hydroxyl groups. They realized that the crystalline domains are not large in diameter; therefore, the surface hydroxyls account for a high percentage of the total volume of a crystallite, as expressed by Eq. (1):

$$F' = \sigma * \alpha + (100 - \alpha) \quad \text{and} \quad \alpha = \frac{100 - F'}{1 - \sigma} \tag{1}$$

where F' is the percentage of all the hydroxyls that react rapidly with D_2O, σ corresponds to the available surface hydroxyls of the crystalline parts, and α is the

Table 1 Available data on the degree of crystallinity for several samples in 1956, as determined by gravimetric analyses

Sample	Accessibility to liquid D_2O (%)					Amorphous material (%)
	Champetier and Villard (1938) [4]	Mark (1948) [5]	Rowen and Plyler (1950) [7]	Mann and Marrinan (1955) [8]		
				First deuteration	Second deuteration	
Viscose		81		83	78	75
Viscose treated with 18% NaOH				74	70	66
Cellophane			<50			
Cellulose from acetate			<50			
Bacterial cellulose				39		30
Cotton linters	100	61				

resulting crystallinity of the sample. At this time the first reports on the dimensions of crystallites were already available from Mark and Kratky [6], whose work indicated edge values between 50 and 100 Å. The authors were aware that wrong assumptions of σ would lead to some deviation; however, the agreement between their obtained degrees of crystallinity and those available nowadays is quite impressive (Table 1).

The differences observed using the Nickelson method [9], described above, were explained by the fact that it depolymerizes cellulose, leading to more mobile chains capable of rearrangement to form laterally ordered structures that undergo recrystallization. However, this was a misconception because the method turned out to be unreliable. Additionally, it was thought that prolonged acid treatment of cellulose, as first described by Ingersol in 1946 [9], induced crystallization. This conclusion was based on Ingersoll's observation of significant sharpening of the X-ray patterns after treatment, possibly the first indirect observation of cellulose nanocrystals.

2 Infrared Efforts

The next breakthrough in the use of D_2O exchange involved the use of infrared (IR) spectroscopy, giving insight into the hydrogen bonding pattern and providing an elegant way to quantify the accessibility and subsequent estimation of crystallinity. Rowan and Plyler [7] employed this technique for the first time on cellophane and regenerated cellulose obtained from cellulose triacetate using regeneration with NaOD. They found very low deuteration degrees, even after treatment in liquid D_2O for several days at 52°C. However, Almin [10] later showed in detailed studies

that the samples were rehydrogenated before analysis, giving rise to low deuteration degrees.

Later, it was shown that the shape of the absorption band can be exploited to directly distinguish between amorphous and crystalline domains during measurement. Mann and Marrinan investigated different aspects of deuteration in a series of publications [8, 11, 12]. The first focused on gas and liquid phase deuteration of several cellulose samples (viscose, bacterial cellulose) using in situ IR spectroscopy. Similar to the observations made by Frillette et al. [5], after 1 h the H/D exchange slowed down and was accompanied by the replacement of a broad OH band with four distinct bands in the area assigned to crystalline cellulose I. There were also bands at ca 2,500 cm^{-1}, corresponding to OD stretching vibrations. Even though the reaction speed was faster in liquid-based systems, deuteration using D_2O vapor yielded the same IR spectra after 4 h. However, the authors noticed distinct differences between deuteration of the viscose sample and the sample derived from bacterial cellulose. Whereas viscose readily exchanged, the bacterial cellulose was deuterated to a much lesser extent. Interestingly, rehydrogenation without drying revealed another difference, namely so-called resistant OD groups, which were exclusively observed in samples of bacterial cellulose and assigned to hydroxyls on the crystal surfaces. As found in Plyler's experiments [7], drying the sample after the D_2O exchange leads to irreversible incorporation of deuterium into the supramolecular structure of viscose. Even extensive exposure to liquid H_2O could not rehydrogenate OD groups. These results clearly indicate that incorporation of water into the crystalline domains of cellulose does not take place. Although this question had been solved unambiguously for cellulose I with X-ray data [13], for cellulose II the situation was unclear because X-ray experiments showed a widening of the (101) reflection during wetting with water, which was interpreted as the formation of stoichiometrically formed hydrates [14]. The authors argued that that the resistant OD groups are located in apparently perfect crystalline domains (sharp bands), and that their resistance to rehydrogenation suggests that their formation cannot take place by penetration into the lattice [11].

Because it was now possible to accurately estimate the amount of hydroxyl exchange, it was possible to determine cellulose accessibly with much higher precision; the same was true for the crystallinity as several assumptions were avoided (see discussion below). The imprecisions were recognized as far as the equilibrium constant K of the exchange reaction (Eq. 2):

$$K = \frac{D_{\mathrm{acc}}/H_{\mathrm{acc}}}{D_{\mathrm{H_2O}}/H_{\mathrm{H_2O}}} = 1 \quad \text{for the equilibrium} \quad \mathrm{HOD} + \mathrm{ROH} \leftrightarrow \mathrm{ROD} + \mathrm{ROH} \quad (2)$$

Mark and coworkers [5] stated that $K = 1$, which was not the case because the zero-point energies are changed by the H/D exchange (at that time K values reported were between 1.04 and 1.10, depending on which hydroxyls were exchanged) [15]. The zero-point energy differences of R–OH and R–OD are connected to the difference in vibrational energies of their ground states and can be, in principle, calculated from their frequencies of vibration. Because the hydroxyls have a wide

Table 2 Percentage of amorphous OH groups obtained by FT-IR spectroscopy [11]

Sample	$\frac{\log(I_0/I)_{OD}}{\log(I_0/I)_{OH}}$	Amorphous OH (%)
Saponified acetate	3.35	75
Viscose oriented	3.18	74
Viscose unoriented	3.10	73.5
Viscose hydrolyzed in H_2SO_4	2.42	68.5
Precipitated cellulose	2.34	68
Mercerized bacterial cellulose	2.28	67
Viscose treated with NaOH	2.20	66.5
Fortisan micelles	0.96	46.5 ± 5
Bacterial cellulose	–	30
Cotton micelles	–	31 ± 5

range of vibrational frequencies, a wide range of K values for these and the overall equilibrium could only be obtained by performing the exchange with extremely high mole fractions of D_2O. Mann and Marrinan proved a difference of about 30–40% between the crystallinity and the accessibility of cellulose for viscose and bacterial cellulose [8]. They recognized that under the condition that all OD groups in the crystalline domains are located on the surface (and not at imperfections in the lattice), it is possible to estimate crystallite size using their approach.

The use of IR spectroscopy and a related definition of crystallinity were introduced by the same authors by employing the ratio of the intensities at a given wavelength for OD and OH, corrected by the extinction coefficient according to the Beer's law (Eq. 3 and Table 2):

$$\log\left(\frac{I_0}{I}\right)_{\lambda} = k_{\lambda} * c * l \tag{3}$$

where I_0 is the intensity of the radiation incident on the film, I the intensity of the transmitted radiation, c the concentration of material absorbing at wavelength λ expressed as a mole fraction, l the path length of the radiation through the film, and k the extinction coefficient per unit mole fraction. As a result, the crystallinities of several cellulose I and II materials (cotton, bacterial cellulose, saponified acetate, viscose oriented/unoriented/hydrolyzed, precipitated cellulose, mercerized bacterial cellulose) were determined and compared with previously determined results, derived from X-ray studies. The same authors were aware that results should be different, because methods based on scattering do not give reasonable results for crystallite surfaces. In all cases, crystallinities lower than those obtained by X-ray were obtained; however, the relative ratios were similar.

Further progress in IR spectroscopy was made by Tsuboi [16], who investigated the effect of polarization (i.e., the orientation of cellulose molecules in response to deuteration). He obtained spectra for ramie cellulose swollen in NaOD that allowed him to assign bands in the OD regime to certain vibrations and to correlate them to

the corresponding OH vibration, most of which are parallel to the fiber axis (Fig. 2). As a result, Tsuboi found that the ratio of νOD/νOH was always between 1.33 and 1.35 (Table 3).

Although Tsuboi was not able to assign which hydroxyls are oriented along the fiber axis and which are perpendicularly oriented, the results gave the first insight into the preferred hydrogen bonding pattern in cellulose.

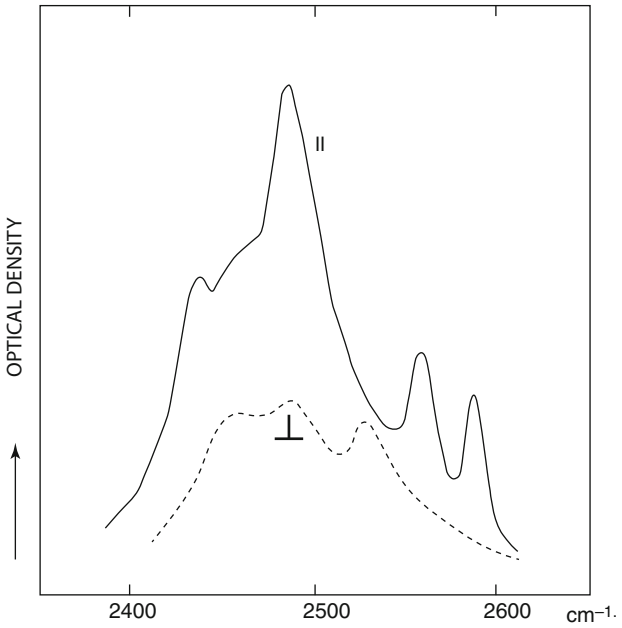

Fig. 2 Infrared spectrum of NaOD-swollen ramie fiber in the O–D stretching region: || electric vector parallel to fiber axis, ⊥ electric vector perpendicular to fiber axis [16]

Table 3 OD band shifts compared with OH band shifts

OD bands observed by Tsuboi [16] (cm^{-1})	OH bands observed by Marrinan and Mann [11] (cm^{-1})		Frequency ratio	Dichroism[a]
	Cellulose I	Cellulose II		
2,585	–	3,484	1.35	||
2,551	–	3,444	1.35	||
2,527	3,410	–	1.35	⊥
2,484	3,350	–	1.35	||
2,462	3,288	–	1.34	||
2,440	3,250	–	1.33	||

[a]|| parallel, ⊥ perpendicular

A rather exotic method was used some time after Tsuboi's report, namely a combination of D_2O and T_2O to determine the accessibility of cellulosic samples [17, 18]. In fact, after incorporation of T_2O the decay of radioactivity over time could be exploited to determine the accessibility of cellulose and other biopolymers. The results the authors obtained were in good agreement with studies of deuterated samples, which was necessary in order to exclude roughness effects that could influence the radioactivity measurements. Furthermore, the H/D and H/T exchange was studied in detail [19] with regard to supramolecular arrangements. As a result, it was shown that heating cellulose leads to a rearrangement of the molecules and results in partial interchange of accessible and inaccessible regions if a variety of drying/wetting procedures are performed. The authors argued that heating can cause mechanical stresses that lead to disruption of crystallites, followed by recrystallization to form new crystalline domains.

A complementary, interesting approach was carried out by Okajima and Kai, who investigated the H/D exchange behavior of native and regenerated cellulose from *Valonia* before and after heat treatment [20]. According to the early definitions of Frilette and coworkers [5], they analyzed the deuteration curves according to the different phases (*a*, *b*, *c*) (see Fig. 1). For native samples, a fast exchange was observed, which corresponded to about 20% of exchange, whereas the decay was down to ca 75% for the mercerized cellulose. Deuteration of the *a* region was considered to occur directly by exchange with diffused D_2O molecules, but this was not yet clear for the *b* and *c* regions. Because of the relation between the amount of OD (OH) and the logarithmic integrated time *t* it was clear that no dominant role of the diffusion of D_2O existed for the *b* region.

3 Scattering and Diffraction

The next milestone in the investigation of deuterated cellulose was the use of neutron scattering. Compared with hydrogen, deuterium is a very good isotope for such studies because it provides a high scattering contrast and provides a way to stain the amorphous domains of cellulose, and (as shown later) to stain the crystalline domains.

Fischer and colleagues were the first to report the long spacing in cellulose [21], which had been postulated but not measured because the electron density differences between the amorphous and the crystalline domains in cellulosic fibers were too small for elucidation using small angle X-ray scattering (SAXS) or small angle neutron scattering (SANS). For this purpose, Fischer employed gas phase deuteration, which mainly takes place in the amorphous domains. As was the case in other reports, the exchange was complete after a short time (30 min) and no increase in scattering intensity was observed after prolonged exposure times. Meridional long spacing was determined for the deuterated samples (16.5 and 19.3 nm for Fortisan and rayon) whereas native cellulose samples (ramie) did not give any result. The authors explained this observation by diffuse scattering, which plays a major role if

the long spacing reach values in the range of 50–70 nm, as found for such materials by electron microscopy. In addition, the experiments gave the cross-section of crystalline arrays in regenerated cellulose (3.4 nm), which compared well with data available from other sources such as electron microscopy (3.5 nm). The results were superior to SAXS data (5.0 nm) available at that time by evaluation and data acquisition at large angles. In addition, a large monodisperse component was identified in the range of 9.8 nm, which was assigned to bundles of eight elementary fibrils. Besides insights into dimensions, these experiments also shed light on how voids and pores could be organized. As a result of the presence of continuous equatorial scattering (which leads to elongated scattering patterns), the authors concluded that elongated microvoids were present in the sample.

After Fischer's findings, there were only isolated reports on deuterated cellulose until the end of the 1990s when Nishiyama, Isogai, Langan, and Chanzy, to name some contributors, revisited the topic. The motivation for related work was probably driven by discoveries some years before when it was demonstrated via ^{13}C solid state NMR spectroscopy [22] that the earlier reported crystal structure of *Valonia* cellulose was imprecise. This was because it was not taken into account that *Valonia* cellulose is composed of cellulose I_α and I_β [23]. The main challenge in the determination of crystal structures of native cellulose is that fibers consist of microcrystallites that are preferentially aligned along the fiber axis, but employ a random orientation. As a consequence, reflection spots tend to overlap in diffractograms as a result of cylindrical averaging, making the separation of distinct reflections from different phases doubtful. Progress has been made by electron microscopy of individual cellulose microcrystals, resulting in the unambiguous identification of two distinct crystal phases corresponding to cellulose I_α and I_β [24]. In a first series of experiments, Nishiyama and coworkers investigated a series of highly crystalline cellulose samples (*Cladophora*, I_α and I_β; *Halocynthia*, exclusively I_β) [25] and mercerized cellulose. They compared the neutron diffraction data before and after deuteration and obtained resolutions of 0.9 (native celluloses) and 1.2 Å (mercerized cellulose). Their report was accompanied by new investigations to elucidate whether deuterium can be incorporated into the crystal structure of these materials [17, 26]. Substrates of choice included acid-hydrolyzed microcrystals that had been processed into oriented films. It was demonstrated by X-ray experiments using synchrotron radiation that exposure to elevated temperature (210°C/30 min) leads to intracrystalline H/D exchange without converting cellulose I_β to I_α. In addition to scattering data, the polarized FT-IR proved that there was no significant amount of OH groups present in the samples. These OH groups nearly quantitatively converted to OD groups that, in turn, were assigned very precisely. On the basis of these results, it was subsequently possible to determine the precise crystal structures and to locate the hydrogen bonding system in cellulose I_β (*Halocynthia*) [27] and later on in I_α (*Glaucocystis*) [28, 29]. A major contribution in these studies was the excellent quality of data from both X-ray and neutron scattering experiments. For example, the use of deuterated samples allowed the precise determination of the atomic coordinates and the localization, with atomic

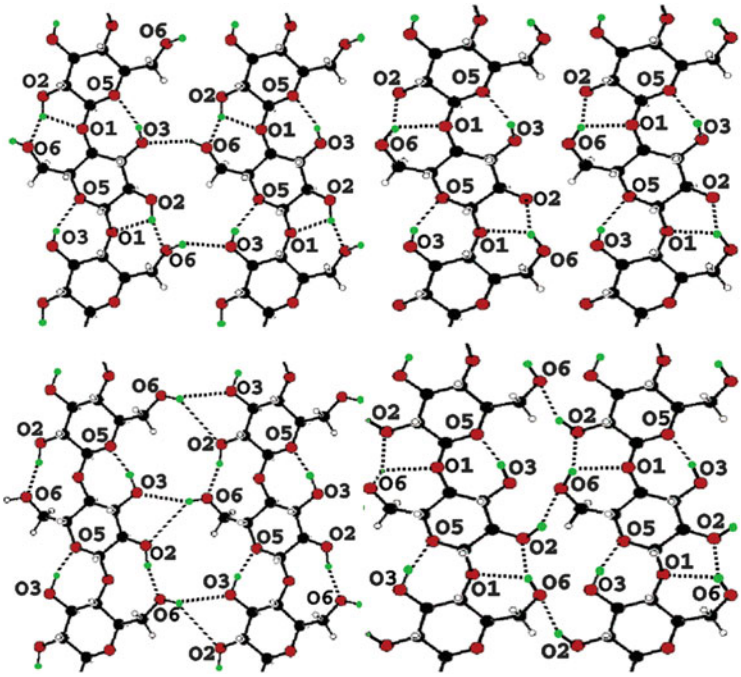

Fig. 3 Hydrogen bonds in the origin (*top*) and center (*bottom*) sheets of cellulose I_β. Carbon, oxygen, hydrogen, and deuterium atoms are colored *black*, *red*, *white*, and *green*, respectively. Hydrogen bonds are represented by *dotted lines*. Only the oxygen atoms involved in hydrogen-bonding have been labeled for clarity. Deuterium atoms D2oA, D3o, and D6oA are included in the *top left view* (O2o–D2oA···O6o, O2o–D2oA···O1o, O3o–D3o···O5o, O6o–D6oA···O3o); D3o and D6oB in the *top right view* (O3o–D3o···O5o, O6o–D6oB···O2o, O6o–D6oB···O1o); D2cA, D3c, and D6cA in the *bottom left view* (O2c–D2cA···O6c, O3c–D3c···O5c, O6c–D6cA···O3c, O6c–D6cA···O2c); and D2cB, D3c, and D6cB in the *bottom right view* (O2c–D2cB···O6c, O3c–D3c···O5c, O6c–D6cB···O2c, O6c–D6cb···O1c) [27]

resolution, of the hydrogen bonded network in Fourier difference maps for both the deuterated and hydrogenated data. The resulting hydrogen bonding pattern and the geometric details are given in Fig. 3 and Table 4 for cellulose I_β. The resulting hydrogen bonding pattern for cellulose I_α is given in Table 5.

It was demonstrated that the intrasheet hydrogen bonding involving O2 and O6 donors is disordered over two possible sites in both cellulose I_α and I_β. Most of the hydrogen bonds in these networks are either strong (D···A: 2.2–2.5 Å) or medium strong (2.5–3.2 Å) according to Steiner [30] and Jeffrey [31] (compare Tables 4 and 5). The situation is complicated because there are at least two different networks, probably in dynamic equilibrium (see Fig. 3). In both networks, the intramolecular O3–H3···O5 hydrogen bonds are relatively strong in both I_α and I_β (H···A: 1.966 and 2.072 Å) featuring in addition DHA angles close to 180° (162.23 and 163.94°). In network I, the intramolecular O2–H2···O6 bonds are quite different (H···A: 1.689

Table 4 Hydrogen bonding parameters for cellulose I_β determined by Nishiyama et al. [27]

D–H	d(D–H)	d(H···A)	∠DHA	d(D··A)	A
O2o–D2oA	0.977	1.832	158.72	2.765	O6o [$-x$, $-y$, $z+½$]
O2o–D2oA	0.977	2.304	110.28	2.797	O1o [$-x$, $-y$, $z+½$]
O3o–D3o	0.979	1.966	137.08	2.764	O5o [$-x$, $-y$, $z-½$]
O6o–D6oA	0.979	2.040	144.26	2.892	O3o [x, $y+1$, z]
O6o–D6oB	0.974	1.876	150.23	2.765	O2o [$-x$, $-y$, $z+½$]
O6o–D6oB	0.974	2.152	121.59	2.789	O1o
O2c–D2cA	0.982	1.904	165.12	2.865	O6c [$-x+1$, $-y+1$, $z+½$]
O2c–D2cA	0.978	2.440	135.44	3.211	O6c [x, $y-1$, z]
O3c–D3c	0.983	1.752	162.23	2.705	O5c [$-x+1$, $-y+1$, $z-½$]
O6o–D6cA	0.985	1.779	156.61	2.711	O3c [x, $y+1$, z]
O6o–D6cA	0.985	2.544	124.98	3.211	O2c [x, $y+1$, z]
O6o–D6cB	0.975	1.967	152.06	2.865	O2c [$-x+1$, $-y+1$, $z-½$]
O6o–D6cB	0.975	2.243	123.21	2.894	O1c

Table 5 Hydrogen bonding parameters for cellulose I_α determined by Nishiyama et al. [28]

D–H	d(D–H)	d(H··A)	∠DHA	d(D··A)	A
O3d–D3d	0.989	1.954	163.94	2.918	O5u [$x-1$, y, z]
O3d–D3d	0.989	2.386	119.05	2.994	O1u [$x-1$, y, z]
O2d–D2dA	0.974	1.689	133.83	2.465	O6u
O2d–D2dB	0.983	2.283	116.94	2.866	O3d
O2d–D2dB	0.983	2.679	157.47	3.606	O6d [x, $y-1$, $z+1$]
O2u–D2uA	0.980	1.763	127.07	2.480	O6d [$x+1$, y, z]
O2u–D2uA	0.980	2.181	118.44	2.784	O1u
O2u–D2uB	0.985	2.357	110.37	2.853	O3u
O2u–D2uB	0.985	3.019	122.21	3.641	O6u [x, $y+1$, $z-1$]
O6d–D6dA	0.977	2.176	122.20	2.821	O3d [x, $y+1$, $z-1$]
O6d–D6dA	0.977	2.791	141.32	3.606	O2d [x, $y+1$, $z-1$]
O6d–D6dB	0.976	1.894	150.36	2.785	O1u [$x-1$, y, z]
O6d–D6dB	0.976	1.967	110.23	2.480	O2u [$x-1$, y, z]
O6u–D6uA	0.983	1.853	153.99	2.770	O3u [x, $y-1$, $z-1$]
O6u–D6uA	0.983	2.881	134.82	3.641	O2u [x, $y-1$, $z-1$]
O6u–D6uB	0.976	1.956	145.03	2.812	O1d
O3u–D3u	0.976	2.072	137.59	2.868	O5d

and 1.763 Å for I_α; 1.832 and 1.904 Å for I_β) as well as the O6–H6···O3 interchain bonds (H···A: 1.853 and 2.176 Å for I_α; 1.779 and 2.040 Å for I_β). In contrast, in network II there is only one intramolecular hydrogen bond for I_α (O6–H6···O2) whereas there are two in I_β. For the interchain hydrogen bond O2–H2···O6, the situation is opposite. For all hydrogen bonds, the distances are shorter (H···A are 2.679, 3.019, and 1.967 Å for I_α; 1.876, 2.440, and 1.967 Å for I_β).

The use of deuteration in cellulose II combined with neutron diffraction allowed the distinction between two conformational models (A and B). Model A features

equivalent backbone conformations, having different conformations at the hydroxymethyl group (tg and gt, respectively). Model B (cellotetraose-like) has different backbone conformations and the hydroxymethyl group always has nearly the same conformation (Fig. 4). Langan and coworkers showed that model B is correct and identified the hydrogen bonding pattern of cellulose II. There are intermolecular hydrogen bonds between the origin and center chains involving O2c (D) and O2o (A) and O6o (D) that form a four-center hydrogen bond, with O6c, O5c, and O3c as potential acceptors. There is a rather strong intramolecular hydrogen bond between O3 and O5 (O3o–O5o: 2.66 Å and O3c–O5c: 2.73 Å) and a much weaker bond between O3 and O6 (O3o–O6o: 3.31 Å and O3c–O6c: 3.22 Å). Both values for these hydrogen bonds are very similar to those reported by Gessler et al. [32], who studied hydrogen bonding in D-cellotetraose (compare O3o–O5o: 2.84 Å, O3c–O5c: 2.91 Å, O3o–O6o: 3.32 Å, and O3c–O6c: 3.09 Å). A summary of hydrogen bonding parameters is given in Table 6.

Although cellulose I and II are the most prominent polymorphs, others are also possible. In a similar approach to that used for cellulose I and II, deuterated cellulose III [33] was produced by employing ND_3 instead of NH_3 for conversion. A comparison of the different polymorphs is depicted in Fig. 5. It is clear that, compared with cellulose I_β, cellulose III has a chain reorientation that significantly reduces the distance between neighboring chains in a sheet (8.20–7.85 Å) and increases sheet separation (from 3.87 to 4.29 Å). Other differences between cellulose I_β and cellulose III_I include the number of weak intersheets in I_β and the tight packing of I_β sheets. Combination of the difference in sheet separation and the nature of intersheet stacking interactions probably contributes to the enhanced accessibility of cellulose III_I for polar guest molecules.

Besides the crystal structures of cellulose, the distribution of the I_α and I_β polymorphs in the elementary fibrils is of great interest from a biological point of view. Horikawa and Sugiyama developed an elegant technique using FT-IR that allows localization of I_α and I_β domains in a single microcrystallite [34]. Their approach converted part of cellulose I_α from *Glaucocystis* into the I_β form by heating to 255°C for 30 min, leading to only partial interconversion. The resulting material included a I_β skin and a I_α core. Afterwards, the procedure was completed by intracrystalline deuteration, as described above. For the sake of comparison, other samples (*Cladophora* and *Valonia*) that contain a large portion of I_β were subjected to intracrystalline deuteration [35]. After rehydrogenation at elevated temperatures, the I_α/I_β localization was predicted according to the H/D exchange rate (faster for the I_β skin) and supported by electron microdiffraction experiments. The authors expected to observe a similar behavior for the native celluloses; however, the H/D exchange rates were identical for the two crystalline phases, meaning that native celluloses do not exhibit a skin–core structure.

Other approaches used neutron scattering of commercial samples, including TENCEL fibers [36] and polysaccharide films [37], but were not aimed at unveiling a deep understanding of cellulose structure and reactivity.

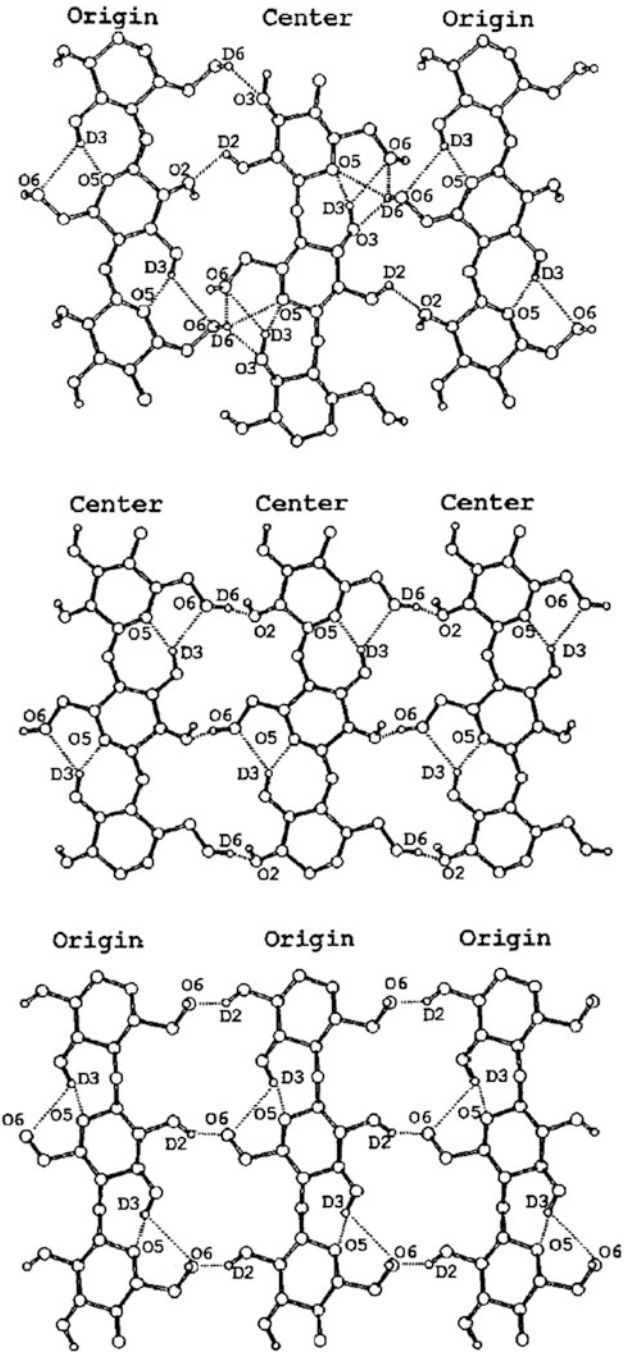

Fig. 4 Hydrogen bonds in cellulose II. Only atoms involved in hydrogen bonding are labeled. Hydrogen bonds are represented by *dotted lines*. Intermolecular hydrogen bonds are O2–D···O6 in sheets containing only origin molecules and O6–D···O2 in sheets containing only center

Table 6 Hydrogen bonding parameters for cellulose II determined by Langan et al. [29]

D–H	d(D–H)	d(H···A)	∠DHA	d(D···A)	A
O2o–D2oA	0.981	2.015	119.75	2.643	O6c [$-x+1, -y, z+½$]
O2o–D2oA	0.981	2.223	141.49	3.053	O3c [$-x, y-1, z$]
O3o–D3o	0.981	2.489	122.08	3.123	O5c [$-x+1, -y, z+½$]
O6o–D6oA	0.980	1.918	130.45	2.660	O5o [$-x, -y, z-½$]
O6o–D6oB	0.980	2.803	113.07	3.312	O6o [$-x, -y, z-½$]
O6o–D6oB	0.979	1.817	150.67	2.713	O6o [$x-1, y, z$]
O2c–D2cA	0.981	1.784	150.44	2.682	O2c [$x+1, y, z$]
O2c–D2cA	0.980	1.848	148.43	2.731	O5c [$-x+1, -y+1, z+½$]
O3c–D3c	0.980	2.500	130.02	3.219	O6c [$-x+1, -y+1, z+½$]
O6o–D6cA	0.981	2.212	115.84	2.783	O2o [$-x, -y+1, z-½$]

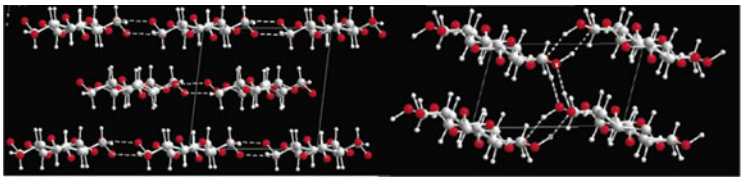

Fig. 5 Projections of the crystal structures of cellulose I_α (*left*) and cellulose III_I (*right*) [33]

4 Current Efforts

Efforts to unravel the crystalline domains of cellulose include those of Kondo and coworkers, who studied the amorphous nature of cellulose. In 1996, they reported a model for amorphous cellulose that featured isotropic hydrogen bonds, whereas some domains exhibited a short-range order via intermolecular hydrogen bonding [38]. However, these interactions are weaker than in crystalline cellulose and lack long-range order. Later, the same authors investigated the deuteration behavior of cast and coagulated cellulose films and calculated 0 and 13.8% crystallinity, respectively, from X-ray diffraction patterns. The amorphous films revealed an interesting behavior in that they did not undergo H/D exchange to a full extent. Although Wadehra [39] and Jeffries [40] had already reported that the materials could probably recrystallize upon D_2O vapor exposure, Kondo and colleagues argued differently. One of their arguments was that, upon recrystallization, the H/D exchange rate changed significantly, as well as the absorption band of the νOH vibrations. Furthermore, the use of different model compounds (methylcelluloses)

Fig. 4 (continued) molecules. In the sheet containing both center and origin molecules there are O6–D···O6 and O2–D···O2 intermolecular hydrogen bonds. The former has minor components involving O5 and O3 as acceptors. Intramolecular hydrogen bonds are O3–D···O5 in each molecule, with a minor component involving O6 as acceptor [29]

allowed the authors to model and determine the possible hydrogen bonding modes of amorphous cellulose [41]. In a subsequent report, the same group employed two-dimensional correlation spectroscopy to characterize amorphous cellulose [42]. They assigned three different noncrystalline domains in the IR spectrum to OH vibrations and were able to distinguish between inter- and intramolecular hydrogen absorption bands. More or less at the same time, inelastic neutron scattering and neutron time-of flight spectroscopy was employed to study this question in more detail [43]. It was shown that the accessible regions can be unambiguously identified with the disordered regions of a specimen, which show universal low frequency dynamic signatures that have a unique response to water molecules [43]. The main result of these studies was that the share of D_2O accessible functional groups in cellulose correlates with disordered domains, whereas the inaccessible groups are assigned to crystalline areas. However, the disordered domains retain a preferential orientation parallel to the microfibril orientation.

Another approach investigated nematically ordered cellulose films, which were obtained by stretching water-swollen, gelatinous cellulose films using a draw ratio of two [44]. As a result, highly oriented films were obtained (crystallinity ca 20%), as shown by high resolution transmission electron microscopy. By using deuteration experiments in combination with polarized IR spectroscopy, Kondo and coworkers showed that the main chains (along the stretching direction) only exhibit a moderate degree of order, whereas the OH groups remained unordered.

After refinement and investigation of the different cellulose crystal structures, revealing the hydrogen bonding pattern in the corresponding polymorphs, the study of cellulose in its native environment (i.e., wood cell walls) became a major focus. In related approaches, the main motivation was to understand the changes that take place during industrial processing steps, namely drying, hydrothermal degradation, and aging, as well as to learn how the cell wall acts in biological systems. Although Tsuchikawa and Siesler had investigated diffusion of D_2O into wood in 2003 [45–47], the first detailed studies on bulk wood were performed by groups in Helsinki in 2010. The same groups used IR spectroscopy to study the influence of drying on the accessibility of fresh wood and never-dried pulp fibers using H/D exchange [48, 49]. The novelty of this work was the fact that changes during drying could be followed in situ (i.e., it was not necessary to process the sample after heat treatment for analysis, which could obviously influence the results). It was found that the behavior of the samples was very similar, particularly in terms of inaccessibility. Therefore, the authors stated that the fundamental mechanisms behind the supramolecular rearrangements in cellulose are qualitatively the same, namely aggregation of microfibrous bundles, which is believed to play a key role in drying of papermaking fibers. In a recent report, the same authors investigated the behavior of fibers during heat treatment [50]. They succeeded in determining the kinetics behind deuteration, allowing them to detect the equilibrium state of accessibility reduction. Furthermore, the effects of pH and temperature were thoroughly studied. Under acidic conditions (pH 3), heat treatment below 100°C caused similar alterations as in wood fibers (reduction by aggregation of microfibrils). Alkaline

treatment (pH 12, $T < 100°C$) led to an equilibrium state of aggregation that originated from either the equilibrium between microfibrils and aggregates or the equilibrium between crystalline and amorphous domains. Based on these results, further details have been investigated by using NaOD for digestion in Kraft processing. It was found that during digestion an irreversible deuteration occurs, which was mainly connected to aggregation of microfibrils caused by heating the wood . The removal of lignin could play a role but this also takes place in other stages of pulping. Therefore, it was suggested that hemicelluloses that are dissolved from the fibers play a crucial role in cellulose microfibril aggregation. Atalla investigated the effects of fiber processing type and compared those that are air-dried to those dried at elevated temperatures [51]. An important finding was that the accessibility, as studied by D_2O exchange, is altered even during air drying, a fact that is often neglected in many studies because drying effects are usually investigated at elevated temperatures. In a related study, Inagaki and coworkers studied the effects of degradation by hydrothermal and aging procedures on crystallite size and microfibril arrangement [52]. Their main interest was to understand how cellulose in old woods (Hinoki wood, in their particular case) crystallized and how various treatments affected the structure over time. XRD and near infrared spectroscopy (NIR) were used, and the different hydroxyl groups from amorphous and crystalline domains, respectively, were well resolved. Mid-infrared has been widely used for analysis of the deuteration process in cellulose. In contrast and despite the possibility to directly distinguish between the amorphous and the crystalline domains, NIR has not been used for this purpose. The reason originates from sample requirements: it must be thick because of the low absorption of cellulose in this region, which is disadvantageous for the investigation of fibers. However, NIR can be exploited for analysis of whole wood samples. Results indicated that hydrothermal treatment leads to an increase in crystallite size, whereas ageing results in smaller crystallites in the microfibrils. On the basis of the data, a morphological model that explains the observed differences was established. Nondegraded wood microfibrils are composed of elementary fibrils, which are glued by hemicelluloses and lignin, whereas in archeological wood these components are depolymerized, oxidized, and finally removed, but the crystalline domains are unaffected in terms of size (2.8 nm). Therefore, gaps are created between the elementary fibrils that, according to the proposed model, are larger than those in native wood (from 0.3 to 0.5 nm). In contrast, the distances between elementary fibrils in hydrothermally altered cellulose are the same as in native cellulose (0.3 nm) whereas the crystallite size increases from 2.8 to 3.3 nm, which is a result of crystallization of amorphous cellulose. In a similar study, “Washi” paper samples were investigated [53]. Washi paper is a very durable form of paper that is mainly used in Japan. The authors were interested in the diffusion of D_2O and the saturation accessibility. They studied archeological papers (AD 1615, AD 1791) and compared their accessibility to D_2O vapor with modern Washi paper (AD 2003). One of their main results was that old papers have much lower accessibility, which probably originates from the beating procedures performed in the past. Beating in combination with oxidative degradation of the hemicelluloses

forms a skin that acts as a diffusion barrier, preventing D_2O penetration into the material.

A different approach was followed by Hofstetter et al. [54] and Sturcova et al. [55], who studied changes in IR spectra upon deuteration during mechanical stress. The main objective was to obtain information on how hydrogen bonding strength is altered during mechanical stress and to provide molecular insights, which are of crucial importance for other fields such as composites. Hofstetter et al. investigated the behavior under dynamic conditions and under a wide range of D_2O vapor pressures, whereas Sturcova et al. mainly focused on the development of a routine under constant mechanical stress. The effects of background fluorescence in Raman spectroscopy and scattering in FT-IR spectra were considered. Changes during mechanical stress were rather small, and interpretation and extraction of bandshifts from complex spectra through background corrections and peak fitting procedures were discussed. As a result, a qualitative description of the dependence of mechanical strain along fiber direction was given. FT-IR absorbance and Raman scattering are dependent on $\cos^2 \alpha$, whereas the strain of the polymer chains varies with $\cos \alpha$, leading to nonlinear effects. Hofstetter et al. investigated oriented sheets from spruce fibers, mounted in a specially designed sample chamber that enabled measurement of IR spectra in parallel and perpendicular modes while (static or dynamic) mechanical analyses were performed. Moreover, the chamber had inlets to vary the D_2O vapor pressure during measurement, which allowed investigation into how the system responded to changes in humidity (Figs. 6 and 7).

The same authors identified several bands, namely the C–O–C bridge (1,160 cm^{-1}), the O5···H3–O3 (3,340 cm^{-1}) and the C–OH bending at 1,435 cm^{-1}; no large differences between high and low humidity conditions were evident. Furthermore, the intensity of the band at 3,230 cm^{-1} (corresponding to the O3–H3···O6 intermolecular hydrogen bonds) slightly increased, meaning that there were rearrangements under mechanical stress. On the other hand, the peak at 3,470 cm^{-1} (assigned to O2–H2···O6) was considerably reduced under high humidity, indicating that this hydrogen bond is not involved as cellulose softens during swelling. In addition to these observations, the authors were able to distinguish

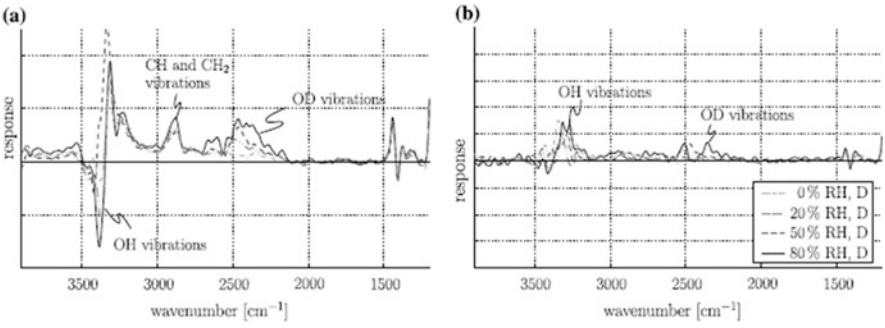

Fig. 6 Dynamic response of cellulose sample in parallel mode during increasing relative humidity to 80% with deuterium vapor: (**a**) in-phase response, (**b**) out-of-phase response [54]

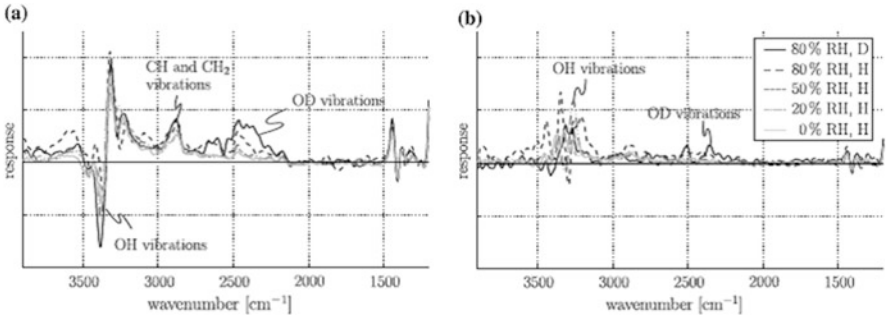

Fig. 7 Dynamic response of cellulose sample in parallel mode during rinsing with normal water vapor and a subsequent decrease of the relative humidity to 0%: (**a**) in-phase response, (**b**) out-of-phase response [54]

Table 7 Wavenumbers of absorption bands in dynamic spectra upon deuteration, assuming pure translation by 850 cm^{-1} and shift by a ratio of 1.34 [54]

Functional group	Wavenumber H (cm^{-1})	Wavenumber D (cm^{-1}) shifted by 850 cm^{-1} (Nishiyama et al. [25])	Wavenumber D (cm^{-1}) shifted by the ratio 1.34 (Jarvis and McCann [56])
Free O–H(2)	3,513–3,560	2,663–2,710	2,622–2,657
Free O–H(6)	3,577–3,579	2,727–2,729	2,669–2,671
O2–H(D) ···O6	3,410–3,455	2,560–2,595	2,545–2,578
O3–H(D) ···O5	3,340–3,375	2,490–2,525	2,492–2,519
O3–H(D) ···O6	3,230–3,310	2,380–2,460	2,410–2,470
Absorbed water (directly bound)	3,200	2,350	2,388
Absorbed water (indirectly bound)	3,600	2,750	2,687

between reorientation and stretching, at least for surface accessible OD groups. As an outcome, the OH bands were assigned to the corresponding vibrations and compared with literature results (Table 7).

Deuterated bacterial cellulose was produced by performing the cultivation in completely deuterated media [57]. By this approach, deuterium was incorporated at positions that are usually not prone to exchange. The exchange of hydrogen for deuterium did not influence accessibility; the molecular weight was not affected, nor the morphology of the material. In addition to the first reports of C–D vibrations determined by IR spectroscopy, ^{2}H NMR spectroscopy was used to characterize the deuterated bacterial cellulose, leading to negligible isotope chemical shifting.

Because these materials possess a large amount of deuterium, they were proposed as model substrates for further studies with SANS.

^{2}H-NMR spectroscopy was employed to investigate cellulose films [58] and fibers, and to gain insights into the residence time and mobility of D_2O in cellulose, which was determined to be about 1.5 ms in oriented fibers [59]. Furthermore, the diffusion behavior of water close to a solid cellulose surface was investigated by the same technique [60–62]. The basis for these measurements is the fact that liquid molecules close to a solid surface have different relaxation profiles to those in the bulk liquid, as a result of interactions at the solid–liquid interface. The main advantage of ^{2}H compared with ^{1}H in this respect is the relaxation mechanism, which is governed by quadrupolar interactions for D_2O ($I = 1$). Therefore, mainly intramolecular relaxation mechanisms are favored, which are hardly affected by paramagnetic impurities as for H_2O. As a consequence, for systems with an intrinsic porosity such as cellulose that contain water, the averaged longitudinal relaxation times are proportional to the surface-area-to-volume ratio of the pores. Models can be employed in order to distinguish between freely moving water and constrained water [62–69]. In a very convenient set of experiments, the change in porosity of biomass samples during sulfuric acid hydrolysis at 160°C was determined. It was shown that the relaxation time of *Populus* biomass decreased from 23.9 to 36.3 ms after exposure for 60 min to H_2SO_4. These values correspond to an increase in pore size by a factor of 3.5 and in pore volume by 6.5. The effect of drying and pressing on the pore size of fibers was also followed [63]. A decrease in water content (e.g., by pressing or drying) leads to a decrease in the average pore size and results in narrowing of the pore size distribution.

Finally, H/D exchange reactions on a variety of thin films were performed in order to determine the water equilibrium content, as measured using a quartz crystal microbalance with dissipation unit. For this purpose, the films are swollen in water for an extensive time before water is exchanged with D_2O. The difference in density and viscosity of D_2O and H_2O leads to a large frequency shift. According to the equations first described by Kazagawa, the water equilibrium content can be simply obtained. The differences in viscosity/density of H_2O and D_2O have an impact on the resonance frequency of the respective solvent fraction, and the changes in the solvent fraction $\Delta f_{\text{solvent}}$ can be expressed by the Kanazawa–Gordon equation (Eq. 4) [70]:

$$\frac{\Delta f_{\text{solvent}}}{n} = -f_0^{3/2}\sqrt{\frac{\eta_l \rho_l}{\pi \rho_p \mu_p}} \tag{4}$$

where n is the overtone number, f_0 the Eigen frequency of the crystal (5 MHz), ρ_l is the density of the liquid (0.9982 g cm^{-3} for H_2O and 1.1050 g cm^{-3} for D_2O at 20°C), η_l is the viscosity of the liquid (1.002 cP for H_2O and 1.25 cP for D_2O at 20°C), and ρ_p and μ_p are the density and shear modulus of the quartz, respectively. The frequency of the bare substrate, Δf_{bare}, can be calculated by subtraction of

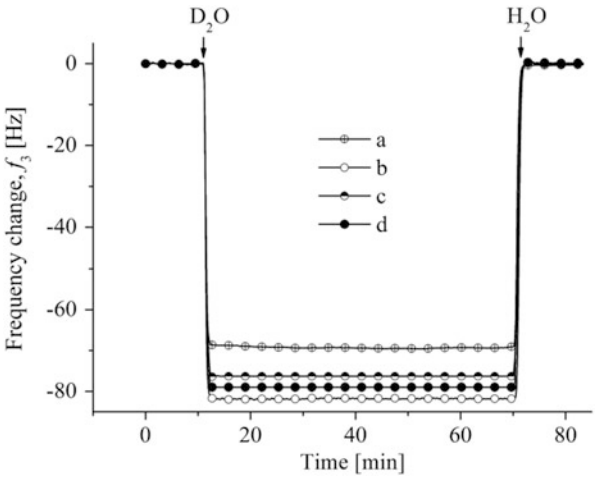

Fig. 8 Effect of H_2O/D_2O solvent exchange on the quartz crystal microbalance resonance frequencies: *a* bare gold substrate, *b* cellulose film (not heat treated), *c* cellulose film (heat treated), and *d* cellulose film (swollen and heat treated) [71]

Δf_{H_2O} from Δf_{D_2O} and the frequency shift caused by the water content can be determined according to (Eq. 5):

$$\frac{\Delta f_{H_2O}}{n} = \frac{\frac{\Delta f_{film}}{n} - \frac{\Delta f_{bare}}{n}}{\frac{\rho_{D_2O}}{\rho_{H_2O}} - 1} \tag{5}$$

The total water content Γ_{water} (also referred to as the surface concentration) can be calculated according to the Sauerbrey equation (Eq. 6) [70]:

$$\Gamma_{water} = -C\frac{\Delta f_{H_2O}}{n} \tag{6}$$

where C is the Sauerbrey constant (17.7 ng cm^{-2} for a 5 MHz crystal). An overview of the behavior of the resonance frequency during H_2O/D_2O solvent exchange is depicted in Fig. 8. The water equilibrium content of amorphous cellulose thin films is about 50–70% relative to the dry mass, whereas pre-dried films and pre-swollen/dried films show lower Γ (30% and 45%, respectively) [71]. Thin films of nanofibrillar cellulose have also been investigated with this approach, yielding values of 70–85% (Fig. 8) [72].

5 Summary and Conclusion

Over the past 80 years, the application of deuteration to cellulose has contributed significantly to an understanding of its supramolecular structure. The developments came in waves and in parallel to advances in analytical techniques. The first studies by Bonhoeffer in 1938 mainly used gravimetric methods, giving the first proof of

the potential of heavy water in cellulose science. The use of FT-IR, however, particularly using polarized waves, allowed band assignment to given hydrogen bonds in cellulose. Neutron scattering provided a tool for distinguishing between amorphous and crystalline domains and later also enabled detailed analysis to unravel the hydrogen bonded network in different cellulose polymorphs. A further wave of efforts focused on more complex systems such as wood samples and on understanding how mechanical properties are influenced by changes at the molecular level. Most recently, the use of D_2O has allowed estimation of the amount of water in cellulose thin films, and opened the way to learn about cellulose hydration and study the behavior of cellulose during adsorption and during interaction with biomolecules.

References

1. Bonhoeffer KF (1934) Z Elektrochem 40:469–474
2. Staudinger H (1920) Ber Dtsch Chem Ges 53:1073–1085
3. Goldfinger G, Siggia S, Mark H (1943) Ind Eng Chem 35:1083–1086
4. Champetier G, Viallard R (1938) Bull Soc Chem 5:1042–1048
5. Frilette VJ, Hanle J, Mark H (1948) J Am Chem Soc 70:1107–1113
6. Kratky O, Mark HZ (1937) Phys Chem B86:129–139
7. Rowen BJW, Plyler EK (1950) J Res Nat Bur Stand 44(3):313–320
8. Mann BYJ, Marrinan HJ (1956) Trans Faraday Soc 52:487–492
9. Nickerson RF (1942) Ind Eng Chem 84:1480–1485
10. Almin KE (1952) Sven Papp-Tidn 55:767–770
11. Mann BYJ, Marrinan HJ (1956) Trans Faraday Soc 52:481–487
12. Mann BYJ, Marrinan HJ (1956) Trans Faraday Soc 52:492–497
13. Hermans PH (1951) Makromol Chem 6:25–29
14. Kratky O, Treiber E (1951) Z Elektrochem 55:716–717
15. Sidgwick NV (1950) Chemical elements and their compounds, vol I. Oxford University Press, London, p 56
16. Tsuboi M (1957) J Polym Sci 25:159–171
17. Sepall O, Mason SG (1961) Can J Chem 39:1934–1943
18. Sepall O, Mason SG (1961) Can J Chem 39:1944–1955
19. Sepall O, Lang ARG, Mason SG (1961) Can J Chem 39:827–834
20. Okajima S, Kai A, Technology F (1968) J Appl Polym Sci 6:2801–2817
21. Fischer EW, Herchenroder P, Manley RSJ, Stamm M (1978) Macromolecules 11:213–217
22. Atalla R, Van der Hart D (1984) Science 223:283–284
23. Gardner KH, Blackwell J (1974) Biopolymers 13:1975–2001
24. Sugiyama J, Chanzy H, Vuong R (1991) Macromolecules 24:4168–4175
25. Nishiyama Y, Okano T, Langan P, Chanzy H (1999) Int J Biol Macromol 26:279–283
26. Wada M, Okano T, Sugiyama J (1997) Cellulose 4:221–232
27. Nishiyama Y, Langan P, Chanzy H (2002) J Am Chem Soc 124:9074–9082
28. Nishiyama Y, Sugiyama J, Chanzy H, Langan P (2003) J Am Chem Soc 125:14300–14306
29. Langan P, Nishiyama Y, Chanzy H (1999) J Am Chem Soc 121:9940–9946
30. Steiner T (2002) Angew Chem 114:50–80
31. Jeffrey GA (1997) An introduction to hydrogen bonding. Oxford University Press, Oxford, p 272

32. Gessler K, Krauss N, Steiner T, Betzl C, Sarko A, Saenger W (1995) J Am Chem Soc 117:11397
33. Wada M, Chanzy H, Nishiyama Y, Langan P (2004) Macromolecules 37:8548–8555
34. Horikawa Y, Sugiyama J (2009) Biomacromolecules 10:2235–2239
35. Horikawa Y, Sugiyama J (2007) Cellulose 15:419–424
36. Crawshaw J, Vickers M, Briggs N, Heenan R, Cameron R (2000) Polymer 41:1873–1881
37. Evmenenko G, Alexeev V, Reynaers H (2000) Polymer 41:1947–1951
38. Kondo T, Sawatari C (1996) Polymer 31:393–399
39. Wadehra IL, Manley R-J (1965) J Appl Polym Sci 9:2627–2630
40. Jeffries R (1968) J Appl Polym Sci 12:425–445
41. Hishikawa Y, Togawa E, Kataoka Y, Kondo T (1999) Polymer 40:7117–7124
42. Hishikawa Y, Inoue S-I, Magoshi J, Kondo T (2005) Biomacromolecules 6:2468–2473
43. Muller M, Czihak C, Schober H, Nishiyama Y, Vogl G (2000) Macromolecules 33:1834–1840
44. Hishikawa Y, Togawa E, Kondo T (2010) Cellulose 17:539–545
45. Tsuchikawa S, Siesler HW (2003) Appl Spectrosc 57:667–674
46. Tsuchikawa S, Siesler HW (2003) Appl Spectrosc 57:675–681
47. Tsuchikawa S, Yonenobu H, Siesler HW (2005) Analyst 130:379–384
48. Suchy M, Virtanen J, Kontturi E, Vuorinen T (2010) Biomacromolecules 11:515–520
49. Suchy M, Kontturi E, Vuorinen T (2010) Biomacromolecules 11:2161–2168
50. Pönni R, Kontturi E, Vuorinen T (2013) Carbohydr Polym 93:424–429
51. Atalla RS, Crowley MF, Himmel ME, Atalla RH (2014) Carbohydr Polym 100:2–8
52. Inagaki T, Siesler HW, Mitsui K, Tsuchikawa S (2010) Biomacromolecules 11:2300–2305
53. Yonenobu H, Tsuchikawa S, Sato K (2009) Vib Spectrosc 51:100–104
54. Hofstetter K, Hinterstoisser B, Salmén L (2006) Cellulose 13:131–145
55. Sturcová A, Eichhorn SJ, Jarvis MC (2006) Biomacromolecules 7:2688–2691
56. Jarvis MC, McCann MC (2000) Plant Physiol Biochem 38:1–13
57. Bali G, Foston MB, O'Neill HM, Evans BR, He J, Ragauskas AJ (2013) Carbohydr Res 374:82–88
58. Matsumura K, Hayamizu K, Yamamoto O (1989) J Polym Sci B Polym Phys 27:2407–2418
59. Li T-Q (1996) Appl Spectrosc 50:1512–1518
60. Foston M, Ragauskas A (2010) Energy Fuels 24:5677–5685
61. Li T-Q, Henriksson U, Eriksson JC, Odberg L (1992) Langmuir 8:680–686
62. Vittadini E, Dickinson LC, Chinachoti P (2001) Carbohydr Polym 46:49–57
63. Haggkvist M, Li T-Q, Odberg L (1998) Cellulose 5:33–49
64. Gallegos D, Munn K, Smith D, Stermer D (1987) J Colloid Interface Sci 119:127–140
65. Gallegos D, Smith D (1988) J Colloid Interface Sci 122:143–153
66. Gallegos D, Smith D, Brinker J (1988) J Colloid Interface Sci 124:186–198
67. Glaves C, Frye G, Smith D, Brinker C, Datye A, Ricco A, Martin S (1989) Langmuir 5:459–466
68. Glaves C, Smith D (1989) J Membr Sci 46:167–184
69. Li T, Henriksson U (1993) Nord Pulp Pap Res J 3:326–330
70. Kanazawa KK, Gordon JG (1985) Anal Chem 57:1770–1771
71. Mohan T, Spirk S, Kargl R, Doliška A, Vesel A, Salzmann I, Resel R, Ribitsch V, Stana-Kleinschek K (2012) Soft Matter 8:9807–9815
72. Kontturi KS, Kontturi E, Laine J (2013) J Mater Chem A 1:13655–13663

Adv Polym Sci (2016) 271: 115–132
DOI: 10.1007/12_2015_320

Published online: 4 July 2015

Correlations of Apparent Cellulose Crystallinity Determined by XRD, NMR, IR, Raman, and SFG Methods

Christopher Lee, Kevin Dazen, Kabindra Kafle, Andrew Moore, David K. Johnson, Sunkyu Park, and Seong H. Kim

Abstract Although the cellulose crystallinity index (CI) is used widely, its limitations have not been adequately described. In this study, the CI values of a set of reference samples were determined from X-ray diffraction (XRD), nuclear magnetic resonance (NMR), and infrared (IR), Raman, and vibrational sum frequency generation (SFG) spectroscopies. The intensities of certain crystalline peaks in IR, Raman, and SFG spectra positively correlated with the amount of crystalline cellulose in the sample, but the correlation with XRD was nonlinear as a result of fundamental differences in detection sensitivity to crystalline cellulose and improper baseline corrections for amorphous contributions. It is demonstrated that the intensity and shape of the XRD signal is affected by both the amount of crystalline cellulose and crystal size, which makes XRD analysis complicated. It is clear that the methods investigated show the same qualitative trends for samples, but the absolute CI values differ depending on the determination method. This clearly indicates that the CI, as estimated by different methods, is not an absolute value and that for a given set of samples the CI values can be compared only as a qualitative measure.

C. Lee, K. Dazen, K. Kafle, and S.H. Kim (✉)
Department of Chemical Engineering and Materials Research Institute, Pennsylvania State University, University Park, PA 16802, USA
e-mail: shkim@engr.psu.edu

A. Moore and S. Park (✉)
Department of Forest Biomaterials, North Carolina State University, Raleigh, NC 27695, USA
e-mail: spark@ncsu.edu

D.K. Johnson
National Renewable Energy Laboratory, 15013 Denver West Parkway, Golden, CO 80401, USA

Keywords X-ray diffraction • Sum frequency generation spectroscopy • Infrared spectroscopy • Raman spectroscopy • Nuclear magnetic resonance • Crystallinity index • Wood pulp

Contents

1 Introduction

Cellulose is the most abundant natural polymer on the planet, and constitutes lignocellulosic biomass along with hemicelluloses and lignin [1]. Cellulose is produced from glucose molecules by photosynthesizing plants such as trees, grasses, and algae as well as by bacteria, fungi, and tunicates (i.e., sea squirts) [2]. Cellulose is a linear macromolecule of repeating 1-4-linked β-D-glucopyranose units. In plants, individual cellulose polymer chains are produced by protein complexes in the plasma membrane and aggregate into microfibrils [3–5]. Hydrogen bonding between and within cellulose chains in cellulose microfibrils leads to formation of ordered crystal structures [6–9]. The crystal structure of cellulose plays a key role in the mechanical strength of plant cell walls as well as deconstruction of lignocellulose biomass [10–14].

Naturally occurring cellulose exists as two polymorphs, cellulose I_α and I_β. Algae and bacteria primarily produce cellulose I_α, whereas land plants tend to produce mostly cellulose I_β [15, 16]. Cellulose can be irreversibly converted into cellulose I_β by heat treatment [17]. Cellulose II is produced via mercerization with a strong alkaline solution or precipitation from a dissolved state [18, 19]. Cellulose I and II can be converted to cellulose III_1 and III_2, respectively, by treatment with dry liquid ammonia [2]. It has been also claimed that cellulose IV_1 and IV_2 can be produced simply by heating cellulose III_1 or III_2, but the products could be a form of

disordered cellulose I_β [20]. These polymorphs of cellulose differ in the size of the unit cell, number of chains included in the crystal unit cell, and orientation of the chains in the crystal (parallel or antiparallel).

Several techniques have been used to measure the amount of crystalline structure and the polymorph type in cellulose samples. Although X-ray diffraction (XRD) is the most widely used technique, infrared spectroscopy (IR), Raman spectroscopy, nuclear magnetic resonance (NMR), and vibrational sum frequency generation (SFG) spectroscopy are also used to investigate the crystal structure of cellulose [21–24]. Because XRD measures coherent scattering from crystalline lattices, it is conceptually easy to understand. However, there are several issues concerned with the practical application of XRD to biomass [25]. In fact, XRD analysis of whole biomass can be challenging because of interference from incoherent X-ray scattering of the amorphous phases, which include hemicelluloses and lignin. Several data processing methods have been proposed and used to extract values for the amount of crystalline cellulose from XRD data of biomass [26]; however, these methods have some limitations that are often neglected in data processing or interpretation. These issues are discussed in this study.

There are several peaks in NMR, IR, and Raman spectra that are characteristic of crystalline cellulose. Cellulose and hemicelluloses share the same organic functional groups (C–C, C–H, C–O–C, and C–O–H); the main differences between them are the monomeric constituents and regioselectivity of glycosidic bonds, which eventually govern the packing of these carbohydrate polymer chains. Structural constraints (such as bond distances and bond angles) imposed by specific polymer chain packing can cause certain peaks in NMR, IR, and Raman spectra to be different for crystalline and amorphous structures [24]. Although many studies have shown that crystalline cellulose can be distinguished from other components in biomass using NMR, IR, and Raman spectroscopy, quantitative analysis is still challenging because of subtle differences between the crystalline and amorphous phases.

Recently, vibrational SFG spectroscopy has been demonstrated to selectively detect crystalline cellulose dispersed in amorphous phases [27, 28]. SFG is a nonlinear optical process for the study of a noncentrosymmetric optical medium. Crystalline cellulose has noncentrosymmetry over several orders of length scales. At the molecular scale, all carbon centers (C1, C2, C3, C4, C5) in the glucopyranose ring are chiral. The symmetry of the crystal unit cells are also noncentrosymmetric (space groups P1 and $P2_1$) [9, 23]. The glucan chains in cellulose I_α and I_β are arranged in parallel fashion, whereas those of cellulose II are arranged in antiparallel fashion [29]. The noncentrosymmetric crystals can be distributed randomly, centrosymmetrically (for example, antiparallel packing), or noncentrosymmetrically (parallel packing) within the amorphous matrices. Thus, the dispersion pattern of cellulose crystals over the characteristic length of the SFG process (so-called coherence length) can also affect the SFG spectra [30]. Although individual chiral centers could generate weak SFG signals, in principle their signals are generally much weaker or negligible compared with SFG signals from noncentrosymmetric crystals. Thus, SFG can selectively detect multiscale

structural aspects (such as crystal structure and mesoscale packing) of crystalline cellulose dispersed in a whole biomass sample without interference from amorphous components [24, 29–33]. This selective detection of crystalline cellulose in its native state is very important for a deep understanding of the role of crystalline cellulose in cell wall properties, both mechanically and chemically. If the packing of crystalline cellulose in biomass remains relatively constant, the SFG signal intensity can be used to estimate crystallinity [28]. However, this becomes challenging if the crystal packing pattern changes drastically between samples [30].

In this paper, we compare the *apparent* crystallinity index (CI) obtained from several structural characterization techniques. In the literature, the CI values obtained from different techniques and/or samples have been compared in a quantitative manner, and in some cases the results have been taken as "accurate" or "absolute." We propose that the CI value should be taken or considered only as a qualitative index to demonstrate a trend between samples, and not as an absolute quantity. The main purpose of this paper is to explain how the CI is obtained by different methods and how different the results can be (even for a given technique when the CI is calculated by different methods). We also attempt to draw a correlation between the different methods. The data presented in this paper provide an insight into the usefulness and limitations of CI estimation.

2 Experimental

2.1 Sample Preparation

Several types of cellulose were used in this study. Cotton linter (Justfiber C10CL FCC) was kindly provided by the International Fiber Corporation; Avicel PH-101 and α-cellulose were purchased from Sigma-Aldrich. Fully bleached hardwood and softwood pulps were obtained from a mill in the southeastern United States. These pulps contained 20.0% and 16.3% noncellulosic carbohydrates, respectively.

Decrystallized samples were prepared using a modified version of the procedure described by Schroeder et al. [12, 34]. Whatman filter paper 1 was used in this study as a reference, highly crystalline, and purified sample. It was first soaked in water and the fibers were dispersed under magnetic stirring overnight. The water was then removed by vacuum filtration over a glass filter. The mat of fibers was removed and re-suspended in a beaker filled with acetone. This dispersion was filtered using vacuum filtration. After the third rinsing with acetone, the fiber mat was suspended in dimethyl sulfoxide (DMSO). Following the same procedure, the DMSO was removed via vacuum and re-suspended three times. The purpose of this solvent exchange was to swell the cellulose fibers and make them more accessible to reaction with formaldehyde. The cellulose and DMSO mixture was then heated to 125°C and paraformaldehyde added. As a result of the reaction, methylol-cellulose was formed, which is soluble in DMSO, and the system became clear. The methylol-cellulose and DMSO solution was filtered through a glass crucible. Amorphous

cellulose was then precipitated in a stirred bath with 0.2 M sodium methoxide in methanol and propanol (1:1). After precipitation, the fibers were washed thoroughly with methanol, 0.1 M hydrochloric acid, and de-ionized water, and then freeze-dried. Partially de-crystallized samples were obtained in a similar manner but not applying solvent exchange so that the cellulose chains only partially dissolved. In addition, no filtration was used so that these chains were preserved. The same procedure was followed to precipitate and wash the dissolved portion.

2.2 X-Ray Diffraction

Freeze-dried cellulose samples were placed on a low-background quartz holder and measured using a Rigaku SmartLab X-ray diffractometer with a Cu tube ($\lambda = 1.5405$ Å). The radiation was generated at 25 mA and 35 kV. A step size of 0.05° and 5 s exposure were used for measuring the scattering angle 2θ in the range 9–41°. The CI was determined by two methods, the peak height (PH) and amorphous subtraction (AS) methods. The PH method, also known as Segal's method, measures the intensity of the crystalline peak (I_{200}–I_{AM}) and the total intensity (I_{200}) after the background spectrum is removed. The ratio of the intensities of these two peaks gives an estimate of the crystallinity of the cellulose sample [35]. The AS method requires the amorphous spectrum to be subtracted from the sample spectrum [36]. This method is challenging because a comparable amorphous sample should be used as a background, and most processes to obtain such a sample (e.g., ball-milling) produce significant modifications. The amorphous background spectrum used here was prepared by utilizing an amorphous cellulose sample from the same given starting material. A scaling factor was used to shift the amorphous spectrum to fit under the sample spectra. The CI was then taken as the area of the crystalline portion (total area minus amorphous background area) divided by the total area.

2.3 X-Ray Diffraction Simulation

To investigate the effect of cellulose crystal size on the CI value using the AS method, simulated diffraction patterns were created from the .cif file obtained for cellulose I_β [9] using the Mercury program v3.3 [37], which is similar to that used in a previous report [38]. Several powder diffraction patterns were obtained by varying the full width at half maximum values. The CI values for each simulated spectra were found by applying the AS method in a manner similar to that used for the experimental spectra described earlier.

2.4 Nuclear Magnetic Resonance Spectroscopy

High-resolution solid-state ^{13}C NMR spectra were collected at 9.4 T with cross-polarization and magic angle spinning (CP/MAS) in a Bruker Avance 400 MHz

spectrometer. ^{1}H and ^{13}C fields were matched at 53.6 kHz, and a 1 dB ramp was applied to the proton rotating-frame during the matching period. Acquisition time was 0.034 s and sweep-width was 30 kHz. Magic-angle spinning was performed at 7,000 Hz. The average was calculated for 3,000 scans using a 2 ms contact time and a delay time of 4.0 s. Crystalline cellulose peaks can be found in the literature [39]. The CI was determined by dividing the total area of crystalline peaks by the area under C4 carbon peaks.

2.5 Fourier-Transform Infrared and Raman Spectroscopies

Fourier-transform infrared (FT-IR) spectroscopy measurements were performed using a Nicolet 8700 FT-IR Spectrometer (Thermo Scientific) with a deuterated triglycine sulfate (DTGS) detector. Data were collected in the region 650–4,000 cm^{-1} with a 4 cm^{-1} resolution, averaged over 100 scans, in reflection mode using a smart iTR diamond plate unit (Thermo Scientific). Each spectrum was baseline-corrected and normalized to the maximum absorbance at 1,030 cm^{-1}. Similar to previous studies, the FT-IR relative crystallinity was calculated using the ratio of the absorption bands at 1,315 and 1,369 cm^{-1} from the filter paper reference samples [40, 41]. The absorbance of each band was measured relative to the valley value at approximately 1,348 cm^{-1}. These two bands were chosen because the 1,315 cm^{-1} peak intensity varies substantially in the reference samples and is located close to the 1,369 cm^{-1} peak, which is used as an internal standard for crystallinity calculations [41]. FT-Raman spectroscopy measurements were taken using a Nicolet NXR Spectrometer (Thermo Scientific) using a 1,064 nm excitation source with a beam power of 1–1.8 W and a germanium detector. Data were collected in the region 250–3,800 cm^{-1} with an 8 cm^{-1} resolution, averaged over 1,000 scans. Each spectrum was baseline-corrected and normalized to the maximum absorbance at 2,894 cm^{-1}. Relative crystallinity from the Raman spectra was calculated using the ratio of the absorbance bands at 380 and 1,096 cm^{-1} [42]. The 380 and 1,096 cm^{-1} peak intensities were measured relative to the minima at 356 and 942 cm^{-1}, respectively.

2.6 Vibrational Sum Frequency Generation Spectroscopy

SFG spectroscopic measurements were carried out by irradiating the sample with picosecond laser pulses in the IR and visible wavelengths and detecting the emitted SFG signals. The SFG spectrometer (EKSPLA) was pumped by a picosecond Nd:YAG laser (1,064 nm at 10Hz). The infrared light was generated with an optical parameter generator/amplifier (OPG/OPA) pumped with 532 and 1064 nm and tuned to 2.3–10 μm with <6 cm^{-1} bandwidth. The polarization of incident IR and visible laser pulses were parallel (p-polarized) and perpendicular (s-polarized) to the plane of laser incidence. The emitted SFG signal (s-polarized) was detected

in the reflection geometry [27]. The visible (60° to surface normal) and IR (56°) laser pulses were overlapped spatially and temporally on each sample. A beam collimator was used to enhance the signal collection efficiency and the SFG signal was filtered through a monochromator and detected with a photomultiplier tube (Hamamatsu Corp.). The SFG intensity was normalized to incident IR and visible laser intensities. SFG spectra were taken at 4 cm^{-1} per step in the CH stretching region (2,700–3,050 cm^{-1}) and 8 cm^{-1} per step in the OH stretching region (3,096–3,800 cm^{-1}). Slight variations in SFG intensity occurred at different locations on the sample pellet, depending on the texture and packing density of the cellulose during sample preparation. Therefore, SFG intensity at the 2,944 and 3,320 cm^{-1} peaks were monitored at multiple locations ($n = 3$–8) on the pellet so that each full-scan spectra was representative of the average SFG intensity at the given locations. No baseline corrections or normalization was performed. The relative crystallinity was calculated by measuring the peak intensity at 2,944 cm^{-1} relative to the minimum at 3,132 cm^{-1} [28].

3 Results and Discussion

3.1 Correlation of "Apparent" Crystallinity Estimated from XRD, IR, Raman, and SFG Analyses of Reference Samples

A set of reference samples with three different crystallinities was prepared as described in the "Sample Preparation" section. We used Whatman filter paper because it is readily and widely available and can be taken as a reference for highly crystalline (as-received filter paper), partially crystalline (prepared by adjusting the decrystallization process), and amorphous cellulose (precipitated from solution) [12, 34]. These samples were analyzed using XRD, IR, Raman, and SFG, as shown in Fig. 1. The filter paper samples were not suitable for ^{13}C solid-state NMR analysis, and thus comparison of CI values obtained using this technique was not possible.

There are many different methods for calculation of the CI from XRD as shown in Fig. 1a [43, 44]. Of the various methods, the most widely used is the peak height (PH) method originally proposed by Segal et al. as a "time-saving empirical measure of relative crystallinity" [35]. This method assumes the background intensity at $2\theta = \sim 18^{\circ}$ to be an amorphous contribution and the peak height at $2\theta = 22.8^{\circ}$ to result from both crystalline and amorpous contributions. In order to quantify and provide a more realistic value, alternative methods such as curve fitting or amorphous subtraction (AS) have been suggested [26]. Depending on the method used to analyze XRD data, the CI value can vary drastically [28]. Note that most of the methods incorrectly assume that X-ray sensitivity to crystalline and amorphous phases is the same. The Rietveld fitting of XRD data can resolve these

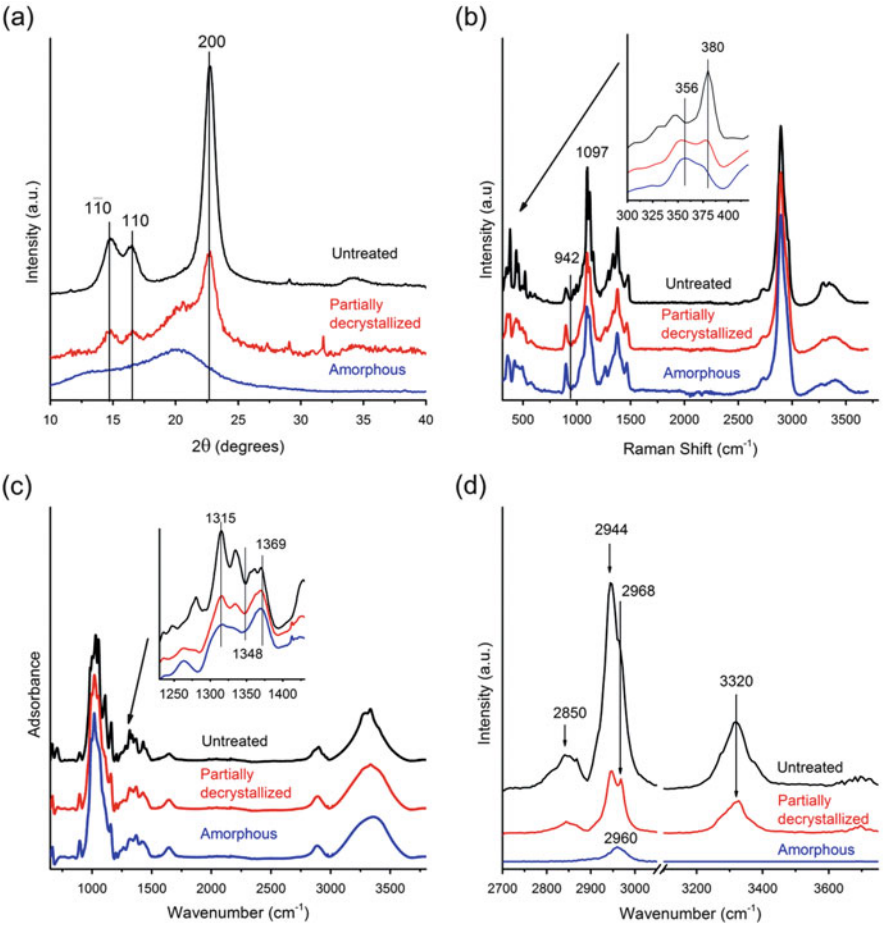

Fig. 1 Characterization of cellulose reference samples using (**a**) XRD, (**b**) Raman, (**c**) IR, and (**d**) SFG. Reference samples were prepared from filter paper and are labeled as untreated (*black*), partially decrystallized (*red*) and amorphous (*blue*). All spectra are offset for clarity. *Insets* in (**b**) and (**c**) show the regions used for CI calculations

uncertainties in the CI calculation [45]. Because these advanced methods are not easily amenable to non-XRD experts, a more user-friendly method has been developed [46].

Figure 1b compares the Raman spectra of the same samples. The 1,480 and 380 cm^{-1} peaks are known to be characteristic of crystalline cellulose [42, 47]. The former is assigned to the CH_2 bending mode of the exocyclic CH_2OH side chain and the latter is speculated to originate from one of the torsion or bending modes of the six-membered ring with respect to the glycosidic bonds [24]. In the case of the 1,480 cm^{-1} peak, the peak deconvolution from the amorphous counterpart (~1,460 cm^{-1}) can be troublesome for calculation of CI. After proper background

correction, good correlation between the 380 cm^{-1} intensity and the XRD CI value has been demonstrated [42]. Hemicelluloses do not show a peak at 380 cm^{-1}, whereas they can show broad peaks in the CH_2 bending vibration region. Thus, use of the 380 cm^{-1} Raman peak intensity is advantageous for CI calculation [48].

Figure 1c displays the IR spectra of the same samples. There are a number of small peaks that vary with the degree of crystallinity. Noticeable peaks are found at 706, 1,056, 1,110, and 1,315 cm^{-1}. The intensities of these peaks are reported to vary in accordance with the XRD CI value [41]. Although the 1,056 and 1,110 cm^{-1} peaks are sharp, they overap with broad and strong background peaks in the C–C and C–O stretch vibration region. For that reason, the peaks at 706 and 1,315 cm^{-1} might work better for CI calculation. The peaks at 1,640 cm^{-1} become larger as the degree of crystallinity decreases. This is a result of the ingress of water into the amorphous cellulose region. For the same reason, the OH stretch peaks (3,000–3,600 cm^{-1}) become broader for the partially and fully decrystallized samples. When applied directly to lignocellulose biomass, the IR method can suffer from peak overlap from noncellulosic components.

Figure 1d exhibits the SFG spectra of the same samples. Although there are many peaks characteristic for crystalline cellulose in the lower wavenumber region, their peak assignment is not straightforward because of substantial coupling between various vibrational modes [31]. The C–H and O–H stretching vibration region alone can provide rich information about the polymorphism (I_α, I_β, II, III) and mesoscale packing pattern of celluose microfibrils [29, 30]. A strong SFG peak at 2944 cm^{-1} and a weaker peak at 3,320 cm^{-1} are characteristic features of antiparallel-packed cellulose I_β microfibrils [30]. The intensities of these peaks decrease in a nonlinear fashion as the crystalline cellulose portion in the sample decreases [28]. The additional peak at 2,968 cm^{-1} for the partially decrystallized sample might be a result of some changes in the cellulose crystal packing [30], which could have occurred during the partial decrystallization process involving incomplete dissolution of cellulose crystals. For the fully decrystallized sample (precipitated from fully dissolved cellulose chains), the OH stretch peak is completely missing and the CH peak is shifted to 2,960 cm^{-1} and is weaker. This implies that a small amount of cellulose II is formed during the precipitation process, because amorphous cellulose chains do not produce measureable SFG signals [29].

Figure 2 presents the correlations between CI values calculated from the data shown in Fig. 1. The XRD data were processed using the PH and AS methods. For the AS method, the XRD data of the fully depolymerized sample (blue curve in Fig. 1a) was used as a reference for CI = 0%. Note that the PH method always gives higher CI values than the AS method. This is an artifact and limitation of the PH method caused by simply reading the height at $2\theta = 22^\circ$ as total diffraction, even though the amorphous phase alters the baseline. For the fully depolymerized sample, the PH method gives 34% CI whereas the AS method gives 0% CI (simply because it is the reference for CI = 0%). The difference between the two methods becomes smaller for samples of higher crystallinity ($CI_{PH} = 94\%$ versus $CI_{AS} = 78\%$ for the as-received filter paper). It should be noted that both methods

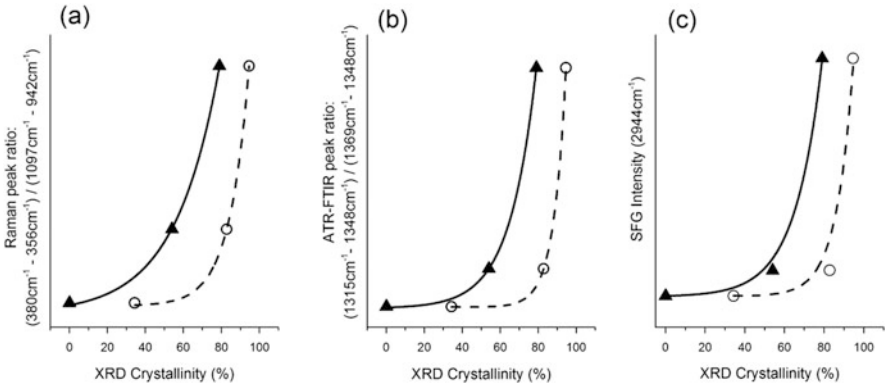

Fig. 2 Correlation between crystalline peak intensities in (**a**) Raman, (**b**) IR, and (**c**) SFG vibration spectroscopy of reference samples with respect to XRD crystallinities calculated using the peak height method (*circles*) and amorphous subtraction method (*triangles*)

ignore the fact that XRD sensitivity to the amorphous background and crystalline peaks are different.

Because there are peaks characteristic for crystalline cellulose in IR, Raman, and SFG spectra, the intensities of these peaks can be correlated with the absolute amount of crystalline cellulose in the sample. However, it is difficult to know the absolute value unless the sample is prepared by mixing known amounts of fully crystalline and fully amorphous cellulose [28]. Thus, we simply compared their intensities with the XRD CI values. Figure 2 shows nonlinear but reasonably good correlation between the CI values obtained using the different techniques. In the case of IR and Raman data, the crystalline peaks appear above the nonzero background or sometimes overlap with the amorphous peaks. Thus, proper background subtraction and intensity normalization using an internal reference (the peak that is not sensitive to crystallinity) is necessary [41, 42]. The nonlinearity of the correlations in Fig. 2 could be a result of improper baseline correction or nonlinearity of the relationship between XRD CI and the true crystallinity of the sample [28]. In the case of SFG, the background from amorphous cellulose is typically zero; thus, the absolute intensity can be used for CI calculations. However, because of the nonlinear nature of the SFG process and scattering of the incident and emitted light from rough samples, as well as birefringence of crystalline cellulose, it is difficult to obtain theoretical predictions of SFG intensity [28].

3.2 Simulation of X-Ray Diffraction Data for Cellulose Crystals of Different Sizes

In plant cell walls, cellulose microfibrils are synthesized by cellulose synthase complexes (CSCs). The CSC consists of a rosette of six subunits, and each subunit

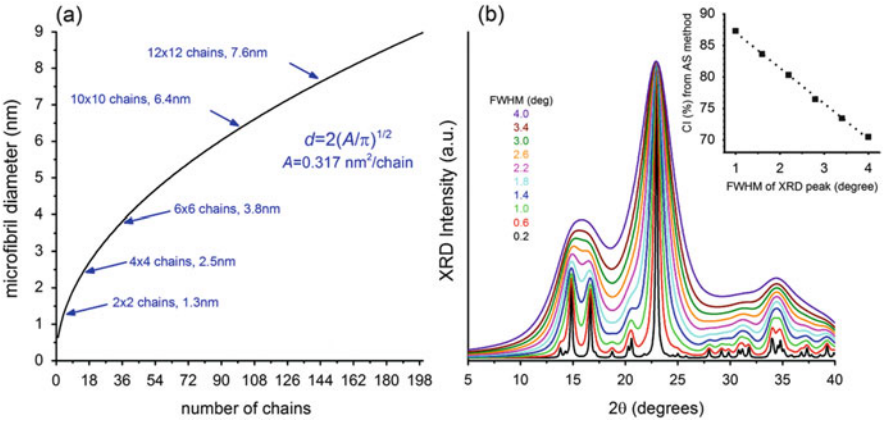

Fig. 3 (**a**) Estimation of the diameter (d) of a cellulose microfibril with circular cross-section (A) as a function of the number of chains in the microfibril. (**b**) Simulated XRD diffractograms using the Mercury program at different peak input values of full width at half maximum (*FWHM*). *Inset* in (**b**) shows the calculated CI value from the amorphous subtraction (*AS*) method versus FWHM value

contains putatively six cellulose synthesis proteins. If all units are active in cellulose synthesis, then cellulose microfibrils would contain 36 chains [49]. However, some models assumed microfibrils with 18 chains [6]. The cross-sectional shape of a cellulose microfibril and the exact number of cellulose chains it contains are difficult to determine [50]. Based on the average cross-section of a glucose chain, the diameter of a microfibril containing 36 chains is estimated to be ~3.8 nm (Fig. 3a). The exact diameter is dependent on an assumption of the shape of the microfibril cross-section. As the number of chains in the crystalline microfibrils varies, the size of the coherent lattice that produce XRD peaks also varies. In plant cell walls, several individual microfibrils have been observed to bundle into larger aggregates called macrofibrils [51]. Some algae and tunicates produce much thicker cellulose crystals (up to 15–20 nm in diameter).

In XRD, the crystal size affects the width of the diffraction peak. The mathematical relationship between the peak width (full width at half maximum, FWHM) of the diffraction peaks and the crystal size (d) is known as the Scherrer equation [52]:

$$\mathrm{FWHM} = \frac{k\lambda}{d\ \cos\theta},$$

where k is the proportionality constant, λ is the X-ray wavelength, and θ is the Bragg diffraction angle. Note that the proportionality constant k has been derived to be about 0.9, assuming Gaussian line profiles of XRD and small perfect cubic crystals of uniform size without any distortion of the lattice [53]. This value is widely used for estimation of cellulose crystal size because it is not sensitive to crystallite shape and symmetry.

In the literature, it is often assumed that the CI and crystal size are independent of each other and are calculated as separate quantities. However, these two terms may not be totally independent but are coupled. In order to demonstrate their dependency, XRD diffractograms were simulated using the Mercury software for the unit cell of cellulose I_β crystal with different FWHM settings (Fig. 3b) [38]. Thus, this data could be considered as 100% crystalline samples with different crystal sizes. In Fig. 3b, the background region close to the assumed amorphous phase rises as FWHM increases. The inset of Fig. 3b shows the CI values calculated for the data in Fig. 3b using the AS method. The CI value decreases in proportion to the FWHM value. This simulation clearly shows that, as cellulose microfibril diameter decreases, the calculated CI values also decrease although the true crystallinity does not change. For a 36-chain cellulose microfibril, the Scherrer equation predicts the FWHM to be around 2.3°, which sets the maximum CI value calculated from the AS method at ~78%. Should 78% CI from AS analysis be taken to correspond to a 100% crystalline sample? To consider the aggregation of individual cellulose microfibrils in plant cell walls, pristine samples of high uniformity are needed [54]. More in-depth analysis with independent experimental design is needed to address this question.

3.3 Comparison of "Apparent" Crystallinity Estimated from XRD, NMR, IR, Raman, and SFG of Isolated and Natural Cellulose Samples

Five different samples containing cellulose were analyzed using XRD, NMR, IR, Raman, and SFG. Cotton linter is one of the purest native (biologically intact) sources of cellulose and contains the highest amount of cellulose (>95% by dry mass). Avicel and α-cellulose are commercially available purified celluloses. Avicel is produced via acid hydrolysis of pulp or cotton linter; thus, the degree of polymerization of cellulose in Avicel is low. α-cellulose is produced via base-catalyzed hydrolysis of wood pulp. Thus, commercial α-cellulose contains mostly cellulose I_β, which should not be confused with cellulose I_α. Bleached hardwood (HW) and softwood (SW) pulps were included in this analysis for comparison with commercial cellulose samples.

Figure 4 and Table 1 compare the XRD, NMR, IR, Raman, and SFG intensity data of the five samples tested. The CI values from XRD were calculated using both PH and AS methods. For the IR, Raman, and SFG data, the signal intensities were converted to values equivalent to the XRD CI values using the calibration curves shown in Fig. 2. In ^{13}C ss-NMR, the C4 peak chemical shifts of amorphous and crystalline cellulose phases were 80–85 ppm and 85–89 ppm, respectively. Thus, their relative intensity can be taken as the CI. The processed CI values are plotted in Table 1. It is clear that all methods show the same qualitative trends for samples (e.g., CI is the highest for cotton linter and lowest for α-cellulose) but that the

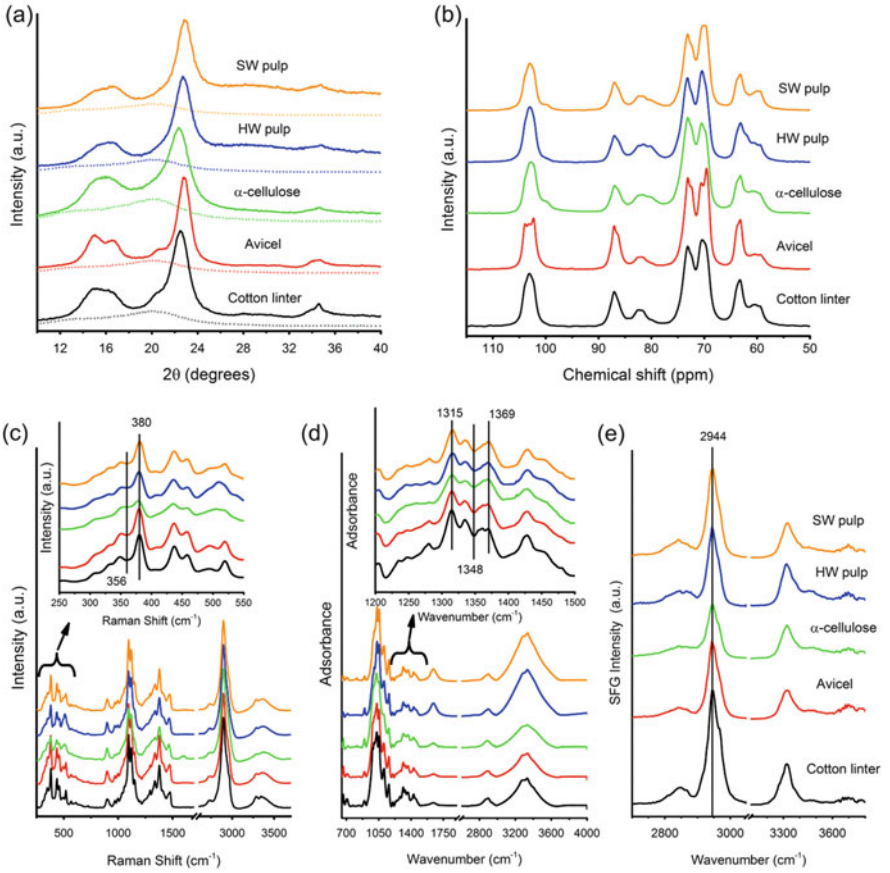

Fig. 4 Characterization of isolated and natural cellulose samples using (**a**) XRD, (**b**) ^{13}C NMR, (**c**) Raman, (**d**) IR, and (**e**) SFG. Samples are cotton linter (*black*), Avicel (*red*), α-cellulose (*green*), hardwood (HW) pulp (*blue*), and softwood (SW) pulp (*orange*). In (**a**) the amorphous standard is plotted as a *dotted line*. *Insets* in (**c**) and (**d**) show the spectral regions used for CI calculations. All spectra are offset for clarity

Table 1 Cristallinity index values obtained for various cellulose-containing samples using different methods

	Calculated crystallinity[a] (%)								
Sample	XRD(PH)	Raman	IR	SFG	XRD(AS)	Raman	IR	SFG	NMR
Cotton linter	85	94	95	93	72	78	80	77	65
Avicel	81	94	93	90	70	77	75	71	58
α-cellulose	65	88	89	86	48	65	67	65	44
Hardwood fiber	84	92	91	90	81	73	72	71	45
Softwood fiber	84	93	92	91	84	76	73	73	52

[a]Values obtained from Raman, IR, and SFG were correlated relative to the XRD values obtained using the peak height method (PH) and amorphous subtraction method (AS)

absolute values are different, depending on the method. This indicates that the CI values estimated using different methods are not "absolute" and should not be compared directly. The CI values obtained for different samples using one method can be compared only qualitatively.

There are a few details that deserve further discussion. First, NMR CI values are much lower than the values calculated from XRD data, even those determined by the AS method. As pointed out earlier, XRD is sensitive to the crystalline phase, but less sensitive to the amorphous phase. Thus, the XRD analysis inevitably discriminates between amorphous and crystalline phases. In contrast, NMR is equally sensitive to both crystalline and amorphous phases. This fundamental difference in detection sensitivity of these two methods might be responsible for the discrepancy between the CI values determined using these methods.

Second, XRD CI values calculated for hardwood and softwood fiber samples with the AS method are high, close to those calculated using the PH method. The source for this high value can be seen in Fig. 4a, which shows the amorphous background portion determined using the AS method. The reference diffractogram used as the amorphous background (blue curve in Fig. 1a) has low intensities at 2θ above 25°, but the hardwood and softwood fiber samples show high background in this region (Fig. 4a). Thus, the AS method cannot properly subtract the background portion in this high 2θ region, adding this difference into the crystalline portion. Figure 3b shows that the background intensities in the $2\theta > 25^{\circ}$ and $2\theta = 18^{\circ}$ regions rise as the FWHM increases. However, the reference sample for the amorphous phase demonstrates negligible intensities at $2\theta > 25^{\circ}$. This makes the CI values calculated using the AS method for the fiber samples much higher than the true mass fraction of crystalline cellulose over the total mass.

4 Conclusions

The apparent CI values of cellulose and biomass samples were evaluated using XRD, solid-state NMR, IR, Raman, and SFG. For a set of filter paper samples, the CI calculated from IR, Raman, and SFG spectra were compared with values from XRD and a nonlinear, positive correlation was observed. The size of cellulose crystals is a factor that can affect the XRD CI value. When different types of cellulose were used, it was clear that all characterization methods show similar trends; but the absolute values are quantitatively different. This indicates that the CI value determined using a given method can be used only as a qualitative and relative measurement.

Acknowledgements This work was supported by the Center for Lignocellulose Structure and Formation (CLSF), an Energy Frontier Research Center funded by the U.S. Department of Energy, Office of Science, and Office of Basic Energy Sciences under Award Number DE-SC0001090. This work was also supported by Subcontract No. XGB-3-23024-01 with the National Renewable Energy Laboratory (NREL), under Contract No. DE-AC36-08-GO28308 with the U.S. Department of

Energy. Sample preparation and XRD and NMR data collection were carried out with funding from the NREL. IR, Raman, and SFG analyses as well as XRD simulation and data analyses were carried out with CLSF support.

References

1. Pauly M, Keegstra K (2008) Cell-wall carbohydrates and their modification as a resource for biofuels. Plant J 54(4):559–568
2. Zugenmaier P (2008) Crystalline cellulose and cellulose derivatives: characterization and structures. Springer, Berlin
3. Cosgrove DJ (2005) Growth of the plant cell wall. Nat Rev Mol Cell Biol 6(11):850–861
4. Paredez AR, Somerville CR, Ehrhardt DW (2006) Visualization of cellulose synthase demonstrates functional association with microtubules. Science 312(5779):1491–1495
5. Somerville C, Bauer S, Brininstool G, Facette M, Hamann T, Milne J, Osborne E, Paredez A, Persson S, Raab T, Vorwerk S, Youngs H (2004) Toward a systems approach to understanding plant cell walls. Science 306(5705):2206–2211
6. Thomas LH, Forsyth VT, Sturcova A, Kennedy CJ, May RP, Altaner CM, Apperley DC, Wess TJ, Jarvis MC (2013) Structure of cellulose microfibrils in primary cell walls from collenchyma. Plant Physiol 161(1):465–476
7. Doblin MS, Kurek I, Jacob-Wilk D, Delmer DP (2002) Cellulose biosynthesis in plants: from genes to rosettes. Plant Cell Physiol 43(12):1407–1420
8. Fernandes AN, Thomas LH, Altaner CM, Callow P, Forsyth VT, Apperley DC, Kennedy CJ, Jarvis MC (2011) Nanostructure of cellulose microfibrils in spruce wood. Proc Natl Acad Sci U S A 108(47):E1195–E1203
9. Nishiyama Y, Langan P, Chanzy H (2002) Crystal structure and hydrogen-bonding system in cellulose 1 beta from synchrotron X-ray and neutron fiber diffraction. J Am Chem Soc 124 (31):9074–9082
10. Himmel ME, Ding S-Y, Johnson DK, Adney WS, Nimlos MR, Brady JW, Foust TD (2007) Biomass recalcitrance: engineering plants and enzymes for biofuels production. Science 315 (5813):804–807
11. Pérez S, Samain D (2010) Structure and engineering of celluloses. In: Derek H (ed) Advances in carbohydrate chemistry and biochemistry, vol 64. Academic, New York, pp 25–116
12. Park S, Johnson DK, Ishizawa CI, Parilla PA, Davis MF (2009) Measuring the crystallinity index of cellulose by solid state 13C nuclear magnetic resonance. Cellulose 16(4):641–647
13. Carroll A, Somerville C (2009) Cellulosic biofuels. Annu Rev Plant Biol 60:165–182
14. Mittal A, Katahira R, Himmel ME, Johnson DK (2011) Effects of alkaline or liquid-ammonia treatment on crystalline cellulose: changes in crystalline structure and effects on enzymatic digestibility. Biotechnol Biofuels 4:41
15. Atalla RH, Vanderhart DL (1984) Native cellulose – a composite of 2 distinct crystalline forms. Science 223(4633):283–285
16. Jarvis M (2003) Cellulose stacks up. Nature 426(6967):611–612
17. Horii F, Yamamoto H, Kitamaru R, Tanahashi M, Higuchi T (1987) Transformation of native cellulose crystals induced by saturated steam at high-temperatures. Macromolecules 20 (11):2946–2949
18. Langan P, Nishiyama Y, Chanzy H (2001) X-ray structure of mercerized cellulose II at 1 angstrom resolution. Biomacromolecules 2(2):410–416
19. Ruan D, Zhang LN, Zhou JP, Jin HM, Chen H (2004) Structure and properties of novel fibers spun from cellulose in NaOH/thiourea aqueous solution. Macromol Biosci 4(12):1105–1112
20. Wada M, Heux L, Sugiyama J (2004) Polymorphism of cellulose I family: reinvestigation of cellulose IVI. Biomacromolecules 5(4):1385–1391

21. Atalla RH, VanderHart DL (1999) The role of solid state C-13 NMR spectroscopy in studies of the nature of native celluloses. Solid State Nucl Magn Reson 15(1):1–19
22. Sugiyama J, Persson J, Chanzy H (1991) Combined infrared and electron diffraction study of the polymorphism of native celluloses. Macromolecules 24(9):2461–2466
23. Nishiyama Y, Sugiyama J, Chanzy H, Langan P (2003) Crystal structure and hydrogen bonding system in cellulose Iα from synchrotron X-ray and neutron fiber diffraction. J Am Chem Soc 125(47):14300–14306
24. Kim SH, Lee CM, Kafle K (2013) Characterization of crystalline cellulose in biomass: basic principles, applications, and limitations of XRD, NMR, IR, Raman, and SFG. Korean J Chem Eng 30(12):2127–2141
25. Ruland W (1961) X-ray determination of crystallinity and diffuse disorder scattering. Acta Crystallogr 14(11):1180–1185
26. Park S, Baker JO, Himmel ME, Parilla PA, Johnson DK (2010) Cellulose crystallinity index: measurement techniques and their impact on interpreting cellulase performance. Biotechnol Biofuels 3:10
27. Barnette AL, Bradley LC, Veres BD, Schreiner EP, Park YB, Park J, Park S, Kim SH (2011) Selective detection of crystalline cellulose in plant cell walls with sum-frequency-generation (SFG) vibration spectroscopy. Biomacromolecules 12(7):2434–2439
28. Barnette AL, Lee C, Bradley LC, Schreiner EP, Park YB, Shin H, Cosgrove DJ, Park S, Kim SH (2012) Quantification of crystalline cellulose in lignocellulosic biomass using sum frequency generation (SFG) vibration spectroscopy and comparison with other analytical methods. Carbohydr Polym 89(3):802–809
29. Lee CM, Mittal A, Barnette AL, Kafle K, Park YB, Shin H, Johnson DK, Park S, Kim SH (2013) Cellulose polymorphism study with sum-frequency-generation (SFG) vibration spectroscopy: identification of exocyclic CH2OH conformation and chain orientation. Cellulose 20 (3):991–1000
30. Lee CM, Kafle K, Park YB, Kim SH (2014) Probing crystal structure and mesoscale assembly of cellulose microfibrils in plant cell walls, tunicate tests, and bacterial films using vibrational sum frequency generation (SFG) spectroscopy. Phys Chem Chem Phys 16(22):10844–10853
31. Lee CM, Mohamed NM, Watts HD, Kubicki JD, Kim SH (2013) Sum-frequency-generation vibration spectroscopy and density functional theory calculations with dispersion corrections (DFT-D2) for cellulose Iα and Iβ. J Phys Chem B 117(22):6681–6692
32. Park YB, Lee CM, Koo B-W, Park S, Cosgrove DJ, Kim SH (2013) Monitoring meso-scale ordering of cellulose in intact plant cell walls using sum frequency generation spectroscopy. Plant Physiol 163(2):907–913
33. Kafle K, Xi X, Lee CM, Tittmann BR, Cosgrove DJ, Park YB, Kim SH (2014) Cellulose microfibril orientation in onion (*Allium cepa* L.) epidermis studied by atomic force microscopy (AFM) and vibrational sum frequency generation (SFG) spectroscopy. Cellulose 21:1075–1086
34. Schroeder LR, Gentile VM, Atalla RH (1986) Nondegradative preparation of amorphous cellulose. J Wood Chem Technol 6(1):1–14
35. Segal L, Creely J, Martin A, Conrad C (1959) An empirical method for estimating the degree of crystallinity of native cellulose using the X-ray diffractometer. Text Res J 29(10):786–794
36. Thygesen A, Oddershede J, Lilholt H, Thomsen AB, Stahl K (2005) On the determination of crystallinity and cellulose content in plant fibers. Cellulose 12:563–576
37. Macrae CF, Bruno IJ, Chisholm JA, Edgington PR, McCabe P, Pidcock E, Rodriguez-Monge-L, Taylor R, Streek JV, Wood PA (2008) Mercury CSD 2.0-new features for the visualization and investigation of crystal structures. J Appl Crystallogr 41(2):466–470
38. French AD, Cintrón MS (2013) Cellulose polymorphy, crystallite size, and the segal crystallinity index. Cellulose 20(1):583–588
39. Atalla RH (1999) Individual structures of native celluloses. In: Proceedings 10th international symposium on wood and pulping chemistry: main symposium, 7–10 June 1999, Yokohama, Japan. Tappi Press, Atlanta, pp 608–614

40. Nelson ML, O'Connor RT (1964) Relation of certain infrared bands to cellulose crystallinity and crystal lattice type. Part II. A new infrared ratio for estimation of crystallinity in celluloses I and II. J Appl Polym Sci 8(3):1325–1341
41. Oh SY, Yoo DI, Shin Y, Kim HC, Kim HY, Chung YS, Park WH, Youk JH (2005) Crystalline structure analysis of cellulose treated with sodium hydroxide and carbon dioxide by means of X-ray diffraction and FTIR spectroscopy. Carbohydr Res 340(15):2376–2391
42. Agarwal UP, Reiner RS, Ralph SA (2010) Cellulose I crystallinity determination using FT–Raman spectroscopy: univariate and multivariate methods. Cellulose 17(4):721–733
43. Bansal P, Hall M, Realff MJ, Lee JH, Bommarius AS (2010) Multivariate statistical analysis of X-ray data from cellulose: a new method to determine degree of crystallinity and predict hydrolysis rates. Bioresour Technol 101(12):4461–4471
44. Terinte N, Ibbett R, Schuster KC (2011) Overview on native cellulose and microcrystalline cellulose I structure studied by X-ray diffraction (WAXD): comparison between measurement techniques. Lenzinger Ber 89:118–131
45. Driemeier C, Calligaris GA (2010) Theoretical and experimental developments for accurate determination of crystallinity of cellulose I materials. J Appl Crystallogr 44(1):184–192
46. Driemeier C (2014) Two-dimensional Rietveld analysis of celluloses from higher plants. Cellulose 21(2):1065–1073
47. Schenzel K, Fischer S, Brendler E (2005) New method for determining the degree of cellulose I crystallinity by means of FT Raman spectroscopy. Cellulose 12(3):223–231
48. Agarwal UP, Reiner RR, Ralph SA (2012) Estimation of cellulose crystallinity of lignocelluloses using near-IR FT-Raman spectroscopy and comparison of the Raman and Segal-WAXS methods. J Agric Food Chem 61(1):103–113
49. Ding SY, Himmel ME (2006) The maize primary cell wall microfibril: a new model derived from direct visualization. J Agric Food Chem 54(3):597–606
50. Newman RH, Hill SJ, Harris PJ (2013) Wide-angle X-ray scattering and solid-state nuclear magnetic resonance data combined to test models for cellulose microfibrils in mung bean cell walls. Plant Physiol 163(4):1558–1567
51. Zhang T, Mahgsoudy-Louyeh S, Tittmann B, Cosgrove DJ (2014) Visualization of the nanoscale pattern of recently-deposited cellulose microfibrils and matrix materials in never-dried primary walls of the onion epidermis. Cellulose 21:853–862
52. Patterson A (1939) The Scherrer formula for X-ray particle size determination. Phys Rev 56 (10):978
53. Oliveira RP, Driemeier C (2013) CRAFS: a model to analyze two-dimensional X-ray diffraction patterns of plant cellulose. J Appl Crystallogr 46(4):1196–1210
54. Fernandes AN, Thomas LH, Altaner CM, Callow P, Forsyth VT, Apperley DC, Kennedy CJ, Jarvis MC (2011) Nanostructure of cellulose microfibrils in spruce wood. Proc Natl Acad Sci 108(47):E1195–E1203

Adv Polym Sci (2016) 271: 133–168
DOI: 10.1007/12_2015_307

Published online: 24 April 2015

Ionic Liquids for the Production of Man-Made Cellulosic Fibers: Opportunities and Challenges

Michael Hummel, Anne Michud, Marjaana Tanttu, Shirin Asaadi, Yibo Ma, Lauri K.J. Hauru, Arno Parviainen, Alistair W.T. King, Ilkka Kilpeläinen, and Herbert Sixta

Abstract The constant worldwide increase in consumption of goods will also affect the textile market. The demand for cellulosic textile fibers is predicted to increase at such a rate that by 2030 there will be a considerable shortage, estimated at ~15 million tons annually. Currently, man-made cellulosic fibers are produced commercially via the viscose and Lyocell™ processes. Ionic liquids (ILs) have been proposed as alternative solvents to circumvent certain problems associated with these existing processes. We first provide a comprehensive review of the progress in fiber spinning based on ILs over the last decade. A summary of the reports on the preparation of pure cellulosic and composite fibers is complemented by an overview of the rheological characteristics and thermal degradation of cellulose–IL solutions. In the second part, we present a non-imidazolium-based ionic liquid, 1,5-diazabicyclo[4.3.0]non-5-enium acetate, as an excellent solvent for cellulose fiber spinning. The use of moderate process temperatures in this process avoids the otherwise extensive cellulose degradation. The structural and morphological properties of the spun fibers are described, as determined by WAXS, birefringence, and SEM measurements. Mechanical properties are also reported.

M. Hummel (✉), A. Michud, S. Asaadi, Y. Ma, L.K.J. Hauru, and H. Sixta (✉)
Department of Forest Products Technology, Aalto University, P.O. Box 16300, 00076 Aalto, Finland
e-mail: michael.hummel@aalto.fi; herbert.sixta@aalto.fi

M. Tanttu
Department of Design, School of Arts, Design and Architecture, Aalto University, P.O. Box 31000, 00076 Aalto, Finland

A. Parviainen, A.W.T. King, and I. Kilpeläinen
Department of Chemistry, University of Helsinki, A.I. Virtasen Aukio 1, 00014 Helsinki, Finland

Further, the suitability of the spun fibers to produce yarns for various textile applications is discussed.

Keywords [DBNH]OAc • Cellulosic fiber • Dry-jet wet fiber spinning • Ionic liquid • Rheology • Yarn spinning

Contents

Abbreviations

[amim]	1-Allyl-3-methylimdazolium
[bmim]	1-Butyl-3-methylimdazolium
[emim]	1-Ethyl-3-methylimdazolium
AS	Acid sulfite
COP	Crossover point
DBN	1,5-Diazabicyclo[4.3.0]non-5-ene
dep	Diethylphosphate
dmp	Dimethylphosphate
DMSO	Dimethyl sulfoxide
FWHM	Full width at half maximum
MCC	Microcrystalline cellulose
NMMO	*N*-Methylmorpholine *N*-oxide
OAc	Acetate
PAN	Polyacrylnitrile
PG	Propyl gallate (propyl 3,4,5-trihydroxybenzoate)
PHK	Prehydrolysis kraft
SEM	Scanning electron microscopy
WAXS	Wide angle X-ray scattering
WLF	Williams–Landel–Ferry

1 Introduction

Rapidly industrializing nations in Asia and South America are closing the prosperity gap between themselves and developed countries. This is reflected by an increased per-capita demand for consumer goods. Accompanied by an estimated population growth of 20% (1.4 billion) over the next two decades, new sustainable resource management strategies are urgently needed. These changes will also affect the textile fiber industry. The demand for textile fibers reached 75.5 million tons in 2010 and is predicted to rise to 133.5 million tons by 2030 (at a growth rate of 3.1% p.a.) [1, 2]. As a result of certain inherent properties of cellulosic fibers (moisture management, breathability), which cannot be met adequately by synthetic fibers, the market share of natural and man-made cellulosic fibers is expected to be between 33 and 37% of the global fiber consumption. The consumption of cellulosic fibers is expected to increase from the current level of 3.7 kg per capita to 5.4 by 2030. The cotton production capacity, however, is no longer expandable. Although the cultivation of cotton hybrids will increase the harvest yield from 800 (2010) to 925 kg/ha (2030), this cannot compensate for the loss of arable land and concomitant increase in demand. Thus, it is estimated that only 3.1 kg of cotton per capita will be available in 2030 [1]. This so-called cellulose gap offers new opportunities for man-made cellulosic fibers. Gradual replacement of cotton by pulp-based fibers is also necessary from an ecological perspective. The production of cotton consumes substantial amounts of water and requires high-grade arable land and thus competes heavily with the cultivation of comestible goods. Further, a recent life-cycle analysis confirmed that the carbon footprint of man-made cellulosic fibers is substantially lower than that of cotton [3]. The pulp industry has already reacted to the anticipated increased demand for dissolving pulp. A number of new dissolving pulp mills have been installed in Asia, and several existing pulp mills in Europe and North America have completed the conversion of (parts of) their production lines to produce dissolving pulp [4].

Currently, approximately three-quarters of the global production of man-made cellulosic fibers is based on the viscose process [5]. Due to the improved wear properties of synthetic fibers and more stringent environmental regulations, substantial viscose capacities were closed in the Northern hemisphere in the early 1980s. Since the beginning of the twenty-first century, however, the installation of new plants and expansion of existing viscose plants in China and in South and Southeast Asia has led to a worldwide increase in production capacity (from 1.5 million tons in 1990 to 3.8 in 2012) [4]. From an environmental point of view, however, it is questionable whether the viscose technique should be further promoted. The utilization of large amounts of CS_2 and caustic soda results in hazardous by-products such as H_2S gas and other volatile thio-compounds, which may cause severe stress to the environment. Consequently, sulfur-free viscose-type alternatives to the wet spinning processes, such as the carbamate [6–8] or BioCelSol [9] processes, have been suggested. However, the moderate fiber properties and the substantial need for auxiliary chemicals have so far prevented

commercialization of these techniques. By dissolving cellulose in non-derivatizing solvents, this problem can be by-passed. Of the several direct cellulose solvents, such as Cuen (cupriethylene diamine) [10], Cuoxam (cuprammonium hydroxide) [10], Cadoxen (CdO/ethylenediamine) [10], DMAc/LiCl [11], DMSO/TBAF [12, 13], ammonia or amine/thiocyante [14–17], and phosphoric acid [18, 19], only *N*-methylmorpholine *N*-oxide (NMMO) monohydrate has been developed to a commercial level. The latter is used for the production of so-called Lyocell fibers [20]. The name Lyocell, given in 1989 for solvent-spun fibers, owes its genesis to the Greek word *lyein* (meaning dissolve) from which *lyo* derives and to *cell* from cellulose. This name was recognized as the generic name by BISFA (International Bureau for the Standardization of Rayon and Synthetic Fibers, Brussels) and the US Federal Trade Commission [21].

In the Lyocell production process, bleached chemical pulps, mainly dissolving pulps, are first suspended in a NMMO–water mixture. Subsequently, the water content of the slurry is gradually decreased at elevated temperature and reduced pressure conditions until the solvent system corresponds to a NMMO monohydrate concentration (13–15 wt% water) in which cellulose is soluble. The resulting spinning dope (cellulose concentration of 8–20%) is then extruded via an air gap into a coagulation bath where solvent exchange takes place, resulting in the regeneration of the cellulosic solute. Typically, water with a small NMMO content is used as coagulation medium [7, 20]. NMMO is then recovered by evaporation of water from the spin bath solution. In contrast to the viscose process, the spinning dope is not extruded directly into the coagulation medium (wet spinning) but passes an air gap and remains as a liquid filament for a short period of time. By drawing the fiber before and in the coagulation zone (i.e., take-up velocity is higher than the extrusion velocity) the filament is stretched up to 10–15 times its original length [22, 23]. The viscoelastic polymer solution is thus subjected to additional extensional stress, which triggers an orientation of the cellulose molecule chains along the fiber axis [24]. This results in the characteristic high tensile strength of Lyocell fibers that, unlike viscose fibers, remains high even in wet conditions [25, 26]. In 2014, the worldwide Lyocell production capacity was expanded to 200,000 tons/year [4]. However, the versatility of the Lyocell process is limited by certain intrinsic properties of NMMO, resulting from its peculiar structure. The N–O moiety impedes the implementation of redox-active agents, whereas the cyclic ether structure is prone to so-called thermal runaway reactions, necessitating appropriate stabilizers [27–29]. An extensive overview of the side reactions and by-product formation in the Lyocell process has been given by Rosenau and coworkers [30].

Alternative direct solvents for pulp cellulose that avoid the problems associated with NMMO would thus be highly attractive from both an environmental and economic point of view.

2 Fiber Spinning based on Ionic Liquids: State of the Art

2.1 Ionic Liquids

Although ionic liquids (ILs) have been known for many decades [31] significant research activity in this field started only in the early 1990s. At that time, ILs still represented a somewhat peculiar substance class that only a handful of research groups were familiar with. But, their unique properties and broad spectrum of application possibilities have promoted intensive research activity. By definition, ILs consist entirely of ions (when adding a molecular co-solvent, the term "electrolyte solution" is more applicable [32]). The combination of bulky organic cations, in which the positive charge is either delocalized and/or sterically shielded, and inorganic anions favors the liquid state of the system in terms of enthalpy and entropy. Thus, these salts display a melting point below 100°C. A first comprehensive overview was given by Welton [33]. Among many different applications, ILs became especially interesting as solvent systems. Because of the virtually endless combination possibilities of cations and anions, ILs can be designed task-specifically (TSILs). Thus, features such as solvent properties can be adjusted to maximize the solubility of one or several target solutes. In 2002, ILs were explored as cellulose solvents [34]. The discovery that ILs were capable of dissolving biopolymers with little or no degradation has afforded numerous publications dealing with the solubilization of cellulosic material and even wood. To date, only a few ILs are known that serve as cellulose solvents. A detailed description of cellulose- and wood-dissolving ILs and their properties can be found in extensive review articles [35–39]. Only few of those have been reported for the production of cellulosic fibers. These so-called first generation spinning ILs typically comprise an imidazolium cation with chloride as the anion. However, their high melting point and the corrosive character of halides toward metal processing equipment have promoted the implementation of alternative anions such as acetate and dialkylphosphate. Figure 1 gives an overview of the structure of these ILs. In Sect. 2, we give a comprehensive review of reported IL-based fiber spinning, including rheological properties of cellulose–IL solutions, and cellulose and IL degradation. Section 3 introduces an ionic liquid suitable for fiber spinning and based on a cation other than imidazolium. The hitherto novel cellulose spinning solvent 1,5-diazabicyclo [4.3.0]non-5-enium acetate ([DBNH]OAc) **4b** shows excellent spin stability, resulting in outstanding fiber properties.

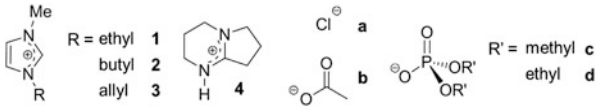

Fig. 1 Constituent ions of ILs used for fiber spinning: **1** 1-ethyl-3-methylimidazolium, **2** 1-butyl-3-methylimidazolium, **3** 1-allyl-3-methylimidazolium, **4** 1,5-diazabicyclo[4.3.0]non-5-enium. Also shown are typical ions, including chloride, acetate, dimethylphosphate, and diethylphosphate (**a**, **b**, **c**, and **d**, respectively). ILs are denoted in the text by a digit representing a cation (**1**–**4**) followed by a letter (**a**–**d**) representing the counter-ion

2.2 Rheology of Cellulose–IL Solutions

Before reviewing the existing literature on fiber spinning from IL solutions, this section addresses the rheological properties of various cellulose–IL solutions. As pointed out later, certain viscoelastic characteristics are decisive for the spinnability of cellulose solutions. Several reports are available describing both shear and oscillatory rheological studies.

Steady shear rheological measurements of microcrystalline cellulose (MCC), sulfite pulp, and bacterial cellulose in 1-butyl-3-methylimdazolium chloride ([bmim]Cl) **2a** and 1-ethyl-3-methylimdazolium acetate ([emim]OAc) **1b** were first reported by Budtova and coworkers [40, 41]. Typically, for polymer melts and solutions, shear thinning was observed at high shear rates, with the onset of shear thinning shifting towards lower shear rates with increasing solute concentration or decreasing temperature. Plotting zero shear viscosity η_0 versus solution concentration, two distinct regions are observed: a linear region in the so-called dilute regime and a power law $\eta_0 \propto c^n$ region above the overlap concentration c^*, which is found to be around 2%. The viscosities of [bmim]Cl **2a** solutions were substantially higher than those of [emim]OAc **1b** analogs. This was attributed to the higher solvent viscosity of the former. Plotting relative viscosity ($\eta_{solution}/\eta_{solvent}$) against concentration, the data of the two IL solutions collapse into one master curve. Neglecting the rather small temperature dependence on the density of [emim]OAc **1b**, the zero shear viscosity of the respective solutions could be converted into the kinematic viscosity, which allowed for the determination of the intrinsic viscosity [η] of the cellulosic solute in [emim]OAc **1b**. Interestingly, Budtova et al. [40, 41] and later Haward et al. [42] showed that by increasing the temperature the intrinsic viscosity decreases and c^* increases, indicating a decline in the polymer's radius of gyration. Thus, the thermodynamic quality of the IL solvent decreases with heating. By analyzing the temperature dependence of the viscosity in an Arrhenius plot, the activation energy of flow can be calculated. Although linear fits of the data had reasonable correlation coefficients, a closer look revealed a concave curvature of the plot. Thus, a fit with the Vogel–Fulcher–Tamman (VFT) equation, which is typically used for "glass-forming" liquids, was found to be more accurate and provided the so-called pseudo-activation energy and glass transition temperature.

The elastic and viscous proportions of cellulose–IL solutions can be assessed via oscillatory rheology measurements [43, 44]. A frequency sweep in the linear viscoelastic range of the solutions provides the complex viscosity $|\eta^*|$ and storage (G') and loss (G'') moduli. Petrovan and coworkers reported a typical shear thinning behavior of $|\eta^*|$ at high angular frequencies ω, with the onset shifting to higher frequencies upon heating the solutions. Master curves covering an extended frequency range can be generated by using temperature shift factors according to the WLF (Williams–Landel–Ferry) theory. Several authors have used this approach to find the right spinning temperature of the respective cellulose–IL solution (vide infra). The complex viscosity curves can be fitted with different model functions to

determine the zero shear viscosity. The Carreau and Cross viscosity models have been proposed, with the latter being more suitable for cellulose–IL solutions and, consequently, predominantly used. However, the validity of the Cox–Merz rule has to be assumed in order to derive the zero shear viscosity from the fit. This empirical postulate indicates that the complex (oscillatory) and dynamic (steady shear) viscosities superimpose at equal values of frequency and shear rate [45]. This has been confirmed by some authors [42], whereas others observed a strong departure, in particular at high cellulose concentration or high shear rates [46, 47].

Storage (G') and loss (G'') moduli reflect the elastic and viscous behavior of the cellulose solution, which are frequency (ω) dependent. At low angular frequency, the loss modulus is usually higher and should scale as $G'' \propto \omega$ wheras the storage modulus scales as $G' \propto \omega^2$. Typically, this is not observed for highly concentrated cellulose solutions (>10%) because such behavior occurs at very low frequencies, outside the accessible measurement range. As the frequency is increased, the storage and loss moduli intersect at the so-called crossover point (COP), after which the solution behaves as predominantly elastic. The COP represents a relaxation time that is related to the molecular weight of the cellulose and is shifted to higher angular frequencies with an increase in temperature or decrease in cellulose concentration [48].

As mentioned in the Introduction, dry-jet wet spinning allows stretching of the liquid filament in the air gap, which exerts extensional stress on the filament, resulting in an orientation of the cellulose polymer chains along the spinning axis. Only two studies are available on the elongational rheology of cellulose–IL solutions. Sammons et al. used a capillary extrusion rheometer with hyperbolic dies of Hencky strains of 5, 6, and 7 [49]. The tested cellulose-[bmim]Cl **2a** solutions exhibited strain hardening and strain rate thinning. The increase in viscosity with higher Hencky strain can be attributed to the gradual extension of the cellulose polymer chains. The temperature effect was more pronounced at high strain rates, although still moderate compared with shear rheology. Haward et al. determined elongational relaxation times and apparent transient extensional viscosities of cellulose-[emim]OAc **1b** solutions by means of a capillary break-up extensional rheometer (CaBER) [42]. In a CaBER measurement, the solution is placed between two plates that are separated rapidly in a step-stretch to create a liquid filament bridge between the two plates. Once the plates have reached their end position, capillary forces act on the filament bridge and cause a continuous thinning of the filament until ultimate break-up. In contrast to the hyperbolic dies, a truly shear-free unidirectional extensional flow, as in the spin line, is generated. The thinning dynamics are governed by the balance between capillary forces and elastic tensile stresses [50, 51]. In the case of a pulp–[emim]OAc **1b** solution, a correlation between the extensional relaxation time of the elastocapillary regime and the cellulose concentration could be established. It was claimed that the solution must exhibit a certain minimum relaxation time to be spinnable in a dry-jet wet process. Also, significant strain hardening was only observed at higher cellulose concentrations.

Although cellulose–IL solutions are in general sensitive to molecular solvents, which mostly act as anti-solvent and induce precipitation of the solute, it is possible to dilute some cellulose–IL solutions to reduce the typical high viscosity. DMSO [52], 1,3-dimethyl-2-imidazolidinone [32], or small amounts of water [53, 54] were reported to reduce the viscosity of the spinning dope. However, the change in the viscoelastic properties and, consequently, the effect on spinnability has not been discussed.

Solutions of cellulose [55, 56] and cellulose derivatives [57, 58] are known to form lyotropic phases under certain circumstances. In the case of cellulose processing, this can lead to outstanding features of the shaped product. As a result of the high orientation of the cellulose chains, the final product can exhibit extraordinary properties, as in the case of cellulose fibers spun from liquid crystalline super-phosphoric acid solutions. Tenacity values of up to 90 cN/tex (centi-Newton per (gram per 1000 meter length)) were reported for these fibers called Fibre B™ or Bocell™ [26, 59]. Liquid crystalline structures have also been observed in cellulose–IL solutions. Kosan et al. showed that distinct lyotropic phases were visible in a transmitted light microscope with cross-polarizers once a certain concentration of beech prehydrolysis kraft (PHK) pulp in [emim]OAc **1b**, [emim]dep **1d**, and [bmim]Cl **2a** was exceeded [60]. Liquid crystalline phases can also be detected by means of different rheological techniques. Isotropic and anisotropic phases have different activation energies for flow. Thus, an Arrhenius plot of the logarithmic viscosity versus the inverse of temperature shows a kink, and the slope of the linear trend changes notably when the solution turns isotropic. Song et al. made similar observations with MCC in [amim]Cl **3a** and [emim]OAc **1b** [61, 62]. They detected the concentration threshold upon which lyotropic phases became visible by means of polarized light microscopy and oscillatory shear-rheological measurements. At concentrations where isotropic solutions turn anisotropic, the damping factor determined in a frequency sweep was found to be independent of the angular frequency, in accordance with Winter and Chambon theory [63, 64]. Comparing related reports, it can be concluded that this threshold concentration is dependent on the cellulosic substrate (particularly on the degree of polymerization, DP) and the ionic liquid: 18.2% beech pulp (DP_{cuoxam} 367) in [bmim]Cl **2a** at 82°C; ca. 25% of the same beech pulp in [emim]OAc **1b** at room temperature; 8.6% of the same beech pulp in [emim]dep **1d** at 40°C; ca. 16% of MCC (DP_{cuen} 200) in [amim]Cl **3a**; and ca. 18% of MCC (DP_{cuen} 220) in [emim]OAc **1b**. However, in all cases the lyotropic phases show a clearing temperature T_c at which the solutions turn isotropic. The reconstitution of the lyotropic phase upon cooling is kinetically hampered and can take several hours to days. So far, all reported lyotropic cellulose–IL systems have a T_c that is lower than their process temperature (i.e., the temperature at which the solution is spun into filaments). Thus, it has not yet been possible to produce Bocell-type fibers using ILs.

2.3 Fiber Spinning

Although the possibility of producing fibers and films from cellulose–IL solutions has already been indicated by Swatloski et al. in their initial patent [65], it was Laus et al. [66] and Bentivoglio et al. [67] who first reported the properties of fibers suitable for textile applications. The authors studied the stability and spinnability of different commercial dissolving pulps dissolved in [bmim]Cl **2a** and [amim]Cl **3a**. All solutions were spun according to the NMMO-based Lyocell technique, that is, in a dry-jet wet spinning process where the liquid filament first passes through an air gap before immersion in the coagulation bath where the solid cellulosic fibers are formed [68]. Gel permeation chromatography (GPC) analyses revealed that ILs **2a** and **3a** degrade the cellulosic solute substantially at 90 and 80°C, respectively. The addition of propyl gallate (PG) as stabilizer showed only minor effects. However, by choosing a lower cellulose concentration the spinning temperature can be reduced, which reduces the degradation. Thus, fibers with high tenacity values can be obtained, partly exceeding those of NMMO-based Lyocell fibers. Related parameters and results are summarized in Table 1, entries 1–9.

High tenacity fibers from IL solution were also reported by Kosan and coworkers [69, 70]. Eucalyptus prehydrolysis sulfate and cotton linters pulps were dissolved in various ILs following the typical Lyocell dissolving protocol. The cellulosic solute was suspended in an IL–water mixture, PG was added as stabilizer, and the water subsequently evaporated under shear resulting in a homogeneous spinning dope [78]. The solutions were analyzed in terms of their viscoelastic properties. This was one of the first attempts to correlate rheological key parameter such as viscosity (both dynamic and complex), storage (G') and loss (G'') moduli, and relaxation times of cellulose–IL solutions with the respective Lyocell–NMMO monohydrate solutions. The polymer solutions were subjected to oscillatory measurements at different temperatures to generate master curves for the complex viscosity and dynamic moduli. Thus, the zero-shear viscosity (η_0) and crossover point of the moduli could be calculated for each spinning dope at the desired temperature. This contributed substantially to the understanding of spinnability of IL-based dopes. Solutions of [bmim]Cl **2a** showed slightly higher η_0 values than the corresponding NMMO monohydrate solutions. This deviation was compensated by a reduced cellulose concentration or by increased spinning temperature. Thus, the viscoelastic properties could be adjusted to the optimum spinning condition for NMMO monohydrate. Michels and Kosan distinguished between solution quality and solution state. The solution state is derived from the rheological properties of the polymer solution and is connected to its spinnability. The solution quality, which is crucial for the spin stability, is related to the amount of undissolved particles in the range 1–100 μm, expressed as particle size distribution or so-called filter index [79–81]. Viscoelastic properties of [bmim]Cl–pulp solutions were also studied by Cai et al. [73]. Solutions (8 wt%) were spun at different draw ratios and the resulting fibers analyzed in terms of strength properties, crystallinity, and – for the first time for IL-spun fibers – in terms of their dyeing properties, which again reflected the

Table 1 Overview of conditions for fiber spinning with ionic liquids and the resultant fiber properties

No	Pulp	DP_w[a]	IL	Conc. (wt%)	Additive (PG, %)	η_0		Spin-temp. (°C)	Nozzle diameter (µm)	Air gap (mm)	DR	Titer (dtex)	Tenacity[b] (cN/tex)	Elongation[b] (%)	Reference
						Pa s	at °C								
1	Beech AS	1,180	[amim] Cl	12.5	0			75	100		10.5	1.3	32.2	8.4	Laus et al. [66]
2	Euca. PHK	815	[amim] Cl	10	0			100	100		8.6	1.6	26.8	10.8	Laus et al. [66]
3	Euca. PHK	920	[amim] Cl	10	0.1			80	100		10.5	1.3	36.8	11.2	Laus et al. [66]
4	Euca. PHK	920	[bmim] Cl	11	0.1			100	100		10.5	1.3	33.1	11.5	Laus et al. [66]
5	Euca. PHK	580	[bmim] Cl	11	0.1			105	100		13.7	1.0	37.9	11.3	Laus et al. [66]
6	Euca. PHK	170	[bmim] Cl	11	0							n.s.			Laus et al. [66]
7	Euca. PHK	920	[bmim] Cl	11	0.1 + NaOH			100	100		15.2	0.9	51.2	8.5	Bentivoglio [67]
8	Euca. PHK	920	[bmim] Cl	11	0.1 + NaOH			100	100		6.5	2.1	45.0	7.5	Bentivoglio [67]
9	Euca. PHK	790	[amim] Cl	11				70	100		6.2	2.2	41.6	12.2	Bentivoglio [67]
10	Euca. PHK	569[c]	[bmim] Cl	10.4					70		2.9	1.7	38.6	13.2	Michels, Kosan [69].
11	Euca. PHK	569[c]	[bmim] Cl	10.4					100		6	1.7	43.8	15.3	Michels, Kosan [69].
12	Euca. PHK	569[c]	[bmim] Cl	10.4					130		10.9	1.6	44.7	12	Michels, Kosan [69].
13	Euca. AS	514	[bmim] Cl	13.6		47,540	85	116	100	80	*10.6*	1.5	53.4	13.1	Kosan et al. [70]
14	Euca. AS	493	[emim] Cl	15.8		24,900	85	99	90	55	*7.9*	1.8	53.1	12.9	Kosan et al. [70]
15	Euca. AS	486	[bmim] OAc	13.2		9,690	85	90	90	60	*7.3*	1.7	44.1	15.5	Kosan et al. [70]

16	Euca. AS	479	[bmim] OAc	18.9		63,630	85	98	90	70	*10.7*	1.6	48.6	12.6	Kosan et al. [70]
17	Euca. AS	515	[emim] OAc	19.6		30,560	85	99	90	40	*10.3*	1.8	45.6	11.2	Kosan et al. [70]
18	Euca. AS	790	[bmim] Cl	12.1	0.2 + NaOH	17,550	85		100	40	*7.8*	1.8	56.8	9.6	Kosan et al. [71]
19	Cotton L.	686[c]	[bmim] Cl	11		~4,500	90	90	145	50			20.7	6.8	Cai et al. [72]
20	Spr. NH_4-S	722[c]	[bmim] Cl	8		~1,350	85	85	145	50	2.4		26.4	8	Cai et al. [73]
21	Spr. NH_4-S	722[c]	[bmim] Cl	8		~1,350	85	85	145	50	3.5		29.3	7	Cai et al. [73]
22	Bamboo	1,120[c]	[emim] OAc	8				85	145	50	3.5		32	7.8	Cai et al. [74]
23	Euca. AS	592[c]	[emim] OAc	10		18,000	20	20	90	10	*2.3*	4.1	24.6	3.8	Ingildeev et al. [75]
24	Euca. AS	592[c]	[emim] OAc	6		33	90	90	40	wet	*0.5*	1.6	22.2	8	Ingildeev et al. [75]
25	Euca. AS	592[c]	[emim] dep	10		18,000	60	60	90	10	*1.9*	4.9	26.4	6	Ingildeev et al. [75]
26	Cotton L.	514[c]	[bmim] Cl	5		50	90	90	150	80	5.0	2.22	35.1	6.6	Jiang et al. [76]
27	Cotton L.	514[c]	[bmim] Cl	5		50	90	90	150	80	5.0	2.22	38.8	6.5	Jiang et al. [76]
28	Cotton L.	514[c]	[bmim] Cl	5		50	90	90	150	80	5.0	2.22	42.1	6.2	Jiang et al. [76]
29	Euca. AS	592[c]	[emim] OAc	6				90	32	Wet	1.0	0.5	17.6	6.5	Hermanutz et al. [77]

DP_w average DP from intrinsic viscosity measurements, *AS* acid sulfite, *Euca* eucalyptus, *PHK* prehydrolysis kraft, *L* linters, *Spr* spruce, *NH_4-S* ammonium sulfite, *n.s.* not spinnable

[a]Average degree of polymerization from intrinsic viscosity measurements; after dissolution (fiber)

[b]Tenacity and elongation in the conditioned state

[c]Given by author

close similarity of IL and NMMO-based Lyocell fibers. Constant draw but different extrusion velocities were adjusted by Jiang et al. using a 5 wt% solution of cotton pulp in [bmim]Cl **2a** (Table 1, entries 26–28) [76]. In this setup, the extensional stress (as a consequence of the draw) on the dope-filament in the air gap was kept constant and the molecular orientation of the cellulose polymer chains increased solely by the augmented shear stress in the spinning capillaries. Indeed, the crystalline orientation of the resulting cellulosic fiber increased directly with the extrusion velocity, resulting in higher tenacities. The crystallographic properties were determined via WAXS and SAXS analyses and compared with those of commercial fibers. The close resemblance to NMMO-based Lyocell fibers was confirmed [82]. Typical for dry-jet wet spinning technology, the overall crystallinity, the degree of crystalline orientation, and the birefringence (total orientation) of NMMO and IL-spun fibers surpassed those of viscose fibers. SAXS measurements showed substantially larger voids in viscose fibers [82]. Furthermore, the Lyocell-type fibers typically have a higher cellulose DP and a fibrillar morphology resulting from coagulation via spinodal decomposition. All these factors contribute to the superior mechanical properties of Lyocell-type fibers compared with viscose.

Recently, Sammons et al. suggested the use of semi-hyperbolically converging dies to spin a pulp–[bmim]Cl **2a** solution [83]. The dies were the same as used in their study of the elongational rheology (vide supra) and are claimed to extrude the spinning dope shear-free [49]. The authors defined an orientation number as the product of the characteristic elongational relaxation time, the Hencky strain, and the elongational strain rate. The orientation number showed a linear correlation with the Herman orientation factor. However, others have doubted the total absence of shear in the spinneret and, thus, shear-induced orientation has to be taken into account [42].

Although fibers spun from first generation ILs (i.e., [bmim]Cl **2a** and [amim]Cl **3a**) showed good tensile properties, use of halide-containing ILs is associated with several drawbacks. The typically high melting points afford high process temperatures, which cause severe cellulose degradation unless appropriate stabilizers are added. Furthermore, halides have a high corrosive potential toward metal processing equipment. Thus, alternative anions such as acetate and dialkylphosphates have been introduced.

It was found that cellulose solutions in acetate-containing ILs, [emim]OAc **1b** and [bmim]OAc **2b**, have a much lower viscosity than the halide analogs or NMMO–Lyocell solutions. Kosan et al. compensated for this by increasing the cellulose concentration (to almost 20 wt%) to obtain spinning dopes with viscoelastic properties comparable with NMMO–Lyocell (Table 1, entries 10–17) [70, 78]. At lower concentration, the fibers can be drawn only to a limited extent, resulting in lower tenacity values, as demonstrated by Cai et al. when spinning bamboo pulp (Table 1, entry 22) [74]. The rheological approach to spinnability was also pursued and further developed by Hermanutz and colleagues [84, 85]. Cellulosic fibers were spun from 10 wt% solutions of a eucalyptus sulfite pulp in [emim]OAc **1b** and [emim]dep **1d** (Table 1, entries 23–25) [75]. The spinning temperature was such that η_0 reached values of 18,000 Pa s, which was determined to be suitable

for the NMMO monohydrate dope. In accordance with Michels and Kosan, the viscosity of the [emim]OAc **1b** dope with the same polymer concentration was considerably lower. Whereas Kosan and Michels responded to the particular low viscosity of [emim]OAc **1b** solutions by increasing the cellulose concentration, Hermanutz and coworkers lowered the spinning temperature. Morphological analysis by means of SEM revealed the typical fibrillar structure of Lyocell fibers. Tenacity values were rather low (around 25 cN/tex), probably as a result of the relative high linear density of 4–5 dtex (grams per 10,000 m length). However, although the NMMO and [emim]OAc **1b** fibers showed typical fibrillation behavior when subjected to mechanical abrasive stress, the fibers spun from [emim]dep **1d** were reported to show no fibrillation (Table 1, entry 25).

In contrast to dry-jet wet spinning, where typically high draw ratios are pursued, the low viscosity of [emim]OAc **1b** is of minor concern when no or only limited draw is desired, as is the case for viscose-type wet spinning. Ingildeev et al. successfully produced fibers of 1.6 dtex via wet-spinning of a 6 wt% [emim]OAc **1b** dope (Table 1, entry 24). The same group reported in 2012 that the same solution can even be spun to microfibers of 0.5 dtex when special spinnerets with holes of 32 μm diameter are used (Table 1, entry 29) [77]. However, in both cases the wet-spun fibers showed tenacity values similar or inferior to commercial viscose fibers. This result was confirmed by other groups [86, 87]. Olsson and Westman studied the influence of the DP of the cellulosic solute on the properties of the final fibers [86]. Different blends of eucalyptus kraft dissolving pulp and MCC were dissolved in [emim]OAc **1b** and spun via a wet-spinning process. Although they could observe a steady increase in tenacity with increasing DP, the values were all in the range of viscose fibers or below.

2.4 Multicomponent Fibers Spun from IL Solutions

Ionic liquids are not only powerful cellulose solvents but are also capable of dissolving various other organic and inorganic solutes. This broad solubility window in combination with a pronounced chemical stability offers the possibility to produce composite fibers. Thus, other synthetic or natural polymers, catalytically actives species, and inorganic compounds can be embedded into a cellulose matrix. Incorporation of inorganic particles into a cellulosic fiber has been reported by several groups. Rogers and coworkers produced magnetic fibers by spinning a cellulose–[emim]Cl **1a** solution with magnetite powder (Fe_3O_4; $\leq$5 μm) suspended therein. They demonstrated that magnetite incorporation did not deteriorate thermal stability. However, the fiber surface became noticeably rougher and fiber strength declined significantly with an increasing proportion of ferromagnetic particles [88, 89]. Later, the authors reported similar results for the thermal stability and tenacity of the composite fibers after adding rutile (TiO_2; $\leq$5 μm) as antibacterial agent to the fiber matrix. Energy dispersive X-ray analysis showed that the surface concentration of TiO_2 particles was slightly elevated, which promoted the desired antibacterial effect [90]. Song et al. added nano-SiO_2 (80 nm diameter) to an

MCC–[amim]Cl **3a** solution and observed a noticeable change in the viscoelastic properties of the resulting mixture. The nano-SiO_2 particles promote interaction between the cellulose polymer chains, resulting in a pronounced elastic behavior. A gel-like structure was confirmed by steady shear and oscillatory measurements. The spun fibers showed improved strength properties up to 8 wt% loading, after which the strength declined [91].

A reinforcing effect was also observed by Zhang et al. [92] and Rahatekar et al. [93] when embedding multiwall carbon nanotubes (MWCNTs) into the cellulosic fiber. Although the groups used different systems (MWCNTs of 50 nm × 50 μm and cellulose of DP 650 in [amim]Cl **3a** [92] and MWCNTs of 80 nm × 100 μm and cellulose of DP 820 in [emim]OAc **1b** [93]) they reported similar results. In both cases the MWCNTs acted as rheological modifier, necessitating an adjustment of the spinning conditions. The carbon modifier caused an increase in crystallinity of the cellulosic matrix. Addition of the carbon additive had only a small influence on thermal stability. However, both studies showed a small increase in fiber tenacity (from 204 to 335 MPa at 4% MWCNT [92] and from 198 to 257 MPa at 7% MWCNT [93]), which started to decline once a certain threshold of MWCNT content was surpassed. Detoxifying and antibacterial properties were imparted to cellulosic fibers by Wendler et al. by adding activated charcoal and silver nanoparticles, respectively [28, 94]. The fibers were spun from [bmim]Cl **2a**, [emim]OAc **1b** and NMMO monohydrate solutions, respectively. Because both particle species possess considerable catalytic activity, the thermal stability of the composite solutions was tested by differential scanning calorimetry (DSC). The IL solutions clearly had superior thermal stability compared with the NMMO analog, as shown by the onset temperatures of the exothermal event: 150, 180, and 200°C for NMMO, [emim]OAc **1b**, and [bmim]Cl **2a**, respectively. Small amounts of micro- and nanosized silver particles in the cellulosic fibers did not impair the structural properties of the fibers but imparted the desired antimicrobial effect. Fibers were spun with 50% charcoal loading for detoxifying nonwoven fabrics, although the tests showed that a certain share of the absorbent material was inactive in the fiber matrix. The mentioned reports all confirmed that a wide spectrum of particles can be incorporated into a cellulosic matrix by regenerating the respective IL suspensions. However, agglomeration occurs if the loading surpasses a particle immanent threshold, which typically has an adverse effect on both the additive activity and the fiber tenacity.

The wide solubility window of ILs also offers the possibility of dissolving two or more polymers simultaneously to form copolymer composites. However, a homogeneous solution does not necessary result in a continuous copolymer phase upon regeneration. Limited interaction between the polymer species can induce phase separation, leading to a discontinuous structure with polymer agglomerates. Kosan et al. mixed eucalyptus pulp and cotton linters with polyacrylnitrile (PAN) in [emim]Cl **1a** and [bmim]Cl **2a** in various ratios and then spun the resulting fibers [95]. Although the addition of PAN had a negative effect on the tenacity, the fibrillation tendency was markedly reduced. The study did not include any morphological analysis to reveal the molecular structure of the copolymer. However, the

authors found that PAN and cellulose can be dissolved selectively by treatment of the composite fibers with dimethyl formamide (DMF) and Cuoxam solution, respectively. This indicates a limited interaction of the polymers. Ingildeev et al. found later that cellulose and PAN do not form a continuous phase in ILs [96]. Studying a series of different synthetic polymers [*m*-aramide, poly(*m*-xyleneadipamide), polyamide, and PAN] the authors reported that only those polymers bearing functional groups capable of interacting with cellulose via hydrogen bonds i.e., *m*-aramide and poly(*m*-xyleneadipamide)] formed homogeneous mixtures with cellulose in IL solutions. Small increments in polyamide and PAN content induced phase separation from cellulose in IL solutions, which led to inhomogeneous and porous fibers with poor mechanical properties. In contrast, *m*-aramide showed complete miscibility with cellulose in [emim]OAc **1b** and [emim]dep **1d**. In accordance with their reports on the spinnability of pure cellulose (vide supra), the low viscosity of the polymer solution in [emim]OAc **1b** only permitted wet spinning, whereas the solutions in [emim]dep **1d** could be processed in a dry-jet wet manner. In essence, the effects of a polymer additive were very similar to those observed for addition of inorganic particles. The polymers had a pronounced effect on the rheological properties of the spinning dopes, necessitating an adjustment of the spinning conditions [97]. The fiber tenacity rose only slightly with an increasing share of *m*-aramide. The fibrillation behavior was improved, probably as a result of the reported decrease in crystallinity.

In two extensive studies, Wendler et al. reported on the miscibility and processability of polysaccharide–polysaccharide mixtures in NMMO, [emim]OAc **1b**, and caustic solution [98, 99]. Xanthan, cellulose carbamate, carboxymethyl cellulose, starch, xylan, carboxymethyl xylan, locust bean gum, guar gum, and gum tragacanth showed good solubility in [emim]OAc **1b** and were thus mixed with cellulose. Despite the molecular similarities of the single polymers, immiscibility and phase separation were observed in most cases. With the exception of cellulose carbamate, none of the polysaccharides revealed anisotropic behavior in the tested concentration range (up to 20 wt%) when dissolved alone. However, anisotropy could be detected by polarized light microscopy and rheological analyses in mixtures of cellulose with xanthan, locust bean gum, and gum tragacanth. Irrespective of the incomplete miscibility, composite fibers could be spun in a dry-jet wet process with [emim]OAc **1b** and NMMO, and in a wet process from the respective caustic solutions. Consequently, [emim]OAc **1b** and NMMO fibers exhibited similar properties. In all cases, the copolymer caused a reduction in the overall crystalline orientation of the fiber, accompanied by a drop in tensile strength. Fibers processed in [emim]OAc **1b** depicted a smoother surface and a higher water contact angle than the NMMO analogs. The water retention value rose slightly with copolymer addition for all fibers.

Lehmann et al. added kraft and organosolv lignin as nonlinear polymers to a solutions of pulp cellulose in [bmim]Cl **2a** and [emim]OAc **1b**. The resulting fibers showed tenacities of 25 and 28 cN/tex and could represent cheap cellulose-based precursors for carbon fibers because of their elevated carbon content [100].

Instead of blending several polymers, Rogers and coworkers suggested direct processing of the world's most abundant natural polymer composite, wood [101].

A comprehensive set of untreated and pretreated lignocellulosic sources was dissolved in [emim]OAc **1b** and spun in a dry-jet wet spinning process. Although their set-up was limited to extrusion of relatively thick filaments (the final fibers were in the range of 60–220 μm diameter), the influence of several parameters could be studied systematically. The tensile strength of the fiber was intimately connected with the cellulose content of the substrate. Pretreated pulps with reduced lignin and hemicellulose content resulted in stronger fibers. In some cases, cellulose enrichment was observed during the spinning process, indicating that some of the lignin and hemicelluloses were not regenerated along with the cellulose matrix but remained in solution. By choosing the right coagulation bath composition, it was possible to amplify the delignification of the lignocellulosic substrate in the spinning process and produce cellulose-enriched strong fibers [102, 103]. Fink and coworkers also reported the production of lignocellulosic fibers from hemp and wheat straw using [bmim]cyclohexylcarboxylate, spinning fibers with a tenacity of 22 and 36 cN/tex, respectively [104].

Ionic liquids also offer the possibility for derivatization of the cellulosic substrate and conversion to shaped products without any solvent exchange. Eucalyptus pulp was acetylated in [amim]Cl **3a**, [bmim]Cl **2a**, and [emim]Cl **1a** by adding acetic anhydride to the homogeneous solutions [105] and then spinning into the respective cellulose acetate fibers [71]. By increasing the relative amount of acetic anhydride, fibers with a degree of substitution (DS) of up to 2.38 could be produced. The viscoelastic properties of the spinning dope were modified notably. Both viscosity and elastic regions decreased with increasing DS. Substitution of the cellulose hydroxyl groups had a similar effect on the fiber properties, as observed when cellulose was blended with another polymer; the tenacity decreased drastically but fibrillation behavior was improved. At low DS values of 0.5, the water retention was increased fivefold.

Ionic liquids are not inert in derivatization reactions such as acylation. In the case of halide-containing ILs, the carboxylic acid anhydride is converted to the respective acid halide, which then acts as the acylating agent. Thus, acylation in [emim]OAc **1b** is limited to acetylation. If a carboxylic acid anhydride other than acetic anhydride is used then the acetate anion of the IL forms a mixed anhydride, which results in a mixed cellulose substitution pattern [106].

It is of little surprise that ILs were also reported to be suitable for forming films and fibers from chitin and chitosan, taking into account their close structural resemblance to cellulose. The IL [emim]OAc **1b** has been identified as powerful solvent for chitin extraction from crustacean shells [107]. The extract was not only purer than the commercially available grade of chitin, but also had higher molecular weight. This was attributed to the enhanced solubility of short-chain chitin in aqueous media. When water was added to the [emim]OAc **1b** solution, short-chain chitin remained dissolved and only high molecular weight chitin was precipitated. The high molecular weight was shown to be necessary for successful dry-jet wet spinning and resulted in fibers with high tensile strength. Chitosan was spun from a mixture of [bmim]Cl **2a** and glycine hydrochloride [108]. It should be noted that the authors claimed a mechanism in which the glycine hydrochloride

protonates the amino group of chitosan, which then becomes soluble in [bmim]Cl **2a**. Strictly speaking, this is not a non-derivatizing dissolution of the polymer, also reflected by the required caustic neutralization bath.

2.5 *Thermal Degradation of the Cellulose–IL System*

The currently used set of imidazolium-based ILs are not inert toward cellulose. As a matter of fact, during heating and processing of the cellulose–IL systems both the biopolymer and the solvent are subjected to degradation reactions that are occasionally severe. Thermal degradation of ILs is known and commonly assessed by DSC or dynamic thermogravimetric analysis (TGA). In the latter, the onset of weight loss is usually defined as the degradation temperature. However, slow decomposition might occur at substantially lower temperatures, not captured during a fast heating ramp [109]. Impurities such as residual precursors left from incomplete synthesis (alkylation and metathesis steps) can further lead to a decrease in decomposition temperature [110]. Impurities can also be introduced by heating ILs of high purity, through various degradation pathways of the imidazolium moiety. For example, the dialkylimidazolium cation can show *trans*-alkylation, resulting in a symmetrical dialkylimidazolium structure, or undergo elimination or retro-alkylation, causing liberation of one alkyl residue and concomitant formation of an alkylimidazole [110, 111]. Similar reactions were observed in a detailed study by Liebner et al., who, in addition to the aforementioned products, also identified methylene-bridged imidazole dimers [112]. The basic amine products can act as catalysts for further degradation reactions or induce secondary side reactions such as deprotonation of the imidazolium C2-H proton, resulting in carbene formation [113]. In particular, nucleophilic anions with a high Kamlet–Taft hydrogen bond basicity value can promote these adverse reactions [114]. Because the same anion properties are required for sufficient cellulose–IL interaction, thermal instability is an intrinsic disadvantage of current cellulose-dissolving ILs.

Degradation products can be reactive toward cellulose or favor cellulose degradation in solution. Using NMR spectroscopy and ^{13}C labeling of ILs and cellulose model compounds, Ebner et al. [115] showed that the dialkylimidazolium moiety can react via an intermediate carbene form with the reducing end of cellulose. Although this might be of little relevance for high DP cellulose, the reaction has to be kept in mind when processing low DP starch or cellulose because the cellulosic product releases the IL moiety over time through hydrolytic cleavage [115].

The synergistic effects of cellulose and ILs are not yet fully understood. The thermal stability of a cellulose–IL system has been reported to be lower than the respective IL itself [116, 117]. Moreover, the detailed mechanisms of cellulose depolymerization in ILs are still unclear. As already mentioned in the section on fiber spinning (Sect. 2.3), halide-containing imidazolium ILs degrade pulp cellulose substantially at elevated temperatures. The extent of degradation during dissolution and processing of the cellulosic solute has been assessed by determining the

intrinsic viscosity of the regenerated cellulose or molar mass distribution of the spun fibers. Bentivoglio et al. reported that the degradation behavior was dependent on the cation, with [amim]Cl **3a** showing the most pronounced degradation [67]. Even the addition of propyl gallate (PG) had only a minor stabilizing effect. In contrast, the stability was improved notably in [bmim]Cl **2a** when PG was added. Gazit and Katz analyzed the degradation behavior of different cellulosic substrates in [emim]Cl **1a**, [bmim]Cl **2b**, and [emim]OAc **1b** [118]. The authors followed the process of cellulose depolymerization using GPC analyses and demonstrated that the degradation in halide-containing ILs was considerably stronger, even under mild conditions (85°C, 5 h), than in [emim]OAc **1b** (110°C, 24 h), with cellulose of high DP being more affected than low DP carbohydrates. Comparing the same IL of different purities, unexpectedly, use of high-purity IL resulted in more pronounced cellulose depolymerization. The authors postulated an acid-catalyzed degradation mechanism caused by the relatively low pK_a of the C2-H in the imidazolium ring. They speculated that residual starting material such as alkylimidazole in the low-purity IL acts as proton scavenger and thus prevents degradation. They confirmed this by adding 5% of 1-methylimidazole to high-purity [bmim]Cl **2b**; degradation was almost completely prevented. The results earlier reported by Kosan et al. seem to be in line with these observations [78]. As mentioned earlier, the authors followed a dissolution protocol adapted from the NMMO–Lyocell process in which water is evaporated under reduced pressure from a solvent–water–cellulose ternary mixture until the solubility window is entered and cellulose dissolution initiated. They showed that cellulose depolymerization is notably reduced if the pH of the IL–water–pulp suspension is initially adjusted to 10.5. However, an accurate adjustment of the pH is only possible following this protocol because the pH is defined for aqueous systems and thus accurate pH adjustment in neat ILs is not possible [78].

In all cases, a reduction in the processing temperature proved most efficient for avoiding extensive degradation [67, 70]. However, because of the high viscosity of halide-based IL systems, processing of these cellulose–IL solutions at lower temperatures is only possible with concomitant reduction of the cellulose concentration, which reduces the economy of the whole process. The low viscosity of [emim]OAc **1b** offers the possibility to spin at lower temperatures while preserving a feasible solute concentration. But even with [emim]OAc **1b**, Ingildeev at al. showed that the cellulosic pulp was degraded heavily during dissolution, despite a moderate temperature of 85°C [75]. This was attributed to a combination of thermal and mechanical degradation induced by high shear forces. Interestingly, the DP of the cellulose was preserved almost completely when the dissolution was performed in an inert gas atmosphere [28, 75, 85], indicating an oxidative degradation mechanism. However, this is only speculation at this point because detailed studies are not yet available.

In the following section, we present detailed results on the spinning of cellulosic fibers using an ionic liquid that is not based on imidazolium. Although 1,5-diazabicyclo[4.3.0]non-5-enium acetate ([DBNH]OAc) **4b** has been reported to be a cellulose solvent, no studies on the spinnability of its cellulose solutions have been conducted [119, 120].

3 [DBNH]OAc as Novel Solvent for Fiber Spinning

3.1 Experimental Details

3.1.1 Materials

Eucalyptus urograndis PHK pulp (intrinsic viscosity in Cuen, according to ISO 5351–1, 468 mL/g; M_n 79.8 kg/mol; M_w 268.7 kg/mol; Bahia pulp, Brazil) was received in the form of sheets and ground by means of a Wiley mill. Viscose fibers were kindly provided by Kelheim Fibres (Germany). 1,5-Diazabicyclo[4.3.0]non-5-ene (99%, Fluorochem, UK) and acetic acid (glacial, 100%, Merck, Germany) were used as received. [DBNH]OAc **4b** was prepared by slowly adding equimolar amounts of acetic acid to DBN while diverting the exothermic reaction enthalpy by active cooling.

3.1.2 Molar Mass Distribution

GPC was performed on samples that were subjected to a solvent exchange sequence in order to remove water and to activate them in *N*,*N*-dimethylacetamide (DMAc) [121]. Finally, the samples were dissolved in a lithium chloride–DMAc solution and analyzed with a Dionex Ultimate 3000 system. Pullulan standards (343 to 708 kDa, Polymer Standard Service, Mainz, Germany, and 1,600 kDa, Fluka, Germany) were used to calibrate the system. The molar masses (MM) of the pullulan standards were converted to correspond to those of cellulose, ($MM_{cellulose} = q^{*}MM_{cellulose}^{p}$), as proposed by Berggren et al. [122]. The coefficients $q = 12.19$ and $p = 0.78$ were found by least-squares fitting using the data published in their report.

3.1.3 Dissolution of Pulp in [DBNH]OAc

[DBNH]OAc **4b** was first liquefied at 70°C in a water bath and then mixed with air-dry eucalyptus PHK pulp to a final consistency of 13 wt%, unless otherwise stated. The sticky pulp–IL mixture was then transferred to a vertical kneader system, which was described in detail in an earlier publication [103, 123]. The mixture was stirred at 80°C and 10 rpm under reduced pressure (50 mbar). Complete dissolution was observed in less than 90 min. The solution was then filtered by means of a hydraulic press filtration device (1–2 MPa, metal filter fleece, 5–6 μm absolute fineness; Gebr. Kufferath AG, Germany) to assure constant solution quality throughout the spinning trials. The solution was shaped to the dimensions of the spinning cylinder and solidified 1–3 days after preparation.

3.1.4 Rheological Measurements

Shear rheology of all solutions was measured on an Anton Paar MCR 300 rheometer with parallel plate geometry (25 mm plate diameter, 1 mm gap size). The viscoelastic domain was determined by performing a dynamic strain sweep test. A strain of 0.5%, which fell well within the linear viscoelastic regime, was chosen for the frequency sweep measurements. A time experiment at constant frequency showed no significant water uptake from the laboratory atmosphere at the plate edges within the required testing time. Thus, it was not necessary to seal the edges with paraffin oil as previously suggested [40, 43]. Each sample was subjected to a dynamic frequency sweep at 70, 75, 80, and 85°C over an angular velocity range of 0.1–100 s^{-1}. Master curves were generated via WLF time–temperature superposition. The shift factor and reduced variables were calculated as described by Sammons et al. [43].

3.1.5 Spinning Trials

Cellulosic fibers were spun using a customized laboratory piston spinning unit (Fourné Polymertechnik, Germany), as depicted in Fig. 2. The cylinder was loaded with solid, shaped [DBNH]OAc–pulp solution, which was then heated to 70°C to form a homogeneous, air bubble-free highly viscous spin dope. The solution was then extruded at 75–80°C through a multihole spinneret (36 holes, capillary diameter 100 µm, L/D 0.2) via a 1-cm air gap into a water coagulation bath. Air gap distance, immersion depth to the first deflection roller, deflection angle, and the retention distance of the filament bundle in the coagulation bath were kept constant throughout all spinning trials. The extrusion rate (v_e) was fixed at 1.6 mL/min (5.7 m/min) while the take-up velocity (v_{tu}) of the godet couple was varied from 5 to 100 m/min, resulting in draw ratios $D_r = v_{tu}/v_e$ of 0.88–17.7. The fibers were washed offline with hot water (60°C) and air dried without tension, resulting in a small natural crimp.

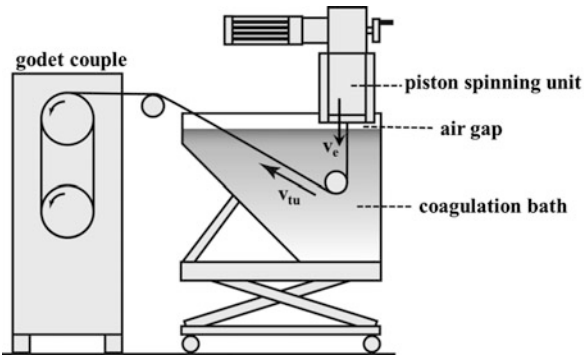

Fig. 2 Illustration of the spinning unit. The filaments are extruded from the piston spinning unit with a velocity v_e (extrusion velocity), pass through the air gap, and are immersed in the coagulation bath. The filaments are stretched in the air gap by the increasing v_{tu} (take-up velocity) of the godet couple

3.1.6 Mechanical Properties

Linear density (titer), conditioned tenacity (i.e., after drying the fibers and equilibrating at the measurement temperature and humidity), and wet tenacity were measured at 23°C and 50% relative humidity using the Lenzing Instrument Vibroskop 400 and Vibrodyn 400 devices.

3.1.7 WAXS and Birefringence Measurements

Wide angle X-ray scattering (WAXS) measurements were performed at the IAP Fraunhofer Institutes (Golm Germany) by means of a two-circle diffractometer D5000 (Fa. Bruker-AXS, Germany) using monochromatic Cu-K_α radiation in symmetric transmission (with Ge(111) as monochromator, $\lambda = 0.15406$ nm; at 30 mA and 40 kV). The step width $\Delta\varphi$ was 0.2° with a measurement time of 180 s/$\Delta\varphi$. The scattering curves were corrected for absorption, polarization, Compton scattering, and parasitic scattering [124, 125]. From the corrected and normalized WAXS curves, the degree of crystallinity x_c and the lattice disorder parameter k according to the Ruland–Vonk method, and the crystallite dimensions $D_{(hkl)}$ from the width of the reflections via the Scherrer equation were determined. The crystallite chain orientation was determined by an azimuthal scan of the meridional main interference taken from well-aligned fiber samples in the longitudinal direction. It is defined by (180° − FWHM)/180°, where FWHM is the full width at half maximum of the (004) reflection plane. The Herman crystalline orientation factor was determined with the IAP software WAXS7 [126]. The average crystallite dimension was calculated from the FWHM of the lateral main peaks according to the Scherrer formula, $D_{(hkl)} = 0.9\lambda/(\text{FWHM} \times \cos\theta)$.

The average orientation of both amorphous and crystalline cellulose in each fiber sample was determined using a polarized light microscope (Zeiss Axio Scope) equipped with a 5λ Berek compensator. The birefringence Δn of the specimen was obtained by dividing the retardation of the polarized light by the thickness of the fiber, which was calculated from the linear density (titer) using a cellulose density value of 1.5 g/cm^3 [127]. The total orientation factor f_t was then derived by dividing Δn by the maximum birefringence of cellulose, 0.062 [128, 129]. A factor $f_t = 1$ means perfect orientation parallel to the fiber axis, $f_t = 0$ for random orientation, and −1 for perfect transverse orientation. Subsequently, the amorphous orientation factor f_a was calculated by:

$$f_a = \frac{f_t - (x_c \times f_c)}{(1 - x_c) \times 0.91}$$

where 0.91 is the ratio of the densities of amorphous and crystalline cellulose, f_c is the crystalline orientation, and x_c is the crystallinity[130–132].

3.1.8 Scanning Electron Microscopy

SEM imaging was performed at the IAP Fraunhofer Institutes (Golm, Germany). For fiber surface analyses, fibers were glued horizontally onto a conductive support. For cryo-fracture, a fiber bundle was dipped into liquid nitrogen, ruptured, and glued vertically on the conductive support. The samples were sputter-coated with a 4-nm platinum layer to enhance the electric conductivity. Images were then obtained using a JSM6330F (Jeol, Japan) scanning electron microscope at 5 kV operating voltage.

3.1.9 Yarn Spinning

The spun continuous filament was cut to staple fibers of 37 mm length, opened, and conditioned at 21°C and 62% for 72 h. The yarn was then spun at the Swedish School of Textiles (University of Borås, Sweden) using a Mesdan laboratory mini-spinning line comprising a Laboratory Carding Machine, a Stiro-Roving-Lab, and a Ring-Lab. Fibers were fed to the carding machine in 25 g batches. All fibers were carded twice. After the first carding, the sliver was cut, folded, and then fed back to the card in perpendicular orientation compared with the first round. Subsequently, the sliver was fed in tube shape to a drafting machine. The sliver was first drafted once, then doubled and drafted again. Finally two of the double-drafted slivers were combined and drafted together to form a roving, which was fed to a spinning unit. A 35 mg ring was used to produce a 30 tex yarn. Finally, yarns were wound together with a twist to make a two-ply yarn using an AGTEKS DirecTwist-2A unit. The yarn was then knitted with a Stoll flat bed knitting machine.

3.2 Results and Discussion

3.2.1 Dissolution and Rheology

Although [DBNH]OAc **4b** is solid at room temperature, its low melting point and immediate low viscosity upon liquefaction (23 mPa s at 65°C) render it an excellent cellulose solvent. Complete dissolution of 13 wt% of the eucalyptus PHK kraft pulp was observed in less than 90 min, even at moderate temperatures. In order to assess possible degradation during the dissolution and filtration steps, part of the solution was regenerated immediately after filtration. Comparison of the molar mass distributions of the substrate and the regenerate (Fig. 3) showed slight degradation of the high molecular weight fraction, resulting in a decline of the polydispersity index (PDI; see inset in Fig. 3). However, the degradation is substantially lower than in previous reports using imidazolium-based ILs or NMMO. The viscoelastic properties of the solutions were assessed by means of oscillatory shear rheology, which provided the complex viscosity and dynamic moduli as a function of angular

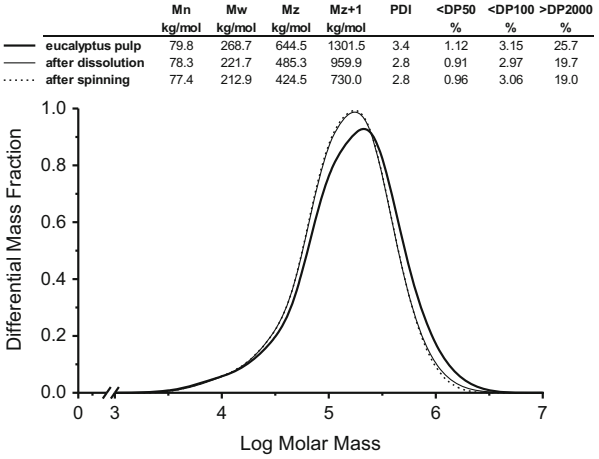

Fig. 3 Molecular weight distribution of eucalyptus PHK kraft pulp, regenerated cellulose after dissolution and filtration, and spun fiber. The average molar masses are summarized in the *inset*; M_n number-average molar mass, M_w weight-average molar mass, M_z Z-average molar mass, *PDI* M_w/M_n

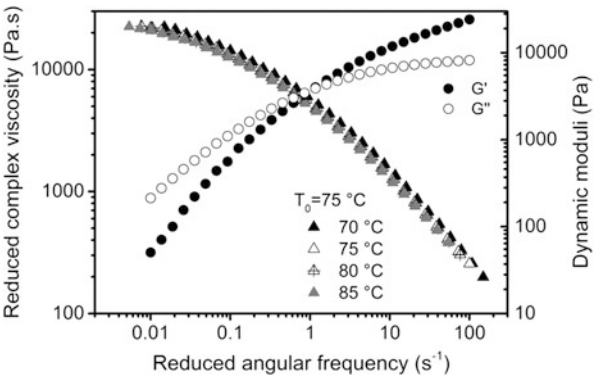

Fig. 4 Storage (G') and loss (G'') moduli (*circles*) and master curve of complex viscosity of eucalyptus pulp-[DBNH]OAc **4b** solution at various temperatures (*triangles*)

frequency. The master curves are depicted in Fig. 4. The shift temperature in Fig. 4 complies with the spinning temperature. As described in Sect. 2.3, stable spinning behavior is observed at temperatures where the complex viscosity and crossover point (COP) of the dynamic moduli are within certain limits. In our case, the solutions were spun at a temperature where the COP was approximately at 1 s^{-1}, crossover modulus was 5,000 Pa and the "zero shear" viscosity was about 30,000 Pa s. Note that the Cross model was used to fit the complex viscosity and calculate the zero shear viscosity, although the Cox–Merz rule failed in some cases (i.e., complex and dynamic viscosity did not superimpose perfectly). Thus, the calculated limiting value of the complex viscosity represents the complex viscosity within the frequency-independent Newtonian plateau but not necessarily the true zero shear viscosity. Also in accordance with earlier reports on highly concentrated cellulose solutions, the regions in which the storage modulus G' scales with ω^2 and $G'' \propto \omega$ were outside the measurement range.

3.2.2 Fiber Spinning

Multifilament bundles of eucalyptus kraft pulp solutions were extruded at 75–80°C. The draw ratio could be increased gradually up to 18, which indicated excellent spin stability. Because of the low processing temperature virtually no cellulose degradation was observed during spinning and the molecular weight distribution was entirely preserved without the addition of stabilizer (Fig. 3).

A combination of WAXS and birefringence measurements is commonly used to provide information about the crystalline structure and orientation of the regenerated fibers. Typical for regenerated cellulose, all fibers showed a cellulose II crystalline structure. The influence of the draw ratio on the crystalline and orientation parameter is summarized in Table 2. In general, all fibers showed a high orientation and similar crystallite size. Even the non-drawn sample ($D_r = 0.88$) showed a crystallinity x_c of 28% and a total orientation f_t of 0.67. This can be attributed to shear-induced orientation of the cellulose polymer chains in the spin capillaries. However, even a small elongational stress on the filament in the air gap increased the crystallinity and orientation notably, as can be seen from the influence of a moderate draw of 2.7, where the crystallinity showed the steepest increase. Further development of the draw increased both crystallinity and crystalline orientation f_c by only a small extent. The total orientation f_t, as determined from fiber birefringence, exhibited the same trend. In contrast, the amorphous orientation f_a increased steadily up to a draw of 5.3. Further draw had little effect on the orientation, which is typical for Lyocell-type fibers [20]. In addition to f_c, the distribution of orientated cellulose molecules along the fiber axis can be expressed by the crystallite chain orientation (OG) derived from the FWHM of the azimuthal scan intensity curves of the (004) lattice plane, with OG ranging from

Table 2 Structural analyses parameters obtained by WAXS and birefringence measurements of fibers spun with different draw ratios

		Draw				
Parameter		0.9	2.7	5.3	12.4	14.1
FWHM (°)		22.16	14.48	13.92	12.89	12.43
OG(004)		0.877	0.920	0.923	0.928	0.931
OGI(004)		0.45	0.75	0.77	0.80	0.81
x_c (%)		28	33	33	35	36
f_c		0.933	0.960	0.960	0.964	0.966
Δn		0.0418	0.0456	0.0502	n/a	0.0506
f_t		0.674	0.735	0.810	n/a	0.816
f_a		0.630	0.686	0.809	n/a	0.803
k (10–2 nm^2)		1.7	1.4	1.3	1.5	1.7
$D_{(hkl)}$ (nm)	(1–10)	4.0	4.3	4.4	4.1	4.2
	(110)	4.2	4.0	4.0	3.9	3.8
	(0–20)	4.1	3.0	3.8	3.8	3.6

See text for description of the analysis parameters

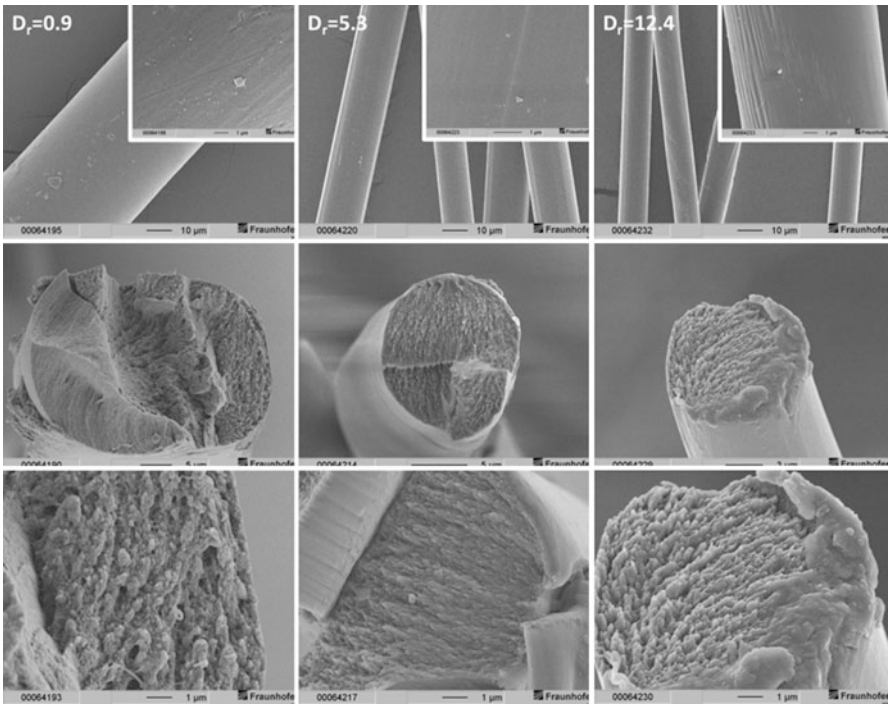

Fig. 5 Electron microscopy images of [DBNH]OAc spun fibers at draw ratio 0.9 (*left*), 5.3 (*middle*), and 12.4 (*right*). The *top row* shows the fiber surface with a tenfold zoom in the *inset*; *middle* and *bottom rows* show the fiber cross-section at different magnifications

0 (no orientation) to 1 (perfect orientation). A steady increase in OG with draw confirmed the trend of the other parameters. Although the OG values were similar to values reported for NMMO-based Lyocell, the orientation parameters f_c, f_a, and f_t of [DBNH]OAc-spun fibers were higher than those reported for NMMO or [emim]OAc **1b** spun fibers [87, 126]. The crystallite dimensions in (1–10), (110), and (020) directions were calculated and shown to be about 4 nm and, thus, slightly higher than reported values for fibers based on [bmim]Cl **2a** [76, 82] and [emim]OAc **1b** [87]. Note that because of the poor resolution of the (110) and (020) peaks they should be interpreted as a sum, and that they show a small decrease with increasing draw.

Lyocell-type fibers have been reported to be characterized by a specific morphology: a smooth fiber surface, round cross-section, and homogeneous, dense fiber bundle structure [20, 26]. Figure 5 combines SEM images of the [DBNH]OAc-spun fibers at no ($D_r = 0.9$), medium ($D_r = 5.3$), and high ($D_r = 12.4$) draw. The undrawn fibers depicted a smooth surface with nodules and small linear depressions in the fiber direction (Fig. 5, left column). The cross-section shows a slightly oval shape. Upon cryo-fracture, a cascaded fracture surface with smooth and coarse domains was formed. The coarse texture resulted from a ductile void structure, which is

characteristic for viscose fibers. A draw of 5.3 reduced the nodules on the smooth fiber surface, but seemed to have little effect on the appearance of the linear grooves (Fig. 5, middle column). The cross-section, however, was round and the fracture surface flat and even. The fiber body depicted a fibrillar structure. On increasing the draw to 12.4 the nodules almost disappeared completely but the grooves along the fiber became more distinct (Fig. 5, right column). This might indicate that the grooves originated from inhomogeneities in the spin capillaries from which filaments with linear defects were extruded. In the case of no draw, the retention time of the filament in the air gap was longer, allowing the filament to relax to a certain extent. When the take-up velocity was increased, the filaments with the linear defects immerse quickly into the water bath where they turn into fibers with the observed grooves upon instantaneous coagulation. The fracture surface of the fibers with $D_r = 12.4$ was again round and even, showing a fibrillar structure.

Subsequently, a denser set of draw ratios was used to evaluate the effect of draw on the mechanical properties of the fibers (Table 3). The absence of draw ($D_r = 0.9$) resulted in a large fiber linear density of 22 dtex. More importantly, the undrawn fibers had a very low tensile strength of 29 cN/tex, which dropped significantly to 18 cN/tex under wet conditions. This viscose-type behavior is in accordance with WAXS and SEM observations. Evidently, the lack of elongational stress in the air gap resulted in a low orientation of the polymer chains (Table 2) and viscose-type morphology of the fiber body (Fig. 5, left column). Consequently, the tenacity values were rather low and not retained in the wet state. The high fiber elongation of 22% is also typical for viscose fibers. However, this might also result from insufficient washing of the thick fiber. Residual IL thus acted as plasticizer. As described earlier in this Sect. 3.2.2, the crystalline and total orientation of the fibers developed quickly with increasing draw. Because the tensile strength is connected to cellulose crystalline structure, this is directly reflected in the resulting tenacity values [128]. Even at small draw ratios the tenacity increased notably, reaching NMMO-based Lyocell values of 40 cN/tex at medium draw ratios of 4.8. With further increase in draw the tenacity of the fibers exceeded even 50 cN/tex. Typical for fibers spun in a Lyocell manner, the high tenacity was retained under wet conditions. The resulting fibers were then cut to staple fibers to produce a textile yarn.

3.2.3 Yarn Spinning

Parallel to the fibers spun from [DBNH]OAc **4b**, commercial viscose fibers were spun to a yarn using the same equipment. Thus, the performance of the IL-based fibers during yarn manufacture and the final yarn properties could be compared with those of commercial fibers. The single process steps are illustrated in Fig. 6. Carding of the IL fibers was slightly more difficult than for the viscose fibers. This can be attributed to the lack of crimp, because the fibers were processed without the additional crimping step that is usually used on the industrial scale. Further, no spin finish was applied to the IL fibers. Nonetheless, drafting proceeded

Table 3 Mechanical properties of fibers spun at different draw in the conditioned and wet states

Conditioned							Wet					
	Titer		Elongation		Tenacity		Titer		Elongation		Tenacity	
Draw	(dtex)	+/−	(%)	+/−	(cN/tex)	+/−	(dtex)	+/−	(%)	+/−	(cN/tex)	+/−
0.9[a]	22.26	0.80	22.00	2.30	28.75	2.17	22.14	3.21	26.3	4.06	18.16	2.11
2.7	7.60	0.96	10.03	1.19	37.49	2.01	9.09	1.37	13.47	1.50	24.92	2.18
4.8	3.49	0.56	9.23	1.43	39.98	4.47	3.55	0.45	11.29	1.61	29.52	4.50
5.3	3.22	0.46	9.15	1.81	41.99	4.95	3.25	0.64	11.63	1.10	37.23	4.70
6.2	3.15	0.30	9.54	1.71	41.85	4.73	2.74	0.44	11.44	0.98	37.46	3.99
7.1	3.03	0.33	9.80	0.87	42.56	3.84	3.05	0.39	11.94	1.56	33.63	3.17
8.3	2.43	0.34	9.52	0.79	48.51	4.68	2.12	0.44	11.18	1.18	44.77	6.64
10.6	1.86	0.21	9.85	1.07	47.16	3.83	1.67	0.20	12.34	1.14	47.58	5.78
17.7	1.21	0.14	8.50	0.83	50.45	4.75	1.18	0.18	9.60	1.13	46.35	5.20

[a]Spun from a 17 weight-% solution

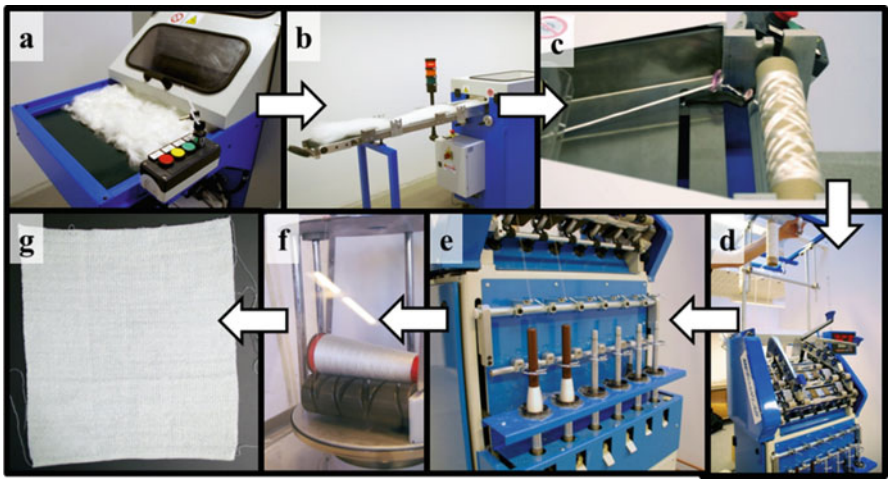

Fig. 6 Single process steps during yarn manufacture and subsequent knitted product: (**a**) carding of [DBNH]OAc-spun staple fibers; (**b**) sliver fed to the drafting machine; (**c**) preparing of roving; (**d**) feeding of the roving; (**e**) ring spinning; (**f**) plying; and (**g**) flat-bed knitted fabric

Table 4 Properties of yarns spun from [DBNH]OAc **4b** and commercial viscose fibers

		[DBNH]OAc	Viscose
Fiber	Linear density (dtex)	1.9	1.5
	Dry tenacity (cN/tex)	47	23
	Elongation (%)	9.4	22.5
	Fiber length (mm)	37	40
	Finish	No	Yes
Yarn	Linear density (tex)	54.3	62.7
	Tenacity (cN/tex)	34.4	17.3
	Elongation (%)	7.4	18.2
	CV (%)	13.6	9.1

smoothly. The resulting sliver from the viscose fibers was shorter after being drafted, indicating that fibers with crimp resisted the draft more than the IL staple fibers. However, no differences were observed during ring spinning and plying. The yarn properties are summarized in Table 4. It should be noted that the yarn processing was not optimized and, thus, the values obtained should only be interpreted relative to each other. The yarn prepared from the IL-spun fibers was slightly thinner and, in accordance with the fiber properties, stronger than the viscose yarn. The coefficient of variation of mass (CV), which indicates the unevenness of the yarn, was slightly higher for the IL yarn. This is a result of inhomogeneities in the carding step deriving from the lack of crimp and the hand-cut IL fibers. The effect of uneven yarn becomes clearer when a fabric is knitted. The thicker and thinner parts in the yarn give the knit a striped appearance in the horizontal direction (see Fig. 7).

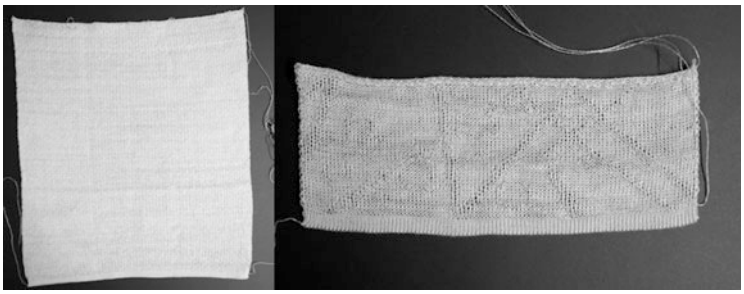

Fig. 7 Flat-bed knitted fabric of viscose reference fiber (*left*), and [DBNH]OAc **4b** spun fibers (*right*). *Stripes* in horizontal direction result from the unevenness of the yarn; *diagonal stripes* derive from the knitting process

4 Conclusions

Promising results have been reported in the field of IL-based fiber spinning. The chemical inertness and ability to dissolve a wide spectrum of substances are probably the biggest advantages of ILs as solvents for biopolymer processing. Various composite fibers of binary polymer mixtures have already been prepared, and incorporation of inorganic and organic particles has been successfully demonstrated. Also, in situ derivatization could open up new routes for the cost- and material-efficient preparation of modified cellulose fibers. Thus, IL-spun fibers could enter the man-made cellulosic fiber market via specialty fibers. However, one has to look at both sides of the IL coin. Imidazolium-based ILs are not inert toward cellulose and can induce cellulose degradation, especially at elevated temperatures. Stabilizers are necessary, as for NMMO. The high solubility of cellulose in certain ILs is sometimes promoted as beneficial in terms of energy consumption during the polymer processing. However, highly concentrated solutions do not necessarily exhibit the targeted rheological properties to enable spinning into highly orientated fibers unless the solutions are heated, which raises the question of the thermal stability of binary cellulose–IL systems (or ternary cellulose–IL–water systems). Doubtless, the biggest challenge for all IL-based process is a viable recycling strategy. The high costs of the designer solvents require a recovery rate similar to that of the NMMO-based Lyocell process (i.e., $>99.9\%$). This means that the IL in question has to be stable under processing conditions and must be removed quantitatively from the regenerated product. If these prerequisites are met, then the overall economy of the process is determined by the energy intensity of anti-solvent removal and purification strategies to isolate possible degradation products. Unfortunately, this topic is still an idle research field.

We have introduced here an alternative IL that is not based on imidazolium. [DBNH]OAc **4b** can dissolve high concentrations of cellulose at moderate temperatures. Moreover, even at high pulp cellulose concentration the viscoelastic properties permitted fiber spinning at temperatures notably lower than in the NMMO-

based Lyocell process. Thus, only negligible cellulose degradation was observed. Results of previous reports indicate that the degradation might be solely shear induced during the dissolution step. The spun fibers had excellent mechanical properties, which makes them suitable as reinforcing material in composite structures and for textile applications. The latter was demonstrated via the manufacture of a textile yarn. Long-term stability tests and recycling runs are difficult on a laboratory scale. However, thermal and hydrolytic stability tests are currently being conducted along with energy balance calculations of water–IL separation via evaporation to evaluate the feasibility of [DBNH]OAc **4b**-based fiber spinning on a pilot scale.

Acknowledgement This study is part of the Future Biorefinery program financed by the Finnish Bioeconomy Cluster (FIBIC) and the Finnish Funding Agency for Technology and Innovation (TEKES). The authors would like to thank Anders Persson and Anders Berntsson from the Swedish School of Textiles (University of Borås, Sweden) for their kind assistance with the yarn preparation.

References

1. Hämmerle FM (2011) The cellulose gap (the future of cellulose fibres). Lenzinger Ber 89: 12–21
2. Eichinger D (2012) A vision of the world of cellulosic fibers in 2020. Lenzinger Ber 90:1–7
3. Shen L, Patel MK (2010) Life cycle assessment of man-made cellulose fibres. Lenzinger Ber 88:1–59
4. The Fiber Year (2013) World survey on textiles & nonwovens. The Fiber Year, Speicher. http://www.thefiberyear.com/. Accessed 20 Dec 2013
5. Bywater N (2011) The global viscose fibre industry in the 21st century – the first 10 years. Lenzinger Ber 89:22–29
6. Mikolajczyk W, Wawro D, Struszczyk H (1998) Cellulose carbamate spinning solutions prepared for the manufacture of fibers. Fibres Text East Eur 6:53–55
7. Fink H-P, Ganster J, Lehmann A (2014) Progress in cellulose shaping: 20 years industrial case studies at Fraunhofer IAP. Cellulose 21(1):31–51. doi:10.1007/s10570-013-0137-7
8. Weigel P, Fink H-P, Doss M (2005) Method for producing nonwovens from cellulose carbamate in a continuous procedure. Patent WO2005080660A1
9. Vehvilaeinen M, Kamppuri T, Rom M, Janicki J, Ciechanska D, Groenqvist S, Siika-Aho M, Elg Christoffersson K, Nousiainen P (2008) Effect of wet spinning parameters on the properties of novel cellulosic fibres. Cellulose 15:671–680. doi:10.1007/s10570-008-9219-3
10. Horvath AL (2006) Solubility of structurally complicated materials: I. Wood. J Phys Chem Ref Data 35(1):77–92
11. Hansen CM, Björkman A (1998) The ultrastructure of wood from a solubility parameter point of view. Holzforschung 52(4):335–344
12. Heinze T, Dicke R, Koschella A, Kull AH, Klohr E-A, Koch W (2000) Effective preparation of cellulose derivatives in a new simple cellulose solvent. Macromol Chem Phys 201(6): 627–631
13. Köhler S, Heinze T (2007) New solvents for cellulose: dimethyl sulfoxide/ammonium fluorides. Macromol Biosci 7(3):307–314
14. Hattori K, Cuculo JA, Hudson SM (2002) New solvents for cellulose: hydrazine/thiocyanate salt system. J Polym Sci A Polym Chem 40(4):601–611. doi:10.1002/pola.10135

15. Hattori K, Abe E, Yoshida T, Cuculo JA (2004) New solvents for cellulose. II. Ethylenediamine/thiocyanate salt system. Polym J 36(2):123–130. doi:10.1295/polymj.36.123
16. Cuculo JA, Smith CB, Sangwatanaroj U, Stejskal EO, Sankar SS (1994) A study on the mechanism of dissolution of the cellulose/NH3/NH4SCN system. II. J Polym Sci A Polym Chem 32(2):241–247. doi:10.1002/pola.1994.080320204
17. Cuculo JA, Smith CB, Sangwatanaroj U, Stejskal EO, Sankar SS (1994) A study on the mechanism of dissolution of the cellulose/NH3/NH4SCN system. I. J Polym Sci A Polym Chem 32(2):229–239. doi:10.1002/pola.1994.080320203
18. Bredereck K, Hermanutz F (2005) Man-made cellulosics. Rev Prog Color 35:59–75
19. Liebert T (2010) Cellulose solvents – remarkable history, bright future. In: Liebert T, Heinze TJ, Edgar KJ (eds) Cellulose solvents: for analysis, shaping and chemical modification. ACS Symposium Series, vol 1033. American Chemical Society, Washington DC, pp 3–54. doi:10.1021/bk-2010-1033.ch001
20. Fink HP, Weigel P, Purz HJ, Ganster J (2001) Structure formation of regenerated cellulose materials from NMMO-solutions. Prog Polym Sci 26(9):1473–1524
21. BISFA (2009) Terminology of man-made fibres. BISFA, Brussels
22. Zikeli S, Ecker F, Schwenninger F, Jurkovic R, Ruef H (1995) Process and apparatus for producing cellulose fibers. Patent WO9501470A1
23. Wilhelm F, Eduard M, Hartmut R, Christoph S (1998) Method for producing cellulose fibres. Patent WO1998058103A1
24. Liu R, Shao H, Hu X (2001) The online measurement of lyocell fibers and investigation of elongational viscosity of cellulose N-methylmorpholine-N-oxide monohydrate solutions. Macromol Mater Eng 286:179–186. doi:10.1002/1439-2054(20010301)
25. Gindl W, Reifferscheid M, Adusumalli RB, Weber H, Roeder T, Sixta H, Schoeberl T (2008) Anisotropy of the modulus of elasticity in regenerated cellulose fibres related to molecular orientation. Polymer 49:792–799. doi:10.1016/j.polymer.2007.12.016
26. Röder T, Moosbauer J, Kliba G, Schlader S, Zuckerstätter G, Sixta H (2009) Comparative characterisation of man-made regenerated cellulose fibres. Lenzinger Ber 87:98–105
27. Buijtenhuijs FA, Abbas M, Witteveen AJ (1986) The degradation and stabilization of cellulose dissolved in N-methylmorpholine N-oxide (NMMO). Papier 40:615–619
28. Wendler F, Kosan B, Krieg M, Meister F (2009) Cellulosic shapes from ionic liquids modified by activated charcoals and nanosilver particles. Lenzinger Ber 87:106–116
29. Kalt W, Maenner J, Firgo H (1995) Molding or spinning material containing cellulose and manufacture of molded or spun articles from. Patent WO9508010A1
30. Rosenau T, Potthast A, Sixta H, Kosma P (2001) The chemistry of side reactions and byproduct formation in the system NMMO/cellulose (Lyocell process). Prog Polym Sci 26(9):1763–1837
31. Walden P (1914) Molecular weights and electrical conductivity of several fused salts. Bull Acad Imp Sci (St Petersburg) 8:405–422
32. Rinaldi R (2011) Instantaneous dissolution of cellulose in organic electrolyte solutions. Chem Commun 47:511–513. doi:10.1039/c0cc02421j
33. Welton T (1999) Room-temperature ionic liquids. Solvents for synthesis and catalysis. Chem Rev 99(8):2071–2083
34. Swatloski RP, Spear SK, Holbrey JD, Rogers RD (2002) Dissolution of cellose with ionic liquids. J Am Chem Soc 124(18):4974–4975
35. Pinkert A, Marsh KN, Pang S, Staiger MP (2009) Ionic liquids and their interaction with cellulose. Chem Rev 109(12):6712–6728
36. Maeki-Arvela P, Anugwom I, Virtanen P, Sjoeholm R, Mikkola JP (2010) Dissolution of lignocellulosic materials and its constituents using ionic liquids-A review. Ind Crops Prod 32:175–201. doi:10.1016/j.indcrop.2010.04.005
37. Brandt A, Grasvik J, Hallett JP, Welton T (2013) Deconstruction of lignocellulosic biomass with ionic liquids. Green Chem 15(3):550–583. doi:10.1039/c2gc36364j

38. Wang H, Gurau G, Rogers RD (2012) Ionic liquid processing of cellulose. Chem Soc Rev 41(4):1519–1537. doi:10.1039/c2cs15311d
39. Singh S, Simmons BA (2013) Ionic liquid pretreatment: mechanism, performance, and challenges. In: Wyman CE (ed) Aqueous pretreatment of plant biomass for biological and chemical conversion to fuels and chemicals. Wiley, Chichester, pp 223–238. doi:10.1002/9780470975831.ch11
40. Gericke M, Schlufter K, Liebert T, Heinze T, Budtova T (2009) Rheological properties of cellulose/ionic liquid solutions: from dilute to concentrated states. Biomacromolecules 10:1188–1194. doi:10.1021/bm801430x
41. Sescousse R, Le KA, Ries ME, Budtova T (2010) Viscosity of cellulose-imidazolium-based ionic liquid solutions. J Phys Chem B 114:7222–7228. doi:10.1021/jp1024203
42. Haward SJ, Sharma V, Butts CP, McKinley GH, Rahatekar SS (2012) Shear and extensional rheology of cellulose/ionic liquid solutions. Biomacromolecules 13(5):1688–1699. doi:10.1021/bm300407q
43. Sammons RJ, Collier JR, Rials TG, Petrovan S (2008) Rheology of 1-butyl-3-methylimidazolium chloride cellulose solutions. I. shear rheology. J Appl Polym Sci 110:1175–1181. doi:10.1002/app.28733
44. Collier JR, Watson JL, Collier BJ, Petrovan S (2009) Rheology of 1-butyl-3-methylimidazolium chloride cellulose solutions. II. Solution character and preparation. J Appl Polym Sci 111:1019–1027. doi:10.1002/app.28995
45. Cox WP, Merz EH (1958) Correlation of dynamic and steady flow viscosities. J Polym Sci 28(118):619–622. doi:10.1002/pol.1958.1202811812
46. Lu F, Cheng B, Song J, Liang Y (2012) Rheological characterization of concentrated cellulose solutions in 1-allyl-3-methylimidazolium chloride. J Appl Polym Sci 124(4):3419–3425. doi:10.1002/app.35363
47. Chen X, Zhang Y, Wang H, Wang S-W, Liang S, Colby RH (2011) Solution rheology of cellulose in 1-butyl-3-methyl imidazolium chloride. J Rheol 55(3):485–494. doi:10.1122/1.3553032
48. Schausberger A, Moslinger R (1999) Rheology of cellulose solutions. A tool for the characterization of cellulose. Papier 53:715–721
49. Sammons RJ, Collier JR, Rials TG, Petrovan S (2008) Rheology of 1-butyl-3-methylimidazolium chloride cellulose solutions. III. Elongational rheology. J Appl Polym Sci 110:3203–3208. doi:10.1002/app.28928
50. Anna SL, McKinley GH (2001) Elasto-capillary thinning and breakup of model elastic liquids. J Rheol 45:115–138. doi:10.1122/1.1332389
51. Stelter M, Brenn G, Yarin AL, Singh RP, Durst F (2002) Investigation of the elongational behavior of polymer solutions by means of an elongational rheometer. J Rheol 46:507–527. doi:10.1122/1.1445185
52. Ma B, Qin A, Li X, He C (2013) Preparation of cellulose hollow fiber membrane from bamboo pulp/1-butyl-3-methylimidazolium chloride/dimethylsulfoxide system. Ind Eng Chem Res 52:9417–9421. doi:10.1021/ie401097d
53. Hummel M, Michud A, Sixta H (2012) Structure formation of cellulosic material upon regeneration from ionic liquid solutions. In: Abstracts 243rd National Meeting American Chemical Society, I&EC Division, San Diego. ACS, Washington DC, pp IEC-17
54. Le KA, Sescousse R, Budtova T (2012) Influence of water on cellulose-EMIMAc solution properties: a viscometric study. Cellulose 19:45–54. doi:10.1007/s10570-011-9610-3
55. Boerstoel H (1998) Liquid crystalline solutions of cellulose in phosphoric acid for preparing cellulose yarns. Dissertation, Universit of Groningen
56. Boerstoel H, Maatman H, Westerink JB, Koenders BM (2001) Liquid crystalline solutions of cellulose in phosphoric acid. Polymer 42(17):7371–7379. doi:10.1016/S0032-3861(01)00210-5

57. Onofrei MD, Dobos AM, Stoica I, Olaru N, Olaru L, Ioan S (2014) Lyotropic liquid crystal phases in cellulose acetate phthalate/hydroxypropyl cellulose blends. J Polym Environ 22(1): 99–111. doi:10.1007/s10924-013-0618-7
58. Boerstoel H, Maatman H, Picken SJ, Remmers R, Westerink JB (2001) Liquid crystalline solutions of cellulose acetate in phosphoric acid. Polymer 42(17):7363–7369. doi:10.1016/S0032-3861(01)00209-9
59. Northolt MG, Boerstoel H, Maatman H, Huisman R, Veurink J, Elzerman H (2001) The structure and properties of cellulose fibres spun from an anisotropic phosphoric acid solution. Polymer 42(19):8249–8264. doi:10.1016/S0032-3861(01)00211-7
60. Kosan B, Schwikal K, Meister F (2010) Solution states of cellulose in selected direct dissolution agents. Cellulose 17(3):495–506. doi:10.1007/s10570-010-9402-1
61. Song H, Zhang J, Niu Y, Wang Z (2010) Phase transition and rheological behaviors of concentrated cellulose/ionic liquid solutions. J Phys Chem B 114(18):6006–6013. doi:10.1021/jp1013863
62. Song H, Niu Y, Wang Z, Zhang J (2011) Liquid crystalline phase and gel–sol transitions for concentrated microcrystalline cellulose (MCC)/1-ethyl-3-methylimidazolium acetate (EMIMAc) solutions. Biomacromolecules 12(4):1087–1096. doi:10.1021/bm101426p
63. Winter HH, Chambon F (1986) Analysis of linear viscoelasticity of a crosslinking polymer at the gel point. J Rheol 30(2):367–382. doi:10.1122/1.549853
64. Chambon F, Winter HH (1987) Linear viscoelasticity at the gel point of a crosslinking PDMS with imbalanced stoichiometry. J Rheol 31(8):683–697. doi:10.1122/1.549955
65. Swatloski RP, Rogers RD, Holbrey JD (2003) Dissolution and processing of cellulose using ionic liquids, cellulose solution, and regenerating cellulose. Patent WO2003029329A2
66. Laus G, Bentivoglio G, Schottenberger H, Kahlenberg V, Kopacka H, Roeder H, Roeder T, Sixta H (2005) Ionic liquids: current developments, potential and drawbacks for industrial applications. Lenzinger Ber 84:71–85
67. Bentivoglio G, Roeder T, Fasching M, Buchberger M, Schottenberger H, Sixta H (2006) Cellulose processing with chloride-based ionic liquids. Lenzinger Ber 86:154–161
68. Vagt U (2010) Cellulose dissolution and processing with ionic liquids. Wiley-VCH, Weinheim, pp 123–136
69. Michels C, Kosan B (2006) Structure of lyocell fibers, spun from aqueous amino oxides and/or ionic liquids. Lenzinger Ber 86:144–153
70. Kosan B, Michels C, Meister F (2008) Dissolution and forming of cellulose with ionic liquids. Cellulose 15:59–66. doi:10.1007/s10570-007-9160-x
71. Kosan B, Dorn S, Meister F, Heinze T (2010) Preparation and subsequent shaping of cellulose acetates using ionic liquids. Macromol Mater Eng 295:676–681. doi:10.1002/mame.201000022
72. Cai T, Yang G, Zhang H, Shao H, Hu X (2012) A new process for dissolution of cellulose in ionic liquids. Polym Eng Sci 52(8):1708–1714. doi:10.1002/pen.23069
73. Cai T, Zhang H, Guo Q, Shao H, Hu X (2010) Structure and properties of cellulose fibers from ionic liquids. J Appl Polym Sci 115:1047–1053. doi:10.1002/app.31081
74. Cai T, Wang YM, Yang YR, Wei M, Wang M (2013) Regenerated bamboo fiber from green solvent. Appl Mech Mater 423–426:370–372. doi:10.4028/www.scientific.net/AMM.423-426.370
75. Ingildeev D, Effenberger F, Bredereck K, Hermanutz F (2013) Comparison of direct solvents for regenerated cellulosic fibers via the lyocell process and by means of ionic liquids. J Appl Polym Sci 128:4141–4150. doi:10.1002/app.38470
76. Jiang G, Yuan Y, Wang B, Yin X, Mukuze KS, Huang W, Zhang Y, Wang H (2012) Analysis of regenerated cellulose fibers with ionic liquids as a solvent as spinning speed is increased. Cellulose 19:1075–1083. doi:10.1007/s10570-012-9716-2
77. Hermanutz F, Ingeldeev D, Effenberger F (2013) Environmentally friendly process for producing continuous micro- or supermicrofibers based on cellulose. Patent DE102012005489A1

78. Kosan B, Schwikal K, Meister F (2012) Effects of pre-treatment and dissolution conditions for improved solution and processing properties of cellulose in ionic liquids. Lenzinger Ber 90:76–84
79. Michels C, Kosan B (2001) The lyocell process – present output limit from the material and technological viewpoint. Lenzinger Ber 80:13–21
80. Michels C, Kosan B (2005) Contribution to the dissolution state of cellulose and cellulose derivatives. Lenzinger Ber 84:62–70
81. Michels C, Kosan B (2000) Lyocell process - material and technological restrictions. Chem Fibers Int 50:556, 558–561
82. Jiang G, Huang W, Li L, Wang X, Pang F, Zhang Y, Wang H (2012) Structure and properties of regenerated cellulose fibers from different technology processes. Carbohydr Polym 87: 2012–2018. doi:10.1016/j.carbpol.2011.10.022
83. Sammons RJ, Collier JR, Rials TG, Spruiell JE, Petrovan S (2013) Orientation of carbon fiber precursors from 1-butyl-3-methylimidazolium chloride cellulose solutions. J Appl Polym Sci 128:951–957. doi:10.1002/app.37906
84. Hermanutz F, Meister F, Uerdingen E (2006) New developments in the manufacture of cellulose fibers with ionic liquids. Chem Fibers Int 56:342, 344
85. Hermanutz F, Gaehr F, Uerdingen E, Meister F, Kosan B (2008) New developments in dissolving and processing of cellulose in ionic liquids. Macromol Symp 262:23–27. doi:10.1002/masy.200850203
86. Olsson C, Westman G (2013) Wet spinning of cellulose from ionic liquid solutions-viscometry and mechanical performance. J Appl Polym Sci 127:4542–4548. doi:10.1002/app.38064
87. Li X, Li N, Xu J, Duan X, Sun Y, Zhao Q (2014) Cellulose fibers from cellulose/1-ethyl-3-methylimidazolium acetate solution by wet spinning with increasing spinning speeds. J Appl Polym Sci 131(9):40225. doi:10.1002/app.40225
88. Sun N, Swatloski RP, Maxim ML, Rahman M, Harland AG, Haque A, Spear SK, Daly DT, Rogers RD (2008) Magnetite-embedded cellulose fibers prepared from ionic liquid. J Mater Chem 18:283–290. doi:10.1039/b713194a
89. Maxim ML, Sun N, Wang H, Sterner JR, Haque A, Rogers RD (2012) Reinforced magnetic cellulose fiber from ionic liquid solution. Nanomater Energy 1:225–236. doi:10.1680/nme.12.00010
90. Maxim ML, Sun N, Swatloski RP, Rahman M, Harland AG, Haque A, Spear SK, Daly DT, Rogers RD (2010) Properties of cellulose/TiO2 fibers processed from ionic liquids. ACS Symp Ser 1033:261–274. doi:10.1021/bk-2010-1033.ch014
91. Song H-Z, Luo Z-Q, Wang C-Z, Hao X-F, Gao J-G (2013) Preparation and characterization of bionanocomposite fiber based on cellulose and nano-SiO2 using ionic liquid. Carbohydr Polym 98:161–167. doi:10.1016/j.carbpol.2013.05.079
92. Zhang H, Wang Z, Zhang Z, Wu J, Zhang J, He J (2007) Regenerated cellulose/multiwalled carbon nanotube composite fibers with enhanced mechanical properties prepared with the ionic liquid 1-allyl-3-methylimidazolium chloride. Adv Mater 19:698–704. doi:10.1002/adma.200600442
93. Rahatekar SS, Rasheed A, Jain R, Zammarano M, Koziol KK, Windle AH, Gilman JW, Kumar S (2009) Solution spinning of cellulose carbon nanotube composites using room temperature ionic liquids. Polymer 50:4577–4583. doi:10.1016/j.polymer.2009.07.015
94. Wendler F, Kosan B, Krieg M, Meister F (2009) Possibilities for the physical modification of cellulose shapes using ionic liquids. Macromol Symp 280:112–122. doi:10.1002/masy.200950613
95. Kosan B, Nechwatal A, Meister F (2008) Cellulose multi-component fibers from ionic liquids. Chem Fibers Int 58:234–236
96. Ingildeev D, Hermanutz F, Bredereck K, Effenberger F (2012) Novel cellulose/polymer blend fibers obtained using ionic liquids. Macromol Mater Eng 297:585–594. doi:10.1002/mame.201100432

97. Yao Y, Mukuze KS, Zhang Y, Wang H (2014) Rheological behavior of cellulose/silk fibroin blend solutions with ionic liquid as solvent. Cellulose 21:675–684. doi:10.1007/s10570-013-0117-y
98. Wendler F, Meister F, Wawro D, Wesolowska E, Ciechanska D, Saake B, Puls J, Le Moigne N, Navard P (2010) Polysaccharide blend fibres formed from NaOH, N-methylmorpholine-N-oxide and 1-ethyl-3-methylimidazolium acetate. Fibres Text East Eur 18:21–30
99. Wendler F, Persin Z, Stana-Kleinschek K, Reischl M, Ribitsch V, Bohn A, Fink H-P, Meister F (2011) Morphology of polysaccharide blend fibers shaped from NaOH, N-methylmorpholine-N-oxide and 1-ethyl-3-methylimidazolium acetate. Cellulose 18: 1165–1178. doi:10.1007/s10570-011-9559-2
100. Lehmann A, Ebeling H, Fink H-P (2012) Method for economical production of lignin-containing precursor fibers for use in further production of carbon fibers. Patent WO2012156441A1
101. Sun N, Li W, Stoner B, Jiang X, Lu X, Rogers RD (2011) Composite fibers spun directly from solutions of raw lignocellulosic biomass dissolved in ionic liquids. Green Chem 13: 1158–1161. doi:10.1039/c1gc15033b
102. Sun N, Rahman M, Qin Y, Maxim ML, Rodriguez H, Rogers RD (2009) Complete dissolution and partial delignification of wood in the ionic liquid 1-ethyl-3-methylimidazolium acetate. Green Chem 11:646–655. doi:10.1039/b822702k
103. Hauru LKJ, Ma Y, Hummel M, Alekhina M, King AWT, Kilpelaeinen I, Penttilae PA, Serimaa R, Sixta H (2013) Enhancement of ionic liquid-aided fractionation of birchwood. Part 1: autohydrolysis pretreatment. RSC Adv 3:16365–16373. doi:10.1039/c3ra41529e
104. Lehmann A, Bohrisch J, Protz R, Fink H-P (2013) Method for preparing lignocellulose spinning solution and spin regenerated fibers from it without any initial preatreatments. Patent WO2013144082A1
105. Cao Y, Wu J, Zhang J, Li H, Zhang Y, He J (2009) Room temperature ionic liquids (RTILs): a new and versatile platform for cellulose processing and derivatization. Chem Eng J 147: 13–21. doi:10.1016/j.cej.2008.11.011
106. Köhler S, Liebert T, Schöbitz M, Schaller J, Meister F, Günther W, Heinze T (2007) Interactions of ionic liquids with polysaccharides 1. Unexpected acetylation of cellulose with 1-ethyl-3-methylimidazolium acetate. Macromol Rapid Commun 28(24):2311–2317. doi:10.1002/marc.200700529
107. Qin Y, Lu X, Sun N, Rogers RD (2010) Dissolution or extraction of crustacean shells using ionic liquids to obtain high molecular weight purified chitin and direct production of chitin films and fibers. Green Chem 12:968–971. doi:10.1039/c003583a
108. Ma B, Qin A, Li X, He C (2013) High tenacity regenerated chitosan fibers prepared by using the binary ionic liquid solvent (Gly · HCl)-[Bmim]Cl. Carbohydr Polym 97:300–305. doi:10.1016/j.carbpol.2013.04.080
109. Kosmulski M, Gustafsson J, Rosenholm JB (2004) Thermal stability of low temperature ionic liquids revisited. Thermochim Acta 412(1–2):47–53. doi:10.1016/j.tca.2003.08.022
110. Meine N, Benedito F, Rinaldi R (2010) Thermal stability of ionic liquids assessed by potentiometric titration. Green Chem 12:1711–1714. doi:10.1039/c0gc00091d
111. Awad WH, Gilman JW, Nyden M, Harris RH Jr, Sutto TE, Callahan J, Trulove PC, DeLong HC, Fox DM (2004) Thermal degradation studies of alkyl-imidazolium salts and their application in nanocomposites. Thermochim Acta 409(1):3–11. doi:10.1016/s0040-6031(03)00334-4
112. Liebner F, Patel I, Ebner G, Becker E, Horix M, Potthast A, Rosenau T (2010) Thermal aging of 1-alkyl-3-methylimidazolium ionic liquids and its effect on dissolved cellulose. Holzforschung 64:161–166. doi:10.1515/hf.2010.033
113. Aggarwal VK, Emme I, Mereu A (2002) Unexpected side reactions of imidazolium-based ionic liquids in the base-catalysed Baylis-Hillman reaction. Chem Commun 2002(15): 1612–1613

114. King AWT, Parviainen A, Karhunen P, Matikainen J, Hauru LKJ, Sixta H, Kilpelaeinen I (2012) Relative and inherent reactivities of imidazolium-based ionic liquids: the implications for lignocellulose processing applications. RSC Adv 2:8020–8026. doi:10.1039/c2ra21287k
115. Ebner G, Schiehser S, Potthast A, Rosenau T (2008) Side reaction of cellulose with common 1-alkyl-3-methylimidazolium-based ionic liquids. Tetrahedron Lett 49(51):7322–7324
116. Wendler F, Todi L-N, Meister F (2012) Thermostability of imidazolium ionic liquids as direct solvents for cellulose. Thermochim Acta 528:76–84. doi:10.1016/j.tca.2011.11.015
117. Dorn S, Wendler F, Meister F, Heinze T (2008) Interactions of ionic liquids with polysaccharides – 7: thermal stability of cellulose in ionic liquids and N-methylmorpholine-N-oxide. Macromol Mater Eng 293:907–913. doi:10.1002/mame.200800153
118. Gazit OM, Katz A (2012) Dialkylimidazolium ionic liquids hydrolyze cellulose under mild conditions. ChemSusChem 5(8):1542–1548. doi:10.1002/cssc.201100803
119. Parviainen A, King AWT, Mutikainen I, Hummel M, Selg C, Hauru LKJ, Sixta H, Kilpelaeinen I (2013) Predicting cellulose solvating capabilities of acid–base conjugate ionic liquids. ChemSusChem 6:2161–2169. doi:10.1002/cssc.201300143
120. Wahlstroem R, King A, Parviainen A, Kruus K, Suurnaekki A (2013) Cellulose hydrolysis with thermo- and alkali-tolerant cellulases in cellulose-dissolving superbase ionic liquids. RSC Adv 3:20001–20009. doi:10.1039/c3ra42987c
121. Froschauer C, Hummel M, Iakovlev M, Roselli A, Schottenberger H, Sixta H (2013) Separation of hemicellulose and cellulose from wood pulp by means of ionic liquid/cosolvent systems. Biomacromolecules 14:1741–1750. doi:10.1021/bm400106h
122. Berggren R, Berthold F, Sjöholm E, Lindström M (2003) Improved methods for evaluating the molar mass distributions of cellulose in kraft pulp. J Appl Polym Sci 88(5):1170–1179. doi:10.1002/app.11767
123. Hauru LKJ, Hummel M, King AWT, Kilpelainen I, Sixta H (2012) Role of solvent parameters in the regeneration of cellulose from ionic liquid solutions. Biomacromolecules 13: 2896–2905. doi:10.1021/bm300912y
124. Röder T, Moosbauer J, Fasching M, Bohn A, Fink H-P, Baldinger T, Sixta H (2006) Crystallinity determination of native cellulose-comparison of analytical methods. Lenzinger Ber 86: 85–89
125. Fink HP, Fanter D, Philipp B (1985) Röntgen-Weitwinkeluntersuchungen zur übermolekularen Struktur beim Cellulose-I-II-Phasenübergang. Acta Polym 36(1):1–8. doi:10.1002/actp.1985.010360101
126. Fink H-P, Weigel P, Ganster J, Rihm R, Puls J, Sixta H, Parajo JC (2004) Evaluation of new organosolv dissolving pulps. Part II: structure and NMMO processability of the pulps. Cellulose 11:85–98. doi:10.1023/B:CELL.0000014779.93590.a0
127. Maenner J, Ivanoff D, Morley RJ, Jary S (2011) TENCEL - new cellulose fibers for carpets. Lenzinger Ber 89:60–71
128. Adusumalli R-B, Keckes J, Martinschitz K, Boesecke P, Weber H, Roeder T, Sixta H, Gindl W (2009) Comparison of molecular orientation and mechanical properties of lyocell fibre tow and staple fibres. Cellulose 16(5):765–772. doi:10.1007/s10570-009-9292-2
129. Lenz J, Schurz J, Wrentschur E (1994) On the elongation mechanism of regenerated cellulose fibers. Holzforschung 48:72–76. doi:10.1515/hfsg.1994.48.s1.72
130. Fink HP, Walenta E (1994) X-ray diffraction investigations of cellulose supramolecular structure at processing. Papier 48(12):739–748
131. Gindl W, Reifferscheid M, Martinschitz KJ, Boesecke P, Keckes J (2008) Reorientation of crystalline and noncrystalline regions in regenerated cellulose fibers and films tested in uniaxial tension. J Polym Sci B Polym Phys 46:297–304. doi:10.1002/polb.21367
132. Hermans PH, Weidinger A (1949) X-ray studies on the crystallinity of cellulose. J Polym Sci 4(2):135–144. doi:10.1002/pol.1949.120040203

Adv Polym Sci (2016) 271: 169–206
DOI: 10.1007/12_2015_305

Published online: 6 May 2015

The Surface and In-Depth Modification of Cellulose Fibers

Alessandro Gandini and Mohamed Naceur Belgacem

Abstract This review updates the most relevant advances achieved in the field of surface and in-depth modification of cellulose fibers during the last 5 years. It reports work dealing with cellulose substrates on the nano- to micrometer scale, namely cellulose nanocrystals (CNCs), cellulose nanofibrils (CNFs), microfibrillated cellulose (MFC), and bacterial cellulose (BC), as well as conventional lignocellulosic fibers. Several approaches have been applied for surface modification of these substrates, namely hydrophobization and oleophobization, physicochemical adsorption, oxidation, cationization, esterification, urethane and siloxane formation, and grafting-from and grafting-onto macromolecular sequences. In-depth modification can be achieved by both partial esterification and partial oxypropylation.

Keywords Bacterial cellulose · Cellulose nanocrystals (CNCs) · Cellulose nanofibrils (CNFs) · In-depth modification of cellulose · Lignocellulosic fibers · Nano- and microfibrillated cellulose · Surface modification of cellulose

Contents

A. Gandini (✉) and M.N. Belgacem
The International School of Paper, Print Media and Biomaterials (Pagora), Grenoble Polytechnic Institute, 38402 Saint Martin d'Hères Cedex, France
e-mail: agandini@iqsc.usp.br

1 Introduction

This review provides an updated description of the state of the art in research dealing with different approaches related to the modification of cellulose fibers using both physical and chemical processes. It covers both classical lignocellulosic fibers from wood and annual plants and the different nanocellulose counterparts that have gained such a prominent status in recent years. Two strategies are covered here, namely alterations limited to the macromolecules present on the surface of the fibers and those involving deeper modifications leading to the formation of a sleeve of modified material, but without transforming the entire thickness of the fiber, which would otherwise generate a bulk cellulose derivative. In other words, the purpose of the latter approach is to induce an in-depth modification, while preserving the pristine morphology of the unmodified inner regions of the fibers and, hence, their original mechanical properties.

The purposes of these investigations are related to a number of alternative outcomes and, hence, to various properties and applications, including hydrophobization; lipophobization; super-absorbency; interfacial compatibilization with other macromolecular materials (mostly for the elaboration of high-performance composites); the selective sequestration of industrial effluents or marine pollutants; hybrid, magnetic, conductive, and other "intelligent" materials; and the possibility of generating single-component composites based exclusively on cellulose. Other types of surface modifications, such as dyeing or the manufacture of chromatography substrates, fall outside the scope of this review.

The literature on cellulose fiber surface modification is very rich and several reviews cover the field up to 2010 [1–5], with particular emphasis on the elaboration of composite materials, although the latest contribution covers a wider scope [5]. Given this quantity of information, only a brief summary is given here on the developments achieved up to about 5 years ago and the review concentrates on the important advances reported since 2010. Although this seems a relatively short period of time, the quantity of original contributions, attesting to the importance of the topic, justifies the need for a detailed and critical update.

The interest in altering the surface of cellulose fibers began in the middle of the last century with studies of graft polymerizations in aqueous media, in which surface-generated free radicals initiated the polymerization of various monomers. Hebeish and Guthrie [6] thoroughly reviewed this field up to 1980. Subsequent work, including excursions into anionic and cationic grafting, was described by Belgacem and Gandini in 2005 [3]. Despite significant efforts, these processes did

not materialize into viable applications. The advent of controlled radicals has reopened this dormant topic with new perspectives, as discussed below.

Revival of the field took place after a lull of a few decades, with a sudden crop of studies at the beginning of the 1990s and the trend has not stopped, nor slackened, since then, enriched moreover by investigations related to the blooming of interest in nanocelluloses [7–11]. In the context of conventional chemical modifications, the obvious reactive moieties are, of course, almost exclusively the hydroxyl functions, usually comprising both the primary and the secondary species. Small molecules, oligomers, and polymers have been appended to the outer layer(s) of the fibers by a variety of mechanisms [5], and the ensuing materials often characterized in a rigorous fashion using a battery of complementary techniques. Physical treatments using a variety of energy sources are covered in a more modest number of studies and, inevitably, also produced structural modifications, albeit in a less predictable and precise fashion [5]. Some reports also described approaches that did not involve any attack on the fiber surface, focusing instead on the building of a polymer cover around it to mask its specific structural features (i.e., the OH groups), which were replaced by those of the coating. Recent progress associated with all these strategies is discussed and subdivided on the basis of the primary aim of each of strategy.

2 Surface Modification

Surface modification dominates the field covered by this review. This section is concerned with investigations in which the depth of the modification is ideally limited to the outer macromolecular layer of the fiber surface. Strictly speaking, it is more realistic to view these treatments as affecting what one could call its "outer skin" (i.e., the most superficial cellulose molecules). Even when the main purpose of the study clearly addresses a specific application, the nature of the modification sometimes generates properties that are also exploitable for other uses, as in the case of certain types of hydrophobization, which create conditions also appropriate for surface compatibilization with a nonpolar polymer matrix in the construction of a composite material. The following subdivision is therefore not entirely univocal, but is nevertheless deemed sufficiently rational to justify its use, with the proviso that broader situations, as defined above, are clearly identified and discussed.

2.1 Hydrophobization and Oleophobization

Making the surface of cellulose fibers hydrophobic can be an end in itself, as in the case of the treatment of paper, or it can combine two aims, such as the decrease in affinity for moisture and the transformation of a polar surface into a nonpolar counterpart in order to improve its compatibility with a similarly nonpolar polymer. An example is the elaboration of a composite material in which the reinforcing

fibers must display a strong interfacial adhesion to the macromolecular matrix by minimizing their interface energy. The publications surveyed in this section often relate to the latter situation.

It is generally acknowledged that in order to generate a highly hydrophobic (or superhydrophobic) surface, two complementary features must be imparted to it, namely a chemical contribution arising from the presence of nonpolar moieties and a morphological complement consisting of the development of micro- or nano-asperities that inhibit wetting of the corresponding valleys and, hence, the spreading of water. The hydrophobic character of a surface can be assessed by measurement of the contact angle formed by a droplet of water deposited on it, although other criteria are also employed. Values higher than 90° conventionally define a surface as hydrophobic. When a contact angle of 150° is reached, the surface is said to be superhydrophobic.

Much research has been devoted to the hydrophobization of cellulose [12, 13] because of its intrinsic affinity to water and, hence, its classical moisture uptake or wicking, which dramatically affects the mechanical properties of the fibers. This is a problem also encountered with starch-based materials and other polysaccharides [14].

The necessity to confer hydrophobic characteristics to fibers or fibrils that assemble into a hydrophilic biopolymer such as cellulose has always been part of the development of papermaking, particularly with respect to the sizing operation. Sizing is generally conducted at the wet-end part of the process in order to reduce the tendency of paper to absorb liquids (e.g., to ensure the drying of an ink without smudging or excessive in-depth penetration, or to retain the mechanical strength of cardboard in a damp atmosphere, as with egg containers). The most common sizing agents used in papermaking are alkenyl succinic acid anhydride (ASA), alkyl ketene dimer (AKD), and rosin, which are added to the fiber suspension in the form of emulsions [15, 16] or delivered from the vapor phase [17].

AKD has also been employed to prepare superhydrophobic papers using three alternative introduction techniques: (1) air-blasting with cryoground micro-particles, (2) crystallizing from organic solvents, and (3) spraying with rapid expansion of supercritical solutions (RESS) [18]. The green character and simplicity of the cryogrinding–airblasting method is favored over the use of an organic solvent, but the RESS technique produces a higher hydrophobicity; moreover, this approach provides the additional advantage of a continuous application (i.e., has potential industrial implementation).

Whether AKD actually reacts with the surface OH groups of the paper cellulose fibers or is simply adsorbed on them through polar interactions is still a source of debate among specialists [15, 16]. However, a recent alternative to conventional sizing [19] involves an entirely physical process consisting of sizing and coating paper with poly(3-hydroxybutyrate), a readily biodegradable material, using a heat press. The high price of this polymer, however, constitutes a serious drawback to possible applications, particularly in the realm of papermaking where cost-effectiveness is paramount.

The interest in making cellulose fibers hydrophobic in a more general context began some 40 years ago with numerous studies on surface esterification using aliphatic and aromatic carboxylic reagents, mostly in organic media, although recent reports also deal with gas–solid reactions using carboxylic anhydrides [12, 13]. Depending on the degree of substitution (DS) and the specific moiety appended, contact angles increased to different levels, reaching values above 90° in the best situations [12, 13]. A particularly detailed study dealing with the use of aliphatic fatty acid chlorides of different chain lengths [20–24] showed that the combined use of two renewable resources as both the fiber substrate and the reagent can open the way to fully green systems with properties that go beyond mere hydrophobization, which is nevertheless attained at good levels. The modified fibers displayed excellent compatibility with polyolefins in the construction of composite materials, given the structural affinity between the grafted aliphatic "hairs" and the matrix macromolecules. Furthermore, these hairs were sufficiently long (C12–C22) to generate physical entanglements with the polymer surrounding them, thus enhancing the strength of the fiber–matrix interface. A later study applied the same approach to cellulose nanocrystals or whiskers instead of conventional fibers [25]. Results showed that long appended aliphatic chains actually crystallized at the surface of the modified cellulose nanocrystals and that their incorporation into poly(ethylene) improved the mechanical properties of the matrix.

Esterification with the perfluorocarbonyl compounds shown in Fig. 1 leads to cellulose surfaces with enhanced hydrophobicity compared with those discussed above, as expected, because of the low surface energy associated with the presence of fluorinated moieties. Indeed, the polar component of the surface energy (γ_s^p) fell to practically zero and the dispersive contribution (γ_{ds}) to values as low as 8 mJ/m^2. This explains the fact that these treatments also generate a strong lipophilicity and thus the fiber surface becomes "omniphobic," with high contact angles for polar and nonpolar liquids. Trifluoroacetylation is readily reversed by hydrolysis following prolonged contact with water, a feature that favors recycling of the original fibers after their life cycle (e.g., in packaging resist to both moisture and grease). Pentafluorobenzoylation, on the other hand, gives surfaces that are much more stable toward hydrolysis [12, 13].

Another coupling reaction involves isocyanates. The most thorough investigation on the preparation of omniphobic cellulose surfaces using this coupling deals with the reaction of (3-isocyanatopropyl)triethoxysilane with cellulose fibers [26], followed by sol–gel treatments with different reagents to generate the most appropriate conditions for superhydrophobicity and superoleophobicity, particularly

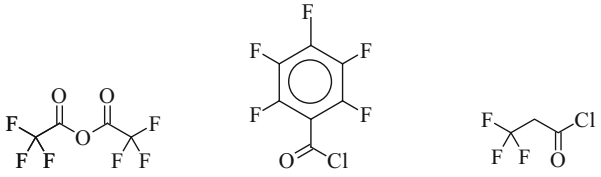

Fig. 1 Three perfluorocarboxyl reagents used for the hydrophobization and lipophobization of cellulose fibers [12, 13]

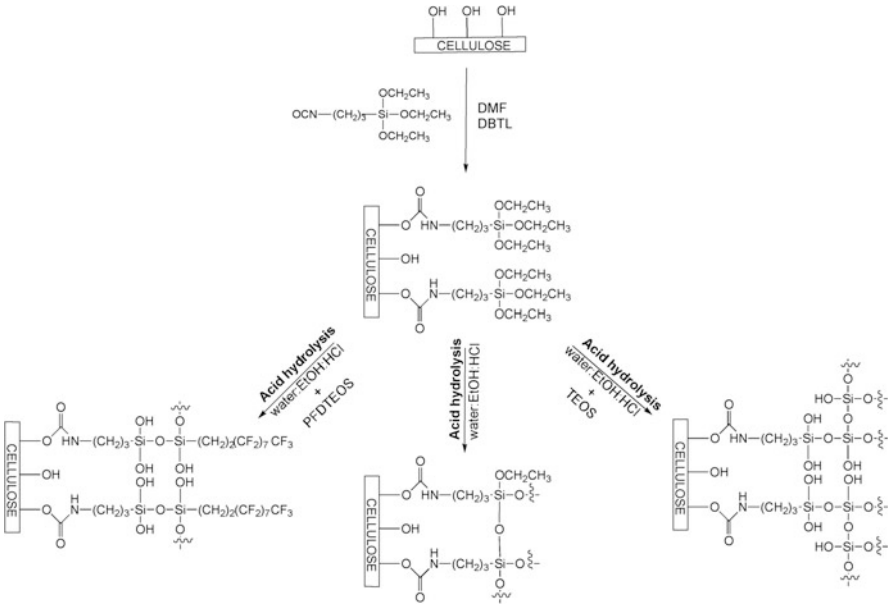

Fig. 2 Pathways implemented to prepare differently modified cellulose fibers, following the initial coupling with (3-isocyanatopropyl)triethoxysilane (reproduced by permission of Elsevier. Copyright 2010. Reprinted from Cunha et al. [26])

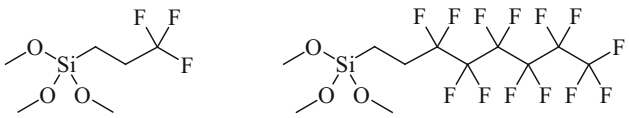

TFPS PFOS

Fig. 3 Chemical structures of 3,3,3-trifluoropropyl trimethoxysilane (*TFPS*) and *1H*,*1H*,*2H*,*2H*-perfluorooctyl trimethosysilane (*PFOS*)

when using perfluorosiloxanes for the final step (see Fig. 2). This process ultimately generates micro- or nanosurface asperities on the fibers, which, when complemented by incorporation of perfluoro moieties, results in strongly biphobic surfaces with contact angles as high as 140° for water and 134° for the nonpolar diiodomethane.

A different treatment involving the siloxane reaction with the cellulose OH groups, aimed at producing a highly hydrophobic surface [27], enabled grafting of the surface of two models for cellulose fibers (Avicell and Whatman paper) with two fluorine-bearing alkoxysilanes, 3,3,3-trifluoropropyl trimethoxysilane (TFPS) and *1H*,*1H*,*2H*,*2H*-perfluorooctyl trimethosysilane (PFOS) (Fig. 3).

These fluorinated moieties append onto the surface of the cellulose macromolecules and produce a strong hydrophobic effect, as revealed by the increase in

water contact angles on both model substrates. Contact angles changed from about 50° before modification to 115° and 125° for TFPS- and PFOS-modified samples, respectively. Moreover, determination of the polar contribution to the surface energy (γ_s^p) using the Owens–Wendt approach showed a dramatic decrease from about 20 mJ/m^2 for the pristine celluloses to practically zero after modification. A similar approach was implemented with the aim of preparing a superhydrophobic and self-cleaning cotton fabric [28] using treatment with *1H*,*1H*,*2H*,*2H*-perfluorooctyl triethoxysilane (FOS). Water contact angle measurements revealed the formation of a highly hydrophobic surface after modification with different concentrations of FOS. A superhydrophobic character was only attained when the FOS concentration was 20% with respect to the cotton weight. The self-cleaning ability of the FOS-modified cotton fabric was also investigated, with encouraging results.

Two original alternative strategies for generating a pronounced hydrophobic character on the surface of cellulose fibers combine the introduction of nonpolar moieties and the formation of micro- to nanoscale topographies. One strategy involved physical adsorption of silica nanobeads onto the fibers (nanoroughness), followed by the reaction of TFPS or FOS with the silica surface (low surface energy structures) [29], as illustrated in Fig. 4. Each modification step was followed by SEM and AFM imaging. Water contact angles close to 150° were attained, confirming the effectiveness of combining the two approaches.

The second strategy has the advantage of a remarkable ease of implementation and green connotations [30]. The cellulose surface was subjected to short contact

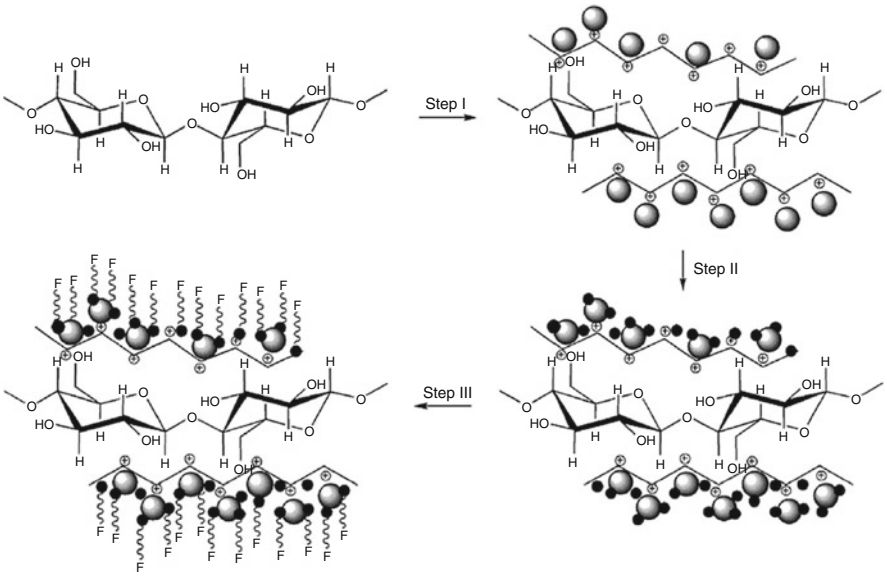

Fig. 4 Sequence of steps applied for preparation of highly hydrophobic rough cellulose surfaces (reproduced by permission of Elsevier. Copyright 2008. Reprinted from Gonçalves et al. [29])

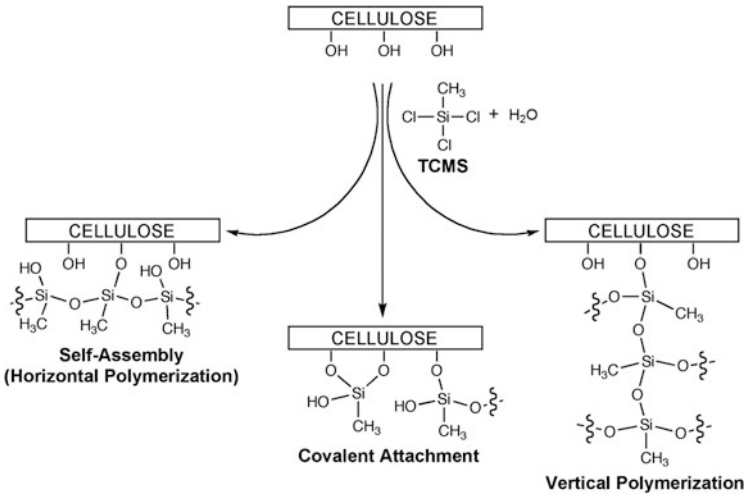

Fig. 5 Alternative structures generated by the reaction of hydrolysed trichloromethylsilane (*TCMS*) with the surface of cellulose fibers (reproduced by permission of Elsevier. Copyright 2010. Reprinted from Reference [30])

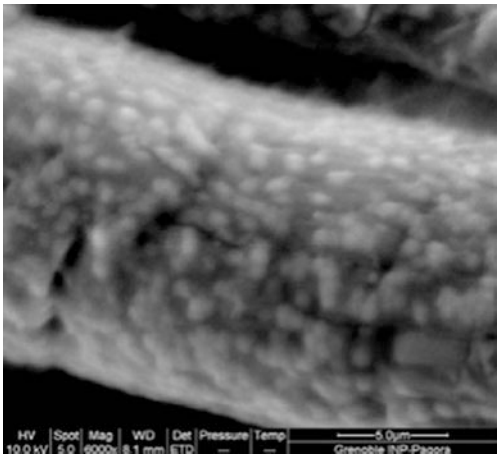

Fig. 6 A cellulose fiber covered by nano-asperities associated with the structures shown in Fig. 5 (reproduced by permission of Elsevier. Copyright 2010. Reprinted from Cunha et al. [30])

with trichloromethylsilane (TCMS) vapor in the presence of moisture at room temperature, and the hydrolyzed silane rapidly reacted with the surface OH of the fibers. The set of structures arising from this process, as shown in Fig. 5, contribute to the generation of nano-asperities on the cellulose fibers (Fig. 6).

In the process of switching to nanocelluloses, the use of aliphatic isocyanates has been reported for appending relatively long methylene sequences onto their

surfaces [31, 32]. The reaction of *n*-octadecylisocyanate was conducted in toluene on both cellulose nanocrystals (CNCs) and cellulose nanofibrils (CNFs) and, despite a fairly low DS as a result of steric hindrance of the appended long aliphatic chains, the water contact angles were raised to values as high as 100°. This study also included incorporation of the modified fibers into a poly(caprolactone) (PCL) matrix and characterization of the ensuing composites. The results clearly showed the benefits of modification in terms of a superior gain in mechanical properties compared with the two untreated nanocelluloses.

An investigation aimed at the synthesis of so-called continuous fiber-reinforced composites led to the elaboration of new cellulose-based hydrophobic materials. The approach involved attaching a polymeric matrix to the surface of cellulose fibers via chemical coupling, in such a way that the long chains appended to the fiber surface formed macromolecular entanglements with those of the polymer matrix. In particular, the grafting of cellulose fibers by PCL followed a reaction pathway in which phenyl isocyanate was used as an OH-blocking agent, and 2,4-toluene diisocyanate (TDI) as the PCL–cellulose coupling mediator (Fig. 7) [33]. After modification, the water contact angle was higher than 90° and was found to be quite stable with time. This material was biodegradable, albeit with slower kinetics than those of the pristine fibers.

The use of high-energy physical sources, such as cold plasma, lasers, and UV light, in the presence of a specifically selected compound in the gas phase has been exploited to increase the hydrophobicity of cellulose surfaces [12, 13]. In all these processes, the mechanisms leading to chemical modification of the fiber surface are ill defined and certainly not confined to a single process [12, 13]. Plasmas involving styrene and a number of its homologs [34] have been tested successfully as sources of hydrophobization. A systematic study using this approach showed that the water contact angle increased up to 100°. There was clear evidence of surface modification, as shown by X-ray photoelectron microscopy (XPS) and elemental analysis. In the case of cold plasmas involving fluorinated reagents, the presence of grafted fluorine moieties or individual atoms were unambiguously detected and considered to be the main cause of the observed increase in hydrophobicity. However, these techniques, with rare exceptions [34], are difficult to control for good reproducibility, although this might not be a major drawback for certain applications where a positive qualitative outcome is considered adequate.

The purely physical deposit of a hydrophobic material onto cellulose fibers is the last type of treatment discussed in this section. The noncovalent attachment of different polymers or nanosized particles has been carried out using several techniques, such as Pickering emulsions, layer-by-layer or multilayer deposition, dip-coating or immersion in the polymer solution, impregnation, physical deposition, or simply heating [12, 13]. The advantages of these techniques stem from their relative simplicity and the possibility of using aqueous media. However, the mechanical stability of these thin coatings following prolonged utilization under mechanical stress raises concerns, which to the best of our knowledge have never been thoroughly addressed.

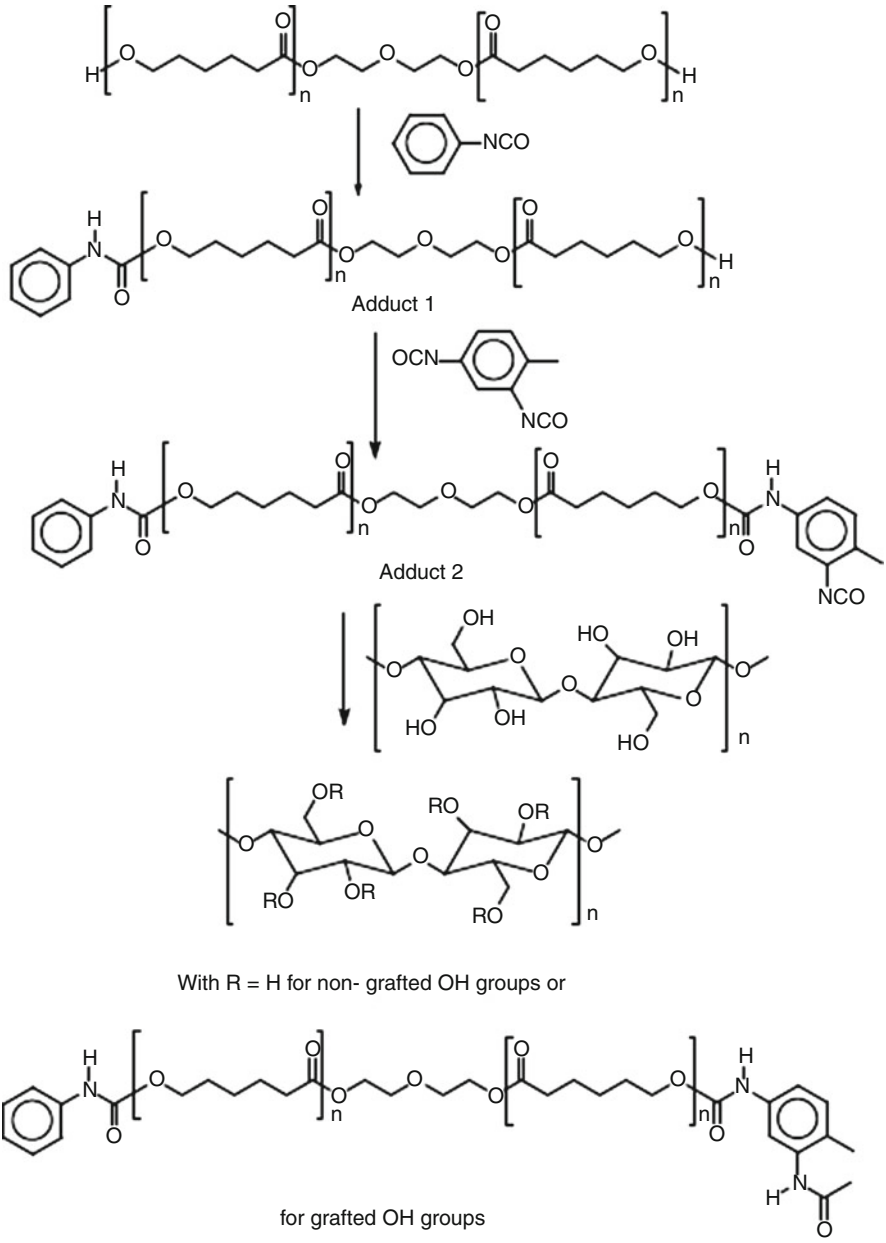

Fig. 7 Process leading to the grafting of poly (caprolactone) onto cellulose fibers (reproduced by permission of Elsevier. Copyright 2010. Reprinted from Paquet et al. [33])

The application of admicellar polymerization to cellulose fibers was first reported more than 10 years ago [35]. The process, formerly used to coat inorganic substrates such as oxides, involves generating an admicellar double layer of surfactant onto the solid surface to be modified and then filling it with a nonpolar monomer from its water suspension. The subsequent free radical polymerization generates a thin sleeve of the corresponding polymer around the substrate. Poly (styrene) and poly(acrylate)s were thus efficiently wrapped around conventional cellulose fibers, with a considerable gain in hydrophobicity after washing and drying the material [35]. Polymers with a low glass transition temperature are obviously preferred in this context in order to ensure flexibility of the sleeved fibers. The purpose of this study was to associate two possible applications, namely the increase in hydrophobicity for packaging papers and the incorporation of the treated fibers into a macromolecular matrix to form a composite material with good interfacial properties. This investigation was not pursued any further until 2013, when the same process was applied successfully to the three types of nanocellulose (CNCs, CNFs, and bacterial cellulose (BC) filaments [36, 37]). This is an original, simple, and green method for enveloping fibers with different polymers of low polarity without recurring to cumbersome techniques involving the transfer of nanofibers from their natural aqueous habitat to an organic medium. Figure 8 shows unpublished SEM images of BC fibers before and after undergoing the admicellar polymerization of styrene, and highlights the formation of a sleeve of poly(styrene) around the fibers.

The rewarding repercussions of this strategy are clearly illustrated by a subsequent study in which poly(styrene)-coated BC nanofibers were incorporated into natural rubber in order to enhance its mechanical properties [36, 37]. The presence of the polymer sleeve around BC improved the quality of its interface with the nonpolar natural matrix and provided a notable improvement in the mechanical properties of the ensuing composites in terms of Young's modulus and tensile strength, even with modest nanofiber loadings. This investigation resulted in the preparation of materials going progressively from typical elastomers to stiff thermoplastics, as a function of the extent of incorporation of modified BC.

2.2 Modification by Physical-Chemical Adsorption

Noncovalent interactions have received much attention in the context of nanocellulose surface modification [7–11], on the one hand to facilitate dispersion in nonpolar media and, on the other hand, to develop viable bioengineering interactions. The former strategy was introduced in 2000 [38] by using surfactants consisting of the mono- and di-esters of phosphoric acid, with alkyl phenols tails to adsorb onto CNCs, with excellent results in terms of ease of dispersion in organic solvents. The incorporation of these surfactant-coated CNCs into either atactic or isotactic polypropylene produced very good compatibilization [39, 40], with specific interactions between charge and matrix in the latter type of composite. The use

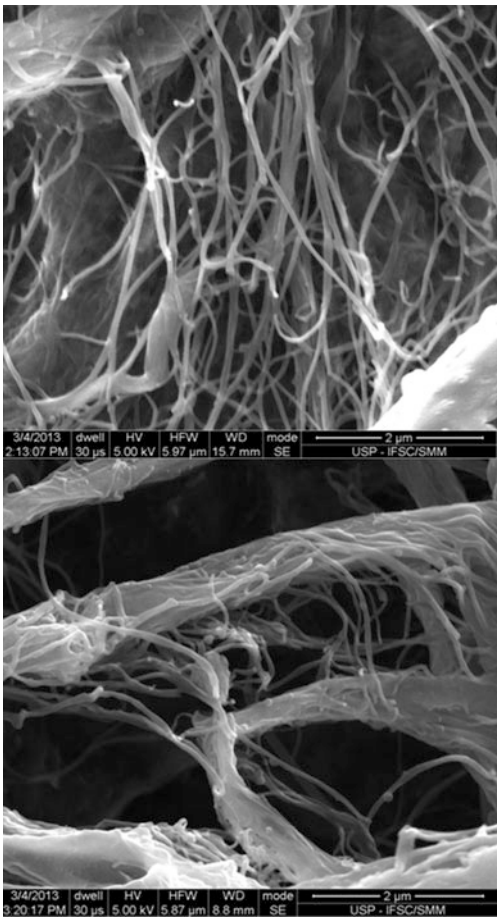

Fig. 8 SEM images of bacterial cellulose fibers before (*above*) and after (*below*) being subjected to the admicellar polymerization of styrene

of anionic surfactants was found to improve the dispersion of the modified CNCs in poly(lactic acid) [41], and nonionic counterparts provided the same beneficial effect when the matrix was poly(styrene) [42, 43]. Macromolecular amphiphilic block copolymers were also tested in this context and found to be an efficient aid for the dispersion of modified CNCs in nonpolar solvents [44]. The deposition of a cationic surfactant, cetyltrimethylammonium bromide, onto oxidized BC enhanced the strength of the interfacial interaction (thanks to the anionic–cationic electrostatic coupling) to such a degree that the surfactant was not removed by repeated aqueous washings [45, 46]. A similar study [47] described the interaction of oxidized CNCs with various cationic surfactants in an aqueous medium, simulating the process of organic modification of layered silicates.

Studies related to biologically inspired composites using nanocelluloses include the interaction of BC with poly(ethylene oxide) (PEO) [48] and hydroxyethylcellulose [49], the association of CNCs with PEO [50], and the adsorption of

carboxymethylcellulose or chitosan on cellulose film surfaces [51]. The treatment of CNCs with a quaternized thermoresponsive acrylic copolymer [52] imparted this important property to the coated nanocrystals.

The by-now classical strategy of assembling monomolecular strata via layer-by-layer (LbL) deposition, based on electrostatic interaction between oppositely charged molecules or polyelectrolytes, has also been applied to both CNCs and microfibrillar cellulose (MFC) [53–59], as well as to carboxymethylated MFC, a highly negatively charged surface [60]. A variety of cationic polyelectrolytes, and even cationized MFC, were used, and the ensuing assemblies characterized in terms of specific structures and properties and, hence, possible applications.

The attachment of inorganic nanoparticles, including metals and oxides, onto the surface of cellulose fibers is another topic of growing interest. The first thorough study described the deposition of Ag, Au, Pt, and Pd particles with a narrow size distribution below 10 nm and the characterization of these novel hybrid materials [61]. Further work on this topic developed progressively [5] and the most notable advances reported the electrostatic deposition of Au nanoparticles on wood pulp and BC [62], the preparation of cellulose/SiO_2 nanocomposites by the LbL process [63], and the surface modification of cellulose fibers with TiO_2 [64] to give solar light photostable nanocomposites. Another promising application involves the antibacterial activity of cellulose/Ag nanocomposites. Ag concentrations as low as 5×10^{-4} wt% provided effective antibacterial action [65]. Further investigations have focused on increasing the fiber surface coverage [66] and exploring alternative deposition processes [67]. The most recent original contributions in this area deal with the use of LbL to first attach various polyelectrolytes to CNFs, in order to use them as attachment sites for the deposition of Ag and ZnO nanoparticles capable of providing antimicrobial properties to the ensuing assemblies [68, 69].

2.3 Chemical Modification of the Surface Chemical Moieties

2.3.1 Oxidation

The most relevant aspect of controlled modification of the chemical structure of cellulose fibers is the 2,2,6,6-tetramethylpiperidine-1-oxyl (TEMPO)-catalyzed oxidation of cellulose to generate carboxylic groups, particularly in view of its usefulness in handling nanocellulose suspensions and their reactivity. The reaction is known to exclusively affect the primary OH groups and is ecologically advantageous because it is carried out in water and in the presence of NaBr and NaOCl and calls upon the strategic role of the stable nitroxyl radical TEMPO to mediate the oxidation. Figure 9 illustrates the mechanism as applied to cellulose.

Isogai's group has been at the forefront of this research area [70] and developed an optimized technique to treat wood and other lignocellulosic fibers under mild basic conditions in order to facilitate their progressive unraveling as a consequence of the electrostatic repulsion generated by the formation of carboxylic groups.

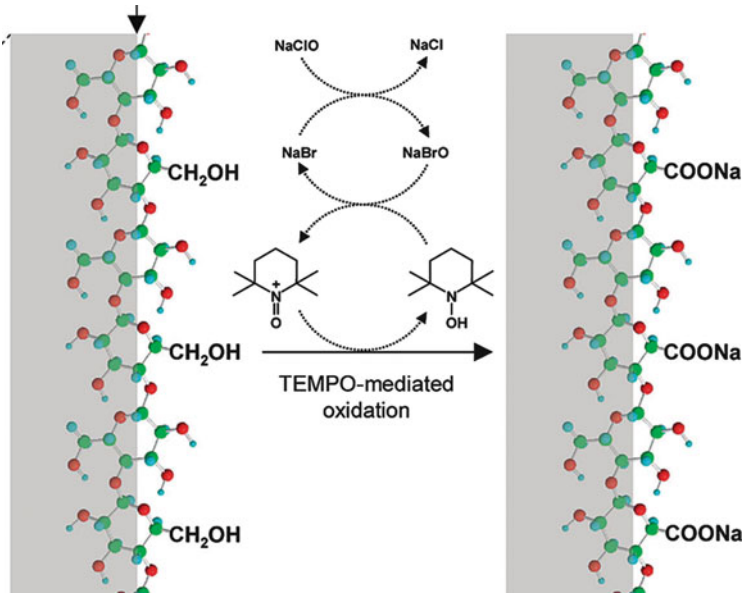

Fig. 9 Mechanism of the TEMPO-catalyzed oxidation of the primary hydroxyl groups of cellulose

Coupled with mechanical shearing, as in the preparation of CNFs, this green process gives rise to individual microfibers in a couple of hours at room temperature. The fibers are typically several nanometers wide, several micrometers long, and have a crystallinity of 70–90%. Numerous applications have been found for this relatively cheap nanocellulose, including nanoelectronics, healthcare, cosmetics and, not least, their incorporation into polymer matrices as reinforcement, to impart gas-barrier properties, and to improve thermal stability [70]. This process has also been applied to CNCs [71] and CNFs [72] with the purpose of facilitating their dispersion in both aqueous and organic media, and also to generate surface COOH groups in order to graft different moieties onto them.

2.3.2 Cationization

The introduction of positive charges on cellulose macromolecules [73, 74] is more cumbersome than similar cationizations of other polysaccharides such as starch and chitosan, because of solubility problems, as highlighted in a recent review [75]. However, this problem is largely alleviated if only the surface of the fibers is involved. The typical reagents used for this purpose are epichlorohydrin in conjunction with tertiary amines (as shown in Fig. 10), or an ammonium oxirane such as epoxypropyltrimethylammonium chloride, via nucleophilic addition of the alkali-activated cellulose hydroxyl groups to the epoxy moiety. As in the case of the

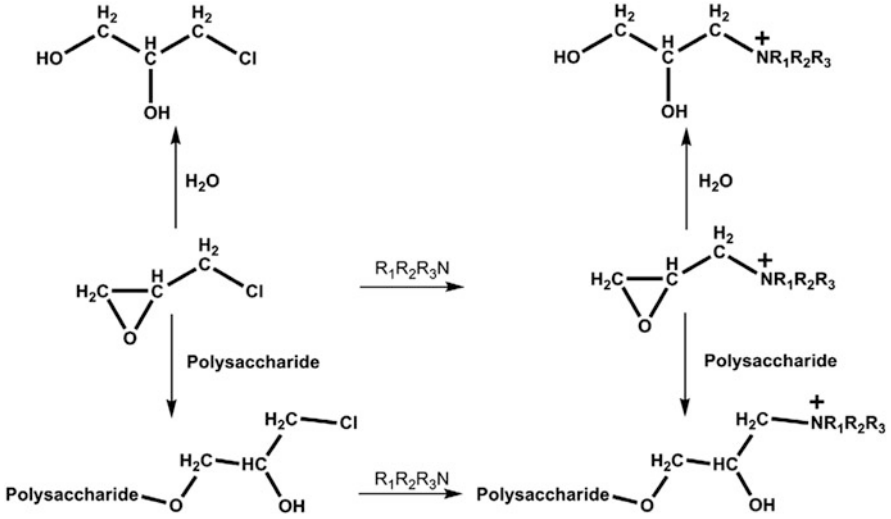

Fig. 10 Synthesis of cationized polysaccharides with epichlorohydrin and tertiary amines

cationization of CNCs [76], the surface grafting of chitin nanocrystals by appended cationic moieties leads to stable aqueous suspensions of these particles with original thixotropic properties. Given the fact that in this process the original anionic sites on the cellulose molecules are preserved, the ensuing fibers can be considered as amphoteric, but, of course, with a predominant cationic character. A similar process was applied to cellulose fibers before their mechanical shearing in order to reduce energy consumption in the preparation of CNFs [77, 78].

2.4 Grafting with Molecular Moieties

The numerous studies dealing with the chemical condensation of nonpolymeric molecular structures at the surface of cellulose fibers have been reviewed on several occasions [1–5], apart from the specific investigations discussed in the section on hydrophobization (Sect. 2.1). Only the advances reported in the last 5 years, which are predominantly related to the use of nanocelluloses as substrates [7–11], are therefore reviewed here. Many of these contributions are concerned with improvements in the compatibilization of the nanocellulose used as a reinforcing element in composites based on polymer matrices, but other strategies have been put forward with a variety of other purposes in mind.

2.4.1 Esterification

This chemical transformation has been discussed in the section on hydrophobization (Sect. 2.1). Work on the acetylation of different CNFs, typically involving acetic anhydride in the presence of strong acids as catalysts, has shown that the morphology of the substrates is not substantially altered, even under rather severe conditions. In general, the purpose of these esterification processes is primarily to improve compatibilization of the ensuing nanofibers with different macromolecular matrices in the construction of nanocomposite materials. The most original idea in this context stems from a pioneering investigation [79, 80] in which the authors coupled the acetylation reaction with the splicing and size reduction of lignocellulosic fibers in order to prepare esterified nanocellulose in a single step, as sketched in Fig. 11.

This approach inspired a recent study in which esterified CNFs were prepared by the application of both the fiber ball milling and chemical processes [81]. The use of different organic media, reagents, and other experimental conditions enabled modified CNFs with various features and properties to be attained.

An alternative way to avoid the laborious aqueous–organic medium change before the chemical transformation, a procedure that typically requires such steps as water–acetone–toluene exchange, has been put forward, namely a gas–solid reaction. CNCs and CNFs were exposed to the in vacuo attack of palmitoyl chloride at 160–190°C [82, 83] and the extent of esterification assessed by SEM and X-ray characterization. By altering the reaction conditions, the authors were able to ensure near-complete surface condensation without affecting the inner layers of the

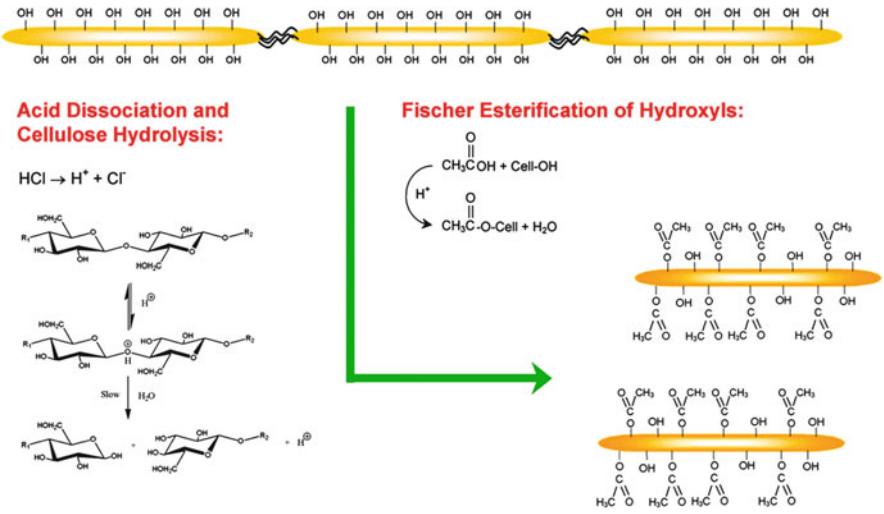

Fig. 11 Concomitant hydrolysis of amorphous regions and acetylation in a single-step process, leading to esterified cellulose nanocrystals (reproduced by permission of the American Chemical Society. Copyright 2010. Reprinted from Braun and Dorgan [79] and Sobkowicz et al. [80])

nanocellulose substrates. Further work by the same group used nanocrystal aerogels as starting cellulose material to provide a convenient way of dispersing the ensuing esterified product in nonpolar media [82, 83].

Exploitation of the classical transacetylation reaction using vinyl acetate was extended to CNCs in a study conducted in DMF suspension with potassium carbonate as catalyst [84]. This simple procedure provided a means to control the extent of esterification, as well as the severity of the attack.

Another interesting strategy with ecological advantages uses an ionic liquid ([bmim][PF6]) as the reaction medium for the surface esterification of CNFs by different aliphatic carboxylic anhydrides [85]. After optimization, surface DS values of around unity were attained, as assessed by XPS. Time-of-flight secondary ion mass spectrometry (ToF-SIMS) was used as a novel complementary tool for the characterization of esterified nanofibers, and the authors also showed that the solvent could be adequately recycled.

2.4.2 Reactions with Isocyanates

The same group that carried out the reactions mentioned above in the context of hydrophobization [31, 32], also pursued reactions with isocyanates on both CNCs and CNFs in bulk at around 100°C [86–88] in order to find the optimal grafting conditions for compatibilization of the modified nanocelluloses with nonpolar matrices.

A more detailed and thorough investigation by another group from the same laboratory [89] was carried out in which a toluene suspension of CNFs was reacted with *n*-octadecyl-isocyanate (with the aid of the classical dibutyltindilaurate catalyst) in order to enhance the degree of surface grafting. One of the interesting outcomes of this study was that the morphology of the nanofiber assemblies was a function of the DS of the long aliphatic chains on their surface, as shown in Fig. 12. At high DS, steric crowding favored their organization to form crystalline domains based on dispersive interactions. This conclusion was reached from X-ray evidence and further corroborated by contact angle and thermogravimetric measurements [89].

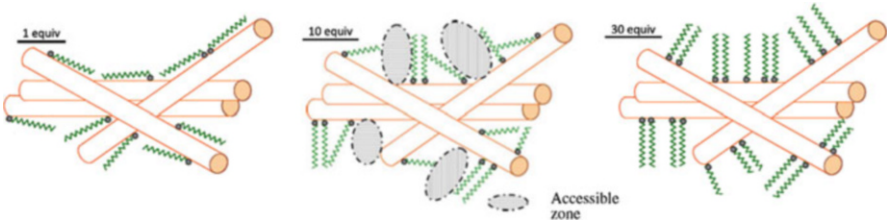

Fig. 12 Morphology of modified cellulose nanofibers as a function of the extent of grafting of octadecyl chains (reproduced by permission of Springer. Copyright 2012. Reprinted from Missoum et al. [89])

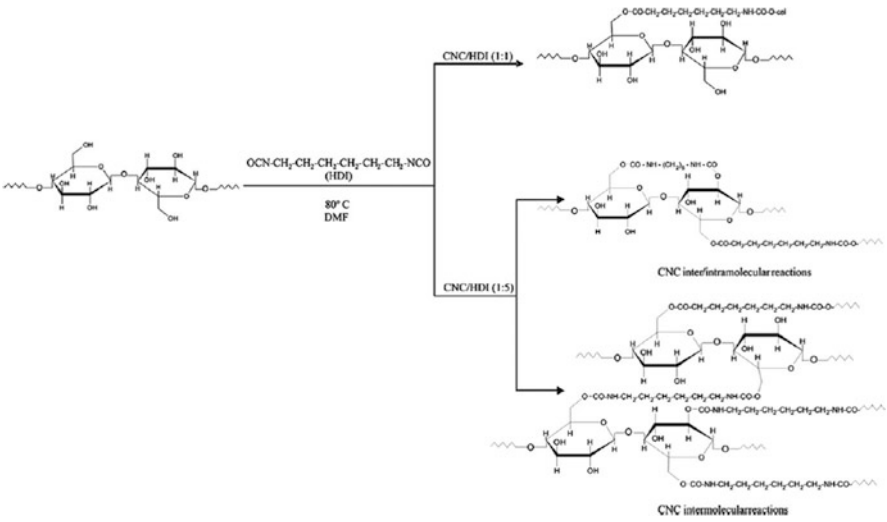

Fig. 13 Reaction between the surface OH groups of cellulose nanocrystals (*CNC*) and hexamethylenediisocyanate (*HDI*) in different molar ratios (reproduced by permission of Elsevier. Copyright 2011. Reprinted from Rueda et al. [92])

An extension of this work used the same aliphatic isocyanate to treat conventional lignocellulosic fibers used for the reinforcement of cement-based composites for roofing and cladding panels. The treated fibers created a protective shield against water swelling and the strongly basic medium of the matrix, which promotes degradation of cellulose [90, 91]. This strategy gave satisfactory results in terms of high chemical and physical stability of the fibers and enhanced mechanical properties.

The use of an aliphatic diisocyanate as the surface-coupling agent for CNCs [92] showed that, as the amount of 1,6-hexamethylene diisocyanate was increased with respect to the available surface OH groups, intra- and inter-CNC condensations took place (see Fig. 13). The incorporation of untreated CNCs into a polyurethane matrix resulted in an even dispersion, yielding a tough material without loss of ductility. Counterparts modified with an excess of diisocyanate appeared to migrate preferentially toward the matrix hard segments, increasing their crystallinity and enhancing the stiffness and thermal stability of the composite.

Another double reagent (3-isocyanatepropyltriethoxysilane), but this time made up of different moieties, was grafted onto CNCs through its more OH-reactive NCO side, thus leaving the siloxane end dangling and awaiting further modification [93]. This occurred as a sol–gel hydrolytic coupling and generated a silica-type coating on the nanocrystals, as shown in Fig. 14.

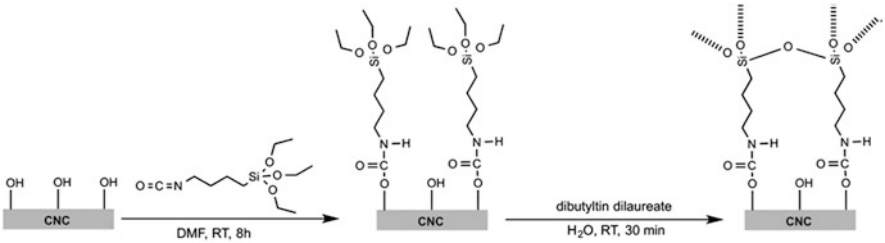

Fig. 14 Double reaction leading to silica-coated cellulose nanocrystals (*CNC*)

2.4.3 Reactions with Silanes and Siloxanes

Pioneering work of Chanzy's group dealt with the treatment of CNCs with a series of alkyldimethylchlorosilanes that resulted in stable suspensions with birefringent behavior. The same modification was applied to CNFs and provided nanocelluloses with a flexibility akin to that of conventional polymers [94, 95]. Research in Stenius' laboratory pursued this topic with the aim of giving the silylated CNFs the capacity of stabilizing water-in-oil emulsions [96, 97].

CNCs functionalized by coupling with *n*-dodecyldimethylchlorosilane gave a good dispersion in poly(L-lactide) and accelerated its crystallization rate [98]. Chemical vapor deposition of perfluorodecyltrichlorosilane or octyltrichlorosilane onto CNF aerogels provided a means to reduce considerably their wetting by nonpolar liquids [99, 100].

Regrettably, there is often some confusion in the literature regarding both the terminology and the reactivity of silicon-based reagents for cellulose. In order to clarify the following observations, it is therefore important to distinguish between *silanes*, where the silicon atom is bound to carbon and halogen atoms, and *siloxanes*, where Si–O bonds are also present. This is not trivial, because the generic use of the term silane for both types of compounds can lead to the wrong assumption of a similar reactivity toward the cellulose hydroxyl groups.

All the systems discussed above are based on the very efficient silylation reaction:

$$\equiv\mathrm{Si-Cl} \;+\; \text{Cell-OH} \;\rightarrow\; \equiv\mathrm{Si-O\text{-}Cell} \;+\; \mathrm{HCl}.$$

This is, however, not the case when the reaction involves an alkoxysilane, despite numerous unverified claims to the contrary:

$$\equiv\mathrm{Si-OR} \;+\; \text{Cell-OH}$$

The latter is an exceedingly sluggish interaction (if it does take place at all), as clearly shown in a thorough study on the issue [101]. However, if the siloxane has been partly hydrolyzed, the condensation reaction does occur, albeit at a lower rate than that involving the Si–Cl link [101]:

$$\equiv Si-OH + \text{Cell-OH} \rightarrow Si-O\text{-Cell} + H_2O$$

It follows that the studies quoted below bear an uncertainty related to whether the used siloxane had undergone some degree of hydrolysis, because otherwise its coupling with the cellulose OH remains doubtful.

The use of the fluoroalkoxysilane TFPS and PFOS (see above) as grafting agents on model cellulose fibers or filter paper was investigated and the coupling clearly shown to occur, because the two reagents had indeed partly hydrolyzed [27]. The reaction of 3-aminopropyltriethoxysilane with both CNCs and CNFs [102] was studied in order to enhance their compatibility with poly(lactic acid), but the proof that it actually took place was not provided convincingly. In contrast, the coupling of CNC with a variety of siloxanes for the same purpose, carried out in an aqueous medium, was shown to occur [103].

An interesting route for the preparation of fluorescent nanocellulose is the reaction of aminosiloxanes with CNCs, followed by grafting of the fluorescent moiety onto the appended amino groups [104]. Additionally, the use of siloxanes bearing SH groups has been described in two studies with the aim of appending thiol functionalities to CNC [105, 106]. In both instances, the first modification was carried out with the purpose of applying the thiol-ene click reaction to the ensuing SH-decorated CNCs, as discussed further in the next section.

2.4.4 Other Molecular Graftings

Two independent approaches have been proposed for attaching pH-sensitive structures onto nanocellulose. The first method used succinimidyl ester dyes introduced onto the surface of CNCs through a thiol-ene reaction [107], whereas the other exploited the azide-alkyne 1,3-dipolar cycloaddition to graft 1,2,3-triazole-4-methanamine to CNFs [108]. The latter click mechanism was also adopted to incorporate cationic porphyrin [109] and an imidazolium salt [110] onto the surface of CNCs for antimicrobial purposes and ion-exchange applications, respectively.

A recent addition to the numerous ways of appending reactive moieties to nanocellulose surfaces is the reaction of TEMPO-oxidized CNFs, embedded in an electrospun poly(acrylonitrile) nanofibrous scaffold, with cysteine [111], as shown in Fig. 15. The aim of this study was to use the material as an efficient scavenger of chromium (VI) and lead (II) pollutants in water.

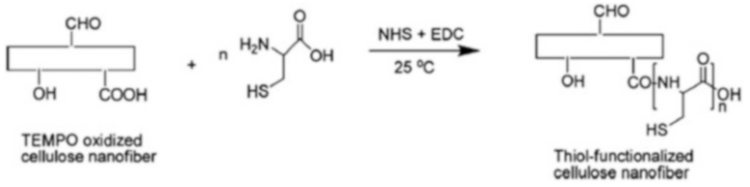

Fig. 15 Reaction of oxidized cellulose nanofibers with cysteine (reproduced by permission of Elsevier. Copyright 2014. Reprinted from Young et al. [111])

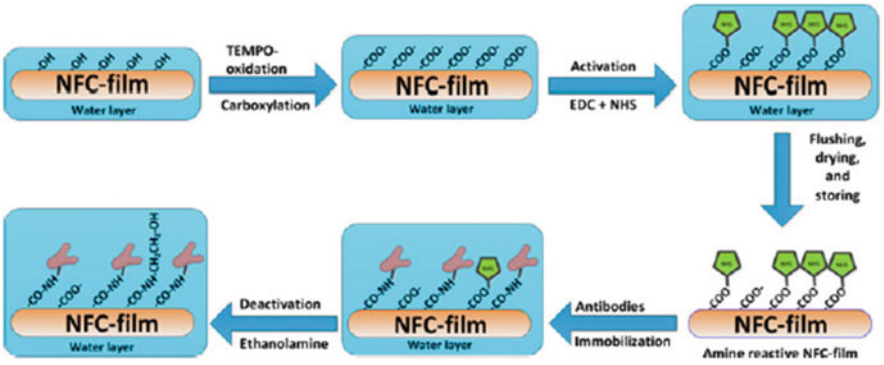

Fig. 16 Sequence of steps for the immobilization of antibodies on the surface of a nanofibrillar-cellulose film (*NFC-film*) (reproduced by permission of AIP Publishing LLC. Copyright 2012. Reprinted from Orelma et al. [113])

The possibility of exploiting nanocelluloses as bioactive surfaces has been carefully reviewed by the group of Rojas [112]. An original example of this strategy [113] deals with the reaction of TEMPO-oxidized CNF thin films with *N*-hydroxysuccinimide (NHS), in the presence of 1-ethyl-3-[3-dimethylamino-propyl]carbodiimide hydrochloride (EDC) to catalyze the condensation reaction. The amino groups thus appended were used to anchor antibodies, as sketched in Fig. 16. The same type of surface modification with NHS and EDC was applied to oxidized CNFs [114], but the purpose of this investigation was to apply the amidation reaction to amino-functionalized carbon dots, which were thus chemically incorporated at the nanofibril surface. The result of this study was the preparation of transparent and fluorescent nanopaper with tunable luminescence.

Another contribution from this USA–Finland research collaboration proposed a general method for attaching a chemical graft onto nanocellulose [115, 116] in an aqueous medium. Carboxymethyl cellulose was functionalized with either azido or propargyl moieties and then adsorbed onto CNFs or ultrathin cellulose films before proceeding to click the grafted moieties with a variety of complementary molecules using the Cu(I)-catalyzed 1,3-dipolar azido-alkyne cycloaddition.

Yet another stimulating piece of research from the same group looked into a strategy for building CNCs bearing a thiol group at one end of their rodlike morphology [117]. The process required the transformation of surface OH groups into sulfate anions, leaving the reducing aldehyde end ready for transformation into an aliphatic thiol tail that could be placed in contact with a gold surface. Under appropriate medium conditions, these end-SH functionalized nanorods could be aligned perpendicularly to a gold surface (as shown in Fig. 17), but other orientations were also available given the flexibility of the SH–gold junction.

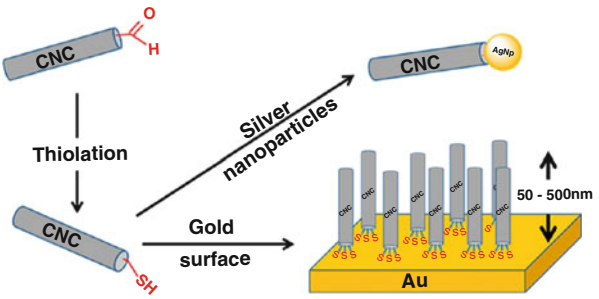

Fig. 17 The principles associated with building cellulose nanopillars on a gold surface (reproduced by permission of the American Chemical Society. Copyright 2013. Reprinted from Lokanathan et al. [117])

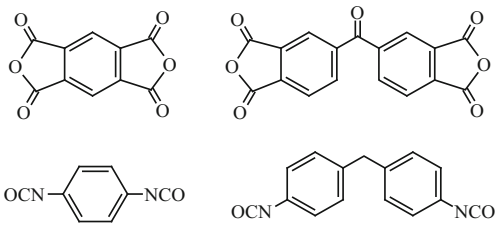

Fig. 18 Stiff bifunctional molecules suitable for reacting with only one of their moieties in heterogeneous contact with cellulose fibers

2.4.5 The Use of Stiff Bifunctional Reagents

Bifunctional reagents have been reviewed before [3–5], but the interest in them and their applications justify a reminder here. The strategy is based on the use of bifunctional molecules with a rigid core, which hinder any flexibility with respect to the availability of both reactive groups [118]. When such reagents are placed in contact with a solid substrate bearing complementary functions in a heterogeneous medium, only one of the active moieties can statistically graft itself onto the solid surface, thus leaving the other available for further exploitation.

In the specific case of a cellulose surface, the obvious reactive moieties are carboxylic anhydrides and isocyanates, as in the structures given in Fig. 18. One of the most obvious applications of this principle is the preparation of composite materials in which the surface of the modified cellulose fibers is covalently linked to the macromolecular matrix, demonstrating the best means of ensuring an optimized interface.

Apart from the examples of applications given in the original study [118], some recent exploitations of this idea include a study in which each of the four molecules shown in Fig. 18 was appended onto the surface of cellulose fibers before incorporating them into a cellulose aceto-butyrate matrix [119].

2.5 *Grafting with Oligomers and Polymers*

The chemical attachment of macromolecular strands to the surface of cellulose fibers has witnessed an important revival. This is because of the opportunities arising from the recent advances in controlled radical and ring-opening polymerization techniques and, also, because of the stimulating perspectives associated with grafting nanocelluloses. Again, given the availability of previous overviews [3–5, 120, 121], the present treatment of this topic concentrates on notable progress in the last few years. The grafting strategies have either exploited the reactivity of the cellulose superficial hydroxyl groups directly, or their preliminary transformation into other functional moieties, following the concepts discussed in the previous section. In both instances, the classical approaches of grafting-from and grafting-onto have been applied. The grafting-through counterpart is not possible in these heterogeneous systems because the cellulose macromolecules are immobilized on the fiber surface and can therefore only provide access to the growth of the appended polymer in the outward direction.

2.5.1 Grafting From

The surface activation of cellulose fibers to generate initiating species for free radical and ionic polymerization of different monomers [3, 6] had lost impetus because of rather unsatisfactory results in terms of the possible applications of the ensuing materials. However, the development of novel quasi-living mechanisms and the current relevance of nanocelluloses have spurred a flurry of fresh research initiatives.

Chain polymerization reactions bearing a free radical nature have been studied using traditional techniques based on the OH-oxidative power of Ce(IV) salts or the persulfate–sulfite couple, applied to different nanocelluloses and acrylic monomers [122–126], but gave rather poor yields because of the important interference of homopolymerization reactions. By contrast, controlled approaches such as atom-transfer radical polymerization (ATRP) and single-electron living radical polymerization (SE-LRP), have provided interesting results. Thus, poly(styrene) [127] and acrylic polymers [128, 129] were efficiently grafted onto nanocellulose surfaces using these procedures, namely, poly(butylacrylate) was attached to MFC [130, 131] and both poly(butylacrylate) and poly(methylmethacrylate) were linked to BC [132]. A variety of specific mechanisms and conditions were selected for these processes and the ensuing degree of branching, as well as the properties of the grafted nanocelluloses, varied accordingly. An interesting example among these studies [129] is that of a two-step procedure to attach isobutyl bromide moieties at the CNC surface, which resulted in optimization of the extent of grafting and relative uniformity in the chain length of poly(*tert*-butylacrylate) chains.

The ring-opening polymerizations (ROP) of ε-caprolactone and L-lactide are other relevant contributions to recent grafting-from investigations, as recently

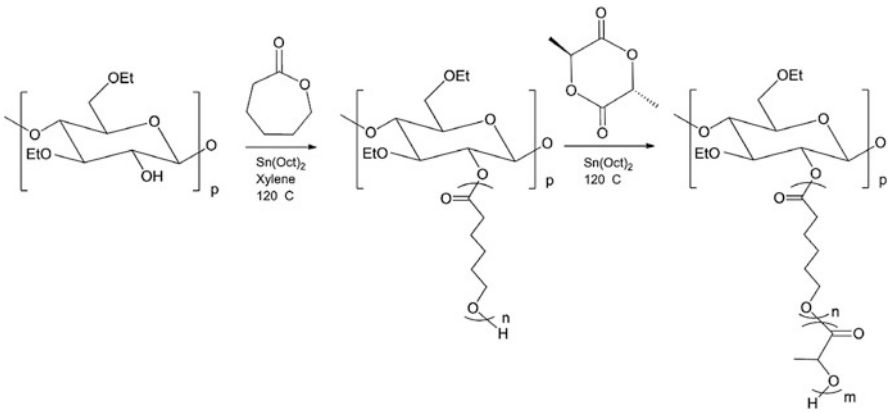

Fig. 19 Example of sequential ring-opening polymerization grafting of a cellulose surface to append block copolymer chains (reproduced by permission of the American Chemical Society. Copyright 2007. Reprinted from Yuan et al. [133] and Goffin et al. [134])

reviewed [120]. The principle of these processes, applicable equally well to conventional lignocellulosic fibers and nanocelluloses, consists of activating the surface OH groups in order to promote the ROP of these cyclic esters. Tin (II) 2-ethylhexanoate, $Sn(Oct)_2$, is by far the preferred catalyst and operates through a coordination–insertion polymerization mechanism, but carboxylic acids have also been utilized. These ROPs do not display any termination reaction and the hydroxyl-bearing end group of each chain can therefore be exploited to initiate the polymerization of a second monomer. This expedient has been applied to cellulose surface grafting (both common fibers and CNCs) by using ε-caprolactone and L-lactide in succession to generate block copolymers [133, 134], as shown in Fig. 19.

The most important aim behind these studies is, of course, optimization of the interface quality arising from the incorporation of the modified fibers or nanofibers into polyester-type matrices, including the attainment of continuous covalent bonding [120, 135].

2.5.2 Grafting Onto

Interestingly, the grafting of PCL chains at the surface of conventional cellulose fibers was also carried out by coupling the polymer bearing isocyanate end-functions with the outer OH groups of the fibers. This is a grafting-onto strategy, which is an alternative to the grafting-from counterpart discussed above [33] and shown in Fig. 7 (a three-step procedure using a PCL macrodiol prepared from diethylene glycol).

The grafting of oligo- or poly-ether chains onto (nano)cellulose fibers is arguably the most investigated item within the present subject. In the first report on this

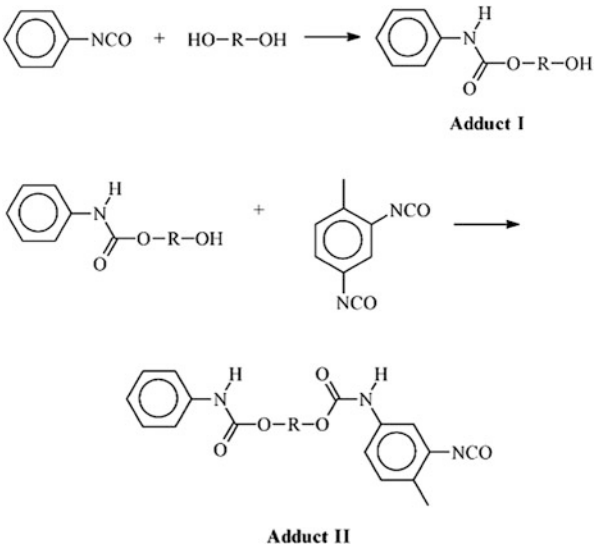

Fig. 20 Synthesis of polyethers bearing an isocyanate end group to be reacted with the superficial cellulose hydroxyl functions (reproduced by permission of Elsevier. Copyright 2010. Reprinted from Ly et al. [136])

topic [136], the surfaces of lignocellulosic fibers were decorated with PEO, poly (propylene oxide), and poly(tetrahydrofuran) (PTHF) with molecular weights of 2,000–4,000, employing the same principle used for grafting PCL chains [33]. More specifically, toluene diisocyanate played the role of coupling agent between the polyether and the OH groups on the fiber surface, as sketched in Fig. 20, where HO-R-OH is the polyether diol. Adduct II was then grafted to the fiber surface.

CNCs were grafted with PEO chains by the condensation reaction of PEO-NH_2 ($M_w = 5{,}000$) with the TEMPO-oxidized surface of nanocrystals bearing COOH groups [137], in order to improve their dispersability in melt-extruded poly(styrene). The same strategy was adopted to append PEO chains (M ~1,000 and ~2,000) to ultrafine CNFs [138], which were then used to prepare poly(L-lactide) composites displaying enhanced mechanical properties.

The direct elaboration of nanocomposites of CNFs chemically linked to a thermoplastic polyurethane (PU) matrix, based on a grafting-onto process, was recently described [139]. A PTHF macrodiol ($M_w = 1{,}000$) was reacted with an excess of an aromatic diisocyanate and the ensuing PU with NCO end groups was mixed in situ with the CNFs, whose surface OH moieties condensed with some of the NCO functions. Chain extension of all the PU chains was then induced by adding 1,4-butanediol to the medium, before casting and solvent evaporation. The procedure is illustrated in Fig. 21. The composites displayed a considerable increase in strength, even with incorporation of only 1% nanocrystal, without loss of extensibility and transparency.

In a similar vein, biomimetic capsules designed to hold liquids were prepared by reacting CNFs directly with an aliphatic diisocyanate using an original one-pot two-phase process, as sketched in Fig. 22 [140].

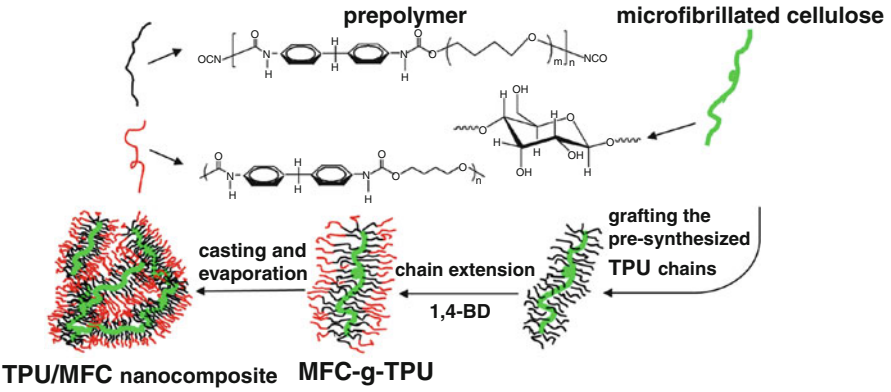

Fig. 21 In situ preparation of a polyurethane/cellulose nanofiber composite (reproduced by permission of the American Chemical Society. Copyright 2014. Reprinted from Yao et al. [139])

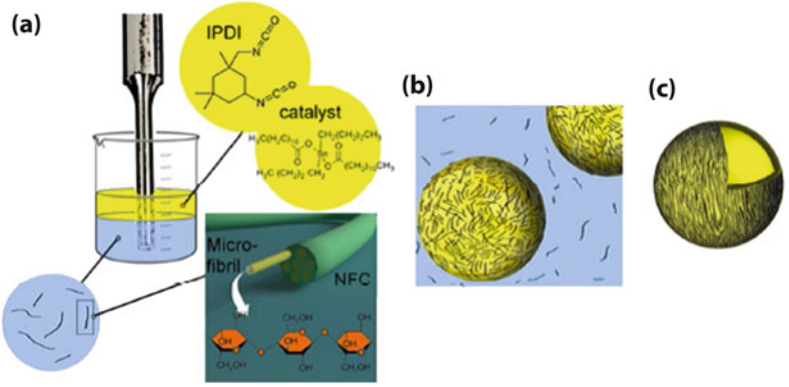

Fig. 22 Preparation of liquid-holding capsules based on cellulose nanofibers (reproduced by permission of the American Chemical Society. Copyright 2014. Reprinted from Svagan et al. [140])

In a different vein, β-cyclodextrin moieties were attached to the surface of various conventional types of celluloses, including paper and cotton bandage. This was accomplished through the catalytic action of citric acid, which played the role of polycondensation agent thanks to its three COOH groups. The growth of cyclodextrin chains was promoted while, at the same time, joining them covalently to the substrate fibers [141]. The cup-like shape of cyclodextrin (see Fig. 23) bearing hydroxyl functions was exploited to insert chlorhexidinedigluconate, a widely used antiseptic molecule whose shape fits appropriately into the cavities. Release of the bioactive agent was studied by immersing the modified cellulose in water and measuring its escape kinetics. This simple procedure, based on a surface grafting-onto mechanism, enabled the performance of bactericidal aids to be

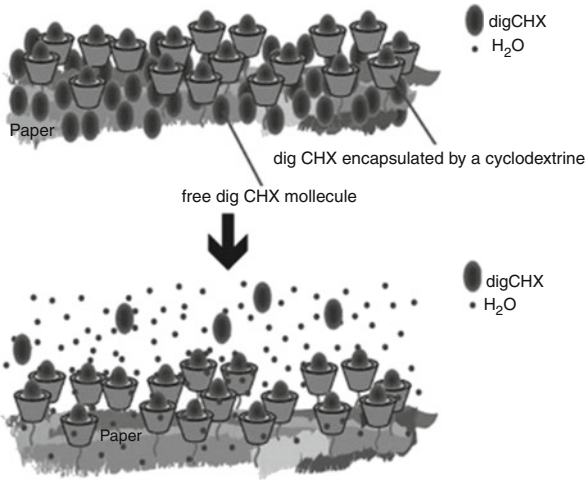

Fig. 23 Massive release of chlorhexidine digluconate (*digCHX*) from cyclodextrin grafted on cellulose (reproduced by permission of Wiley Periodicals, Inc. Copyright 2012. Reprinted from Cusola et al. [141])

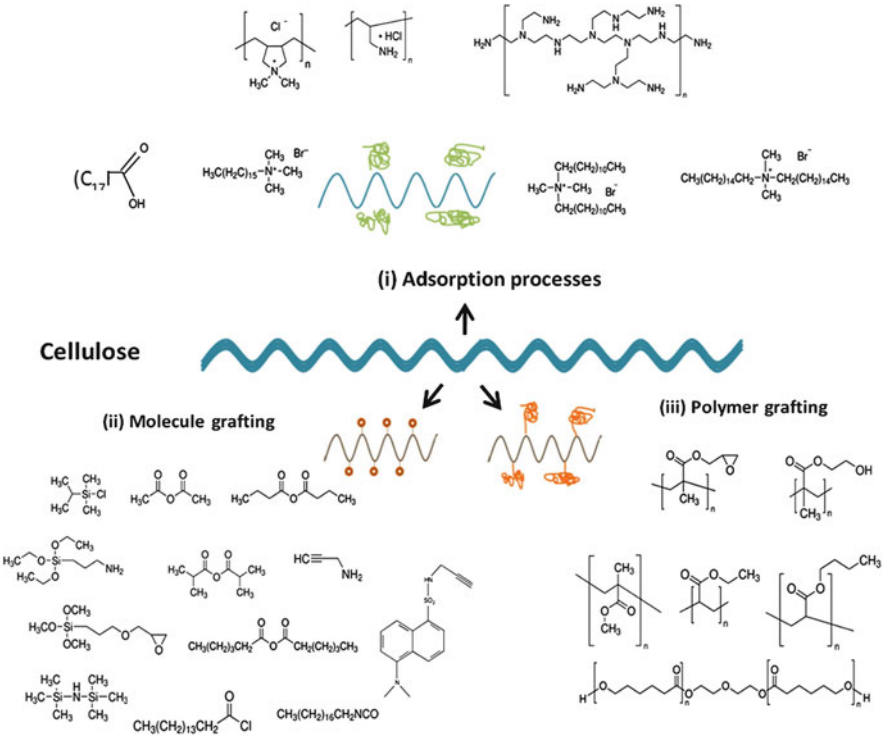

Fig. 24 Strategies for cellulose surface modification: (*i*) adsorption processes, (*ii*) molecule grafting, and (*iii*) polymer grafting (adapted from Missoum et al. [142])

optimized without affecting the mechanical properties of their inner cellulose structure and morphology.

Before introducing in-depth modification of cellulose, we finalize this section by presenting a summary of the different approaches and main moieties that can be used for cellulose surface modification. Figure 24 displays graphically the various approaches discussed in Sect. 2, including physical adsorption as well as molecular and polymer grafting.

3 In-Depth Modification

In contrast to the working hypothesis discussed in Sect. 2, which is based on limiting any cellulose modification to the surface, or to a few outer molecular layers, the strategy discussed here consists in carrying out modification reactions that proceed through part of the fiber thickness, in a controlled fashion. Although these ideas have generated relatively few concrete results up to now, further implementation seems likely given the potential development of interesting novel materials, hence our decision to incorporate this topic in the review.

3.1 Physical Modification

The idea of elaborating a composite material in which both the matrix and the reinforcing elements are from the same polymer was originally proposed by Ward and Hine [143,144], who applied it to poly(ethylene). Reports about the application of this concept to cellulose [145–148] describe the impregnation of uniaxially aligned cellulose fibers with a cellulose solution, selectively dissolving the surface of cellulose fibers and then compressing and drying the system. This gives rise to an all-cellulose composite in which the crystalline inner core of undissolved fibers is surrounded by an amorphous sleeve. Similar approaches have been implemented, all based on embedding highly crystalline fibers into a matrix of regenerated cellulose, albeit using different solvents and fibers [149–152]. The modulus of elasticity and the strength of these original materials in some instances reached values well above those of the best cellulose-reinforced thermoplastics, namely more than 10 GPa and about 100–500 MPa, respectively.

An extension of these concepts to the preparation of cellulose aerogels involves the partial and controlled dissolution of microcrystalline cellulose in a LiCl/ *N*,*N*-dimethylacetamide (DMAc) solvent system, followed by precipitation of the ensuing gels and freeze-drying to preserve their open morphology [153]. These highly porous materials had densities of 100–350 kg m^{-3}, flexural strengths as high as 8 MPa, and a maximum stiffness of 280 MPa.

3.2 Chemical Modification

To the best of our knowledge, two different methods for in-depth chemical modification of cellulose fibers have been tackled successfully. The first is an extension of the study on surface esterification with fatty acid chlorides discussed above [20–24], in which the reaction medium was changed from toluene (which does not swell cellulose) to the cellulose-swelling *N*,*N*-dimethylformamide. Under these conditions, the esterification reaction could proceed beyond the surface of the fibers and thus produce a thermoplastic sleeve around them. The crucial aspect of this process is careful control of the extent of penetration, to avoid the total transformation of cellulose into its corresponding esters. Optimization of the system gave a morphology consisting of an inner core of untouched residual fibrous cellulose, which therefore preserved its pristine mechanical properties, and an outer shell of thermoplastic material. Hot pressing this two-layer product generated a novel composite arising entirely from the starting cellulose fibers in a one-pot operation. Figure 25 illustrates this sequential transformation.

The second approach is a variation on the theme of oxypropylation. This process has received considerable attention as a very useful way of valorizing biomass rejects by turning them into useful polyols for rigid polyurethane foams [155]. Any OH-bearing solid substrate can be readily converted into a viscous polyol by the straightforward grafting-from of propylene oxide (PO) through its anionic oligomerization. Figure 26 shows the principle of this reaction, which is always accompanied by some PO homopolymerization. The green aspects of the process are coupled with the interest in using a straightforward method of exploiting a large number of industrial side products associated with vegetable resources such as sugarbeet pulp, lignin, cork rejects, olive stones, low-quality chitin, and chitosan.

In these applications, the substrate is treated in order to be converted entirely into the corresponding oxypropylated polyol, whereas the partial reaction provides an original means of turning cellulose fibers into a source of one-component composite. The system was thoroughly studied [156–158] and yielded interesting fiber morphologies, characterized by a sleeve of thermoplastic poly(PO) surrounding the inner unreacted core (as shown in Fig. 27), which could be hot-pressed into a composite. The same treatment was also applied to starch granules, with similar results [157].

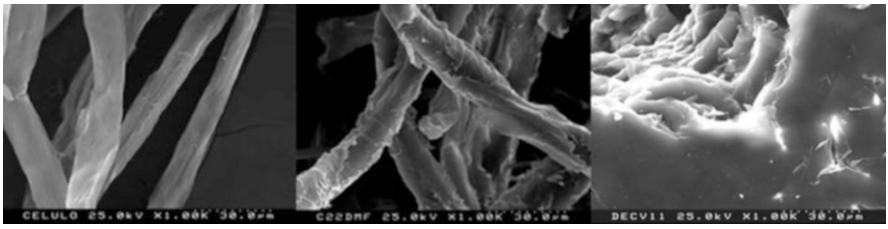

Fig. 25 In-depth esterification of cellulose fibers and formation of a composite. Pristine fibers (*left*), esterified fibers before (*center*) and after (*right*) hot pressing (reproduced by permission of Elsevier. Copyright 2005. Reprinted from Gandini et al. [154])

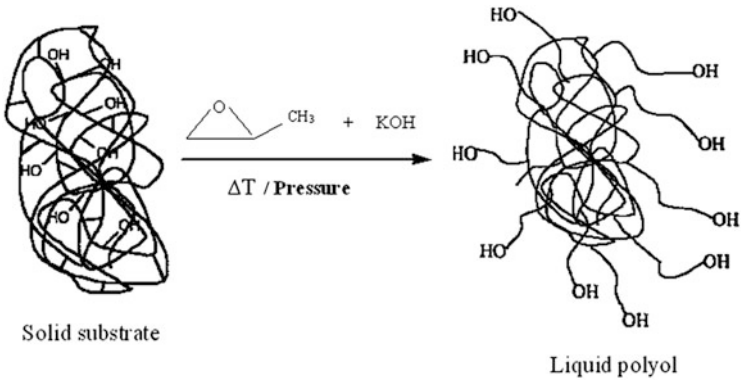

Fig. 26 Oxypropylation of an OH-bearing solid substrate by gaseous propylene oxide

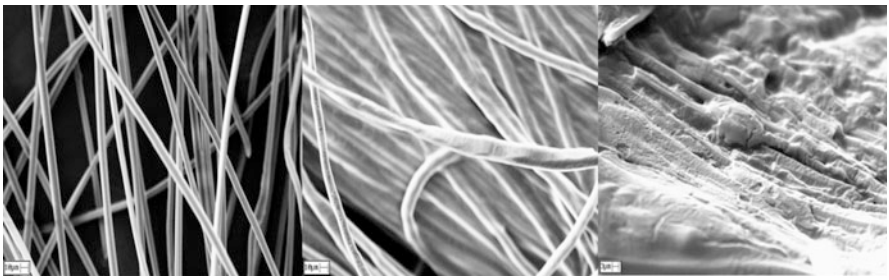

Fig. 27 From *left* to *right*: regenerated cellulose fibers before and after partial oxypropylation, and after hot pressing (reproduced by permission of Elsevier. Copyright 2005. Reprinted from Belgacem and Gandini [155])

4 Conclusions

This review shows clearly that modification of cellulose substrates, either limited to their surface or involving a sleeve of numerous macromolecular layers, is a steadily growing area of research and development that is applicable to conventional fibers and, more importantly, to their nanocellulose counterparts. This trend is driven by the benefits associated with the large specific surface area offered by the latter, which results in enhanced mechanical performance and other properties of macromolecular matrices when nanofibers are incorporated. The various strategies for surface modification discussed here can bring about an improvement in properties and widen the domains of application of the ensuing materials in such fields as packaging, composites, selective adsorption, optoelectronics, biomedicine, and catalysis.

References

1. Gassan J, Bledzki AK (1999) Composites reinforced with cellulose based fibres. Prog Polym Sci 24:221–274
2. Mohanty AK, Misra M, Hinrichsen G (2000) Biofibres, biodegradable polymers and biocomposites: an overview macromolecular. Mater Eng 276(277):1–24
3. Belgacem MN, Gandini A (2005) Physical, chemical and physico-chemical modification of cellulose fibers. Compos Interfaces 12:41–75
4. Belgacem MN, Gandini A (2008) Surface modification of cellulose fibers. In: Belgacem MN, Gandini A (eds) Monomers, polymers and composites from renewable resources. Elsevier, Amsterdam, pp 385–400
5. Gandini A, Belgacem MN (2011) Modifying cellulose fiber surface in the manufacture of natural fiber composites. In: Zafeiropoulos NE (ed) Interface engineering of natural fiber composites for maximum performance. Woodhead, Oxford, pp 3–42
6. Hebeish A, Guthrie JT (1981) The chemistry and technology of cellulosic copolymers. Springer, Berlin
7. Klemm D, Kramer F, Moritz S, Lindstrom T, Ankerfors M, Gray D, Dorris A (2011) Nanocelluloses: a new family of nature-based materials. Angew Chem Int Ed 50:5438–5466
8. Siró I, Plackett D (2010) Microfibrillated cellulose and new nanocomposite materials: a review. Cellulose 17:459–494
9. Habibi Y, Lucia LA, Rojas OJ (2010) Cellulose nanocrystals: chemistry, self-assembly, and applications. Chem Rev 110:3479–3500
10. Eichhorn S, Dufresne A, Aranguren M, Marcovich N, Capadona J, Rowan S, Weder C, Thielemans W, Roman M, Renneckar S, Gindl W, Veigel S, Keckes J, Yano H, Abe K, Nogi M, Nakagaito A, Mangalam A, Simonsen J, Benight A, Bismarck A, Berglund L, Peijs T (2010) Review: current international research into cellulose nanofibres and nanocomposites. J Mater Sci 45:1–33
11. Trovatti E (2013) The future of bacterial cellulose and other microbial polysaccharides. J Renew Mater 1(1):28–41
12. Gandini A, Cunha AG (2010) Turning polysaccharides into hydrophobic materials: a critical review. Part 1. Cellulose. Cellulose 17:875–889
13. Song J, Rojas OJ (2013) Approaching superhydrophobicity based on cellulosic materials: a review. Nord Pulp Pap Res J 28:216–238
14. Gandini A, Cunha AG (2010) Turning polysaccharides into hydrophobic materials: a critical review. Part 2. Hemicelluloses, chitin/chitosan, starch, pectin and alginates. Cellulose 17:1045–1065
15. Roberts JC (1996) Paper chemistry, 2nd edn. Chapman & Hall, London
16. Lindstrom T, Larsson PT (2008) Alkyl Ketene Dimer (AKD) sizing – a review. Nord Pulp Pap Res J 23(2):202–209
17. Zhang H, Kannangara D, Hilder M, Ettl R, Shen W (2007) The role of vapour deposition in the hydrophobization treatment of cellulose fibres using alkyl ketene dimers and alkenyl succinic acid anhydrides. Colloid Surf A 297(1–3):203–210
18. Werner O, Quan C, Turner C, Petterson B, Wågberg L (2010) Properties of superhydrophobic paper treated with rapid expansion of supercritical CO_2 containing a crystallizing wax. Cellulose 17(1):187–198
19. Bourbonnais R, Marchessault RH (2010) Application of polyhydroxyalkanoate granules for sizing of paper. Biomacromolecules 11(4):989–993
20. Freire CSR, Silvestre AJD, Neto CP, Belgacem MN, Gandini A (2006) Controlled heterogeneous modification of cellulose fibers with fatty acids: effect of reaction conditions on the extent of esterification and fiber properties. J Appl Polym Sci 100(2):1093–1102
21. Freire CSR, Silvestre AJD, Pascoal Neto AC, Gandini A, Fardim P, Holmbom B (2006) Surface characterization by XPS, contact angle measurements and ToF-SIMS of cellulose fibers partially esterified with fatty acids. JCIS 301:205–209

22. Pasquini D, Belgacem MN, Gandini A, Curvelo AAS (2006) Surface esterification of cellulose fibers: characterization by DRIFT and contact angle measurements. J Colloid Interface Sci 295:79–83
23. Pasquini D, Teixeira EM, Curvelo AAS, Belgacem MN, Dufresne A (2008) Surface esterification of cellulose fibres: processing and characterisation of low-density polyethylene/cellulose fibres composites. Compos Sci Technol 68(1):193–201
24. Freire CSR, Silvestre AJD, Pascoal Neto C, Gandini A, Martin L, Mondragon I (2008) Composites based on acylated cellulose and low-density polyethylene: effect of the fiber content, degree of substitution and fatty acid chain length on final properties. Compos Sci Technol 68:3358–3364
25. de Menezes AJ, Siqueira G, Curvelo AAS, Dufresne A (2009) Extrusion and characterization of functionalized cellulose whiskers reinforced polyethylene nanocomposites. Polymer 50: 4552–4563
26. Cunha AG, Freire CSR, Silvestre AJD, Neto CP, Gandini A (2010) Preparation and characterization of novel highly omniphobic cellulose fibers organic–inorganic hybrid materials. Carbohydr Polym 80(4):1048–1056
27. Ly B, Belgacem MN, Bras J, Salon MCB (2009) Grafting of cellulose by fluorine-bearing silane coupling agents. Mater Sci Eng C 30(3):343–347
28. Erasmus E, Barkhuysen FA (2009) Superhydrophobic cotton by fluorosilane modification. Indian J Fibre Text Res 34:377–379
29. Gonçalves G, Marques PAAP, Trindade T, Neto CP, Gandini A (2008) Superhydrophobic cellulose nanocomposites. J Colloid Interf Sci 324(1–2):42–46
30. Cunha AG, Freire C, Silvestre A, Neto CP, Gandini A, Belgacem MN, Chaussy D, Beneventi D (2010) Preparation of highly hydrophobic and lipophobic cellulose fibers by a straightforward gas–solid reaction. J Colloid Interf Sci 344(2):588–595
31. Siqueira G, Bras J, Dufresne A (2009) Cellulose whiskers versus microfibrils: influence of the nature of the nanoparticle and its surface functionalization on the thermal and mechanical properties of nanocomposites. Biomacromolecules 10:425–432
32. Siqueira G, Bras J, Dufresne A (2010) New process of chemical grafting of cellulose nanoparticles with a long chain isocyanate. Langmuir 26:402–411
33. Paquet O, Krouit M, Bras J, Thielemans W, Belgacem MN (2010) Surface modification of cellulose by PCL grafts. Acta Mater 58(3):792–801
34. Costa AP, Belgacem MN, Santos Silva M, Thielemans W, Gaiolas C (2013) Cold-plasma assisted hydrophobisation of cellulosic fibers. Curr Org Chem 17:892–899
35. Boufi S, Gandini A (2001) Formation of polymeric films on cellulosic surfaces by admicellar polymerization. Cellulose 8(4):303–312
36. Trovatti E, Ferreira AM, Carvalho AJF, Lima Ribeiro SJ, Gandini A (2013) Sleeving nanocelluloses by admicellar polymerization. J Colloid Interface Sci 408:256–258
37. Trovatti E, Carvalho AJF, Lima Ribeiro SJ, Gandini A (2013) Simple green approach to reinforce natural rubber with bacterial cellulose nanofibers. Biomacromolecules 14: 2667–2674
38. Heux L, Chauve G, Bonini C (2000) Nonflocculating and chiral-nematic self-ordering of cellulose microcrystals suspensions in nonpolar solvents. Langmuir 16:8210–8212
39. Ljungberg N, Bonini C, Bortolussi F, Boisson C, Heux L, Cavaillé JY (2005) New nanocomposite materials reinforced with cellulose whiskers in atactic polypropylene: effect of surface and dispersion characteristics. Biomacromolecules 6:2732–2739
40. Ljungberg N, Cavaillé JY, Heux L (2006) Nanocomposites of isotactic polypropylene reinforced with rod-like cellulose whiskers. Polymer 47:6285–6292
41. Bondeson D, Oksman K (2007) Dispersion and characteristics of surfactant modified cellulose whiskers nanocomposites. Compos Interfaces 14:617–630
42. Kim J, Montero G, Habibi Y, Hinestroza JP, Genzer J, Argyropoulos DS, Rojas OJ (2009) Dispersion of cellulose crystallites by nonionic surfactants in a hydrophobic polymer matrix. Polym Eng Sci 49:2054–2061

43. Rojas OJ, Montero GA, Habibi Y (2009) Electrospun nanocomposites from polystyrene loaded with cellulose nanowhiskers. J Appl Polym Sci 113:927–935
44. Zhou Q, Brumer H, Teeri TT (2009) Self-organization of cellulose nanocrystals adsorbed with xyloglucan oligosaccharide-poly(ethylene glycol)-polystyrene triblock copolymer. Macromolecules 42:5430–5432
45. Syverud K, Xhanari K, Chinga-Carrasco G, Yu Y, Stenius P (2011) Films made of cellulose nanofibrils: surface modification by adsorption of a cationic surfactant and characterization by computer-assisted electron microscopy. J Nanopart Res 13:773–782
46. Xhanari K, Syverud K, Chinga-Carrasco G, Paso K, Stenius P (2011) Reduction of water wettability of nanofibrillated cellulose by adsorption of cationic surfactants. Cellulose 18: 257–270
47. Salajkova M, Berglund LA, Zhou Q (2012) Hydrophobic cellulose nanocrystals modified with quaternary ammonium salts. J Mater Chem 22:19798–19805
48. Brown EE, Laborie M-PG (2007) Bioengineering bacterial cellulose/poly(ethylene oxide) nanocomposites. Biomacromolecules 8:3074–3081
49. Zhou Q, Malm E, Nilsson H, Larsson PT, Iversen T, Berglund LA, Bulone V (2009) Nanostructured biocomposites based on bacterial cellulosic nanofibers compartmentalized by a soft hydroxyethylcellulose matrix coating. Soft Matter 5:4124–4130
50. Changsarn S, Mendez JD, Shanmuganathan K, Foster EJ, Weder C, Supaphol P (2011) Biologically inspired hierarchical design of nanocomposites based on poly(ethylene oxide) and cellulose nanofibers. Macromol Rapid Commun 32:1367–1372
51. Orelma H, Filpponen I, Johansson L-S, Laine J, Rojas OJ (2011) Modification of cellulose films by adsorption of CMC and chitosan for controlled attachment of biomolecules. Biomacromolecules 12:4311–4318
52. Larsson E, Sanchez CC, Porsch C, Karabulut E, Wagberg L, Carlmark A (2013) Thermo-responsive nanofibrillated cellulose by polyelectrolyte adsorption. Eur Polym J 49: 2689–2696
53. Podsiadlo P, Choi SY, Shim B, Lee J, Cuddihy M, Kotov NA (2005) Molecularly engineered nanocomposites: layer-by-layer assembly of cellulose nanocrystals. Biomacromolecules 2005(6):2914–2918
54. Cranston ED, Gray DG (2006) Morphological and optical characterization of polyelectrolyte multilayers incorporating nanocrystalline cellulose. Biomacromolecules 7:2522–2530
55. Podsiadlo P, Sui L, Elkasabi Y, Burgardt P, Lee J, Miryala A, Kusumaatmaja W, Carman MR, Shtein M, Kieffer J, Lahann J, Kotov NA (2007) Layer-by-layer assembled films of cellulose nanowires with antireflective properties. Langmuir 23:7901–7906
56. Li F, Biagioni P, Finazzi M, Tavazzi S, Piergiovanni L (2013) Tunable green oxygen barrier through layer-by-layer self-assembly of chitosan and cellulose nanocrystals. Carbohydr Polym 92:2128–2134
57. Eronen P, Laine J, Ruokolainen J, Osterberg M (2012) Comparison of multilayer formation between different cellulose nanofibrils and cationic polymers. J Colloid Interface Sci 373: 84–93
58. Shim BS, Podsiadlo P, Lilly DG, Agarwal A, Leet J, Tang Z, Ho S, Ingle P, Paterson D, Lu W, Kotov NA (2007) Nanostructured thin films made by dewetting method of layer-by-layer assembly. Nano Lett 7:3266–3273
59. de Mesquita JP, Donnici CL, Pereira FV (2010) Biobased nanocomposites from layer-by-layer assembly of cellulose nanowhiskers with chitosan. Biomacromolecules 11:473–480
60. Wågberg L, Decher G, Norgren M, Lindstrom T, Ankerfors M, Axnas K (2008) The build-up of polyelectrolyte multilayers of microfibrillated cellulose and cationic polyelectrolytes. Langmuir 24:784–795
61. He J, Kunitake T, Nakao A (2003) Facile in situ synthesis of noble metal nanoparticles in porous cellulose fibers. Chem Mater 15:4401–4406
62. Pinto RJB, Marques PAAP, Martins MA, Pascoal Neto C, Trinidade T (2007) Electrostatic assembly and growth of gold nanoparticles in cellulosic fibres. J Colloid Interface Sci 312: 506–512

63. Pinto RJB, Marques PAAP, Barros-Timmons A, Trinidade T, Pascoal Neto C (2008) Novel SiO2/cellulose nanocomposites obtained by in situ synthesis and via polyelectrolyte assembly. Compos Sci Technol 68:1088–1093
64. Gonçalves G, Marques PAAP, Pinto RJB, Trindade T, Pascoal Neto C (2009) Surface modification of cellulosic fibers for multi-purpose TiO_2 based nanocomposites. Compos Sci Technol 69:1051–1056
65. Pinto RJB, Marques PAAP, Pascoal Neto C, Trinidade T, Daina S, Sadocco P (2009) Antibacterial activity of nanocomposites of silver and bacterial or vegetable cellulosic fibers. Acta Biomater 5:2279–2289
66. Dong H, Hinestroza JP (2009) Metal nanoparticles on natural cellulose fibers: electrostatic assembly and in situ synthesis. ACS Appl Mater Interfaces 1:797–803
67. Ferraria AM, Boufi S, Battaglini N, Botelho do Rego AM, Rei Vilar M (2010) Hybrid systems of silver nanoparticles generated on cellulose surfaces. Langmuir 26:1996–2001
68. Martins N, Freire C, Pinto R, Fernandes S, PascoalNeto C, Silvestre A, Causio J, Baldi G, Sadocco P, Trindade T (2012) Electrostatic assembly of Ag nanoparticles onto nanofibrillated cellulose for antibacterial paper products. Cellulose 19:1425–1436
69. Martins NCT, Freire CSR, Neto CP, Silvestre AJD, Causio J, Baldi G, Sadocco P, Trindade T (2013) Antibacterial paper based on composite coatings of nanofibrillated cellulose and ZnO. Colloids Surf A 417:111–119
70. Isogai A, Saito T, Fukuzumi H (2011) TEMPO-oxidized cellulose nanofibers. Nanoscale 3: 71–85
71. Habibi Y, Chanzy H, Vignon M (2006) TEMPO-mediated surface oxidation of cellulose whiskers. Cellulose 13:679–687
72. Okita Y, Saito T, Isogai A (2010) Entire surface oxidation of various cellulose microfibrils by TEMPO-mediated oxidation. Biomacromolecules 2010(11):1696–1700
73. Ott G, Schempp W, Krause T (1989) Production of cationic cellulose ofhigh substitution grades in the system lithium-chloride/dimethylacetamide. Papier 43:694–699
74. Song Y, Sun Y, Zhang X, Zhou J, Zhang L (2008) Homogeneous quaternization of cellulose in NaOH/urea aqueous solutions as gene carriers. Biomacromolecules 9:2259–2264
75. Prado HJ, Matulewicz MC (2014) Cationization of polysaccharides: a path to greener derivatives with many industrial applications. Eur Polym J 52:53–75
76. Hasani M, Cranston ED, Westman G, Gray DG (2008) Cationic surface functionalization of cellulose nanocrystals. Soft Matter 4:2238–2244
77. Ho T, Zimmermann T, Hauert R, Caseri W (2011) Preparation and characterization of cationic nanofibrillated cellulose from etherification and high-shear disintegration processes. Cellulose 18:1391–1406
78. Olszewska A, Eronen P, Johansson L-S, Malho J-M, Ankerfors M, Lindström T, Ruokolainen J, Laine J, Österberg M (2011) The behaviour of cationic nanofibrillar cellulose in aqueous media. Cellulose 18:1213–1226
79. Braun B, Dorgan JR (2009) Single-step method for the isolation and surface functionalization of cellulosic nanowhiskers. Biomacromolecules 10:334–341
80. Sobkowicz MJ, Braun B, Dorgan JR (2009) Decorating in green: surface esterification of carbon and cellulosic nanoparticles. Green Chem 11:680–682
81. Huang P, Wu M, Kuga S, Wang D, Wu D, Huang Y (2012) One-step dispersion of cellulose nanofibers by mechanochemical esterification in an organic solvent. ChemSusChem 2012(5): 2319–2322
82. Berlioz S, Molina-Boisseau S, Nishiyama Y, Heux L (2009) Gas-phase surface esterification of cellulose microfibrils and whiskers. Biomacromolecules 10:2144–2151
83. Fumagalli M, Sanchez F, Boisseau SM, Heux L (2013) Gas phase esterification of cellulose nanocrystal aerogels for colloidal dispersion in apolar solvents. Soft Matter 9:11309–11317
84. Çetin NS, Tingaut P, Oezmen N, Henry N, Harper D, Dadmun M, Sebe G (2009) Acetylation of cellulose nanowhiskers with vinyl acetate under moderate conditions. Macromol Biosci 9: 997–1003

85. Missoum K, Belgacem MN, Barnes JP, Brochier-Salon MC, Bras J (2012) Nanofibrillated cellulose surface grafting in ionic liquid. Soft Matter 8:8338–8349
86. Siqueira G, Fraschini C, Bras J, Dufresne A, Prud'hommeand R, Laborie MP (2011) Impact of the nature and shape of cellulosic nanoparticles on the isothermal crystallization kinetics of poly(ε-caprolactone). Eur Polym J 47:2216–2227
87. Siqueira G, Bras J, Follain N, Belbekhouche S, Maraisand S, Dufresne A (2013) Thermal and mechanical properties of bio-nanocomposites reinforced by *Luffacylindrica* cellulose nanocrystals. Carbohydr Polym 91:711–717
88. Follain N, Belbekhouche S, Bras J, Siqueira G, Maraisand S, Dufresne A (2013) Water transport properties of bio-nanocomposites reinforced by *Luffacylindrica* cellulose nanocrystals. J Membr Sci 427:218–229
89. Missoum K, Bras J, Belgacem M (2012) Organization of aliphatic chains grafted on nanofibrillated cellulose and influence on final properties. Cellulose 19:1957–1973
90. Tonoli GHD, Belgacem MN, Siqueira G, Bras J, Savastano H Jr, Rocco Lahr FA (2013) Processing and dimensional changes of cement based composites reinforced with surface-treated cellulose fibres. Cem Concr Compos 37:68–75
91. Tonoli GHD, Mendes RF, Siqueira G, Bras J, Belgacem MN, Savastano H Jr (2013) Isocyanate-treated cellulose pulp and its effecton the alkali resistance and performance of fiber cement composites. Holzforschung 67:853–861
92. Rueda L, Fernández d'Arlas B, Zhou Q, Berglund LA, Corcuera MA, Mondragon I, Eceiza A (2011) Isocyanate-rich cellulose nanocrystals and their selective insertion in elastomeric polyurethane. Compos Sci Technol 71:1953–1960
93. de Oliveira Taipina M, Ferrarezi M, Yoshida I, Goncalves MD (2012) Cellulose 20:217–226
94. Goussé C, Chanzy H, Cerrada ML, Fleury E (2004) Surface silylation of cellulose microfibrils: preparation and rheological properties. Polymer 45:1569–1575
95. Goussé C, Chanzy H, Excoffier G, Soubeyrand L, Fleury E (2002) Stable suspensions of partially silylated cellulose whiskers dispersed in organic solvents. Polymer 43:2645–2651
96. Andresen M, Johansson L-S, Tanem BS, Stenius P (2006) Properties and characterization of hydrophobized microfibrillated cellulose. Cellulose 13:665–677
97. Andresen M, Stenius P (2007) Water-in-oil emulsions stabilized by hydrophobized microfibrillated cellulose. J Dispers Sci Technol 28:837–844
98. Pei A, Zhou Q, Berglund LA (2010) Functionalized cellulose nanocrystals as biobased nucleation agents in poly(L-lactide) (PLLA) – crystallization and mechanical property effects. Compos Sci Technol 70:815–821
99. Aulin C, Netrval J, Wagberg L, Lindstrom T (2010) Aerogels from nanofibrillated cellulose with tunable oleophobicity. Soft Matter 6:3298–3305
100. Cervin NT, Aulin C, Larsson PT, Waagberg L (2012) Ultra porous nanocellulose aerogels as separation medium for mixtures of oil/water liquids. Cellulose 19:401–410
101. Castellano M, Gandini A, Fabbri P, Belgacem MN (2004) Modification of cellulose fibres with organosilanes: under what conditions does coupling occur? J Colloid Interface Sci 273(2):505–511
102. Frone AN, Berlioz S, Chailan JF, Panaitescu DM, Donescu D (2011) Cellulose fiber-reinforced polylactic acid. Polym Compos 32:976–985
103. Raquez JM, Murena Y, Goffin AL, Habibi Y, Ruelle B, DeBuyl F, Dubois P (2012) Surface-modification of cellulose nanowhiskers and their use as nanoreinforcers into polylactide: a sustainably-integrated approach. Compos Sci Technol 72:544–549
104. Yang Q, Pan X (2010) A facile approach for fabricating fluorescent cellulose. J Appl Polym Sci 117:3639–3644
105. Tingaut P, Hauert R, Zimmermann T (2011) Highly efficient and straightforward functionalization of cellulose films with thiol-ene click chemistry. J Mater Chem 21:16066–16076
106. Huang J-L, Li C-J, Gray DG (2014) Functionalization of cellulose nanocrystals films via "thiol-ene" click reaction. RSC Adv 4:6965–6969

107. Nielsen LJ, Eyley S, Thielemans W, Aylott JW (2010) Dual fluorescent labelling of cellulose nanocrystals for pH sensing. Chem Commun 46:8929–8931
108. Pahimanolis N, Hippi U, Johansson L-S, Saarinen T, Houbenov N, Ruokolainen J, Seppala J (2011) Surface functionalization of nanofibrillated cellulose using click-chemistry approach in aqueous media. Cellulose 18:1201–1212
109. Feese E, Sadeghifar H, Gracz HS, Argyropoulos DS, Ghiladi RA (2011) Photobactericidal porphyrin-cellulose nanocrystals: synthesis, characterization, and antimicrobial properties. Biomacromolecules 12:3528–3539
110. Eyley S, Thielemans W (2011) Imidazolium grafted cellulose nanocrystals for ion exchange applications. Chem Commun 47:4177–4179
111. Young R, Aubrecht KB, Ma H, Wang R, Grubbs RB, Hsiao BS, Chu B (2014) Thiol-modified cellulose nanofibrous composite membranes for chromium (VI) and lead (II) adsorption. Polymer 55:1167–1176
112. Zhang Y, Nypelö T, Salas C, Arboleda J, Hoeger IC, Rojas OJ (2013) Cellulose nanofibriels: from strong materials to bioactive surfaces. J Renew Mater 1:195–211
113. Orelma H, Filpponen H, Johansson L-S, Österberg M, Rojas OJ, Laine J (2012) Surface functionalized nanofibrillar cellulose (NFC) film as a platform for immunoessays and diagnostics. Biointerphases 7:61–72
114. Junka K, Guo J, Filpponen I, Laine J, Rojas OJ (2014) Modification of cellulose nanifibrils with luminescent carbon dots. Biomacromolecules 15(3):876–881
115. Filpponen I, Kontturi E, Nummelin S, Rosilo H, Kolehmainen E, Ikkala O, Laine J (2012) Generic method for modular surface modification of cellulosic materialsin aqueous medium by sequential "click" reaction and adsorption. Biomacromolecules 13(3):736–742
116. Junka K, Filpponen I, Johansson LS, Kontturi E, Rojas OJ, Laine J (2014) A method for the heterogeneous modification of nanofibrillar cellulose in aqueous media. Carbohydr Polym 100:107–115
117. Lokanathan AR, Nykänen A, Seitsonen J, Johansson L-S, Campbell J, Rojas OJ, Ikkala O, Laine J (2013) Cilia-mimetic hairy surfaces based on end-immobilized colloidal rods. Biomacromolecules 14:2807–2813
118. Gandini A, Botaro VR, Zeno E, Bach S (2001) Activation of solid polymer surfaces with bifunctional reagents. Polym Int 50:7–11
119. Ly B, Thielemans W, Dufresne A, Chaussy D, Belgacem MN (2008) Surface functionalization of cellulose fibers and their incorporation in renewable polymeric matrices. Compos Sci Technol 68:3193–3201
120. Carlmark A, Larsson E, Malmstrom E (2012) Grafting of cellulose by ring-opening polymerisation – a review. Eur Polym J 48:1646–1659
121. Roy D, Semsarilar M, Guthrie JT, Perrier S (2009) Cellulose modification by polymer grafting: a review. Chem Soc Rev 38:2046–2064
122. Stenstad P, Andresen M, Tanem B, Stenius P (2008) Chemical surface modifications of microfibrillated cellulose. Cellulose 15:35–45
123. Littunen K, Hippi U, Johansson L-S, Österberg M, Tammelin T, Laine J, Seppälä J (2011) Free radical graft copolymerization of nanofibrillated cellulose with acrylic monomers. Carbohydr Polym 84:1039–1047
124. Zhou C, Wu Q, Yue Y, Zhang Q (2011) Application of rod-shaped cellulose nanocrystals in polyacrylamide hydrogels. J Colloid Interface Sci 353:116–123
125. Zhou C, Wu Q, Zhang Q (2011) Dynamic rheology studies of in situ polymerization process of polyacrylamide–cellulose nanocrystal composite hydrogels. Colloid Polym Sci 289: 247–255
126. Yang J, Han C-R, Duan J-F, Ma M-G, Zhang X-M, Xu F, Sun R-C, Xie X-M (2012) Studies on the properties and formation mechanism of flexible nanocomposite hydrogels from cellulose nanocrystals and poly(acrylic acid). J Mater Chem 22:22467–22480

127. Morandi G, Heath L, Thielemans W (2009) Cellulose nanocrystals grafted with polystyrene chains through surface-initiated atom transfer radical polymerization (SI-ATRP). Langmuir 25:8280–8286
128. Zoppe JO, Habibi Y, Rojas OJ, Venditti RA, Johansson L-S, Efimenko K, Osterberg M, Laine J (2010) Poly(N-isopropylacrylamide) brushes grafted from cellulose nanocrystals via surface-initiated single-electron transfer living radical polymerization. Biomacromolecules 11: 2683–2691
129. Majoinen J, Walther A, McKee JR, Kontturi E, Aseyev V, Malho JM, Ruokolainen J, Ikkala O (2011) Polyelectrolyte brushes grafted from cellulose nanocrystals using Cu-mediated surface-initiated controlled radical polymerization. Biomacromolecules 12:2997–3006
130. Li S, Xiao M, Zheng A, Xiao H (2011) Cellulose microfibrils grafted with PBA via surface-initiated atom transfer radical polymerization for biocomposite reinforcement. Biomacromolecules 12:3305–3312
131. Xiao M, Li S, Chanklin W, Zheng A, Xiao H (2011) Surface-initiated atom transfer radical polymerization of butyl acrylate on cellulose microfibrils. Carbohydr Polym 83:512–519
132. Lacerda PSS, Barros-Timmons AMMV, Freire CSR, Silvestre AJD, Neto CP (2013) Nanostructured composites obtained by ATRP sleeving of bacterial cellulose nanofibers with acrylate polymers. Biomacromolecules 14:2063–2073
133. Yuan W, Yuan J, Zhang F, Xie X (2007) Syntheses, characterization, and in vitro degradation of ethyl cellulose-graft-poly (e-caprolactone)-block-poly (L-lactide) copolymers by sequential ring-opening polymerization. Biomacromolecules 8(4):1101–1108
134. Goffin A-L, Habibi Y, Raquez J-M, Dubois P (2012) Polyester-grafted cellulose nanowhiskers: a new approach for tuning the microstructure of immiscible polyester blends. ACS Appl Mater Interfaces 4:3364–3371
135. Goffin A-L, Raquez J-M, Duquesne E, Siqueira G, Habibi Y, Dufresne A, Dubois P (2011) From interfacial ring-opening polymerization to melt processing of cellulose nanowhisker-filled polylactide-based nanocomposites. Biomacromolecules 12:2456–2465
136. Ly EB, Bras J, Sadocco P, Belgacem MN, Dufresne A, Thielemans W (2010) Surface functionalization of cellulose by grafting oligoether chains. Mater Chem Phys 120:438–445
137. Lin N, Dufresne A (2013) Physical and/or chemical compatibilization of extruded cellulose nanocrystal reinforced polystyrene nanocomposites. Macromolecules 46:5570–5583
138. Fujisawa S, Saito T, Kimura S, Iwata T, Isogai A (2013) Surface engineering of ultrafine cellulose nanofibrils toward polymer nanocomposite materials. Biomacromolecules 14:1541–1546
139. Yao X, Qi X, He Y, Tan D, Chen F, Fu Q (2014) Simultaneous reinforcing and toughening of polyurethane via grafting on the surface of microfibrillated cellulose. ACS Appl Mater Interfaces 6:2497–2507
140. Svagan AJ, Musyanovych A, Kappl M, Bernhardt M, Glasser G, Wohnhaas C, Berglund LA, Risbo J, Landfester K (2014) Cellulose nanofiber/nanocrystal reinforced capsules: a fast and facile approach toward assembly of liquid-core capsules with high mechanical stability. Biomacromolecules 15:1852–1859
141. Cusola O, Tabary N, Belgacem MN, Bras J (2013) Cyclodextrin functionalization of several cellulosic substrates for prolonged release of antibacterial agents. J Appl Polym Sci 129:604–613
142. Missoum K, Belgacem MN, Bras J (2013) Nanofibrillated cellulose surface modification: a review. Materials 6:1745–1766
143. Ward IM, Hine PJ (1997) Novel composites by hot compaction of fibers. Polym Eng Sci 37: 1809–1814
144. Ward IM, Hine PJ (2004) The science and technology of hot compaction. Polymer 45: 1413–1427
145. Nishino T, Matsuda I, Hirao K (2004) All-cellulose composite. Macromolecules 37: 7683–7687

146. Nishino T, Arimoto N (2007) All-cellulose composite prepared by selective dissolving of fiber surface. Biomacromolecules 8:2712–2716
147. Soykeabkaew N, Arimoto N, Nishno T, Peijs T (2008) All-cellulose composites by surface selective dissolution of aligned ligno-cellulosic fibres. Compos Sci Technol 68:2201–2207
148. Soykeabkaew N, Sian C, Gea S, Nishno T, Peijs T (2009) All-cellulose nanocomposites by surface selective dissolution of bacterial cellulose. Cellulose 16:435–444
149. Gindl W, Keckes J (2005) All-cellulose nanocomposite. Polymer 2005(46):10221–10225
150. Gindl W, Schoberl T, Keckes J (2006) Structure and properties of a pulp fibre-reinforced composite with regenerated cellulose matrix. J Appl Phys A Mater Sci Proc 83:19–22
151. Duchemin B, Newman R, Staiger M (2007) Phase transformations in microcrystalline cellulose due to partial dissolution. Cellulose 14:311–320
152. Duchemin BJC, Newman RH, Staiger MP (2009) Structure–property relationship of all-cellulose composites. Compos Sci Technol 69:1225–1230
153. Duchemin BJC, Staiger MP, Tucker N, Newman RH (2010) Aerocellulose based on all-cellulose composites. J Appl Polym Sci 115:216–221
154. Gandini A, Curvelo AAS, Pasquini D, de Menezes AJ (2005) Direct transformation of cellulose fibres into self-reinforced composites by partial oxypropylation. Polymer 46: 10611–10613
155. Belgacem MN, Gandini A (2008) Partial or total oxypropylation of natural polymers and the use of the ensuing materials as composites or polyolmacromonomers. In: Belgacem MN, Gandini A (eds) Monomers, polymers and composites from renewable resources. Elsevier, Amsterdam
156. DeMenezes AJ, Pasquini D, Curvelo AAS, Gandini A (2008) Self-reinforced composites obtained by the partial oxypropylation of cellulose fibers. 1. Characterization of the materials obtained with different types of fibers. Carbohydr Polym 76:437–442
157. de Menezes AJ, Pasquini D, Curvelo AAS, Gandini A (2007) Novel thermoplastic materials based on the outer-shelloxypropylation of corn starch granules. Biomacromolecules 8: 2047–2050
158. de Menezes AJ, Pasquini D, Curvelo AAS, Gandini A (2009) Self-reinforced composites obtained by the partial oxypropylation of cellulose fibers. 2. Effect of catalyst on the mechanical and dynamic mechanical properties. Cellulose 16:238–246

Adv Polym Sci (2016) 271: 207–224
DOI: 10.1007/12_2015_322

Published online: 1 August 2015

Nanocellulose and Proteins: Exploiting Their Interactions for Production, Immobilization, and Synthesis of Biocompatible Materials

Consuelo Fritz, Benjamin Jeuck, Carlos Salas, Ronalds Gonzalez, Hasan Jameel, and Orlando J. Rojas

Abstract Nanocellulose has been used with promising results as reinforcement material in composites, many of which include hydrophobic polymers. However, the hydrophilic nature of nanocellulose can be better exploited in composites that incorporate high surface energy systems as well as in applications that can benefit from such properties. In fact, proteins can be ideal components in these cases. This paper reviews such aspects, which are based on the remarkable mechanical properties of nanocellulose. This material also exhibits low density, high aspect ratio, high surface area, and can be modified by substitution of its abundant hydroxyl groups. It also shows biocompatibility, low toxicity, and biodegradability. Convenient biotechnological methods for its production are of interest not only because of the possible reduction in processing energy but also because of positive environmental aspects. Thus, enzymatic treatments are favorable for effecting fiber deconstruction into nanocellulose. In addition to reviewing nanocellulose production by enzymatic routes, we discuss incorporation of enzyme activity to produce biodegradable systems for biomedical applications and food packaging. Related applications have distinctive features that take advantage of protein–cellulose interactions and the possibility of changing nanocellulose properties via enzymatic or protein treatments.

C. Fritz (✉), B. Jeuck, C. Salas, R. Gonzalez, and H. Jameel
Department of Forest Biomaterials, North Carolina State University, Raleigh, NC, USA
e-mail: cfritz@ncsu.edu

O.J. Rojas (✉)
Departments of Forest Biomaterials and Chemical and Biomolecular Engineering, North Carolina State University, Raleigh, NC, USA

Bio-based Colloids and Materials (BiCMat), Department of Forest Products Technology, School of Chemical Technology, Aalto University, Espoo, Finland
e-mail: orlando.rojas@aalto.fi

Keywords Bacterial cellulose (BC) • Biocompatibility • Cellulose nanocrystal (CNC) • Cellulose nanofibril (CNF) • Enzyme • Immobilization • Microcrystalline cellulose (MCC) • Microfibrillated cellulose (MFC) • Protein

Contents

1 Enzymatic Production of Nanocellulose

The production of nanocellulose through mechanical treatments requires high energy consumption [1], therefore a combination of different treatments has been suggested. One strategy to reduce the energy needed during these processes involves the use of different types of enzymes to improve accessibility and cellulose hydration and swelling. Also, reduction of the degree of polymerization of cellulose in fibers has been attempted by using cellulolytic enzymes. Specifically, endoglucanase enzymes are of interest because they preferentially attack the less crystalline regions within the fiber cell walls and cause their swelling and softening [2]. There are several studies highlighting the advantage of using enzymatic treatments for nanocellulose production (Table 1). In some cases, a reduction in yield as a result of cellulose loss is an important issue, for example, as reported in the case of fungal treatments [13].

An environmentally friendly method was developed by Henriksson et al. [3], who obtained microfibrillated cellulose (MFC) or nanofibers from bleached fibers after enzymatic hydrolysis with endoglucanases, followed by mechanical refining. The main advantage of this treatment compared with acid hydrolysis is the high aspect ratio of the nanofibers obtained after disintegration as a result of a decrease in the degree of polymerization of cellulose and an increase in swelling caused by endoglucanase action. These results were confirmed by another study that used a combination of high pressure shear forces and mild enzymatic hydrolysis to prepare MFC [4]. The material that resulted from using only mechanical shearing was not homogenous, in part because of blockages within the system. In contrast, when enzymatic hydrolysis steps were used between mechanical refining stages, the MFC obtained displayed a more uniform and smaller characteristic width and a high aspect ratio. This effect was mainly ascribed to cell wall delamination promoted by enzymatic action. The resulting material had higher elastic modulus than the material obtained using acid hydrolysis. Another interesting finding was the more

Table 1 Summary of some reported approaches to produce nanocellulose by using cellulolytic enzyme systems

Material	Pre/post-treatment	Enzymes used	Enzymatic hydrolysis conditions	Reference
Bleached wood sulfite pulps (*Picea abies*)	PFI-mill before and after enzymatic hydrolysis, mild acid hydrolysis (50°C, 1 h), stronger acid hydrolysis (NaOH 50°C, 10 min plus HCl 90°C, 2 h	Endoglucanase (commercial enzyme)	3% pulp, pH 7, 50°C, 2 h	[3]
Bleached sulfite softwood pulp	Refining before and after enzymatic hydrolysis plus homogenization	Endoglucanase	4% pulp, pH 7, 50°C, 2 h	[4]
Microcrystalline cellulose from cotton fibers	Hydrochloric acid hydrolysis (4 N)	*Trichoderma reseei* cellulases	5% inoculum, 1% MCC, 25 and 30°C, 150 rpm, 5 days	[5]
Recycled pulp (1% lignin)	Conventional and microwave heating after enzymes addition	Endoglucanase	1% pulp, 50°C, 60 min	[6]
Microcrystalline cellulose from cotton fibers	Hydrochloric acid hydrolysis (4 N)	Anaerobic microbial consortium (*Clostridium* sp. and coccobacillus)	1% MCC, 35°C, 5–15 days	[7]
Microcrystalline cellulose from *Cladophora* sp.		Exoglucanase	0.1% MCC, 38°C, pH 4.8, 2–3 days	[8]
Bacterial cellulose from *Acetobacter xylinum*		*Trichoderma reseei* cellulases	10% cellulose, pH 5, 50°C, 24 h	[9]
Bleached kraft eucalyptus pulp	Mechanical homogenization (microfluidizer) after enzymatic hydrolysis	Endo- and exoglucanase (commercial enzymes)	10% pulp, 5 and 10 FPU, 50°C, pH 4.8, 48 h	[10]
Bleached native sisal fibers	Mechanical shearing before and after enzymatic hydrolysis followed by mild acid hydrolysis	Endo- and exoglucanase (commercial enzymes)	2 and 5% pulp, 0.5 and 1% enzymes, 50°C, 2 h	[11]
Bleached native sisal fibers	Mechanical shearing before or after enzymatic hydrolysis followed by mild acid hydrolysis	Endo- and exoglucanase (commercial enzymes)	0.1% enzymes, 50°C, 2 h	[12]

entangled network formed by cellulose fibrils obtained enzymatically compared with those obtained by acid hydrolysis, which showed little or no entanglement. Siqueira and coworkers [12] took advantage of the combination of enzymatic hydrolysis followed by a mechanical shearing to produce nanocomposite films with good thermomechanical properties. A comparative study between commercial endo- and exoglucanases was performed earlier by same authors [11]. The enzymes were responsible for a much higher reduction in the degree of polymerization because they attacked specific sites on the chain and released small moieties in the form of nanoparticles, the morphology of which depended on the treatment used.

Fungi such as *Trichoderma reseei* have been used to prepare cellulose nanocrystals (CNC) from microcrystalline cellulose (MCC) from cotton [5], which was prepared by a conventional method employing hydrochloric acid. After controlled enzymatic hydrolysis, the slurry was subjected to additional fermentation stages to obtain CNC. It was found that the fungus consumed significant amounts of MCC for its own growth, as expected from the fact that cellulose was the only carbon source available for the microorganisms. In contrast to materials obtained after acid hydrolysis, fungal treatment produce no significant changes in surface chemistry. In fact, enzymatic or fungal methods do not install negatively charged groups on the surface (e.g., sulfate half ester groups from sulfuric acid hydrolysis) and result in material with negative zeta potential, less than −15 mV, making the material suitable for biomedical and related applications.

An integrated production of both cellulose nanofibrils (CNF) and bioethanol was developed by Zhu and coworkers [10]. The cellulosic material presented a decreased degree of polymerization after enzymatic hydrolysis, as found by other researchers, which facilitated the production of CNF by subsequent mechanical methods (microfluidization). The fiber length was significantly affected by cellulases, as observed in Fig. 1. The opacity and mechanical properties of nanopapers made from CNFs were better than those obtained from eucalyptus fibers. Moreover,

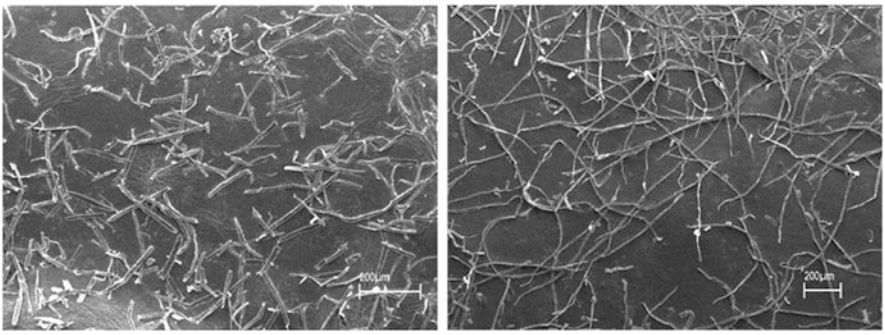

Fig. 1 SEM image of cellulosic material resulting from 48 h of enzymatic hydrolysis under enzyme loading of 5 FPU/g cellulase (*left*), and the original bleached Kraft eucalyptus fibers (*right*). Reproduced from Zhu et al. [10] with permission of The Royal Society of Chemistry (RSC)

and as a side advantage, the residual sugar stream was fermented by typical microorganisms to produce bioethanol with an efficiency of 92%.

Recently, Satyamurthy and Vigneshwaran [7] produced spherically shaped nanocellulose particles by using MCC subjected to degradation by an anaerobic microbial consortium of *Clostridium* sp. and coccobacillus. The nanocellulose obtained preserved its structure without any chemical modification, which makes it suitable for applications that demand minimum chemical changes to cellulose, such as biomedical, drug delivery and other applications requiring biocompatibility.

A major drawback of most methods for producing nanocellulose materials is the characteristic low yield. Satyamurthy and coworkers prepared CNC with a yield of 22% [5], whereas the same group reported a maximum yield of ~12% using an anaerobic microbial consortium [7]. In contrast, Filson et al. [6] studied the enzymatic hydrolysis of recycled paper using endoglucanases, following by microwave or conventional heating to produce related materials. The presence of nanocrystals was confirmed by flow birefrigerence and it was demonstrated that the heating method gave a higher yield (~38%) than conventional methods giving typical yields of ~ 29%. The authors highlighted the stability of the obtained crystals as nanofillers for reinforced polymer composites. They attributed the high negative zeta potential to the long-term stability of aqueous dispersions of CNC.

Although the production of nanocellulose from lignocellulosic materials has been heavily studied, other sources of cellulose could be useful. An exoglucanase (CBH I) was applied to produce shortened MCC from algal cellulose of *Cladophora* sp. [8]. These short elements exhibited high crystallinity because the cellulose allomorph I_α was preferentially degraded by the enzymes, leaving the highly ordered crystalline I_β domains unaffected. As an application, the authors indicated that the short elements could act as nano-ordered bioparticles.

Bacterial cellulose (BC) is a promising source for producing CNC. George et al. [9] prepared CNC from *Acetobacter xylinum* using cellulases from *Trichoderma reseei*. The amorphous domains were removed, whereas the crystalline portion was unaltered, in part because of better stability of this nanomaterial compared with material obtained by acid hydrolysis. Moreover, nanocomposites were produced using poly(vinyl alcohol) matrices. It was found that, even at low loading of CNC from BC (1 wt%), the mechanical and thermal stability was favorably affected.

Having discussed several prominent methods for producing CNF, MFC, and CNC, the following sections evaluate the functionality and application of these biobased nanomaterials. Not only does nanocellulose possess outstanding thermal and mechanical properties, it is also naturally biocompatible, which gives it tremendous potential in biomedical applications. Considered together, the mechanical properties, malleable nature, and biocompatibility render CNF, MFC, and CNC exceptional candidates in related fields.

2 Nanocellulose, Proteins, and Enzymes: Interactions and Immobilization

Nanocellulose is suitable for immobilization of different proteins. An inexpensive, simple, and direct immobilization method is desirable so that the nanocellulose can display its promising features [14]. Immobilization can be carried out by different mechanisms, involving covalent or noncovalent attachment, biochemical affinity, and physical adsorption (van de Waals forces, hydrogen bonds, electrostatic and hydrophobic interactions).

The immobilization of enzymes onto a material can help to increase their thermal and pH stability and provide relative longevity and reusability [15]. This could also allow substrates to be modified for biosensors, industrial applications, and continuous catalytic processes [15–17], as discussed in the next sections.

Ong et al. [14] demonstrated as early as 1989 that cellulosic materials offer a strong and stable noncovalent binding capacity for the carbohydrate binding domains (CBD) of certain cellulase enzymes, simplifying their immobilization onto the substrate. This technique was shown to extend enzyme activity (although decreased to 42% by immobilization) and helped to stabilize it against thermal and pH fluctuations [14]. Since the undertakings of Ong et al. [14], other successful studies utilizing covalent attachment have also been conducted [15, 18, 19]. Arola et al. [15] used CNF to covalently immobilize two types of proteins (alkaline phosphatase and anti-hydrocortisone antibody). Specialized techniques were utilized to conjugate the proteins to three CNF-derived substrates based on their prominent functional groups (epoxy, amine, and carboxylic acid) [15]. The study concluded that hydrophilic substrates can support immobilization better than their hydrophobic counterparts, and that certain kinds of covalent immobilization have a distinct advantage over nonspecific adsorption of proteins. Using this covalent approach, Mahmoud and coworkers [18] were able to attach an enzyme to a CNC matrix conjugated with gold particles. In this system, the specific enzyme activity and stability were improved [18]. Incani et al. [19] have similarly produced materials for use in biosensor applications by covalently immobilizing glucose oxidases (GOx) to CNC that had been previously modified with gold nanoparticles (AuNP), with their deposition being controlled using cationic polyethylenimine (PEI) at various pH levels [19] (see Fig. 2).

Adsorption interaction has been studied on cellulose-based aerogels with promising results [20–23]. The immobilized proteins tended to show increased thermal stability, probably as a result of noncovalent interactions. As a consequence, storage stability was improved [22]. Drug delivery based on nanocellulose has been studied [24]. The relative size of the drugs compared with the porous nature of CNF substrates was crucial, and electrostatic forces were found to be a primary mechanism of interaction. Such interactions were studied in the case of soybean protein adsorption on cellulose [25]. The storage proteins in soybean, glycinin, and β-conglycinin were found to interact with cellulose surfaces by different mechanisms (see Fig. 3). For instance, the adsorption of glycinin increased with

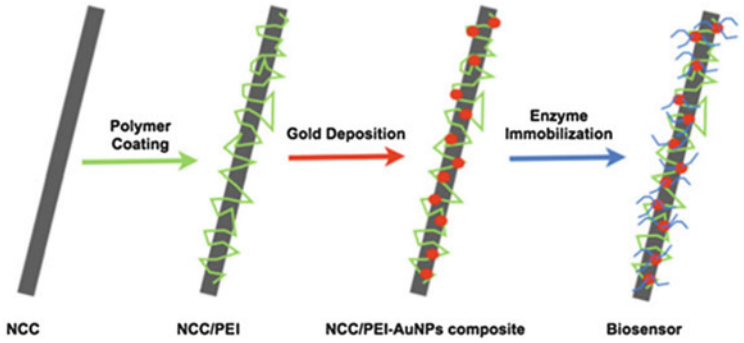

Fig. 2 Synthesis of a biosensor based on cellulose nanocrystals (here denoted as NCC) by modification with polyethylenimine and thiol-functionalized gold that is conjugated to glucose oxidase. Reprinted from reference [19], with kind permission from Springer Science and Business Media

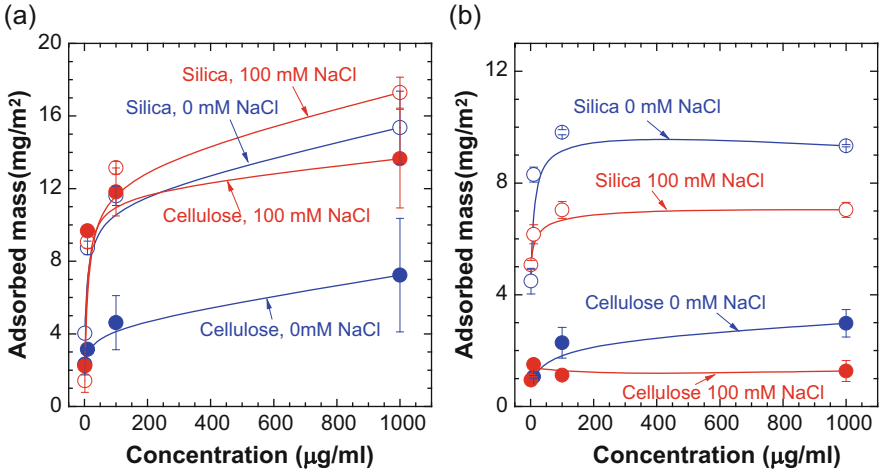

Fig. 3 Adsorption isotherms for (**a**) soy glycinin and (**b**) β-conglycinin on cellulose, as determined from quartz crystal microbalance measurements. Note the contrasting adsorption behavior of each protein as a function of ionic strength. Silica surfaces were used as reference, as indicated. Adapted from Salas et al. [25]. Reproduced with permission. Copyright © 2012 American Chemical Society

ionic strength but β-conglycinin adsorption was reduced. In addition, changes in pH and the use of a reducing agent (2-mercaptoethanol) were found to significantly reduce the adsorption of both proteins. For instance, 2-mercaptoethanol, a reducing agent of the disulfide bonds in proteins, unfolds the protein to expose their hydrophobic groups. The results highlight the fact that protein–cellulose interactions can be tuned by considering the protein structure and its response to physicochemical changes in the surrounding environment.

3 Nanocellulose–Protein Hybrids in 3D Structures: Gels/Hydrogels and Fibers

CNF surface modification via electrostatic interaction, adsorption, bioconjugation, or enzymatic catalysis can increase the versatility of CNF applications and result in increased material benefits. Examples of this include the production of bioinert or biospecific surfaces [26], cell adhesion on scaffolding [27], immobilization of proteins and enzymes for increased stability [14, 15, 19, 22], or production of novel nanocomposites for thin films, aerogels, and fibers.

Interactions between proteins and nanocellulose have been exploited in the development of hydrogels, which can also serve as template material for the preparation of aerogels (e.g., for drug encapsulation). One approach included coating of drug nanoparticles with hydrophobic proteins and embedding them in hydrogels that were subsequently freeze-dried into aerogels [28].

Although CNF is biocompatible, aerogels produced for cell scaffolding tend to have a relatively low affinity for cell attachment and require some protein-based modification to enhance this feature [27]. For instance, fibronectin and collagen type I were conjugated onto the surface of BC using 1-cyano-4-dimethylamino-pyridinium (CDAP) as crosslinking agent. This approach enhanced the adhesion and growth of human umbilical vein endothelial cells and mouse mesenchymal stem cell line C3H10T1/2 on bacterial nanocellulose [27].

CNF hydrogels can serve as three-dimensional (3D) cell culture scaffolds for the growth of human hepatic cells (HepaRG and HepG2). The approach included culturing the cells on the hydrogels. Evaluation of injectability of CNF hydrogels indicated that they can flow, even through very small needles, without damaging the cells. In addition, cell viability on CNF hydrogels was similar to that using conventional cell cultures, although cell growth was different for each type of cell studied. For example, HepG2 exhibited nonexponential growth and HepaRG showed less proliferation. Both cell types showed 3D multicellular spheroids (see Fig. 4) [29]. More recently, Lou et al. [30] used CNF hydrogels to create a 3D environment for proliferation and differentiation of human pluripotent stem cells (hPSCs). This new flexible culture system was able to maintain the pluripotency of hPSCs for up to 26 days, demonstrating that it could be a useful approach for research and regenerative medicine.

In related efforts, the ability of BC for cartilage regeneration was evaluated. Bovine cartilage samples were punched and BC inserted inside the cartilage cavity, followed by immersion in culture media for 8 weeks. The results indicated that cartilage cells still exhibited vital morphology after that period, with growth of chondrocytes on the surface of BC but not inside the pores. The chondrocytes at the nanocellulose surface showed successful re-differentiation [31].

BC nanofiber 3D networks, with pore sizes between 150 and 500 μm, were prepared by culturing *Gluconacetobacter xylinus* on medium containing paraffin beads that helped to create a uniform porous structure. These 3D networks served as

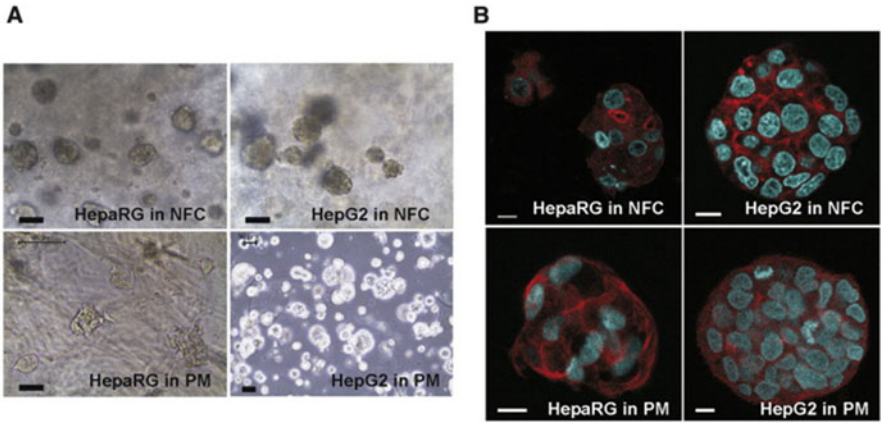

Fig. 4 Evidence of HepaRG and HepG2 cell spheroid formation in cellulose nanofibril (CNF) and peptide nanofiber (Puramatrix™, PM) hydrogel cultures. (**a**) Phase contrast microscopy and (**b**) confocal microscopy with structural staining of filamentous actin (*red*) and nuclei (*blue*). Reproduced with permission from reference [29]. Copyright © Elsevier

scaffolds for culture of human nasal and auricular chondrocyte cells and produced cartilaginous matrix protein for cartilage tissue engineering applications [32].

A different approach used unidirectional and 3D laser perforation with a CO_2 laser system to produce uniform, round-shaped pores (pore size ~220 μm) on never-dried BC hydrogels. The method included production of rectangular 3D porous structures that were used to grow bovine (24 h) and human (7–21 days) chondrocytes. The results indicated colonization of the BC nanofiber surface and of the laser-perforated channels with vital cells, with both unidirectional and 3D perforated channels, and allowed the re-differentiation of chondrocytes (see Fig. 5). The mechanical properties of the hydrogels were not significantly different from those of nonperforated hydrogels [33].

CNF hydrogels were used to culture HepaRG liver progenitor cells, which induced formation of 3D multicellular spheroids structures. Compared with hyaluronan gelatin hydrogels, the CNF hydrogels proved to be more effective for cell growth of undifferentiated cells and for maintaining differentiation of cells [34]. Likewise, BC hydrogels with high protein loads were prepared using a vortexing method, which took less time (10 min, uptake capacity of $8.4 \pm 0.1\%$) than the adsorption method (24 h, uptake capacity of $7.9 \pm 0.7\%$). The hydrogels produced by the faster method exhibited a denser fiber network morphology, slower protein release, and lower water holding capacity than conventional BC hydrogels [35].

Composites of BC with fish gelatin were prepared by immersing alkali-treated-BC pellicles in gelatin solutions and crosslinking the gels with different chemical agents (transglutaminase, genipin, and 1-ethyl-3-(3-imethylaminopropyl) carbodiimide hydrochloride, EDC). The results indicated an enhancement of the gel elastic behavior with increased protein content. In addition, the morphology of the

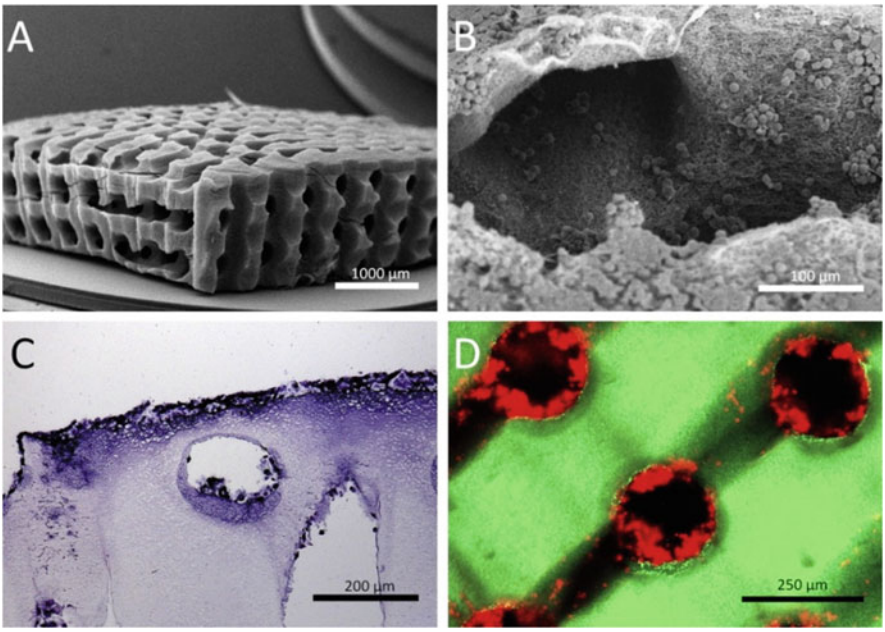

Fig. 5 (**a**, **b**) Scanning electron micrographs, (**c**) histological cross-section, and (**d**) laser scanning micrograph of 3D modified BC hydrogels (stained with 5-[(4,6-dichlorotriazin-2-yl)amino]fluorescein hydrochloride, DTAF) seeded with bovine chondrocytes. (**a**) View of 3D hydrogel channels. (**b**) Side view of channels showing chondrocytes (labeled with CellTracker Orange CMRA) adhered to inner surface after 24 h of culture. (**c**) Histological sections and (**d**) laser scanning micrographs of BC nanofiber surface and laser channels after seeding with cells of round morphology. Reproduced with permission from reference [33]. Copyright © Elsevier

composites indicated the formation of a dense porous network with gelatin covering the nanocellulose fiber network; after crosslinking, the gelatin improved the rehydration capacity of the material [36].

Widely available and inexpensive proteins from soy bean have been utilized to produce hydrogels and, subsequently, aerogels. For instance, soy protein isolate with a high protein content was used to prepare CNF–soy protein aerogels. The results indicated good synergy between the proteins and nanocellulose in the porous aerogels, which displayed mechanical properties comparable to those of aerogels obtained from pure nanocellulose. In addition, because of the hydrophilic nature of cellulose, these materials showed enhanced water absorption and, interestingly, similar absorption of nonpolar fluids [37]. Similarly, biocomposite porous scaffolds of ovalbumin/poly(vinyl alcohol) reinforced with CNC were prepared recently [38]. The addition of CNC as reinforcement increased the strength and flexibility of the porous scaffolds. The changes were explained by the different morphology of the aerogels obtained after addition of nanocrystals.

In addition to hydrogels, nanocellulose/protein composite fibers have been developed. CNC was used to reinforce prolamin protein (hordein/zein) electrospun

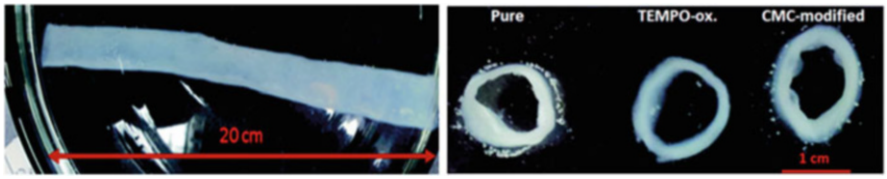

Fig. 6 Longitudinal (*left*) and cross-section (*right*) images of bacterial cellulose (BC) tubes. Tubes of pure BC, TEMPO-oxidized BC, and carboxymethyl cellulose (CMC)-modified BC were produced. Adapted from Orelma et al. [40] with permission from The Royal Society of Chemistry

nanofibers. The addition of cationically modified (using phenyltrimethylammonium chloride) CNC helped to increase the tensile strength, Young's modulus, water resistance, and alignment of the fibers. In addition, these fibers were encapsulated with a model drug (riboflavin) and were found to be effective for controlled release within a period of 24 h [39].

The potential of BC for selective biofiltration of blood proteins has been explored [40] by growing and modifying BC (from *Gluconacetobacter medellinensis*) in the presence of CMC. Such CMC-modified BC was used to synthesize tubules of given sizes. Synthesis was carried out using a silicon tube template through which air was supplied for bacterial growth. Also, 2,2,6,6,-tetramethylpiperidine-1-oxyl (TEMPO) oxidation was used to produce TEMPO-oxidized BC tubes. The CMC-modified BC tubes exhibited thicker walls than tubes of pure BC or TEMPO-oxidized BC (see Fig. 6). In addition, CMC not only reduced the irreversible structural changes in BC that occur upon drying but also facilitated the immobilization of anti-human serum albumin (anti-HSA) Affibodies via EDC-NHS conjugation. Interestingly, the CMC-modified BC carrying anti-HSA had better affinity for HSA than TEMPO-oxidized BC.

4 Biocompatible CNF/Polymer Systems

Nonspecific protein adsorption begins instantly after introduction of intracorporeal implants, marking the implant as a foreign or invasive entity needing to be destroyed or isolated [26, 41]. In either event, the effectiveness of the implant is obstructed by layers of protein or a fibrous avascular capsule growth that completely isolate it from the rest of the tissue [26]. Therefore, it is of extreme interest in the field of bionics to develop materials that are biocompatible. "Biocompatibility" can be described as the property of a material that provides an explicit purpose within an organism while, or by, suppressing or expressing all, most, or specifically few natural immunological or foreign body reactions by the organism [26]. Figure 7 illustrates a simplified model of immunoresponsive protein marking on bio-incompatible surfaces through adsorption and denaturation, and how polymer-coated surfaces can intervene in this interaction by making the

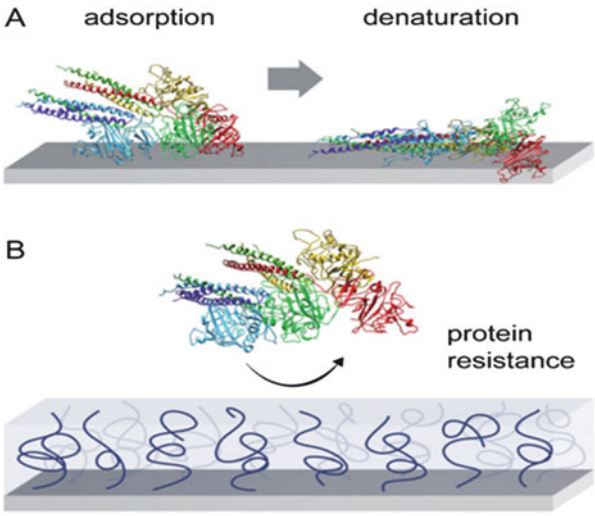

Fig. 7 (**a**) Dynamic adsorption and denaturation of proteins on a nonbiocompatible surface. (**b**) Protein resistance of a biocompatible polymer-coated surface. Reproduced from reference [26] by permission of John Wiley & Sons Ltd

surface more biocompatible [26]. The prevention of nonspecific protein adsorption is the key factor for biocompatibility of a material [26]. The surface characteristics responsible for preventing protein adsorption, referred to as "Whitesides rules," involve both the presence of polar and H-bond acceptor groups as well as the absence of net charge or H-bond donor groups [26]. This rule applies to cellulosic materials given their extreme hydration properties, which roughly compensate for the presence of H-bond acceptors in the form of hydroxyl groups [26].

In practice, CNF has been shown to be biocompatible [42–45]. Helenius et al. [46] demonstrated that subcutaneous implants of BC nanofibrils developed very little, if any, inflammation (both acute and chronic) and induced no foreign body responses, such as capsule formation or fibrosis [46]. CNF has been used in cell growth scaffolding for surrogate carotid arteries [42], tissue engineered blood vessels [44], cartilage [43], and burn tissue regeneration [45], to give a few examples.

Table 2 shows techniques that have been used for protein and enzyme immobilization on various cellulose–polymer matrices. Kuzmenko et al. [27] showed that cell adhesion to CNF scaffolds can be increased through bioconjugation of fibronectin and collagen proteins to its surface; these proteins are responsible for cell interactions [48]. This technique modifies CNF surfaces by adhering the cell binding domains of these proteins to the hydroxyl groups extending from the polysaccharides [27]. Crosslinking to produce an intermediate radical, followed by a nucleophilic substitution reaction with the protein amine groups, resulted in a stable, covalently bound protein. This, in turn, improved cell culture binding to the scaffolding, a crucial aspect for healthy tissue development [27]. Others have developed similar methods for different tissues, as each tissue type requires specific proteins for proper tissue adhesion and development [48–50].

Table 2 Techniques for protein/enzyme immobilization on nanocellulose/polymer systems

Protein(s)/ enzyme(s)	Polymer system	Method	Reference
Pancreatic serine protease trypsin	Poly(acrylic acid)-modified poly(glycidylmethacrylate)-grafted nanocellulose (PAPGNC)	PAPGNC-protein adsorption	[22]
Hemoglobin	Poly(methacrylic acid-*co*-vinyl sulfonic acid)-grafted–magnetite nanocellulose composite (P(MAA-*co*-VSA)-*g*-MNCC)	(P(MAA-co-VSA)-*g*-MNCC)-protein adsorption	[23]
Alkaline phosphatase/ anti-hydrocortisone antibody	TEMPO-/amine-/epoxy-functionalized CNF	Bioconjugation	[15]
Glucose oxidase	Nanocrystalline cellulose adorned with gold nanoparticles	Carbodiimide coupling	[19]
β-Casein	Nanocrystalline cellulose with functionalized reducing end	Click chemistry	[47]
Fibronectin and collagen type I	Bacterial nanocellulose	Bioconjugation using 1-cyano-4-dimethylaminopyridinium (CDAP) tetrafluoroborate as intermediate catalyst	[27]
Exoglucanase (from *Cellulomonas fimi*)	Cellulose material	Adsorption via cellulose-binding domain	[14]
Bovine serum albumin/antihuman IgG	TEMPO-oxidized CNF films	EDC/NHS activation	[16]

Protein adsorption has been studied on nanocellulose-based aerogels, and promising results for biomedical applications have been obtained [20, 22, 23]. Anirudhan and Rejeena [22] immobilized pancreatic serine protease trypsin (TRY) on a composite nanocellulose-based aerogel matrix through adsorption, resulting in increased thermal stability of the protein [22]. Storage shelf-life of the material was also improved by protein immobilization [22]. TRY is a protease enzyme used industrially for various applications and is notoriously unstable, making the enhancement of thermal and storage stabilities perspicuous advantages in the biomedical and food industries [22].

CNF has been investigated for the immobilization of proteins and subsequent film formation. In one study, nanofibers were first functionalized using different chemistries (amination, epoxydation, and TEMPO oxidation) then, alkaline phosphatase (AP) was conjugated in solution to each of the modified CNF, followed by spin-coating of these solutions onto silicon surfaces. Multiple layers of spin-coating

gave an increased amount of AP-conjugated CNF on the surface, as revealed by atomic force microscopy (AFM) imaging, which supports the hypothesis of higher enzyme immobilization. The results also indicated an increased stability of the AP-conjugated CNF at temperatures of 21°C and 37°C within a period of 168 h, which indicated biocompatibility for proteins [15].

The development of paper-based biosensors has been investigated. Orelma et al. [16] used TEMPO-oxidized CNFs, activated by EDC/NHS treatment, to conjugate antibodies and proteins. The adsorption of a human blood protein (human immunoglobulin G, hIgG) and bovine serum albumin was tested, demonstrating the use of this surface for the detection and diagnosis of biomolecules. Similarly, Zhang et al. [17] immobilized acetylated HWRGWVA peptide onto bioactive cellulose nanofibrils using the copolymer poly(2-aminoethyl methacrylate hydrochloride-*co*-2-hydroxyethylmethacrylate) as spacer and support layer. This modified-CNF network exhibited a high specific binding capacity for hIgG and high nonspecific protein resistance.

5 Enzymatic Modification of CNF

The natural hydrophilicity and ability of CNF to hydrogen bond into agglomerates makes it difficult to evenly disperse them amid nonpolar polymers in composites without some previous surface modification [51]. One technique uses TEMPO-mediated oxidation to increase the electronegative charge of CNF through the addition of anionic carboxylate groups [51]. Although TEMPO and its derivatives work as catalysts, they are continually reoxidized by primary oxidants, such as NaBr/NaClO or NaClO/$NaClO_2$ reagents in alkali conditions [52]. Oxidative enzymes have shown promise in replacing these primary oxidants while simultaneously maintaining milder reaction conditions. TEMPO-mediated oxidation using laccase enzymes with high oxidation rates was studied for the benefits of milder conditions and potential economic and ecological soundness [52, 53]. It was discovered that when using laccases as the primary oxidant, the percentage of aldehydes produced during oxidation increased between three- and fivefold compared with the chemical system. There were insignificant changes to the nanofibrillar structures, which could prove useful for various composites [52]. The investigation also revealed that site-specific surface modification produced a unique nanocellulose-derived product that could be of use in a number of novel nanocomposites [52]. Application of enzymatic modification of TEMPO-oxidized materials was investigated by Li et al. [54], who prepared nanocomposites through polymerization of phenol enzymatically in the presence of TEMPO-oxidized CNF. Polyphenols formed globular clusters on the nanocellulose, which improved the thermal stability and toughness of the composites and decreased their solubility in organic solvents [54].

Other work utilizing laccases has also been conducted. Garcia-Ubasart et al. [55] showed that the hydrophobicity of nanofibrillated cellulose can be controlled

through laccase-mediated coupling of different short, hydrophobic chains to its surface. The coupling reaction, catalyzed by laccase, showed that hydrophobization could be maximized by coupling dodecyl 3,4,5- trihydroxybenzoate (HB-C12) with flax fiber-based nanofibrillated cellulose [55]. The resulting water contact angles of the fiber webs were found to be 80–96° degrees, significantly greater than those of the control [55]. Cusola et al. [56] also manipulated surface hydrophobicity through applying a novel, multicomponent colloidal system comprised of laccase, hydrophobic dodecyl 3,4,5-trihydroxybenzoate (LG), and dispersant (sulfonated lignin) to couple LG onto the surface of CNF. It was observed that the low surface energy of LG was imparted to the composite and that the surface roughness greatly diminished, as shown by a 90° increase in water contact angle and AFM imaging on spin-coated thin films, respectively [56]. These reports concluded that laccase is capable of modifying the surface of cellulose-derived materials through the coupling of hydrophobic materials.

6 Final Remarks

The production of nanocellulose materials from lignocelluloses or other sources is still at the developmental and demonstration scale. According to the discussion presented here and literature on the subject, there is a large interest in the incorporation of biologically derived macromolecules. Examples include enzymes to decrease the energy demand of nanocellulose production, proteins and other molecules for development of bioactive cellulose, and novel materials. In these fields, chemical stability, (anti)fouling properties, swelling, and water resistance are central aspects that affect the full realization of these approaches involving proteins in their various forms.

References

1. Spence K, Venditti R, Rojas O, Habibi Y, Pawlak J (2011) A comparative study of energy consumption and physical properties of microfibrillated cellulose produced by different processing methods. Cellulose 18:1097–1111
2. Josefsson P, Henriksson G, Wågberg L (2008) The physical action of cellulases revealed by a quartz crystal microbalance study using ultrathin cellulose films and pure cellulases. Biomacromolecules 9:249–254
3. Henriksson M, Henriksson G, Berglund LA, Lindström T (2007) An environmentally friendly method for enzyme-assisted preparation of microfibrillated cellulose (MFC) nanofibers. Eur Polym J 43:3434–3441
4. Pääkkö M, Ankerfors M, Kosonen H, Nykänen A, Ahola S, Österberg M, Ruokolainen J, Laine J, Larsson PT, Ikkala O, Lindström T (2007) Enzymatic hydrolysis combined with mechanical shearing and high-pressure homogenization for nanoscale cellulose fibrils and strong gels. Biomacromolecules 8:1934–1941

5. Satyamurthy P, Jain P, Balasubramanya RH, Vigneshwaran N (2011) Preparation and characterization of cellulose nanowhiskers from cotton fibres by controlled microbial hydrolysis. Carbohydr Polym 83:122–129
6. Filson PB, Dawson-Andoh B, Schwegler-Berry D (2009) Enzymatic-mediated production of cellulose nanocrystals from recycled pulp. Green Chem 11:1808–1814
7. Satyamurthy P, Vigneshwaran N (2013) A novel process for synthesis of spherical nanocellulose by controlled hydrolysis of microcrystalline cellulose using anaerobic microbial consortium. Enzym Microb Technol 52:20–25
8. Hayashi N, Kondo T, Ishihara M (2005) Enzymatically produced nano-ordered short elements containing cellulose Iβ crystalline domains. Carbohydr Polym 61:191–197
9. George J, Ramana KV, Bawa AS, Siddaramaiah (2011) Bacterial cellulose nanocrystals exhibiting high thermal stability and their polymer nanocomposites. Int J Biol Macromol 48:50–57
10. Zhu JY, Sabo R, Luo X (2011) Integrated production of nano-fibrillated cellulose and cellulosic biofuel (ethanol) by enzymatic fractionation of wood fibers. Green Chem 13: 1339–1344
11. Siqueira G, Tapin-Lingua S, Bras J, da Silva Perez D, Dufresne A (2010) Morphological investigation of nanoparticles obtained from combined mechanical shearing, and enzymatic and acid hydrolysis of sisal fibers. Cellulose 17:1147–1158
12. Siqueira G, Tapin-Lingua S, Bras J, da Silva Perez D, Dufresne A (2011) Mechanical properties of natural rubber nanocomposites reinforced with cellulosic nanoparticles obtained from combined mechanical shearing, and enzymatic and acid hydrolysis of sisal fibers. Cellulose 18:57–65
13. Janardhnan S, Sain M (2006) Isolation of cellulose microfibrils – an enzymatic approach. Bioresources 1(2):176–188
14. Ong E, Gilkes NR, Warren RAJ, Miller RC, Kilburn DG (1989) Enzyme immobilization using the cellulose-binding domain of a *Cellulomonas fimi* exoglucanase. Nat Biotechnol 7:604–607
15. Arola S, Tammelin T, Setälä H, Tullila A, Linder MB (2012) Immobilization–stabilization of proteins on nanofibrillated cellulose derivatives and their bioactive film formation. Biomacromolecules 13:594–603
16. Orelma H, Filpponen I, Johansson L, Österberg M, Rojas OJ, Laine J (2012) Surface functionalized nanofibrillar cellulose (NFC) film as a platform for immunoassays and diagnostics. Biointerphases 7:61
17. Zhang Y, Carbonell RG, Rojas OJ (2013) Bioactive cellulose nanofibrils for specific human IgG binding. Biomacromolecules 14:4161–4168
18. Mahmoud KA, Male KB, Hrapovic S, Luong JHT (2009) Cellulose nanocrystal/gold nanoparticle composite as a matrix for enzyme immobilization. ACS Appl Mater Interfaces 1:1383–1386
19. Incani V, Danumah C, Boluk Y (2013) Nanocomposites of nanocrystalline cellulose for enzyme immobilization. Cellulose 20:191–200
20. Sannino A, Demitri C, Madaghiele M (2009) Biodegradable cellulose-based hydrogels: design and applications. Mater 2:353–373
21. Anirudhan TS, Tharun AR, Rejeena SR (2011) Investigation on poly(methacrylic acid)-grafted cellulose/bentonite superabsorbent composite: synthesis, characterization, and adsorption characteristics of bovine serum albumin. Ind Eng Chem Res 50:1866–1874
22. Anirudhan TS, Rejeena SR (2012) Adsorption and hydrolytic activity of trypsin on a carboxylate-functionalized cation exchanger prepared from nanocellulose. J Colloid Interface Sci 381:125–136
23. Anirudhan TS, Rejeena SR (2013) Selective adsorption of hemoglobin using polymer-grafted-magnetite nanocellulose composite. Carbohydr Polym 93:518–527
24. Kolakovic R, Peltonen L, Laukkanen A, Hellman M, Laaksonen P, Linder MB, Hirvonen J, Laaksonen T (2013) Evaluation of drugs interactions with nanofibrillar cellulose. Eur J Pharm Biopharm 85(3):1238–1244

25. Salas C, Rojas OJ, Lucia LA, Hubbe MA, Genzer J (2012) Adsorption of glycinin and β-conglycinin on silica and cellulose: surface interactions as a function of denaturation, pH, and electrolytes. Biomacromolecules 13:387–396
26. Wei Q, Becherer T, Angioletti-Uberti S, Dzubiella J, Wischke C, Neffe AT, Lendlein A, Ballauff M, Haag R (2014) Protein interactions with polymer coatings and biomaterials. Angew Chem Int Ed 53:8004–8031
27. Kuzmenko V, Sämfors S, Hägg D, Gatenholm P (2013) Universal method for protein bioconjugation with nanocellulose scaffolds for increased cell adhesion. Mater Sci Eng C 33:4599–4607
28. Valo H, Arola S, Laaksonen P, Torkkeli M, Peltonen L, Linder MB, Serimaa R, Kuga S, Hirvonen J, Laaksonen T (2013) Drug release from nanoparticles embedded in four different nanofibrillar cellulose aerogels. Eur J Pharm Sci 50:69–77
29. Bhattacharya M, Malinen MM, Lauren P, Lou Y, Kuisma SW, Kanninen L, Lille M, Corlu A, GuGuen-Guillouzo C, Ikkala O, Laukkanen A, Urtti A, Yliperttula M (2012) Nanofibrillar cellulose hydrogel promotes three-dimensional liver cell culture. J Control Release 164: 291–298
30. Lou Y, Kanninen L, Kuisma T, Niklander J, Noon LA, Burks D, Urtti A, Yliperttula M (2014) The use of nanofibrillar cellulose hydrogel as a flexible three-dimensional model to culture human pluripotent stem cells. Stem Cells Dev 23:380–392
31. Pretzel D, Linss S, Ahrem H, Endres M, Kaps C, Klemm D, Kinne R (2013) A novel in vitro bovine cartilage punch model for assessing the regeneration of focal cartilage defects with biocompatible bacterial nanocellulose. Arthritis Res Ther 15:R59
32. Feldmann E, Sundberg J, Bobbili B, Schwarz S, Gatenholm P, Rotter N (2013) Description of a novel approach to engineer cartilage with porous bacterial nanocellulose for reconstruction of a human auricle. J Biomater Appl 28:626–640
33. Ahrem H, Pretzel D, Endres M, Conrad D, Courseau J, Müller H, Jaeger R, Kaps C, Klemm DO, Kinne RW (2014) Laser-structured bacterial nanocellulose hydrogels support ingrowth and differentiation of chondrocytes and show potential as cartilage implants. Acta Biomater 10:1341–1353
34. Malinen MM, Kanninen LK, Corlu A, Isoniemi HM, Lou Y, Yliperttula ML, Urtti AO (2014) Differentiation of liver progenitor cell line to functional organotypic cultures in 3D nanofibrillar cellulose and hyaluronan-gelatin hydrogels. Biomaterials 35:5110–5121
35. Müller A, Wesarg F, Hessler N, Müller FA, Kralisch D, Fischer D (2014) Loading of bacterial nanocellulose hydrogels with proteins using a high-speed technique. Carbohydr Polym 106: 410–413
36. Chang S, Chen L, Lin S, Chen H (2012) Nano-biomaterials application: morphology and physical properties of bacterial cellulose/gelatin composites via crosslinking. Food Hydrocoll 27:137–144
37. Arboleda JC, Hughes M, Lucia LA, Laine J, Ekman K, Rojas OJ (2013) Soy protein-nanocellulose composite aerogels. Cellulose 20:2417–2426
38. Kumar A, Negi YS, Choudhary V, Bhardwaj NK (2014) Effect of modified cellulose nanocrystals on microstructural and mechanical properties of polyvinyl alcohol/ovalbumin biocomposite scaffolds. Mater Lett 129:61–64
39. Wang Y, Chen L (2014) Cellulose nanowhiskers and fiber alignment greatly improve mechanical properties of electrospun prolamin protein fibers. ACS Appl Mater Interfaces 6: 1709–1718
40. Orelma H, Morales LO, Johansson L, Hoeger IC, Filpponen I, Castro C, Rojas OJ, Laine J (2014) Affibody conjugation onto bacterial cellulose tubes and bioseparation of human serum albumin. RSC Adv 4:51440–51450
41. Lynch I, Salvati A, Dawson KA (2009) Protein-nanoparticle interactions: what does the cell see? Nat Nanotechnol 4:546–547
42. Klemm D, Schumann D, Udhardt U, Marsch S (2001) Bacterial synthesized cellulose-artificial blood vessels for microsurgery. Prog Polym Sci 26:1561–1603

43. Svensson A, Nicklasson E, Harrah T, Panilaitis B, Kaplan DL, Brittberg M, Gatenholm P (2005) Bacterial cellulose as a potential scaffold for tissue engineering of cartilage. Biomaterials 26:419–431
44. Bäckdahl H, Helenius G, Bodin A, Nannmark U, Johansson BR, Risberg B, Gatenholm P (2006) Mechanical properties of bacterial cellulose and interactions with smooth muscle cells. Biomaterials 27:2141–2149
45. Czaja WK, Young DJ, Kawecki M, Brown RM (2007) The future prospects of microbial cellulose in biomedical applications. Biomacromolecules 8:1–12
46. Helenius G, Bäckdahl H, Bodin A, Nannmark U, Gatenholm P, Risberg B (2006) In vivo biocompatibility of bacterial cellulose. J Biomed Mater Res A 76A:431–438
47. Karaaslan MA, Gao G, Kadla JF (2013) Nanocrystalline cellulose/β-casein conjugated nanoparticles prepared by click chemistr. Cellulose 20:2655–2665
48. Kleinman HK, Luckenbill-Edds L, Cannon FW, Sephel GC (1987) Use of extracellular matrix components for cell culture. Anal Biochem 166:1–13
49. Yeh H-Y, Lin J-C (2008) Surface characterization and in vitro platelet compatibility study of surface sulfonated chitosan membrane with amino group protection–deprotection strategy. J Biomater Sci Polym Ed 19:291–310
50. López-Pérez PM, da Silva RMP, Serra C, Pashkuleva I, Reis RL (2010) Surface phosphorylation of chitosan significantly improves osteoblast cell viability, attachment and proliferation. J Mater Chem 20:483–491
51. Kalia S, Boufi S, Celli A, Kango S (2014) Nanofibrillated cellulose: surface modification and potential applications. Colloid Polym Sci 292:5–31
52. Jaušovec D, Vogrinčič R, Kokol V (2015) Introduction of aldehyde vs. Carboxylic groups to cellulose nanofibers using laccase/TEMPO mediated oxidation. Carbohydr Polym 116:74–85
53. Aracri E, Vidal T (2012) Enhancing the effectiveness of a laccase-TEMPO treatment has a biorefining effect on sisal cellulose fibres. Cellulose 19:867–877
54. Li Z, Renneckar S, Barone JR (2010) Nanocomposites prepared by in situ enzymatic polymerization of phenol with TEMPO-oxidized nanocellulose. Cellulose 17:57–68
55. Garcia-Ubasart J, Vidal T, Torres AL, Rojas OJ (2013) Laccase-mediated coupling of nonpolar chains for the hydrophobization of lignocellulose. Biomacromolecules 14:1637–1644
56. Cusola O, Roncero MB, Vidal T, Rojas OJ (2014) A facile and green method to hydrophobize films of cellulose nanofibrils and silica by laccase-mediated coupling of nonpolar colloidal particles. ChemSusChem 7:2868–2878

Adv Polym Sci (2016) 271: 225–240
DOI: 10.1007/12_2015_318

Published online: 4 July 2015

Layer-by-Layer Assembly for Biofunctionalization of Cellulosic Fibers with Emergent Antimicrobial Agents

Ana P. Gomes, João F. Mano, João A. Queiroz, and Isabel C. Gouveia

Abstract Coating with polyelectrolyte multilayers has become a generic way to functionalize a variety of materials. In particular, the layer-by-layer (LbL) technique allows the coating of solid surfaces to give them several functionalities, including controlled release of bioactive agents. At present there are a large number of applications of the LbL technique; however, it is still little explored in the area of textiles. In this review we present an overview of LbL for textile materials made from synthetic or natural fibers. More specifically, LbL is presented as a method for obtaining new bioactive cotton (as in cellulosic fibers) for potential application in the medical field. We also review recent progress in the embedding of active agents in adsorbed multilayers as a novel way to provide the system with a "reservoir" where bioactive agents can be loaded for subsequent release.

A.P. Gomes
Optical Center and Electron Microscopy Center, University of Beira Interior, Covilhã 6201-001, Portugal
e-mail: anapaula@ubi.pt

J.F. Mano
3B's Research Group – Biomaterials, Biodegradables and Biomimetics, European Institute of Excellence on Tissue Engineering and Regenerative Medicine, University of Minho, AvePark, Taipas, Guimarães 4806-909, Portugal

ICVS/3B's – PT Government Associate Laboratory, Braga/Guimarães, Portugal
e-mail: jmano@dep.uminho.pt

J.A. Queiroz
Health Sciences Research Center, University of Beira Interior, Covilhã 6201-001, Portugal
e-mail: jqueiroz@ubi.pt

I.C. Gouveia (✉)
FibEnTech – Fiber Materials and Environmental Technologies Research Unit, Faculty of Engineering, University of Beira Interior, Covilhã 6201-001, Portugal
e-mail: igouveia@ubi.pt

Keywords Bioactive agents · Bioactive textiles · Cellulosic fibers · Cotton · Layer-by-layer

Contents

1 Introduction

1.1 Antimicrobial Textiles

The number of textiles functionalized for antimicrobial activity has increased considerably over the last few years. Antimicrobial textiles were first created to prevent damage to textiles under adverse environmental conditions during their storage or use. Textiles are widely used in daily life and there has been a growing need to develop associated finishes that can offer improved protection to users, for example, from microbes (bacteria, fungi) that could pose a threat to health. Hence, there is a pressing need to develop functionalized textiles that are resistant to microbes, especially for use in healthcare activities. Synthetic antimicrobial compounds used in textile articles are very effective against a wide range of microorganisms. However, the continuous use of antimicrobial compounds can lead to bacterial resistance and desensitization of users, as well as produce a negative environmental impact [1–4].

To minimize these risks, there is currently a high demand for antimicrobial textiles produced with environmentally friendly, nontoxic natural compounds. The low incidence of adverse effects of natural compounds, compared with their synthetic counterparts, has led to such textiles being explored as attractive and promising alternatives [5–7].

Cotton is the textile substrate most widely used in the health sector. In the form of cellulose fibers [3, 4], it is known for its versatility, natural comfort, softness, breathability, and ability to absorb moisture [8]. Cotton is often used to make a

variety of clothing for industrial and biomedical purposes. Because of its properties, cotton is also ideally suited as wound dressing material. In fact, cotton gauze is still the most commonly used textile for wound dressing in hospitals; however, new products have emerged for wound healing and for protection against entry of bacteria. For exudative wounds, there are a range of absorptive products (including various hydrophilic foam dressings, hydrogels, and alginates) that can absorb up to 20 times their weight [9] and can be formulated in combination with cotton substrates. At the same time, cotton is prone to act as host for the growth and development of microorganisms, making biofunctionalization with antimicrobial agents a necessity.

1.2 Current Functionalization Processes in Textile Materials

Coating is an important technique for adding value to technical textiles and a generic method of surface functionalization. In its most generic form, coatings involve polymer layers that are applied directly to one or both surfaces of a given fabric. A number of nanotechnologies have received special attention in the textile industry for fiber or fabric modification and to endow the substrates with new properties that are revealed at the nanoscale, especially multifunctional properties [10] that include antimicrobial activity to reduce the risk of microorganism transmission.

Several processes are available for coating textile materials, depending upon the requirement of the end product. The most significant processes include techniques such as sol–gel, which is a wet process that is broadly employed in the textile field and involves a simple pad or dip coating; magnetron sputter coating, which is one of several physical vapor deposition methods; plasma, which is a suitable technique for modifying the structure and topography of the surface; and others involving composite and hybrid systems [11].

These methods have a number of disadvantages, the most significant being the need for expensive solvents and equipment and the requirement for multistep and complex processing. In addition, under certain conditions it is necessary to use high temperatures, and the success of modification is often dependent on the substrate topography. It is apparent that new strategies are needed and the LbL technique, in particular, is as an attractive option because of its relative simplicity and efficiency.

The prerequisite for the success of LbL coating is the presence of a minimal surface charge on the substrate. In such cases, the LbL technique provides coatings on the surface of textiles to enable a wide range of functionalities [12]. Despite its technological appeal, the LbL deposition process has not been extensively implemented in the textile industry, particularly for natural fibers. The main reason for the slow introduction of LbL for natural fibers is their unique characteristics, including surface chemical heterogeneity, which complicates the application of such coatings.

2 LbL Assembly Technique

LbL is a simple and versatile method that can provide new types of coatings for textile materials. It was proposed by Decher and collaborators in the early 1990s [13] and the interest it has generated since then can be judged by the growing number of published papers on the subject.

LbL assembly can be applied on many kinds of charged surfaces [14], mainly to deposit multilayers of controlled architecture and composition from aqueous solutions. Electrostatic interactions are the main driving force for assembly within the neighboring layers of polyelectrolytes. Generally, LbL assembly proceeds as follows: (1) a charged substrate is immersed in a solution of an oppositely charged colloid that adsorbs as the first monolayer; (2) a washing cycle removes excess and unbound material; and (3) the coated substrate is submerged again to deposit a second layer to form a bilayer structure [15]. These cycles can be repeated as often as needed, and crosslinking is often applied to convert the obtained LbL multilayers into surface-bound hydrogels [16]. The number of deposition cycles and the type of polyelectrolyte used in the LbL construction allow full control of the thickness and roughness of the multilayered film [17]. Usually, multilayered films based on electrostatic interaction are affected by environmental conditions such as, pH, polyelectrolyte concentration, nature of solvents, and ionic strength [14, 18, 19].

LbL materials can be selected from a large variety of materials other than polyelectrolytes: small organic molecules, polymers, natural proteins, inorganic clusters, clay particles, and other colloids. In such cases, LbL can open new possibilities because a myriad of component combinations can be formulated in single devices with designed features and architectures. Importantly, the resulting functions might not be associated with those of the native (substrate) material. Surface functionality, for example, can be controlled directly by choosing appropriate polyelectrolyte combinations. This allows modification of electrical, optical, magnetic, physicochemical, and biological properties of the materials. Multilayer coating with bioactive, natural polyelectrolytes has become a new process for surface biofunctionalization.

Advantages of the LbL technique are that the process is inexpensive, relatively fast and simple, does not require sophisticated equipment and precise stoichiometry, or rely on complicated chemical reactions to deposit successive layers [20]. Another advantage of LbL deposition is its insensitivity to the size and shape of the substrate in producing comfortable coatings. This means that an LbL assembly can be realized not only on planar substrates, but also on substrates with different shapes and curvatures. For example, Caruso et al., (1998) demonstrated LbL deposition on a spherical template. After template dissolution, microcapsules were obtained [21]. Theoretically, LbL substrates can be of any size, shape, topography, or topology, and no stoichiometric control is necessary to maintain surface functionality and avoid propagation of defects [22].

In LbL deposition, pH can be used to adjust the strength of interlayer bonding and, therefore, multilayer thickness. As stated before, this requires the presence of a minimal surface charge, which, if absent, can be induced by different means [23].

Most knowledge about the LbL method has been developed in the field of drug delivery systems, allowing the creation of sophisticated materials and the production of capsules as carriers of drugs that can be released gradually. A major challenge in drug delivery is to produce controlled, sustained or triggered release systems for small encapsulated drug molecules. A discussion of these processes can be found in a review article by Wohl and Engbersen [24].

Several biomedical engineering studies have reported the creation of multilayer coatings by the LbL technique involving synthetic and natural polyelectrolytes [25]. Related multilayers have a characteristic low packing density to facilitate diffusion of bioactive agents, which in most cases are embedded throughout the multilayer. In fact, various parameters such as pH, ionic strength, temperature, light, and chemical or electrochemical stimuli have been used to tune the release and/or retention of bioactive agents within the multilayers. This allows control of drug dose, and delivery on demand with reduced toxicity and increased efficacy [16].

Using the concept of diffusion from multilayers, several authors have immobilized more than ten different water-soluble proteins in multilayers, ensuring the inhibition of protein denaturation [26–28]. Appropriate preservation of the functional characteristics of given compounds have ensured good results for effective incorporation of proteins and drugs between the multilayers, and their diffusion and subsequent release [29–33].

Several researchers have reported bioactive proteins, peptides, hormones, growth factors, and drugs that can be directly integrated into LbL architectures, without any covalent bonding with a polyelectrolyte and while maintaining their native structures and activities [29, 34–41]. The strategy described in all these efforts can be valuable in the application of a variety of drugs/bioactive agents. This opens a route for substrate functionalization via multilayers with embedded bioactive agents, in which the multilayers act as a reservoir for bioactive agents that can be gradually released and controlled.

A recent review provides an exhaustive account of the potential uses of the LbL method in biomedical engineering [42]; however, the technique is still in its infancy for textile applications. In recent years, researchers have used the LbL process to modify the surface of textile fabrics to impart or improve numerous surface properties, including UV protection [43, 44], hydrophobicity/hydrophilicity [45, 46], flame retardancy [47–49], and antimicrobial activity [50–54].

Our aim in this review is to assess the feasibility of employing the LbL method to obtain functionalized cellulose (cotton) with antimicrobial properties by incorporating bioactive agents between the layers for subsequent controlled release. This approach is supported by the work of Caridade et al., who studied the production of thick membranes by LbL assembly of chitosan and alginate and the control of membrane permeability to bioactive agents [55].

3 LbL in Textile Materials

The LbL process has been widely used to create multilayer films on various substrates. However, it has not been extensively employed for textile fibers. Textile fibers present some unique challenges for LbL assembly, such as the chemical heterogeneity and irregular shape of their surfaces [56]. Because LbL is a relatively new method for material functionalization, there are only a few reports concerning its adoption for textiles. For simplicity, this review divides textile substrates into two categories, synthetic and natural fibers.

3.1 LbL Coatings on Synthetic Fiber Materials

Synthetic fibers play an important role in the textile industry. There are many different types of synthetic fibers, but the most used are polypropylene, polyethylene, polyester, polyamide (nylon), and polyvinyl alcohol. A great disadvantage of some synthetic fibers is low hydrophilicity. This affects the LbL process because the fiber surface is not easily wetted. Table 1 shows a summary of the state of the art in application of the LbL method for textile materials involving synthetic fibers, mainly polypropylene, polyester, and polyethylene terephthalate (PET). The deposition of several layers endows the textile material with several features; however, attempts to impart antimicrobial properties to synthetic textiles have been introduced only recently.

3.2 LbL Coating of Cellulose-Based Textiles

Cotton, as one of the most commonly used materials in textiles, is suitable for medical usage, especially for wound dressings as a result of its high liquid absorbency and hygienic nature. However, cotton is characterized by its heterogeneity, which causes problems in conventional coatings but creates an opportunity for application of the LbL technique. Currently, only a few reports exist on the application of the LbL method to cotton. In this section we present the most important developments in terms of functionalized cotton using the LbL technique. A special note on antimicrobial cotton obtained by LbL is discussed at the end of this section.

There are many early reports on the application of the LbL technique to cellulosic fibers, mainly wood fibers. Hyde et al. reported application of LbL to cotton substrates. They found that the cationization process produced a cotton surface capable of supporting polyelectrolyte films via LbL deposition. They observed that the LbL deposition process is more dependent on the nature of the polyelectrolytes than on the nature of the original substrate; the analyses revealed

Table 1 Summary of main milestones in LbL application to synthetic fibers in textiles

Author (year)	Substrate	Polyelectrolytes	Notes
Polowinski (2005) [57]	Polypropylene	PAH/PAA	The dyeing technique allows the type of external layers deposited in succession to be identified. The LbL method deposits layers of polymeric complexes, not only onto polypropylene, but also onto other textile materials with smooth surfaces.
Dubas et al. (2006) [58]	Nylon	PDADMAC/anionic scarlet dye	The LbL of PDADMAC/anionic scarlet dye has a high dependence on the number of layers, salt concentration, and concentration of chemicals but is almost independent of dipping time.
Polowinski (2007) [59]	Polypropylene, polyester	PAH/PAA	The LbL method was used to deposit thin polymeric layers on textile fabrics. A necessary condition for using this method is a smooth surface on the fibers in the fabric.
Jantas et al. (2007) [60]	Polyester	PAA/PVP	The surface of fibers in the fabric becomes smoother after depositing PAA/PVP nanolayers.
Polowinski (2007) [61]	Polypropylene	PAA/PDAMA/PAH Nanoparticles: Au, Pt, Ag	The LbL method is a convenient way of depositing colloidal particles of silver, gold, or platinum onto textiles.
Stawski et al. (2009) [62]	Polypropylene	PAH/PAA	Deposition of successive polyelectrolyte layers fails to provide complete coverage of the modified surface.
Park et al. (2009) [63]	Nylon 6	Alginic acid sodium salt and chitosan	The morphology of a polyelectrolyte multilayer coated on nylon 6 fibers was uniform and smooth. The surface morphology, stiffness, and hydrophilicity of the system was controlled by regulating the number of polyelectrolyte nanocoats.
Carosio et al. (2011) [48]	PET	Silica nanoparticles	PET fabrics were coated with silica nanoparticles. This study demonstrates the ability to impart flame retardant behavior using a water-based, environmentally friendly protective coating.
Martin et al. (2013) [65]	Non-woven PET	MB/chitosan/polyCD (cyclodextrin polyelectrolyte)	The aim of this work was to develop an antibacterial multilayer coating activated with methylene blue (MB). The authors prepared two types of samples, MB-free and MB-loaded.

(continued)

Table 1 (continued)

Author (year)	Substrate	Polyelectrolytes	Notes
Martin et al. (2013) [64]	Non-woven PET	Chitosan/polyCTR-beta CD (beta cyclodextrin polymer)	This work developed the formation of a multilayered coating onto a PET textile support in order to obtain reservoir and sustained release properties towards bioactive molecules.

PAH poly(allylamine hydrochloride), *PAA* poly(acrylic acid), *PDADMAC* poly(diallyldimethylammonium chloride), *PVP* poly(vinyl pyrrolidone), *PDAMA* poly(diallylamine-*co*-maleic acid), *PET* polyethylene terephthalate, *PSS* poly(sodium styrene sulfonate), *MB* methylene blue

conformal and uniform coating of the cotton fibers [66]. From this work, there is indication that various functionalities can be developed for a given substrate, depending on the combinations of polyelectrolytes used. It is noteworthy that the nature of the substrate in LbL deposition has a relatively minor role, allowing the LbL to be applied smoothly onto cotton. Other publications report methods of analysis of samples obtained by the LbL technique [67]. Studies were also carried out to unveil the influence of physical parameters such as pH, concentration, ionic strength of polyelectrolytes, and cationization level of the substrate [56, 68]. In general, it was concluded that the deposition process was not significantly influenced by the degree of cotton cationization. In contrast, physical parameters were found to have a major influence on the success of LbL coating.

Protection against UV irradiation has been approached by using LbL coating of cotton fabrics [43, 44, 69, 70]. High UV protection factors were obtained as well as good resistance to washing, revealing the stability of the layers obtained by LbL on cotton. In fact, durability of the coating is often associated with the LbL technique. Another important property often reported for cotton is that of hydrophobicity [45, 71]. In this case, LbL coating is an easy method for fabrication of hydrophobic cotton fabrics.

More recently, several authors have used the LbL technique to coat cotton with specific polymers in order to enhance its flame retardancy properties. The studies showed that flame retardant coatings can be readily applied to textile fabrics for commercial and industrial applications [47–49, 72].

Providing antimicrobial properties to textiles is an effective way to prevent disease transmission in applications involving consumer and healthcare markets. Many textiles are treated to afford protection against bacteria, fungi, and other related microorganisms. During the past few years, several studies have aimed at functional antimicrobial modification via LbL assembly onto cotton fibers. Using *N*-halamine polyelectrolyte deposition on cotton fibers via LbL, cotton textiles were obtained with antimicrobial properties and potential application as medical textiles [73, 74]. A similar effect was obtained in our work group using chitosan and alginate as polyelectrolytes [52, 53, 75]. Other approaches for obtaining antimicrobial cotton have used chitosan [50, 51], copper [76], and ZnO [70] nanoparticles. In

these works, the nanoparticles were coated via LbL onto cotton fabric to form a nanocoating.

The LbL technique also offers new opportunities for the preparation of functionalized biomaterial coatings and the possibility of incorporating bioactive molecules between the layers [77–79]. Peptides, proteins, and active agents adsorbed or embedded in multilayer films have been shown to retain their biological activities [41], whereas covalent attachment to the active agents can reduce or even destroy their biochemical activity [79]. Thus, with the LbL technique, active agents can be directly integrated into the architecture without the need for covalent bonding.

Based on this concept, Gomes et al. investigated methods for the functionalization of cotton with polyelectrolyte multilayer films that incorporated a bioactive amino acid (L-cysteine, L-Cys). In this work, the strategy was based on the use of multilayer films as reservoirs of L-Cys [80]. These kinds of systems are promising for use in biomedical textiles, specifically for wound dressings. Cotton fiber is the basis of many wound dressings, and wound dressings containing antibiotics have been developed for the inhibition of wound infection [81–83]. Note that the continuous use of antibiotics has resulted in multiresistant bacterial strains; consequently, there is an urgent for alternatives to antibiotics.

4 Antimicrobials of the Future: Antimicrobial Peptides

Antibacterial resistance is a natural biological phenomenon that occurs in microorganisms and is potentiated by indiscriminate use of antibacterial agents. If the microorganism becomes resistant to a particular antibacterial agent, when an infection occurs, the effect of the antibacterial agent is reduced or nullified. Therefore, it is urgent that new antibacterial agents are discovered and used. Recently, a large group of low molecular weight natural compounds that exhibit antimicrobial activity were isolated from animals and plants, resulting in a new generation of antibacterial agents, named antimicrobial peptides (AMPs).

AMPs are promising agents because they are natural compounds [84, 85]; have a broad spectrum of action [86, 87]; exhibit high activity, even at low concentrations [87, 88]; have a low tendency to develop resistance as a result of their different mechanism of action [84, 85, 89–91]; act quickly and efficiently against bacterial agents [87, 91]; are generally of small size; and have low mammalian toxicity [87, 91]. The ability of AMPs to kill multidrug-resistant microorganisms has gained considerable attention and clinical interest. An alternative approach to wound healing with AMPs is related to the function of AMPs in removing destructive proteases from the wound. These proteases cause considerable destruction of growth factors and connective tissue proteins during the prolonged inflammatory phase of a chronic wound [92]. The 2010 review paper by Gouveia refers to AMPs for the first time as promising antimicrobial agents for textiles [93]. AMPs can be incorporated into textiles to produce nontoxic antimicrobial textiles. AMPs

produced in bacteria, insects, plants, invertebrates, and vertebrates are important components of the natural defenses of most living organisms. AMPs exhibit potent ability to kill a broad range of microorganisms, including Gram-negative and Gram-positive bacteria, fungi, and viruses [90, 94, 95].

4.1 AMPs: Characterization and Classification

Currently, databases (e.g., http://aps.unmc.edu/AP) list over 2,400 AMPs. Their characterization is complicated as a result of their great diversity, but can be simplified if based on their secondary structure. AMPs are mainly grouped into four classes: β-sheet, α-helical, loop, and extended peptides [96]. There are AMPs with positive [97] and negative [98] charges, or they can be amphipathic molecules (with both hydrophobic and hydrophilic regions). Some have sequences of less than 10 amino acids, whereas others contain nearly 100 amino acids [99]. In general, the AMPs are described as small molecules containing 12–50 amino acids with a cationic charge between +4 and +6 (as a result of the presence of the amino acids lysine and arginine) [91, 100]. Anionic AMPs generally have a net charge in the range of −1 to −7, as a result of the presence of glutamic and aspartic acids. AMPs are mainly cationic and interact with membranes in a general mechanism that involves interaction between charged residues of the peptides and anionic components of the membrane surface.

4.2 Mechanisms of Action

The AMPs in bacteria can cause disruption of the membrane, resulting in lysis or pore formation, allowing efflux of essential ion and nutrients. In this case, the AMPs are transported into the cell and inhibit DNA and RNA synthesis, inhibit ribosomal function and protein synthesis, and target mitochondria [101]. Many models of antimicrobial action at the membrane level have been proposed. Models that have greater acceptance in the scientific community include the carpet model, toroidal pore, and barrel-stave [88].

AMPs also possess antiviral properties. They inhibit viral fusion and egress, thus preventing infection and viral spread via direct interaction with the viral membranes and host cell surface molecules [101]. These properties, combined with the broad range of activity and short contact time required to induce killing, have led to the consideration of AMPs as novel therapeutic agents.

4.3 Applications of AMPs

AMPs applications are not limited to the development of new drugs, because there are also other medical, environmental, and industrial applications. Some potential medical applications of AMPs include:

- Prevention and treatment of eye disease, and in antimicrobial coatings for contact lenses [102]
- Antimicrobial coating on polymeric materials, such as implants and catheters, for prevention of bacterial colonization and biofilm formation on the surfaces of the implants [88]
- Functionalization of biomedical materials (e.g., in heart valves) and other textile materials such as socks for diabetics, gauze for chronic wounds, etc. [88]
- Wound healing, treating fibrosis, acne, Crohn's disease [90]

Recently, our research group found AMP applications in textiles, particularly in cotton gauzes for wound dressings [95, 103]. Incorporation is the most popular method for preparing immobilized AMPs on a variety of surfaces and retaining their ability to kill bacteria [104, 105]. Gomes et al. (2015) developed a new strategy for the biofunctionalization of cotton by incorporation of AMPs, with possible application in medical textiles such as wound dressings. This study demonstrated that cotton functionalized with chitosan/alginate loaded with AMPs is effective against pathogenic bacterial strains. The results demonstrated antimicrobial activity as well as low cytotoxicity. The main advantage of using AMPs is a result of their natural existence, meaning that they are well tolerated by the human body and that low concentrations are required. In addition, their synergistic biocide mechanism of action is effective against multiresistant bacteria.

5 Concluding Remarks and Future Prospects

Successful deposition of multilayers onto the surfaces of textile fibers, especially those based on cellulose, by the LbL technique can open opportunities for the development of functional textiles in a broad range of applications. The LbL technique in textiles is entirely new and is a simple and effective method, with a strong possibility of industrial implementation.

Bioactive agents can be directly embedded between polyelectrolyte layers without the need for covalent bonding, which facilitates the development of strategies to produce antimicrobial cotton by using AMPs in polyelectrolyte multilayer films. These coatings on cellulose surfaces are new and potentially useful as antibacterial materials in a wide variety of biomedical applications. In addition, LbL deposition allows easy fabrication of multimaterial films, in which different layers carry different functionalities or control the quality and quantity of active

agents. Overall, the reviewed work lays the groundwork for scale-up in cellulose-based materials and opens new avenues towards the development of nontoxic and safe biomedical textiles.

Acknowledgments The authors would like to thank Fundação para a Ciência e Tecnologia (FCT) for the funding granted for the project PTDC/EBB-BIO/113671/2009 (FCOMP-01-0124-FEDER-014752) Skin2Tex. Also, we would like to thank Fundo Europeu de Desenvolvimento Regional (FEDER) through COMPETE – Programa Operacional Factores de Competitividade (POFC) for co-funding.

References

1. Gouveia IC, Sa D, Henriques M (2012) Functionalization of wool with L-cysteine: process characterization and assessment of antimicrobial activity and cytotoxicity. J Appl Polym Sci 124(2):1352–1358
2. Gouveia IC (2012) Synthesis and characterization of a microsphere-based coating for textiles with potential as an in situ bioactive delivery system. Polym Adv Technol 23(3):350–356
3. Caldeira E et al (2013) Biofunctionalization of cellulosic fibers with L-cysteine: assessment of antibacterial properties and mechanism of action against Staphylococcus aureus and Klebsiellapneumoniae. J Biotechnol 168(4):426–435
4. Nogueira F et al (2014) Covalent modification of cellulosic-based textiles: a new strategy to obtain antimicrobial properties. Biotechnol Bioprocess Eng 19(3):526–533
5. Singh R et al (2005) Antimicrobial activity of some natural dyes. Dyes Pigments 66 (2):99–102
6. Gao Y, Cranston R (2008) Recent advances in antimicrobial treatments of textiles. Text Res J 78(1):60–72
7. Papaspyrides CD, Pavlidou S, Vouyiouka SN (2009) Development of advanced textile materials: natural fiber composites, anti-microbial, and flame-retardant fabrics. Proc Inst of Mech Eng L J Mater Des Appl 223(2):91–102
8. Chang SC et al (2014) Surface coating for flame-retardant behavior of cotton fabric using a continuous layer-by-layer process. Ind Eng Chem Res 53(10):3805–3812
9. Murphy PS, Evans GR (2012) Advances in wound healing: a review of current wound healing products. Plast Surg Int 2012:190436
10. Gowri S et al (2010) Polymer nanocomposites for multifunctional finishing of textiles – a review. Text Res J 80(13):1290–1306
11. MazeyarGashti FA, Song G, Kiumarsi A (2012) Characterization of nanocomposite coating on textiles: a brief review on microscopic technology. Curr Microsc Contrib Adv Sci Technol 2:1424–1437
12. Lee H et al (2008) Substrate-independent layer-by-layer assembly by using mussel-adhesive-inspired polymers. Adv Mater 20(9):1619–1623
13. Decher G, Hong JD, Schmitt J (1992) Buildup of ultrathin multilayer films by a self-assembly process. 3. Consecutively alternating adsorption of anionic and cationic polyelectrolytes on charged surfaces. Thin Solid Films 210(1–2):831–835
14. Decher G (1997) Fuzzy nanoassemblies: toward layered polymeric multicomposites. Science 277(5330):1232–1237
15. Lvov Y et al (1999) A careful examination of the adsorption step in the alternate layer-by-layer assembly of linear polyanion and polycation. Colloids Surf A Physicochem Eng Asp 146(1–3):337–346
16. Pavlukhina S, Sukhishvili S (2011) Polymer assemblies for controlled delivery of bioactive molecules from surfaces. Adv Drug Deliv Rev 63(9):822–836

17. Picart C et al (2001) Determination of structural parameters characterizing thin films by optical methods: a comparison between scanning angle reflectometry and optical waveguide lightmode spectroscopy. J Chem Phys 115(2):1086–1094
18. Li Y, Wang X, Sun JQ (2012) Layer-by-layer assembly for rapid fabrication of thick polymeric films. Chem Soc Rev 41(18):5998–6009
19. Such GK, Johnston APR, Caruso F (2011) Engineered hydrogen-bonded polymer multilayers: from assembly to biomedical applications. Chem Soc Rev 40(1):19–29
20. de Villiers MM et al (2011) Introduction to nanocoatings produced by layer-by-layer (LbL) self-assembly. Adv Drug Deliv Rev 63(9):701–715
21. Caruso F, Caruso RA, Mohwald H (1998) Nanoengineering of inorganic and hybrid hollow spheres by colloidal templating. Science 282(5391):1111–1114
22. Chen W, McCarthy TJ (1997) Layer-by-layer deposition: a tool for polymer surface modification. Macromolecules 30(1):78–86
23. Caruso F et al (2000) Microencapsulation of uncharged low molecular weight organic materials by polyelectrolyte multilayer self-assembly. Langmuir 16(23):8932–8936
24. Wohl BM, Engbersen JFJ (2012) Responsive layer-by-layer materials for drug delivery. J Control Release 158(1):2–14
25. Mano JF et al (2007) Natural origin biodegradable systems in tissue engineering and regenerative medicine: present status and some moving trends. J R Soc Interface 4 (17):999–1030
26. Onda M et al (1996) Sequential actions of glucose oxidase and peroxidase in molecular films assembled by layer-by-layer alternate adsorption. Biotechnol Bioeng 51(2):163–167
27. Onda M et al (1996) Sequential reaction and product separation on molecular films of glucoamylase and glucose oxidase assembled on an ultrafilter. J Ferment Bioeng 82 (5):502–506
28. Lvov Y et al (1996) Molecular film assembly via layer-by-layer adsorption of oppositely charged macromolecules (linear polymer, protein and clay) and concanavalin a and glycogen. Thin Solid Films 284:797–801
29. Caruso F et al (1997) Assembly of alternating polyelectrolyte and protein multilayer films for immunosensing.2. Langmuir 13(13):3427–3433
30. Cai P et al (2013) Adsorbed BMP-2 in polyelectrolyte multilayer films for enhanced early osteogenic differentiation of mesenchymal stem cells. Colloids Surf A Physicochem Eng Asp 434:110–117
31. Divyalakshmi TV et al (2013) Subpicomolar sensing of hydrogen peroxide with ovalbumin-embedded chitosan/polystyrene sulfonate multilayer membrane. Anal Biochem 440 (1):49–55
32. Guillot R et al (2013) The stability of BMP loaded polyelectrolyte multilayer coatings on titanium. Biomaterials 34(23):5737–5746
33. Anandhakumar S, Raichur AM (2013) Polyelectrolyte/silver nanocomposite multilayer films as multifunctional thin film platforms for remote activated protein and drug delivery. Acta Biomater 9(11):8864–8874
34. Ladam G et al (2001) Protein adsorption onto auto-assembled polyelectrolyte films. Langmuir 17(3):878–882
35. Jessel N et al (2003) Bioactive coatings based on a polyelectrolyte multilayer architecture functionalized by embedded proteins. Adv Mater 15(9):692–695
36. Vodouhe C et al (2006) Control of drug accessibility on functional polyelectrolyte multilayer films. Biomaterials 27(22):4149–4156
37. Chluba J et al (2001) Peptide hormone covalently bound to polyelectrolytes and embedded into multilayer architectures conserving full biological activity. Biomacromolecules 2 (3):800–805
38. Caruso F, Schuler C (2000) Enzyme multilayers on colloid particles: assembly, stability, and enzymatic activity. Langmuir 16(24):9595–9603

39. Vodouhe C et al (2005) Effect of functionalization of multilayered polyelectrolyte films on motoneuron growth. Biomaterials 26(5):545–554
40. Tezcaner A et al (2006) Polyelectrolyte multilayer films as substrates for photoreceptor cells. Biomacromolecules 7(1):86–94
41. Leguen E et al (2007) Bioactive coatings based on polyelectrolyte multilayer architectures functionalized by embedded proteins, peptides or drugs. Biomol Eng 24(1):33–41
42. Costa RR, Mano JF (2014) Polyelectrolyte multilayered assemblies in biomedical technologies. Chem Soc Rev 43(10):3453–3479
43. Wang Q, Hauser PJ (2010) Developing a novel UV protection process for cotton based on layer-by-layer self-assembly. Carbohydr Polym 81(2):491–496
44. Iamphaojeen Y, Siriphannon P (2012) Immobilization of zinc oxide nanoparticles on cotton fabrics using poly 4-styrenesulfonic acid polyelectrolyte. Int J Mater Res 103(5):643–647
45. Wang LL et al (2011) Superhydrophobic and ultraviolet-blocking cotton textiles. ACS Appl Mater Interfaces 3(4):1277–1281
46. Zhao Y et al (2010) Superhydrophobic cotton fabric fabricated by electrostatic assembly of silica nanoparticles and its remarkable buoyancy. Appl Surf Sci 256(22):6736–6742
47. Carosio F et al (2013) Green DNA-based flame retardant coatings assembled through layer by layer. Polymer 54(19):5148–5153
48. Carosio F et al (2011) Layer-by-layer assembly of silica-based flame retardant thin film on PET fabric. Polym Degrad Stab 96(5):745–750
49. Li YC et al (2010) Flame retardant behavior of polyelectrolyte-clay thin film assemblies on cotton fabric. ACS Nano 4(6):3325–3337
50. Joshi M et al (2011) Chitosan nanocoating on cotton textile substrate using layer-by-layer self-assembly technique. J Appl Polym Sci 119(5):2793–2799
51. Ali SW, Joshi M, Rajendran S (2011) Novel, self-assembled antimicrobial textile coating containing chitosan nanoparticles. AATCC Rev 11(5):49–55
52. Gomes AP et al (2012) Layer-by-layer deposition of antibacterial polyelectrolytes on cotton fibers. J Polym Environ 20(4):1084–1094
53. Gomes AP et al (2013) Layer-by-layer deposition of antimicrobial polymers on cellulosic fibers: a new strategy to develop bioactive textiles. Polym Adv Technol 24(11):1005–1010
54. Dubas ST, Kumlangdudsana P, Potiyaraj P (2006) Layer-by-layer deposition of antimicrobial silver nanoparticles on textile fibers. Colloids Surf A Physicochem Eng Asp 289 (1–3):105–109
55. Caridade SG et al (2013) Free-standing polyelectrolyte membranes made of chitosan and alginate. Biomacromolecules 14(5):1653–1660
56. Hyde K, Dong H, Hinestroza JP (2007) Effect of surface cationization on the conformal deposition of polyelectrolytes over cotton fibers. Cellulose 14(6):615–623
57. Polowinski S (2005) Polyelectrolyte layer-by-layer processed coated textiles. Fibers Text East Eur 13(6):50–52
58. Dubas ST et al (2006) Assembly of polyelectrolyte multilayers on nylon fibers. J Appl Polym Sci 101(5):3286–3290
59. Polowinski S (2007) Deposition of polymer complex layers onto nonwoven textiles. J Appl Polym Sci 103(3):1700–1705
60. Jantas R, Polowinski S (2007) Modifying of polyester fabric surface with polyelectrolyte nanolayers using the layer-by-layer deposition technique. Fibers Text East Eur 15(2):97–99
61. Polowinski S, Stawski D (2007) Thermogravimetric measurements of poly(propylene) nonwovens containing deposited layers of polyelectrolytes and colloidal particles of noble metals. Fibers Text East Eur 15(4):82–85
62. Stawski D, Bellmann C (2009) Electrokinetic properties of polypropylene textile fabrics containing deposited layers of polyelectrolytes. Colloids Surf A Physicochem Eng Asp 345 (1-3):191–194
63. Park JH et al (2009) Polyelectrolyte multilayer coated nanofibrous mats: controlled surface morphology and cell culture. Fibers Polym 10(4):419–424

64. Martin A et al (2013) Multilayered textile coating based on a beta-cyclodextrin polyelectrolyte for the controlled release of drugs. Carbohydr Polym 93(2):718–730
65. Martin A et al (2013) Build-up of an antimicrobial multilayer coating on a textile support based on a methylene blue-poly(cyclodextrin) complex. Biomed Mater 8(6):065006
66. Hyde K, Rusa M, Hinestroza J (2005) Layer-by-layer deposition of polyelectrolyte nanolayers on natural fibers: cotton. Nanotechnology 16(7):S422–S428
67. Wang Q, Hauser PJ (2009) New characterization of layer-by-layer self-assembly deposition of polyelectrolytes on cotton fabric. Cellulose 16(6):1123–1131
68. Ali SW, Rajendran S, Joshi M (2010) Effect of process parameters on layer-by-layer self-assembly of polyelectrolytes on cotton substrate. Polym Polym Compos 18(5):175–187
69. Zhao Y et al (2013) Superhydrophobic and UV-blocking cotton fabrics prepared by layer-by-layer assembly of organic UV absorber intercalated layered double hydroxides. Appl Surf Sci 286:364–370
70. Ugur SS et al (2010) Modifying of cotton fabric surface with nano-ZnO multilayer films by layer-by-layer deposition method. Nanoscale Res Lett 5(7):1204–1210
71. Zhao Y et al (2012) Photoreactive azido-containing silica nanoparticle/polycation multilayers: durable superhydrophobic coating on cotton fabrics. Langmuir 28(15):6328–6335
72. Apaydin K et al (2013) Polyallylamine-montmorillonite as super flame retardant coating assemblies by layer-by layer deposition on polyamide. Polym Degrad Stab 98(2):627–634
73. Cerkez I (2013) Rapid disinfection by N-halamine polyelectrolytes. J Bioact Compat Polym 28(1):86–96
74. Cerkez I et al (2011) N-halamine biocidal coatings via a layer-by-layer assembly technique. Langmuir 27(7):4091–4097
75. Gomes A, Mano J, Queiroz J, Gouveia I (2010) Assessment of bacteria-textile interactions using scanning electron microscopy: a study on LbL chitosan/alginate coated cotton. In: Méndez-Vilas A, Diaz J (eds) Microscopy: science, technology, applications and education. Formatex, Badajoz, pp 286–292
76. Cady NC, Behnke JL, Strickland AD (2011) Copper-based nanostructured coatings on natural cellulose: nanocomposites exhibiting rapid and efficient inhibition of a multi-drug resistant wound pathogen, A. baumannii, and mammalian cell biocompatibility in vitro. Adv Funct Mater 21(13):2506–2514
77. Sanders W, Anderson MR (2009) Electrostatic deposition of polycations and polyanions onto cysteine monolayers. J Colloid Interface Sci 331(2):318–321
78. Pedrosa VA et al (2007) Studies on the electrochemical behavior of a cystine self-assembled monolayer modified electrode using ferrocyanide as a probe. J Electroanal Chem 602 (2):149–155
79. Martins GV et al (2010) Crosslink effect and albumin adsorption onto chitosan/alginate multilayered systems: an in situ QCM-D study. Macromol Biosci 10(12):1444–1455
80. Gomes AP et al (2014) New biomaterial based on cotton with incorporated biomolecules. J Appl Polym Sci 131(15):40519
81. Wang YC et al (2003) Fabrication of a novel porous PGA-chitosan hybrid matrix for tissue engineering. Biomaterials 24(6):1047–1057
82. Rujitanaroj PO, Pimpha N, Supaphol P (2008) Wound-dressing materials with antibacterial activity from electrospun gelatin fiber mats containing silver nanoparticles. Polymer 49 (21):4723–4732
83. Dong Y et al (2010) A novel CHS/ALG bi-layer composite membrane with sustained antimicrobial efficacy used as wound dressing. Chin Chem Lett 21(8):1011–1014
84. Seo MD et al (2012) Antimicrobial peptides for therapeutic applications: a review. Molecules 17(10):12276–12286
85. Bulet P, Stocklin R, Menin L (2004) Anti-microbial peptides: from invertebrates to vertebrates. Immunol Rev 198:169–184
86. Reddy KVR, Yedery RD, Aranha C (2004) Antimicrobial peptides: premises and promises. Int J Antimicrob Agents 24(6):536–547

87. Brogden NK, Brogden KA (2011) Will new generations of modified antimicrobial peptides improve their potential as pharmaceuticals? Int J Antimicrob Agents 38(3):217–225
88. Costa F et al (2011) Covalent immobilization of antimicrobial peptides (AMPs) onto biomaterial surfaces. Acta Biomater 7(4):1431–1440
89. Maroti G et al (2011) Natural roles of antimicrobial peptides in microbes, plants and animals. Res Microbiol 162(4):363–374
90. Zasloff M (2002) Antimicrobial peptides of multicellular organisms. Nature 415 (6870):389–395
91. Li YM et al (2012) Overview on the recent study of antimicrobial peptides: origins, functions, relative mechanisms and application. Peptides 37(2):207–215
92. Edwards JV et al (1999) Synthesis and activity of NH2- and COOH-terminal elastase recognition sequences on cotton. J Pept Res 54(6):536–543
93. Gouveia IC (2010) Nanobiotechnology: a new strategy to develop non-toxic antimicrobial textiles. In: Méndez-Vilas A (ed) Current research, technology and education topics in applied microbiology and microbial biotechnology. Formatex, Badajoz, pp 407–414
94. da Silva FP, Machado MCC (2012) Antimicrobial peptides: clinical relevance and therapeutic implications. Peptides 36(2):308–314
95. Pedrosa M et al. (2014) Comparison of the antibacterial activity of modified-cotton with magainin I and LL-37 with potential as wound-dressings. J Appl Polym Sci 131(21):40997. doi: 10.1002/app.40997
96. Giuliani A, Pirri G, Nicoletto SF (2007) Antimicrobial peptides: an overview of a promising class of therapeutics. Cent Eur J Biol 2(1):1–33
97. Zhang LJ, Rozek A, Hancock REW (2001) Interaction of cationic antimicrobial peptides with model membranes. J Biol Chem 276(38):35714–35722
98. Harris F, Dennison SR, Phoenix DA (2009) Anionic antimicrobial peptides from eukaryotic organisms. Curr Protein Pept Sci 10(6):585–606
99. Zhang XJ, Clark CA, Pettis GS (2003) Interstrain inhibition in the sweet potato pathogen streptomyces ipomoeae: purification and characterization of a highly specific bacteriocin and cloning of its structural gene. Appl Environ Microbiol 69(4):2201–2208
100. Hassan M et al (2012) Natural antimicrobial peptides from bacteria: characteristics and potential applications to fight against antibiotic resistance. J Appl Microbiol 113(4):723–736
101. Peters BM, Shirtliff ME, Jabra-Rizk MA (2010) Antimicrobial peptides: primeval molecules or future drugs? PLoS Pathog 6(10), e1001067
102. Silva NC, Sarmento B, Pintado M (2013) The importance of antimicrobial peptides and their potential for therapeutic use in ophthalmology. Int J Antimicrob Agents 41(1):5–10
103. Gomes AP, Mano JF, Queiroz JA, Gouveia IC (2015) Incorporation of antimicrobial peptides on functionalized cotton gauzes for medical applications. Carbohydr Polym 127:451–461
104. Shukla A et al (2010) Controlling the release of peptide antimicrobial agents from surfaces. Biomaterials 31(8):2348–2357
105. Sobczak M et al (2013) Polymeric systems of antimicrobial peptides-strategies and potential applications. Molecules 18(11):14122–14137

Adv Polym Sci (2016) 271: 241–286
DOI: 10.1007/12_2015_308

Published online: 18 April 2015

Liquid Crystals of Cellulosics: Fascinating Ordered Structures for the Design of Functional Material Systems

Yoshiyuki Nishio, Junichi Sato, and Kazuki Sugimura

Abstract This article surveys progress in both fundamental and applied research related to cellulosic liquid crystals, mainly of chiral nematic order. These liquid crystals are divided into two different classes, namely cellulosic macromolecules and cellulose nanocrystals (CNCs), depending on the mesogenic constituent. We start with a review of the fundamental and chiroptical characteristics of molecular liquid crystals of representative cellulose derivatives and then discuss recent efforts on the design and construction of functional material systems (such as stimuli-sensitive optical media and novel hybrids with minerals). These systems make use of the liquid crystalline molecular assembly of cellulosics. The survey of the other class of cellulosic liquid crystals deals with colloidal suspensions of CNCs obtained by acid hydrolysis of native cellulose fibers. Following the review of fundamental aspects related to the isotropic–anisotropic phase separation behavior of CNC suspensions, attention is directed to current applications of free-standing colored films, polymer composites reinforced with CNCs as mesofiller, and inorganic hybridizations using CNC chiral nematics as template. Some comments and the outlook for future explorations are also offered.

Keywords Cellulose · Chirality · Composites · Derivatives · Functional materials · Hybrids · Liquid crystal · Nanocrystal · Phase behavior · Polysaccharides

Contents

Y. Nishio (✉), J. Sato, and K. Sugimura
Division of Forest and Biomaterials Science, Graduate School of Agriculture, Kyoto University, Kyoto 606-8502, Japan
e-mail: ynishio@kais.kyoto-u.ac.jp

Abbreviations

(E-CE)C	Ethyl cyanoethyl cellulose
3-CF_3-CTC	Cellulose 3-(trifluoromethyl)phenycarbamate
3-Cl-CPC	Cellulose 3-chlorophenylcarbamate
4-Cl-CPC	Cellulose 4-chlorophenylcarbamate
5FPEC	Pentafluoropropionyl ethyl cellulose
AA	Acetic acid
AEC	Acetyl ethyl cellulose
AGU	Anhydroglucose unit
APC	Acetoxypropyl cellulose
ATBC	Amylose tris(*n*-butylcarbamate)
ATEC	Amylose tris(ethylcarbamate)
ATHC	Amylose tris(*n*-hexylcarbamate)
ATPC	Aamylose triphenylcarbamate
ATRP	Atom transfer radical polymerization
BC	Bacterial cellulose
BEC	Butyryl ethyl cellulose
CD	Circular dichroism
ChtNC	Chitin nanocrystal
CNC	Cellulose nanocrystal (or nanocrystallite)
CPC	Cellulose phenylcarbamate
CTC	Cellulose triphenylcarbamate (or tricarbanilate)
CtsPC	Chitosan phenylcarbamate
DCA	Dichloroacetic acid
DEME	Diethylene glycol monoethyl ether
DEMM	Diethylene glycol monomethyl ether
DMA	Dynamic mechanical analysis
DMAc	*N*,*N*-Dimethylacetamide
DMF	*N*,*N*-Dimethyformamide
DMSO	Dimethyl sulfoxide
DP_s	Degree of polymerization (or polyaddition) in the side chain
DS	Degree of substitution
DS_{acyl}	Degree of acyl substitution
EC	Ethyl cellulose

FTIR	Fourier transform infrared spectroscopy
HAp	Hydroxyapatite
HPC	Hydroxypropyl cellulose
IL	Ionic liquid
IPN	Interpenetrating network
LCST	Lower critical solution temperature
MS	Molar substitution
ORD	Optical rotatory dispersion
P	Chiral nematic (or cholesteric) pitch
PAA	Poly(acrylic acid)
PEC	Propionyl ethyl cellulose
PEDOT	Poly(3,4-ethylenedioxythiophene)
PEG	Poly(ethylene glycol)
PEO	Poly(ethylene oxide)
PHEMA	Poly(2-hydroxyethyl methacrylate)
POM	Polarized optical microscope
PVP	Poly(*N*-vinyl pyrrolidone)
SEM	Scanning electron microscope
T_c	Cloud point
TEM	Transmission electron microscope
TEMPO	2,2,6,6-Tetramethylpiperidine-1-oxyl
TEOS	Tetraethyl orthosilicate (or Tetraethoxysilane)
T_g	Glass transition temperature
THF	Terahydrofuran
T_i	Isotropization temperature
TMOS	Tetramethl orthosilicate (or Tetramethoxysilane)
TRIMM	Triethylene glycol monomethyl ether
WAXD	Wide angle X-ray diffraction
λ_M	Wavelength of maximum light reflectance

1 Introduction

Earnest research on cellulose-based liquid crystals started in 1976 when Werbowyi and Gray found a clear liquid crystallinity of hydroxypropyl cellulose in concentrated solutions in water [1]. Since then, it has been revealed by a number of investigations that many cellulosic polymers are capable of forming an optically anisotropic mesophase in a condensed fluid state (including a melt), most probably as a result of the inherent semirigidity of the carbohydrate backbone of β(1→4)-linked glucans. The general features of the mesomorphic states and ensuing optical or chiroptical behavior of cellulosics have been well described by several reviews [2–8] published in the middle of the 1990s. The supramolecular structure in the mesophase is usually "cholesteric," or "chiral nematic" as synonym (see Fig. 1),

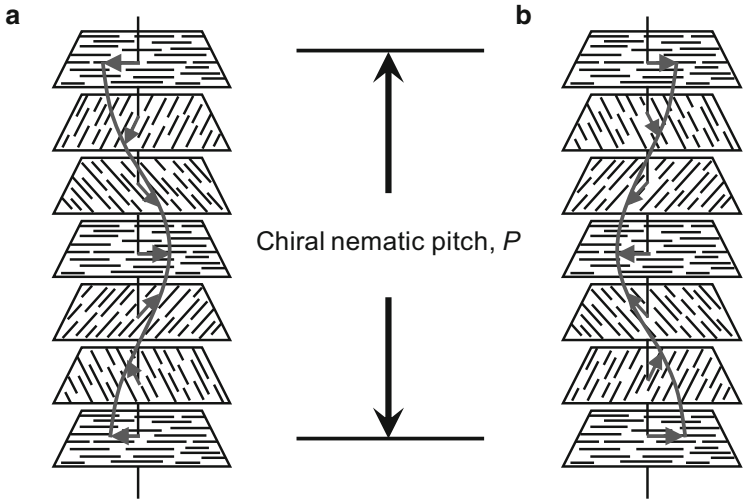

Fig. 1 Illustration showing chiral nematic mesophases with helicoidal pitch *P*: (**a**) *left-handed* and (**b**) *right-handed* helical twisting arrangements of nematic layer stack

with possible exceptions such as a columnar phase claimed for thermotropic cellulose trialkanoates [5, 6].

As indicated in Fig. 1, the chiral nematic phase is characterized by the director of nematic orientation, which propagates rotationally along one direction to form a helical arrangement of pitch *P*; therefore, this structure can be taken as a distorted form of the nematic phase of $P = \infty$ [9]. Liquid crystalline molecules that prefer this type of assembly are all chiral, each different from its mirror image, and are readily exemplified by nonracemic polypeptides and cholesterol esters. Molecular chains of polypeptides can assume an α-helical conformation to form a rigid rod. The mesogenic nucleus of cholesterol derivatives is a steroid ring system with a nonplanar structure; however, the annular sequence is rigid and forms a twisted rod (see, for instance, figure 1.8 in [9]). In contrast to these representatives, the molecular secondary structure of liquid crystalline cellulosics in fluid media seems not to be firmly established, as yet, because of the lack of clear observation linking directly to an asymmetry of the cellulosic molecules. However, judging from supporting evidence from computational and experimental work that points to molecular asymmetry, it seems natural to accept the existence of a helical or twisted conformation in the molecular chains [2].

In the chiral nematic cellulose derivatives, the pitch *P* (including the magnitude and the helix direction of rotation) should depend on a large number of factors such as the side chain structure (linkage and length), degree of substitution (DS), temperature, solvent nature, and solvent concentration (for lyotropic systems). The large number of factors affecting *P* reflects the diversity of chemical modifications of cellulose and its high side group reactivity. Thus, compared with other liquid crystalline polymer substances, cellulosic systems seem to be somewhat

intractable and challenging for a detailed structural elucidation. However, from a practical standpoint, it follows that many opportunities exist for the design and fabrication of new materials based on cellulosic polymers by using their respective mesomorphic order [10].

Meanwhile, although different to macromolecular cellulosics, the fragmented microfibrils of fibrous celluloses (i.e., cellulose nanocrystallites or nanocrystals, typically of ~100 nm length and ~5 nm width) also assume a self-assembling character and form liquid crystals in aqueous suspensions [2, 3, 11–13]. Somewhat surprisingly, the resulting mesophase is again of a chiral nematic type, as first reported by Revol et al. in 1992 [11]. The rodlike cellulose nanocrystal (CNCs) are conventionally obtained by hydrolysis with sulfuric acid of native cellulose fibers (e.g., cotton or wood pulp), resulting in CNC surfaces that are sulfated. In water, therefore, the CNC particles are negatively charged by sulfate half-esters and show adequate dispersion, yielding a stable colloidal suspension. With a small increase in CNC concentration, typically to 3–5 wt%, the visually homogeneous suspension phase-separates into an isotropic upper phase and an anisotropic lower phase in the course of quiescent standing of the sample. The anisotropic phase is birefringent and exhibits a fingerprint pattern under a polarized optical microscope. This pattern is characteristic of a chiral nematic mesophase of relatively long helical pitch.

The phase behavior stated above is in qualitative accordance with the anisotropic–isotropic phase separation of rodlike particles predicted by Onsager [14] and also by Flory [15]. Thus, the primary driving force for mesophase formation is undoubtedly the rigid rod shape of the CNC particles. It should be stressed, however, that the stability of such CNC suspensions is greatly influenced by the surface charge of the CNC rods, and some appropriate modifications of their surface can also change the anisotropic–isotropic phase equilibrium condition of the suspensions. Such modifications include addition of electrolytes and surface grafting, in addition to the standard control of sulfate charge density in the purification process after acid hydrolysis [12, 13, 16, 17]. The effective dimensions and aspect ratios of the CNC rods can be varied according to the chemical treatment used. The chiral stacking of CNCs in the mesophase can be ascribed to a certain twisted habit in the dispersoid unit. Nevertheless, problems still remain unresolved: What is the origin of the structural asymmetry of CNC rods themselves? Does the distribution of charges or other modifiers on CNC surfaces contribute to the chiral asymmetry? [12].

CNCs are rod-shaped fragments of highly crystalline microfibrils extracted from cellulose fibers that excel in tensile mechanical strength. Therefore, as demonstrated [18] early on, CNCs can work as a stiff nanofiller to effectively reinforce bulk matrices of other polymers. In view of the liquid crystallinity of CNCs, their use as reinforcing agent is promising, because they are able to behave in an ordered assemblage under external force fields (as shown by their behavior under a magnetic field [19]). Furthermore, the chiral nematic architecture of CNCs can be carried over into the solid materials, usually as a film [13] or as solids (including composites with other polymeric or inorganic components [12]). This also applies to the case of molecular liquid crystals of cellulose derivatives [10].

The present article describes the up-to-date strategies available for the design and fabrication of novel cellulosic-based materials displaying high functionality or performance, mainly derived from their mesomorphic characteristics. In connection with this, the review covers recent progress in basic studies of the structure and properties of cellulosic chiral nematics, with the description divided according to the two different assembly scales, namely polymeric molecules and CNCs. Reference studies and preliminary observations for related polysaccharides are also cited.

2 Molecular Liquid Crystals of Cellulosics

2.1 Fundamental Aspects

Figure 2 shows structural formulae of representative liquid crystalline cellulose derivatives: hydroxypropyl cellulose (HPC), ethyl cellulose (EC), and cellulose phenylcarbamate (CPC). These derivatives are industrially well-established cellulosic products and are also often employed in research concerning liquid crystalline materials. An important structural parameter, in addition to molecular weight, that characterizes these derivatives is the degree of substitution (DS) of the side chain group. It is defined as the average number of substituted hydroxyls per anhydroglucose unit (AGU). If a repeatable chain growth is considered for the respective substituents, the secondary molar substitution (MS) is defined as the average number of substituent groups introduced per AGU; this is the case for HPC and, strictly, the same holds for CPC. Highly substituted HPC, EC, and CPC (usually with DS = 2–3 and MS > 3 for HPC) form chiral nematic mesophases (Fig. 1) in good solvents and at concentrations typically exceeding ~40 wt% (~0.35 in volume fraction).

For liquid crystalline cellulose derivatives, the so-called persistence length (q), which is an index related to the stiffness of polymer chains, is estimated to be about 6–12 nm [20–22]. This is considerably smaller than the corresponding data for other liquid crystalline polymers [e.g., q = ~37 nm for poly(*n*-hexyl isocyanate) in toluene at 25°C and q = ~150 nm for α-helical poly(γ-benzyl-L-glutamate) in *N*,

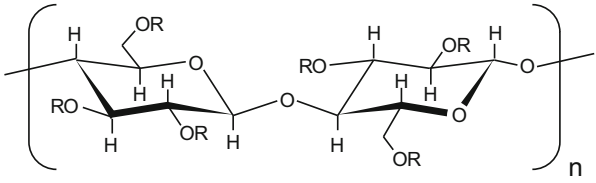

(a) HPC: R = H or CH_2-CH(CH_3)OR

(b) EC : R = H or CH_2CH_3

(c) CPC: R = H or CONR-C_6H_5

Fig. 2 Structural formulae of representative liquid crystalline cellulose derivatives: (*a*) hydroxypropyl cellulose (HPC), (*b*) ethyl cellulose (EC), and (*c*) cellulose phenylcarbamate (CPC)

N-dimethyformamide (DMF)] [22]. The moderate degree of chain stiffness of cellulose derivatives is responsible for the requirement for such a high polymer concentration for mesophase formation in lyotropic systems. If the semirigid cellulosic molecules are depicted in terms of a Kuhn chain composed of freely jointed rods of length $l_K = 2q$ and diameter a, the critical volume fraction V_p^* for incipient mesophase appearance can be approximated by the following Flory formulation [20]:

$$V_p^* \approx (8/x)(1 - 2/x) \tag{1}$$

with

$$x = l_K/a \tag{2}$$

where x is an aspect ratio of the rod segment. The diameter a can be calculated from a solid geometry, assuming the chain segment to be cylindrical in shape; roughly, $a = \sim 1.1$ nm for HPC, ~0.9 nm for EC, and ~1.3 nm for CPC, but their specific volumes are all taken to be nearly equal to 0.80 $cm^3\ g^{-1}$. For instance, taking $l_K = 20$ nm and $a = 1.1$ nm for HPC, one obtains $V_p^* = 0.39$ from Eq. (1). Thus, the semiquantitative estimate seems to be in good agreement with commonly observed data.

Regarding the molecular liquid crystal features of cellulose, in the 1980s some investigators observed the lyotropic mesophase in a few cellulose solutions, using solvent systems such as *N*-methylmorpholine-*N*-oxide/water, trifluoroacetic acid/chlorinated alkane, ammonium thiocyanate (NH_4SCN)/liquid ammonia, and LiCl/*N*,*N*-dimethylacetamide (DMAc) [2, 8]. In most cases, however, a stable, pure anisotropic solution of unmodified cellulose molecules was not obtained because of limited solubility at high concentrations (>15 wt%). Some factors that might have prevented precise determination of the nature of the observed mesophases include degradation, derivatization, and agglomeration or complex formation in the cellulose dissolution process. In 2002, Swatloski et al. [23] reported that several ionic liquids (ILs) can act as direct solvents for chemically unmodified cellulose and, especially, that the use of 1-butyl-3-methylimidazolium chloride led to a viscous cellulose solution displaying optical birefringence at polymer concentrations of more than 10 wt%; however, detailed characterization of the anisotropic phase has not been made available. In 2011, it was reported that cellulose forms a molecular liquid crystalline phase in 1-ethy-3-methyimidazolium acetate solutions of >10 wt% concentration, whereas a critical gelation point was detected at a concentration slightly higher (by ~2 wt%) than the anisotropic phase transition point [24].

Of interest in liquid crystals obtained from cellulose derivatives are the optical characteristics related to the helicoidal supermolecular structure constructing the chiral mesophases, as schematically shown in Fig. 1. For example, the liquid crystals often exhibit beautiful colors of reflective light, whose wavelength is

correlated with the pitch P. The wavelength λ_M giving a maximal intensity in normal reflection can be connected to P by the de Vries equation [25]:

$$\lambda_M = \tilde{n}P \tag{3}$$

where $\tilde{n}$ is the average refractive index of the mesophase. In such light reflection, there is another selectivity, which is associated with polarization of the reflective light. The left-handed chiral nematic mesophase (Fig. 1a) reflects left-handed circularly polarized light, whereas the right-handed chiral nematic mesophase (Fig. 1b) reflects right-handed circularly polarized light. Such an effect can be distinguished by circular dichroism (CD) or optical rotatory dispersion (ORD) spectrophotometry.

A few structural parameters, besides P, that characterize chiral nematic supramolecular assemblies are described in Fig. 3. As depicted in Fig. 3a, d denotes the normal distance between adjacent nematic layers stacking in the mesophase; φ is the twist angle, defined as the azimuth difference between adjacent nematic directors; and φ/d (equal to $360°/P$) expresses the twisting power of the chiral mesophase. The angle φ is usually small ($<360° \times 10^{-2}$), and the short-range distance d can be determined in practice by wide angle X-ray diffractometry (WAXD), in terms of a pseudo-hexagonal packing of molecular chains, as depicted in Fig. 3b. Figure 3c illustrates changing pitch P as a result of variation in the twist angle φ, in terms of a threaded rod model [26] for a twisting molecule of cellulose derivative [27].

An excellent review by Zugenmaier [8] lists many cellulose derivatives that form a chiral nematic mesophase and describes the dependence of P on various factors such as temperature, solvent, concentration, molecular mass, and additional substitution of the derivatives. The next section (Sect. 2.2) is a complementary review and deals with the optical or chiroptical properties deriving from the helical periodicity of chiral nematic liquid crystals, with reference to recent studies employing mostly HPC, EC, CPC, and their modified derivatives as well as related molecules. Section 2.3 is concerned with the design and construction of functional material systems by making use of the liquid crystalline assemblies of cellulose derivatives.

2.2 *Optical and Chiroptical Properties of Chiral Nematics*

2.2.1 HPC-Core Mesomorphic Systems

(a) **Typical Lyotropics**. In solution and with a variety of conventional solvents, HPC forms a chiral nematic mesophase usually in a right-handed helicoidal fashion (Fig. 1b). Of particular significance is the fact that water as a typical lyotropic medium readily provides a diversity of ionic media by dissociating various electrolytes (acid, base, and salt compounds). A phase diagram of the

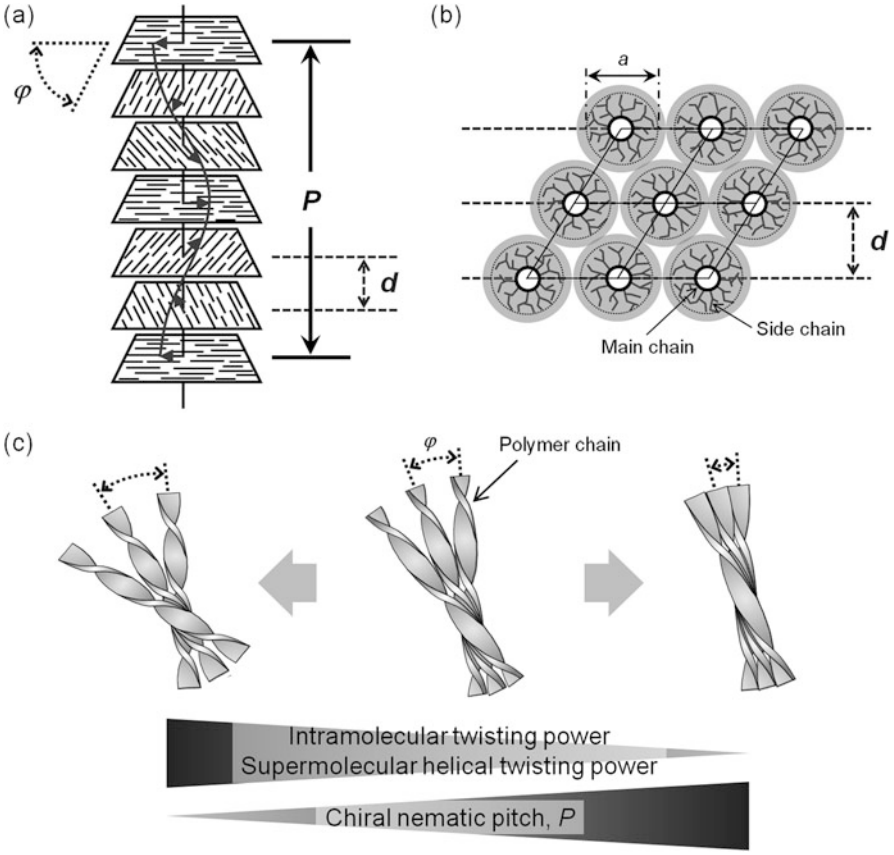

Fig. 3 Structural models and parameters for characterizing the chiral nematic arrangement of pitch P: (*a*) definition of the nematic layer spacing d and twist angle φ; these satisfy a relation $\varphi/d = 360°/P$; (*b*) pseudo-hexagonal packing of molecular chains of diameter a, tolerated as a short-range order of the mesophase; (*c*) changing manner of P with variation in the angle φ between adjacent nematic directors, in terms of a threaded rod model [26] for a twisting molecule of cellulose derivative [27]

HPC/water system has been established as a function of composition and temperature [28, 29]. In brief, at HPC concentrations of $\geq$45 wt%, the polymer solution is optically anisotropic and, particularly at 50–70 wt%, has a vivid color because of the selective reflection of visible light with a wavelength comparable to P (see Eq. 3). This pitch P decreases with increasing polymer concentration and with decreasing temperature. The binary system also shows a unique phase-separation behavior with a lower critical solution temperature (LCST). The so-called cloud point (T_c) is situated around 40°C for isotropic HPC solutions ($\leq$40 wt%) and it is reduced at higher HPC concentrations, giving mesophase formation.

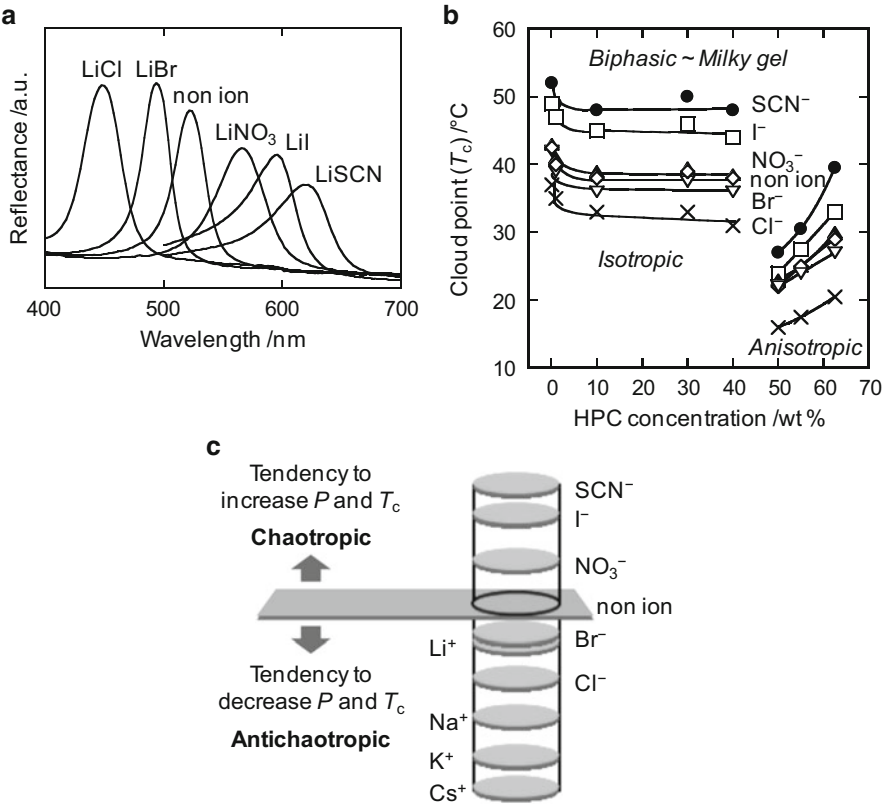

Fig. 4 Addition effects of alkali-metallic salts on the HPC/water lyotropic system: (**a**) selective light-reflection spectra for a lithium salt-containing series (HPC concentration 62.5 wt%; salt concentration 0.5 M; temperature 22°C); (**b**) plots of cloud point (T_c) versus polymer concentration, representing a phase diagram, for the HPC lyotropic series containing 0.5 M lithium salt; (**c**) ranking of the relative effectiveness of various inorganic ions in altering the chiral nematic pitch P and cloud point T_c of aqueous HPC lyotropics. The total effect of a given salt on P or T_c obeys the algebraic addition of the respective effects of the constituent ions (reproduced from Nishio et al. [30])

The periodicity of the chiral mesophase and LCST-type phase boundary, and the ensuing optical properties of the HPC/water lyotropic system, are significantly affected by addition of a third component, such as a small amount of inorganic neutral salts [30] or ILs such as imidazolium salts [31]. For instance, when LiCl is dissolved in the lyotropic system, the wavelength of selective reflection (λ_M) shifts to the blue region and T_c decreases. In contrast, the presence of LiSCN results in a red shift in λ_M and an elevation in T_c (see Fig. 4a, b). As a universal rule, the optical quantity λ_M and T_c (and therefore the pitch P and the phase-separation temperature) vary systematically with a change in the specific chaotropic strength of the ions constituting the salt additive. Figure 4c illustrates the rank order of the chaotropic/antichaotropic

potential of various ions of alkali-metallic halides. Generally, an increase in the ionic chaotropicity tends to disrupt the hydrophobic interaction of the side chains of water-soluble polymers. Regarding the effect of salt on the HPC mesophase, it is inferred that salt addition subtly alters the conformational state of the molecular chain and, as a consequence, induces a marked change in twisting power ($2\pi P^{-1}$) of the chiral stack of nematic layers [30]. Using the model shown in Fig. 3c, we find that a small change in the degree of twisting habit of the cellulose derivative molecule gives rise to a large variation in P.

In the case where ILs of N-alkyl-substituted methylimidazolium salts [CnMim][X] (Fig. 5a, b) are employed as additives in aqueous HPC lyotropics, particular attention should be paid to the amphiphilic structure and possible surfactant-like action of the organo-cation moiety CnMim$^+$ [31]. In mesophase formation at $\geq$50 wt% HPC, the helicoidal pitch P shifts upward according to the chaotropic strength of X^- of the added IL (e.g., in a manner satisfying the order $Cl^- < Br^- < NO_3^- < I^-$) if the salt is well dissociated. The organo-cations generally raise P relative to the nonionic reference, with effectiveness according to the N-alkyl chain length, that is, C2Mim$^+$ < C4Mim$^+$ < C6Mim$^+$ (Fig. 6a). In spite of their specific volume,

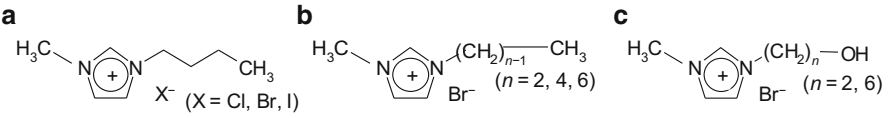

Fig. 5 Examples of N-alkyl-substituted methylimidazolium salts: (**a**) [C4Mim][X]; (**b**) [CnMim][Br]; (**c**) [CnOHMim][Br]

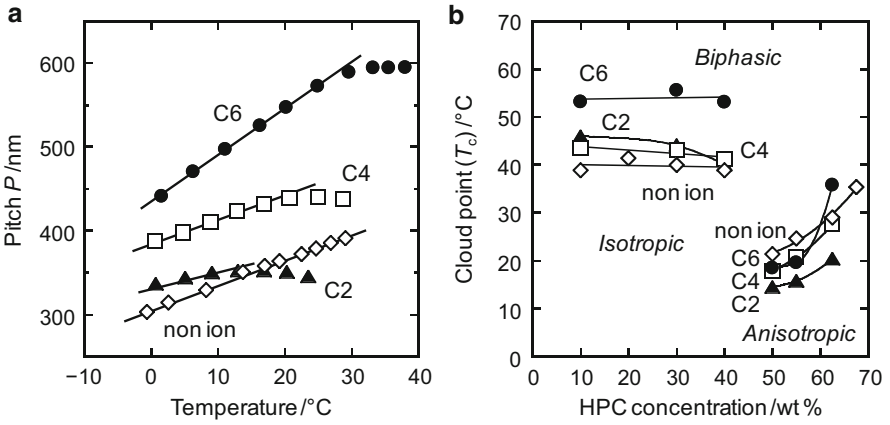

Fig. 6 Effect of the addition of imidazolium salts on the HPC/water lyotropic system (salt concentration 2.5×10^{-4} mol/g HPCaq): (**a**) plots of P versus temperature [CnMim][Br]-containing series (at 62.5 wt% HPC); (**b**) plots of T_c versus HPC concentration for [CnMim][Br]-containing series. Using [C6OHMim][Br] instead of [C6Mim][Br] as additive, the observed T_c closely approaches the data points for the salt-free system, in both the isotropic region and the anisotropic region of the diagram (quoted from Chiba et al. [31])

any of the added ILs cause only a small expansion of the nematic layer spacing (d) in the mesophase, as estimated by WAXD. Therefore, the rise in P with increasing carbon number n is principally a result of the reduced twist angle φ in the nematic layer stack (see Fig. 4a). The *N*-alkyl substituents seem to merge into the hydrophobic side chain region of each oriented HPC molecule. If the well-balanced amphiphilic nature of C*n*Mim$^+$ is quenched by OH attachment to the *N*-alkyl terminal (Fig. 5c), the *P*-elevating effect is seriously suppressed.

With regard to LCST behavior, imidazolium additives of the [C*n*Mim][X] type raise the cloud point T_c in isotropic solutions of $\leq$40 wt% HPC, whereas the T_c of a mesomorphic solution is lowered by the addition (Fig. 6b) [31]. In the isotropic region, the surfactant-like action of the organo-cations on HPC molecules works as a T_c-elevating factor, because of the gain in electrostatic stability of the solute polymer. In anisotropic, condensed HPC solutions, however, self-aggregation of imidazolium salts might be partly possible in the nondissociated form, but with coupled water molecules. This should operate as a T_c-depressing factor, heightening the hydrophobic character of the HPC solute. Thus, the [C*n*Mim][X]-containing aqueous HPC lyotropic system is equilibrated under the multiple effects of mutually competitive electrostatic and hydrophobic factors involving organo-cations and the additional chaotropic effect of isolated anions.

The use of ILs as a single solvent directly dissolving HPC could also be possible. In fact, HPC is solubilized in some imidazolium salts, as shown in Fig. 5. However, as yet, the appearance of a homogeneously anisotropic fluid of HPC/IL has not been observed. Usually, gelation comes before mesophase formation. In a rheological study of HPC in 1-butyl-3-methyimidazolium acetate ([C4Mim][CH_3COO]) [32], an anisotropic phase was observed at a concentration of ~7 wt%, which, nevertheless, was preceded by sol–gel transition at 6 wt%. The anionic counterpart [X] is the key to acquiring a real mesophase in an IL.

(b) **Typical Thermotropics**. Acetoxypropyl cellulose (APC) prepared by acetylating HPC was first reported by a Canadian group to be a thermotropic cellulose derivative that displays iridescent colors over a range of temperatures (ca. 85–125°C as for APC) [33]. Subsequently, the same group indicated that several ethers and esters of HPC obtained by etherifying or esterifying the hydroxyl groups of HPC can form stable chiral nematic phases (typically with a right-handed twisted), some of which imparted reflection colors at ambient temperatures [3, 4]. In the 2000s, a few efforts on thermotropic behavior were conducted for longer alkyl esters [34, 35] and ethers [36] of HPC (see Scheme 1).

Yamagishi et al. [36] prepared butyl ether (C4-*O*-PC), pentyl ether (C5-*O*-PC), and butyl/pentyl mixed ether (C4/C5-*O*-PC) derivatives of HPC at DS $\approx$ 3 (for the newly introduced substituent) and examined the temperature dependence of the pitch P of their chiral nematic thermotropics. All the thermotropics indicated a positive dependence of P with increasing

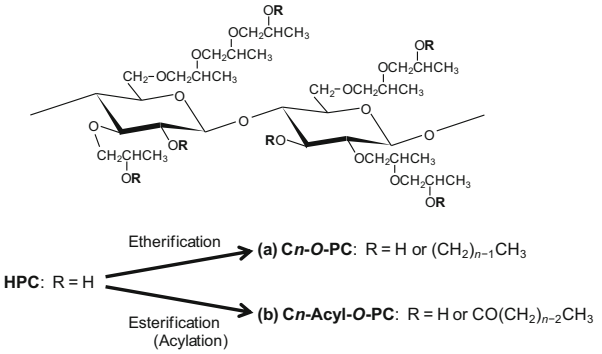

Scheme 1 Derivatives of HPC: (*a*) alkyl ethers, HPC-*O*-$(CH_2)_{n-1}CH_3$ (abbreviated as C*n*-*O*-PC); (*b*) alkyl esters (normal acylates), HPC-*O*-CO$(CH_2)_{n-2}CH_3$ (abbreviated as C*n*-Acyl-*O*-PC)

temperature. The thermal range involving cholesteric coloration shifted systematically upwards with an increasing proportion of butyl in the side chain (i.e., from 20–70°C observed for C5-*O*-PC to 80–120°C for C4-*O*-PC). These temperature ranges are lower than that observed for ethoxypropyl cellulose (C2-*O*-PC), namely 130–160°C [37]. It follows, therefore, that C*n*-*O*-PC of larger n forms a chiral mesophase of longer P for a given temperature.

Hou et al. [35] prepared a series of alkyl esters of HPC, C*n*-Acyl-*O*-PC ($n = 2$–7, 10) of DS = 2.6–2.7. The ester derivatives showed a definite chiral nematic mesophase between their glass transition (T_g) and isotropization (T_i) temperatures ($T_g = -10$°C and $T_i = 162$°C for $n = 2$; $T_g = -63$°C and $T_i = 89$°C for $n = 10$). As the methylene unit number n increased, the pitch P increased at a constant temperature. This elevation in P was a result of both an increase in the nematic layer spacing d and a decrease in the twist angle φ (see Fig. 3a). In the thermotropics of C4-Acyl-*O*-PC of different DS (ranging from 2.20 to 2.96 [34]), P decreased with increasing DS at room temperature; the layer spacing d was almost constant, whereas the twist angle φ increased. These HPC ether/ester series can serve as media for a color display or light reflection system and their usage can be adapted to various temperature conditions in the −60 to 160°C range.

2.2.2 EC-Core Mesomorphic Systems

Commercially available EC (typically, $DS_{ethyl} = 2.5$) forms chiral nematic mesophases in some organic solvents such as chloroform ($CHCl_3$), acetic acid (AA), and dichloacetic acid (DCA). The helicoidal supermolecular structure is left-handed in $CHCl_3$ and AA, and right-handed in DCA [2, 8]. Acyl ethyl cellulose (Acyl EC) obtained by acylation of the residual hydroxyl groups of EC shows a unique mesomorphic behavior; the chiroptical property of the formed mesophase is strongly influenced by the degree of acyl substitution (DS_{acyl}) and the solvent. In the lyotropics of acetyl ethyl cellulose (AEC) in $CHCl_3$ and AA, the twisting power $2\pi P^{-1}$ of the chiral nematic mesophase decreases (the absolute value of P increases) with increasing acetyl content, and the originally left-handed

helicoidal structure changes into a right-handed arrangement above a certain value of DS_{acyl}. The observed value of this critical DS_{acyl} (DS_{acyl}*) is ~0.19 in $CHCl_3$ and ~0.37 in AA [38, 39]. On the other hand, AEC mesophases in DCA assume a right-handed helical twisting, regardless of the acetyl content [39]. These effects of acylation affecting EC mesophases vary according to the type of acyl group employed.

For lyotropics of propionyl ethyl cellulose (PEC) and hexanoyl ethyl cellulose in $CHCl_3$, an optical study [40] suggested that the specific DS_{acyl}* for the handedness inversion of their chiral nematic mesophases appeared to be considerably lower (~0.1) than that observed for the AEC/$CHCl_3$ system (~0.19). However, such estimation may have been based on poor CD data for a few samples. In a supplementary work on PEC and butyryl ethyl cellulose (BEC) lyotropics [41], such an inversion in handedness of their respective chiral nematic phases was detected at a relatively higher value of DS_{acyl} compared with the case of AEC lyotropics, both in $CHCl_3$ and in AA. As listed in Table 1, DS_{acyl}* increased with increasing alkyl chain length (acetyl < propionyl < butyryl) of the acyl substituent. Possibly, the gain in chain flexibility and/or van der Waals intermolecular interactions, accompanied by an increase in the length of the alkyl side chain, could prevent the elevation in pitch of the Acyl EC mesophases with increasing DS_{acyl}. In connection with this, the use of a pentafluoropropionyl (5FP) group as the modifier of EC resulted in a noticeable decrease in DS_{acyl}* for mesomorphic solutions of pentafluoropropionyl ethyl cellulose (5FPEC) in $CHCl_3$ and AA, compared with the corresponding series of PEC and even that of AEC (Table 1) [42]. This is probably because the 5FP substituent is relatively rigid and has a much weaker cohesive energy as a result of the strong electronegativity of fluorine atoms. Additional attention should be directed to the fact that the DS_{acyl}* values obtained for $CHCl_3$ solutions were appreciably lower than those for AA solutions. Furthermore, in DCA, any acylated EC formed right-handed chiral nematic phases without giving $DS_{acyl}^* > 0$ (expediently, $DS_{acyl}^* < 0$). In a general trend, therefore, the

Table 1 Twist-handedness of the chiral nematic helicoidal structure and the critical degree of acylation (DS_{acyl}*) for the handedness inversion observed for lyotropic liquid crystals[a] of various acyl derivatives of EC in $CHCl_3$, AA, and DCA

Solvent		EC	AEC[b]	PEC	BEC	5FPEC
$CHCl_3$	DS_{acyl}*	–	~0.19[c]	0.20–0.26[d]	0.27–0.34[d]	<0.12[d]
	Handedness	L	L → R	L → R	L → R	L → R
AA	DS_{acyl}*	–	~0.37[c]	0.40–0.44[c]	0.45–0.50[c]	0.33–0.34[c]
	Handedness	L	L → R	L → R	L → R	L → R
DCA	DS_{acyl}*	–	×	×	×	×
	Handedness	R	R	R	R	R

Notations: *L* left-handed, *R* right-handed, × not observed
[a]Polymer concentration 40 wt% in $CHCl_3$, 50 wt% in AA, and 30 wt% in DCA
[b]Quoted from [38, 39]
[c]Data at 20°C
[d]Data at 5°C (at 20°C, DS_{acyl}* assumes larger values, e.g., 0.26–0.30 for PEC)

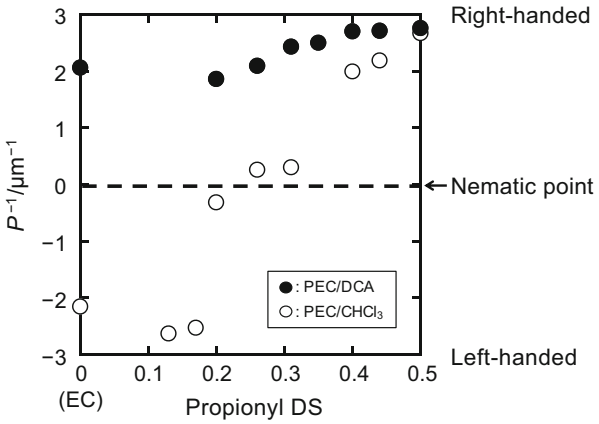

Fig. 7 Reciprocal pitch (P^{-1}) as a function of propionyl DS for chiral nematic liquid crystalline solutions of 40 wt% PEC/$CHCl_3$ (5°C) and 30 wt% PEC/DCA (20°C). Positive and negative values of P^{-1} correspond to the right-handed and left-handed helical twist, respectively. When the measurement temperature is raised, the location of the data points shifts downward (based on data from Nada et al. [41])

higher polar covalent bonds originating from the larger electronegativity of halogens (regardless of whether the atoms are in the acyl substituent or in the solvent for EC) could contribute to the lowering of DS_{acyl}*for handedness inversion of the chiral mesophase.

In Fig. 7, values of the reciprocal pitch (P^{-1}) are plotted as a function of propionyl DS for 40 wt% PEC/$CHCl_3$ and 30 wt% PEC/DCA lyotropics; the pitch P here is taken to be a pseudo-scalar that is assumed to be, respectively, positive or negative for right-handed or left-handed helical chiral nematics. It is observed for both lyotropic systems that P^{-1} substantially increases with increasing propionyl DS, regardless of the handedness. This was also the case for lyotropics of the other pairs of Acyl EC (AEC [38, 39], PEC [41], BEC [41], or 5FPEC [42])/organic solvent ($CHCl_3$, AA, or DCA). As a general rule, it can be said that the increase in DS_{acyl} reinforces a "right-handed twisting power" in each lyotropic series of the respective acyl derivatives of EC.

The EC/$CHCl_3$ and EC/AA chiral nematics (left-handed) show a negative temperature dependence of the pitch (the absolute value of P decreases with increasing temperature) [2, 8, 38], whereas the EC/DCA chiral nematics (right-handed) show a positive temperature dependence of the pitch (P increases with temperature) [39]. Regarding the lyotropics of AEC [38, 39] and those of the EC acylates, PEC, BEC, and 5FPEC [41, 42] in $CHCl_3$ and AA, the pitch of the left-handed helicoidal structure formed in the range $DS_{acyl} < DS_{acyl}$* decreases with temperature, whereas the pitch of the right-handed helicoidal structure ($DS_{acyl} > DS_{acyl}$*) increases with temperature. In DCA, these EC derivatives form right-handed chiral nematics, indicative of a positive temperature dependence of the pitch, irrespective of DS_{acyl}. To summarize, it can be assumed that a

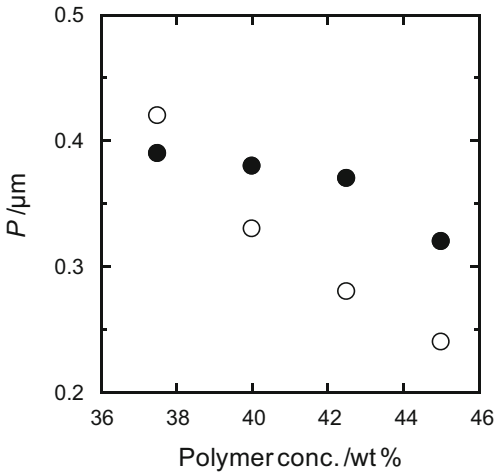

Fig. 8 Concentration dependence of pitch (P) for PEC/$CHCl_3$ chiral nematic liquid crystals (5°C): *open circles*, data for the left-handed series of propionyl DS = 0.13; *filled circles*, data for the right-handed series of propionyl DS = 0.50 (based on data from Nada et al. [41])

temperature elevation generally strengthens a "left-handed twisting power" in each lyotropic series of the acyl derivatives of EC.

All the chiral nematics of EC and its derivatives mentioned above show a negative concentration dependence of the pitch (P decreases with increasing concentration), regardless of the twist handedness. This correlation seems to be a natural phenomenon, taking into consideration the increase in relative density of the solute polymer in the mesophase. However, caution should be exercised in this interpretation because the opposite case (i.e., positive correlation) is actually known, for instance, for a lyotropic system of cellulose triphenylcarbamate/diethylene gycol monoethyl ether [7, 8]. Here, it is interesting that the concentration dependence of P for left-handed chiral nematics is larger than that for right-handed nematics. This is exemplified by the PEC/$CHCl_3$ system in Fig. 8, where P of the left-handed series (propionyl DS = 0.13) varies with polymer concentration more markedly than that of the right-handed series (propionyl DS = 0.50). Essentially the same result is reported for the former AEC/$CHCl_3$ system [43].

2.2.3 CPC-Core Mesomorphic Systems

(a) **CTC Lyotropics**. Zugenmaier organized a large number of studies of the helicoidal pitch and chiroptical properties of chiral nematic mesophases formed by cellulose carbamates, mostly triphenylcarbamate (CTC) or slightly altered compounds thereof, in various glycols and related solvents [7, 8, 44]. The temperature and concentration gradients of the pitch, and the twist handedness, were tabulated for each pair of phenylcarbamate/solvent explored. A small difference in chemical modification of the aromatic substituent strongly influences the solubility in solvents and the chiral nematic twist of the liquid crystalline phenylcarbamate derivatives. To mention only a few

characteristics: Both CTC and cellulose tri(4-chrolophenyl)carbamate (4Cl-CTC) form a left-handed mesophase in diethylene (or triethylene) glycol monomethyl ether (DEMM or TRIMM), whereas cellulose tri (3-chrolophenyl)carbamate (3Cl-CTC) in the same solvents forms a right-handed mesophase. In a ternary system of CTC/3Cl-CTC/TRIMM, phase separation can occur, as indicated by spectrophotometric studies showing two discrete pitches in the vicinity of the 1:1 polymer mixture condition. However, the CTC-3-Cl-CTC copolymer in TRIMM forms essentially a single chiral nematic mesophase; the handedness is right for 3-chlorophenylcarbamate group-rich compositions and left for phenylcarbamate group-rich compositions, and their random distribution at a 1:1 ratio leads to a balanced structure of $P^{-1} = 0$.

(b) **Chitinous Phenylcarbamate Lyotropics**. Chitin and chitosan are widely distributed in crusts of marine crustaceans as well as in exoskeletons of many species of insects. These polysaccharides are structurally similar to cellulose. Chitin consists of 2-acetamido-2-deoxy-β-D-glucose units linked together through a $\beta(1\rightarrow4)$ linkage, and chitosan is an *N*-deacetylated derivative of chitin. In contrast to the situation for cellulose derivatives, there have been only a limited number of studies of the liquid crystalline behavior of chitin or chitosan derivatives [45–49], except for the mesophase characterization of chitin nanocrystals (microfibrils) [3, 50]. The authors' group synthesized chitosan phenylcarbamate (CtsPC) samples of varying DS (2.7–3.7) and examined the liquid crystalline characteristics in polar aprotic solvents [49]. In the characterization of the molecular structure of CtsPC, not only the DS (possibly exceeding a value of 3) but also the MS and the average degree of phenylcarbamoyl polyaddition in the side chains (DP_s) were taken into consideration. The phenylcarbamation of chitin and chitosan with phenyl isocyanate, in general, gives rise to diverse substitutions, as shown in Scheme 2. The use of CtsPCs of $DP_s \geq 1.1$ displayed lyotropics that assumed a blurred cholesteric coloration; therefore only CtsPC products of $DP_s < 1.1$ were used to investigate the mesomorphic behavior.

CtsPCs of $DS > 2.8$ dissolve in DMF, DMAc, and dimethyl sulfoxide (DMSO) at high concentrations (>44 wt%) and the resulting solutions form a left-handed chiral nematic type of mesophase and mostly impart vivid colors. The mesophase shows a negative concentration dependence and positive DS dependence of the absolute value of *P*, as does the left-handed chiral nematic lyotropics of acylated EC (Sect. 2.2.2). However, the temperature dependence of *P* makes a positive correlation in the CtsPC/aprotic solvent systems (Fig. 9), differing from the case in the left-handed lyotropic systems of EC and acylated EC.

In a recent extensive study [51], 1-ethyl-3-methylimidazolium dicyanamide ([C2Mim][$N(CN)_2$]) was found to be a novel solvent for CtsPC ($DS = 2.3$–3.5). The concentrated polymer solutions formed a right-handed chiral nematic mesophase, mostly colorful at CtsPC concentrations of ca. 35–45 wt %. The dependence of the absolute value of *P* on the three variables (DS,

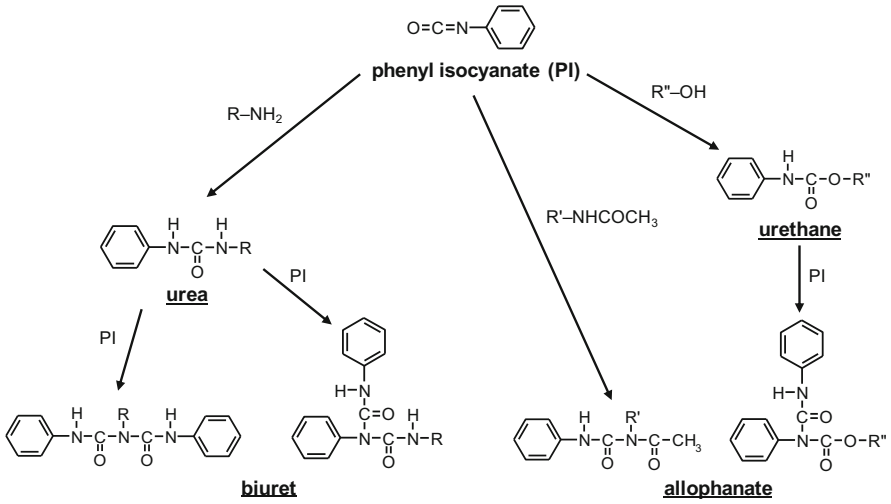

Scheme 2 Diverse substitutions via phenylcarbamation of chitin/chitosan with phenyl isocyanate (*PI*). Carbohydrate backbones are represented by *R* (for chitosan), *R′* (for chitin), and *R″* (for both)

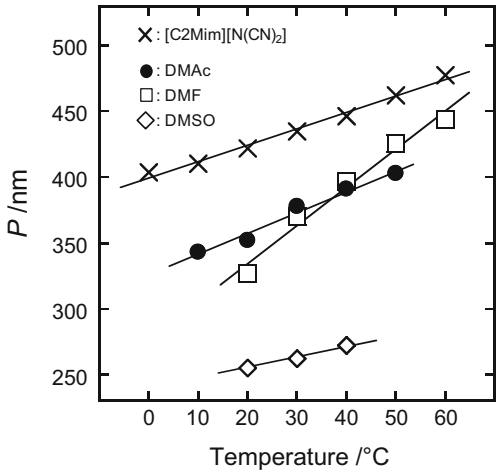

Fig. 9 Temperature dependence of pitch (*P*) for 48 wt% CtsPC (DS = 2.91) lyotropics in DMAc (*filled circles*), DMF (*open squares*), and DMSO (*open diamonds*) [49], and for 40 wt% CtsPC (DS = 2.84) lyotropics in [C2Mim][$N(CN)_2$] (*crosses*) [51]

concentration, and temperature) was essentially the same as that found in the CtsPC/aprotic solvent systems; therefore, the positive temperature dependence of *P* (see Fig. 9) is similar to that observed for the right-handed chiral nematics of acylated EC. A positive correlation of *P* with DS was not observed in the case of right-handed systems of acylated EC. Figure 10 illustrates the DS dependence of *P* for 40 wt% CtsPC solutions in [C2Mim][$N(CN)_2$] (25°C); the

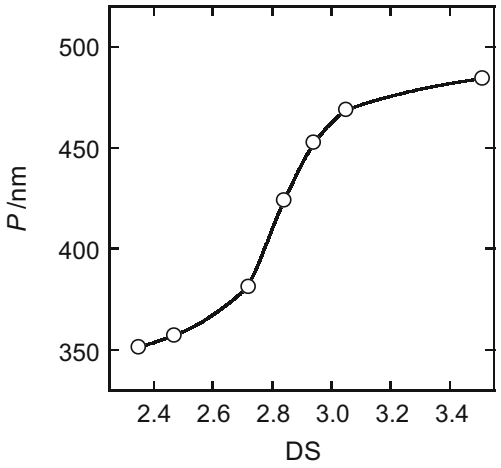

Fig. 10 DS dependence of pitch (P) for 40 wt% CtsPC chiral nematics in [C2Mim][$N(CN)_2$] at 25°C [51]

increase in DS from 2.35 to 3.5 leads to a marked rise in P. A notable observation is the steep increase in P in the DS range 2.75–2.95, followed by saturation at higher DS values of $\geq$3.0. Thus, the supermolecular helicoid of CtsPC of DS = 2.8 (MS = 3.0) is particularly sensitive as far as the twisting power is concerned for small fluctuations in DS. It should be added that the observed correlations of P with phenylcarbamoyl DS and temperature were assigned mainly to the responsiveness of the twist angle φ between adjacent nematic layers, whereas the variation in the layer spacing d was negligible.

In view of the difference in handedness of chiral nematics between the two lyotropic systems of CtsPC/polar aprotic solvent and CtsPC/[C2Mim][$N(CN)_2$], we can expect to observe a handedness inversion by using a mixed solvent of the two types. In Fig. 11, P^{-1} is plotted against the proportion of [C2Mim][$N(CN)_2$] in the mixed solvent for a ternary series of CtsPC (DS = 2.72)/[C2Mim][$N(CN)_2$]/DMF (polymer concentration 46 wt%). As can be seen from the graph, the increase in IL content correlates with handedness conversion from left to right in the chiral supermolecular arrangement, and the nematic state of $P^{-1} = 0$ can occur at a composition of [C2Mim][$N(CN)_2$]:DMF = 0.55:0.45. A similar inversion of the helical twist has been observed for a lyotropic series of CTC in a mixture of diethylene glycol monoethyl ether (DEME) and 2-pentanone [8, 44].

It is difficult at the present time to clarify the reason why the handedness of chiral nematics changes depending on solvent species, this is mainly due to the lack of lucid data linking the chiral supermolecular arrangement of cellulosic and chitinous derivatives to their possible asymmetrical molecular structures. However, it should be noted that the compensation phenomenon of chiral nematic pitch using a solvent mixture has been reported for polypeptide lyotropic liquid crystals [52–54] and discussed in terms of the relative dielectric constants of the solvent and solute molecules [52, 55].

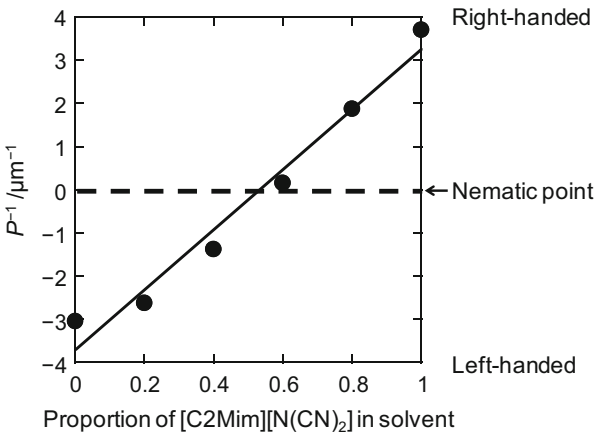

Fig. 11 Plots of P^{-1} as a function of solvent composition for a chiral nematic series of 46 wt% CtsPC (DS = 2.72) in the mixed solvent [C2Mim][N(CN)$_2$]/DMF at 25°C. Positive and negative signs of P indicate the right-handed and left-handed helical twist, respectively; $P^{-1} = 0$ corresponds to a nematic state of the mesophase (quoted from Sato et al. [51])

2.2.4 Other Related Systems and Outlook

According to an earlier work by Zugenmaier and Voihsel [56], triethyl amylose in chloroform can most probably form a right-handed chiral nematic mesophase of large pitch (e.g., ~10 μm). Since then, however, few reports have been made available on the liquid crystallinity of amylose derivatives having an α(1→4)-linked pyranose sequence. Actually, the lyotropic liquid crystallinity of amylose triphenylcarbamate (ATPC) would be difficult to investigate because of the extremely high viscosity of the concentrated solutions. Recently, Terao et al. performed an interesting study [57] of lyotropic mesophase behavior of three amylose alkylcarbamates: amylose tris(ethylcarbamate) (ATEC), amylose tris(*n*-butylcarbamate) (ATBC), and amylose tris(*n*-hexylcarbamate) (ATHC). They were prepared from enzymatically synthesized amylose with no branching. The three tris(alkylcarbamate)s assume a tightly wound helical conformation stabilized by intramolecular hydrogen bonds in THF [58] and have liquid crystallinity in the solvent [57]. The mesophase of ATBC in THF is a definite chiral nematic type, exhibiting selective reflection of visible light; the twist sense is left-handed and the absolute value of P increases with increasing temperature and decreasing concentration, as in the case of CtsPC/DMF lyotropics (Sect. 2.2.3). By using ethyl lactates as lyotropic solvent, intriguingly, any of the amylose derivatives can form a smectic type of mesophase, as judged from small angle X-ray scattering.

In studies of the correlation of chiroptical properties with the pitch of the chiral nematic liquid crystals of cellulosics and derivatives (as summarized in Sect. 2.2), CD and ORD are powerful tools that can detect the selective reflection of circularly polarized light as a pseudo-Cotton effect. In the usual CD instrumentation, however, spectra measurement is restricted to a wavelength range of about 250–850 nm, where no direct signal characterizing chiral molecular conformation of cellulosics appears to exist. In recent years, vacuum-ultraviolet CD (VUVCD) spectrophotometry using synchrotron radiation has been developed, whereby CD spectra for

saccharides in solution have been possible in a range from ~240 to 160 nm [59, 60]. The saccharides explored included familiar aqueous monosaccharides (e.g., D-glucose and D-mannose) and disaccharides (e.g., cellobiose and maltose), and even polysaccharides (glycosaminogycans). Although the accumulated spectral data characteristic of the individual saccharides have not yet been completely elucidated for peak assignments, they can serve as important bases for understanding their molecular structures, reflecting the intersaccharide linkages and constituent functional side groups. In the future, synchrotron radiation VUVCD spectroscopy will possibly develop as a significant technique for elucidating the relation between molecular conformation and liquid crystalline chirality in cellulosics.

2.3 Application in Functional Material Systems

2.3.1 Dynamic Control of Chiral Nematic Pitch and Optical Properties

(a) **Electric Field-Assisted Control and the Electro-optical Effect**. As described in Sect. 2.2.1 for salt-added aqueous HPC systems, the pitch P (and λ_M) and cloud point T_c of chiral nematics can be controlled by selecting the combination of cation and anion species in the added salt (see Figs. 4 and 6). A significant example of such functional development is the ion-mediated dynamic manipulation of cholesteric coloration and optical turbidity by using electrical stimulation of HPC lyotropics, including swollen gels [10, 61–64]. In the first demonstration [61], conventional metallic salts were employed as additive ions to shift P and/or T_c. Such a dynamic concept is based on the possible electrophoretic migration of the dissociated ionic particles, as represented diagrammatically in Fig. 12.

A similar electro-optical phenomenon was observed in aqueous HPC liquid crystals containing an IL additive of the ([C*n*Mim][X]) type [64]. A time-evolving gradation in reflective color or optical clarity of the lyotropics was attained by imposing a relatively weak electromotive force (e.g., ~4.5 V) onto appropriate electrodes (e.g., twins of carbon plate) in contact with the sample sealed in a cell. Figure 13 illustrates the temporal variation in visual appearance for HPC lyotropics containing added [C4Mim][Br] or [C4Mim][I]. This behavior is phenomenologically parallel to that found in previous experiments [61] using conventional alkali-metallic salts and was interpreted as being primarily a result of the generation of a disproportional dislocation of $CnMim^+$ and X^- as P and/or T_c shifters. In fact, the ionic fluctuation gives rise to an inner gradient of electric potential in the concentrated polymer medium. However, before distinct formation of an imbalanced distribution of cations and anions, there would need to be sufficient dissociation of the ion pair and orientational re-allocation of the organo-cation initially stabilizing the HPC solute in a surfactant-like fashion; these pre-actions should be promoted by the external electric force. Thus, the effect of an electric field on the salted

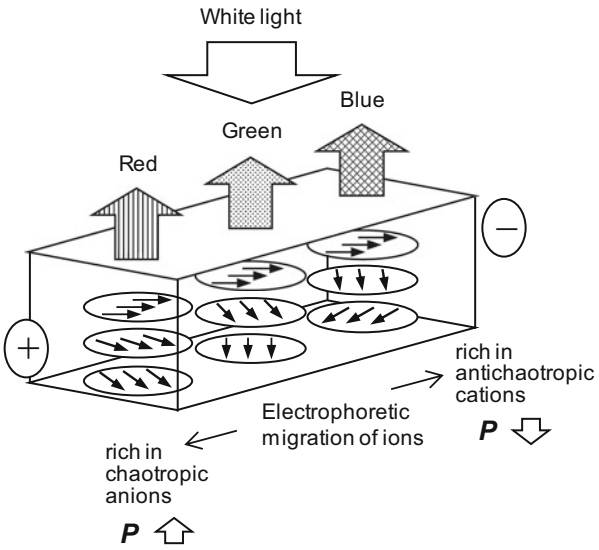

Fig. 12 Dynamic control of the visual appearance of aqueous HPC liquid crystals containing salt ions as *P*-shifting agent by an external electric field. The liquid crystals can display color gradation with an elapse of time from the initial monocolor stage if electrophoretic migration of the dissociated ionic particles advances

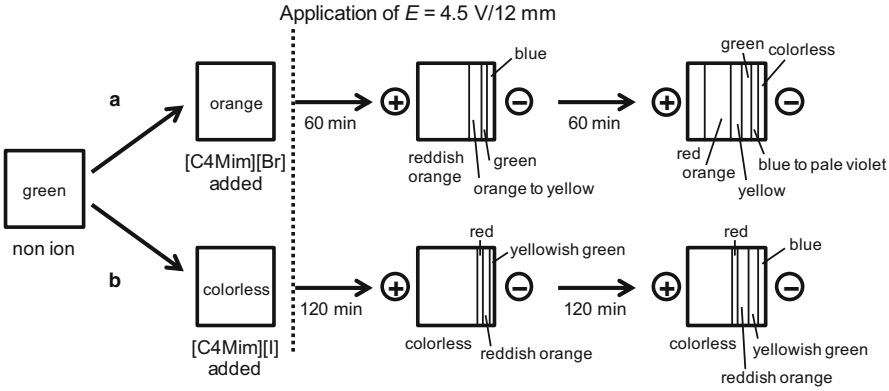

Fig. 13 Time-evolving color gradations observed for (*a*) [C4Mim][Br]-added and (*b*) [C4Mim][I]-added HPC aqueous liquid crystals (HPC concentration 62.5 wt%; salt concentration 2.5×10^{-4} mol/g-HPCaq) at 23°C under application of $E = 4.5$ V/12 mm. Each anisotropic solution was sealed in a layer between slide glasses spaced by a pair of carbon electrodes (500 μm thick) (rearranged using data from Ito et al. [64])

HPC liquid crystals is remarkable, although their response is influenced by the electrochemical reaction.

Note that even after the electric field is ceased, an appreciable potential difference remains in the color-gradated samples. It is suggested that the salt-containing liquid crystalline system behaves like a quasi-capacitor, as a viscous electrolytic medium of high resistance.

The electro-optical function found for such an ionic system of HPC liquid crystals is potentially relevant to some displays that do not require short response times. The color patterning could also be diversified by alteration of the sort and shape of the electrodes contacting the viscous sample.

(b) **Magnetic Field-Assisted Control**. As described in a previous review by Nishio [10], there have been several attempts to observe the effect of magnetic fields on the chiral nematic structure of liquid crystals of cellulose derivatives. The diamagnetic anisotropy of cellulosic molecules is usually negative and, therefore, the molecular director of nematic orientation tends to be perpendicular to the applied magnetic field and the supramolecular helix axis is aligned parallel to the field vector. In a (~9 T) magnetic field-imposed lyotropic system of ethylcyanoethyl cellulose [(E-CE)C]/DCA [65], it was observed that the orientation regularity and helicoidal pitch of the chiral nematic mesophase were strongly influenced by the polymer concentration of the solution and, in the lower concentration range (biphasic state), particularly by the surface tension of the discrete domains of the mesophase.

Application of a magnetic field can be more effective in control of alignment for the chiral nematics of cellulose and chitin nanocrystals than for molecular liquid crystals of cellulose derivatives. In synthesis of polymer composites reinforced with rodlike mesogen fillers (see Sect. 3.2.2), the application of a field serves as a powerful pretreatment for regulating the orientation of the crystallite assembly.

2.3.2 Mesomorphic Order-Retaining Polymer Solids

(a) **Fixation of Chiral Nematic Structure**. The chiral nematic supramolecular structure of cellulose derivatives can be made permanent in polymer films or gels. Typical methods employ crosslinking of cellulosic molecules with reactive side groups in the liquid crystalline state, or polymerization of solvent monomers constituting the lyotropics of cellulosics. The major examples that appeared before 2006 are listed in Nishio's article [10], in connection with the structural design of microcompositional materials based on cellulosics. Since then, there have been a few studies of the synthesis of colorful optical materials retaining the chiral nematic mesomorphy of cellulosic polymers (mostly phenylcarbamate derivatives).

Wenzlik, Zentel, and coworkers made a novel attempt to prepare spherical particles (microbeads of ~300 μm diameter) having an opalescent look from a chiral nematic sample of cellulose 3-(trifluoromethyl)phenycarbamate

Table 2 Pitch P, layer spacing d, and twist angle φ for a 50 wt% CtsPC[a] chiral nematic liquid crystalline solution in DMAc/VP (1:1 in weight), and their changes following the polymerization[b] and washing[c] processes

State	P (nm)	d (nm)	φ (°)
Solution	396	1.61	1.46
Gel film before DMAc removal (as-polymerized)	385	1.55	1.45
Film after DMAc removal (washed and dried)	368	1.45	1.41

[a]DS = 3.08 and MS = 3.36
[b]Initiator, 2-hydroxy-2-methylpropiophenone; crosslinker, *N*,*N*-methylenebisacrylamide
[c]Washing agent, ethyl acetate

(3-CF_3-CTC) in hexyl acrylate/diethylene glycol dimethacrylate, by photo-initiated polymerization of the acylic solvent in a microfluidic setup [66]. The derivative 3-CF_3-CTC in such an acrylic monomer forms a right-handed chiral nematic mesophase, imparting vivid reflection colors. The same group made efforts to tune the reflection colors of 3-CF_3-CTC chiral nematics by careful choice of the polymerizing monomer solvent, and also to regulate other conditions for film preparation [67]. As a consequence, they acquired free-standing chiral nematic films of high optical quality, which gave a very sharp, selective reflection band (half width of ~25 nm).

We often meet with the case where liquid crystalline cellulosic or chitinous derivatives dissolve poorly at high concentrations in a given monomer. There are also cases where the derivatives form a liquid crystal in a monomer solvent, but the lyotropics are never colored; for example, this situation applies to anisotropic solutions of CtsPC (see Sect. 2.2.3b) in *N*-vinyl pyrrolidone (VP) or *N*,*N*-diethylacrylamide. In these cases, a combination of standard solvent and vinyl monomer could be available; the solvent leads to chiral nematics and polymerization of the monomer fixes the mesomorphic structures into the resulting solid. Uniformly colored films composed of CtsPC/poly (*N*-vinyl pyrrolidone) (PVP) can be obtained via photopolymerization of chiral nematic solutions in a mixed solvent of DMAc (or DMF) and VP monomer containing a suitable crosslinker and photo-initiator. However, this polymerization process is inevitably followed by washing to remove DMAc (or DMF), whereupon the chiral nematic pitch P and therefore λ_M (equal to $\tilde{n}P$) of selective light reflection usually decreases, with accompanying shrinkage of the film sample. This is exemplified in Table 2 for the preparation of a colored film (yellowish green) from a CtsPC chiral nematic solution (orange to red) in DMAc/VP of 1:1 (w/w). As seen in the example, the decrease in P of the liquid crystal following polymerization and washing can be ascribed to a reduction in the nematic layer spacing d. The angular parameter φ is less variable and, as a matter of course, the twist of the chiral mesophase remains unchanged (left-handed in this system). The extent of the reduction in P is generally controllable by altering the composition of the monomer and DMAc mixture.

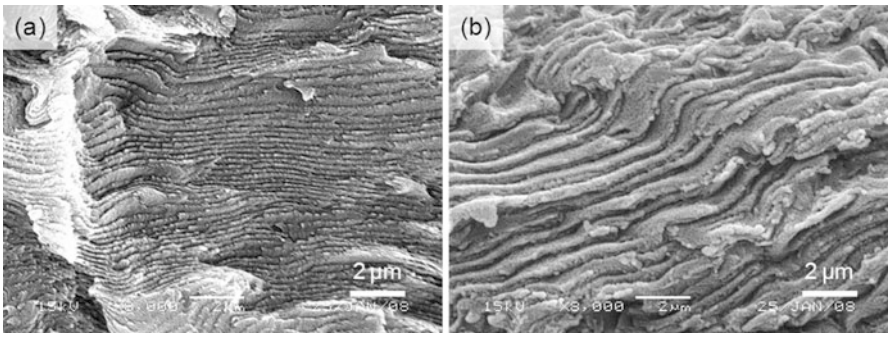

Fig. 14 SEM photographs of fracture surface morphology for CtsPC/PVP films prepared from 50 wt% CtsPC solutions in the mixed solvents: (**a**) DMF/VP of 1:1 (w/w); (**b**) DMAc/VP of 1:4 (w/w). The fracture surfaces were spattered with Au

Figure 14 shows scanning electron microscope (SEM) images of fracture surface morphologies for CtsPC/PVP films prepared from 50 wt% CtsPC chiral nematics formed in DMF/VP (1:1) or DMAc/VP (1:4) mixed solvents. A beautiful periodic layered architecture can be observed in the films. The periodicity of the lamellar structure appearing in the SEM images is roughly in agreement with half of *P*, as estimated by optical measurements. Several morphological studies have referred to this point for similar chiral nematic films obtained from liquid crystals of cellulose derivatives [68, 69].

(b) **Stimuli Responsive Materials**. In addition to the ion-mediated electro-optical HPC lyotropic systems described in Sect. 2.3.1a, in the past two decades there have been some attempts to fabricate stimuli-responsive smart materials based on liquid crystalline cellulose derivatives. Noteworthy advances in this area were reported intensively from the middle of the 1990s until 2005 [10], mainly concerning manipulation of the selective light reflection of chiral nematics by various external stimuli, targeting mechanical compression-sensitive, photo-sensitive, temperature-sensitive, and humidity-sensitive materials, or dealing with nonlinear optical media for optoelectronic devices. The chiral nematic orders were fixed into soft films or gels, mostly of CPC- or HPC-cored derivatives or their composites with acrylate polymers. The efforts of Zentel and coworkers to fine-tune cholesteric reflection colors (see Sect. 2.3.2a) can be included here.

An interesting attempt has been made to prepare chiral conductive polymer films using HPC liquid crystals as a chiral template [70]. Goto and Akagi synthesized a polymer composite of poly(3,4-ethylenedioxythiophene) with HPC (PEDOT/HPC) by electrochemical polymerization of EDOT monomer in a 65 wt% HPC aqueous solution containing tetrabutylammonium perchloride (~0.1 M) as a supporting salt. The PEDOT/HPC film exhibited an optically active electrochromism ("electro-chiroptical effect"), that is, color switching between a dark blue reduced state and sky blue oxidized state with corresponding changes in the Cotton signal of CD through the electrochemical redox process.

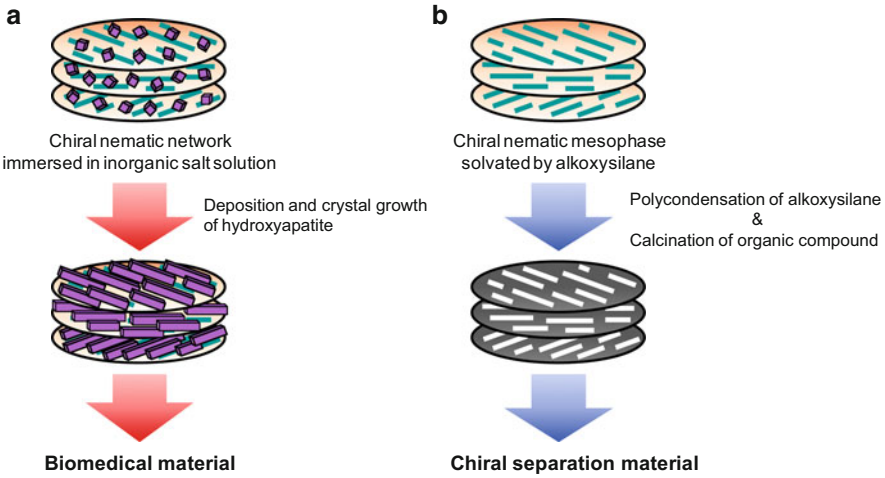

Fig. 15 Design of new cellulosic polymer/inorganic hybrid materials: (**a**) deposition of hydroxyapatite (calcium phosphate) onto the cellulosics-derived chiral nematic stratums as scaffold; (**b**) hybridization of silica using a similar liquid crystalline organization as template

2.3.3 Inorganic Hybridization and Outlook

A remarkably growing field in materials research is the development of polymer/inorganic nanocomposites showing high mechanical performance or other specific functionalities. As part of this research field involving cellulosics, attention is being dedicated to a novel class of hybrid materials that use the mesomorphic ordered structure of cellulosics as a scaffold or template for confined growth of inorganic ingredients. Strategic schemes for design of such hybrids are presented in Fig. 15. Figure 15a shows hydroxyapatite (HAp) deposition onto chiral nematic stratums as scaffold, and Fig. 15b illustrates silica hybridization using a similar organization as template. In both cases, the layered matrices are provided by liquid crystalline cellulosics.

In a later example, mineralization behavior was investigated using chiral nematic liquid crystalline gels of EC/poly(acrylic acid) (PAA) as a scaffolding medium for deposition of HAp [71]. The EC/PAA samples were obtained in film form from EC/acrylic acid liquid crystals (left-handed chiral nematics) by polymerization of the monomer solvent [72, 73]. The mineralization was conducted in a batch process or by alternate soaking of the liquid crystalline films in immersion baths of the relevant inorganic salt solutions. For instance, the resulting HAp-deposited EC/PAA composites retained cholesteric reflective coloration that shifted to the red side with increasing time of mineralizing treatment, and they also showed noticeably improved thermomechanical properties relative to those of the respective original EC/PAA films. As a related example from preceding work, Nishimura et al. succeeded in inducing unidirectional crystal growth of calcium carbonate ($CaCO_3$) using an oriented nematic liquid crystalline phase of chitin

phenylcarbamate that was adopted as the template [74]. First, a lyotropic sample of chitin phenylcarbamate/DMSO/DMF was converted to a free-standing gel film by soaking in methanol. The resultant gel was drawn to 200% elongation and subjected to a 2-h treatment in NaOH/methanol to cleave the carbamoyl groups. Then, the oriented chitin film was immersed in an aqueous solution of calcium chloride in the presence of PAA while ammonium carbonate vapor was diffused into the solution. As a consequence, rods of $CaCO_3$ were aligned parallel to the draw direction of the chitinous gel film. The polymorph of the formed crystal was confirmed to be calcite by FTIR and Raman spectroscopy and transmission electron microscopy (TEM).

Concerning silica hybridization (Fig. 15b), as briefly reviewed [10], an earlier report by Thomas and Antonietti [75] included an iridescently colored hybrid material of HPC/silica produced by sol–gel conversion of tetramethyl orthosilicate (TMOS), used as a solvent component of aqueous lyotropics of HPC. The hybrid was further transformed into silica glass retaining a chiral nematic pore structure by post-treatment of calcination to remove the organic template. In 2013, Sato et al. attempted to synthesize optically chiral silica monoliths based on hydrophobic liquid crystalline CPC derivatives, cellulose 3-chlorophenylcarbamate (3-Cl-CPC) and 4-chlorophenylcarbamate (4-Cl-CPC) [76]. A right-handed chiral nematic hybrid series of 3-Cl-CPC/silica and a left-handed series of 4-Cl-CPC/silica were both successfully prepared via the vitrification of alkoxysilanes selected as a lyotropic solvent suitable for the respective parent liquid crystalline systems. The CPC family is known to possess a chiral resolution power for enantiomers. Therefore, this study is of great significance, not only for development of materials that are optically active but also for chiral separation.

A recent trend in the cellulose research field is the preparation of related inorganic hybrids using templates from the chiral mesomorphic assemblies of CNCs and of related natural polymer microfibrils. This will be discussed in Sect. 3.2.3.

3 Liquid Crystals of Cellulose Nanocrystals

3.1 Fundamental Aspects

3.1.1 Phase Separation Behavior of CNC/Water Suspensions

Hydrolysis of native cellulose fibers, commonly using sulfuric acid, yields highly crystalline rodlike particles (i.e., cellulose nanocrystals, CNCs), as a result of the cleavage and destruction of the more readily hydrolyzable amorphous regions of cellulose microfibrils [2, 11]. The crystal size along the longitudinal direction of cellulose chains is thought to correlate with the so-called level-off degree of polymerization. Scheme 3 illustrates a typical procedure for the preparation of CNC/water suspensions. In the case where sulfuric acid is the hydrolyzing agent, the surface hydroxyl groups of cellulose fibrils can react with the agent to produce

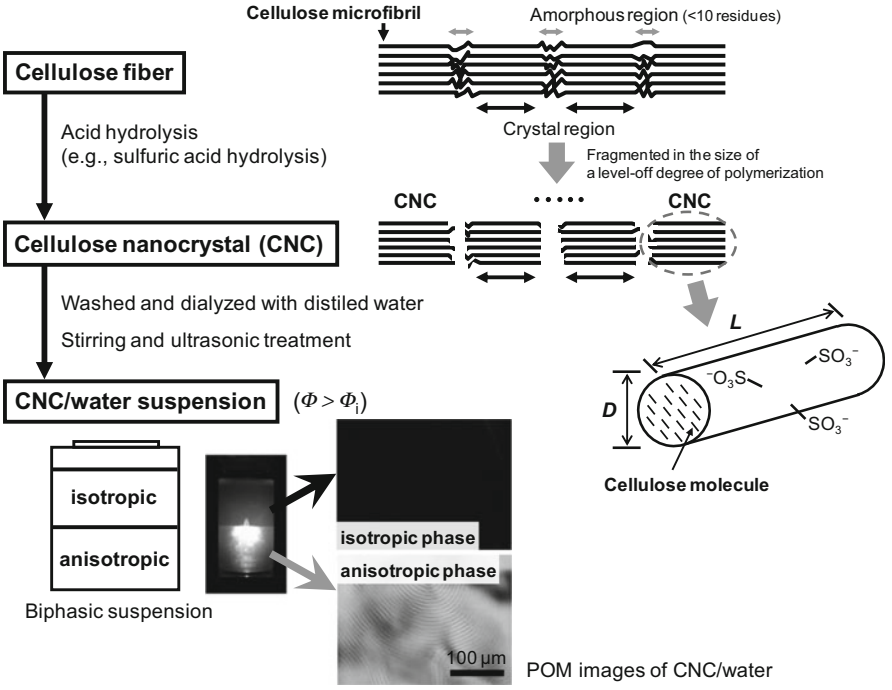

Scheme 3 Flow chart illustrating a typical procedure for preparation of CNC suspensions in water

negatively charged sulfate half-esters. In water, therefore, the resulting CNC particles show adequate dispersibility via electrostatic repulsions and yield a stable colloidal suspension. When the CNC concentration exceeds a certain critical value, the suspension spontaneously separates into an upper isotropic phase and a lower anisotropic phase in the course of quiescent standing of the sample vial. Under a polarized optical microscope (POM), the anisotropic phase exhibits fingerprint-like retardation lines that are characteristic of a chiral nematic mesophase of long P (e.g., 20–80 μm). In contrast to the behavior of molecular liquid crystals of cellulose derivatives, only the left-handed helicoidal arrangement has been reported for chiral nematic mesophases of CNC suspensions [77, 78].

Onsager theorized on the liquid crystal phase transition for a disperse system of perfect rigid rods of length L and width D [14]. According to classical theory, the critical volume fraction of rods for isotropic–biphasic transition (Φ_i) and for biphasic–wholly anisotropic transition (Φ_a) are given by the following equations:

$$\Phi_i \approx 3.3D/L \tag{4}$$

$$\Phi_a \approx 4.5D/L \tag{5}$$

For example, for a dispersion of CNCs having an aspect ratio $L/D = 100$, the theory predicts biphase separation at ~3.5 vol.%, which corresponds to ~5.5 wt%, assuming the density of CNCs to be 1.6 g/cm^3. For a CNC suspension of $L/D = 25$, the

critical concentration is estimated to be ~14 vol% or ~21 wt%. These calculated values of critical concentration are evidently higher than experimental data observed for the charged CNC suspensions with given polydispersity (e.g., critical concentration of 3–5 wt% for CNC particles of $L/D = 10–30$). Refinements of the Onsager theory were developed by Odijk et al. [79] to precisely describe the phase separation of rodlike polyelectrolytes, taking into account two factors: (i) the increased effective diameter of a rod and (ii) a twisting factor working between rods as a result of electrostatic repulsion. Dong et al. applied the refined theory by Odijk et al. to explain the isotropic–chiral nematic phase transition behavior of CNC suspensions with addition of electrolytes (NaCl, KCl, and HCl) and found a relatively good agreement between experimental results and theoretical predictions [16]. It turned out that the isotropic–anisotropic transition boundary of colloidal CNC suspensions depends primarily on the (effective) aspect ratio L/D, and also strongly on the surface charge density and resulting electrostatic interparticle repulsion. The influence of the cellulose source, hydrolysis conditions, and added electrolyte on the resulting CNCs is discussed in more detail below.

(a) **Cellulose Source and CNC Dimensions**. The material source used to produce the CNCs can fix the approximate limits of the aspect ratio of the dispersed rods. Different cellulose materials (cotton, tunicate, etc.) produce different CNC sizes, even under similar experimental conditions [12] (see Table 3). For instance, CNCs from wood and cotton are 5–10 nm in width and 100–350 nm in length, whereas tunicate gives CNCs of ca. 10–20 nm in width and 500–2,000 nm in length. Thus, the aspect ratio of CNC spans a broad range, roughly from 10–30 (for higher plants) to >70 (for tunicate). As the above-mentioned theories indicate, CNCs of higher aspect ratios should drive their suspensions to the liquid crystal phase transition at lower concentrations. Indeed, aqueous suspension of CNCs from tunicate require a much lower concentration

Table 3 Dimensions of CNCs obtained from different cellulose materials and values of the critical concentration (Φ_i) for isotropic to anisotropic phase transition

Source	Length (L) (nm)[a]	Width (D) (nm)[a]	L/D	Φ_i (wt %)	References
Higher plants					
Wood	100–200	~5	20–40	~3	[11]
Cotton	150–350	5–10	10–30	4–7	[16, 17, 77]
Tunicate	1,000–3,000	15–30	50–100	<2	[19]
	500–2,000	10–20	>70	<1	[80]
	500–2,000	~15	70	~0.5	[97]
	~2,000	~20	~100	0.3–0.7	[98]
Bacteria (*Acetobactor*)	100–2,000	5–10 × 30–50	50–100	<0.3	[81]
	600–1,800	~8 × 40–55	40–90	0.4–0.8	[82]

[a]From TEM observation

(<<1 wt%) for the transition [80] than cotton-derived CNCs (4–7 wt%) [16, 17]. Bacterial cellulose (BC) nanocrystals have a flat ribbon shape and, usually, the rectangular cross-section is about 5–10 × 30–50 nm and the length ranges from 100 nm to a few micrometers, typically with an average of ~1 μm. Because of such high aspect ratios, aqueous suspensions of BC-derived CNCs separate into isotropic and anisotropic phases at a low concentration, just exceeding 0.4 wt% [81, 82]. One reference [81] reports that the anisotropic phase was of a "nonchiral" nematic order, unlike the chiral nematic assemblies usually observed for CNCs from higher plants.

(b) **Effect of Hydrolysis Treatment**. As stated above, the surface charge density strongly affects the effective CNC aspect ratio. The electric charge of the CNC surface is primarily controlled by the conditions used to hydrolyze the cellulose fibers [17]. Because the hydrolysis process with sulfuric acid is heterogeneous, higher acid concentrations, higher reaction temperatures, and longer reaction times promote diffusion of sulfuric acid into the fibers and subsequent cleavage of glycosidic linkages in the amorphous regions, resulting in a higher extent of sulfation on the CNC surface. However, the hydrolysis conditions must be mild enough to avoid complete hydrolysis to glucoses and possible side reactions such as dehydration.

If hydrochloric acid is used instead of sulfuric acid to hydrolyze native celluloses, nanocrystals having almost no charged side groups are obtained. Their dispersibility is significantly limited and the aqueous suspensions tend to flocculate as a result of limited electrostatic repulsion between the crystal particles [83]. However, hydrochloric acid treatment offsets the lack of thermal stability [84] of the conventional surface-sulfated CNC particles. That is, prehydrolysis of cellulose fibers in hydrochloric acid followed by post-treatment with sulfuric acid could be a means of controlling the surface charge density of CNC particles [85, 86]. In an analogous route, hydrochloric acid-hydrolyzed tunicin CNCs were successfully dispersed in water by post-oxidation with a stable nitroxyl radical, 2,2,6,6-tetramethylpiperidine-1-oxyl (TEMPO), in the presence of sodium bromide and sodium hypochlorite [87]; the TEMPO-mediated oxidation converts the surface hydroxymethyl groups of cellulose into negatively charged carboxyl groups that have better thermal stability. The resulting suspensions (~0.5 wt%) of the TEMPO-oxidized CNCs (from tunicate) displayed a liquid crystalline birefringent phase over the whole area of the sample, but the optical image was indicative of a less chiral nematic character. In connection with this study, quite recently Castro-Guerrero and Gray prepared CNCs with surface carboxyl groups by oxidation of lignocellulosic materials with ammonium persulfate, according to a similar procedure [88], and demonstrated by POM observations a clear, chiral nematic mesophase formation for the CNC suspensions in water [89].

As an additional remark on acid hydrolysis of cellulose, there was a report [90] indicating that a combination of sulfuric acid and hydrochloric acid under ultrasonic treatment generated spherical CNCs rather than rodlike CNCs; the cellulose material used was commercial microcrystalline cellulose. The acid

regents seem to quickly penetrate the fibrous cellulose as a result of ultrasonic treatment. Of interest was the observation of a liquid crystalline phase (but not a chiral nematic phase) appearing in suspensions of spherical CNCs with high polydispersity (49%) at concentrations above 3.9 wt%, in spite of the poor anisotropic shape of the dispersoids.

(c) **Effect of Added Electrolytes**. Dong et al. systematically studied the effect of added electrolytes on the isotropic–chiral nematic phase equilibrium of sulfated CNC suspensions [16, 91]. For a biphasic sample, at a fixed total CNC concentration, increasing the amount of added electrolyte (KCl, NaCl, or HCl of <2.5 mM) diminishes anisotropic phase formation [16]. The chiral nematic pitch P of the anisotropic phase decreases, that is, the phase becomes more highly twisted with increasing concentration of the added trace electrolyte. It can be assumed that the electric double layer on the crystallite rods regresses at higher ionic strengths, resulting in a stronger chiral interaction between the crystallites so as to diminish P. The phase separation behavior also depends strongly on the nature of the counterions present in the sulfated CNC suspensions [91]. For inorganic counterions, the critical concentration for ordered phase formation increases as a function of increasing van der Waals radius, in the order $H^+ < Na^+ < K^+ < Cs^+$. For organic counterions such as NH_4^+, $(CH_3)_4N^+$, $(CH_3CH_2)_4N^+$, $(CH_3CH_2CH_2)_4N^+$, $(CH_3CH_2CH_2CH_2)_4N^+$, $(CH_3)_3HN^+$, and $(CH_3CH_2)_3HN^+$, the critical concentration generally increases with increasing counterion size; but it is suggested that the equilibrium is governed by a balance between hydrophobic attraction and steric repulsion forces. The chemical nature of the counterions also influences the suspension stability, the temperature dependence of the phase separation and chiral nematic pitch, and the re-dispersibility of dried CNC samples made from the suspensions.

Additive effects of electrolytes have also been described for CNC suspensions (0.2–1.6 wt%) prepared by sulfuric acid hydrolysis of BC [81]. Interestingly, addition of <1 mM NaCl induced cholesteric chirality in the originally nematic BC phase. This phenomenon was explained by the change in the effective particle shape from a cylinder to a clearly twisted rod as a result of screening of the surface charge, which might conform with the observations by Dong et al. [16]. The presence of electrolyte also significantly decreased the volume fraction of the anisotropic phase, an observation made after addition of 0.1–1.0 mM NaCl for a fixed CNC concentration of 1.58 wt%. Hirai et al. performed a similar phase study for BC-derived CNC suspensions (0.2–4.0 wt% CNC) in an expanded range of NaCl addition (0–5.0 mM) [82]. In their report, the anisotropic phase situated in the lower layer of biphasic suspensions (>0.42 wt%) was evidently "chiral nematic" even in the electrolyte-free condition. For a salt-added biphasic series of 3 wt% CNCs, it was shown that the volume fraction of the anisotropic phase decreased with increasing NaCl concentration, reached a minimum at ~1.0 mM, and then increased with further added NaCl. Correspondingly, the chiral nematic pitch P decreased from 16.5 μm for the electrolyte-free suspension to a minimum

value of 12 μm at ca. 0.75 mM NaCl, and then increased sharply to ~19 μm with an elevation in NaCl concentration up to 2.0 mM. In the concentration range of 2.0–5.0 mM NaCl, no biphasic separation occurred and the suspensions became entirely liquid crystalline, but poor in chiral nematic character.

Besides simple 1:1 electrolytes (e.g., NaCl), polyvalent dyes also affect the phase equilibrium of liquid crystalline CNC suspensions. For instance, addition of anionic dyes of varying charge to completely anisotropic suspensions of cotton-derived CNCs (concentration of ~14 wt%) caused phase separation of the isotropic phase [92]. This anisotropic to biphasic transition was interpreted as being a result of their polyvalent character and larger hydration radius, which raised the upper limit of CNC concentration required for the formation of a completely anisotropic suspension. By contrast, neutral, cationic, and cellulose-binding anionic dyes did not cause phase separation in the anisotropic CNC suspensions. Related preceding work [93, 94] reported that the anisotropic-to-biphasic transition was also induced by addition of blue dextran (actually by the presence of a sulfonated triazine dye bound covalently to hydroxyl groups on the dextran chain). In this phase separation, blue dextran was partitioned preferentially into the upper isotropic phase; however, the lower dextran-poor chiral nematic phase exhibited a rather distorted fingerprint texture with numerous disclinations. Further investigation of these lines demonstrated that the "isotropic–isotropic–chiral nematic" phase equilibrium developed when an undyed neutral dextran was added along with the anionically charged blue dextran to a biphasic CNC suspension (e.g., 8.7 wt%) [95]. The concentrations of the two dextrans needed to produce the three-phase equilibrium were strongly influenced by their molecular weights and overall charge density. The mechanism of the observed phase behavior was not clear, but the phase behavior seemed to be governed by the complex interplay of repulsive electrostatic and attractive entropic forces.

3.1.2 CNC Dispersions in Organic Solvents and Surface Graft Modifications

As mentioned in Sect. 3.1.1, the stability of CNCs in water and their liquid crystalline formation are greatly influenced by the surface charge of the CNC rods. Adequate control of the surface condition of CNCs is also a key factor in obtaining their stable dispersions in organic solvents. The use of organic solvents as suspending media is of great importance for the production of well-dispersed CNC/polymer composites of various types.

(a) **Organic Dispersion Systems**. There have been some attempts at preparing stable CNC dispersions in polar organic solvents of high dielectric constant, such as DMF and DMSO [96, 97]. The typical procedure used is as follows: dilute aqueous suspensions of CNCs obtained by sulfuric acid hydrolysis of cellulose materials are freeze-dried, and subsequently sonicated in the organic solvent of interest; incompletely dispersed clumps are filtered out. For example [96], it was reported that cotton-derived CNC suspensions of 0.6 and

1.8% w/v in DMSO exhibited strong shear birefringence between crossed polars. The presence of a small amount of water (~0.1 wt%) in the polar organic solvent seems to be critical for homogeneous re-suspension. Similarly, a stable suspension of 0.5 wt% tunicin CNC was attained in DMF [97]. Both the high dielectric constant of DMF and the medium wettability of the (charged) CNC were thought to control the stability of the suspension. Lyophilized tunicate-derived CNC was also well re-dispersed in other organic solvents such as *N*-methyl pyrrolidone, formic acid, and *m*-cresol [98]. Furthermore, mixtures of water with hydrophilic or amphiphilic (meth)acrylic monomers can serve as solvents for CNC dispersion; some examples are given in Sect. 3.2.2.

For the dispersion of CNCs in nonpolar organic media, however, the electrostatic repulsion character is not efficient, and hydrogen-bonding interactions preferentially work between CNC particles, resulting in rapid aggregation of the colloidal suspension. Therefore, the stabilization of CNC suspensions in nonpolar solvents requires some additive or chemical modification that is capable of altering the surface condition of the CNC rods used. Heux et al. demonstrated the stable dispersion and liquid crystalline formation of CNCs (cotton- and tunicate-derived) in apolar solvents such as toluene and cyclohexane using the surfactant BNA [phosphoric ester of poly(ethylene oxide)(9) nonylphenyl ether] [99, 100]. The surfactant molecules covered the CNC rods and thus exchanged the strong repulsive electrostatic interaction for smoother steric repulsion. As a consequence, the suspensions spontaneously phase-separated into an isotropic–anisotropic biphasic state above a critical concentration (e.g., ~17 wt% for cotton-derived CNC in cyclohexane). The critical concentrations for liquid crystalline formation (Φ_i and Φ_a) were generally higher than those in water without any additive, but still lower than the values predicted by the Onsager theory (Eqs. 4 and 5). In this regard, Heux et al. also claimed an attractive interaction between the BNA-coated CNC rods [100]. The observed anisotropic phases were commonly chiral nematic, and the helicoidal pitch was found to be ca. 2–4 μm, which is evidently smaller than that estimated for aqueous suspensions ($P = 20$–80 μm). These results indicate that the steric stabilization exerted by the surfactant coating screens out the electrostatic repulsion and induces a stronger chiral interaction between CNC rods in a low dielectric constant medium (e.g., cyclohexane). Chiral nematic self-organization behavior of CNCs in nonpolar media was also reported for a toluene suspension of CNCs adsorbed with an amphiphilic triblock copolymer, xyloglucan oligosaccharide–poly(ethylene glycol)–polystyrene [101]; the system assumed a biphasic state at a total dispersoid concentration of ~20 wt%, with the copolymer and net cellulose at a weight proportion of 45:55.

(b) **Surface Graft Modifications**. Chemical modifications such as esterification, etherification, oxidation, silylation, and polymer grafting onto the surface of CNCs can improve their dispersibility in various media, including organic solvents and polymers of low polarity. Many successful or promising methods

for surface modification of CNCs and some examples of their stable dispersions in both aqueous and nonaqueous media are summarized in other reviews [12, 102–104]. Here, we briefly summarize several reports dealing with the liquid crystalline behavior of CNCs grafted with longer chains.

Sulfated tunicin CNCs were partially silylated with a series of alkyldimethylchlorosilanes, the alkyl moieties of which ranged from isopropyl to *n*-butyl, *n*-octyl, and *n*-dodecyl (Scheme 4a) [105]. It was demonstrated that when the CNCs were modified at an adequate degree of silylation (depending on the introduced alkyl moiety), they became dispersible in THF and the resulting suspensions were wholly birefringent. However, formation of a chiral nematic phase was not referred to in the report. In advance of this work, Araki et al. realized a stable dispersion of cotton-derived CNCs in chloroform by grafting poly(ethylene gycol) (PEG) onto the nanorods [106]; the optical data for the suspension solely indicated flow birefringence and provided no evidence of chiral nematic character. This surface modification was made by TEMPO-mediated oxidation (oxidative carboxylation) of hydrochloric acid-hydrolyzed CNCs and subsequent grafting (amidation reaction) of a terminally aminated PEG (Scheme 4b). The PEG-grafted CNCs showed enhanced dispersion stability in water without precipitating, even in the presence of 2 M NaCl, unlike the situation in ungrafted CNC suspensions. Concentrated aqueous suspensions of the PEG-grafted CNCs (above 5% solid content) formed a chiral nematic mesophase through a biphasic separation similar to that of the nongrafted samples, but the chiral nematic pitch was relatively smaller. In interpreting these results in terms of the steric stabilization effect, caution should be exercised because of the following points: (i) the PEG-grafted samples still contained an appreciable amount of unreacted surface carboxyl groups, and (ii) the grafted PEG chains were relatively short and possibly unable to completely shield the effect of surface charge. In this context, Kloser and Gray also carried out surface grafting of CNCs with poly(ethylene oxide) (PEO) [107]; first, CNC suspensions prepared by sulfuric acid hydrolysis were desulfated with sodium hydroxide and then the surfaces of the crystals were functionalized with epoxy-terminated PEO under alkaline conditions (Scheme 4c). Aqueous suspensions of the PEO-grafted CNCs (sulfur content was ~0.06 mmol/g cellulose) were stable over time and indicated the onset of chiral nematic phase separation when condensed to ~5 wt%. To the present reviewers, however, development of the optical fingerprint texture appeared to be limited, compared with the clear-cut texture commonly observed for sulfated CNC suspensions.

There are some studies of CNC graft modifications using atom transfer radical polymerization (ATRP). In the lines of cellulosic liquid crystals, polystyrene (PS)-grafted CNC (~68 wt% PS) [108], poly{6-[4-(4-methoxyphenylazo)phenoxy] hexyl methacrylate} (PMMAZO)-grafted CNC (~75 wt% PMMAZO) [109], poly(*N*,*N*-dimethylaminoethyl methacrylate) (PDMAEMA)-grafted CNC (~53 wt% PDMAEMA) [110], etc. were synthesized by surface-initiated ATRP (see Scheme 4d) and examined for their lyotropic and/or thermotropic liquid

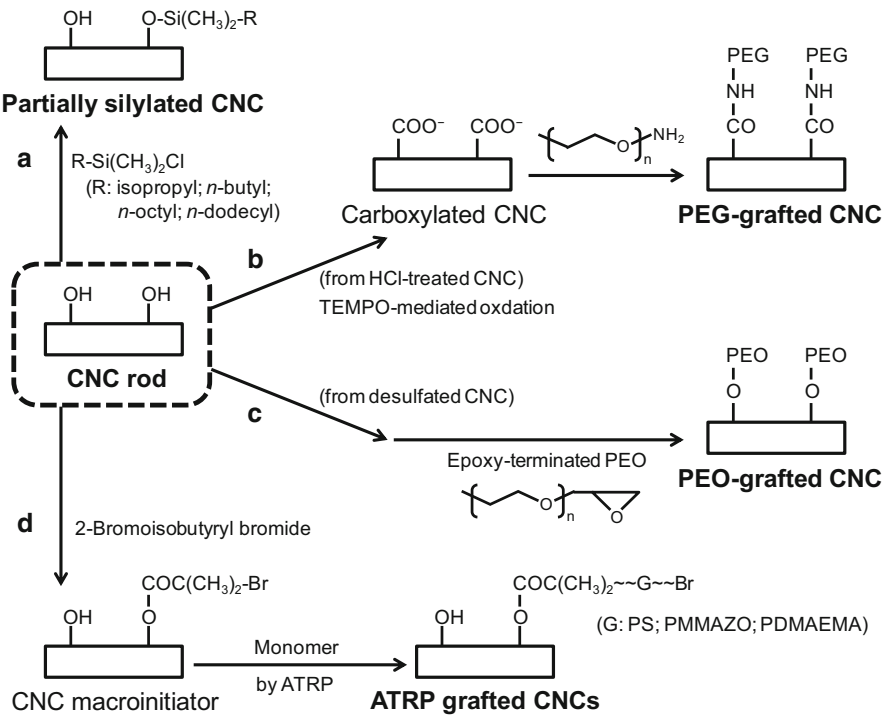

Scheme 4 Chemical modifications of CNC surfaces with (*a*) alkyldimethylchlorosilanes [105], (*b*) amine-terminated PEG [106], (*c*) epoxy-terminated PEO [107], and (*d*) various polymers obtained by ATRP [108–110]

crystallinities. Zhang et al. reported that DMF suspensions of PS-grafted CNCs and aqueous suspensions of PDMAEMA-grafted CNCs formed a chiral nematic phase ($P = 1$–2 μm) at dispersoid concentrations of 4.5–6 wt%, whereas PMMAZO-grafted CNCs exhibited a nonchiral nematic phase when dispersed in chlorobenzene at concentrations above ~5 wt%. They also reported thermotropicity of the PS-grafted and PMMAZO-grafted CNC samples; however, the optical and thermal data appear to be insufficient for elucidating the phase behavior and assembly structure. In order to carry out this kind of grafting study, it is desirable to prepare a series of samples through assessment of the graft density on the considered CNC surface as well as the precise molecular weight and polydispersity of the graft chains. Looking over the research results summarized in this section, particularly those involving polymer adsorption or grafting onto CNCs, we find it disputable whether the origin of the chiral nematic order is the (twisted) geometry of CNC particles or the (asymmetric) distribution of surface charges.

3.2 Solid Materials from CNC Liquid Crystals

There has been considerable effort over the last 15 years to acquire solid materials that exhibit optical functionality or high mechanical performance from CNC liquid crystals. The main material targets include chiral nematic films consisting of essentially pure cellulose, and similar mesomorphic or uniaxially oriented composites of CNCs with other organic polymers or inorganic substances. Some highlights along these lines are reviewed next, in consideration of future advances.

3.2.1 Chiral Nematic CNC Films

In 1998, Revol et al. reported that iridescent films were successfully obtained by simple evaporation of chiral nematic liquid crystalline aqueous suspensions of acid-hydrolyzed CNCs [77]. The pitch P of the resulting left-handed chiral nematic films, and therefore the wavelength λ_M of the selective light reflection, was tailored by changing the ionic strength of the starting suspensions by addition of NaCl or KCl. The liquid crystalline CNC suspensions can be oriented by applying a magnetic field (e.g., ~7 T), whereby the chiral nematic axis aligns parallel to the field direction, because of the negative diamagnetic susceptibility of the cellulose crystallites [111]. Thereby, unique reflective films were prepared under appropriate conditions of suspension casting with magnetic alignment [77].

The microstructure and morphology of such chiral nematic films of CNCs were well characterized in a short paper by Majoinen et al. [112]; the explanation of SEM images (e.g., arcing and fan-like texture) for the film fracture surfaces was especially useful as an indication of the pitch, handedness, and direction of the chiral nematic director. Earlier, an elaborate work [113] reported the characterization of a parabolic focal conic structure trapped in chiral nematic CNC films using computer-aided modeling combined with polarized-light and atomic force microscopy. The distinctive defect structure was observed by POM in slowly cast, thin CNC films as well as in molecular liquid crystals of polymers and oligomers.

A few papers have provided insight into several parameters (such as NaCl addition, drying temperature, suspension concentration, and exposure to a magnetic field) that affect the chiral nematic pitch and reflection properties of CNC films obtained by casting from aqueous suspensions. Pan et al. [114] demonstrated by CD and POM measurements that the pitch P (absolute value) of CNC cast films decreased with increasing NaCl concentration and with elevating drying temperature, whereas P increased with increasing concentration of the initial suspension ($\leq$2 wt%) and with increasing time of exposure to an applied magnetic field (0.2 T). Beck et al. [115] showed that ultrasonication pretreatment increased the chiral nematic pitch of CNC suspensions and moved the reflection spectral band of the cast, iridescent films to longer wavelengths. This effect of sonication was cumulative and permanent; hence, it was possible to obtain CNC films exhibiting various colorations by using different ultrasonic energy inputs or by accumulation of the

inputs. The same research group proposed a procedure to locally shift the reflection color band in solid chiral nematic CNC films [116]. In the method, pattern-forming objects were used during film casting to modify the heat transfer kinetics to different areas of the evaporating CNC suspension.

With regard to film-making from CNC dispersions in polar organic solvents such as DMSO and DMF, Viet et al. prepared wholly birefringent films both by drying under vacuum (a relatively rapid process) and by drying under ambient conditions (slower process) [96]; however, they found no evidence of a chiral nematic structure.

The following examples [117, 118] are concerned with the production of uniaxially oriented CNC films from isotropic suspensions, not from mesomorphic suspensions; however, the electric field-assisted control of orientation could be important and is worthy of special mention. Bordel et al. [117] attained a high degree of orientation of tunicin CNCs dispersed at ~0.5% w/v in cyclohexane [99] (see Sect. 3.1.2a) by application of an alternating current (AC) electric field (e.g., 2,000 V/cm and 1 kHz). Evaporation of the CNC suspension under the electric field allowed the system to dry into a thin film of CNCs aligned parallel to the electric field. Thus, the behavior of CNCs differs from that (perpendicular alignment) during the application of a strong magnetic field. The optimum conditions for preparing oriented films of tunicin and ramie CNCs from their aqueous suspensions under an AC electric field, by varying the field strength and frequency, were also explored [118]. The orientation of CNCs seems to be more homogeneous with an electric field higher than 2,000 V/cm, with an AC frequency ranging between 10^4 and 10^6 Hz.

3.2.2 Polymer Composites with Liquid Crystalline CNCs

(a) **High-Performance Materials**. A number of studies have been conducted to design and develop high-performance polymer composites reinforced with CNCs as stiff filler [13, 102] since the report by Favier et al. in 1995 [18, 119]. In many cases, CNCs were compounded with thermoplastic polymers by simple mechanical mixing. As another route to microcomposition of CNCs, Tatsumi et al. demonstrated a successful synthesis of polymer composites containing a fixed liquid crystalline arrangement of CNCs via bulk polymerization of monomer solvent [120]. From phase-separated suspensions of cotton CNCs in an aqueous 2-hydroxyethyl methacrylate (HEMA) monomer solution (water to HEMA ratio was 0.5–1.2:1 by volume), polymer composites PHEMA-CNC_{iso} and PHEMA-CNC_{aniso} coming from the upper isotropic phase and the lower anisotropic phase, respectively, were prepared in film form by photopolymerization of HEMA followed by oven-curing and drying. The synthesized composites were transparent (see Fig. 16a), and the fingerprint texture characteristic of chiral nematic liquid crystals prevailed widely in PHEMA-CNC_{aniso} (Fig. 16b), but only appeared locally in PHEMA-CNC_{iso}. Field emission-SEM (FE-SEM) images of the fracture surfaces of PHEMA-

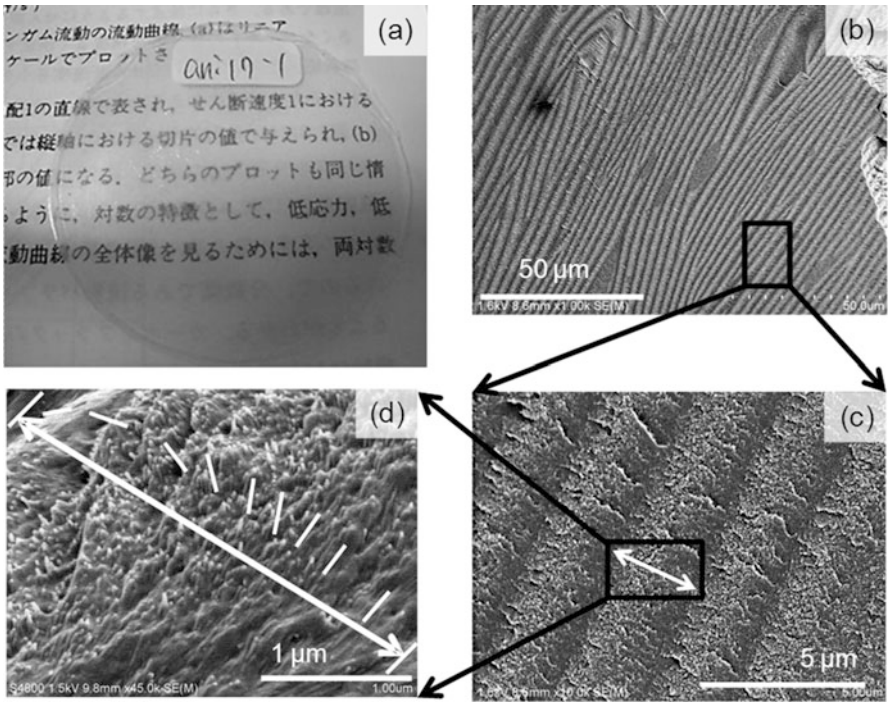

Fig. 16 Morphology of PHEMA-CNC_{aniso} composite film (CNC ≥ 7 wt%): (**a**) visual appearance; (**b–d**) FE-SEM images of the fracture surfaces. The composite film was obtained by polymerization of HEMA from the anisotropic phase of a CNC/water/HEMA suspension (~5.0 wt% CNC; water/HEMA = 0.46:1 by weight) (quoted from Tatsumi et al. [120] with an adequate modification)

CNC_{aniso} revealed a left-handed helicoidal arrangement of fibrous entities assembled in the polymer matrix (Fig. 16c, d). In dynamic mechanical analysis (DMA), the locking-in of the CNC assembly gave rise to an increase in the glassy modulus E' of PHEMA as well as a marked suppression of the E'-drop at temperatures higher than T_g (~110°C) of the vinyl polymer, as exemplified in Fig. 17. These reinforcement effects were usually more pronounced in PHEMA-CNC_{aniso} than in PHEMA-CNC_{iso}. The re-rise of modulus observed at 150–190°C was a secondary effect resulting from crosslinking of PHEMA catalyzed by the acidic CNC filler.

The synthetic strategy for PHEMA-CNC composites substantially follows two works by Nishio et al.; one dealt with an interpenetrating network (IPN)-type of polymer composite from cellulose gels [121], and the other was concerned with locking-in of a chiral nematic mesophase of HPC into polymer composites [122].

An extensive effort was made to synthesize further novel composites from similar CNC suspensions in water/monomer using a magnetic alignment

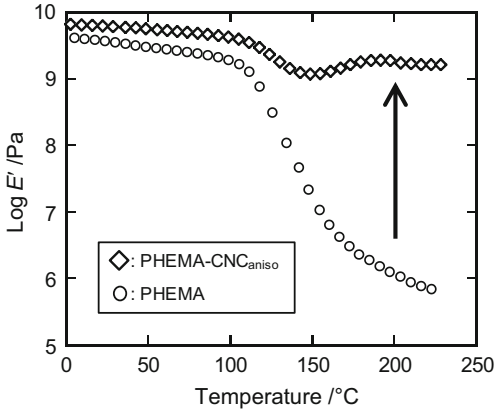

Fig. 17 Dynamic mechanical analysis data for film samples of PHEMA and PHEMA-CNC_{aniso}. Plots of modulus E' versus temperature are compared for the two samples(quoted from Tatsumi et al. [120])

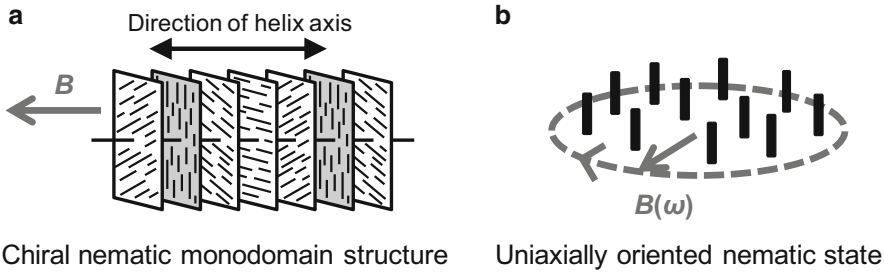

Fig. 18 Control of orientation of CNC assembly under different magnetic fields: (**a**) static magnetic field, whereby one can expect a chiral nematic monodomain structure with the helix axis aligned parallel to the applied field B; (**b**) rotating magnetic field, whereby one can expect an oriented nematic state with the longer axis of CNCs oriented perpendicular to the rotating field $B(\omega)$

technique [123]. As shown in Fig. 18, ideally, the application of a static magnetic field can produce a chiral nematic monodomain structure, and the use of a rotating magnetic field can realize an oriented nematic state (i.e., uniaxial alignment of CNCs) [19, 124]. PHEMA-CNC oriented composites were successfully obtained via photopolymerization of CNC/HEMA aqueous suspensions after treatment with either type of magnetic field. The composites showed definite mechanical anisotropy, reflecting the different arrangements of CNC assembly as mesofiller.

(b) **Multifunctional Materials**. As described in Sect. 2.3.2 for cellulosic molecular liquid crystals, the fixing of chiral nematic CNC mesomorphy into polymeric films or gels is a promising route for production of multifunctional

composites that can exhibit structural colors. Novel chiral nematic hydrogels have been prepared by photopolymerization of hydrogel-forming monomer (acrylamide, *N*-isopropylacrylamide, etc.) dissolved in a concentrated CNC aqueous suspension [125]. The CNC/polymer hydrogels obtained showed changes in iridescence in response to external stimuli such as solvent, pH, or temperature.

Iridescent CNC/polymer composites were also produced solely by slow evaporation of chiral nematic dispersions of CNC (~3.5 wt%) in DMF, which were mixed in advance with a commodity polymer such as polystyrene or poly(methyl methacrylate) [126]. To obtain the stable liquid crystalline suspensions of CNCs in such a polar organic solvent, sulfuric acid-hydrolyzed CNCs were neutralized with a strong base (LiOH, NaOH, KOH, etc.) and freeze-dried before the usual processes of stirring and sonication. The chiral nematic CNC assembly was also immobilized into a crosslinked polymeric network, which allowed synthesis of iridescent and flexible thermosetting resins of CNC/melamine-urea-formaldehyde composite [127]. The coloration of the resins was controlled not only by addition of salt to the initial suspension but also by application of external pressure on the resins. Furthermore, flexible mesoporous phenol-formaldehyde resins with iridescent color were produced by removing CNC entities from chiral nematic CNC/phenol-formaldehyde composites through alkaline treatment at high temperatures (e.g., 70°C) [128]. CNC removal resulted in a blue shift of the iridescent color, probably as a result of the decrease in pitch following volume shrinkage, in addition to the lowered refractive index as a porous material.

3.2.3 CNC/Inorganic Nanohybrids and Outlook

Cellulosic polymer/inorganic hybrid composites imprinted with the chiral nematic liquid crystalline structure of the cellulosic are described in Sect. 2.3.3. The strategic scheme shown in Fig. 15 is also applicable to the design of CNC/inorganic nanocomposites with a helical internal architecture. Recently, the chiral mesomorphic assembly of CNCs has been used as a structural template [104, 129, 130].

Mann et al. presented the first report on the use of CNC liquid crystals as template, particularly for the production of chiral nematic porous silicas by the sol–gel conversion of alkoxysilane and subsequent calcination treatment [131]. Monolithic silicas with such a chiral pore structure were successfully obtained by condensation of prehydrolyzed TMOS precursors in a liquid crystalline aqueous suspension of CNCs, followed by removal of the organic template at 400°C. The resulting silica replica was cracked, but remained birefringent. TEM observations confirmed the chiral imprint of a helically ordered CNC assembly on the silica matrix. It was also revealed that the diameter (~15 nm) of the aligned cylindrical pores was comparable to the width of CNC rods.

More recently, MacLachlan and coworkers synthesized a wide variety of iridescent mesoporous silicas using a chiral nematic CNC liquid crystalline template

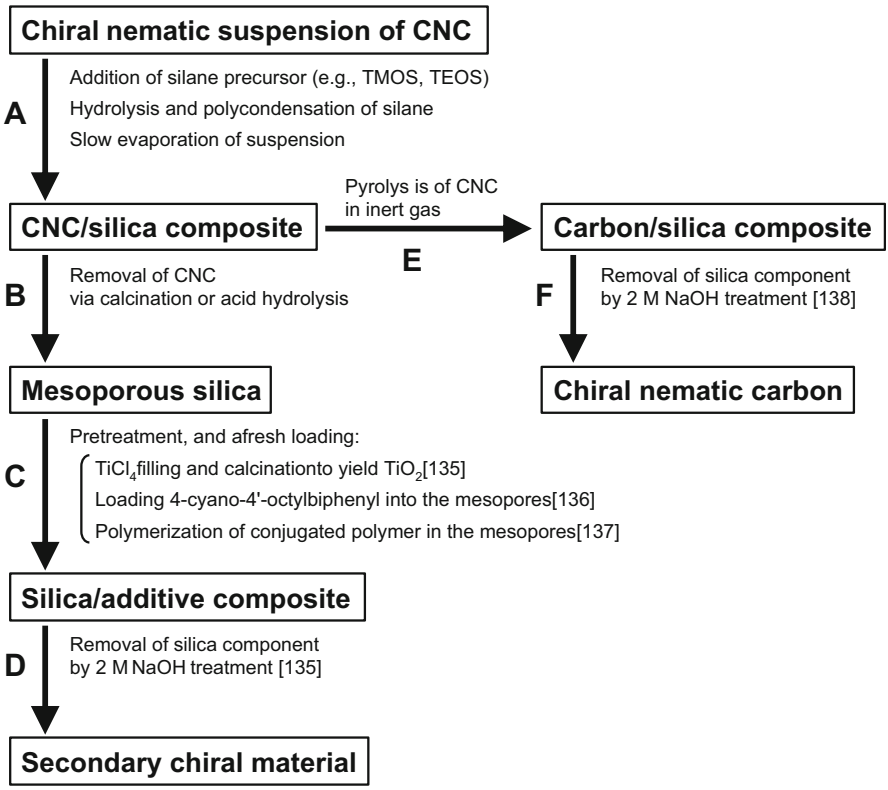

Scheme 5 Various materials prepared by chiral template techniques from liquid crystalline CNC suspensions. Representative examples following the approaches *A*–*F* used by the MacLachlan Group are included[135–138]

[132–134]. It was possible to vary the structural color, derived from the chiral nematic pitch of the hybrids, across the entire visible spectrum by simply changing the CNC/silica composition or by modifying the preparation conditions. They successfully assigned diverse functionalities to the chiral nematic mesoporous silicas by loading organic or inorganic functional guest substances into the mesopores [135–137]. Scheme 5 outlines the preparation protocol used. A sequence of routes (B, C, and D in Scheme 5) correspond to the replacement process of CNC with another guest ingredient. Chiral nematic free-standing carbon films were also prepared from CNC/silica composites via pyrolysis of the CNC component (e.g., at 900°C in N_2 gas) and subsequent removal of the silica component (e.g., with NaOH aqueous solution) [138]. This conversion of CNCs into carbon corresponds to the sequential routes E and F in Scheme 5.

The above results demonstrating many colorful materials could hold much appeal, but attention should be called to the fact that all the materials based on CNC chiral mesomorphy share the common feature of preserving a left-handed

helical structure. By contrast, in the solid materials obtained from cellulosic molecular liquid crystals, the handedness of the chiral nematic twist is exchangeable depending on the side chain structure and substitution degree of the cellulose derivative, as well as on the lyotropic solvent used.

There are also some examples of chitin nanocrystal (ChtNC)/silica hybridization associated with mesomorphic assemblage of ChtNC rods [139, 140]. Here, we refer only to the preparation of an oriented ChtNC composite with silica using an external electric field [140]. In the work, ChtNCs were dispersed in an ethanol/hydrochloric acid aqueous mixture containing siloxane oligomer (from tetraethoxysilane, TEOS) and the resulting co-suspensions of nanorod/siloxane oligomer exposed to an AC electric field (~140 V/mm). The alignment of ChtNCs was monitored by in situ small-angle X-ray scattering and POM observation. When the starting co-suspension was in an anisotropic liquid crystalline state, a higher alignment of ChtNC rods was achieved right after the electric field was applied, resulting in instantaneous formation of a nematic monodomain. The oriented nematic phase was stably preserved for several weeks, even after the electric field was switched off. Therefore, further solvent evaporation induced sol–gel transition of the siloxane oligomer component and, eventually, uniaxially anisotropic chitin/silica nanocomposites were produced in the dried film state.

In comparison with silica hybridizations, few papers have dealt with the deposition and crystal growth of minerals onto CNC or ChtNC rods assembling in a liquid crystalline formation. To mention an example, there was a successful attempt to prepare $CaCO_3$/ChtNC hybrids by a mineralization process from chiral nematic chitin gels [141]. The anisotropic gels were obtained from concentrated aqueous suspensions of ChtNC (acid-hydrolyzed α-chitin from crab) by exposure to ammonium carbonate vapor. The gels were then immersed in an aqueous solution of calcium chloride, whereby polycrystalline calcite deposited in the gel matrix to form a three-dimensional interpenetrated structure. However, the $CaCO_3$/ChtNC composites obtained were not mechanically stable hybrid materials exhibiting high strength. This work could be a step toward the exploitation of new biomimetic mineralization methods. In the future, a number of systematic studies are expected on the nano-aggregation and stabilization of biorelated minerals in the presence of mesoscopically arranged chitinous or cellulosic polysaccharides.

4 Concluding Remarks

In addition to covering the progress in basic studies of cellulosic liquid crystals, this article has given examples of recent approaches to the preparation of cellulosic-based novel materials displaying high functionality or mechanical performance derived from their mesomorphic structure and properties. Related efforts using other polysaccharides were also quoted for reference. Looking over the many comprehensive efforts summarized here, the authors would like to add the following concluding thoughts: Despite the fact that the origin of chiral helicoidal

stacking is still unclear and regardless of whether the mesogenic constituent is a cellulosic molecule or a CNC, the typically formed chiral nematic assemblies in these systems involve fascinating phenomena that can be exploited in the design of advanced cellulosic materials. Luckily, cellulose is endowed with a broad chemical modification capacity through its side group reactivity. In view of its predominance, a wide spectrum of derivatives of both cellulosic polymers and CNCs will revitalize related research fields in the coming decade. In parallel with this, instrumentation, theoretical, and computational work are expected to provide further insights into the chiral asymmetry of cellulosic constituents.

Acknowledgements One of the authors (YN) is grateful to Professor O. J. Rojas of Aalto University for his encouragement and helpful suggestions as well as for his kind invitation to contribute to this special volume. The authors also wish to convey many thanks to Professor Y. Teramoto of Gifu University, and to the graduate students K. Horikiri, T. Ogiwara, and T. Hirata in our laboratory for their assistance in the preparation of this chapter.

References

1. Werbowyj RS, Gray DG (1976) Mol Cryst Liq Cryst (Lett) 34:97
2. Guo J-X, Gray DG (1994) In: Gilbert RD (ed) Cellulosic polymers, blends and composites. Carl Hanser, Munich
3. Gray DG (1994) Carbohydr Polym 25:277
4. Gray DG, Harkness BR (1994) In: Shibaev VP, Lam L (eds) Liquid crystalline and mesomorphic polymers. Springer, New York, 298 p
5. Fukuda T, Takada A, Miyamoto T (1994) In: Gilbert RD (ed) Cellulosic polymers, blends and composites. Carl Hanser, Munich
6. Fukuda T, Tsujii Y, Miyamoto T (1995) Macromol Symp 99:257
7. Zugenmaier P (1994) In: Gilbert RD (ed) Cellulosic polymers, blends and composites. Carl Hanser, Munich
8. Zugenmaier P (1998) In: Demus D, Goodby J, Gray GW, Spiess H-W, Vill V (eds) Handbook of liquid crystals, vol 3. Wiley-VCH, Weinheim
9. de Gennes PG (1975) The physics of liquid crystals. Oxford University Press, Oxford
10. Nishio Y (2006) Adv Polym Sci 205:97
11. Revol J-F, Bradford H, Giasson J, Marchessault RH, Gray DG (1992) Int J Biol Macromol 14:170
12. Habibi Y, Lucia LA, Rojas OJ (2010) Chem Rev 110:3479
13. Klemm D, Kramer F, Moritz S, Lindström T, Ankerfors M, Gray DG, Dorris A (2011) Angew Chem Int Ed 50:5438
14. Onsager L (1949) Ann N Y Acad Sci 51:627
15. Flory PJ (1956) Proc R Soc Lond A 234:73
16. Dong XM, Kimura T, Revol J-F, Gray DG (1996) Langmuir 12:2076
17. Dong XM, Revol J-F, Gray DG (1998) Cellulose 5:19
18. Favier V, Chanzy H, Cavaillé JY (1995) Macromolecules 28:6365
19. Kimura F, Kimura T, Tamura M, Hirai A, Ikuno M, Horii F (2005) Langmuir 21:2034
20. Flory PJ (1984) Adv Polym Sci 59:1
21. Gray DG (1985) Faraday Discuss Chem Soc 79:257
22. Sato T, Teramoto A (1996) Adv Polym Sci 126:85
23. Swatloski RP, Spear SK, Holbrey JD, Rogers RD (2002) J Am Chem Soc 124:4974

24. Song H, Niu Y, Wang Z, Zhang J (2011) Biomacromolecules 12:1087
25. de Vries H (1951) Acta Crystallogr 4:219
26. Straley JP (1976) Phys Rev A 14:1835
27. Osipov MA (1988) Nuovo Cimento 10D:1249
28. Werbowyj RS, Gray DG (1980) Macromolecules 13:69
29. Fortin S, Charlet G (1989) Macromolecules 22:2286
30. Nishio Y, Chiba R, Miyashita Y, Oshima K, Miyajima T, Kimura N, Suzuki H (2002) Polym J 34:149
31. Chiba R, Ito M, Nishio Y (2010) Polym J 42:232
32. Rwei S-P, Lyu M-S, Wu P-S, Tseng C-H, Huang H-W (2009) Cellulose 16:9
33. Tseng SL, Valente A, Gray DG (1981) Macromolecules 14:715
34. Hou H, Reuning A, Wendorff JH, Greiner A (2000) Macromol Chem Phys 201:2050
35. Huang B, Ge JJ, Li Y, Hou H (2007) Polymer 48:264
36. Yamagishi T, Nakamoto Y, Sixou P (2006) Cellulose 13:205
37. Ritcey AM, Gray DG (1988) Macromolecules 21:1251
38. Guo J-X, Gray DG (1989) Macromolecules 22:2086
39. Guo J-X, Gray DG (1994) J Polym Sci B Polym Phys 32:2529
40. Ties JC, Cowie JMG (2001) Polymer 42:1297
41. Nada T, Teramoto, Y, Nishio Y (2010) 17th annual meeting of the cellulose society of Japan, Preprints 17:61
42. Horikiri K, Aoki D, Teramoto, Y, Nishio Y (2014) 21st annual meeting of the cellulose society of Japan, Preprints 21:98
43. Shimamoto S, Gray DG (1998) Chem Mater 10:1720
44. Zugenmaier P (1998) In: Dumitriu S (ed) Polysaccharides: structural diversity and functional versatility. Marcel Dekker, New York
45. Rout DK, Barman SP, Pulapura SK, Gross RA (1994) Macromolecules 27:2945
46. Asahina D, Miyashita Y, Nishio Y (1999) Sen'I Gakkaishi 55:28
47. Asahina D, Matsubara T, Miyashita Y, Nishio Y (2000) Sen'I Gakkaishi 56:435
48. Dong Y, Yuan Q, Wu Y, Wang M (2000) J Appl Polym Sci 76:2057
49. Kuse Y, Asahina D, Nishio Y (2009) Biomacromolecules 10:166
50. Revol J-F, Marchessault RH (1993) Int J Biol Macromol 15:329
51. Sato J, Morioka N, Teramoto Y, Nishio Y (2014) Polym J 46:559
52. Uematsu I, Uematsu Y (1984) Adv Polym Sci 59:37
53. Robinson C (1961) Tetrahedron 13:219
54. Duke RW, Du Pré DB, Hines WA, Samulski ET (1976) J Am Chem Soc 98:3094
55. Samulski TV, Samulski ET (1977) J Chem Phys 67:824
56. Zugenmaier P, Voihsel M (1984) Macromol Chem Rapid Commun 5:245
57. Oyamada K, Terao K, Suwa M, Kitamura S, Sato T (2013) Macromolecules 46:4589
58. Terao K, Maeda F, Oyamada K, Ochiai T, Kitamura S, Sato T (2012) J Phys Chem B 116:12714
59. Matsuo K, Gekko K (2004) Carbohydr Res 339:591
60. Matsuo K, Namatame H, Taniguchi M, Gekko K (2009) Biosci Biotechnol Biochem 73:557
61. Chiba R, Nishio Y, Miyashita Y (2003) Macromolecules 36:1706
62. Nishio Y, Chiba R (2003) Ekisho 7:218
63. Chiba R, Nishio Y, Sato Y, Ohtaki M, Miyashita Y (2006) Biomacromolecules 7:3076
64. Ito M, Teramoto Y, Nishio Y (2012) Biomacromolecules 13:569
65. Wang L, Huang Y (2003) Macromol Symp 192:207
66. Wenzlik D, Ohm C, Serra C, Zentel R (2011) Soft Matter 7:2340
67. Wenzlik D, Zentel R (2013) Macromol Chem Phys 214:2405
68. Arrighi V, Cowie JMG, Vaqueiro P, Prior KA (2002) Macromolecules 35:7354
69. Wang L, Huang Y (2004) Macromolecules 37:303
70. Goto H, Akagi K (2006) Chem Mater 18:255

71. Ogiwara T, Teramoto Y, Nishio Y (2013) 62nd annual meeting of the society of polymer science, Japan. Polym Preprints Jpn 62:1049
72. Nishio Y, Susuki S, Takahashi T (1985) Polym J 17:753
73. Nishio Y, Fujiki Y (1991) J Macromol Sci Phys B30:357
74. Nishimura T, Ito T, Yamamoto Y, Yoshio M, Kato T (2008) Angew Chem Int Ed 47:2800
75. Thomas A, Antonietti M (2003) Adv Funct Mater 13:763
76. Sato J, Teramoto Y, Nishio Y (2013) 3rd European Polysaccharide Network of Excellence (EPNOE) international polysaccharide conference, Nice, France. Book of abstracts, p 120
77. Revol J-F, Godbout L, Gray DG (1998) J Pulp Paper Sci 24:146
78. Edgar CD, Gray DG (2001) Cellulose 8:5
79. Odijk T (1986) Macromolecules 19:2313
80. Lima MMD, Borsali R (2004) Macromol Rapid Commun 25:771
81. Araki J, Kuga S (2001) Langmuir 17:4493
82. Hirai A, Inui O, Horii F, Tsuji M (2009) Langmuir 25:497
83. Araki J, Wada M, Kuga S, Okano T (1998) Colloids Surf A 142:75
84. Roman M, Winter WT (2004) Biomacromolecules 5:1671
85. Araki J, Wada M, Kuga S, Okano T (2000) Langmuir 16:2413
86. Araki J, Wada M, Kuga S, Okano T (1999) J Wood Sci 45:258
87. Habibi Y, Chanzy H, Vignon MR (2006) Cellulose 13:679
88. Leung ACW, Hrapovic S, Lam E, Liu Y, Male K, Mahmoud KA, Luong JHT (2011) Small 7:302
89. Castro-Guerrero CF, Gray DG (2014) Cellulose 21:2567
90. Wang N, Ding E, Cheng R (2008) Langmuir 24:5
91. Dong XM, Gray DG (1997) Langmuir 13:2404
92. Beck-Candanedo S, Viet D, Gray DG (2006) Cellulose 13:629
93. Edgar CD, Gray DG (2002) Macromolecules 35:7400
94. Beck-Candanedo S, Viet D, Gray DG (2006) Langmuir 22:8690
95. Beck-Candanedo S, Viet D, Gray DG (2007) Macromolecules 40:3429
96. Viet D, Beck-Candanedo S, Gray DG (2007) Cellulose 14:109
97. Azizi Samir MAS, Alloin F, Sanchez J-Y, El Kissi N, Dufresne A (2004) Macromolecules 37:1386
98. van den Berg O, Capadona JR, Weder C (2007) Biomacromolecules 8:1353
99. Heux L, Chauve G, Bonini C (2000) Langmuir 16:8210
100. Elazzouzi-Hafraoui S, Putaux J-L, Heux L (2009) J Phys Chem B 113:11069
101. Zhou Q, Brumer H, Teeri TT (2009) Macromolecules 42:5430
102. Moon RJ, Martini A, Nairn J, Simonsen J, Youngblood J (2011) Chem Soc Rev 40:3941
103. Araki J (2013) Soft Matter 9:4125
104. Habibi Y (2014) Chem Soc Rev 43:1519
105. Goussé C, Chanzy H, Excoffier G, Soubeyrand L, Fleury E (2002) Polymer 43:2645
106. Araki J, Wada M, Kuga S (2001) Langmuir 17:21
107. Kloser E, Gray DG (2010) Langmuir 26:13450
108. Yi J, Xu Q, Zhang X, Zhang H (2008) Polymer 49:4406
109. Xu Q, Yi J, Zhang X, Zhang H (2008) Eur Polym J 44:2830
110. Yi J, Xu Q, Zhang X, Zhang H (2009) Cellulose 16:989
111. Revol J-F, Godbout L, Dong XM, Gray DG, Chanzy H, Maret G (1994) Liq Cryst 16:127
112. Majoinen J, Kontturi E, Ikkala O, Gray DG (2012) Cellulose 19:1599
113. Roman M, Gray DG (2005) Langmuir 21:5555
114. Pan J, Hamad W, Straus SK (2010) Macromolecules 43:3851
115. Beck S, Bouchard J, Berry R (2011) Biomacromolecules 12:167
116. Beck S, Bouchard J, Chauve G, Berry R (2013) Cellulose 20:1401
117. Bordel D, Putaux J-L, Heux L (2006) Langmuir 22:4899
118. Habibi Y, Heim T, Douillard R (2008) J Polym Sci B Polym Phys 46:1430

119. Favier V, Canova GR, Cavaillé JY, Chanzy H, Dufresne A, Gauthier C (1995) Polym Adv Technol 6:351
120. Tatsumi M, Teramoto Y, Nishio Y (2012) Biomacromolecules 13:1584
121. Nishio Y, Hirose N (1992) Polymer 33:1519
122. Nishio Y, Yamane T, Takahashi T (1985) J Polym Sci Polym Phys Ed 23:1043
123. Tatsumi M, Kimura F, Kimura T, Teramoto Y, Nishio Y (2014) Biomacromolecules 15:4579
124. Kimura F, Kimura T (2008) Sci Technol Adv Mater 9:024212
125. Kelly JA, Shukaliak AM, Cheung CCY, Shopsowitz KE, Hamad WY, MacLachlan MJ (2013) Angew Chem Int Ed 52:8912
126. Cheung CCY, Giese M, Kelly JA, Hamad WY, MacLachlan MJ (2013) ACS Macro Lett 2:1016
127. Giese M, Khan MK, Hamad WY, MacLachlan MJ (2013) ACS Macro Lett 2:818
128. Khan MK, Giese M, Yu M, Kelly JA, Hamad WY, MacLachlan MJ (2013) Angew Chem Int Ed 52:8921
129. Lin N, Huang J, Dufresne A (2012) Nanoscale 4:3274
130. Lagerwall JPF, Schütz C, Salajkova M, Noh J, Park JH, Scalia G, Bergström L (2014) NPG Asia Mater 6:e80
131. Dujardin E, Blaseby M, Mann S (2003) J Mater Chem 13:696
132. Shopsowitz KE, Qi H, Hamad WY, MacLachlan MJ (2010) Nature 468:422
133. Nguyen T-D, Hamad WY, MacLachlan MJ (2013) Chem Commun 49:11296
134. Shopsowitz KE, Kelly JA, Hamad WY, MacLachlan MJ (2014) Adv Funct Mater 24:327
135. Shopsowitz KE, Stahl A, Hamad WY, MacLachlan MJ (2012) Angew Chem Int Ed 51:6886
136. Giese M, Witt JCD, Shopsowitz KE, Manning AP, Dong RY, Michal CA, Hamad WY, MacLachlan MJ (2013) ACS Appl Mater Interfaces 5:6854
137. Mehr SHM, Giese M, Qi H, Shopsowitz KE, Hamad WY, MacLachlan MJ (2013) Langmuir 29:12579
138. Shopsowitz KE, Hamad WY, MacLachlan MJ (2011) Angew Chem Int Ed 50:10991
139. Nguyen T-D, Shopsowitz KE, MacLachlan MJ (2013) Chem Eur J 19:15148
140. Boltoeva MY, Dozov I, Davidson P, Antonova K, Cardoso L, Alonso B, Belamie E (2013) Langmuir 29:8208
141. Yamamoto Y, Nishimura T, Saito T, Kato T (2010) Polym J 42:583

Adv Polym Sci (2016) 271: 287–328
DOI: 10.1007/12_2015_323

Published online: 11 September 2015

Photonic and Semiconductor Materials Based on Cellulose Nanocrystals

Wadood Y. Hamad

Abstract Cellulose nanocrystals (CNCs) are renewable, sustainable nanomaterials, typically produced by strong sulfuric acid hydrolysis of lignocellulosic biomass. CNCs can self-assemble in aqueous, and other, suspensions at a critical concentration, or under evaporation, into chiral nematic organization to exhibit anisotropic structural color. The degree of sulfation is critical for producing both stable colloidal suspensions and iridescent films by evaporation-induced self-assembly. CNCs also possess electromagnetic and piezoelectric properties, as well as active surface groups that render them suitable for tailored functionalization. This chapter presents a framework of how CNCs can be used to (i) template in/organic mesoporous photonic and electronic materials and structures, and (ii) develop sustainable, flexible electronics. Using a novel supramolecular co-templating approach, the first example of functional, mesoporous, photonic cellulose films, or nanopaper, has been produced. The CNC-templating approach is a scalable, effective tool for imparting long-range chirality in a number of distinct materials (polymer, silica, metal oxides, carbon) with promising applications in, for example, optoelectronics, biosensors, actuators, functional membranes, 3D printing, and tissue engineering.

Keywords Cellulose • Mesoporous • Nanocrystals • Optoelectronics • Photonics • Sensors • Supramolecular

Contents

W.Y. Hamad (✉)
Cellulosic Biomaterials Group, FPInnovations, Department of Chemistry, University of British Columbia, Vancouver, BC, Canada
e-mail: wadood.hamad@fpinnovations.ca

1 Introduction

Cellulose nanocrystals (CNCs), produced using strong acid hydrolysis (typically sulfuric acid) of wood, plant, or marine animal biomass, are transformative materials that are nontoxic and sustainable [1, 2]. CNCs possess fascinating electromagnetic and photonic properties. The piezoelectric effect[1] in wood was first reported by Bazhenov over half-a-century ago; however, it was shown that the magnitude of the piezoelectric constant was small in wood fibers, primarily as a result of the random, heterogeneous distribution of fibers and the relatively small amount of crystalline cellulose in the amorphous hemicellulose-and-lignin matrix [3]. Native cellulose (cellulose I) in plant and wood cell walls has been shown to possess a non-centrosymmetric structure, as the cellulose chains have a chemical polarity and all point in the same direction [4].

Recently, Frka-Petesic et al. [5] employed the transient electric birefringence (TEB) method to probe the electric properties of CNC colloids and obtain quantitative information on the rotational diffusion, size, and polarization properties of CNCs dispersed in an organic solvent. They showed experimental evidence, for the first time, of remarkable re-orientation of cellulose nanocrystals in response to electric field reversal [5]. This re-orientation presents a strong argument for the existence of a permanent dipolar moment inside the CNCs (i.e., permanent polarization of CNCs) or cellulose I [5]. The permanent dipolar moment for CNCs has been experimentally determined as equal to $4{,}400 \pm 400$ Debye [5], or one order of magnitude higher than that measured for some widely researched and commercially available quantum-dot nanocrystals, such as cadmium sulfide (CdS) nanocrystals [6]. Frka-Petesic et al. [5] explained the origin of the permanent dipolar moment in CNCs by a combination of factors: (1) the asymmetric nature of the polar

[1] Piezoelectricity is related to the change in polarization density and the occurrence of dipole moments within a material.

glucopyranosyl monomers, (2) the chemical polarity of the cellulose chains, and (3) the parallel, non-centrosymmetric structure of the chains in cellulose I inside each CNC. These findings can contribute to an understanding of the underlying mechanisms of CNC self-assembly, as well as advance strategies for advanced material design (e.g., using CNCs to template nonlinear optical materials for applications in photonics and optoelectronics).

The asymmetric, crystalline structure of CNCs can also display inhomogeneous deformation of strain gradients, associated with the piezoelectric response to an applied electrical field [7]. Csoka et al. [7] provided experimental evidence for a large piezoelectric response associated with CNCs, and prepared ultrathin CNC films that could induce high electromechanical actuation and strain dependence on CNC alignment. As such, CNCs could effectively be used as sustainable materials for applications requiring the design and fabrication of high mechano-electrical energy transfer [7]. On a relevant note, anisotropic, homogeneously oriented ultrathin films of CNCs can be obtained using a convective assembly set-up coupled with a low-strength external AC electric field [8, 9]. The orientation and degree of alignment of the spindle-like nanoparticles can be controlled by the applied field strength and frequency used during thin film formation [8, 9].

Biological communication by means of structural color has existed for at least half-a-millennium, whereby layered transparent photonic stacks are responsible for brilliant colors in a variety of living organisms [10–12]. Although the structure and, hence, color are locked in these naturally occurring photonic materials, some animals, flowers, and fruits have the capacity to show tunable iridescence (e.g., the longfin inshore squid *doryteuthis pealeii*) [13–15]. Biomimetic replication of such natural phenomena can not only contribute to a more fundamental understanding of structural color in plants and animals, but also assist in the design of sustainable advanced materials for applications in, for instance, photonics and optoelectronics.This contribution specifically focuses on the utilization of CNCs for developing proof-of-concept material platforms. We discuss a number of novel approaches describing the advancement, over the past decade or so, of (1) chiral nematic mesoporous polymer films and hydrogels; (2) chiral nematic mesoporous silica, metal oxides, and hybrid materials and structures templated by CNCs; and (3) flexible organic semiconductor materials based on CNCs.

2 Mesoporous Photonic Cellulose Films

An innovative form of *active* paper with a mesoporous chiral nematic structure, referred to as photonic nanopaper or mesoporous photonic cellulose (MPC) film, has recently been developed for the first time using an elegant and conceptually new supramolecular co-templating strategy [16]. MPC films are flexible, display dynamic photonic properties, and undergo rapid, reversible color changes in response to variation in solvent polarity or pressure [16]. The bio-inspired, selective color tuning (from red to blue and vice versa; see Sect. 3) of MPCs can potentially

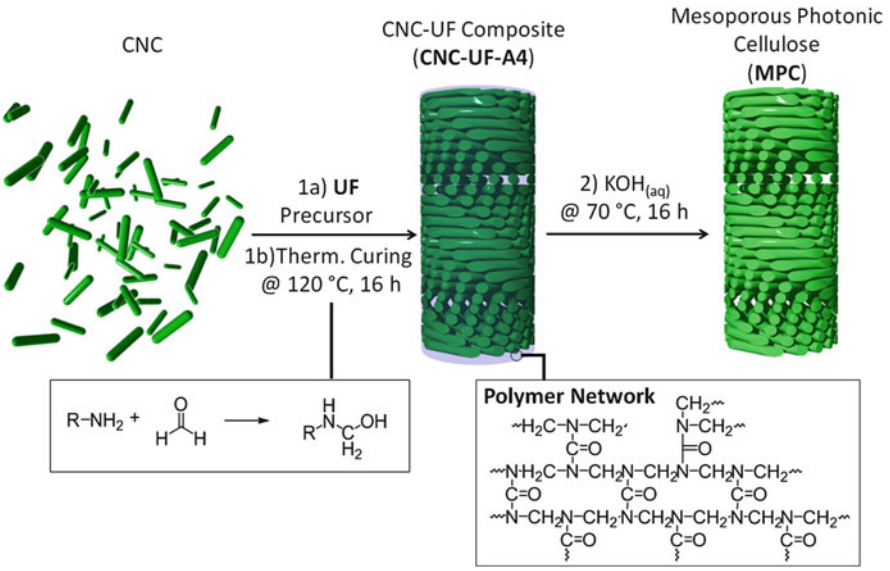

Fig. 1 Synthetic route to photonic nanopaper or mesoporous photonic cellulose (MPC) films. Initially, an aqueous suspension of cellulose nanocrystals (CNCs) is combined with a urea-formaldehyde (UF) precursor. Following evaporation-induced self-assembly, a CNC–UF composite with chiral nematic order is obtained. Thermal curing of the composite is followed by treatment with aqueous KOH to yield MPC films (after Giese et al. [16])

provide the basis for dynamically controlled optical filters and sensors. They can also be used as a novel, sustainable hard templates to access diverse mesoporous materials for applications in gas separation, membranes, and drug delivery.

MPC films are produced via a (relatively) facile, scalable, two-step synthesis [16]. In the first step (Fig. 1), chiral nematic composite films are synthesized by self-assembly of lyotropic CNCs in the presence of a urea-formaldehyde (UF) precursor. The UF/CNC mixture is dried overnight at ambient conditions, followed by heat curing at 120°C to complete the polymerization. In the second step, alkaline treatment of the composite films with 15% $KOH_{(aq)}$ at 70°C removes UF[2] and results in iridescent and insoluble cellulose films (MPC). This method represents a novel approach for creating functional cellulosic materials by supramolecular co-templating, whereby UF and CNCs act as synergetic templates: CNCs first serve as a template to construct CNC–UF composite films, and the UF functions as a secondary template. Removal of the secondary template affords a

[2] Giese et al. [16] confirmed complete removal of UF using three analytical methods: (1) elemental analysis, showing no nitrogen was present; (2) IR spectroscopy, showing that the diagnostic carbonyl vibration of UF at 1,664 cm^{-1} was absent; and (3) solid-state ^{13}C CP/MAS NMR, showing that the carbonyl and methylene groups assigned to the UF resin were clearly present in the ^{13}C NMR spectrum of the composites, but inexistent in the CMP spectrum.

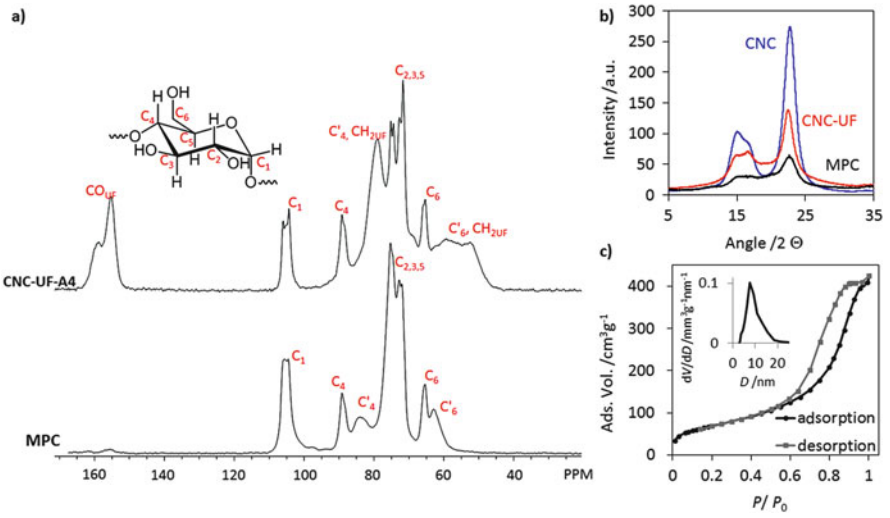

Fig. 2 Structural characterization of MPC films. (**a**) Solid-state ^{13}C CP/MAS NMR spectra of the CNC–UF composite and MPC. (**b**) PXRD pattern of pristine CNCs (cellulose I), CNC–UF composite, and MPC. (**c**) Isothermal N_2 adsorption of MPC dried from EtOH with supercritical CO_2 (BET surface area), as well as the corresponding BJH pore-size distribution calculated from the adsorption branch of the isotherm (*inset*) (adapted from Giese et al. [16])

cellulose film with chiral nematic order and enhanced stability, flexibility, and mesoporosity [16].

Structural characterization of MPC films confirms that they maintain the cellulose I structure, exactly as with CNCs. The solid-state ^{13}C cross-polarization/magic-angle spinning (CP/MAS) NMR spectrum of MPC shows all the expected peaks for crystalline cellulose (Fig. 2a). However, reduced crystallinity of the MPC films relative to the starting CNCs is confirmed from signal broadening as well as new peaks at ~84 and ~62 ppm, assigned to amorphous or surface cellulose (C4′ and C6′, respectively) [17]. Powder X-ray diffraction (PXRD) patterns further indicate (Fig. 2b) that MPC films have a substantially lower degree of crystallinity (~70%) than pure CNCs (>90%), but maintain the cellulose I structure [16].[3] Moreover, MPC films exhibit similar thermal stability to Na-CNCs and CNC–UF composites, but show enhanced stability relative to pristine CNCs. MPC films are stable in water, including boiling water, for weeks and undergo no decomposition, whereas CNCs disperse in water within 1–2 h [16]. The enhanced stability of MPCs

[3] Giese et al. [16] confirmed that there was no experimental evidence for methylene ether crosslinking between surface hydroxyl groups of the CNCs. They also carried out a control experiment in which pristine CNCs (with no UF) were treated with 15% $KOH_{(aq)}$ solution under identical conditions. The control experiment produced, as expected [18], mercerized cellulose, or the conversion from cellulose I to cellulose II.

can be explained by desulfation of the CNCs surfaces, leading to nonpolar and nondispersible cellulose films.[4]

The color reflected by a chiral nematic structure can be modulated by manipulating the pitch or refractive index of the medium. This stems from the fact that chiral nematic structures reflect light with a wavelength (λ_{max}) that depends on the helical pitch (P), the angle of incident light (θ), and the average refractive index (n_{avg}), of the material according to the following equation [19]:

$$\lambda_{max} = n_{avg} \cdot P \cdot \sin(\theta) \quad (1)$$

Thus, a red shift is observed with increasing polymer content in the CNC–UF composites, , whereas a blue shift occurs with increasing ionic strength. Coloration of the MPC films can be varied in the range 500–1,300 nm [16]. The composite film appears nearly transparent and colorless (reflecting at 1,300 nm; see Fig. 3a), whereas the MPC film (dried from water) is colorless with faint blue iridescence (reflecting at 331 nm; Fig. 3b). However, if the MPC film is dried with supercritical CO_2, then iridescence is clearly visible (reflecting at 500 nm; Fig. 3c). A red-shifted reflectance, compared with the water-dried MPC film, indicates that the pitch of the chiral nematic order (P) increases with the introduction of mesoporosity [16]. Scanning electron microscopy (SEM) images of water-dried and supercritically dried MPC films (Fig. 3b, c) illustrate a layered structure that is typical of chiral nematic order. However, the microstructure after supercritical drying appears less ordered than that of water-dried MPC films, and this heterogeneity could contribute to the apparent opacity of the former [16].

Mesoporosity (indicated by the translucent appearance) in MPC films originates from removal of the space-filling polymer co-template. Films dried in air from water or ethanol show no porosity; however, supercritical CO_2 drying of ethanol-soaked films preserves the porosity in MPC films [16]. These MPC films possess a type IV isotherm with a Brunauer–Emmett–Teller (BET) surface area of ca. 250 m^2/g and an average pore volume of 0.6 cm^3/g (Fig. 2c). The calculated Barrett–Joyner–Halenda (BJH) average pore size is ca. 8 nm (Fig. 2c, inset).

MPC films show a rapid and visible red-shift of the reflection peak from 330 nm (dry) to 820 nm when immersed in water (Fig. 4c). This is a significantly faster response than reported for photonic hydrogels [20, 21] and polymer composites with tunable photonic properties [22]. Moreover, the degree of swelling is sensitive to the solvent used [22]. For example, immersing MPC films in a mixture of water and ethanol permits tuning from blue (reflection at 430 in pure ethanol) to colorless (reflection at 840 nm in pure water) (see Fig. 4a, b). Because ethanol and water have

[4] Giese et al. [16] registered a substantial drop in sulfate groups, as inferred from elemental sulfur, after alkaline treatment to remove UF. However, it is remarkable that MPC films retain chiral nematic organization, perhaps as a result of simultaneous desulfation and UF decomposition. It is worth pointing out that desulfated CNC nanoparticles and CNCs prepared by means that do not give a surface charge (e.g., free-radical oxidation) are unable to form chiral nematic lyotropic phases.

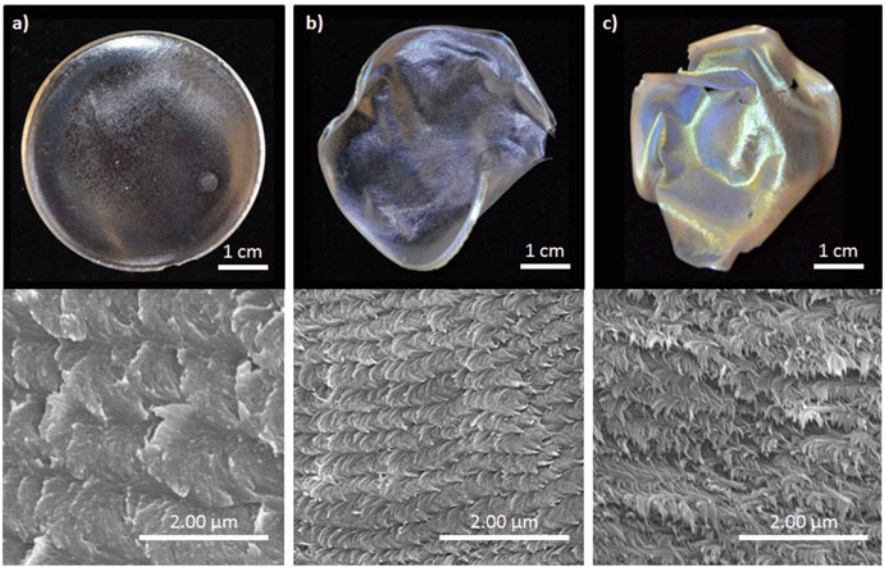

Fig. 3 Optical characterization of the CNC–UF composite and resulting MPC film. (**a**) Photograph of composite film after curing, with its SEM image *below*. (**b**) Photograph of MPC air-dried from H_2O, with its SEM image *below*. (**c**) Photograph of MPC dried from EtOH with supercritical CO_2, with its SEM image *below* (adapted from Giese et al. [16])

refractive indices similar to that of cellulose, the color change is primarily attributed to a change in helical pitch upon swelling [22], which can reliably be detected via ultraviolet–visible (UV-vis) or circular dichroism (CD) spectroscopy (Fig. 4b).

The combination of flexibility and fast swelling behavior renders MPC films pressure sensitive. Giese et al. [16] detected a distinctive color change when, for instance, a water-soaked CMP film sandwiched between two glass slides was subjected to moderate external pressure. This is essentially akin to various examples of naturally occurring structural color changes, such as the tunable iridescence of a squid's iridophores under external applied pressure [14]. In this case, as with MPC films, the applied macroscopic pressure is transferred to the nanoscale level, leading to compression of the layers and consequent reduction in the helical pitch of the chiral nematic structure [13, 16]. MPC films blue-shift an approximately 100 nm reflectivity range from 630 to 520 nm when subjected to external pressures up to 7.8×10^6 N m^{-2} (Fig. 4d). The change in photonic color of MPC films as a function of applied pressure (Fig. 4e) can be used to produce a rough estimate of Young's modulus, ~0.02 GPa, which is in the range of rubber materials [13, 16]. It is important to note that coloration under pressure is completely reversible; once external pressure is removed, the film relaxes and reverts to its initial colorless state [13, 16]. This can form the basis for developing reliable, accurate, and cost-effective sensors.

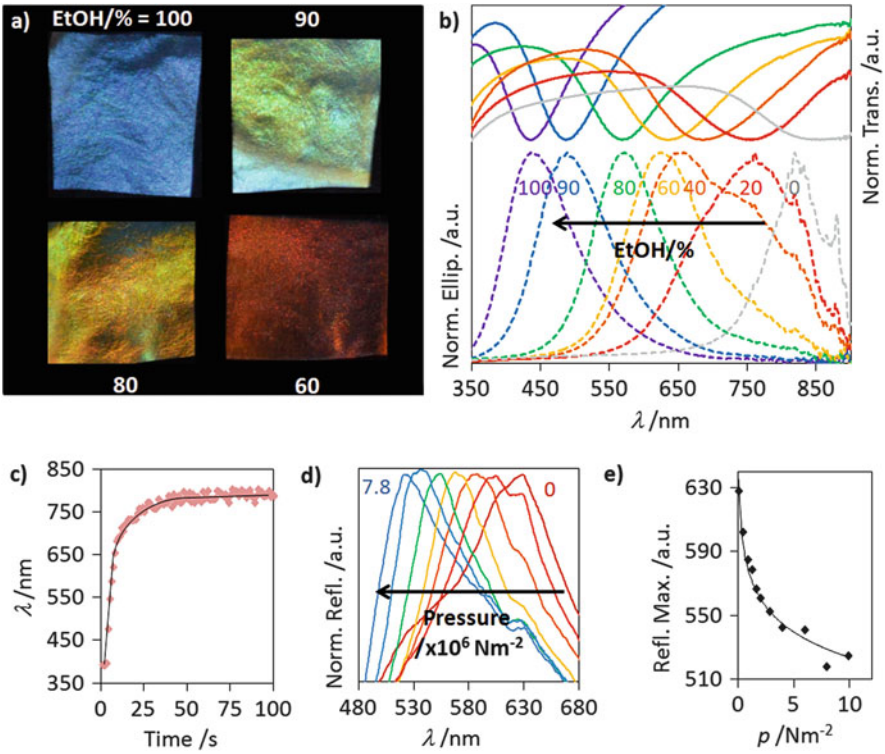

Fig. 4 Sensing performance of the functional MPC films. (**a**) Photographs of MPC soaked in different EtOH/H_2O mixtures, as indicated. (**b**) UV-vis (*solid lines*) and CD spectra (*dashed lines*). (**c**) Swelling kinetics of MPC, showing the dependence of wavelength on time when a dry sample is immersed in water. (**d**) Pressure response of MPC at 0, 0.4, 0.8, 1.6, 2.7, 5.9 and 7.8 × 10^6 N m^{-2} (first and final values are indicated), showing a clear blue-shift of the peak reflectance wavelength. (**e**) Peak reflection wavelength plotted versus pressure; data were fit with an exponential curve (adapted from Giese et al. [16])

In summary, mesoporous photonic cellulose films can be prepared using a scalable, supramolecular co-templating approach, whereby two components (CNCs and a suitable polymer) function as synergetic templates. MPC films, the first example of an active cellulosic material, are obtained by removing the polymer through alkaline treatment to produce flexible films of pure cellulose I, albeit at lower crystallinity than starting CNCs. MPC films display dynamic photonic properties and show rapid responses to external stimuli such as pressure and solvent polarity, thereby having application as potentially effective sensors or optical filters [16]. The mesoporous chiral nematic structure of MPC films can also be used to stabilize monodisperse metal nanoparticles (NPs) such as Au NPs [23]. Au NPs formed within the MPC film show a NP-based plasmonic chiroptical activity arising from interaction with the chiral nematic environment of the MPC film [23].

MPC films can also be used as a novel hard template to access diverse mesoporous materials for a variety of applications ranging from gas separation to drug delivery.[5]

3 Mesoporous Plastics with Tunable Photonic Properties

CNC self-assembly into chiral nematic structures that can be used as removable templates for synthesizing inorganic mesoporous materials with tunable photonic properties. Similarly, the approach can be extended to produce mesoporous polymer resins with tunable photonic properties. Khan et al. [22] used an aqueous mixture of dispersed CNCs and ethanol solution of phenol-formaldehyde (PF) precursor at neutral pH.[6] Brilliantly iridescent polymer films were produced after air-drying (under ambient conditions) and curing (for 24 h at 75°C to enhance PF crosslinking) the composite films, followed by treatment with aqueous NaOH solution to remove the CNC template, and supercritical drying of methanol-soaked films with CO_2. The color of the composite film (prior to CNC removal) could be controlled by increasing the ratio of PF precursor (resulting in a red shift) or the addition of salts such as NaCl (leading to a blue shift) [22]. Both approaches affect the helical pitch (P) of the chiral nematic CNC phase, which – in combination with the average refractive index (n_{avg}) of the material – shifts the peak wavelength (λ_{max}) of the light reflected by the chiral nematic structure.[7]

Mesoporosity of these chiral nematic polymer films was evident after CNC removal by base treatment and subsequent supercritical drying (to remove methanol). The BET surface area was estimated to be in the range 310–365 m^2/g, with a

[5] Chiral nematic mesoporous cellulose (CNMC) materials can also be synthesized from CNC–silica composites (see Sect. 5 for details on CNC templating of chiral nematic mesoporous silica). The optical and physical properties of the final CNMC material can be readily adjusted to produce different helical pitches but identical porosity [24]. The CNMC materials have been shown to have very high surface areas (up to 314 $m^2\ g^{-1}$) and large average pore widths (up to 15.7 nm). Characteristically, the CNMC materials show a high degree of crystallinity that is comparable to pure CNC films, indicating no adverse effect of the preparation process. In addition, the materials were used to stabilize gold nanoparticles, which can be controlled by changing the concentration of the gold precursor solution. These composite materials show chiroptical properties as a result of interaction between the surface plasmon resonance of the gold nanoparticles and the chiral nematic environment provided by the CNMC host. The new CNMC and Au@CNMC composite materials have potential utility in novel biosensors, security features, membranes, and chromatography materials [24].

[6] Low molecular weight polymers, $M_w = 500–5{,}000$, work best for this approach [22].

[7] CD and UV-vis spectroscopy, as well as polarized optical microscopy (POM) and SEM, are typically used to confirm the CNC-imparted twisted layer structure of the left-handed chiral nematic organization of both composite and mesoporous photonic polymer films [22]. Furthermore, removal of the CNC template to produce chiral nematic mesoporous polymer films was confirmed by IR and CP/MAS NMR spectra, indicating removal of 85–90% of the CNCs during base treatment [22]. Moreover, PXRD has been used to confirm CNC removal by a significant drop in the intensity of the reflection peaks assigned to CNCs relative to the composite films, combined with loss of crystallinity in the remaining cellulose in the resin films [22].

pore volume average of 0.5–0.7 cm^3/g [22].[8] CNC-templated polymer films exhibit unique photonic properties precisely because of the combination of chiral nematic ordering, mesoporosity, and responsive behavior, while retaining the mechanical and thermal performance of the polymer resin. The systematic shift in color upon swelling in mixtures of ethanol and water with varying ratios can be easily followed with the naked eye (Fig. 5). The response is reversible, characteristically fast (within seconds; see Fig. 5c), and shows a large range (Fig. 5d). This demonstrates the general potential of these chiral nematic mesoporous polymers as unique optical sensors [22]. One particular advantage of these plastics is that the CD spectrum rather than the UV-vis spectrum can be used as a measure of concentration, implying that colored impurities do not substantially interfere.

Khan et al. [25] employed chiral nematic mesoporous plastics as substrate to produce latent photonic images that are only revealed upon swelling (i.e., controlled, reversible patterning of the mesoporous phenol-formaldehyde resins; see Fig. 6). The films can be manipulated either by acid or formaldehyde treatment, and the photonic resins show red-shifted color upon swelling in polar solvents [25]. With acidification, the films show enhanced crosslinking, lower density of surface methylol groups, and hence lower hydrophilicity; the converse is true for formaldehyde-treated plastic films [25]. By writing on the film with chemical inks, the density of the methylol groups in the resin changes, subsequently affecting the degree of swelling of the mesoporous plastic film and, in turn, its color [25]. Changes in the extent of swelling of the films in polar solvents lead to changes in the pitch of the chiral nematic structure and, hence, in the reflected color. By selectively applying acid or formaldehyde to regions of the mesoporous photonic plastic film, it therefore becomes possible to produce latent images that are presented only upon swelling (Fig. 6). Using ink-jet printing, it is possible to make high-resolution photonic patterns both as text or image that can be visualized by swelling and erased by drying [25]. This novel approach to printing photonic patterns in polymer films can find potential applications in anticounterfeiting tags, signage, and decorative applications.

In a related development, Giese et al. [26, 27] synthesized composites of CNCs and amino resins for the construction of photonic crystals that can be structurally colored and/or mechanically manipulated.[9] The new family of amino resin

[8] Note that the CNC–PF composite possesses no mesoporosity, akin to the case of CNC–silica composites. Only after removal of the CNCs (and any residual solvent) is mesoporous formation also imparted by the CNC spindles. For mesoporous PF films, the calculated BJH pore-size distributions are about 7 nm [22], which is close to the diameter of individual CNC spindles removed from the composite.

[9] This works builds on findings by Cheung et al. [28], who carefully and systematically showed how neutral-form sulfated CNCs could form lyotropic chiral nematic liquid crystalline phases when dispersed in polar organic media, using no surface functionalization. Self-assembly of organic CNC dispersions can be employed to prepare iridescent polymeric composites simply by solution-casting the CNC dispersion with a suitable polymer soluble in the organic solvent. As is well known, the photonic properties of these CNC–polymer composites can be controlled by varying the ratio of CNCs to polymer or the ionic strength of the CNC dispersion through salt addition.

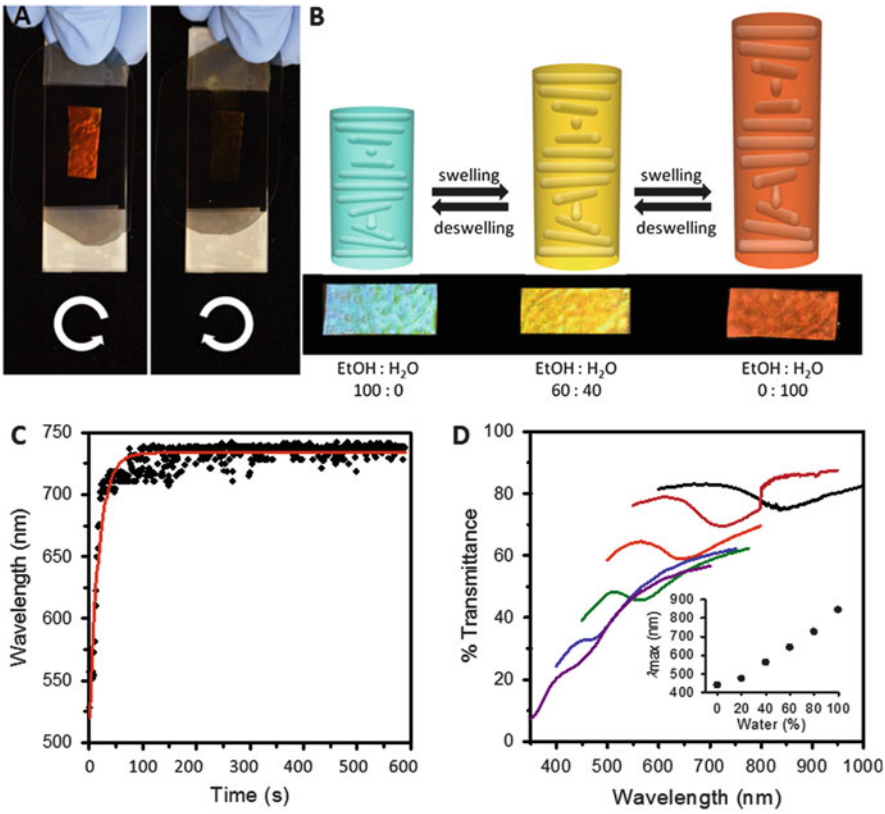

Fig. 5 Demonstration of the potential application of mesoporous photonic plastics in security features or optical sensors. (**a**) The mesoporous films appear bright red-colored under a left-handed circular polarizer (*left*), whereas the color disappears under a right-handed polarizer (*right*). (**b**) Swelling behavior of the mesoporous plastics in mixtures of water and ethanol is shown by the photographs (*below*) and schematic illustrations (*above*). Swelling of the material leads to a change in helical pitch that affects the color of the chiral nematic polymer films. (**c**) The swelling kinetics of the samples in water reveals a fast response of the material to solvent changes. (**d**) UV-vis spectra show a systematic shift of the reflection signal of the chiral nematic resin during swelling in different mixtures of water and ethanol (adapted after Khan et al. [22])

composites can be derived from the condensation of melamine, urea, and formaldehyde in the presence of CNCs [26, 27]. The melamine-urea-formaldehyde (MUF)–CNC composites capture the chiral nematic organization of self-assembled aqueous CNCs and integrates the chiral nematic structure into the crosslinked polymer network, leading to the production of colorful films with tunable optical properties. As seen earlier, the color of the composite films can be controlled either by changing the ratio of polymer to CNCs, or by adjusting the ionic strength of the CNC aqueous dispersion through salt addition (to tune the color from red to blue). Significantly, structural coloration of these composite films can be manipulated by

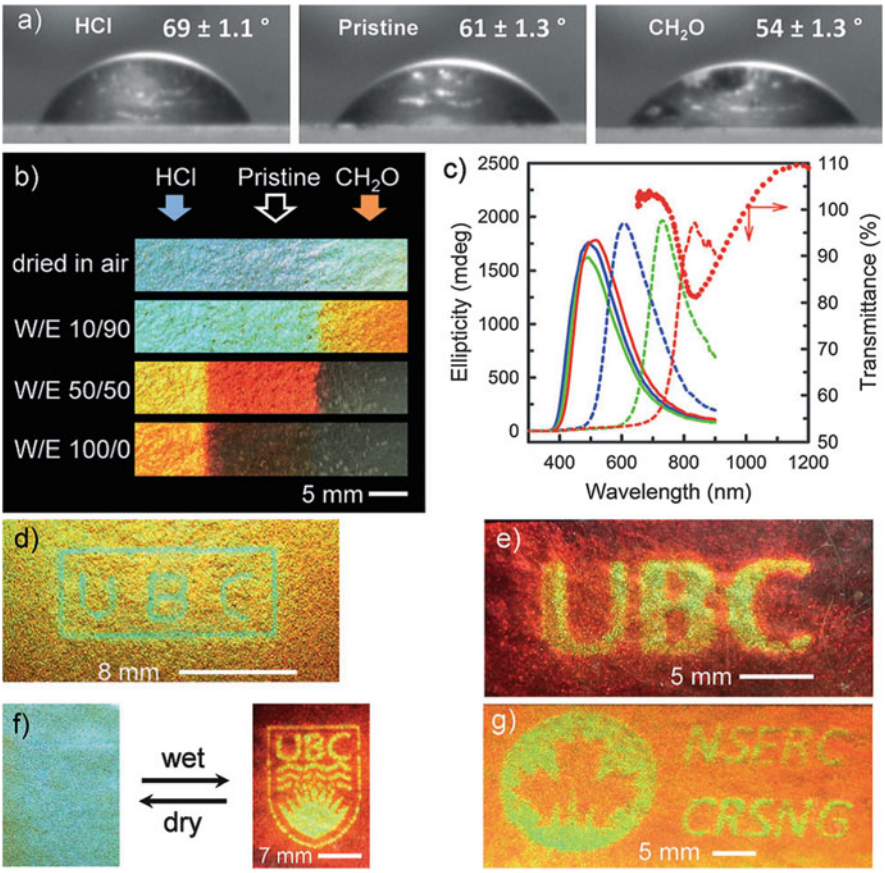

Fig. 6 (**a**) Images from static contact angle measurements of CNC-templated phenol-formaldehyde resin films treated with HCl (*left*), pristine (*middle*), and treated with CH_2O (*right*). (**b**) Photographs of a strip of the resin films illustrating changes in color in water/ethanol binary solvent mixtures of different proportions. The *left* and *right ends* of the strip were treated with HCl and CH_2O, respectively, whereas the *middle part* remained untreated. (**c**) CD spectra of the untreated (*green*), HCl-treated (*blue*), and CH_2O-treated (*red*) resin films in dry state (*solid lines*) and after swelling in water (*dashed lines*). Because the CD spectrometer that was used could not measure beyond 900 nm, the reflection peak of the CH_2O-treated film in the swollen state was confirmed with complementary UV-vis spectroscopy (*red dotted line*). (**d–g**) Inkjet printing of photonic patterns on mesoporous-resin films: (**d**) pattern printed as the letters *UBC* on the mesoporous resin film, (**e**) *UBC* patterned as an image, (**f**, **g**) more complicated images patterned on another resin film. The pattern in (**f**) was revealed by swelling in water whereas the pattern in (**g**) was revealed in 20/80 (v/v) water/ethanol mixture. The appearance and disappearance of the patterns upon swelling and drying, respectively, are completely reversible (adapted after Khan et al. [25])

applying pressure to the films, causing a blue shift in the wavelength of light reflected from the material. Pressure-induced chiral nematic patterns can also be imprinted into these composite films [26, 27].

4 Actuators and Sensors

Besides having one of the highest strength-to-weight ratios of natural or synthetic materials, lignocellulosic fibers have various useful functional attributes. The cellulosic helix predominant in the largest layer of the fiber wall (the S_2 layer) is crucial for maintaining structural integrity of the hollow fiber and for guiding the buckling of thin-walled fibers, a phenomenon known as tension buckling in which the spirally wound tube buckles under axial strain [29, 30]. More recently, Plaza et al. [31] examined how a bundle of wood cells can function as efficient moisture-activated torsional activators that twist multiple revolutions per centimeter length in direct proportion to moisture content. The specific torque generated during both twisting and untwisting is 10 N m kg^{-1}, which is characteristically higher than that of an electric motor. These wood bundles were shown to also exhibit a moisture-activated, shape-memory twist effect, whereby over 70% of the twist in a wetted bundle could be locked-in by drying under constraint and then released by re-wetting the bundle [31]. The study by Plaza et al. [31] offers proof of the capabilities of natural materials, which can provide powerful insights for bio-inspired synthetic actuators possessing high angles of rotation, high specific torque, and shape memory twist behavior. These properties could be simultaneously incorporated into engineered smart materials and structures for industrial applications, most notably micro-actuators, sensors, and energy harvesters.

Dumanli et al. [32] investigated the conditions for evaporation-induced self-assembly (EISA) of CNC films in controlled humidity conditions to tune the optical properties of the films and distinguish different phases of CNC organization into chiral nematic order. From the detailed scattering studies and quantification of disorder within the film, Dumanli et al. [32, 33] concluded that color fluctuations were principally a result of nonuniform helical pitch, rather than misalignment of the chiral nematic director. This suggests that CNC self-assembly is affected by surface preparation and, hence, new biomimetic film formation methods could be conceived to produce advanced optical materials, and shed light onto the assembly of chiral cellulose stacks within plants [32, 33]. Controlled CNC self-assembly into photonic films has also been explored for covert optical encryption [34] and reversible color humidity indicators in a mechanism that resembles band tuning in classical chiral nematic liquid crystals [21].

The discussions thus far offers a glimpse of the possibilities for developing advanced functional materials, based on cellulose nanocrystals, with tunable photonic properties for a multitude of crucial applications for the information age in the twenty-first century. Combining stimuli-responsive mechanical behavior with tunable photonic properties for the development of flexible photonic materials capable of multicolor reflections can seriously expand their technological applicability in sensors and optoelectronics. Building on the discussion of CNC-templated mesoporous photonic materials, we highlight next two relevant developments for potential applications in photonics and optoelectronics.

4.1 Responsive Chiral Actuators

Khan et al. [35] proposed a facile and scalable layer-by-layer fabrication method for the development of mesoporous bilayer phenol-formaldehyde (PF) resin films with chiral nematic organization (Fig. 7). The method is based on the approach used to prepare (single-layer) mesoporous photonic plastics, as developed by Khan et al. [22] and discussed in Sect. 3.

Bilayer mesoporous films have two layers in which the chiral nematic structures have different helical pitches and, hence, reflect light at two different wavelengths. These bilayer mesoporous photonic films also show interesting actuator behavior. Unlike the usual bilayer materials for actuation obtained by combination of an active layer on a substrate [36], bilayer mesoporous PF films consist of two active layers of the same material that differ only in their nanostructures [35]. In line with relevant discussions on factors affecting photonic properties, the color of the individual layers of the bilayer composite films can be red-shifted by increasing the ratio of PF precursor to CNCs, or blue-shifted by the addition of salts (e.g., NaCl) [35]. Variation in the color of the individual layers arises from the change in helical pitch of the chiral nematic CNC phase,[10] and can thus be tuned across the UV and visible regions of the spectrum [35]. Moreover, structural differences in the pore size and density between the two layers leads to asymmetric swelling

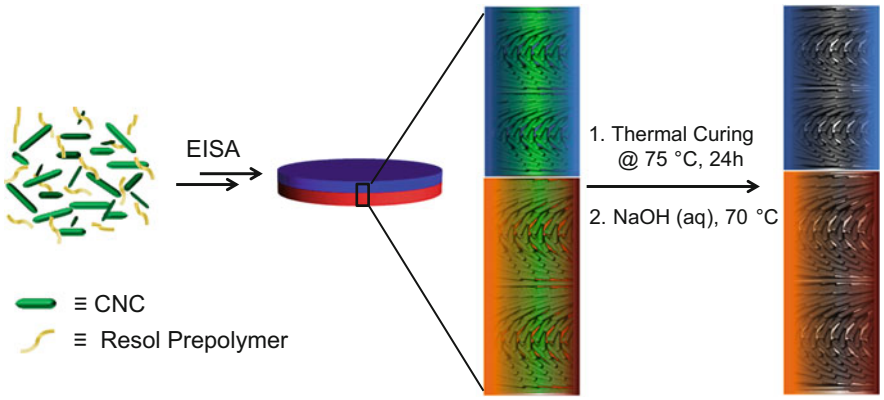

Fig. 7 Synthesis of the mesoporous chiral nematic bilayer phenol-formaldehyde (PF) resin films. A suspension of CNCs is mixed with an aqueous solution of the PF polymer precursor. Layer-by-layer film fabrication results in bilayer composite films with chiral nematic organization upon evaporation-induced self-assembly (EISA) of the CNC–PF mixture followed by thermal curing. Treatment with alkaline solution removes (most of) the CNC template, yielding highly iridescent, bilayer mesoporous photonic resins after supercritical drying (adapted from Khan et al. [35])

[10] Salt addition to aqueous CNC suspension decreases the helical pitch of the anisotropic chiral nematic phase [37].

behavior, which imparts actuator properties. Detailed investigations by Khan et al. [35] revealed that the layer with longer helical pitch and larger pore size swells more than the layer with shorter helical pitch, which essentially leads to directional curling and uncurling upon drying and swelling in polar solvents. This was further confirmed by selective swelling of one layer with water vapor, causing curling in the direction of the opposite layer (as illustrated in Fig. 8). For instance, a dry, uncurled film gradually uncurls upon swelling in water within 10 s, whereas re-curling in acetone is slightly slower (~14 s), with insignificant mechanical stress [35]. These response times are appreciably faster than those reported for hydroxypropylcellulose (HPC)-based actuators [38] or polymer microgels that mimic muscles [39], with response times ranging from minutes to hours, respectively. The reversible bending of these bilayer mesoporous photonic polymer films can be attributed to the difference in the permeability between the individual layers and the consequent difference in the expansion/shrinkage rate of the bilayer chiral nematic structure, which leads to color change [35]. The rapid dynamic mechanical and photonic responses of the bilayer mesoporous chiral nematic polymer are the first example of a bilayer material with tunable photonic properties for potential applications in optics and soft robotics.

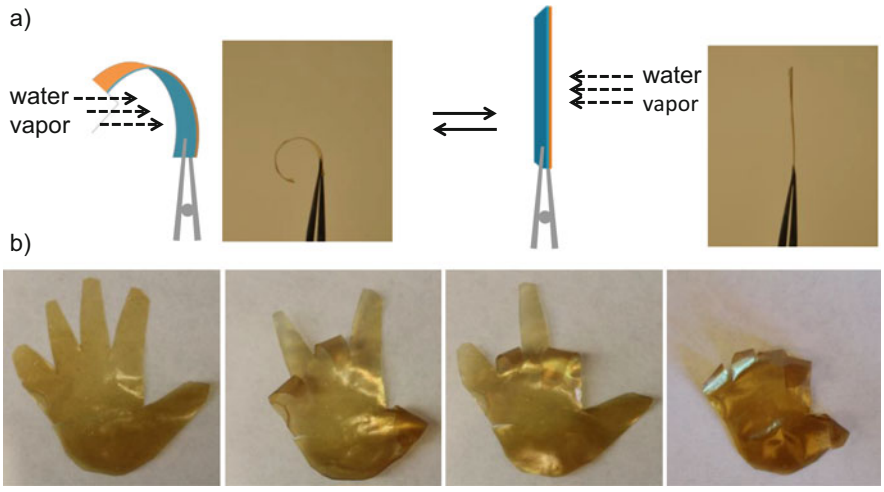

Fig. 8 (**a**) Schematics (*left*) and corresponding photographs (*right*) of bilayer film showing selective swelling of one layer, causing actuation to the direction of the opposite layer. (**b**) Site-selective actuation of the bilayer resin film cut into a hand shape. All fingers are straight when the film is swollen in water (*left*). Alternate fingers bend when drops of acetone are put on the respective fingers and allowed to dry (*middle panels*). All fingers curl when the film is completely dry (*right*). The light yellow color of the bilayer films originates from the resin, and is apparent when the films are viewed on a white background (adapted from Khan et al. [35])

4.2 Responsive Photonic Hydrogels for Chiral Optoelectronics

Conventional hydrogels essentially undergo dimensional changes when swollen in water. Photonic hydrogels, on the other hand, possess the ability to show large color changes in response to variations in osmotic pressure, leading to their ability to function as sensors for analytes [40, 41]. Photonic hydrogels can have a wide range of tunable functionality through judicious selection of suitable hydrogel monomer(s) [41, 42]. A general approach to instituting a broad range of stimuli-responsiveness to, for instance, pH, temperature, or solvent polarity, in photonic hydrogels is, however, still in early development. Cellulose nanocrystals thus seem a fitting component for instilling functionality, tunable photonic properties, and, potentially, stimuli-responsiveness.

Tatsumi et al. [43] were first to employ CNCs to create hydrogels with liquid crystalline order but, alas, their hydrogels showed no photonic properties. Kelly et al. [20, 44] were, however, first to develop responsive photonic hydrogels based on CNCs and a series of suitable monomers: acrylamide (AAm), *N*-isopropylacrylamide (NIPAm), acrylic acid (AAc), 2-hydroxyethylmethacrylate (HEMa), polyethylene glycol methacrylate (PEGMa), *N*,*N*′-methylenebisacrylamide (bis), and polyethylene glycol dimethacrylate (DiPEGMa). A key criterion for successful synthesis of photonic hydrogels using CNCs is to find suitable conditions for polymerization of the hydrogel precursors while retaining formation of the CNC chiral nematic phase, which is very sensitive to pH and ionic strength [20].[11] The precursor composition and evaporation time can be varied to access a wide range of nanocomposite hydrogels with chiral nematic organization. Basically, any CNC concentration can be used that is greater than the threshold for full anisotropy, ca. 10–12 w/w% in sulfated CNC aqueous suspensions [20]. For example, polymerizing a suitable monomer in the presence of relatively low CNC concentration, [CNC] = 10.5 w/w%, [AAm] = 17.4 w/w%, and [bis] = 0.34 w/w%, results in a flexible, transparent film with a large helical pitch observable by polarized optical microscopy (POM) (Fig. 9b). Composite hydrogels with iridescence (arising from their helical pitch being in the order of the wavelength of visible light) can, however, be prepared at high CNC concentrations while allowing the dispersion to evaporate to dryness before polymerization, yielding a final composition of, for example, [CNC] = 64.4 w/w%, [AAm] = 33.5 w/w%, and [bis] = 2.1 w/w% [20]. Increasing the ionic strength of the dispersion by adding salts such as NaCl, which decrease the helical pitch of the chiral nematic phase of CNCs, yields composite hydrogels with iridescence spanning the near-infrared (IR) and visible regions of the electromagnetic spectrum (Fig. 9c). Note that the reflection bands for CNC–polymer composite hydrogels are broad compared with those of molecular planar chiral nematic liquid crystals. This is characteristic of the chiral nematic

[11] These considerations are akin to procedural nuances for preparing, for instance, CNC-templated mesoporous silica with long-range chiral nematic organization. Please refer to Sect. 5.

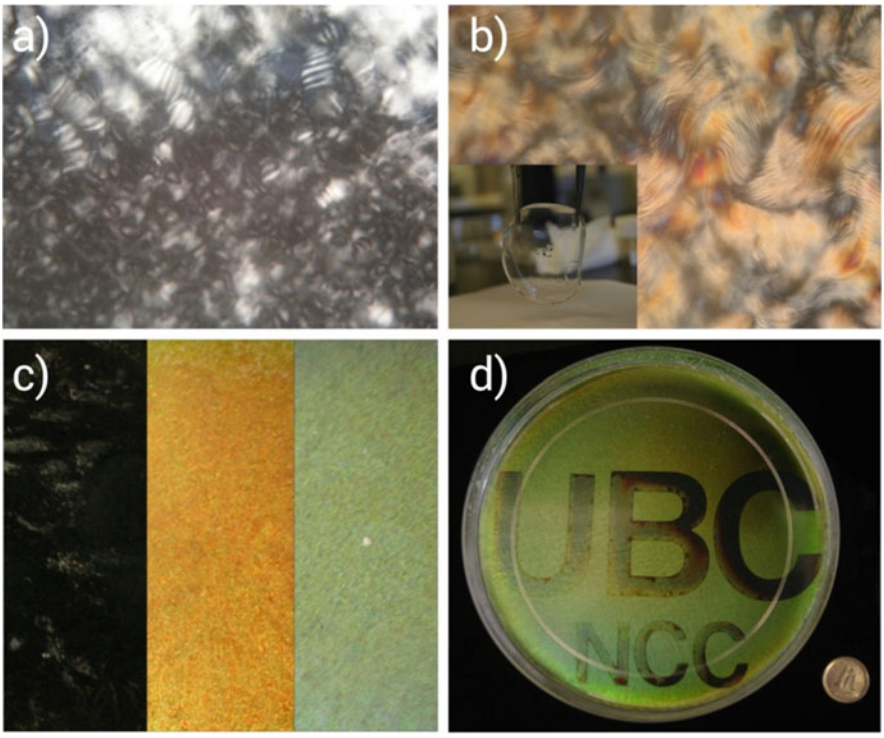

Fig. 9 Formation of the chiral nematic structure in nanocomposite hydrogels of varying compositions. (**a**) Polarized optical microscopy (POM) image of a CNC/acrylamide dispersion during evaporation, showing the formation of fingerprint texture characteristic of chiral nematic ordering. (**b**) POM of a PAAm composite prepared with high acrylamide loading soaked in water, showing fingerprint texture locked in place by photopolymerization (*inset*: photograph of the swollen transparent hydrogel). (**c**) Photographs of iridescent PAAm composite hydrogels prepared with high CNC loading and different amounts of NaCl; increasing the ionic strength blue-shifts the reflectance across the visible region. (**d**) Photograph of an iridescent photopatterned PAAm composite as the film swells in water. The masked region swells at a much faster rate, producing a latent image (adpated from Kelly et al. [20, 44])

phases of EISA CNCs and probably originates from the polydispersity of the CNC mesogens and misalignment of the chiral nematic domains [20].

CNC–polymer nanocomposite hydrogels undergo fast and reversible swelling in water and other polar solvents, and respond to variations in swelling with a change in the helical pitch of the chiral nematic phase, accompanied by a change in iridescence [20]. For example, immersing a blue iridescent CNC–PAAm composite hydrogel in water causes an immediate red-shift as the film swells, reaching equilibrium in the near-IR after ca. 150 s (Fig. 10a). The extent and rate of swelling have been shown to correlate with the polymerization time, such that increasing UV radiation time reduces the extent and rate of swelling [20]. However, films prepared without photopolymerization swell very rapidly with near-IR iridescence, yet

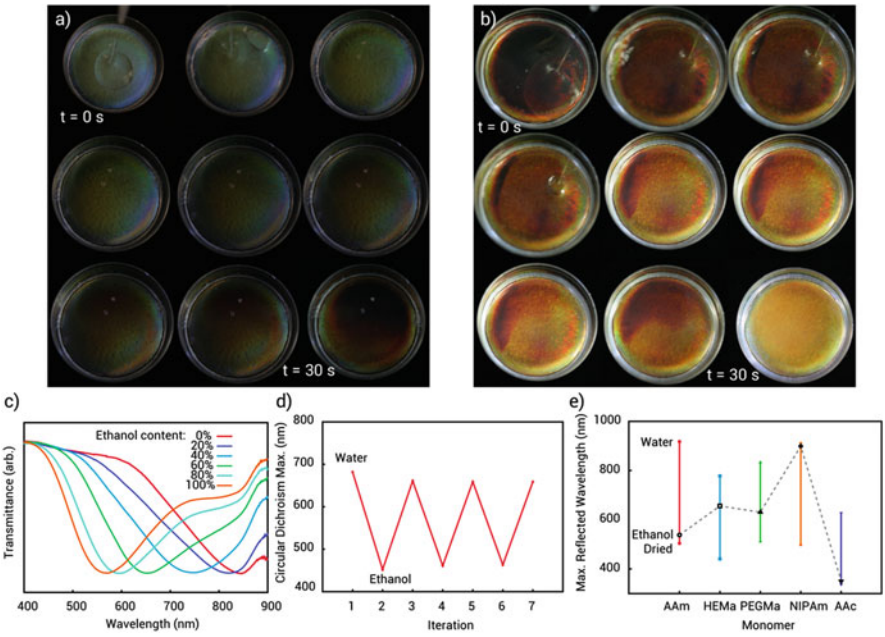

Fig. 10 Swelling of composite hydrogels, Photographs of a 6-cm diameter PAAm hydrogel as it (**a**) swells in water and (**b**) contracts in ethanol. (**c**) Transmission spectra of a PAAm composite in varying concentrations of aqueous ethanol. (**d**) Change in maximum reflected wavelength measured by circular dichroism of a PAAm hydrogel soaked in water and ethanol iteratively. (**e**) Maximum reflected wavelength as a function of hydrogel monomer in dry, aqueous and ethanolic states (adapted from Kelly et al. [20])

remain intact [20]. This can be used to produce a latent image that appears when the film swells in water as the masked nonpolymerized region rapidly red-shifts (Fig. 9d), and can be the basis for application as a security feature or patterned sensor [20].

The reflected color of CNC-based nanocomposite hydrogels can be reversibly controlled by swelling in various media (Fig. 10d). The hydrogels show strong positive ellipticity arising from the reflection of the left-handed circularly polarized light from the CNC chiral nematic phase [20]. For example, a rapid blue-shift for a hydrated PAAm nanocomposite is observed upon immersion in pure ethanol (Fig. 10b), reaching equilibrium in ~150 s. However, soaking a swollen PAAm nanocomposite in water/ethanol mixtures causes a gradual blue-shift with increasing ethanol content (Fig. 10c). The swelling response of the iridescent hydrogel nanocomposites can further be tailored through selection of hydrogel monomer. For instance, PNIPAm and PAAm nanocomposites have similar near-IR iridescence after swelling in water, but PNIPAm nanocomposites do not de-swell upon immersion in ethanol, retaining a maximum reflected wavelength of ca. 900 nm, and PAAm nanocomposites de-swell, showing a maximum reflected wavelength at ca. 550 nm (Fig. 10e). Nanocomposite hydrogels made with PHEMa (a polymer

known to exhibit increased swelling in ethanol as a result of favorable free energy of mixing) show a blue-shift in their reflected color upon immersing a water-swollen nanocomposite in ethanol [20]. Conversely, the swelling response in water from CNC-based nanocomposite hydrogels is more stable towards changes in ionic strength. Given the significant cellulosic content in these hydrogels, the potential for strong hydrogen bonding interactions between CNCs and the hydrogel polymers probably contributes to their unique swelling behavior [20].

It is important to note that major limitations to the commercial implementation of photonic hydrogels have been their slow swelling kinetics (it can take several hours to reach equilibrium) and poor mechanical properties [45]. These deficiencies have been overcome by the development of CNC-based nanocomposite hydrogels, where the fast swelling response of CNC-based hydrogels is related to their toughness and high Young's modulus [20], which has been shown to correlate with hydrogel network diffusion kinetics [46].[12]

In closing this section, it is essential to point out the possibility of installing responsive functionality in nanocomposite hydrogels through CNC surface functionalization after hydrogel polymerization. The as-synthesized CNC–polymer nanocomposite hydrogels discussed contain acidic sulfate ester surface groups,[13] which readily undergo cation exchange within the nanocomposite hydrogel in response to neutralization of the gel in dilute basic solution [49]. The nanocomposite hydrogels exhibit increased swelling (and red-shifted color) in methanol, ethanol, acetone, and isopropanol as the size and hydrophobicity of the cations increase [20] (see Fig. 11c). Simple cation exchange allows a variety of tailored photonic hydrogels to be prepared, and the ability to carry out CNC surface functionalization inside a pre-assembled chiral nematic phase (i.e., post-synthesis modification) offers a promising approach for preparation of new functional materials that are incompatible with the EISA method.

5 Mesoporous Photonic Materials from Cellulose Nanomaterial Liquid Crystal Templates

There is considerable interest in materials that combine porosity with photonic structure for advanced applications in, for instance, sensors, lasing, and photovoltaics. This can serve as a bottom-up approach for tailoring the resulting optical or electronic properties of such materials by infiltrating the pores with a suitable guest

[12] Iridescent CNC-based hydrogels, which have high stiffness and tensile strength relative to conventional photonic hydrogels, exhibit a decrease in Young's modulus from 11.3 GPa to 20.9 MPa upon swelling in water from dryness [20]. The dramatic change in mechanical properties during swelling resembles the response of other CNC-reinforced polymer nanocomposites [47, 48].

[13] Of course, these ester groups arise from the sulfuric acid hydrolysis process.

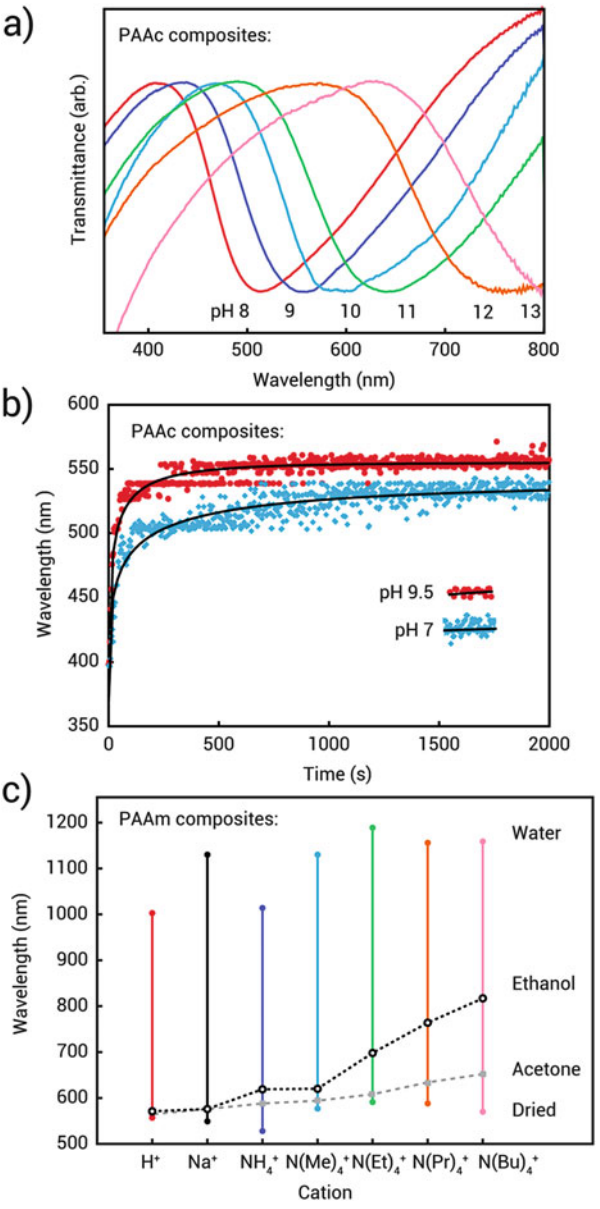

Fig. 11 Responsive behavior of CNC-based nanocomposite hydrogels. (**a**) Transmission spectra of PAAc composite in different basic solutions, showing a red-shift with increasing pH. (**b**) Time-dependence of the reflected color from PAAc nanocomposite immersed in pH 7 and 9.5 (*lines* drawn to guide the eye). (**c**) Maximum reflected wavelength of a cation-exchanged PAAm/CNC nanocomposite as a function of cation in dry, aqueous, ethanol-swollen, and acetone-swollen states (adapted from Kelly et al. [20])

species [41]. This could allow development of, for example, mesoporous silicon prepared by chemical etching [50], one-dimensional Bragg stacks prepared by spin-coating alternate layers of metal oxide nanoparticles [51], opals prepared by self-assembly of mesoporous silica nanoparticles [52], and inverse opals [53]. Bottom-up approaches enabled by advances in nanotechnology offer advantages over

top-down methods such as milling and lithography by allowing precise control of the final morphology and composition of the resulting nanomaterial [41, 54].

One effective bottom-up approach for setting structural features at the nanometric scale and permit precise control of dimensions, periodicity, and structure is to employ self-assembly of templates with the desired structural architecture [54]. Templates can vary from hard templates (e.g., carbon and silica) to soft templates (e.g., biomolecules and polymers). Liquid crystals have been widely employed as templates for their ability to self-assemble into transferrable superstructures [41].[14] Lyotropic liquid crystals (LLCs), of which CNCs are one example, are widely used in templating because their liquid crystalline phase is compatible with many precursors [56]. Kresge et al. [57] pioneered the synthesis of mesoporous silica via LLC templating, and the approach has since been extended by researchers worldwide to develop porous materials of various structures and materials.

Thomas and Antonietti [58] used hydroxypropylcellulose (HPC) as a soft template to synthesize mesoporous silica via a nanocasting approach.[15] In their approach, Thomas and Antonietti [58] obtained silica composites by mixing aqueous HPC with the precursor tetramethyl orthosilicate (TMOS) in the presence of HCl. The mixture was stored for several days to weeks in a sealed tube to allow formation of the LLC phase. After observing iridescence of the mesophase, the solvent was slowly evaporated under vacuum to obtain chiral nematic composites. The chiral nematic order of the HPC was clearly maintained in the composite; however, the retention of chiral nematic long-range order was not observed in the calcined silica [58]. Wang et al. [59] synthesized porous silica by mixing 3-(methacryloyloxy)propyltrimethoxysilane (MPTOS), divinylbenzene (DVB, as crosslinker), and an initiator with ethylcyanoethyl cellulose in acetic acid. However, their findings revealed that the morphology of the silica materials was dependent on the silica precursor content in the composite, and no long-range order could be observed in the final product. In yet another approach, Qi et al. [60] synthesized cellulose/metal nitride complexes via self-assembly of

[14] Liquid crystals are organic molecules with an anisotropic shape, such as mono- and disaccharides, biphenylalkyl compounds, surfactants, and their polymeric analogus. Biopolymers such as DNA, silk, amyloids, chitin, collagen, cellulose, and some microorganisms can also exhibit liquid crystalline behavior [55]. As a consequence of their shape anisotropy, liquid crystals form characteristic mesophases – a state of matter that combines the long-range order of crystals with the mobility of an isotropic liquid [55]. Diverse mesogens are known that vary in molecular shape (e.g., rod-like, orcalamitic, and disc-like, discotic) and thermal behavior (thermotropic liquid crystals). Others only form liquid–crystalline phases in solvents (lyotropic liquid crystals, LLC) whose phase behavior depends on concentration, temperature, pH, and the ionic strength of the solution [55].

[15] Although cellulose derivatives such as ethylcellulose (EC) and hydroxypropylcellulose (HPC) can be used as templates to form nanostructured materials, very high concentrations are required to form the chiral nematic phase. These high concentrations would present grave challenges for rheological handling and necessitate the use of special equipment. Highly viscous suspensions, in turn, slow the process of self-assembly.

cellulose in liquid NH_3/NH_4SCN solution. Their approach produced nanoporous titanium or vanadium nitride, but with no long-range chiral nematic order [60]. Furthermore, nanocrystalline chitin (NCh) was used to form a LLC phase to produce nanocomposite materials of NCh and silica or organosilica; however, there was no evidence of chiral nematic order in the composite materials [61–63].

In conclusion, none of the cellulose derivatives investigated by various researchers could produce porous materials that possessed long-range chiral nematic order. This is a unique feature of CNCs when used as LLC templates for synthesizing mesoporous chiral materials, as discussed in detail in the next section.

5.1 Chiral Nematic Mesoporous Silica and Organosilica Films

The first example of the use of CNCs in templating was reported by Dujardin et al. [64]. CNC–silica composites were obtained via EISA of a mixture of CNC aqueous suspension and a pre-hydrolyzed suspension of TMOS. The resulting composite material appeared birefringent before and after calcination; however, the imprint of the chiral nematic phase could not unequivocally be proven in the final mesoporous silica [64]. Shin and Exarhos [65] prepared porous titania films by CNC templating using a modified approach, but without being able to maintain chiral nematic organization in the final titania film.

Successful use of the self-assembly of CNC-based templates to produce nanostructured composite materials with long-range chiral nematic organization (characteristic of the CNC template) in the mesoporous matrix after removal of the template was first reported in a seminal paper by Shopsowitz et al. [66]. In their ground-breaking discovery, Shopsowitz et al. employed alkoxysilane precursors, such as TMOS or tetraethyl orthosilicate (TEOS), with compatible self-assembly of CNC aqueous suspensions to produce composites with vibrant iridescent colors [66]. Negatively charged CNCs, obtained from the conversion of the CNC –OH group to $–OSO_3H$ with a conversion rate of about one sulfate group per 20 glucose units [1], are essential for the formation of a chiral nematic phase (in the final mesoporous films) and for producing stable colloidal suspensions (during the reaction).[16] The compatibility (crucial for the subsequent reaction) of the CNC aqueous suspensions and the alkoxysilane precursors primarily stems from the followings considerations: (1) the isoelectric point of silica is near the pH of the as-prepared acidic CNC dispersions; (2) hydrolysis of alkoxysilanes generates the corresponding alcohol, which does not perturb EISA; and (3) the high water

[16] The pH of CNC aqueous suspensions used for producing chiral nematic mesoporous films via nanocasting is critical, as is concentration, typically pH = 2.4 and [CNC] = 3 w/w% [66]. EISA occurs within a narrow pH range of the suspension (pH 2.4–4), outside of which achiral and opaque composites are obtained.

concentration and pH of the CNC dispersions suppress silica polymerization until the later stages of evaporation [66, 67].

The reflected color of the resulting mesoporous silica films could be tuned from the UV to the near-IR region of the electromagnetic spectrum by changing the ionic strength (salt addition) or changing the ratio of silica to CNCs [67]. The tunable color is an excellent indication of intimately homogeneous CNC–silica composites. Because the refractive indices of CNCs and silica are relatively close, the shift in the reflected wavelength is predominantly a result of an increase in the helical pitch [67]. CD spectroscopy has been extensively used to show that the reflection is exclusively left-handed, as expected from a CNC chiral nematic phase, with strong positive ellipticity matching the reflected wavelengths measured by UV-vis spectroscopy (Fig. 12). The self-assembly behavior occurs within a narrow pH range, as indicated above.

The incorporation of organic functionality into mesoporous silicas provides a way to further fine tune their properties. An important advance in this area took place with the discovery that, by using bridged silsesquioxane precursors of the type $R(Si(OR')_3)_2$, periodic mesoporous organosilicas (PMOs) with integral organic groups could be directly synthesized using liquid crystal templating [72–75].

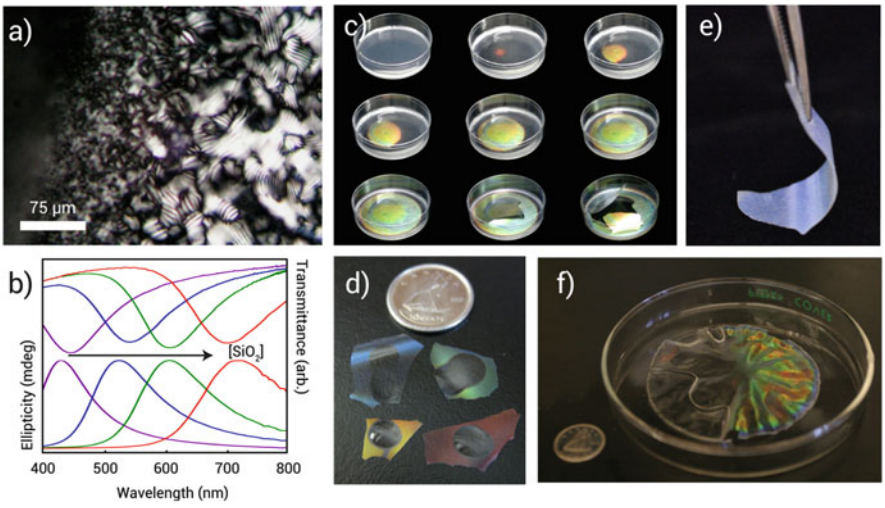

Fig. 12 (**a**) Self-assembly of CNCs with silica sol–gel precursors indicates the fingerprint-like texture characteristic of the formation of a chiral nematic phase, as illustrated by polarized optical microscopy. (**b**, **c**) Evaporation of the mixture to dryness yields an iridescent composite whose structural color depends on the silica loading. (**d**) After calcination of the composite to remove the CNC template, mesoporous sol–gel derived films are obtained that retain their intense structural color. (**e**) The use of organosilica precursors yields flexible films after acid hydrolysis to remove the CNC template from the composite. (**f**) Cracking observed during evaporation can be eliminated in the mesoporous silica films by the addition of polyols such as glucose, leading to large, crack-free films. Relevant references are Shopsowitz et al. [66–68] and Kelly et al. [44, 69]. Constellation of images is adapted, from Kelly et al. [70, 71]

The direct use of bridged organosilica precursors provides a distinct advantage compared with post-synthetic grafting by allowing precise stoichiometric control over the relative amounts of inorganic and organic components within the hybrid material [76]. Also, by incorporating the organic groups as integral components of the crosslinked structure, it is possible not only to change the chemical environment within the pores but also to modify material properties such as mechanical strength, hydrothermal stability, and molecular organization [77, 78]. The sol–gel process for these precursors is similar to using TMOS; EISA with CNCs produces analogous iridescent composites [68]. However, the bridging organic group cannot withstand calcination to remove the CNC template, and an alternative removal method was developed by Shopsowitz et al. [68]. Treating ethylene-bridged organosilica composites with hot 6 M sulfuric acid, followed by rinsing with piranha solution (a mix of sulfuric acid and hydrogen peroxide), completely removes the CNCs without damaging the organosilica pore walls, as confirmed by solid-state NMR [68].[17] In comparison with brittle silica films produced from TMOS, films prepared with bridging ethylene groups are flexible and can easily be picked up and handled (Fig. 12e).

The surface areas of the mesoporous organosilica films are high, and consistent with complete template removal. However, these films have higher pore volume than calcined mesoporous silica films, and pore diameters that more closely resemble those of CNCs [68]. This suggests that acid extraction does not induce the significant contraction experienced with calcination, and can thus pose as an indirect method for controlling pore diameter and volume. High-resolution electron microscopy of these sol–gel-derived materials (both silica and organosilica) reveals the presence of helically twisting structures replicating the left-handed chiral nematic organization in CNCs. Using helium ion microscopy (HIM), which allows direct, high-resolution imaging without sputter coating, ethylene-bridged films appear as a porous, woven network of whisker-like organosilica [79] (see Fig. 13a–d).

It is apposite to point out at this juncture that the generation of significant capillary pressure gradients during evaporation (as observed in other mesoporous materials) contributes to the formation of cracks in the final stages of preparing chiral nematic mesoporous silica (CNMS) and organosilica films. Kelly et al. [44] overcame the issue of cracking by the addition of polyols (e.g., glucose) to the CNC suspension before EISA, which altered the sol–gel curing kinetics (Fig. 12f). This seems to work for producing crack-free silica films, but not in the case of organosilica films, probably because perturbation of the sol–gel equilibria does not provide sufficient condensation to survive the acid extraction process [44].[18]

[17] In another publication, Terpstra et al. [79] prepared mesoporous organosilica films with a bridging benzene precursor, and the CNC template was effectively and completely removed using hot HCl followed by washing with silver-activated hydrogen peroxide.

[18] Using both enantiomers of glucose resulted in films with left-handed chiral nematic organization, indicating that self-assembly is probably not driven by hydrogen bonding on the surface of the cellulose nanocrystals [44].

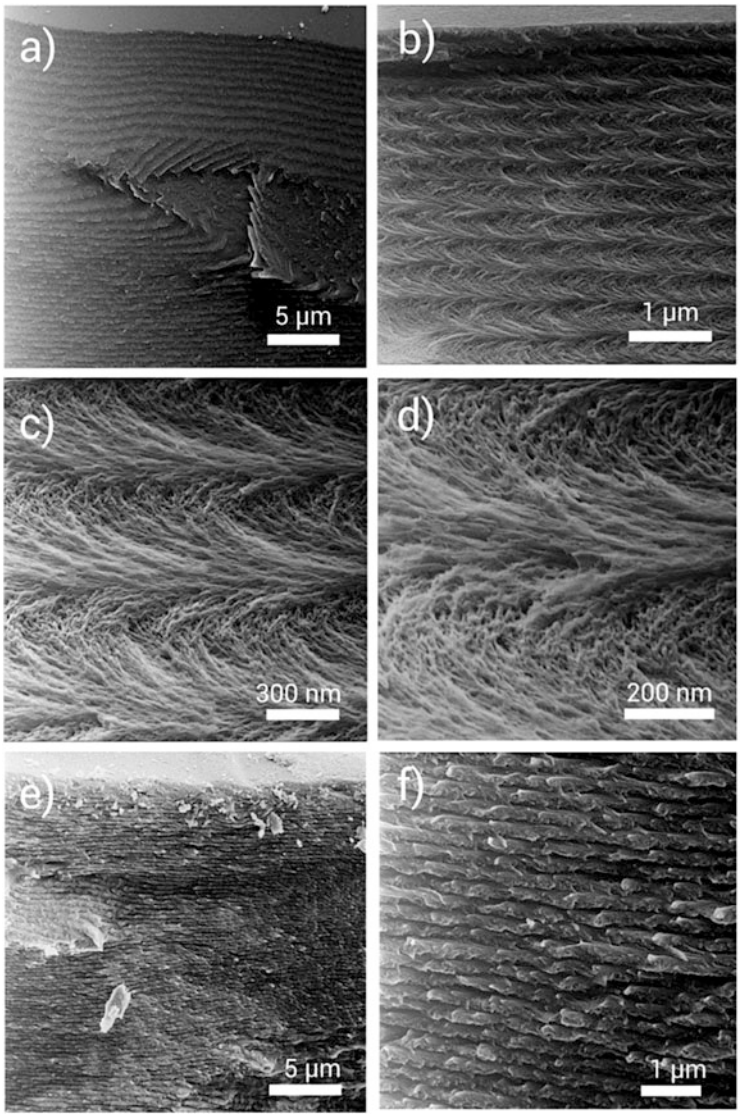

Fig. 13 Helium ion microscopy of chiral nematic mesoporous (**a**–**d**) ethylene-bridged organosilica and (**e**, **f**) silica at varying magnifications (adapted from Terpstra et al. [79])

5.2 Refractive Index Sensing

The combination of porosity and chiral nematic photonic properties in CNMS materials is intriguing for their use in refractive index-based sensors. When immersed in water and other liquids, the films rapidly become transparent and colorless (see Figs. 12d and 14a). A similar effect has also been reported for other

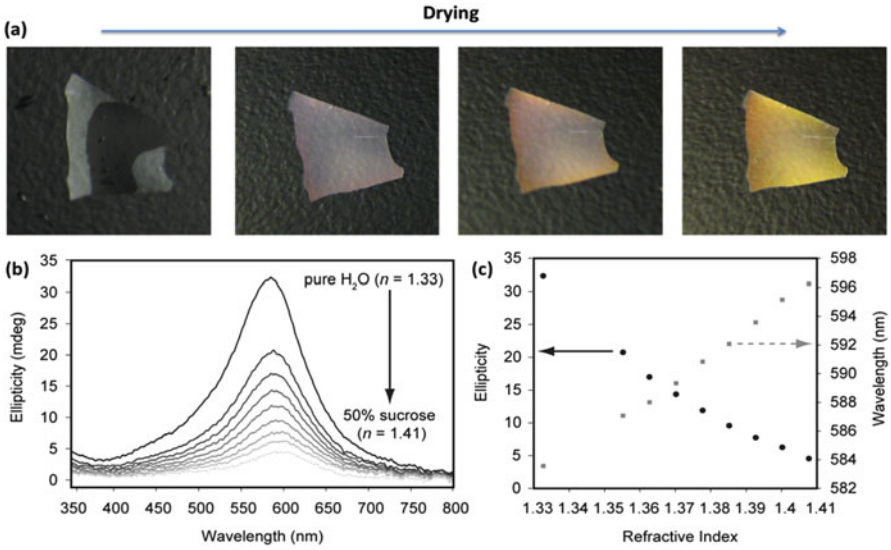

Fig. 14 Effect of refractive index changes on the photonic properties of CNMS films. (**a**) Series of photographs showing the reversible color change that occurs upon wetting and drying a CNMS film. (**b**) Circular dichroism spectra of a CNMS film at different sucrose concentrations, ranging from 0 to 50 wt%. (**c**) Plots of peak intensity and position versus refractive index for the series of CD spectra shown in (**b**) (adapted from Shopsowitz et al. [67])

porous photonic nanostructures, such as helical inorganic nanostructures prepared by glancing angle deposition (GLAD) or silica inverse opals, and has been attributed to approximate refractive index matching between the isotropic liquid in the pores and the walls of the material [80, 81]. Because the silica pore walls are locally isotropic, the strong iridescence and birefringence of the CNMS films entirely originate from the anisotropic mesoscopic ordering induced by CNC self-assembly, a phenomenon long-known as form birefringence [82]. As a result, the mesoporous silica films appear transparent to the eye when the pores are filled with a liquid such as water whose refractive index ($n_{(H_2O)} = 1.33$) is a close match to that of silica ($n_{(SiO_2)} = 1.46$), regaining their iridescence as the liquid evaporates [66] (see Fig. 12d). A residual signal, after water infiltration, can still be observed using CD spectroscopy[19] from the optically transparent films because the refractive indices are not perfectly matched [67]. This signal gradually decreases and red-shifts as the refractive index inside the pores increases and becomes closer to that of silica [67].

The CD signal of the films is reduced by two orders of magnitude to ~30 mdeg after infiltration with water (Fig. 14b). The CD peak is also red-shifted relative to the reflectance peak for the dry film, as expected from an increase in n_{avg}. Increasing the refractive index by infiltration with a range of aqueous sucrose solutions

[19] The residual peak is too small to be detected by transmission spectra. However, the chiral origin of the reflectance peak allows optical changes in the films to be probed using circular dichroism.

(a common approach for testing the sensitivity of refractive index-based sensors) shows a gradual decrease in CD signal and red-shift of the maximum wavelength (Fig. 14c). The sensitivities of the mesoporous silica in CD signal intensity and peak position to changes in refractive index are ca. 200 mdeg/refractive index unit (RIU) and ca. 170 nm/RIU, respectively [67], which are comparable to the sensitivity of porous silicon-based photonic sensors (based on reflectivity measurements) [83]. These results suggest that there are opportunities to employ these materials in optical sensing applications where small changes in the refractive index within the pores result in changes in both the intensity and position of the CD peak. This takes advantage of the increased sensitivity of CD and the unique combination of chirality, photonic properties, and mesoporosity in these materials. Thus, this could form the basis for a chiral photonic sensor because the observed sensitivity is comparable to that of state-of-the-art refractive index-based sensors.

5.3 Nanocasting Chiral Nematic Mesoporous Metals

Nanocasting, or hard templating, has emerged as a versatile and powerful technique for constructing new solid-state materials with periodic order [84, 85]. It typically employs preformed mesoporous materials to prepare structures that cannot be accessed through conventional lyotropic template synthesis (e.g., because of hydrolytic instability of precursors) [84, 85]. Nanocasting essentially involves the infiltration of successive loadings of a precursor into a stable mesoporous support, usually followed by calcination to build an interconnected network of the desired product [84, 85]. A variety of ordered mesoporous materials (e.g., carbon, metal oxides, and polymers) can be prepared through hard templating; however, mesoscopically ordered titania has attracted particularly intense interest for its (1) photocatalytic activity, (2) incorporation into dye-sensitized solar cells, and (3) high refractive index ($n \sim 2.5$) for photonic applications [86].

Shopsowitz et al. [87] were first to show that CNMS could be used as a template to synthesize titania. In this hard templating method, structural features are replicated at several length scales: (1) the titania is mesoporous, with surface area and pore size determined by the porosity of the starting CNMS template; (2) the material obtained selectively reflects left-handed circularly polarized light, which indicates a chiral nematic organization of the titania crystallites; and (3) the titania is obtained as films with similar dimensions as the original silica films. These novel, highly porous thin films of titania could be excellent materials for application in dye-sensitized solar cells, photocatalysts, sensors, and batteries.

Shopsowitz et al. [87] employed a novel strategy to prepare chiral nematic mesoporous titania films by repeatedly loading a peptized $TiCl_4$ solution (a precursor that instantaneously gels aqueous CNCs dispersions) into CNMS films (by the procedure described above), followed by annealing. After four cycles of loading, the silica–titania composite was calcined at 600°C and the silica support was removed by etching in 2 M NaOH to yield freestanding, chiral nematic

mesoporous titania films whose iridescence was exclusively left-handed circularly polarized (Fig. 15a). Hard templating of titania films could be carried out using CNMS films prepared through either calcination or acid extraction to give mesoporous titania with varying pore diameters, pore volumes, and surface areas [87]. Both types of CNMS films reproduced the characteristic iridescence typical of chiral nematic organization in the resulting titania films. However, films prepared using acid-extracted silica appeared to possess larger dimensions and qualitatively more intense iridescence, suggesting that the larger mesopores obtained through acid extraction allowed more effective diffusion of the titania precursor [87]. Importantly, SEM images of the hard-templated titania confirmed mimicking of the original helical chiral nematic structure of CNCs, with a globular morphology evident at higher magnification that was probably a result of crystallization of titania (Fig. 15b, c). Moreover, Shopsowitz et al. [87] confirmed, via XRD analysis, that the obtained chiral nematic mesoporous titania films were composed of nanocrystalline anatase, rather than the thermodynamically favored rutile phase, as a result of confinement inside the mesopores during crystallization. The successful replication of chiral nematic order in titania through nanocasting confirms the interconnected nature of the pore network in these CNC-derived materials, and is

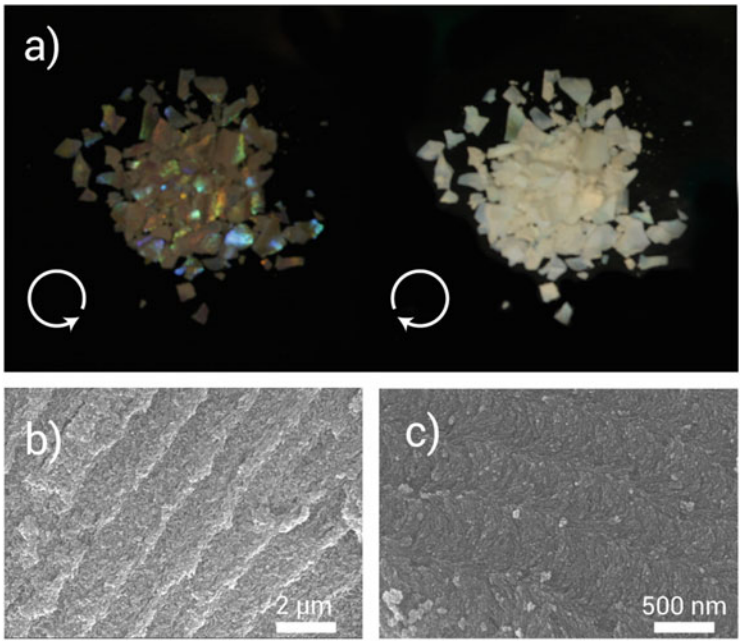

Fig. 15 (**a**) Chiral nematic mesoporous titania thin films prepared by nancasting appear iridescent through a left-handed circularly polarized filter and opaque white through a right-handed filter, illustrating the selective reflection in these materials. (**b**, **c**) SEM images of the thin films confirm mimicking of the helical, twisting structure of CNCs, with globules probably introduced by titania crystallization (adapted from Shopsowitz et al. [87])

proof-of-concept for a general strategy for preparation of other mesoporous metal oxide structures with chiral nematic organization.

5.4 *Mesoporous Scaffolds for Chiral Optical Effects*

The high surface area and mesoporosity of CNC-templated sol–gel-derived materials facilitates their use as scaffolds for guest species exhibiting novel chiral optical properties through chiral nematic organization [70]. Relevant examples are given next that can serve as proof-of-concept for applications in catalysis, sensing, and optoelectronics.

Noble metal nanoparticles (NPs) are attractive for developing biochemical sensors that generate a change in the surface plasmon resonance (SPR)[20] upon binding of a desired analyte [88]. Chiral assemblies of NPs are especially promising candidates because the CD of the SPR gives rise to excellent sensitivity and detection limits [89, 90]. Qi et al. [91] demonstrated the first example of chiral metal NP assemblies without the use of a chiral ligand or biotemplate. They prepared silver NPs by in situ reduction of $AgNO_3$ inside the pores of calcined CNMS, and the resulting materials showed a strong CD signal for the SPR peak that varied with the helical pitch [91] (see Fig. 16b). Qi et al. [91] proved, through detailed CD spectroscopic investigations and control experiments, that the observed chirality originated from the helical pitch of the mesoporous material rather than the molecular chirality of CNC imprinting in the silica. Subsequently, Kelly et al. [69] employed a one-pot synthesis to make CNMS films decorated with assemblies of gold, silver, and platinum metal NPs. In their method, compatible precursors of metal NPs were co-assembled with the CNC–silica composites, leading to the corresponding CNMS films decorated with metal NPs upon calcination [69] (see Fig. 16a).[21] Considering the importance of the SPR of metal NPs in biochemical sensing, these novel chiral nematic NP composite materials open up new directions in chemical sensing applications based on the CD response of the chiral assemblies of NPs in chiral nematic mesoporous hosts.

[20] Surface plasmon resonance (SPR) is defined as the light-stimulated resonant oscillation of conduction electrons at the interface between negative and positive permittivity materials, also known as surface magnetic waves [88]. When the frequency of incident photons matches the natural frequency of surface electrons oscillating against the restoring force of positive nuclei, resonance is established. SPR is the basis of many standard tools for measuring adsorption of material onto planar metal (usually Ag and Au) surfaces, or onto the surface of metal nanoparticles. In subwavelength-scale nanostructures, SPR can be polaritonic or plasmonic [88]. SPR is the fundamental principle behind many color-based biosensor applications and different lab-on-a-chip sensors.

[21] CD spectroscopy of the Ag and Au NP hybrid materials demonstrates that metal NPs can induce CD spectra of their SPR bands as a result of their chiral organization [91]. Furthermore, significant changes in both CD and UV-vs spectra in response to changes in the environment (e.g., different solvents or the introduction of surface-bound ligands) can be observed [91].

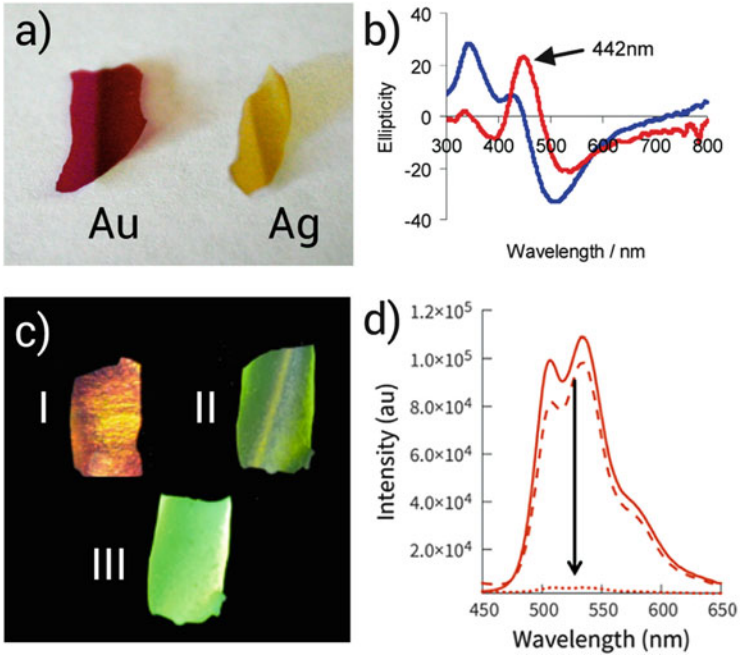

Fig. 16 Photographs and characterization of new hybrid materials templated by CNCs. (**a**) Silica films doped with Au and Ag NPs depicting characteristic colors arising from the plasmon resonance of the NPs [69]. (**b**) CD spectra clearly demonstrate the induction of chirality to the plasmon resonance by the chiral nematic surroundings [91]. (**c**) Photographs showing chiral nematic organosilica films before (*I*) and after doping with PPV (*II*), as well as fluorescence from PPV composites under UV illumination (*III*) [92]. (**d**) Fluorescence quenching of the PPV composites by diluted solutions of TNT, demonstrating their potential use in sensing [92] (adapted from Kelly et al. [69], Qi et al. [91] and Mehr et al. [92])

Chiral nematic ordering in conjugated polymers can also give rise to novel magnetic, electronic, and optical properties [93]. For example, Mehr et al. [92] formed poly(phenylene vinylene) (PPV) within chiral nematic mesoporous organosilica by surface-induced polymerization of xylene bis(tetrahydrothiophenium bromide) in chiral nematic mesoporous organosilica films. The synthesis yielded bright yellow, iridescent PPV–organosilica composites with long-range chiral alignment of the PPV inside the mesoporous host (Fig. 16c). The polymer was accessible to analytes and underwent fluorescence quenching (Fig. 16d) when exposed to electron-deficient aromatic guests (e.g., TNT). This is a new approach to the organization of conjugated polymers within a chiral host and might potentially have an impact on the development of novel devices based on the anisotropic ordering of these hybrid materials.

The development of devices such as reflective displays, optical filters, or sensors requires reversible control of the optical properties of photonic materials by

tackling either their periodicity or refractive index contrast [94]. For instance, stimuli-induced changes in refractive index can be initiated by embedding responsive guests within the channels of a chiral nematic mesoporous host, leading to dynamic modification of the optical properties [94]. In this vein, thermotropic liquid crystals can be incorporated as guests because they show large changes in their refractive indices and molecular alignment in response to temperature changes, for instance [94]. Giese et al. [26] infiltrated octyl-functionalized chiral nematic organosilica films with 4-cyano-4′-octylbiphenyl (8CB), a well-studied thermotropic liquid crystal, whereby the 8CB acts as a thermal switch to control reflection in the chiral nematic mesoporous organosilica films. The films showed strong iridescence at room temperature and underwent a rapid change to colorless when heated to near the nematic-to-isotropic transition temperature for 8CBof ~40°C [26]. The changes in optical properties could be illustrated by complete loss of the reflection signal in the UV-vis spectra for the liquid crystal-loaded films (Fig. 17).[22] Thus, thermoresponsive materials with tunable properties can potentially prove suitable for the development of switchable components in displays and sensors.

6 Sustainable Electronics Based on Cellulose Nanocrystals

The synthesis and design of one-dimensional (1D) organic semiconductors are important for the development of nanostructured thin films, which can enable large, robust, and low-cost electronic devices to be constructed. This section seeks to shed light on considerations germane to the fundamental electromagnetic and piezoelectric properties of CNCs, as well as provide a summary of how CNCs can be used, in conjunction with conjugated polymers, to synthesize flexible semiconducting films or to template mesoporous carbon structures.

6.1 Flexible, Organic, Semiconducting Materials

Polyaniline (PANI), a prototypical conducting polymer, also referred to as an inherently conducting polymer (ICP), has emerged as a promising 1D material. It is particularly attractive for electronic devices because of its facile chemical and electrochemical synthesis, environmental stability, unique electronic properties, and simple acid/base doping/de-doping chemistry [95]. PANI has also been used

[22] Giese et al. [26] investigated the correlation between the observed color change and the alignment of the 8CB molecules using variable-temperature solid-state NMR spectroscopy of a ^{15}N-labeled 8CB derivative, and revealed alignment of the rod-shaped guests with the pores in the liquid-crystalline state. Upon reaching the isotropic phase, the solid-state NMR spectra proved the liquid-like nature of the mesogen within the channels [26].

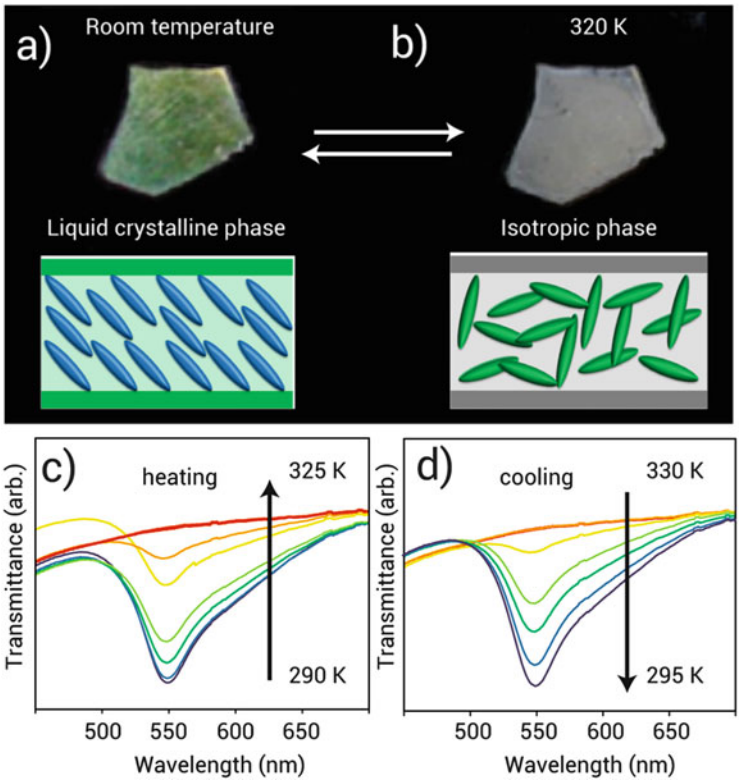

Fig. 17 Infiltration of chiral nematic organosilica films with thermoresponsive liquid crystals (LCs) reversibly changes the color from (**a**) green to (**b**) transparent upon heating from the liquid crystalline phase to the isotropic phase. The change in color and its reversibility can be quantified by UV-vis studies showing (**c**) the decrease in photonic signal upon heating the LC-infiltrated composite material to 50°C and (**d**) the return of the photonic signal upon cooling to room temperature (adpated from Giese et al. [26])

in many other applications, including anticorrosion coatings, batteries, sensors, separation membranes, and antistatic coatings [95, 96]. However, despite its unique chemical and electronic properties, PANI has major processing limitations and inferior mechanical properties compared with conventional polymers. To date, great research efforts have been expended to overcome these limitations and to produce conductive nanocomposite materials and films based on ICPs such as polyaniline, polypyrrole, polythiophene, polyacetylene, and poly(*p*-phenylene vinylene) combined with nanomaterials such as carbon nanotubes [97], nanoclay [98], and graphene oxide [99] for application in supercapacitors, light-emitting composites, or low-cost disposable sensors.

Burgeoning interest in developing sustainable organic electronics has given impetus to exploration of different forms of cellulosic materials. van der Berg et al. [100] reported the preparation of a blended mixture of PANI or poly(*p*-

phenylene ethylene), PPE, camphorsulfonic acid, and sulfate-functionalized tunicate CNCs in formic acid to produce a conductive film (electrical conductivity in the range 1.3×10^{-2} to 5×10^{-2} S cm^{-1}) with good mechanical stiffness (elastic modulus 9.5 GPa at 99.4% w/w of tunicate CNCs for PANI-CNCs and ~2.5 GPa for PPE-CNCs). Moreover, CNCs have been used with poly(3,4-ethylenedioxythiophene)/poly(styrene sulfonate) (PEDOT/PSS) [101] or PEDOT alone [102] to produce conductive films. It was found that the electrical percolation threshold of PEDOT/PSS could be reduced by the addition of CNCs as a result of their templating effect [101].[23] Different protonic acids could be used in such constructs, such as *p*-toluenesulfonic acid, [106, 107] and dodecylbenzene sulfonic acid (DBSA) [108, 109], as well as different oxidizing agents such as $(NH_4)_2S_2O_8$ and $FeCl_3{\cdot}6H_2O$ [103, 110]. Practically all reported methods for preparation of CNC-based conductive nanocomposites primarily involve physical blending, layer-by-layer (LbL) deposition, electrochemical co-deposition, latex technology, or in situ oxidative polymerization [100–102, 111, 112]. Hamad and Atifi [113] reported the first application of emulsion polymerization of aniline in the presence of CNCs, and investigated the mechanism involved, to promote the formation of organic nanocomposite materials with tunable electrical and mechanical properties.

Aqueous emulsion polymerization (a scalable, green process) has successfully been used to prepare flexible, organic, semiconducting CNC-PANI-DBSA nanocomposite films in which the original chiral nematic organization of CNCs could be preserved [113] (see Fig. 18a, b). The authors showed that the mechanical and conductive properties could be tailored to suit the desired end-use application in electronics and optoelectronics [113]. CNCs – strong acid polyelectrolytes – and the micelles formed by DBSA act as effective templates for aniline before initiation of the polymerization process. A stable suspension of the CNC-PANI-DBSA nanocomposite was obtained, whose mechanical and electrical properties could be tailored by changing the concentration of the surfactant and CNCs used [113]. Furthermore, doping with HCl has been shown to alter the structural organization of CNCs in the nanocomposite film as a result of the high ionic strength, but without affecting the conductive and mechanical performance [113]. It is possible, of course, to use different dopants and produce flexible, organic semiconducting films that retain chiral, nematic organization.

Doped CNC-PANI-DBSA nanocomposite films are mechanically distinct from the PANI-DBSA polymer. The former are flexible smooth films after doping and drying at room temperature (Fig. 18c), whereas PANI-DBSA is obtained as a

[23] Other forms of cellulose, primarily fibrous webs such as bacterial cellulose (BC), microfibrillated cellulose, and cellulose nanofibrils, have been examined as flexible substrates for electronic materials. For instance, BC has been used to prepare (1) flexible PANI–BC membranes via in situ oxidative polymerization [103], (2) electroactive cellulose-based polythiophene composites via $FeCl_3$-initiated oxidation copolymerization with thiophene comonomers [104], and (3) core–sheath hybrid composites with polypyrrole via in situ oxidative polymerization in a miscible two-phase system of dimethyl formamide and water using ferric chloride as oxidant catalyst [105].

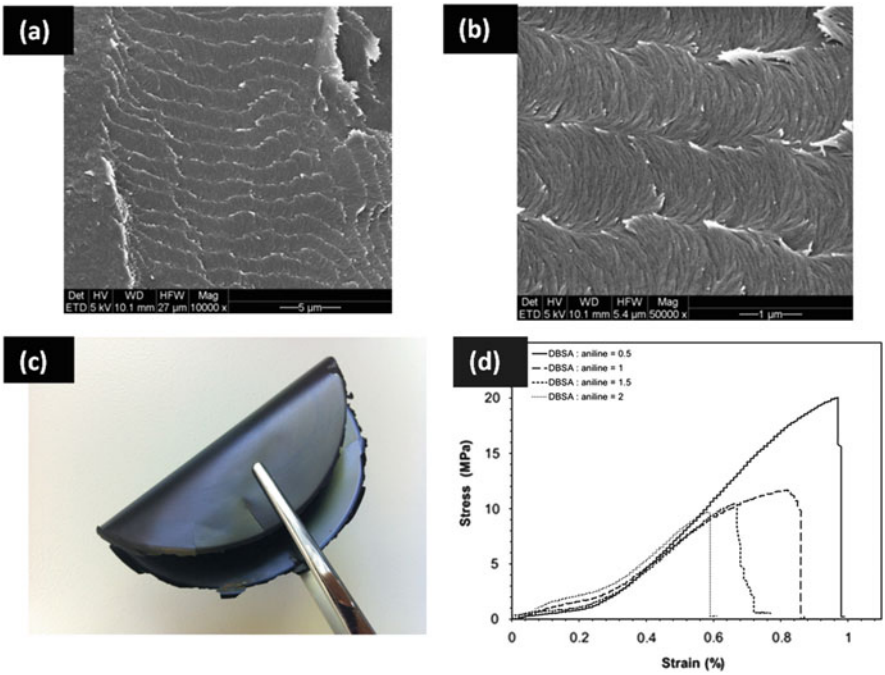

Fig. 18 (**a**, **b**) SEM micrographs of air-dried CNC-PANI-DBSA nanocomposite films depicting preservation of the chiral nematic organization after emulsion polymerization. Further doping with, for instance, HCl disrupts the chiral nematic order, but maintains good conductive and mechanical properties. (**c**) Photograph showing the flexibility of these semiconducting nanocomposite films. (**d**) Viscoelastic stress versus strain response of the films at constant mass ratio (CNC:aniline = 2) but different molar ratios of DBSA:aniline (adapted after Hamad and Atifi [113])

powder or a film with limited structural integrity. The mechanical properties of CNC-PANI-DBSA nanocomposite films change significantly with increasing DBSA content (Fig. 18d). At a molar ratio of DBSA to aniline of 0.5, the nanocomposite shows maximum stress and strain values of 22 ± 2.16 MPa and $0.89 \pm 0.20\%$, respectively, whereas at a higher molar ratio of 2, the tensile strength and strain decrease to 8 MPa and 0.56%, respectively [113]. Furthermore, increasing the CNC content in the system at a constant DBSA concentration expectedly leads to enhancement of the nanocomposite strength [113]. The decrease in tensile strength for CNC-PANI-DBSA nanocomposites at high DBSA concentration could be a result of the steric effect of the long alkyl chains of DBSA, which in turn limit CNCs from connecting with each other and thus result in a relatively weakened system [113]. However, when the CNC concentration is increased, CNCs act as an efficient scaffold for PANI as a result of the intermolecular and hydrogen bonds existing between CNC nanoparticles [101, 113]. A similar effect was observed with nanocomposites of cellulose nanofibrils and polypyrrole (CNF–PPy), where

postsynthetic inclusion of pristine CNFs into the composite enhanced the mechanical strength as a result of hydrogen bonding between adjacent pristine CNFs [112].

It is worthwhile noting that CNC-DBSA-PANI nanocomposite films are stronger and more flexible films than, for instance, graphene/polyaniline composite paper or graphene paper, with tensile strengths of 12.6 and 8.8 MPa, and maximum strains of 0.11 and 0.08%, respectively [114].

Large-scale CNCs coatings can, in principle, be developed using electrophoretic deposition (EPD) of different grades of CNCs (H-Form, Na-Form and carboxylated CNCs) for use in a variety of value-added industrial products [115]. With proper pulse EPD parameters, one can control the uniformity of CNC films and obtain smooth and bubble-free CNC deposits. The chiral nematic organization can be preserved in electrodeposited CNC films, and aqueous CNCs dispersions can further be used to suitably trap electropolymerized conjugated polymers, for instance, to make CNC–PANI nanocomposite films [115]. These deposited nanocomposite films exhibit good adherence to the substrate after drying, and possess tunable conductivities and photonic properties [115].

6.2 Chiral Mesoporous Carbon Films

The development of porous carbon materials with high specific surface areas, large pore volumes, and large adsorption capacities has been driven by interest in applications such as electrode materials, sorbents in separation processes, and catalyst supports [116]. In particular, their use as high surface area electrodes in electric-double layer supercapacitors has led to devices with promising high specific capacitance values [117]. In all of these applications, two often-encountered drawbacks of porous carbon materials are (1) slow mass transport properties as a result of significant microporosity inherent to their preparation, and (2) elaborate, time-consuming, or expensive synthetic methods that are impractical for commercial-scale operations [71].

Iridescent, mesoporous silica films prepared via CNC templating can be used to prepare freestanding mesoporous carbon films, simply by pyrolysis under nitrogen at 900°C (instead of calcining under air), followed by etching of the silica [118]. The resulting glossy black films are obtained in about 30% yield as amorphous carbon and are semiconducting at room temperature. The porosity of the films varies with the silica loading, ranging from largely microporous for pure CNC-derived samples to completely mesoporous for 65 w/w% CNC samples [118]. The surface area and pore volume of the CNC-templated mesoporous carbon films are comparable to those of carbon materials prepared by hard templating, and their morphology remarkably corresponds to CNC-templated mesoporous silica with helical twisting, indicative of chiral nematic ordering (Fig. 19a, b).

Because of their freestanding nature, mesoporous carbon films can be used directly as supercapacitor electrodes without a binding agent, typically needed for other mesoporous carbon electrodes (Fig. 19c). In a symmetrical capacitor with

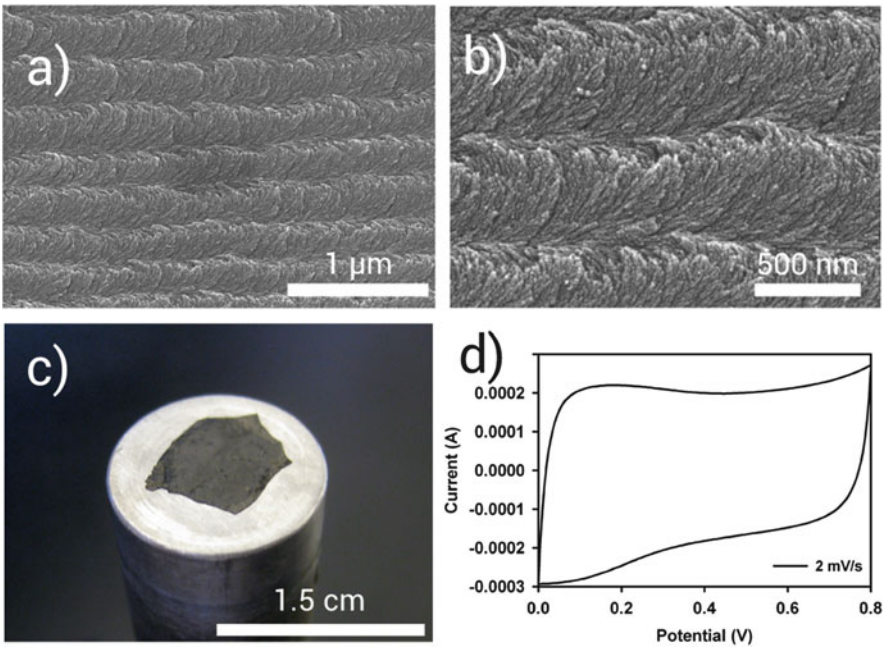

Fig. 19 (**a**, **b**) SEM images of chiral nematic mesoporous carbon films prepared by pyrolysis of CNC–silica composites show similar helical twisting morphologies. (**c**) The freestanding films can be used directly without any binders as electrodes in electrical double-layer supercapacitors. (**d**) Films display near-ideal capacitor behavior, with specific capacitances comparable with those of other state-of-the-art carbon-based supercapacitors (adapted from Shopsowitz et al. [118])

aqueous sulfuric acid as the electrolyte, mesoporous carbon films display near-ideal capacitor behavior (Fig. 19d). Their specific capacitance is 170 F g^{-1} at a current load of 230 mA g^{-1}, with performance decreasing at higher power loads [118].

7 Conclusions and Outlook

The chiral structure of CNCs, which derives from the chirality of the glucose subunits, enables them to form a chiral nematic liquid crystalline phase when dispersed in various solvents. This spontaneous self-assembly process occurs above a critical concentration and is influenced by many factors, including the choice of solvent, the aspect ratio of the particles, surface charge, pH, and ionic strength. The slow drying of aqueous CNC suspensions can result in solid films that retain the chiral nematic ordering of the liquid crystal phase. These films often have brilliant iridescent colors as a result of the 1D photonic properties of chiral nematic liquid crystals. These cause the films to selectively reflect circularly polarized light with wavelengths that depend on the helical pitch of the chiral nematic structure.

CNCs also possess unique piezoelectric properties and can potentially be used in conjunction with conjugated polymers to produce sustainable, organic semiconducting materials.

The potential to mimic the chiral nematic organization of natural helicoidal structures featuring strong optical signatures with unique polarization-dependence through CNC self-assembly has ushered exciting new research directions with promising commercialization prospects. Liquid crystal templating techniques have been shown to successfully transfer the chiral nematic organization of CNCs to solid-state composite materials based on silica and organosilica. The resulting CNC–(organo)silica composites can be transformed into a range of new materials, including highly porous semiconducting carbon films with chiral nematic order that function as supercapacitor electrodes. Alternatively, the CNC template can be removed to yield flexible, iridescent, mesoporous, large-scale (organo)silica films potentially suitable for application as reflectors, sensors, membranes, and sorbents. We have also shown similar approaches for the preparation of photonic hydrogels and polymers, as well as mesoporous cellulose films with tunable optical and mechanical properties (the first example of a functional, active cellulosic material). Moreover, encapsulation of functional guests (e.g., quantum dots) [119] within the chiral channels offers opportunities to produce new functional, responsive materials and to transfer chiral nematic order to other solid-state compositions.

References

1. Hamad WY, Hu TQ (2010) Structure-process-yield interactions in nanocrystalline cellulose extraction. Can J Chem Eng 88(3):392–402
2. Kovacs T, Naish V, O'Conner B, Blaise C, Gagne F, Hall L, Trudeau V, Martel P (2010) An ecotoxicological characterization of nanocrystalline cellulose (NCC). Nanotoxicology 4 (3):255–270
3. Bazhenov VA (1961) Piezoelectric properties of wood. Consultants Bureau, New York
4. Nishiyama Y, Langan P, Chanzy H (2002) Crystal structure and hydrogen-bonding system in cellulose I_β from synchrotron x-ray and neutron fiber diffraction. J Am Chem Soc 124:9074–9082
5. Frka-Petesic B, Jean B, Heux L (2014) First experimental evidence of a giant permanent electric-dipole moment in cellulose nanocrystals. Europhys Lett 107(2):28006. doi:10.1209/0295-5075/107/28006
6. Li L-S, Alivisatos AP (2003) Origin and scaling of the permanent dipole moment in CdSe nanorods. Phys Rev Lett 90:097402
7. Csoka L, Hoeger IC, Rojas OJ, Peszlen I, Pawlak JJ, Peralta PN (2012) Piezoelectric effect of cellulose nanocrystals thin films. ACS Macro Lett 1:867–870
8. Habibi Y, Heim T, Douillard R (2008) AC electric field-assisted assembly and alignment of cellulose nanocrystals. J Polym Sci B Polym Phys 46:1430–1436
9. Csoka L, Hoeger IC, Peralta P, Peszlen I, Rojas OJ (2011) Dielectrophoresis of cellulose nanocrystals and alignment in ultrathin films by electric field-assisted shear assembly. J Colloid Interface Sci 363:206–212
10. Vignolini V, Rudall PJ, Rowland AV, Reed A, Moyroud E, Faden RB, Baumberg JJ, Glover BJ, Steiner U (2012) Pointillist structural color in Pollia fruit. Proc Natl Acad Sci USA 109 (39):15712–15715

11. Burresi M, Cortese L, Patteli L, Kolle M, Vukusic P, Wiersma DS, Steiner U, Vignolini S (2014) Bright-white beetle scales optimise multiple scattering of light. Sci Rep 4:6075. doi:10.1038/srep06075
12. Wilts BD, Whitney HM, Glover BJ, Steiner U, Vignolini S (2014) Natural helicoidal structures: morphology, self-assembly and optical properties. Mater Today Proc 1S:177–185
13. Lee DW (1991) Ultrastructural basis and function of iridescent blue colour of fruits in *Elaeocarpus*. Nature 394:260–262
14. Kinoshita S, Yoshioka S, Miyazaki J (2008) Physics of structural colors. Rep Prog Phys 71:076401
15. Doucet SM, Meadows MG (2009) Iridescence: a functional perspective. J R Soc Interface 6: S115–S132
16. Giese M, Blusch LK, Khan MK, Hamad WY, MacLachlan MJ (2014) Responsive mesoporous photonic cellulose films by supramolecular contemplating. Angew Chem Int Ed 53(34):8880–8884
17. Lemke CH, Dong RY, Michal CA, Hamad WY (2012) New insights into nano-crystalline cellulose structure and morphology based on solid-state NMR. Cellulose 19:1619–1629
18. Chuang IS, Maciel GE (1992) ^{13}C CP/MAS NMR study of the structural dependence of urea-formaldehyde resins on formaldehyde-to-urea molar ratios at different urea concentrations and pH values. Macromolecules 25:3204–3226
19. de Vries HI (1951) Rotary power and other optical properties of certain liquid crystals. Acta Crystallogr 4:219–226
20. Kelly JA, Shukaliak AM, Cheung C, Shopsowitz KE, Hamad WY, MacLachlan MJ (2013) Responsive photonic hydrogels based on nanocrystalline cellulose. Angew Chem Int Ed 52 (34):8912–8916
21. Zhang YP, Chodavarapu VP, Kirk AG, Andrews MP (2013) Structured color humidity indicator from reversible pitch tuning in self-assembled nanocrystalline cellulose films. Sens Actuators B 176:692–697
22. Khan MK, Giese M, Yu M, Hamad WY, MacLachlan MJ (2013) Flexible mesoporous photonic resins with tunable chiral nematic structures. Angew Chem Int Ed 52 (34):8921–8924
23. Schlesinger M, Giese M, Blusch LK, Hamad WY, MacLachlan MJ (2015) Chiral nematic cellulose–gold nanoparticle composites from mesoporous photonic cellulose. Chem Commun 51:530–533
24. Schlesinger M, Hamad WY, MacLachlan MJ (2015) Optically tunable chiral nematic mesoporous cellulose films. Soft Matter 11(23):4686–4694
25. Khan MK, Bsoul A, Walus K, Hamad WY, MacLachlan MJ (2015) Photonic patterns printed in chiral nematic mesoporous resins. Angew Chem Int Ed. doi:10.1002/anie.201410411
26. Giese M, De Witt JC, Shopsowitz KE, Manning AP, Dong RY, Michal CA, Hamad WY, MacLachlan MJ (2013) Thermal switching of the reflection in chiral nematic mesoporous organosilica films infiltrated with liquid crystals. ACS Appl Mater Interfaces 5 (15):6854–6859
27. Giese M, Khan MK, Yu M, Hamad WY, MacLachlan MJ (2013) Imprinting of photonic patters with novel thermosetting amino-formaldehyde-cellulose composites. ACS Macro Lett 2(9):818–821
28. Cheung CCY, Giese M, Kelly JA, Hamad WY, MacLachlan MJ (2013) Iridescent chiral nematic cellulose nanocrystals (CNCs)/polymer composites assembled in organic solvents. ACS Macro Lett 2(11):1016–1020
29. Page DH, El-Hosseiny F, Winkler K (1971) Behaviour of single wood fibres under axial tensile strain. Nature 229:252
30. Page DH, El-Hosseiny F, Winkler K, Lancaster APS (1977) Elastic modulus of single wood pulp fibers. TAPPI J 60(4):114
31. Plaza N, Zelinka SL, Stone DS, Jakes JE (2013) Plant-based torsional actuator with memory. Smart Mater Struct 22, 072001 (7 pages)

32. Dumanli AG, Kamita G, Landman J, van der Kooij H, Glover BJ, Baumberg JJ, Steiner U, Vignolini S (2014) Controlled, bio-inspired self-assembly of cellulose-based chiral reflectors. Adv Opt Mater 2:646–650
33. Dumanli AG, van der Kooij HM, Kamita G, Reisner E, Baumberg JJ, Steiner U, Vignolini S (2014) Digital color in cellulose nanocrystal films. ACS Appl Mater Interfaces 6:12302–12306
34. Zhang YP, Chodavarapu VP, Kirk AG, Andrews MP (2012) Nanocrystalline cellulose for covert optical encryption. J Nanophotonics 6, 063516. doi:10.1117/1.JNP. 6.063516
35. Khan MK, Hamad WY, MacLachlan MJ (2014) Tunable mesoporous bilayer photonic resins with chiral nematic structures and actuator properties. Adv Mater 26(15):2323–2328
36. Lee W-E, Jin Y-J, Park L-S, Kwak G (2012) Fluorescent actuator based on microporous conjugated polymer with intramolecular stack structure. Adv Mater 24:5604–5609
37. Dong XM, Kimura T, Revol J-F, Gray DG (1996) Effects of ionic strength on the isotropic – chiral nematic phase transition of suspensions of cellulose crystallites. Langmuir 12(8):2076–2082
38. Geng Y, Almeida PL, Fernandes SN, Cheng C, Palffy-Muhoray P, Godinho MH (2013) A cellulose liquid crystal motor: a steam engine of the second kind. Sci Rep 3:1–4
39. Islam MR, Li X, Smyth K, Serpe MJ (2013) Polymer-based muscle expansion and contraction. Angew Chem Int Ed 52:10330–10333
40. Asher S, Holtz J, Weissman J, Pan G (1998) Mesoscopically periodic photonic-crystal materials for linear and nonlinear optics and chemical sensing. MRS Bull 23:44–50
41. von Freymann G, Kitaev V, Lotsch BV, Ozin GA (2013) Bottom-up assembly of photonic crystals. Chem Soc Rev 42:2528–2554
42. Ge J, Yin Y (2011) Responsive photonic crystals. Angew Chem Int Ed 50:1492–1522
43. Tatsumi M, Teramoto Y, Nishio Y (2012) Polymer composite reinforced by locking-in liquid-crystalline assembly of cellulose nanocrystallites. Biomacromolecules 13:1584–1591
44. Kelly JA, Yu M, Hamad WY, MacLachlan MJ (2013) Large, crack-free freestanding films with chiral nematic structures. Adv Opt Mater 1(4):295–299
45. Ben-Moshe M, Alexeev VL, Asher SA (2006) Fast responsive crystalline colloidal array photonic crystal glucose sensors. Anal Chem 78:5149–5157
46. Tanaka T, Fillmore DJ (1979) Kinetics of swelling of gels. J Chem Phys 70:1214–1218
47. Capadona JR, van den Berg O, Capadona LA, Schroeter M, Rowan SJ, Tyler DJ, Weder C (2007) A versatile approach for the processing of polymer nanocomposites with self-assembled nanofiber templates. Nat Nanotechnol 2(12):765–769
48. Capadona JR, Shanmuganathan K, Tyler DJ, Rowan SJ, Weder C (2008) Stimuli-responsive polymer nanocomposites inspired by the sea cucumber dermis. Science 319:1370–1374
49. Dong XM, Gray DG (1997) Effect of counterions on ordered phase formation in suspensions of charged rodlike cellulose crystallites. Langmuir 13(8):2404–2409
50. Lin VS, Motesharei K, Dancil KP, Sailor MJ, Ghadiri MR (1997) A porous silicon-based optical interferometric biosensor. Science 278:840–843
51. Choi SY, Mamak M, von Freymann G, Chopra N, Ozin GA (2006) Mesoporous bragg stack color tunable sensors. Nano Lett 6:2456–2461
52. Yamada Y, Nakamura T, Ishi M, Yano K (2006) Reversible control of light reflection of a colloidal crystal film fabricated from monodisperse mesoporous silica spheres. Langmuir 22:2444–2446
53. Petkovich ND, Stein A (2013) Controlling macro- and mesostructures with hierarchical porosity through combined hardand soft templating. Chem Soc Rev 42:3721–3739
54. Lee YS (2008) Self-assembly and nanotechnology: a force balance approach. Wiley, Hoboken
55. Chandrasekhar S (1992) Liquid crystals, 2nd edn. Cambridge University Press, Cambridge
56. Friberg SE, Yang CC, Goubran G, Partch RE (1991) Ammonia microemulsions and ammonolysis of silicon tetrachloride. Langmuir 7:1103–1106

57. Kresge CT, Leonowicz ME, Roth WJ, Vartuli JC, Beck JS (1992) Ordered mesoporous molecular sieves synthesized by a liquid-crystal template mechanism. Nature 359:710–712
58. Thomas A, Antonietti M (2003) Silica nanocasting of simple cellulose derivatives: towards chiral pore systems with long-range order and chiral optical coatings. Adv Funct Mater 13:763–766
59. Wang W, Liu R, Liu W, Tan J, Liu W, Kang H, Huang Y (2010) Hierarchical mesoporous silica prepared from ethyl-cyanoethyl cellulose cholesteric liquid crystalline phase. J Mater Sci 45:5567–5573
60. Qi H, Roy X, Shopsowitz KE, Hui JKH, MacLachlan MJ (2010) Liquid-crystal templating in ammonia: a facile route to micro- and mesoporous metal nitride/carbon composites. Angew Chem Int Ed 49:9740–9743
61. Alonso B, Belamie E (2010) Chitin-silica nanocomposites by self-assembly. Angew Chem Int Ed 49:8201–8204
62. Belamie E, Boltoeva MY, Yang K, Cacciaguerra T, Alonso B (2011) Tunable hierarchical porosity from self-assembled chitin-silica nanocomposites. J Mater Chem 21:16997–17006
63. Nguyen TD, Shopsowitz KE, MacLachlan MJ (2013) Mesoporous silica and organosilica films templated by nanocrystalline chitin. Chem Eur J 19:15148–15154
64. Dujardin E, Blaseby M, Mann S (2003) Synthesis of mesoporous silica by sol-gel mineralization of cellulose nanorod nematic suspensions. J Mater Chem 13:696–699
65. Shin Y, Exarhos GJ (2007) Template synthesis of porous titania using cellulose nanocrystals. Mater Lett 61:2594–2597
66. Shopsowitz KE, Qi H, Hamad WY, MacLachlan MJ (2010) Free-standing mesoporous silica films with tunable chiral nematic structures. Nature 468:422–425
67. Shopsowitz KE, Kelly JA, Hamad WY, MacLachlan MJ (2013) Biopolymer template glass with a twist: controlling the chirality, porosity and photonic properties of silica with cellulose nanocrystals. Adv Funct Mater 24(3):327–338
68. Shopsowitz KE, Hamad WY, MacLachlan MJ (2012) Flexible and iridescent chiral nematic mesoporous organosilica films. J Am Chem Soc 134(2):867–870
69. Kelly JA, Shopsowitz KE, Ahn J, Hamad WY, MacLachlan MJ (2012) Chiral nematic stained glass: controlling the optical properties of nanocrystalline cellulose-templated materials. Langmuir 28(50):17256–17262
70. Kelly JA, Kyle Manchee CP, Cheng S, Ahn JM, Shopsowitz KE, Hamad WY, MacLachlan MJ (2014) Evaluation of form birefringence in chiral nematic mesoporous materials. J Mater Chem C 2:5093–5097
71. Kelly JA, Giese M, Shopsowitz KE, Hamad WY, MacLachlan MJ (2014) The development of chiral nematic mesoporous materials. Acc Chem Res 47(4):1088–1096
72. Asefa A, MacLachlan MJ, Coombs N, Ozin GA (1999) Periodic mesoporous organosilicas with organic groups inside the channel walls. Nature 402:867–871
73. Mizoshita N, Ikai M, Tani T, Inagaki S (2009) Hole-transporting periodic mesostructured organosilica. J Am Chem Soc 131:14225–14227
74. Haffer S, Tiemann M, Fröba M (2010) Periodic mesoporous organosilica (PMO) materials with uniform spherical core-shell structure. Chem Eur J 16:10447–10452
75. Wang H, Roman M (2011) Formation and properties of chitosan-cellulose nanocrystal polyelectrolyte-macroion complexes for drug delivery applications. Biomacromolecules 12:1585–1593
76. Lim MH, Stein A (1999) Comparative studies of grafting and direct syntheses of inorganic-organic hybrid mesoporous materials. Chem Mater 11:3285–3295
77. Lu Y, Fan H, Doke N, Loy DA, Assink RA, LaVan DA, Brinker CJ (2000) Evaporation-induced self-assembly of hybrid bridged silsesquioxane film and particulate mesophases with integral organic functionality. J Am Chem Soc 122:5258–5261
78. Inagaki S, Guan S, Ohsuna T, Terasaki O (2002) An ordered mesoporous organosilica hybrid material with a crystal-like wall structure. Nature 416:304–307

79. Terpstra AS, Shopsowitz KE, Gregory CF, Manning AP, Michal CA, Hamad WY, Yang J, MacLachlan MJ (2013) Helium ion microscopy: a new tool for imaging novel mesoporous silica and organosilica materials. Chem Commun 49(16):1645–1647
80. Robbie K, Broer DJ, Brett MJ (1999) Chiral nematic order in liquid crystals imposed by an engineered inorganic nanostructure. Nature 399:764–766
81. Burgess IB, Koay N, Raymond KP, Kolle M, Loncar M, Aizenberg J (2012) Wettingin color: calorimentric differentiation of organic liquids with high selectivity. ACS Nano 6:1427–1437
82. Bragg WL, Pippard AB (1953) The form birefringence of macromolecules. Acta Crystallogr 6:865–867
83. Anderson MA, Tinsley-Bown A, Allcock P, Perkins EA, Snow P, Hollings M, Smith RG, Reeves C, Squirrell DJ, Nicklin S, Cox TI (2003) Sensitivity of the optical properties of porous silica layers to the refractive index of liquid in the pores. Phys Status Solidi A 197:528–533
84. Lu A, Scüth F (2006) Nanocasting: a versatile strategy for creating nanostructured porous materials. Adv Mater 18:1793–1805
85. Lu AH, Zhao D, Wan Y (2009) Nanocasting: a versatile strategy for creating nanostructured porous materials. The Royal Society of Chemistry, Cambridge
86. Zhang R, Elzatahry AA, Al-Deyab SS, Zhao D (2012) Mesoporous titania: from synthesis to application. Nano Today 7:344–366
87. Shopsowitz KE, Stahl A, Hamad WY, MacLachlan MJ (2012) Hard templating of nanocrystalline titanium dioxide with chiral nematic order. Angew Chem Int Ed 51(28):6886–6890
88. Zeng S, Baillargeat D, Ho H-P, Yong K-T (2014) Nanomaterials enhanced surface plasmon resonance for biological and chemical sensing applications. Chem Soc Rev 43:3426–3452
89. Gautier C, Buergi T (2009) Chiral gold nanoparticles. ChemPhysChem 10:483–492
90. Govorov AO, Gun'ko YK, Slocik JM, Gerard VA, Fan Z, Naik RR (2011) Chiral nanoparticle assemblies: circular dichroism, plasmonic interactions, and exciton effects. J Mater Chem 21:16806–16818
91. Qi H, Shopsowitz KE, Hamad WY, MacLachlan MJ (2011) Chiral nematic assemblies of silver nanoparticles in mesoporous silica thin films. J Am Chem Soc 133(11):3728–3731
92. Mehr SHM, Giese M, Qi H, Shopsowitz KE, Hamad WY, MacLachlan MJ (2013) Poly(*p*-phenylenevinylene) in chiral nematic mesoporous organosilica. Langmuir 29 (40):12579–12584
93. Akagi K, Piao G, Kaneko S, Sakamaki K, Shirakawa H, Kyotani M (1998) Helical polyacetylene synthesized with a chiral nematic reaction field. Science 282:1683–1686
94. Ruda H, Matsuura N (2007) Nano-engineered tunable photonic crystals in the near-IR and visible electromagnetic spectrum. Springer, Boston, pp 997–1019
95. Chandrasekhar P (1999) Conducting polymers, fundamentals and applications: a practical approach. Kluwer Academic, Boston, pp 434–435
96. Skotheim TG, Elsenbaumer RL, Reynolds JR (1998) Handbook of conducting polymers, 2nd edn. Marcel Dekker, New York, pp 883–1007
97. Liao Y, Zhang C, Zhang Y, Strong V, Tang J, Li XG, K-Zadeh K, Hoek EMV, Wang KL, Kaner RB (2011) Carbon nanotube/polyaniline composite nanofibers: facile synthesis and chemosensors. Nano Lett 11:954–959
98. Lin J, Tang Q, Wu J, Sun H (2008) Synthesis, characterization and properties of polyaniline/expanded vermiculite intercalated nanocomposite. Sci Technol Adv Mater 9(2), 025010
99. Zhu C, Zhai J, Wen D, Dong S (2012) Graphene oxide/polypyrrole nanocomposites: one-step electrochemical doping, coating and synergistic effect for energy storage. J Mater Chem 22:6300–6306
100. van der Berg O, Schroeter M, Capadona JR, Weder C (2007) Nanocomposites based on cellulose whiskers and (semi)conducting conjugated polymers. J Mater Chem 17:2746–2753
101. Tkalya E, Ghislandi M, Thielemans W, van der Schoot P, de With G, Koning C (2013) Cellulose nanowhiskers templating in conductive polymer nanocomposites reduces electrical percolation threshold 5-fold. ACS Marco Lett 2:157–163

102. Fan J, Shao W, Xu G, Cui XT, Luo X (2014) Preparation and electrochemical catalytic application of nanocrystalline cellulose doped poly(3,4-ethylenedioxythiophene) conducting polymer nanocomposites. RSC Adv 4:24328–24333
103. Hu W, Chen S, Yang Z, Liu L, Wang H (2011) Flexible electrically conductive nanocomposite membrane based on bacterial cellulose and polyaniline. J Phys Chem B 115:8453–8457
104. Sakakibara K, Rosenau T (2012) Polythiophene-cellulose composites: synthesis, optical properties and homogeneous oxidative co-polymerization. Holzforschung 66:9–19
105. Wang H, Bian L, Zhou P, Jian T, Tang W (2013) Core-sheath structured bacterial cellulose/polypyrrole nanocomposites with excellent conductivity as supercapacitors. J Mater Chem A 1:578–584
106. Mattoso LHC, Medeiros ES, Baker DA, Avloni J, Wood DF, Orts W (2009) Electrically conductive nanocomposites made from cellulose nanofibrils and polyaniline. J Nanosci Nanotechnol 9:2917–2922
107. Byoung-Ho L, Hyun-Joong K, Han-Seung Y (2012) Polymerization of aniline on bacterial cellulose and characterization of bacterial cellulose/polyaniline nanocomposite films. Curr Appl Phys 12:75–80
108. Nyström G, Mihranyan A, Razaq A, Lindström T, Neyholm L, Strømme M (2010) A nanocellulose polypyrrole composite based on microfibrillated cellulose from wood. J Phys Chem B 114:4178–4182
109. Marins JA, Soares BG, Dahmouche K, Ribeiro SJL, Barud H, Bonemer D (2011) Structure and properties of conducting bacterial cellulose-polyaniline nanocomposites. Cellulose 18:1285–1294
110. Müller D, Mandelli JS, Marins JA, Soares BG, Porto LM, Rambo CR, Barra GMO (2012) Electrically conducting nanocomposites: preparation and properties of polyaniline (PAni)-coated bacterial cellulose nanofibers (BC). Cellulose 19:1645–1654
111. Liew SY, Shariki S, Vuorema A, Walsh DA, Marken F, Thielmans W (2012) Cellulose nanowhiskers in elechtrochamical applications. In: Liebner F et al (eds) Functional materials from renewable sources, ACS symposium series. American Chemical Society, Washington DC, pp 75–106. ISBN 9-78084122789-7
112. Mihranyan A, Esmaeili M, Razaq A, Alexeichlik D, Lindtröm T (2012) Influence of the nanocellulose raw material characteristics on the electrochemical and mechanical properties of conductive paper electrodes. J Mater Sci 47:4463–4472
113. Hamad WY, Atifi S (2015) Flexible, semiconducting nanocomposite materials based on nanocrystalline cellulose and polyaniline. CA Patent No. 2,831,147
114. Wang D-W, Li F, Zhao J, Ren W, Chen ZG, Tan J, Wu ZS, Gentle I, Lu GQ, Cheng HM (2009) Fabrication of graphene/polyaniline composite paper via in situ anodic electropolymerization for high performance flexible electrod. ACS Nano 3(7):1745–1752
115. Hamad WY, Atifi S, Stead N (2013) Cellulose nanocrystal (CNC) films and CNCs-based polymer films using electrochemical techniques. USPTO Application 61/819,905 filed on May 6, 2013
116. Lee J, Kim J, Hyeon T (2006) Recent progress in the synthesis of porous carbon materials. Adv Mater 18:2073–2094
117. Zhang LL, Zhao XS (2009) Carbon-based materials as supercapacitor electrodes. Chem Soc Rev 38:2520–2531
118. Shopsowitz KE, Hamad WY, MacLachlan MJ (2011) Chiral nematic mesoporous carbon derived from nanocrystalline cellulose. Angew Chem Int Ed 123(46):11183–11187
119. Nguyen TD, Hamad WY, MacLachlan MJ (2014) CdS quantum dots encapsulated in chiral nematic mesoporous silica: new iridescent and luminescent materials. Adv Funct Mater 24 (6):777–783

Index